Carbon Nanostructures

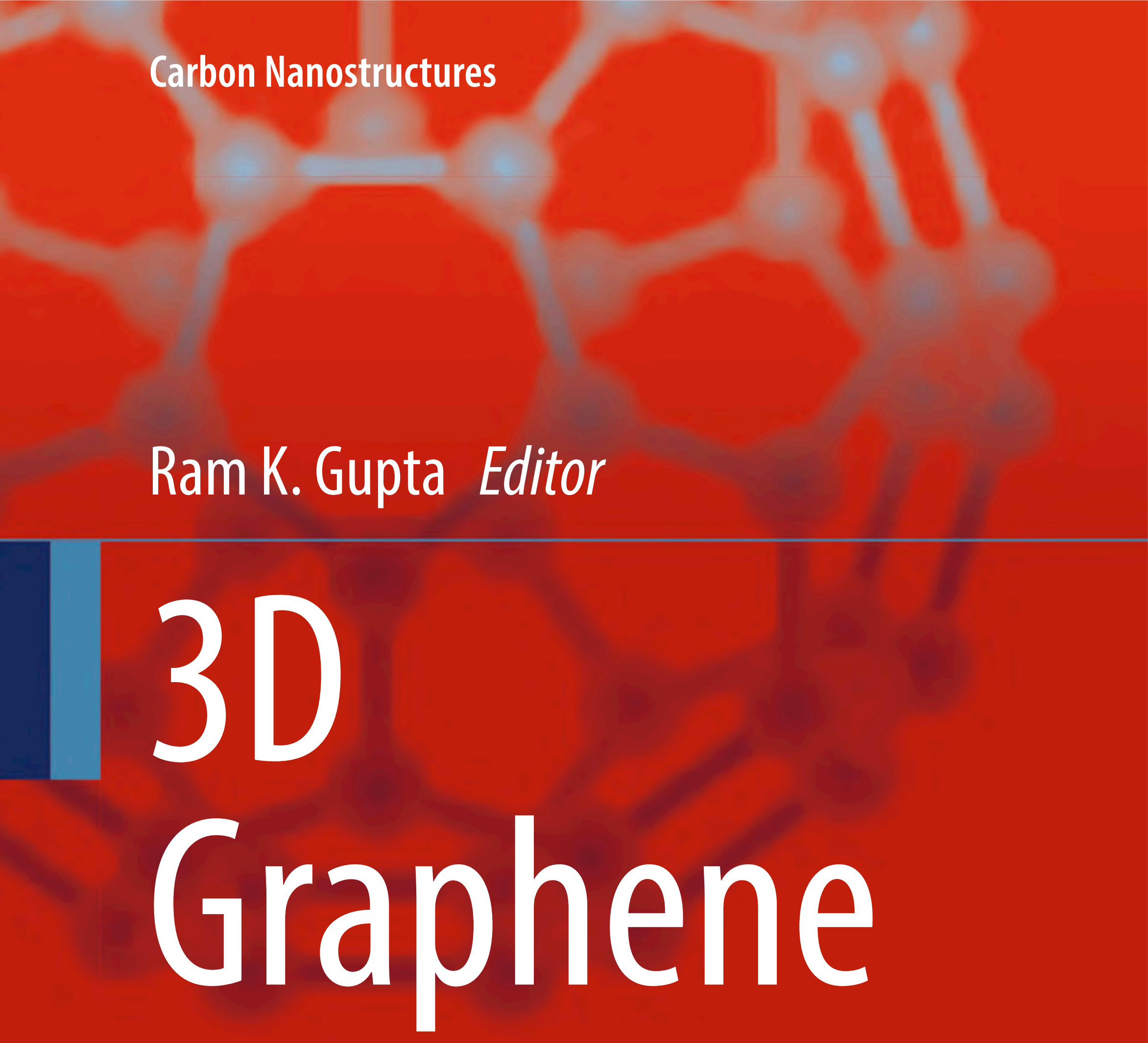

Ram K. Gupta *Editor*

3D Graphene

Fundamentals, Synthesis, and Emerging Applications

Springer

Carbon Nanostructures

Series Editor

Paulo Araujo, The University of Albama, Tuscaloosa, AL, USA

Editorial Board

Antonio Gomes Sousa Filho, Universidade Federal do Ceara—UFC, Fortaleza, Brazil

Stephen K. Doorn, Los Alamos National Laboratory—LANL, Los Alamos, NM, USA

Aaron D. Franklin, Electrical and Computer Engineering, Hudson Hall 129, Duke University, Durham, NC, USA

Achim Hartschuh, Ludwig-Maximilians-Universität, München, Germany

Carbon is intimately connected to almost everything we deal with in a daily basis. Due to its outstanding properties, such as high stability at environmental conditions, different hybridizations, strong covalent bond formation and easy of compounds formation, carbon has been a topic of scientific interest in several areas. Indeed, starting in the 19th century, chemists have devoted a whole field to study carbon-based compounds, which is, nowadays, known as Organic Chemistry. Remarkably, the last 30 years have been witnessing an exponential advance in the science involving carbon and carbon structures. Since the discovery of Fullerenes in 1985, which was awarded the Nobel Prize in Chemistry in 1996, carbon nanostructures have been attracting a great deal of attention from the research community. This public interest dramatically increased after the publications by the Iijima and Bethune groups on single-wall carbon nanotubes in 1993 and found a “new research era” with the isolation of a monolayer of carbon atoms, also called graphene, which conducted groundbreaking experiments demonstrating outstanding phenomena such as the Klein-Tunneling and the fractional quantum hall effect. No wonder, graphene was the object of the 2010 Nobel Prize in Physics.

The “Carbon Nanostructures” book series covers the state-of-art in the research of nanocarbons and their applications. Topics related to carbon allotropes such as diamond, graphite, graphene, fullerenes, metallofullerenes, solid C60, bucky onions, foams, nanotubes and nanocones, including history, theory, synthesis, chemistry & physics, Biophysics & engineering, characterization methods, properties and applications are welcome. Within the “Carbon Nanostructures” book series, the reader will find valuable, up-to-date account of both the newer and traditional forms of carbon. This book series supports the rapid expansion of this field and is a valuable resource for students and professionals in several different areas.

Springer welcomes new book ideas from potential authors. If you are interested in publishing your book in this series, please contact us via mayra.castro@springer.com

**** Indexed by Scopus (2018) ****

Ram K. Gupta
Editor

3D Graphene

Fundamentals, Synthesis, and Emerging Applications

Springer

Editor
Ram K. Gupta
Department of Chemistry
Pittsburg State University
Pittsburg, PA, USA

ISSN 2191-3005 ISSN 2191-3013 (electronic)
Carbon Nanostructures
ISBN 978-3-031-36248-4 ISBN 978-3-031-36249-1 (eBook)
https://doi.org/10.1007/978-3-031-36249-1

© The Editor(s) (if applicable) and The Author(s), under exclusive license to Springer Nature Switzerland AG 2023

This work is subject to copyright. All rights are solely and exclusively licensed by the Publisher, whether the whole or part of the material is concerned, specifically the rights of translation, reprinting, reuse of illustrations, recitation, broadcasting, reproduction on microfilms or in any other physical way, and transmission or information storage and retrieval, electronic adaptation, computer software, or by similar or dissimilar methodology now known or hereafter developed.
The use of general descriptive names, registered names, trademarks, service marks, etc. in this publication does not imply, even in the absence of a specific statement, that such names are exempt from the relevant protective laws and regulations and therefore free for general use.
The publisher, the authors, and the editors are safe to assume that the advice and information in this book are believed to be true and accurate at the date of publication. Neither the publisher nor the authors or the editors give a warranty, expressed or implied, with respect to the material contained herein or for any errors or omissions that may have been made. The publisher remains neutral with regard to jurisdictional claims in published maps and institutional affiliations.

This Springer imprint is published by the registered company Springer Nature Switzerland AG
The registered company address is: Gewerbestrasse 11, 6330 Cham, Switzerland

Dedicated to Dr. Tim Dawsey for his support, encouragement, and guidance. Thank you for always being there since the beginning and supporting me to complete this book.

Contents

Introduction to 3D Graphene

Chuanyin Xiong, Tianxu Wang, Yongkang Zhang, and Qing Xiong

Abstract The 3D graphene-based materials fabricated by various methods not only effectively prevent mutual re-stacking between the graphene layers to make full use of its specific surface area, but also obtain excellent functional characteristics via introducing other functional materials. This part briefly summarizes the types, preparation methods, application fields, existing problems, and development trends of 3D graphene-based materials with different structures and components. The purpose is to provide methods and theoretical references for the research and efficient utilization of 3D graphene-based materials.

Keywords 3D graphene · Classification · Preparation · Application

1 Classification of Graphene

Graphene is a 2D carbon material with a hexagonal honeycomb lattice structure hybridized by carbon atoms connected by sp^2 [1] and is the basic building block of fullerene, carbon nanotubes, and 3D graphene. Andre Geim and Konstantin Novoselov successfully prepared 2D graphene sheets by mechanical stripping for the first time in 2004. Because of its excellent conductivity (electron mobility of 150,000 $cm^2\ V^{-1}\ s^{-1}$) [2], ultra-high theoretical specific surface area (2630 $m^2\ g^{-1}$) [3], high mechanical strength (Young's modulus 1.1 Tpa, tensile strength 125 GPa) [4], and good thermal conductivity (thermal conductivity of 5300 $W\ m^{-1}\ K^{-1}$) [5], it has attracted wide attention of researchers around the world.

Although the 2D graphene nanosheets with a single thickness of about 0.35 nm have excellent performance, in practical applications, due to the van der Waals force and π–π bond between the graphene layers [6], it is very easy to often stack between the graphene layers to form graphite powder. This seriously affects the surface utilization of 2D graphene nanosheets and reduces their inherent excellent performance. For

---

C. Xiong (✉) · T. Wang · Y. Zhang · Q. Xiong
College of Bioresources Chemical and Materials Engineering, Shaanxi University of Science and Technology, Xi'an, China
e-mail: xiongchuanyin@126.com; xiongchuanyin@sust.edu.cn

© The Author(s), under exclusive license to Springer Nature Switzerland AG 2023

R. K. Gupta (ed.), *3D Graphene*, Carbon Nanostructures,
https://doi.org/10.1007/978-3-031-36249-1_1

example, when graphene is used as an energy storage material, the stacking between the layers will lead to a decrease in the electrochemical reaction site and a decrease in the efficiency of electrolyte ion conduction inside the electrode material, which seriously affects the energy storage performance of the device [7]. In view of the above problems, the construction of graphene matrix composites with 3D structure by certain methods is an effective solution. Figure 1a summarizes the relationship between 3D graphene and 2D graphene [8].

As shown in Fig. 1b, according to the currently reported work, the types of 3D graphene can be divided into 3D graphene nanoribbons, 3D graphene powder, 3D graphene spheres, 3D graphene fibers, 3D graphene with a layered structure, 3D graphene foam, 3D graphene aerogels, etc.

1.1 3D Graphene Nanoribbons

Graphene nanoribbons refer to graphene nanomaterials with a width of less than 50 nm, which can be prepared to form 3D graphene nanoribbons through the interaction between carbon-containing molecules. As shown in Fig. 2a, Kawai et al. [9] synthesized 3D graphene nanoribbons using surface chemical reactions of organic molecules. The 3D graphene nanoribbon is a periodic out-of-plane substructure by controlling the addition reaction of a single molecule on the adsorption surface of the local probe at low temperatures. This work has a certain reference value for the precise synthesis of 3D graphene nanoribbons.

1.2 3D Graphene Powder

3D graphene powder appears macroscopically in a powder state, but microscopically has a 3D structure. Cao et al. [10] used CH_4 as a carbon source to prepare 3D graphene powder with different particle sizes by combining CVD and physical crushing. As shown in Fig. 2b, thanks to the excellent microporous structure of 3D graphene powder and the embedding of Pt atoms. The prepared 3D graphene powder is beneficial to the transport of oxygen and lithium ions when applied to $Li–O_2$ batteries, thereby reducing the decomposition barrier of Li_2O_2.

1.3 3D Graphene Spheres

3D graphene spheres can be prepared by a template method and self-assembly. Zhang et al. [11] converted benzene rings into high-purity 3D few-layer graphene microspheres by sulfur-assisted methods. The structure of this 3D graphene microsphere is shown in Fig. 2c, and it can be clearly seen that the 3D graphene microsphere

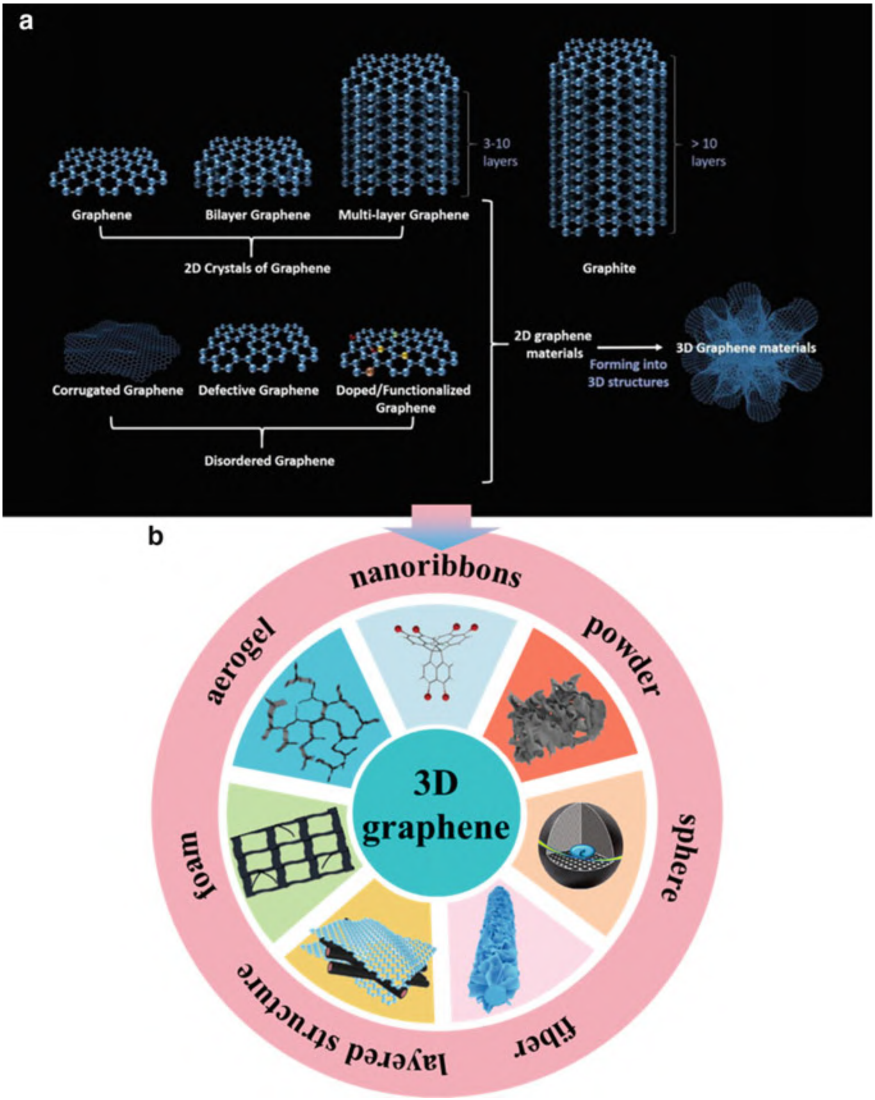

Fig. 1 **a** Schematic diagram of the relationship between graphite, graphene, and 3D graphene. Adapted with permission [8], Copyright (2020), American Chemical Society. **b** Classification diagram of 3D graphene

shows a distinct spherical fluffy state due to the interconnection between several layers of graphene. This provides an excellent energy storage structure for its application in high-performance potassium–ion batteries. In addition, Hirani et al. [12] prepared nitrogen-doped 3D graphene particles (Fig. 2d) by self-assembly, and the microspheres showed excellent wastewater treatment performance.

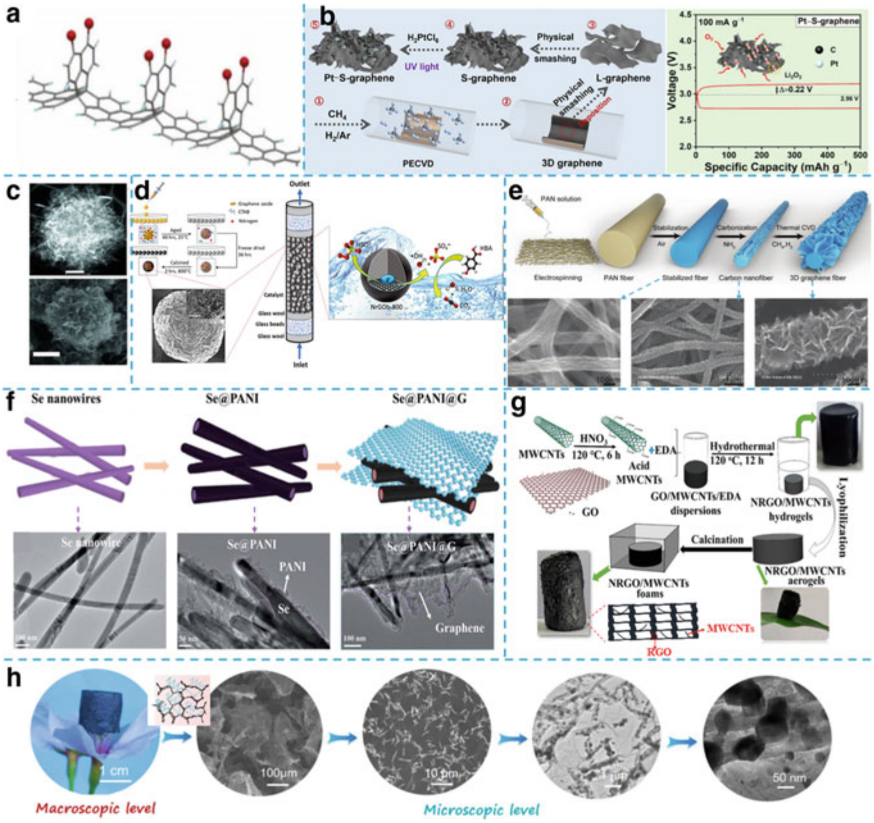

Fig. 2 **a** Schematic representation of the structure of 3D graphene nanoribbons. Adapted with permission [9], Copyright (2020), American Association for the Advancement of Science. **b** Schematic diagram of the preparation process of 3D graphene powder and its properties as a battery cathode material. Adapted with permission [10], Copyright (2022), American Chemical Society. **c** Microscopic image of 3D few-layer graphene microspheres. Adapted with permission [11], Copyright (2021), Royal Society of Chemistry. **d** Fabrication process of 3D nitrogen-doped graphene particles. Adapted with permission [12], Copyright (2022), Elsevier. **e** Preparation of 3D graphene fibers and their SEM images. Adapted with permission [13], Copyright (2018), Wiley–VCH. **f** Preparation process of 3D graphene with hierarchical structure and its corresponding SEM microscopic image. Adapted with permission [14], Copyright (2022), Royal Society of Chemistry. **g** Schematic diagram of the preparation process of MWCNTs enhanced 3D graphene foam and its structure. Adapted with permission [15], Copyright (2020), American Chemical Society. (H) SEM image of Ni-doped 3D-Fe_3O_4@C/rGO aerogel. Adapted with permission [16], Copyright (2022), Springer Nature

1.4 3D Graphene Fibers

3D graphene fibers can be prepared by electrospinning, wet spinning, electrophoresis, and fiber surface coating. Zeng et al. [13] prepared tightly arranged 3D graphene fibers by electrospinning, NH_3 etching, and CVD combination. The preparation process is shown in Fig. 2e, which mainly includes electrospinning PAN nanofibers, etching under NH_3 conditions, and CH_4 and H_2 mixtures to grow 3D graphene by CVD. It is worth mentioning that the etching of NH_3 makes a great number of fringed structures on the surface of carbonized fibers, which provides rich sites for the growth of 3D graphene.

1.5 3D Graphene with a Hierarchical Structure

The preparation of 3D graphene with layered structure by separating 2D graphene nanosheets by introducing the second component is also a relatively simple and efficient method to solve the stacking phenomenon between 2D graphene nanosheets. Lei et al. [14] used polyaniline-coated selenium nanowires as a separating agent to improve the stacking between 2D graphene sheets. The preparation process is shown in Fig. 2f, first polyaniline is coated on the surface of Se nanowires by in situ polymerization to obtain a Se@PANI composite with core–shell structure, and then graphene and Se@PANI nanowires are uniformly dispersed to obtain 3D graphene-based composites. Thanks to the layered structure of the material, the power of the electrochemical reaction is accelerated, so that the material has excellent cycle stability and energy storage characteristics when used as an aluminum–selenium battery.

1.6 3D Graphene Foam

3D graphene foam has the advantages of 3D network structure, high porosity, and ultra-low density, and has been widely used in energy storage, electromagnetic shielding, and wave absorption. As shown in Fig. 2g, Shu et al. [15] prepared an N-doped 3D RGO/multi-walled carbon nanotube (MWCNTs) composite foam by hydrothermal and high-temperature carbonization methods. Thanks to the 3D network structure formed between the RGOs in this material, the material has excellent absorption properties.

1.7 3D Graphene Aerogel

3D graphene aerogels have attracted more and more attention from material scientists due to their good properties. According to existing reports, the preparation methods of 3D graphene aerogels are diverse, mainly including hydrothermal methods, chemical reduction, chemical crosslinking, 3D printing, and self-assembly. Huang et al. [16] prepared Ni-doped 3D-Fe_3O_4@C/rGO aerogels with excellent absorption performance by the hydrothermal method. Figure 2h is a schematic diagram of the microstructure of a 3D graphene composite aerogel. It can be seen that 3D graphene aerogels have rich porous structures and can provide rich loading sites for active materials to prepare high-performance composites.

2 Preparation of Graphene

This section systematically summarizes and classifies the preparation methods of 3D graphene, as shown in Fig. 3. The preparation methods of 3D graphene are mainly divided into CVD growth, self-assembly, 3D printing, 3D laser induction, pyrolysis of organic precursors, and other methods [7]. Templates are also used to assist in the preparation process as required. At present, CVD and self-assembly are used in most studies.

2.1 CVD Growth of 3D Graphene

2.1.1 CVD Growth Based on a Metal Template

Metal templates can be used as catalysts to accelerate the decomposition of hydrocarbons and the nucleation of graphene, making the lattice arrangement of graphene more perfect [8]. Chen et al. [17] first used template-based CVD to synthesize 3D

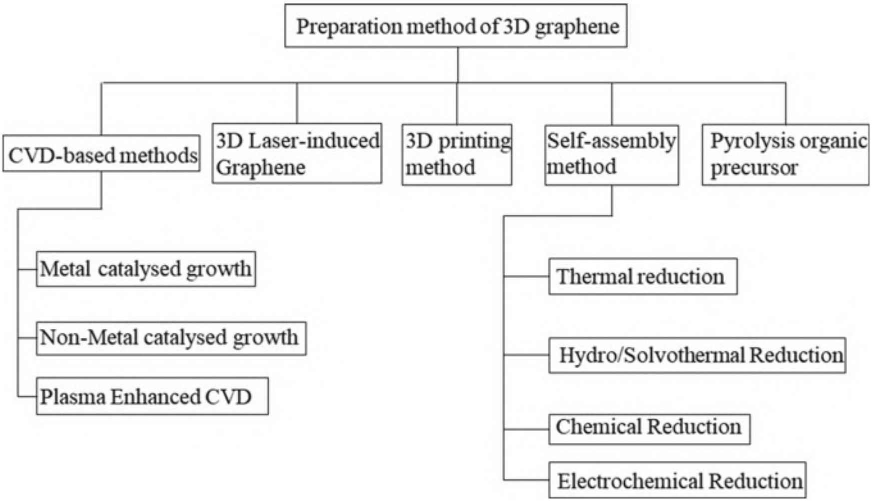

Fig. 3 Preparation method of 3D graphene

porous graphene structure on nickel foam and used methane as carbon precursor nickel foam as a metal template to grow graphene. Graphene was coated on the surface of nickel foam in a tubular furnace at 1000 °C, then etched the nickel foam with $FeCl_3$/HCl solution, and added acetone to remove the PMMA support layer. Finally, 3D porous graphene flexible network structure with the original nickel foam structure was formed. Lin et al. [18] designed a kind of 3D nanoporous graphene based on 12 component ultra-high entropy nanoporous alloy (Fig. 4a), and synthesized a self-contained 3D nanoporous graphene with high N-doping by CVD growth. However, there are some defects in the selection of metal templates, and the etching of the metal template cannot be completely removed, resulting in the preparation of 3D porous graphene being greatly limited in the use process.

2.1.2 CVD Growth Based on a Non-metal Template

Compared with the metal template, the non-metal template has more diversity in morphology, high melting point, and low cost [6]. As shown in Fig. 4b, Shi et al. [19] first calcined the shell (calcium carbonate (CaO)) to porous CaO at 1050 °C, then CVD graphene on porous CaO as a non-metal template, and finally prepared 3D porous graphene structure by removing CaO with hydrochloric acid. In the process of calcining calcium carbonate at high temperatures, the release of CO_2 can form an interconnected porous structure in the shell, which provides favorable conditions for the growth of porous graphene. At the same time, porous CaO as a support structure provides a template for the CVD growth of graphene. The 3D graphene prepared by this method completely retained the porous structure of CaO template, showing ultra-low density and ultra-high porosity. As mentioned in the above section, Zeng et al. [13] used carbon material as a template, carbonized PAN nanofibers by electrospinning under NH_3 etching conditions, and CVD-grown vertically aligned 3D graphene fibers with CH_4 as a carbon source.

2.1.3 Growth of 3D Graphene by PECVD

Through PECVD, hydrocarbons can be pyrolyzed at relatively low temperatures, and 3D graphene can be grown without metal catalysts or even templates. According to the plasma energy source, PECVD can be divided into DC-PECVD, MW-PECVD, and RF-PECVD. No matter which discharge method is used, the formation mechanism of 3D graphene is similar. Yin et al. [20] as shown in Fig. 4c used Si_3N_4 nanowire film as a template to obtain 3D graphene microtubules (3DGMTs) by PECVD and subsequent heat treatment.

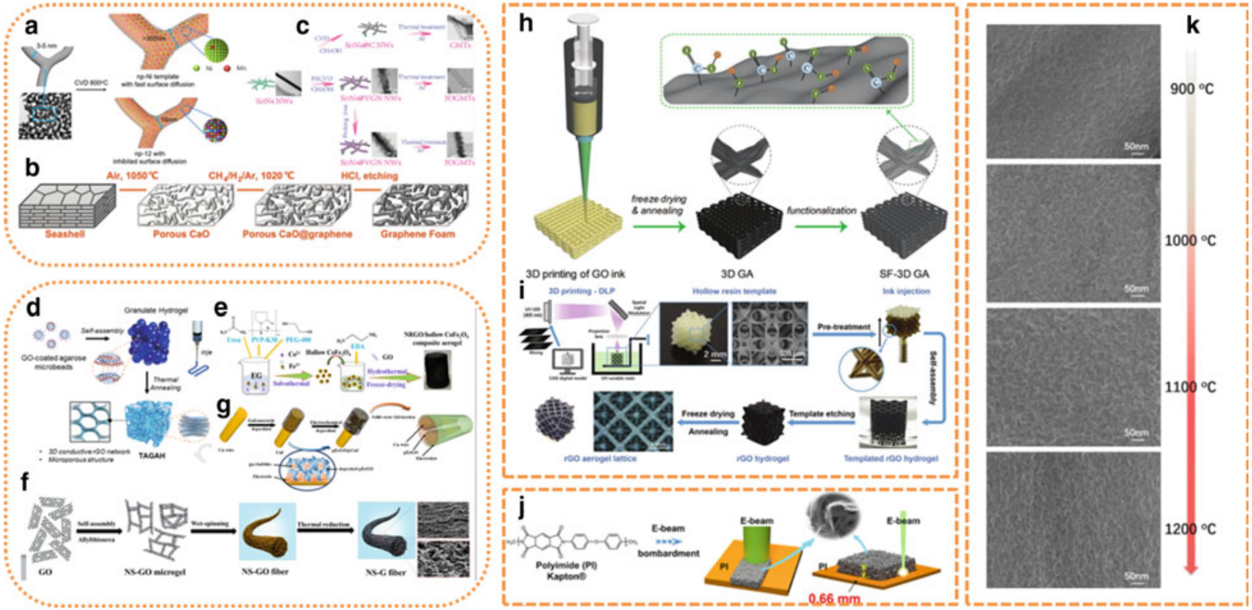

Fig. 4 **a** Schematic diagram of CVD process using NP-12 and NP-Ni as templates. Adapted with permission [18], Copyright (2022), American Chemical Society. **b** Schematic diagram of graphene foam formation. Adapted with permission [19], Copyright (2016), American Chemical Society. **c** Schematic diagram of manufacturing 3D GMTs and CMTs films. Adapted with permission [20], Copyright (2020), Elsevier. **d** A schematic illustration of the fabrication of a TAGAH using granulate hydrogel (GH) self-assembled with graphene-coated agarose microbeads (GAMs). Adapted with permission [21], Copyright (2022), Elsevier. **e** Schematic diagram of the structure of NRGO/hollow $CoFe_2O_4$ composite aerogel. Adapted with permission [22], Copyright (2023), Elsevier. **f** Schematic diagram of the manufacturing route of NS-G fiber. Adapted with permission [23], Copyright (2020), Royal Society of Chemistry. **g** 3G rGO@Cuf/Schematic diagram of overall design and process flow of step-by-step manufacturing of copper supercapacitors. Adapted with permission [25], Copyright (2018), Springer Nature. **h** Schematic diagram of SF-3D GA preparation. Adapted with permission [26], Copyright (2020), Wiley–VCH. **i** Schematic diagram and SEM image of 3D RGO aerogel prepared by DLP method. Adapted with permission [27], Copyright (2022), Wiley–VCH. **j** Process of graphene formation on PI by electron beam bombardment. Adapted with permission [28], Copyright (2021), Elsevier. **k** SEM image of 3D vertical graphene prepared at different temperatures. Adapted with permission [30], Copyright (2021), Elsevier

2.2 Preparation of 3D Graphene by Self-Assembly Method

Self-assembly is a method of self-assembly of 2D graphene materials into 3D graphene structures through a bottom-up strategy.

2.2.1 Thermal Reduction

Thermal reduction, the elimination of oxygen-containing functional groups on GO by thermal annealing, is the most conventional, direct, and effective method. As shown in Fig. 4d, Park et al. [21] used GO-coated agarose beads as precursors to self-assemble into the granular hydrogel and then reduced GO to rGO by thermal annealing to form a thermal annealing graphene channel agarose (TAGAH) hydrogel composed of 3D conductive rGO network. TAGAH has high conductivity, low impedance, and good biocompatibility, and has great potential in soft bioelectrode, pressure sensors, strain sensors, and conductive tissue scaffolds.

2.2.2 Hydro/Solvothermal Reduction

The initial purpose of hydrothermal reduction is to reduce GO to rGO tablets. With the development of research, it has gradually become a method to self-assemble 3D rGO hydrogels while reducing GO. These reactions usually need to be carried out at medium–high temperatures in the high-pressure reactor. During these reactions, the thermally induced solvent acts as a reductant, most carboxyl groups are removed, and rGO sheets are assembled into a 3D rGO framework. Xu et al. [22] prepared nitrogen-doped reduced GO/hollow cobalt ferrite composite aerogels with 3D network structures through simple solvothermal and hydrothermal self-assembly processes. Figure 4e shows the preparation process of composite aerogel.

2.2.3 Chemical Reduction Induction

The chemical reduction was first used to reduce GO to rGO using a strong reductant represented by hydrazine. Then, it was used in the synthesis of 3D graphene hydrogel, and the reductant used was also milder. Compared with hydrothermal reduction, chemical reduction has mild conditions, a higher reduction degree, and easier doping of heteroatoms into 3D rGO. As shown in Fig. 4f, Ma et al. [23] showed a scalable and low-cost microgel spinning method for preparing nitrogen sulfur co-doped 3D porous graphene fibers. Firstly, nitrogen sulfur co-doped GO (NS-GO) microgels with the 3D structure were prepared by chemical reduction-induced self-assembly method. Then, NS-GO fibers were prepared by wet spinning using microgel as a spinning stock solution. Finally, NS-GO fibers were reduced to NS-GF by the thermal reduction method. Jha et al. [24] used copper chloride (I) (CuCl) to reduce GO, and then removed copper ions through HCl to obtain 3D mesoporous rGO, which has significant supercapacitor performance in the field of all-solid-state supercapacitors.

2.2.4 Electrochemical Reduction

GO sheets will be electrochemically reduced near the cathode and deposited on the cathode. The layers support each other to form an interconnected 3D graphene network. As shown in Fig. 4g, Purkait et al. [25] first prepared foamed copper by constant current electrodeposition and then electrodeposited GO with GO suspension containing 1 M phosphoric acid solution as electrolyte. The GO sheet was reduced to a conductive 3D porous rGO network structure at a constant potential. The 3D porous rGO can be directly used to prepare solid-state supercapacitors.

2.3 3D Printing

3D printing is an efficient method to directly construct large-volume objects. First, the target product is designed by using relevant software, and then 3D structural materials are prepared by heating and deposition layer by layer under the control of the computer. The combination of nanotechnology and 3D printing can produce 3D large volumes of materials with unique properties and versatility. Yao et al. [26] prepared a new surface functionalized 3D-printed graphene aerogel electrode material. In Fig. 4h, the GO ink prepared by mixing a single-layer GO sheet with hydroxypropyl methylcellulose is sprayed through a nozzle, heated, and deposited layer by layer, and then freeze-dried to obtain 3D GO aerogel. Finally, the 3D GO aerogel is transformed into a 3D graphene aerogel by thermal annealing at 1050 °C. In addition, 3D graphene aerogels were prepared by the template-assisted method. The ideal shape was designed by software. The hollow templates were arranged into interconnected 3D structures by 3D printing. GO or chemically modified graphene was injected into the hollow template, and the 3D graphene structure was obtained by subsequent processing. As shown in Fig. 4i, Zhou et al. [27] designed and prepared 3D graphene aerogel inheriting a high-resolution polyacrylate resin template by combining digital light processing technology and 3D printing.

2.4 3D Laser-Induced Graphene (3D LIG)

3D LIG is a kind of 3D graphene formed by laser irradiation of polymer precursors to induce photochemical and thermal conversion. It naturally presents a 3D porous structure, which is usually called 3D LIG or 3D laser-scribed graphene (LSG). The quality of LIG is slightly inferior to that of 3D graphene prepared by other methods, but low cost and relatively simple are the advantages of laser-induced graphene.

Han et al. [28] directly synthesized 3D graphene on polymer-based polyimide by a high-energy electron beam. The preparation process is shown in Fig. 4j. The final 3D graphene film has a thickness of 0.66 mm and a specific surface area of 363 m^2 g^{-1}. At present, most studies use macromolecular synthetic resins or natural polymers as laser irradiation precursors, but this largely limits the geometry and size of 3D graphene. Yu et al. [29] used 10.6 μm CO_2 laser to irradiate liquid precursors to prepare 3D laser-induced graphene materials and synthesized non-polymer precursors by introducing aromatic units conducive to high carbonization and oxazine rings with high flame retardancy. Then it is directly converted into graphene by laser irradiation.

2.5 Pyrolytic Organic Precursors

Pyrolysis of organic precursors is a method of direct pyrolysis of organic molecules to obtain 3D graphene materials. Generally speaking, some organic molecules will be mixed through the sol–gel process to form organic polymer carbon precursors before pyrolysis, but organic molecules can also be directly pyrolyzed without sol–gel treatment. Li et al. [30] prepared disordered molecular chain foam as a precursor by thermally induced phase separation and then pyrolyzed it at 900–1200 °C. With the increase of carbonization temperature, the surface roughness of carbon increases, and 3D vertical graphene gradually forms. SEM at different temperatures is shown in Fig. 4k.

3 Application of 3D Graphene

3.1 Energy Conversion

3.1.1 Solar-Thermal Conversion

The best way to collect solar energy is to convert photons into heat directly through the solar heat absorber. It can achieve higher conversion efficiency because it uses a wider bandwidth in the solar spectrum, and is environmentally friendly. Lin et al. demonstrated structured graphene metamaterials (SGM), as shown in Fig. 5a [31]. The structured graphene metamaterials exploit the wavelength selectivity of the base-grooved metal structures. Moreover, the ultra-thin graphene metamaterial membrane has the characteristics of broadband optical dispersion-free and excellent thermal conductivity. The photothermal conversion efficiency is up to 90.1%, the total efficiency is 68.9%, the water evaporation rate is 1.5 kgm^{-2} h^{-1}, and the solar-steam efficiency is up to 96.2%, to realize the high-efficiency solar photothermal conversion at large angles.

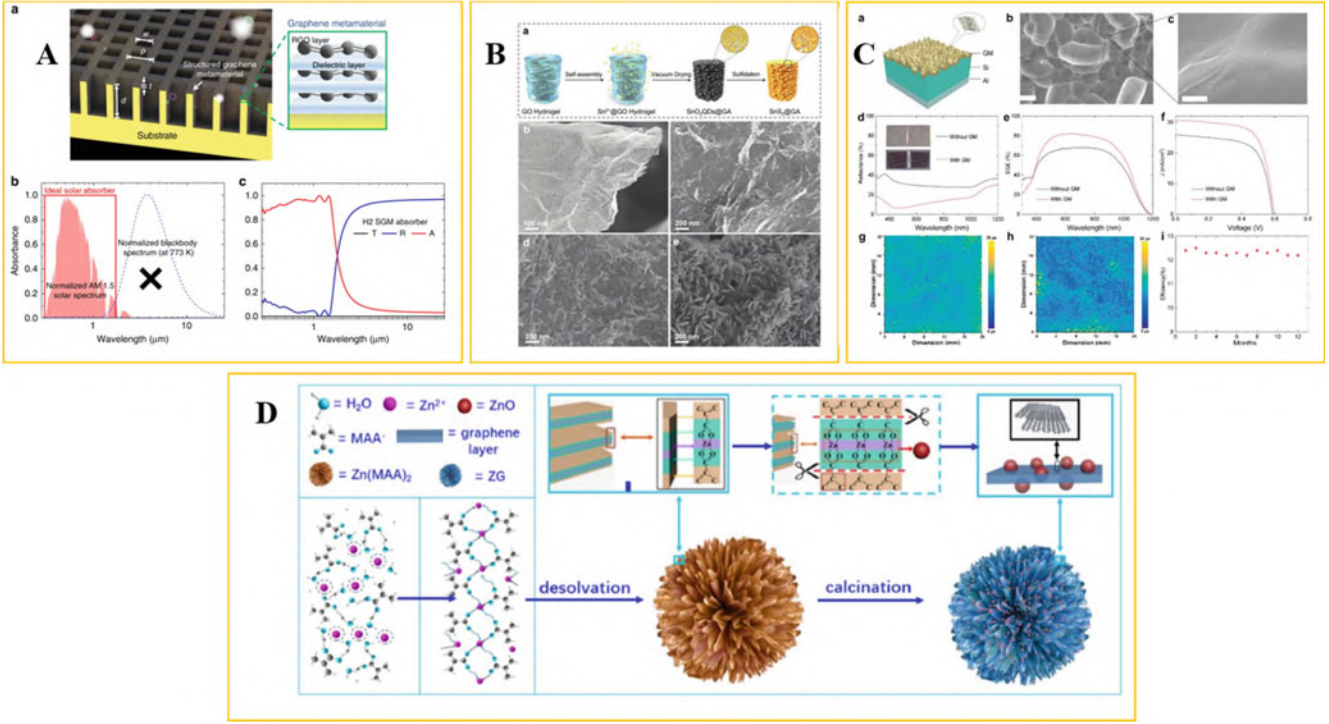

Fig. 5 **a** SGM solar selective absorber. Adapted with permission [31], Copyright (2020), Nature. (B) (a) Schematic diagram of the synthetic route for preparing the SnS2@GA heterostructure. **b** SEM image of SnO2@GA. SEM image of the final product vulcanized at **c** 300 1C, **d** 350 1C, **e** 400 1C. Adapted with permission [34], Copyright (2022), Chinese Chemical Society and Royal Society of Chemistry. (C) Genetically modified enhanced solar cells. Adapted with permission [35], Copyright (2022), American Chemical Society. (D) The structural models and preparation routes of Zn (MAA) 2 and ZG HS are described. Adapted with permission [36], Copyright (2023), Elsevier

3.1.2 Photocatalysis

Graphene photocatalytic composites have developed rapidly in recent years and have great application value in solving energy and environmental problems. On the basis of achieving uniform dispersion of photocatalyst, the construction of 3D graphene has many new advantages: the internal porous structure increases the adsorption of materials on reactants; good mechanical strength makes the material easy to recover after catalytic reaction, which is particularly important in the field of sewage purification. These characteristics make graphene composite photocatalyst materials with a 3D structure more prominent and practical. Wang et al. designed a new method to modify UIO-66-NH_2 metal–organic framework material for efficient photocatalytic reduction of CO_2 by building a 3D graphene framework [32]. Through theoretical calculation and experimental research, it is confirmed that the rearrangement of charge carriers has occurred at the interface of different materials. During the photocatalysis process, the charge transfer and separation can be effectively carried out, which effectively promotes the photocatalytic reduction of the CO_2 conversion process. It provides a promising way to explore the application of nano-composite materials based on MOFs in environmental governance and other related fields.

3.2 Energy Storage

3.2.1 Batteries

Li–ion batteries (LIBs)

In recent years, lithium batteries have developed rapidly to meet the application of rechargeable batteries in various fields (such as portable electronic devices and electric vehicles). As the core of LIB, electrode active materials generally require high capacity and energy density, long-term cycle stability, and safety. Mo and others showed a 3D hierarchical metal hydride/graphene composite ($LiNa_2AlH_6$/3DG) [33]. And $LiNa_2AlH_6$/3DG have significantly better lithium storage performance in solid-state batteries than previously reported aluminate negative electrodes. $LiNa_2AlH_6$ nanoparticles are uniformly anchored on graphene nanosheets. The graphene nanosheets self-assemble to form a 3D flower hierarchical structure, which shows excellent cycle stability when $LiBH_4$ is used as a solid electrolyte. At the current density of 5 Ag^{-1}, its capacity reaches 861 mA h g^{-1}, its cycle life reaches 500 times, and its capacity retention rate reaches 97%.

Sodium–ion battery (SIBs)

Sodium–ion battery (SIBs) has shown great potential application value in the field of energy storage and power transportation due to their advantages of rich resources, low cost, and environmental friendliness. As shown in Fig. 5b, Guo and others show a 2D heterostructure, in which dense SnS_2 nanosheets are uniformly and vertically fixed on graphene aerogel(SnS_2@GA) for high-performance sodium–ion batteries [34]. The composite exhibits enhanced electrochemical reaction kinetics and enhanced structural stability based on the charge storage mechanism dominated by pseudocapacitance. SnS_2@GA The negative electrode provides a high reversible capacity of 690 $mAhg^{-1}$ at 0.2 Ag^{-1}, excellent rate performance, and long cycle life, and the capacity retention rate reaches 83% after 1000 cycles.

Other Batteries

The emergence of silicon solar cells provides feasible and effective solutions to challenges such as energy and environmental crisis. The high reflection and surface recombination loss caused by the silicon interface and its nanometer processing technology are the main obstacles to achieving high energy conversion efficiency. Jia et al. proposed a 3D conformal coating concept for graphene metamaterials [35], as shown in Fig. 5c. Among them, 2D graphene can perfectly adapt to 3D silicon structural surfaces, reducing optical reflection by 20%, and improving surface passivation performance by 60%. Subsequently, the graphene metamaterial 3D conformal coating concept was then further applied to standard silicon solar cells, resulting in an overall 23% increase in solar energy conversion efficiency. Moreover, the concept of 3D conformal coating can be easily extended to a variety of optoelectronic and semiconductor devices with excellent performance, opening a practical and promising way to achieve efficient energy acquisition and storage.

3.2.2 Supercapacitor

Supercapacitors have become one of the most promising energy storage devices due to their high-power density and long cycle life. Due to the advantages of 3D Graphene such as high surface area, high conductivity, high carrier mobility and rich pore structure, many researchers have begun to explore the electrochemical properties of 3D graphene materials in the application of supercapacitors. As shown in Fig. 5d, Ma et al. investigated a novel and efficient molecular self-assembly strategy to prepare 3D flower-like ZG microstructures by calcination of self-assembled precursors (directly deriving three-dimensional amphiphilic $Zn(MAA)_2$ precursors with well-layered structure into three-dimensional graphene mixtures to produce high-quality three-dimensional graphene microstructures with uniform metal oxide (ZnO) nanoparticles) [36]. ZnO NP generated from carboxylic acid groups of Zn $(MAA)_2$ molecules permeates into graphene. The resulting ZG-500 HS as a supercapacitor electrode has a specific capacitance of 272.1 Fg^{-1} at 1 Ag^{-1}. In addition, an asymmetric supercapacitor based on ZG-500 HS and activated carbon provides an energy density of 13.4 $Whkg^{-1}$ at a power density of 387.5 Wkg^{-1}. This opens up a green route for the preparation of high-quality 3D graphene composite supercapacitors.

3.3 Environment

With the rapid development of global industrialization and urbanization, environmental problems have become one of the most worldwide threats. 3D graphene has a large specific surface area, suitable pore size, controllable hydrophilicity and conductivity, and 3D interconnection structure, which shows great potential in environmental treatment such as water purification, seawater desalination, and gas purification.

3.3.1 Water Decontamination

Nowadays, domestic sewage, industrial and agricultural wastewater, and other problems have led to serious water pollution, economic and efficient removal of various pollutants in water needs to be solved immediately.

As one of the widely used water treatment methods, 3D graphene has the advantages of a large specific surface area, good chemical stability, and can easy realize solid–liquid separation. It can also be used as a catalyst carrier to catalyze the degradation of pollutants in water [37]. It is a good new type of economic and efficient adsorption material. 3D graphene composite can be used for water treatment through permeability, π–π interaction, electrostatic interaction, and surface complexation, and becomes a potential adsorbent for treating oil, organic solvents, dyes, metal ions, and other pollutants. It is reported that the adsorption capacity of 3D graphene is tens to hundreds of times that of traditional adsorption materials. 3D graphene has broad application prospects in water environmental pollution treatment.

3.3.2 Gas Adsorption

With the deepening of human industrialization, the problem of natural environmental pollution has gradually emerged. Volatile organic compounds (VOCs) are harmful pollutants and are released from various experimental sources, including the petroleum industry, oil refineries, and the cleaning process of silicon chips. Even at very low concentrations, long-term exposure can cause serious health problems. The adsorption method is considered to be the most reasonable and effective method to control air pollution. The adsorption of gas molecules onto the graphene surface mainly depends on electrostatic adsorption, dispersion interaction, van der Waals force, and charge transfer.

3.4 Catalyst

The traditional catalysts are generally noble metal-based materials, such as Pt, Ru, and alloy. Although they are often used as catalysts in oxygen reduction reactions, their high cost, sensitivity, and poor stability have largely prevented their large-scale commercialization. Doped graphene can be a metal-free, anti-toxic, and durable electrocatalyst to reduce costs [38]. Xie et al. successfully prepared nitrogen-doped graphene aerogel (NGA) by a simple one-pot hydrothermal method. Selecting small-size graphene oxide as a precursor, dopamine as a nitrogen source and the crosslinking agent is conducive to the formation of micropores [39]. When NGA was used as an electrocatalyst in an oxygen reduction reaction, NGA showed higher electrocatalytic performance than Pt/C catalyst. It is due to the high active N atom doping amount and abundant microporous structure.

3.5 Sensor

With the progress of the Internet of Things technology, sensors are becoming increasingly important in life in the information age. They are widely used in industrial manufacture, space exploration, ocean exploration, and other fields of our life. Currently, scientists are working on developing 3D graphene sensors with a wide strain sensing range, high sensitivity, and high cyclic stability. Common types of graphene sensors include gas, strain, optical, magnetic field, mechanical sensor, etc.

3.5.1 Gas Sensor

After graphene adsorbs the target gas, its conductivity changes. By determining the relationship between the conductivity change and the target surface gas concentration, the concentration of the target gas can be measured by measuring the conductivity change of graphene. The detection of graphene material gas is mainly based on the adsorption of the sensing material and its conductivity change. For example, as shown in Fig. 6a, Bag and others studied the effect of the concentration of mesoporous $ZnFe_2O_4$ particles on the gas sensing performance [40]. Due to the defect site of mesoporous particles being relatively high density, the introduction of $ZnFe_2O_4$ in graphene oxide (rGO)-based chemical resistance sensors shows a rapid detection performance of nitrogen dioxide (NO_2) in a wide range from 50 to 4000 ppb. Compared with the original rGO sensor, the sensitivity is higher and the lower detection limit is lower. RGO-$ZnFe_2O_4$-based gas sensor shows good reproducibility and stable dynamic response under static and dynamic tension.

3.5.2 Strain Sensor

Graphene can be used appropriately as a strain and pressure sensor. In graphene strain and pressure sensors, the perception of physical signals (including strain and pressure) is carried out using graphene as an active material. Because of its high electrical conductivity, graphene materials are often used as conductive layers or

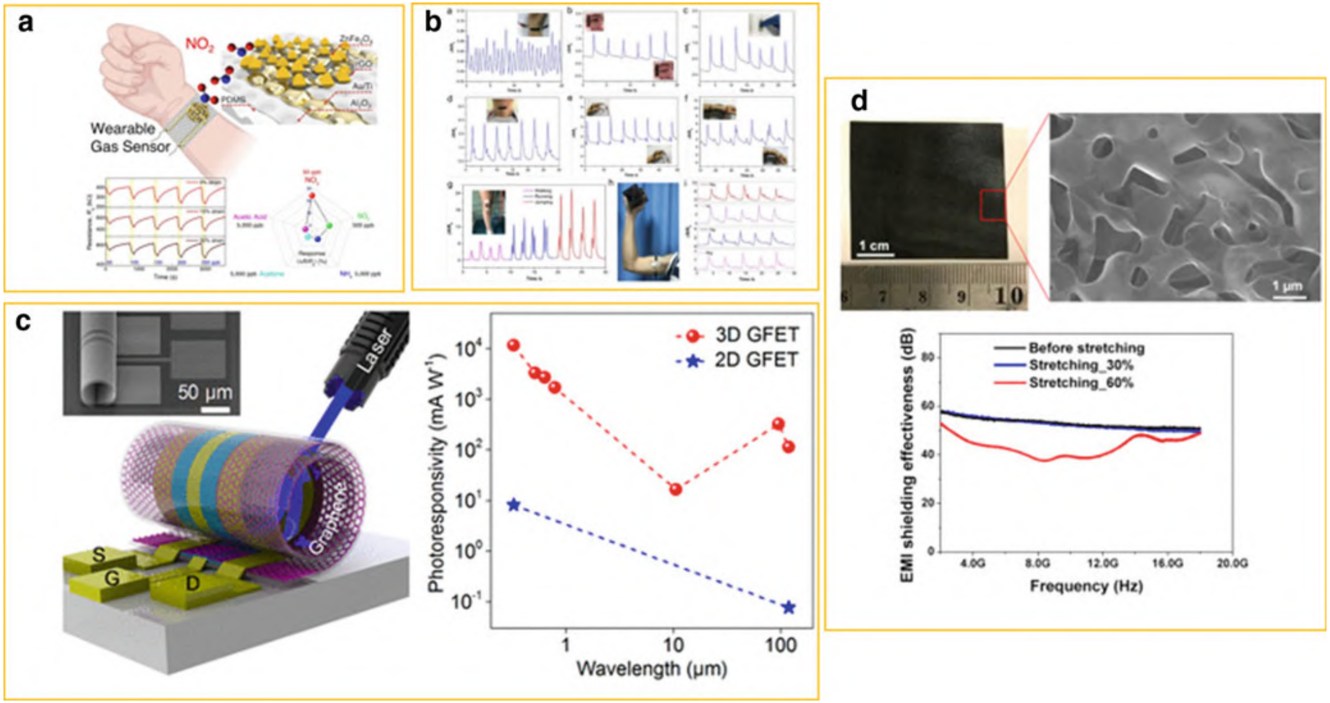

Fig. 6 **a** An extendable, body-attached NO$_2$ gas sensor based on rGO and ZnFe$_2$O$_4$ hollow octahedra. Adapted with permission [40], Copyright (2021), Elsevier. **b** The G/CB/Ni-$_2$ strain sensor is used to monitor human movement in real time. Adapted with permission [41], Copyright (2020), Royal Society of Chemistry. **c** Schematic diagram of high-performance photoelectric sensor based on 3D graphene field-effect tube. Adapted with permission [42], Copyright (2019), American Chemical Society. **d** Demonstration of 3D bi-continuous nanoporous graphene. Adapted with permission [43], Copyright (2019), Cell Press

electrodes for graphene-based strain and pressure sensors. As shown in Fig. 6b, Sun et al. integrated graphene (G), carbon black (CB), and polydimethylsiloxane (PDMS) into a 3D frame of a commercial nickel sponge using a simple, cost-effective, and scalable drip coating method [41]. The G/CB/Ni strain sensor shows good flexibility, high sensitivity (strain coefficient 138 at 16% strain), and long-term stability. The G/CB/Ni sensor can not only accurately monitor the pulse, blink, swallow, and other subtle human movements, but also has broad application prospects in muscle strength detection.

3.5.3 Other Sensors

Due to graphene's excellent electronic and optical properties, it has become an ideal material for high-performance photodetectors. As shown in Fig. 6c, Deng et al. showed a method of using a silicon nitride stress layer to drive 2D graphene field-effect tube to self-curl into a microtubule 3D graphene field-effect tube (3D GFET) structure, and first manufactured the number of curl layers (1–5) and radius (30–65 μm) Precise and controllable 3D GFET device array [42]. The 3D GFET photodetector can detect ultraviolet, visible, mid-infrared, and Hertz (THz) regions at room temperature. The light response of ultraviolet and visible light exceeds 1 AW $^{-1}$, and the light response at 3.11 THz is 0.232 AW $^{-1}$. It realizes ultra-high sensitivity and ultra-fast detection of ultraviolet light, visible light, medium infrared light, and terahertz waves.

3.6 Electromagnetic Interference (EMI)

With the wide use of advanced electronic and communication equipment, electromagnetic radiation seriously affects the precision and sensitivity of precision electrical equipment and causes serious environmental pollution. It is urgent to solve the problem of electromagnetic interference and pollution. Graphene has attracted wide attention because of its excellent electrical and thermal conductivity as well as mechanical properties. The electromagnetic interference (EMI) shielding performance of 3D graphene materials relies strongly on the porous structure. The ideal 3D structure would avoid damaging graphene's electrical conductivity. As shown in Fig. 6d, Kashani's group demonstrated highly conductive bi-continuous nanoporous graphene with excellent EMI shielding performance of 50.9 dB and 83 dB at film thicknesses of 150 mm and 300 mm, respectively [43]. This high shielding efficiency value from light and flexible nanoporous membranes gives the superhigh EMI shielding performance of up to 75,407 and 61630 dB cm^{2}g^{-1} with superior shielding efficiency due to the abundant absorbing interface at a minimum thickness in the bi-continuous porous 3D nanostructures and the high conductivity from the interconnected graphene networks.

References

1. Cui, H.J., Guo, Y.B., Zhou, Z.: 3D graphene-based macrostructures for electrocatalysis. Small **17**, 2005255 (2021)
2. Choi, M.S., Nipane, A., Kim, B.S.Y., Ziffer, M.E., Datta, I., Borah, A., Jung, Y.H., Kim, B., Rhodes, D., Jindal, A., Lamport, Z.A., Lee, M., Zangiabadi, A., Nair, M.N., Taniguchi, T., Watanabe, K., Kymissis, I., Pasupathy, A.N., Lipson, M., Zhu, X.Y., Yoo, W.J., Hone, J., Teherani, J.T.: High carrier mobility in graphene doped using a monolayer of tungsten oxyselenide. Nat. Electron. **4**, 731–739 (2021)
3. Zhi, D.D., Li, T., Li, J.Z., Ren, H.S., Meng, F.B.: A review of 3D graphene-based aerogels: synthesis, structure and application for microwave absorption. Compos. Part B-Eng. **211**,108642 (2021)
4. Xiao, W., Li, B., Yan, J., Wang, L., Huang, X.W., Gao, J.F.: Three dimensional graphene composites: preparation, morphology and their multi-functional applications. Compos. Part A-Appl. Sci. Manuf. **165**, 107335 (2023)
5. Zhao, H.Y., Yu, M.Y., Liu, J., Li, X.F., Min, P., Yu, Z.Z.: Efficient preconstruction of 3D graphene networks for thermally conductive polymer composites. Nano-Micro Lett. **14**, 129 (2022)
6. Chen, K., Shi, L.R., Zhang, Y.F., Liu, Z.F.: Scalable chemical-vapour-deposition growth of 3D graphene materials towards energy-related applications. Chem. Soc. Rev. **47**, 3018–3036 (2018)
7. Qiu, B.C., Xing, M.Y., Zhang, J.L.: Recent advances in 3D graphene based materials for catalysis applications. Chem. Soc. Rev. **47**, 2165–2216 (2018)
8. Sun, Z.X., Fang, S.Y., Hu, Y.H.: 3D graphene materials: from understanding to design and synthesis control. Chem. Rev. **120**, 10336–10453 (2020)
9. Kawai, S., Krejci, O., Nishiuchi, T., Sahara, K., Kodama, T., Pawlak, R., Meyer, E., Kubo, T., Foster, A.S.: 3D graphene nanoribbons as a framework for molecular assembly and local probe chemistry. Sci. Adv. **6**, eaay8913 (2020)
10. Cao, D., Hao, Y.Z., Wang, Y.H., Bai, Y., Li, Y., Wang, X.R., Chen, J.H., Wu, C.: Platinum nanocrystals embedded in 3D graphene for high-performance Li–O_2 batteries. ACS Appl. Mater. Interfaces. **14**, 40921–40929 (2022)
11. Zhang, Q.F., Cheng, X.L., Wang, C.X., Rao, A.M., Lu, B.G.: Sulfur-assisted large-scale synthesis of graphene microspheres for superior potassium-ion batteries. Energy Environ. Sci. **14**, 965–974 (2021)
12. Hirani, R.A.K., Asif, A.H., Rafique, N., Wu, H., Shi, L., Zhang, S., Duan, X.G., Wang, S.B., Saunders, M., Sun, H.Q.: 3D nitrogen-doped graphene oxide beads for catalytic degradation of aqueous pollutants. Chem. Eng. J. **446**, 137042 (2022)
13. Zeng, J., Ji, X.X., Ma, Y.H., Zhang, Z.X., Wang, S.G., Ren, Z.H., Zhi, C.Y., Yu, J.: 3D graphene fibers grown by thermal chemical vapor deposition. Adv. Mater. **30**, 1705380 (2018)
14. Lei, H.P., Tu, J.G., Li, S.Q., Huang, Z., Luo, Y.W., Yu, Z.J., Jiao, S.Q.: Graphene-encapsulated selenium@polyaniline nanowires with 3D hierarchical architecture for high-capacity aluminum-selenium batteries. J. Mater. Chem. A **10**, 15146–15154 (2022)
15. Shu, R.W., Wan, Z.L., Zhang, J.B., Wu, Y., Liu, Y., Shi, J.J., Zheng, M.D.: Facile design of 3D nitrogen-doped reduced graphene oxide/multi-walled carbon nanotube composite foams as lightweight and highly efficient microwave absorbers. ACS Appl. Mater. Interfaces. **12**, 4689–4698 (2020)
16. Huang, X.G., Wei, J.W., Zhang, Y.K., Qian, B.B., Jia, Q., Liu, J., Zhao, X.J., Shao, G.F.: Ultralight magnetic and dielectric aerogels achieved by metal-organic framework initiated gelation of graphene oxide for enhanced microwave absorption. Nano-Micro Lett. **14**, 107 (2022)
17. Chen, Z.P., Ren, W.C., Gao, L.B., Liu, B.L., Pei, S.F., Cheng, H.M.: 3D flexible and conductive interconnected graphene networks grown by chemical vapour deposition. Nat. Mater. **10**, 424–428 (2011)

18. Lin, X.R., Hu, Y.X., Hu, K.L., Lin, X., Xie, G.Q., Liu, X.J., Reddy, K.M., Qiu, H.J.: Inhibited surface diffusion of high-entropy nano-alloys for the preparation of 3D nanoporous graphene with high amounts of single atom dopants. ACS Mater. Lett. **4**, 978–986 (2022)
19. Shi, L.R., Chen, K., Du, R., Bachmatiuk, A., Rümmeli, M.H., Xie, K.W., Huang, Y.Y., Zhang, Y.F., Liu, Z.F.: Scalable seashell-based chemical vapor deposition growth of 3D graphene foams for oil–water separation. J. Am. Chem. Soc. **138**, 6360–6363 (2016)
20. Yin, X.M., Li, H.J., Han, L.Y., Meng, J.C., Lu, J.H., Zhang, L.L., Li, W., Fu, Q.G., Li, K.Z., Song, Q.: Lightweight and flexible 3D graphene microtubes membrane for high-efficiency electromagnetic-interference shielding. Chem. Eng. J. **387**, 124025 (2020)
21. Park, J., Jeon, N., Lee, S., Choe, G., Lee, E., Lee, J.Y.: Conductive hydrogel constructs with 3Dly connected graphene networks for biomedical applications. Chem. Eng. J., 137344 (2022)
22. Xu, J., Shu, R., Wan, Z., Shi, J.J.: Construction of 3D hierarchical porous nitrogen-doped reduced graphene oxide/hollow cobalt ferrite composite aerogels toward highly efficient electromagnetic wave absorption. J. Mater. Sci. Technol. **132**, 193–200 (2023)
23. Ma, W.J., Li, W.F., Li, M., Mao, Q.H., Pan, Z.H., Zhu, M.F., Zhang, Y.G.: Scalable microgel spinning of a 3D porous graphene fiber for high-performance flexible supercapacitors. J. Mater. Chem. A **8**, 25355–25362 (2020)
24. Jha, P.K., Gupta, K., Debnath, A.K., Rana, S., Sharma, R., Ballav, N.: 3D mesoporous reduced graphene oxide with remarkable supercapacitive performance. Carbon **148**, 354–360 (2019)
25. Purkait, T., Singh, G., Kumar, D., Singh, M., Dey, R.S.: High-performance flexible supercapacitors based on electrochemically tailored 3D reduced graphene oxide networks. Sci. Rep. **8**, 1–13 (2018)
26. Yao, B., Chandrasekaran, S., Zhang, H.Z., Ma, A., Kang, J.Z., Zhang, L., Lu, X.H., Qian, F., Zhu, C., Duoss, E.B., Spadaccini, C.M., Worsley, M.A., Li, Y.: 3D-printed structure boosts the kinetics and intrinsic capacitance of pseudocapacitive graphene aerogels. Adv. Mater. **32**, 1906652 (2020)
27. Zhou, J.Z., Wu, X., Chen, Y., Yang, C., Yang, R., Tan, J.Y., Liu, Y.L., Qiu, L., Cheng, H.M.: 3D printed template-directed assembly of multiscale graphene structures. Adv. Func. Mater. **32**, 2105879 (2022)
28. Han, S., Li, N., Song, Y.P., Chen, L.Q., Liu, C., Xi, M., Yu, X.L., Qin, Y., Xu, T.T., Ma, C., Zhang, S.D.: E-beam direct synthesis of macroscopic thick 3D porous graphene films. Carbon **182**, 393–403 (2021)
29. Yu, W.J., Zhao, W.W., Wang, S.P., Chen, Q., Liu. X.Q.: Direct conversion of liquid organic precursor into 3D laser-induced graphene materials. Adv. Mater. (2022)
30. Li, G.Z., Wang, S.S., Zeng, J., Yu, J.: In-situ formation of 3D vertical graphene by carbonizing organic precursor in ammonia. Carbon **171**, 111–118 (2021)
31. Lin, K.T., Lin, H., Yang, T.S., Jia, B.H.: Structured graphene metamaterial selective absorbers for high efficiency and omnidirectional solar thermal energy conversion. Nat. Commun. **11**, 1389 (2020)
32. Wang, X.J., Liu, Y.P., Chai, G.D., Yang, G.R., Wang, C.Y., Yan, W.: Interfacial charge modulation via in situ fabrication of 3D conductive platform with MOF nanoparticles for photocatalytic reduction of CO_2. Chem. Europ. J. **28**, e202200583 (2022)
33. Mo, F.J., Chi, X.W., Yang, S.P., Wu, F.L., Song, Y., Sun, D.L., Yao, Y., Fang, F.: Stable three-dimensional metal hydride anodes for solid-state lithium storage. Energy Storage Mater. **18**, 423–428 (2019)
34. Guo, X., Wang, S., Yu, L.P., Guo, C.Y., Yan, P.G., Gao, H., Liu, H.: Dense SnS2 nanoplates vertically anchored on a graphene aerogel for pseudocapacitive sodium storage. Mater. Chem. Front. **6**, 325–332 (2022)
35. Yang, Y.Y., Zhang, Y.N., Zhang, J., Zheng, X.R., Gan, Z.X., Lin, H., Hong, M.H., Jia, B.H.: Graphene metamaterial 3D conformal coating for enhanced light harvesting. ACS Nano (2022)
36. Ma, Q.H., Liu, M.F., Cui, F., Zhang, J.J., Cui, T.Y.: Fabrication of 3D graphene microstructures with uniform metal oxide nanoparticles via molecular self-assembly strategy and their supercapacitor performance. Carbon **204**, 336–345 (2023)

37. Wang, H.T., Mi, X.Y., Li, Y., Zhan, S.H.: 3D graphene-based macrostructures for water treatment. Adv. Mater. **32**, 1806843 (2019)
38. Shi, C.J., Maimaitiyiming, X.: FeNi-functionalized 3D N, P doped graphene foam as a noble metal- free bifunctional electrocatalyst for direct methanol fuel cells. J. Alloy. Compd. **867**, 158732 (2021)
39. Xie, B.B., Zhang, Y., Zhang, R.J.: Pure nitrogen-doped graphene aerogel with rich micropores yields high ORR performance. Mater. Sci. Eng. B **242**, 1–5 (2019)
40. Bag, A., Kumar, M., Moon, D.B., Hanif, A., Sultan, M.J., Yoon, D.H., Lee, N.E.: A room-temperature operable and stretchable NO_2 gas sensor composed of reduced graphene oxide anchored with MOF-derived $ZnFe_2O_4$ hollow octahedron. Sens. Actuat. B Chem. **346**, 130463 (2021)
41. Sun, S.B., Liu, Y.Q., Chang, X.T., Jiang, Y.C., Wang, D.S., Tang, C.J., He, S.Y., Wang, M.W., Guo, L., Gao, Y.: Wearable, waterproof, and highly sensitive strain sensor based on three-dimensional graphene/carbon black/Ni sponge for wirelessly monitoring human motions. J. Mater. Chem. C **6**, 2074–2085 (2020)
42. Deng, T., Zhang, Z.H., Liu, Y.X., Wang, Y.X., Su, F., Li, S.S., Zhang, Y., Li, H., Chen, H.J., Zhao, Z.R., Li, Y., Liu, Z.W.: Three-dimensional graphene field-effect transistors as high-performance photodetectors. Nano Lett. **19**, 14940–21503 (2019)
43. Kashani, H., Giroux, M., Johnson, I., Han, J.H., Wang, C., Chen, M.W.: Unprecedented electromagnetic interference shielding from three-dimensional bi-continuous Nanoporous graphene. Matter **1**, 1077–1087 (2019)

Synthesis and Printing of 3D Graphene

Arash Ghazitabar and Malek Naderi

Abstract In this chapter, we discuss the various synthesis routes of 3D graphene, also known as Graphene Aerogel (GA). This material, owing to its special structure, provides unique features such as ultra-low density and high surface area. These features meet the requirements, which are fundamental for different applications including supercapacitors, sensors, batteries, and sorbents. This chapter describes the main synthesis methods of hydrothermal, direct self-assembly, chemical reduction, cross-linking agents, template-based, and 3D printing. Graphene oxide (GO), in most of these methods, is almost the main precursor to produce 3D Graphene Hydrogel (GH), which is followed by the GA structure fabrication process achieved through the application of special drying methods like supercritical drying or freeze-drying. In some cases, the post-treatments such as heat treatment are employed to improve the physiochemical properties of GA. Nevertheless, the target application and desired properties are the critical factors in guiding the researchers to choose the most proper synthesis method.

Keywords Freeze-drying · Graphene aerogel · Hydrogel · Hydrothermal · 3D printing

---

A. Ghazitabar · M. Naderi (✉)
Department of Materials and Metallurgical Engineering, Amirkabir University of Technology, No. 350, Hafez Ave., Tehran, Iran
e-mail: mnaderi@aut.ac.ir

Graphene and Advanced Materials Laboratory (GAMLab), Amirkabir University of Technology, No. 7, Balavar Alley, Tehran, Iran

A. Ghazitabar
e-mail: Arash_Ghazitabar@aut.ac.ir

A. Ghazitabar
Department of Inorganic Pigments and Glazes, Institute for Color Science and Technology (ICST), No. 55, Vafamanesh St., Tehran, Iran

© The Author(s), under exclusive license to Springer Nature Switzerland AG 2023

R. K. Gupta (ed.), *3D Graphene*, Carbon Nanostructures,
https://doi.org/10.1007/978-3-031-36249-1_2

1 Introduction

Aerogels are structurally amazing porous synthetic materials, which provide ultra-low density as well as very high specific surface area. Graphene is, also, a miraculous material that has created a tremendous revolution in the field of engineering materials. Considering these definitions, it is obvious that scientists and researchers were looking to produce and synthesize a novel material that combines with the above-mentioned material, i.e., Graphene Aerogel (GA). The graphene-based aerogels have provided an effective way to engineer graphene or Graphene Oxide (GO) into the three-dimensional networks, which provides a high specific surface area with no obligation to restack the graphene sheets. The resulting structure is mostly expected to provide distinguished features including ultra-low density, very high specific surface area, and good mechanical stability. In fact, Wang et al. were the pioneers to produce GA using a conventional hydrothermal synthesis method. First of all, GO is added to a Teflon-lined autoclave reactor vessel, and then the temperature is increased to 200 °C to form the graphene hydrogel (GH). After drying the GH, the GA is formed with a 3D porous interconnected structure [1]. This unique resulting material consists of 2–5% solid materials (i.e., carbon atoms) as well as more than 95% air entrapped in the pores. A theoretical density of 16 g/m^3 is expected.

The drying process is regarded as one of the main steps when producing GA. While drying graphene hydrogel conventionally, the graphene network collapses due to the high capillary force imposed by solvent evaporation. This is why an alternative method of drying should be sought. Supercritical drying and freeze-drying are the most promising proposed methods, which greatly prevent such collapse in the GA structure. Due to π–π interaction, graphene sheets in GA are prone to slip during the supercritical drying process. This results in high shrinkage, and consequently, the reduction in density is not obtained as low as expected in GA. Freeze-drying is the most appropriate method for graphene hydrogel production. It is an effective process to eliminate capillary forces, which are generated during drying. In this method, first, the solvent is replaced with water in the wet gel. Second, the hydrogel is frozen applying low temperatures (i.e., ~60 °C), and finally ice is sublimated into vapor by implying a vacuum. Due to the generation of several micropores in graphene hydrogels, the scaffold of GA remains unchanged, almost no shrinkage occurs, and the density is achieved in the range of expected limits. However, freeze-drying is proposed as the most suitable method, but it is not cost- and energy-effective when it comes to scaling up the GA production, due to the need for applying the high vacuum and very low operating temperature, along with being time-consuming process [2].

The researchers have focused on developing the GA synthesis methods due to the outstanding properties of GA, and their composite materials. In majority of these methods, the GO is the most preferred precursor to begin with because of its functional structure. The main synthesis methods are

- Hydrothermal.
- Direct self-assembly.
- Chemical reduction.

- Cross-linking agents.
- Template-based.
- 3D printing.

All the synthesis methods are briefly discussed in the following sections.

2 Hydrothermal Method

Hydrothermal method was the first process employed to synthesize the graphene aerogel. In this method, the GO suspension is used as a main starting material, which can be mixed with other components such as polymers (cross-linking agents), metal salts (nickel nitrate and cobalt acetate), and reducing agents (ascorbic acid and sodium bisulfite) to fabricate the various types of graphene aerogel. Herein, the most effective parameters that should be considered are including concentration of GO suspension, time and temperature of reaction, and the ratio of free volume (or occupied volume) to total volume of autoclave. The application of hydrothermal method is preferred by researchers since it is a simple one-step process that can be used to produce wide range of composites with high repeatability. However, someone may believe not only it is time-consuming, but also specific equipment is required, and there is a limitation to minimum GO concentration (that should be higher than 2 mg.mL^{-1}) [3–5].

Xu et al. employed hydrothermal method to produce one of the earliest graphene aerogels. They used graphene oxide (2 mg.mL^{-1}) as starting material in a sealed Teflon-lined autoclave at 180 °C for 12 h to make the 3D hydrogel structure [6]. The resulting hydrogel showed high mechanical strength, which could bear the load of 100 g with the lowest deformation. This excellent mechanical stability was due to $\pi-\pi$ stacking interactions between graphene sheets. Three main factors that affected the final structure of produced graphene aerogel were initial GO concentration, processing time, and temperature [7].

3 Direct Self-Assembly of GO

Gelation process of GO is the simplest route to produce graphene oxide aerogel. However, it occurs at higher concentration of GO suspension (higher than 10 mg.mL^{-1}). It requires a simple and cost-effective equipment compared to other GA synthesis routes. Furthermore, the more oxygen functional groups could be maintained in the final 3D graphene structure (without any reduction), which is the main advantage of this method especially when the purpose is to produce an adsorbent/absorbent material in sorption of heavy metals ions or dyes. Qin et al. produced a 3D graphene oxide using self-assembly method to be applied as an organic dye rhodamine B adsorbent. A dispersion of 20–50 mg of dried GO was prepared in 1 mL of deionized water, which was followed by 1 min ultrasonication to generate the 3D graphene oxide hydrogel (GOH). The GOH was either freeze- or vacuum-dried while producing graphene oxide aerogels [8].

In the early research, scientists proposed a novel self-assembly method of 2D GO structure to form the 3D graphene by stimuli-responsive polymers, which could be categorized as a smart material fabrication. These 3D objects can offer reversible, visible, and tangible reactions in response to external stimuli such as mechanical stress, heat, light, gas, electricity, and pH. Zhao et al. used poly (N-isopropylacrylamide) (PNIPAM) and poly (propylene oxide) (PPO) as stimuli-responsive polymers to convert the GO and RGO to 3D graphene structure in order to be used as flexible/foldable supercapacitor electrode [9]. In this work, GO and PNIPAM or PPO polymers were mixed and kept at temperature of 3 °C. Then, the temperature was raised to 50 °C to fabricate 3D hydrogel. The obtained hydrogel was reduced to RGO hydrogel by immersing the hydrogel in sodium ascorbate solution at 80 °C. Freeze-dried hydrogel was used as flexible/foldable electrode for supercapacitor. The electrode exhibited good photo/thermal reversibility thanks to the low critical solution temperature (LCST) of the cross-linking polymers which were used as smart polymers [10].

4 Chemical Reduction Method

Hydrothermal method has some limitations such as high temperature and high amount of residual oxygen-containing groups, which cause reduction in hydrophobicity and conductivity of final graphene aerogel. Moreover, high-pressure autoclave equipment is necessary for hydrothermal process to make the graphene aerogels. Researchers have proposed the chemical reduction method as a highly controllable process to overcome these limitations while fabricating an engineered GA structure. In this method, reducing agents are used to make the 3D graphene hydrogel. The main reducing agents are including L-Ascorbic Acid (LAA) [11], oxalic acid–NaI [12], sodium bisulphite ($NaHSO_3$) [13], sodium sulfide (Na_2S) [14], LAA + $NaHSO_3$ [15], and L-cysteine [16] that can do both chemical self-assembly and reduction of GO at low temperature and under atmospheric pressure.

For instance, Chen et al. investigated the time needed for graphene hydrogel formation, which was affected by the type of applied reducing agents. Vitamin C and Na_2S needed only 10 min to form graphene hydrogel while for $NaHSO_3$ this time was about 30 min. The higher degree of reduction for graphene aerogel was obtained by HI (80%, v/v in acetic acid), which provided high electrical conductivity of 110 $S.m^{-1}$ [14]. Ghazitabar et al. showed that chemical reduction method using L-Ascorbic Acid (L-AA) as reducing agent can form the graphene aerogel/cobalt oxide composites with high specific surface area (215 $m^2.g^{-1}$) along with an amazing load-bearing performance (compression load), which was higher than 2000 times of its own weight [17]. Some researchers claimed that the highest electrical conductivity and lowest density of graphene aerogels may be gained by using simultaneously the mixture of two or more reducing agents in chemical reduction method. A mixture of hypophosphorous acid and iodine is used in dilute GO suspension to form an ultra-low-density graphene aerogel with superior electrical conductivity of 500 $S.m^{-1}$ [18]. Shadkam et al. introduced a high electrochemical performance of graphene aerogel, which was reduced by using the combined reducing agents of L-Ascorbic Acid (L-AA) and $NaHSO_3$. The aerogel exhibited high specific capacitance with superb retention of 91% after 1000 charge/discharge cycles [19]. Their proposed mechanisms of reduction are presented in Fig. 1.

One of the important challenges to make ultra-low-density graphene aerogel applying chemical reduction method is its limitation in using lower concentration of GO (below 0.5 $mg.mL^{-1}$). Zhang et al. [12] could design a new reducing agent mixture to form a stable 3D graphene aerogel. In their research, oxalic acid and NaI were used as reducing agents. The formation of hydrogen bonding between GO (0.1–4.5 $mg.mL^{-1}$) and carboxylic acid groups on oxalic acid was the main reason to result in making a stable 3D structure [12]. In most cases, the functional groups of reducing agents act as cross-linkers between graphene sheets to form graphene aerogel. Ghazitabar et al. reported the cross-linking capability of L-Ascorbic Acid (LAA) when it was used as reducing agent. By-products of LAA oxidation in GO suspension form hydrogen bonding with edge of graphene sheets to form the 3D structure of graphene aerogel [20].

5 Cross-Linking Agents

As said, self-assembly of graphene sheets employing cross-linking agents (for instance, some functional groups on reducing agents as discussed in Sect. 3) is one of the mechanisms to form graphene aerogel structure. These methods are divided to three sub-categories based on the type of the used cross-linking agents.

5.1 Hydrogen Bonding

GO suspension is the stable form of colloid dispersion in water since it contains hydrophilic functional groups on its sheets. In the acidic form, the protonation of carboxyl groups causes reduction in electrostatic repulsion of graphene sheets, and enhances the hydrogen bonding to make an unstable graphene suspension in water. Ghazitabar et al. investigated the effect of the pH of GO suspension on formation of graphene hydrogel in presence of LAA as reducing agent. They selected three different pH values (3, 7, and 10), and concluded that the acidic suspension (with pH value of 3) was the best to form high-strength 3D graphene hydrogel when using chemical reduction method (Fig. 2a), resulting in a porous structure (Fig. 2b) [17].

On the contrary, some studies reported that the alkaline suspension was the proper condition for GA formation. Hu et al. investigated the susceptible mechanisms engaged in formation of 3D graphene hydrogel in both acidic and alkaline media

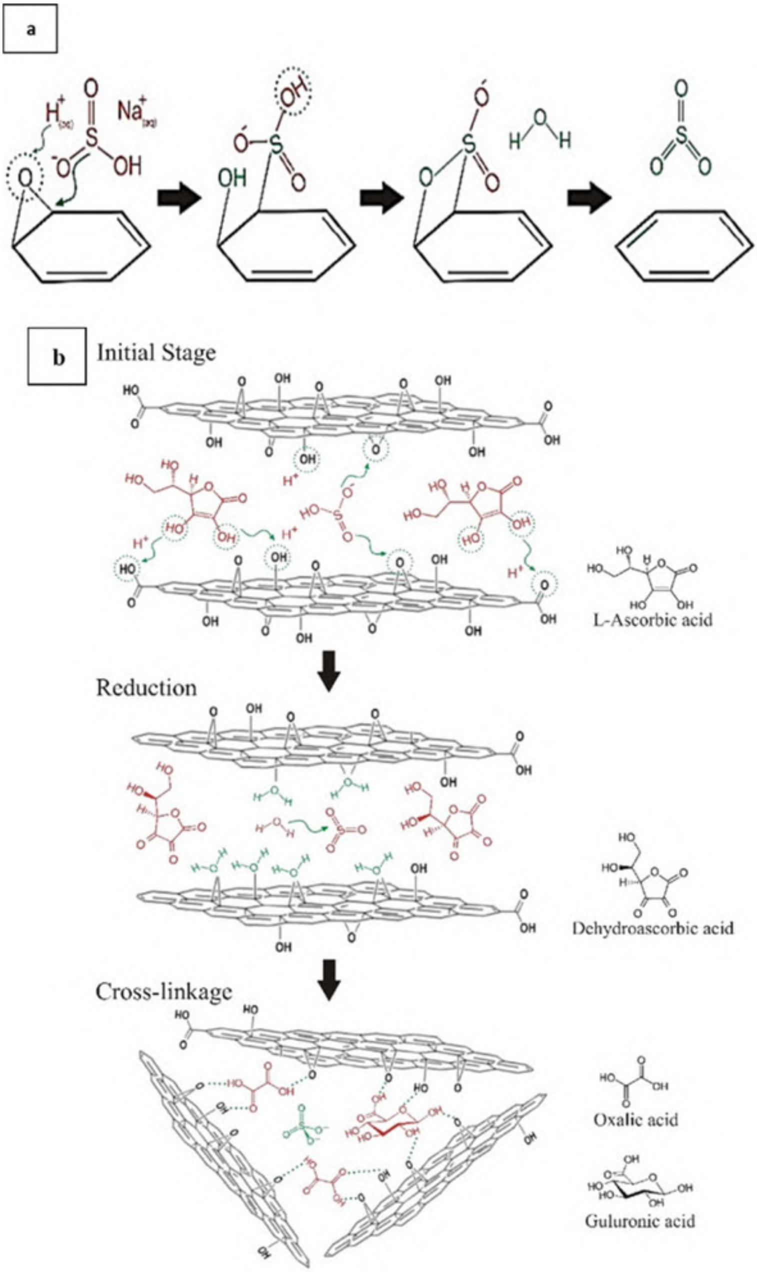

Fig. 1 **a** The mechanism of $NaHSO_3$ in reduction process; ring-opening reaction and **b** Schematic of the reduction reaction and cross-linking effect [19]. Adapted with permission [19], Copyright (2023), Elsevier

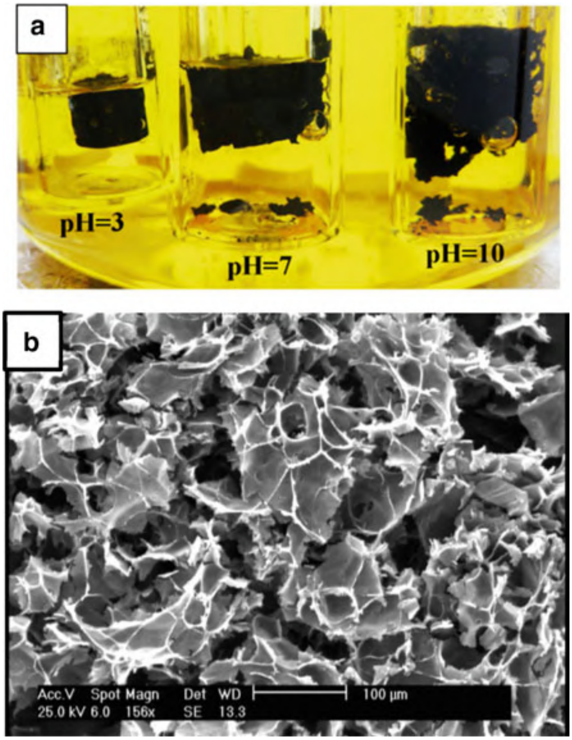

Fig. 2 **a** Hydrogel formation at pH of 3, 7, and 10, **b** SEM image of 3D porous structure of GA which was prepared at pH of 3 [17]. Adapted with permission [17], Copyright (2023), Elsevier

(with pH values of 3 and 10). They reported that the CO_2 bubbles evolved from acidic media of hydrogel led to the formation of macroscopic voids in hydrogel. While in alkaline media, no formation of macroscopic voids was observed due to the conversion of CO_2 into ionic species, which generated a compressible graphene hydrogel that was a good candidate for applications such as supercapacitor and battery electrodes [21]. Therefore, the condition of media (to be acidic or alkaline suspension) relies on the target applications (such as energy storage or adsorption) and the expected features (such as conductivity and mechanical properties) to obtain the proper structure. This, also, is applicable to both hydrothermal and chemical reduction methods.

In general, two factors are the most effective to produce high-quality 3D graphene aerogels: first, enhancing the bonding forces, and second, decreasing the repulsion forces between graphene sheets. Researchers also proposed some polymeric organic materials, which can act as cross-linking agents to form the graphene aerogels, such as PVA, PEI, and EDA. These materials possess functional groups, which are bonded to graphene sheets through hydrogen bonding to facilitate the formation of a high mechanical strength 3D graphene hydrogel [22–24].

5.2 Multivalent Metal Ions

Inducing the metal ions into the GO structure is one of the novel methods in graphene aerogel production. Divalent (Ca^{2+}, Mg^{2+}, and Cu^{2+}) and trivalent ions (Cr^{3+}, Fe^{3+}) provide better interaction with GO to encourage self-assembly of graphene sheets to make 3D graphene hydrogel. X. Jiang et al. showed that Ca^{2+}, Ni^{2+}, and Co^{2+} act as linker resulting in formation of stable 3D graphene hydrogel. The authors optimized the mass ratio of metal ions to GO, and concluded that the mass ratio of 0.1 was the best to form 3D graphene hydrogel due to the cross-linking effect of divalent ions [25].

The effect of using two different types of divalent metal ions on formation and properties of graphene aerogels was studied by Ghazitabar et al. In this research, Zn^{2+} and Co^{2+} were introduced to 3D graphene structure to make the interconnected mesoporous structure, which was the best choice for electrochemical energy storage application. In graphene aerogel structure, the high surface area along with high mesoporous volume was obtained in the presence of both Zn^{2+} and Co^{2+}. In this proposed model, zinc and cobalt ions were converted to oxide forms without forming any clusters or agglomerates. This structure had specific and separated sites on graphene sheets because of adsorption of metal ions on oxygen functional groups on GO sheets [20]. The proposed mechanism of composite formation is shown in Fig. 3a The TEM and FESEM images of final composite are illustrated in Fig. 3b, c, respectively. Due to available separated and monodispersed nanoparticles on graphene sheets, it is highly recommended to use this method for sensing and catalytic applications such as electrochemical hydrogen evolution.

5.3 Biomacromolecules

Some of organic materials can interact with graphene oxide sheets to form 3D porous interconnected structure of graphene hydrogel through hydrogen bonding (in some cases, covalent or non-covalent interactions), such as polysaccharide [26], polyvinyl alcohol (PVA) [27], protein [28], and chitosan [29]. The GA, which was synthesized by this route, represented good mechanical stability and compressibility with less aggregated graphene sheets, becoming suitable for use as sorbent to absorb the organic and inorganic pollutants. The mechanical stability provided by this method can facilitate the sorption process in large-scale operations.

Chitosan, as a natural biopolymer, acts as a cross-linking agent through hydrogen bonding with functional groups on GO sheets to make the 3D graphene aerogel, providing good potential for organic and inorganic adsorption applications [30]. Cellulose fibers are another potential biomaterials, which have been used as building blocks in graphene aerogel composites applicable in various applications such as heavy metal ions adsorption and flexible supercapacitors. Cellulose has numerous hydroxyl groups, which can form hydrogen bonding to functional groups on graphene

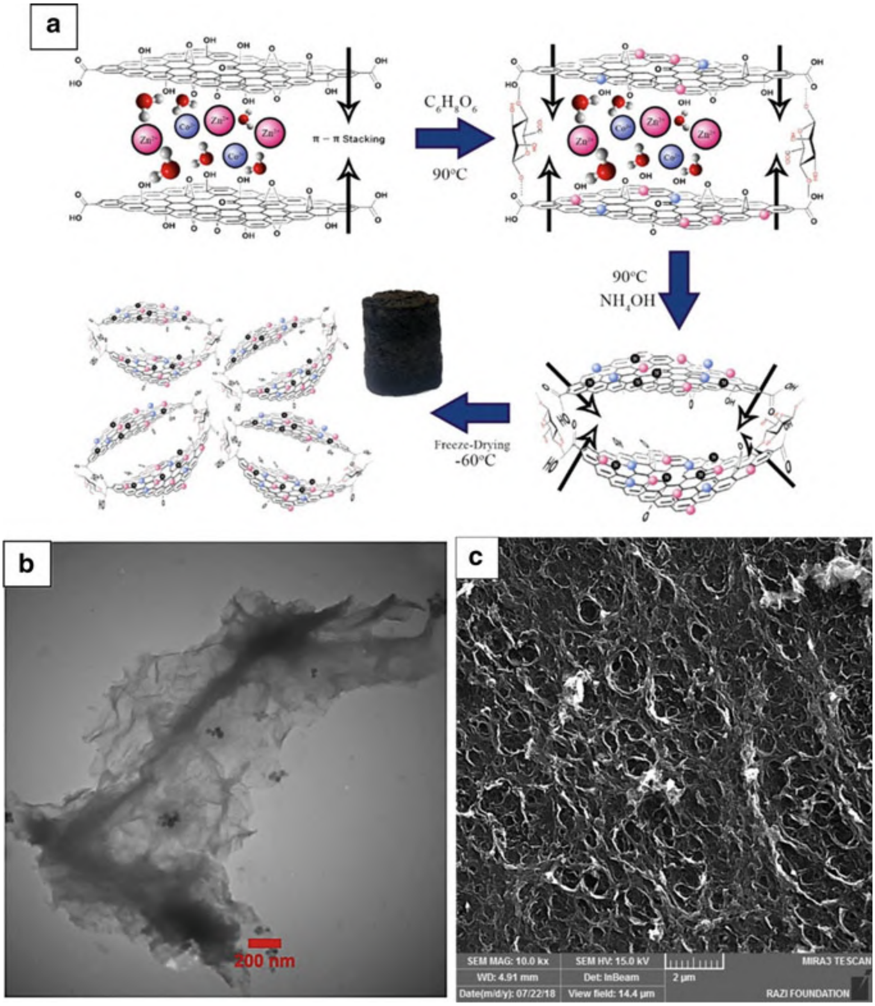

Fig. 3 **a** Mechanism of composite formation, **b** TEM image of composite aerogel, and **c** FESEM image of composite aerogel [20]. Adapted with permission [20], Copyright (2023), Elsevier

sheets in order to enhance the formation of 3D interconnected porous structure in graphene aerogel, as given in Fig. 4a. Researchers used the cellulose fibers and magnetite nanoparticles in graphene aerogel structure to make the specific Au adsorbent from cyanide solution. Cellulose fibers increased the compression strength (at the 50% strain) of graphene aerogel more than 27% (Fig. 4b). The authors reported that the adsorption capacity of this adsorbent was 112 mg Au per 1 g of graphene aerogel composite, which was higher than the results reported in previous studies due to cross-linking role of cellulose fibers [31].

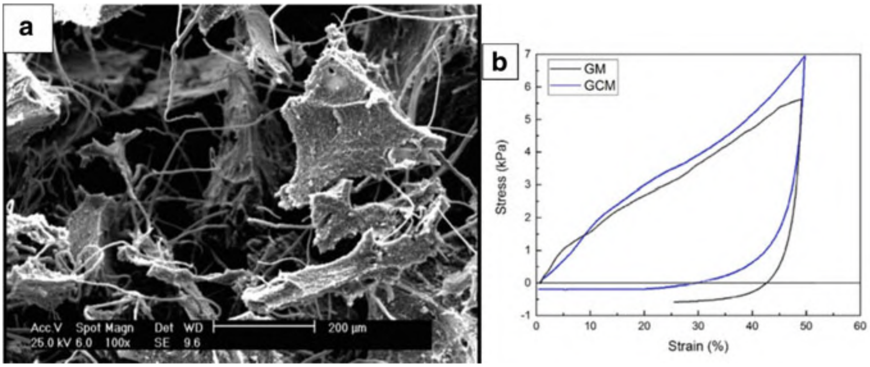

Fig. 4 **a** SEM image of cellulose/Fe_3O_4 nanoparticle/graphene aerogel composite (GCM) and **b** compression test of Fe_3O_4 nanoparticle/graphene aerogel (GM) and GCM composites [31]. Adapted with permission [31], Copyright (2023), Elsevier

In the recent work, researchers evaluated different types of cellulose fibers to be used as cross-linking agent for 3D graphene structure. Microfiber and nanofiber of cellulose were dispersed separately in GO solution, and chemically were reduced by reducing agents to form graphene aerogel composites to use as sorbent for organic pollutants removal (Fig. 5a, b). In the microfiber cellulose-bearing composite, the reduced graphene sheets were folded around the cellulose fibers, (Fig. 5c), which resulted in increasing the hydrophobicity of final structure. However, in the case of cellulose nanofibers, graphene sheets were converted to 3D porous structure with well-dispersed nanofibers between the sheets to make a hydrophilic sorbent (Fig. 5d) [15].

6 Template-Based Method

The porous structure of graphene aerogels, which was mentioned in previous sections, had an irregular shape and randomly arrangements. The template-based method is introduced to obtain the specific shape and size of pores in graphene aerogel structure. In this method, the resulting macropores are uniform as a replica of the template. Indeed, the template and its porous morphology structure can predict the shape and size of pores in 3D graphene aerogel. Three sub-categories for this method are briefly introduced in the following.

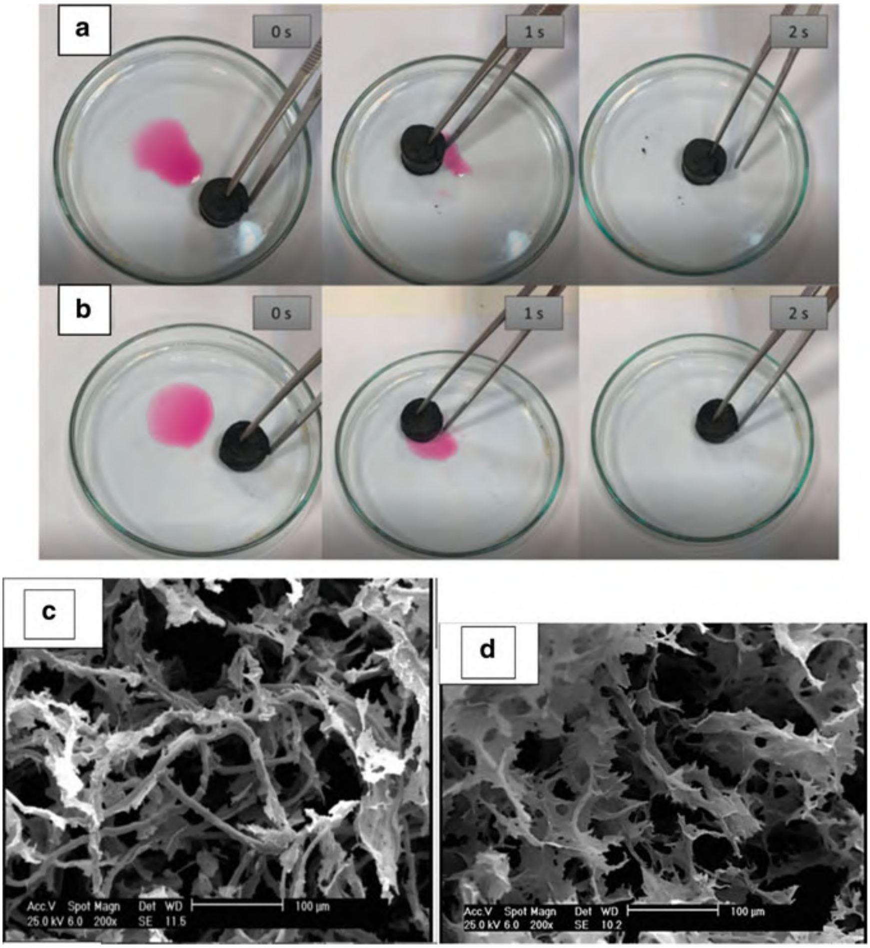

Fig. 5 **a** Sorption process of toluene stained with Sudan red by GA with cellulose microfibers (top) and **b** cellulose nanofibers (bottom), SEM images of **c** GA with cellulose microfibers and (d) GA with cellulose nanofibers [15]. Adapted with permission [15], Copyright (2023), Elsevier

6.1 Chemical Vapor Deposition (CVD)

In this method, a foam, such as nickel foam, is used as template to grow the 3D graphene by means of chemical deposition of carbon in gas phase followed by etching the metallic foam in acidic solution to obtain the 3D structure of graphene [32]. The porous structure obtained in final 3D graphene is related to the initial design of the template. The porous metallic frameworks (nickel foam), oxides (silica nanospheres and MgO nanoparticles), crystalline aluminosilicate minerals (zeolites), biomorphic templates (seashells), and dielectric substrate (Al_2O_3) are the common sacrificed templates, which are used in 3D graphene fabrication by CVD process.

Banciu et al. synthesized a 3D graphene structure for energy-related applications by means of CVD process on a nickel foam template. Carbon sources for this purpose were chosen from gaseous (methane, ethylene, and acetylene), liquid (ethanol, benzene, styrene, and petroleum asphalt), and solid (polyvinyl alcohol and camphor) phase. CVD process was carried out at 1000 °C under a hydrogen and argon atmosphere. The nickel foam was etched by 3 M HCl, after completing the graphene growth process, in order to prepare a 3D graphene applicable in supercapacitor as electrode material [33]. In another study, porous MgO was used as sacrificed template to fabricate 3D graphene structure. In this study, methane was selected as a carbon precursor to make the graphene nanomesh with large surface area (1654 $m^2.g^{-1}$) in order to use as electrode material for supercapacitor [34]. The similar research was performed by Shi et al. to fabricate 3D N-doped graphene in order to find use in catalytic applications due to its extraordinary large surface area (1531 $m^2.g^{-1}$) as well as being dominant pyrrolic type for nitrogen doping (1.3 wt% N content). In this research, a mixture of pyridine (C_5H_5N) and methane (CH_4) was used as nitrogen and carbon sources, respectively, for CVD process at 900 °C to grow the N-doped graphene on MgO template [35].

6.2 *Template-Directed Self-Assembly*

The directional-freezing route is one of the proposed methods to fabricate a highly compressible graphene aerogel due to providing an anisotropic porous structure. Liu et al. proposed directional-freezing of graphene hydrogel, followed by freeze-drying, to obtain a graphene aerogel with a high compressive strength, which made it a promising highly recyclable material for oil absorption applications [36]. A progressive method was introduced by Oh et al. They used the directional-freezing to fill the polyurethane foam with graphene oxide aerogel to use as sound absorber. This 3D aerogel composite had high resilient properties under cyclic loads, and presented full sound absorption with thickness of 45 mm at 2000 Hz frequency [37]. The anisotropic structure of graphene aerogel, which is synthesized by directional-freezing or ice-templated method is a good candidate for Electromagnetic Interference (EMI) shielding application due to highly arranged tubular pores formed in its microstructure. Anisotropic polyimide (PI)/graphene composite aerogel was fabricated by unidirectional freezing of the mixture of GO, poly (amic acid) (PAA) ammonium salt, and trimethylamine followed by freeze-drying and thermal imidization process. The obtained density of the aerogel was 76 $mg.cm^{-3}$ with EMI shielding effectiveness (SE) of 26.1–28.8 dB when 13 wt% of the final aerogel was graphene [38].

Some researchers synthesized a graphene aerogel composite to improve its elasticity and conductivity, applying porous template. Mohsenpour et al. proposed a novel synthesis route for graphene aerogel composite. They used cellulose and carbon aerogel (Fig. 6a, b) as a template to fabricate the carbon/graphene aerogel composite by immersion of monolithic carbon aerogel in GO suspension followed by chemical reduction and freeze-drying. The synthesized monolithic carbon/graphene aerogel presented a great electrochemical performance thanks to its high-strength binder-free electrodes, as shown in Fig. 6c [11].

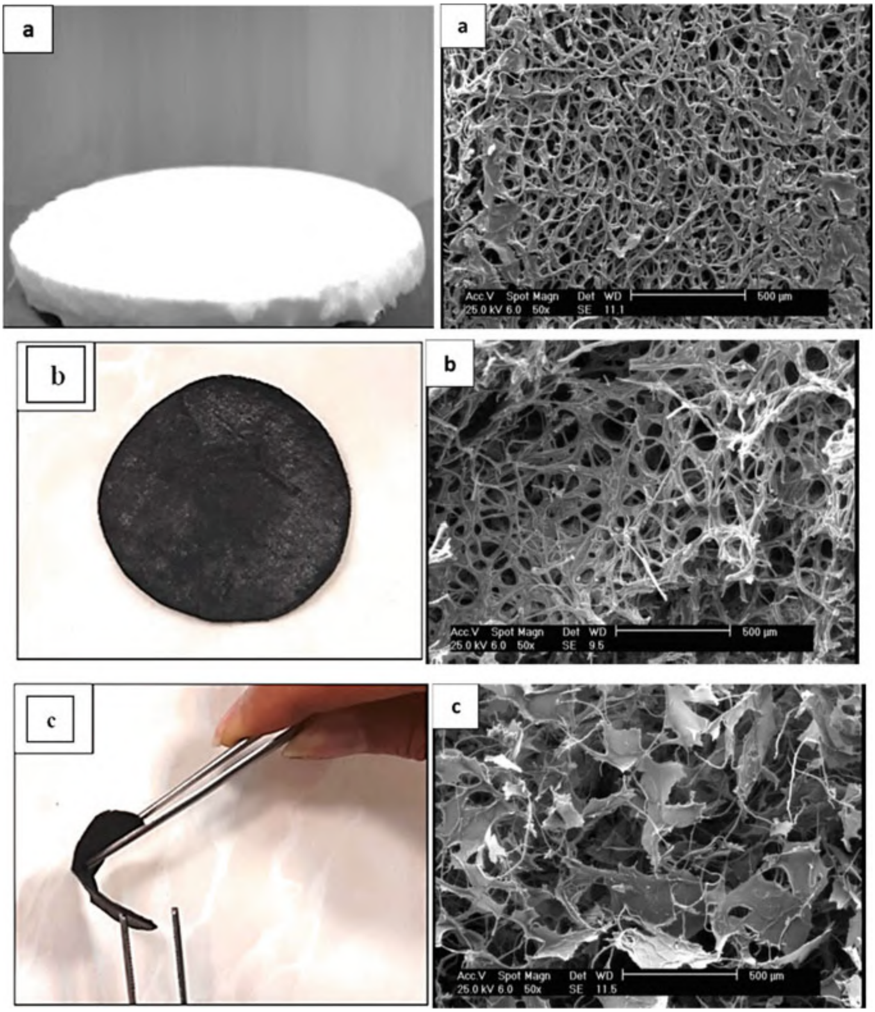

Fig. 6 The photograph and SEM images of **a** Cellulose aerogel, **b** Carbon aerogel, and **c** Graphene/carbon aerogel [11]. Adapted with permission [11], Copyright (2023), Elsevier

6.3 Bubble-Based Method

The latest template-based method is using the bubbles as a template to form manageable porous structure of GA. The bubbles can be made by fabricating an organic/inorganic emulsion or purging air bubbles at high shear rate. The earliest attempt for this method was proposed by Zhang et al. who made a GO/cyclohexane emulsion under ultrasonication to fabricate oil phase droplets. They also used $NaHSO_3$ in that mixture, and kept the mixture at 70 °C for 12 h to reduce GO. The GO was reduced to RGO that led to decrease in hydrophilicity, and gathered around the oil phase droplets to form a honeycomb network. The time and power of ultrasonication operation, and the volume ratio of GO:Cyclohexane were the additional parameters to tailor the porous structure of GA along with other usual synthesis parameters including time and temperature of the GO mixture as well as the type and amount of reducing agent. After freeze-drying the obtained hydrogel, the produced GA had an ultra-light weight (<3 mg.cm^{-3}), and exhibited a high mechanical strength in order to function as a reusable oil absorbent material [39].

In recent works, Zhang et al. proposed the synthesis of ultra-light and superelastic GA by means of air bubble-templated method. In this process, at first the emulsified foam of GO/sodium dodecyl sulfonate (SDS)/LAA mixture was created at the high speed of 2040 rpm. SDS was added to stabilize the bubbles to make a pupil-like rings structure wherein the graphene sheets were located on the bubbles' outer layer. After partially reduction at 75 ºC, the aerogel was obtained by drying at atmospheric pressure. The final aerogel was heat-treated at 500 ºC for further reduction. The uniform honeycomb-like porous structure was templated by the closely packed air bubbles. The regular arrangement graphene cell walls provided supercompression resilience property at compressive strain of 99% at high compressive stress of 87.5 kPa [40]. In summary, bubble-templated method is one of the major methods to fabricate superelastic ultra-low-density GA in order to make materials such as absorbents widely applicable for oil removal, soft robot, and flexible devices.

7 3D Printing

Recently, some of the research groups have introduced 3D printing method for graphene aerogel fabrication. In 3D printing, the parts are built up layer by layer as depositing materials according to digital 3D design data. This procedure has several advantages such as proper flexibility, good durability, and high feasibility for complex designs. Three different sub-categories of 3D printing technique proposed to fabricate the 3D graphene aerogels are Direct Ink Writing (DIW), Inkjet printing, and Stereolithography (SLA).

7.1 Direct Ink Writing (DIW)

This method is one of the extrusion-based 3D printing techniques that has been used to fabricate the lightweight structure. In this technique, extruding the ink through a micronozzle is done continuously in a three-axis motion stage to make the 3D structure. The main challenge for this method is to form a proper gel-based viscoelastic ink, possessing shear-thinning behavior to facilitate the flow under pressure, and a rapid pseudoplastic characteristic to recover after printing. Therefore, the resulting graphene aerogel, which is fabricated by this technique, is highly dependent on the ink formulation and its properties. Graphene oxide (GO) is the main precursor for ink preparation. Printable GO ink is fabricated by engineering its composition and rheology to get it applicable for nozzle of DIW technique. As reported in some studies, the minimum concentration of 5 $mg.mL^{-1}$ of GO was needed to generate the required rheological behavior for a 3D printable ink [41]. There are many reports in which the concentrated alkaline GO suspension, more than 10 $mg.mL^{-1}$ using ammonia as pH-adjusting agent, was used as printable ink due to the good gelation of GO under this condition [3].

Some of the researchers proposed application of cross-linking organic materials such as resorcinol–formaldehyde (R–F) solution in order to induce the gelation to high concentrated GO suspensions. A few studies indicated that addition of hydrophilic fumed silica or alumina powders to the GO suspensions caused an increase in viscosity, and provided non-Newtonian fluid with a shear-thinning behavior, applicable as a printable ink [42]. As discussed in Sect. 4–2, Ca^{2+} as a divalent ion can enhance the graphene aerogel formation by increasing the GO suspension viscosity, and enhancing the gelation of GO suspension. This method was used for ink preparation by Jiang et al. [43]. Guo et al. fabricated highly recoverable elastic porous material in 3D form by means of ink-printing solution of GO and multi-walled carbon nanotubes (MWNTs). In this study, a post-treatment, such as reduction process, was implemented to accomplish more desired mechanical properties in final 3D-printed material [44].

Partially reduced GO suspension is another favorite material for being used as printable ink to fabricate the 3D graphene aerogel. Ultra-light, with the density of 8.5 $mg.cm^{-3}$, and elastic 3D graphene aerogel was printed by Peng et al. They used partially reduced GO inks, prepared by mixing ascorbic acid aqueous solution and GO suspensions at various mass ratios [45]. In most studies that used DIW technique, investigating the viscoelasticity of the printed graphene aerogels was the main research subject. However, some challenges have remained unanswered so far. One of the challenges is how to print properly a complex and miniature design. In this case, a small syringe nozzle hole size is needed, meaning that we must incorporate nanoparticles into the ink. Gue et al. investigated 3D printing of graphene aerogel using DIW technique in order to function in energy storage devices, and to address the challenge faced in printing the nano-size graphene ink [46].

7.2 Inkjet Printing

Zhang et al. introduced a novel technique to assemble graphene sheets into macroscopic 3D structure by combining inkjet printing and directional-freezing methods followed by freeze-drying process. The desired printable ink of graphene oxide was charged into the inkjet printer syringe, and then ejected onto the cold plate (heat sink) to complete the first layer of designed path. Printing the second layer initiated when the freezing of first layer was completed at −20 °C to ensure the layer-by-layer formation of 3D structure. The resulting 3D graphene structure was then emerged into a liquid nitrogen followed by freeze-drying for 48 h to produce the 3D graphene aerogel. Heat-treatment process was conducted at 1000 °C, under argon atmosphere, to increase the conductivity and lightweight of printed graphene aerogel [47]. Such assemblies have been designed and developed in Graphene and Advanced Materials Laboratory (GAMLab) in Amirkabir University of Technology to fabricate graphene hydrogel and aerogel by means of LaserJet and inkjet technologies, respectively (Fig. 7a, b). The cold base is frozen up to −30 °C to make the frozen graphene in order to add later layers to form the 3D structure of graphene hydrogel (Fig. 7c). The fabricated frozen hydrogel is then transferred to the Freeze-dryer (FD-10 V freeze-dryer, Tajhizat Sazan Pishtaz Co., Iran) to produce the final GA (Fig. 7d).

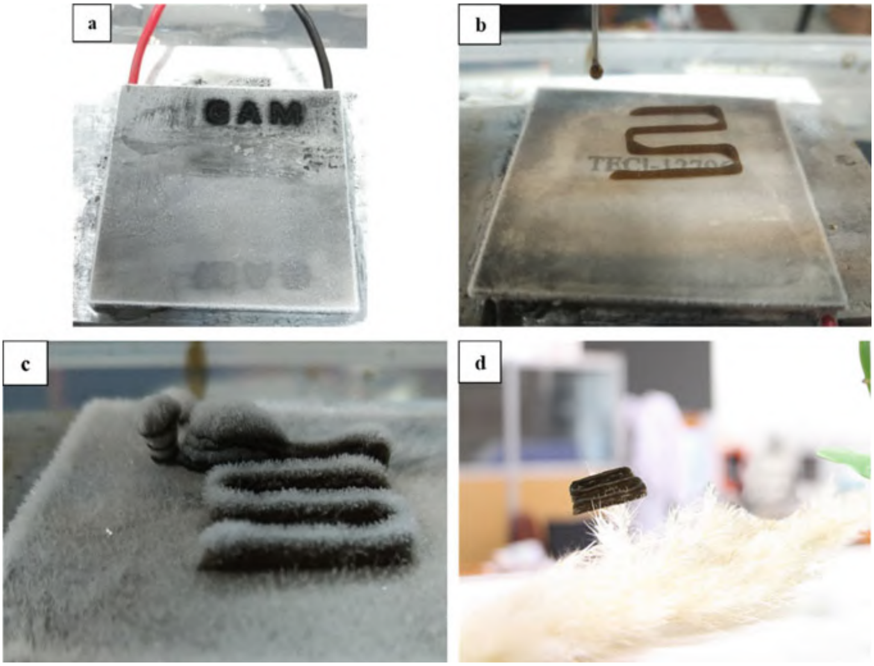

Fig. 7 Photograph images of **a** LaserJet and **b** inkjet technologies of GA formation, **c** the frozen 3D graphene hydrogel is freeze-dried to make **d** the ultra-light 3D GA

7.3 Stereolithography (SLA)

In this method, the 3D structure of graphene is made layer by layer employing laser light that exposes a photocrosslinkable resin to cure it, and to make the 3D graphene. Herein, the right selection of photocrosslinkable resin materials, to form GO in 3D structure, is the critical point. Korhonen et al. used GO and the commercial PIC100 as precursors for graphene and photocrosslinkable resin, respectively, to print the 3D graphene by SLA method. At the first step, GO and PIC100 were stirred in different mass ratios to make the printable suspension. 3D model was prepared by CAD software, and the printing was performed by self-made projection stereolithography (PSLA) system, which used the light intensity of 3900 μW.cm^{-2} along with various curing times. The thermal reduction of 3D-printed graphene/polymer was carried out under nitrogen atmosphere to gain higher electrical conductivity required for electrical applications [48].

Markandan et al. suggested the SLA method to print a 3D graphene lattice by graphene at lower concentration, which was reported as disadvantage in previous similar works. The objective of this work was to achieve the mechanical properties suitable for various applications including aerospace, automotive, and sports equipment, while fabricating the 3D graphene structure. Graphene platelets were dispersed in a gray resin, used as photosensitive agent, to make the printable mixture. The 3D SLA printing was done by 405 nm laser to cure the liquid polymer resin followed by a thermal reduction process. The authors indicated that SLA technique encouraged the incorporation of aligned graphene platelets to make 3D graphene structure with higher mechanical properties [49].

8 Summary

In this chapter, the main 3D graphene synthesis methods were briefly introduced. Herein, researcher finds the preliminary knowledge and the most probable findings related to synthesize GA, while using different methods as discussed. However, the selection of the most proper synthesis method mainly relies on the target application as well as the available facilities. Of course, the related cost and mass production feasibilities are the matter of concerns as well. To simplify the decision-making, and to contribute to the better understanding of all discussed 3D graphene synthesis methods, the main synthesis parameters along with the properties of the GA produced employing different synthesis methods are summarized in Table 1.

Table 1 Summary of different GA synthesis methods

Synthesis methods	Main synthesis parameters	Main features of GA	Application areas
Hydrothermal	Temperature, time, and GO concentration	Partially reduced GO without any macroscopic voids and good mechanical stability	Adsorption and wearable devices
Direct self-assembly of GO	GO concentration	Highest functional groups and hydrophilic structure	Adsorption
Chemical reduction	Temperature, type, and concentration of reducing agent, and GO concentration	Highly reduced graphene, good conductivity, lowest oxygen functional groups, and hydrophobic structure	Electrodes for energy storage devices
Cross-linking agents	Type and concentration of cross-linking agent	Extraordinary mechanical stability and compressive strength	Adsorption, wearable devices and soft robots
Template-based	Precursor composition and type of template	Highest conductivity, uniform porous structure, and high elasticity	Adsorption, wearable devices and soft robots
3D printing	Type of printing method and graphene-based charging material	Desirable and complex shape and size	Electronic sensing

References

1. Wang, J., Ellsworth, M.W.: Graphene aerogels. ECS Trans. **19**(5), 241–247 (2009)
2. Ding, M., Li, C.: Recent advances in simple preparation of 3D graphene aerogels based on 2D graphene materials **10**, 1–9 (2022)
3. Kondratowicz, I., Żelechowska, K., Nadolska, M., Jażdżewska, A., Gazda, M.: Comprehensive study on graphene hydrogels and aerogels synthesis and their ability of gold nanoparticles adsorption. Colloids Surfaces A Physicochem. Eng. Asp. **528**, 65–73 (2017)
4. Huang, Y., Li, C., Lin, Z.: EDTA-induced self-assembly of 3D graphene and its superior adsorption ability for paraquat using a teabag. ACS Appl. Mater. Interfaces **6**(22), 19766–19773 (2014)
5. Liu, H., Qiu, H.: Recent advances of 3D graphene-based adsorbents for sample preparation of water pollutants: a review. Chem. Eng. J. **393**, 124691 (2020)
6. Yuxi Xu, G.S., Sheng, K., Li, C.: Self-assembled graphene hydrogel via a one-step hydrothermal process. ACS Nano **4**(7), 4324–4330 (2010)
7. Nguyen, S.T., Nguyen, H.T., Rinaldi, A., Nguyen, N.P.V., Fan, Z., Duong, H.M.: Morphology control and thermal stability of binderless-graphene aerogels from graphite for energy storage applications. Colloids Surfaces A Physicochem. Eng. Asp. **414**, 352–358 (2012)
8. Qin, S., Liu, X., Zhuo, R., Zhang, X.: Microstructure-controllable graphene oxide hydrogel film based on a pH-responsive graphene oxide hydrogel, 1–8
9. Zhao, Z., Wang, X., Qiu, J., Lin, J., Xu, D.: Three-dimensional graphene-based hydrogel/aerogel materials. Rev. Adv. Mater. Sci **36**(2), 137–151 (2014)
10. Li, K., Xu, Y., Angeles, L.: Reversible 3D self-assembly of graphene oxide and stimuli-responsive polymers and its enabled high-performance graphene-based supercapacitors (2017)

11. Mohsenpour, M., Naderi, M., Ghazitabar, A., Aghabararpour, M., Haghshenas, D.F.: Fabrication of paper based carbon/graphene/ZnO aerogel composite decorated by polyaniline nanostructure: investigation of electrochemical properties. Ceram. Int. (2021)
12. Zhang, L., Chen, G., Hedhili, M.N., Zhang, H., Wang, P.: Three-dimensional assemblies of graphene prepared by a novel chemical reduction-induced self-assembly method. Nanoscale **4**(22), 7038 (2012)
13. Du, A., Zhou, B., Zhang, Z., Shen, J.: A special material or a new state of matter: a review and reconsideration of the aerogel, 941–968 (2013)
14. Chen, W., Yan, L.: In situ self-assembly of mild chemical reduction graphene for three-dimensional architectures. Nanoscale **3**(8), 3132 (2011)
15. Hoviatdoost, A., Naderi, M., Ghazitabar, A., Gholami, F.: Fabrication of high-performance ultralight and reusable graphene aerogel/cellulose fibers nanocomposite to remove organic pollutants. Mater. Today Commun. **34**, 105077 (2023)
16. Qiao, Y., Wen, G.-Y., Wu, X.-S., Zou, L.: l—Cysteine tailored porous graphene aerogel for enhanced power generation in microbial fuel cells. RSC Adv. **5**(72), 58921–58927 (2015)
17. Ghazitabar, A., Naderi, M., Fatmehsari Haghshenas, D.: A facile chemical route for synthesis of nitrogen-doped graphene aerogel decorated by Co3O4 nanoparticles. Ceram. Int. **44**(18), 23162–23171 (2018)
18. Pham, H.D., Pham, V.H., Cuong, T.V.: ChemComm Synthesis of the chemically converted graphene xerogel with superior electrical conductivity w, c, 9672–9674 (2011)
19. Shadkam, R., Naderi, M., Ghazitabar, A., Asghari-Alamdari, A., Shateri, S.: Enhanced electrochemical performance of graphene aerogels by using combined reducing agents based on mild chemical reduction method. Ceram. Int. **46**(14), 22197–22207 (2020)
20. Ghazitabar, A., Naderi, M., Haghshenas, D.F., Rezaei, M.: Synthesis of N-doped graphene aerogel/Co 3 O 4/ZnO ternary nanocomposite via mild reduction method with an emphasis on its electrochemical characteristics. J. Alloys Compd. **794**, 625–633 (2019)
21. Hu, K., Xie, X., Szkopek, T., Cerruti, M.: Understanding Hydrothermally Reduced Graphene Oxide Hydrogels: From Reaction Products to Hydrogel Properties (2016)
22. Wang, X., Nie, S., Zhang, P., Song, L., Hu, Y.: Superhydrophobic and superoleophilic graphene aerogel for ultrafast removal of hazardous organics from water. J. Mater. Res. Technol., 1–8 (2019)
23. Simón-Herrero, C., Peco, N., Romero, A., Valverde, J.L., Sánchez-Silva, L.: PVA/nanoclay/graphene oxide aerogels with enhanced sound absorption properties. Appl. Acoust. **156**, 40–45 (2019)
24. Sui, Z.Y., Cui, Y., Zhu, J.H., Han, B.H.: Preparation of Three-dimensional graphene oxide-polyethylenimine porous materials as dye and gas adsorbents. ACS Appl. Mater. Interfaces **5**(18), 9172–9179 (2013)
25. Jiang, X., Ma, Y., Li, J., Fan, Q., Huang, W.: Self-assembly of reduced graphene oxide into three-dimensional architecture by divalent ion linkage. J. Phys. Chem. C **114**(51), 22462–22465 (2010)
26. Guastaferro, M., Reverchon, E., Baldino, L.: Polysaccharide-based aerogel production for biomedical applications: a comparative review. Materials (Basel) **14**(7) (2021)
27. Rapisarda, M., Malfense Fierro, G.P., Meo, M.: Ultralight graphene oxide/polyvinyl alcohol aerogel for broadband and tuneable acoustic properties. Sci. Rep. **11**(1), 1–10 (2021)
28. Zhuang, Y., Yu, F., Ma, J., Chen, J.: Facile synthesis of three-dimensional graphene–soy protein aerogel composites for tetracycline adsorption. Desalin. Water Treat. **57**(20), 9510–9519 (2016)
29. Pinelli, F., Nespoli, T., Rossi, F.: Graphene oxide-chitosan aerogels: Synthesis, characterization, and use as adsorbent material for water contaminants. Gels **7**(4), (2021)
30. Luo, J., Fan, C., Xiao, Z., Sun, T., Zhou, X.: Novel graphene oxide/carboxymethyl chitosan aerogels via vacuum-assisted self-assembly for heavy metal adsorption capacity. Colloids Surfaces A **578**, 123584 (2019)
31. Ghazitabar, A., Naderi, M., Haghshenas, D.F., Ashna, D.A.: Graphene aerogel/cellulose fi bers/magnetite nanoparticles (GCM) composite as an effective Au adsorbent from cyanide solution with favorable electrochemical property. J. Mol. Liq. **314**, 113792 (2020)

32. Jiang, W., Xin, H., Li, W.: Microcellular 3D graphene foam via chemical vapor deposition of electroless plated nickel foam templates. Mater. Lett. **162**, 105–109 (2016)
33. Banciu, C.A., Florin Nastase, L.M.V.: Anca-Ionela Istrate, “3D graphene foam by chemical vapor deposition: synthesis, properties, and energy-related applications. Molecules **27**, 3634 (2022)
34. Ning, G., Fan, Z., Wang, G., Gao, J., Qian, W., Wei, F.: Gram-scale synthesis of nanomesh graphene with high surface area and its application in supercapacitor electrodes. Chem. Commun. **47**(21), 5976–5978 (2011)
35. Le Shi, J., Tang, C., Huang, J.Q., Zhu, W., Zhang, Q.: Effective exposure of nitrogen heteroatoms in 3D porous graphene framework for oxygen reduction reaction and lithium–sulfur batteries. J. Energy Chem. **27**(1), 167–175 (2018)
36. Liu, T., Huang, M., Li, X., Wang, C., Gui, C., Yu, Z.: Beijing Key Laboratory on Preparation and Processing of Novel Polymer Materials, Beijing,” Carbon N. Y., (2016)
37. Oh, J.H., Kim, J., Lee, H., Kang, Y., Oh, I.K.: Directionally antagonistic graphene oxide-polyurethane hybrid aerogel as a sound absorber. ACS Appl. Mater. Interfaces **10**(26), 22650–22660 (2018)
38. Yu, Z., Dai, T., Yuan, S., Zou, H., Liu, P.: Electromagnetic interference shielding performance of anisotropic polyimide/graphene composite aerogels. ACS Appl. Mater. Interfaces **12**(27), 30990–31001 (2020)
39. Zhang, B. et al.: Cellular graphene aerogel combines ultralow weight and high mechanical strength: a highly efficient reactor for catalytic hydrogenation. Sci. Rep. **6,** 25830 (2016)
40. Xiaofang Zhang, J.Z., Zhang, T., Wang, Z., Ren, Z., Yan, S., Duan, Y.: Ultralight , superelastic and fatigue resistant graphene aerogel templated by graphene oxide liquid crystal stabilized air bubbles. Appl. mat (2018)
41. Palaganas, J.O., Palaganas, N.B., Ramos, L.J.I., David, C.P.C.: 3D printing of covalent functionalized graphene oxide nanocomposite via stereolithography. ACS Appl. Mater. Interfaces **11**(49), 46034–46043 (2019)
42. Zhu, C., et al.: Highly compressible 3D periodic graphene aerogel microlattices. Nat. Commun. **6**, 1–8 (2015)
43. Jiang, Y., et al.: Direct 3D printing of ultralight graphene oxide aerogel microlattices. Adv. Funct. Mater. **28**(16), 1–8 (2018)
44. Guo, F., et al.: Highly stretchable carbon aerogels. Nat. Commun. **9**(1), 1–9 (2018)
45. Peng, M., et al.: 3D printing of ultralight biomimetic hierarchical graphene materials with exceptional stiffness and resilience. Adv. Mater. **31**(35), 1–9 (2019)
46. Guo, B., Liang, G., Yu, S., Wang, Y., Zhi, C., Bai, J.: 3D printing of reduced graphene oxide aerogels for energy storage devices: a paradigm from materials and technologies to applications. Energy Storage Mater. **39**, 146–165 (2021)
47. Zhang, F., Yang, F., Lin, D., Zhou, C.: Parameter study on 3D-printing graphene oxidize based on directional freezing. ASME 2016 11th Int. Manuf. Sci. Eng. Conf. MSEC 2016, vol. 3, pp. 1–11 (2016)
48. Korhonen, H., et al.: Fabrication of graphene-based 3D structures by stereolithography. Phys. Status Solidi Appl. Mater. Sci. **213**(4), 982–985 (2016)
49. Markandan, K., Lai, C.Q.: Enhanced mechanical properties of 3D printed graphene-polymer composite lattices at very low graphene concentrations. Compos. Part A **129**, 105726 (2020)

Synthesis and Characteristics of 3D Graphene

Hiran Chathuranga, Ishara Wijesinghe, Ifra Marriam, and Cheng Yan

Abstract Three-dimensional (3D) graphene structures have high electrical conductivity, excellent mechanical properties, high porosity, and large surface area, demonstrating great potential for broad applications, including sensors, absorbents , solar cells, flexible batteries, supercapacitors, and fuel cells. Their physical and chemical properties are mainly determined by the synthesis methods. Numerous fabrication methods have been successfully developed to tailor the structures and properties of 3D graphene structures. In general, the synthesis approaches can be categorized as template-assisted methods (e.g., chemical vapor deposition, template-assisted graphene oxide (GO) reduction, soft template techniques, and ice templating) and template-free methods (e.g., GO crosslinking, assembly of GO by reduction, 3D printing, and sugar blowing). In addition, 3D graphene structures can be also produced using other techniques like roll-to-roll (R2R) manufacturing and 3D laser-induced manufacturing. Therefore, in this chapter, the recent advances in the synthesis and characteristics of 3D graphene structures are discussed.

Keywords 3D graphene · 3D graphene synthesis · Methods · Template-assisted synthesis · Template-free synthesis

1 Introduction

Graphene, a two-dimensional material (2D) containing sp^2-hybridized carbon atoms arranged into a honeycomb-like structure, has attracted unprecedented research interest in recent years owing to its remarkable properties, including high electron mobility (250,000 cm^2V^{-1}), excellent thermal conductivity (2000–5000 $Wm^{-1}\ K^{-1}$), and strong mechanical strength (Young's modulus of ~1 TPa) [1, 2]. Despite these extraordinary properties, the use of graphene in practical applications has been hindered due to the challenges like high contact resistance

---

H. Chathuranga · I. Wijesinghe · I. Marriam · C. Yan (✉)
School of Mechanical, Medical and Process Engineering, Faculty of Engineering, Queensland University of Technology, 2 George St, Brisbane, QLD 4000, Australia
e-mail: c2.yan@qut.edu.au

© The Author(s), under exclusive license to Springer Nature Switzerland AG 2023

R. K. Gupta (ed.), *3D Graphene*, Carbon Nanostructures,
https://doi.org/10.1007/978-3-031-36249-1_3

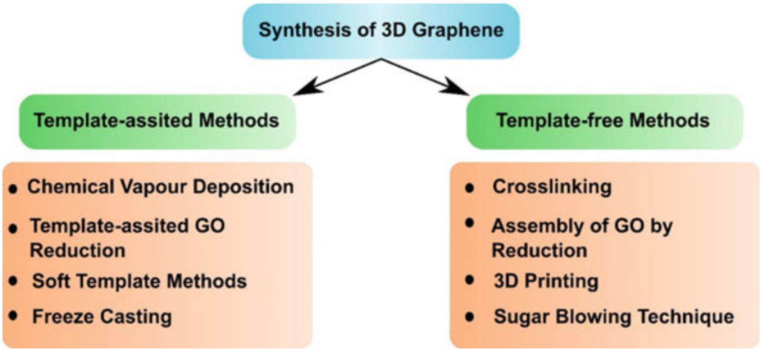

Fig. 1 Synthesis methods of 3D graphene structures

between individual graphene sheets and agglomeration of graphene due to strong van der Waals interactions. Many efforts have been made to address these issues, and the assembly of graphene into 3D structures has been identified as one of the promising solutions [3–6].

In recent years, extensive efforts have been devoted to fabricating 3D graphene structures with outstanding physical and chemical properties. In general, the fabrication of 3D graphene structures can be divided into two main categories: template-assisted methods and template-free methods (Fig. 1) [7, 8]. In template-assisted methods, a template is used to assemble the 3D graphene network. The commonly used template-assisted methods are chemical vapor deposition, template-assisted GO reduction, soft template techniques, and ice templating. On the other hand, 3D graphene structures can also be synthesized without using a template. Here, GO or its derivatives are directly assembled into 3D structures using physical and/or chemical methods such as GO crosslinking, assembly of GO by reduction, and 3D printing [9–13]. Furthermore, manufacturing techniques like R2R manufacturing and 3D laser-induced manufacturing can be used to synthesize 3D graphene structures in large quantities. Thus, the fabrication of 3D graphene structures using these methods is discussed in this chapter.

2 Synthesis of 3D Graphene

2.1 Template-Assisted Synthesis Methods

2.1.1 Chemical Vapor Deposition

Chemical vapor deposition (CVD) is a process that involves decomposing a carbon precursor onto a metal substrate to form single- or multilayer graphene sheets. 3D graphene structures can be synthesized by CVD using prefabricated 3D metal templates as the substrate [3]. The commonly applied metal substrates to grow 3D graphene are copper (Cu) and nickel (Ni), and the growth mechanisms of graphene on these two substrates are different. Graphene growth on the Cu substrate is mainly governed by surface growth, resulting in the formation of single-layer graphene sheets. As a result of the weak connectivity of single-layer graphene sheets, forming 3D graphene networks using Cu substrate is difficult, and these 3D graphene structures break down easily during handling. Graphene has two growth mechanisms when grown on Ni substrate: surface growth and carbon dissolution–precipitation. Thus, multiple layers of graphene can be grown on the Ni substrate, improving the strength and stability of the 3D graphene structure [4, 14].

Synthesis of 3D graphene using Ni substrate is first demonstrated by Chen and co-workers in 2011 [15]. In their pioneering work, commercial Ni foam was used as the 3D substrate and graphene was grown on this substrate by introducing methane gas (CH_4) at 1000 °C under atmospheric pressure. Next, the surface of the 3D structure was coated with a thin layer of poly (methyl methacrylate) (PMMA) to prevent the graphene structure from collapsing during Ni etching. Subsequently, Ni was etched using hot hydrochloric acid (HCl) or ferric chloride ($FeCl_3$), and a free-standing 3D graphene structure was obtained after removing PMMA using acetone (Fig. 2a). The as-prepared 3D graphene structure demonstrated high porosity (99.7%), excellent specific surface area (850 m^2 g^{-1}), and low density (5 mg cm^{-3}). However, these 3D graphene structures often suffer from drawbacks like large pore size (200–500 μm), structural properties determined by the commercial Ni foam, and porous structure collapsing during handling.

Meanwhile, Ito et al. developed a nano-porous 3D graphene structure using a nano-porous Ni substrate [16]. The nano-porous Ni substrate was produced by leaching Mn from the $Ni_{30}Mn_{70}$ alloy. Graphene was grown on this nano-porous substrate using benzene, argon (Ar), and hydrogen (H_2) precursors at 900 °C, and nano-porous 3D graphene was obtained by etching Ni substrate using HCl (Fig. 2b, c). In comparison to commercial Ni foam-based 3D graphene, nano-porous Ni substrate-based 3D graphene has a homogeneous porosity, and the pore size of nano-porous 3D graphene structure can be tailored by altering the temperature and graphene growing time of the CVD process. For instance, the average pore sizes of the nano-porous 3D graphene structures grown at 800 °C for 5 min and 1000 °C for 10 min were ~250 nm and ~3 μm, respectively [17, 18]. Moreover, these 3D graphene structures have better structural and mechanical stabilities owing to the bi-continuous architecture.

In addition to Ni and Cu templates, several other oxides have also been employed as porous substrates for the CVD synthesis of 3D graphene, including SiO_2[19], CaO [20], Al_2O_3[21], and MgO [22]. For example, Nishihara et al. employed Al_2O_3 nanoparticles for the CVD growth of 3D graphene [21]. The resulting graphene structure demonstrated a large surface area (1940 m^2 g^{-1}), high electrical conductivity (~8 S cm^{-3}), and low density (0.4 g cm^{-3}). In this process, first, graphene was grown on the Al_2O_3 nanoparticles using CH_4 gas at 900 °C. Afterward, 3D graphene or graphene mesosponge (GMS) was obtained by removing Al_2O_3 using NaOH. Finally, the 3D structure was annealed at 1800 °C for 2 h to improve the crystallinity (Fig. 2d). The Al_2O_3 substrate-based 3D graphene has fine mesopores (~5.8 nm).

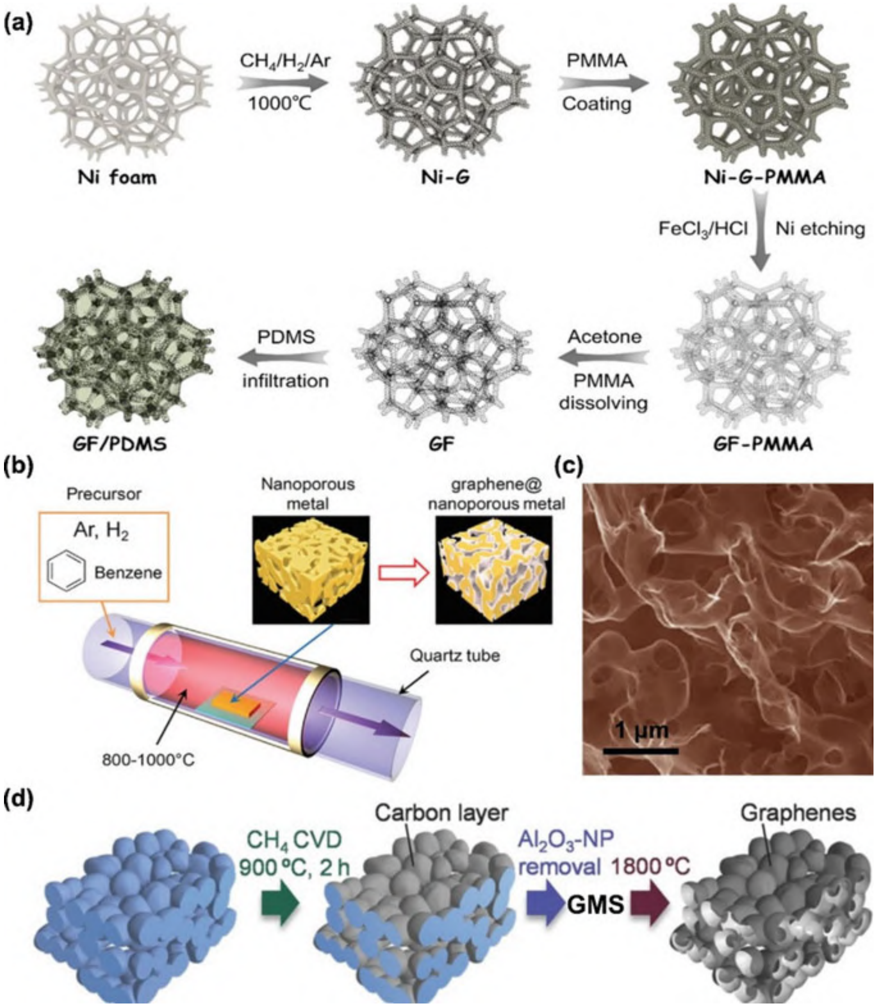

Fig. 2 Schematic illustration of the fabrication process of 3D graphene using **a** commercial Ni foam substrate. Adapted with permission [14]. Copyright (2021) © The Authors, some rights reserved; exclusive licensee John Wiley and Sons. Distributed under a Creative Commons Attribution License 4.0 (CC BY) and **b** nano-porous Ni substrate. Adapted with permission [4]. Copyright (2022) John Wiley and Sons. **c** SEM image of the nano-porous 3D graphene. Adapted with permission [16]. Copyright (2014) John Wiley and Sons. **d** Schematic demonstration of the synthesis steps of 3D graphene using Al_2O_3 substrate. Adapted with permission [21]. Copyright (2016) John Wiley and Sons

However, these mesopores have a spherical shape, and the interconnectivity of these pores is poor.

2.1.2 Template-Assisted GO Reduction Process

In this synthesis method, first, the templates were soaked in GO solution. Next, these templates were chemically or physically treated to convert GO into reduced graphene oxide (rGO). Finally, the 3D graphene structure was obtained by removing the template skeleton using chemical etching (for metallic templates) or thermal decomposition (for polymeric templates). Su et al. used this technique to synthesize a 3D graphene structure for the non-invasive detection of tumor cells [23]. The 3D graphene structure was fabricated by immersing a Ni foam in an aqueous GO solution, converting GO into rGO with hydrazine ($N_2H_4.H_2O$), followed by the removal of Ni foam using HCl (Fig. 3a). In another study, Yang and co-workers immersed a polyurethane (PU) sponge in a GO dispersion and annealed it at 900 °C for 2 h in an inert environment to achieve a sponge-shaped 3D graphene structure with a high specific surface area (305 $m^2\ g^{-1}$), good pore size distribution (>3.5 nm), and excellent electrosorptive capacity (4.95 mg g^{-1}) (Fig. 3b) [24]. Although the synthesis of 3D graphene using this technique is straightforward, the resulting 3D graphene structures are associated with issues like poor quality owing to the stacking of GO sheets and difficulty in controlling the pore size.

2.1.3 Freeze-Casting or Ice Templating

In freeze-casting, first, an aqueous slurry of GO is subjected to freezing, which causes ice crystals to form on the freezing side of the slurry and advance along the temperature gradient. Once the freezing has ended, the solid structure is freeze-dried to remove the ice crystal, and the resulting samples will have pores similar to sublimated crystals. Finally, the 3d structure is thermally treated to enhance physical properties [25, 26]. The freeze-casting method has numerous benefits, including a simple operating procedure, low cost, and the ability to adjust the pore structure. For example, Zhang and colleagues utilized the freeze-casting technique to develop a vertically aligned graphene membrane as a solar thermal converter to produce clean water (Fig. 3c) [27]. This converter exhibited maximum solar thermal conversion efficiency of 94.2%. In another study, Wu et al. fabricated a 3D graphene/polyaniline composite for supercapacitor electrodes [28]. The 3D graphene structure was designed using the freeze-casting method. After freeze-drying and reducing GO, polyaniline was introduced into the 3D structure by in situ polymerization. The graphene/polyaniline electrode demonstrated improved specific capacitance (538 F g^{-1} at 1.0 A g^{-1}) and cycle stability (74% specific capacitance after 1000 cycles).

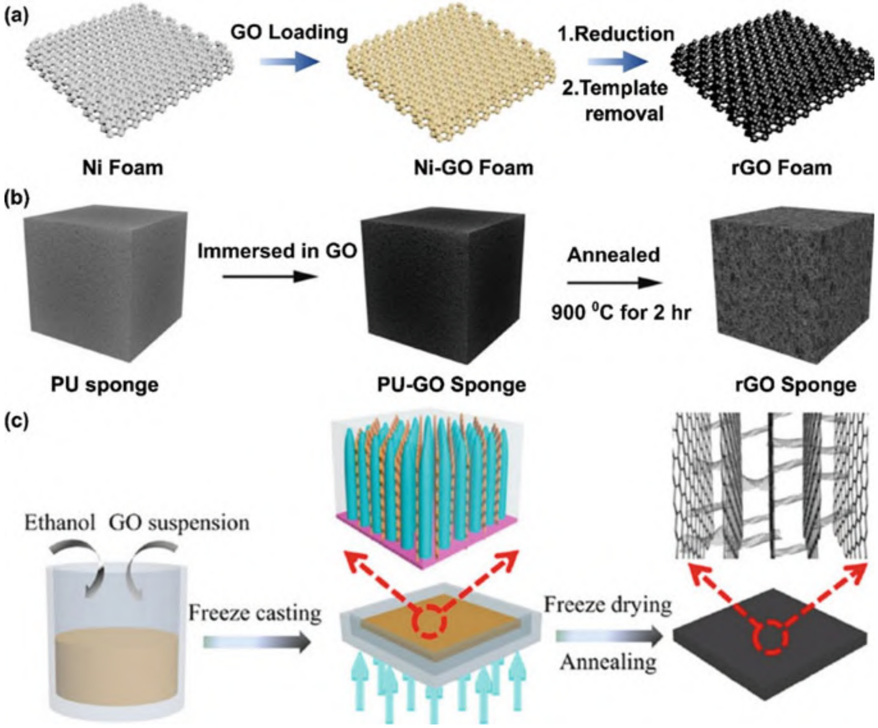

Fig. 3 Schematic diagrams of the preparation process of the **a** Ni-Foam (adapted with permission [23]. Copyright (2021) Elsevier) and **b** PU sponge (adapted with permission [24]. Copyright (2014) John Wiley and Sons)-assisted 3D graphene structure. **c** 3D graphene synthesis using freeze-casting method. Adapted with permission [27]. Copyright (2017) American Chemical Society

2.1.4 Soft Template Techniques

Soft templates like emulsions or gases can also be employed to develop 3D graphene structures. When compared with hard template methods, soft template approaches have numerous advantages like low cost, facile manufacturing steps, and the ability to alter the pore diameter of 3D graphene structure from nano-scale to micro-scale [29, 30]. For instance, Yeo et al. developed a rhombic dodecahedral honeycomb 3D graphene structure using a hierarchical design strategy [31]. First, GO was functionalized with alkylating agents. The alkylated GO sheets were micro-fluidically treated to generate micro-scale spherical solid-shelled bubbles. Subsequently, these homogeneous bubbles were assembled into a 3D structure through post-treatment. Finally, the thermal reduction process was used to obtain the 3D graphene framework (Fig. 4a, b). The as-prepared 3D graphene structure demonstrated a rhombic dodecahedral honeycomb structure (Fig. 4c). Furthermore, it exhibited high Young's modulus (300 kPa), low density (7.7 mg cm^{-3}), and excellent compressive strain (87%). Meanwhile, Barg et al. also fabricated a 3D graphene structure by combing

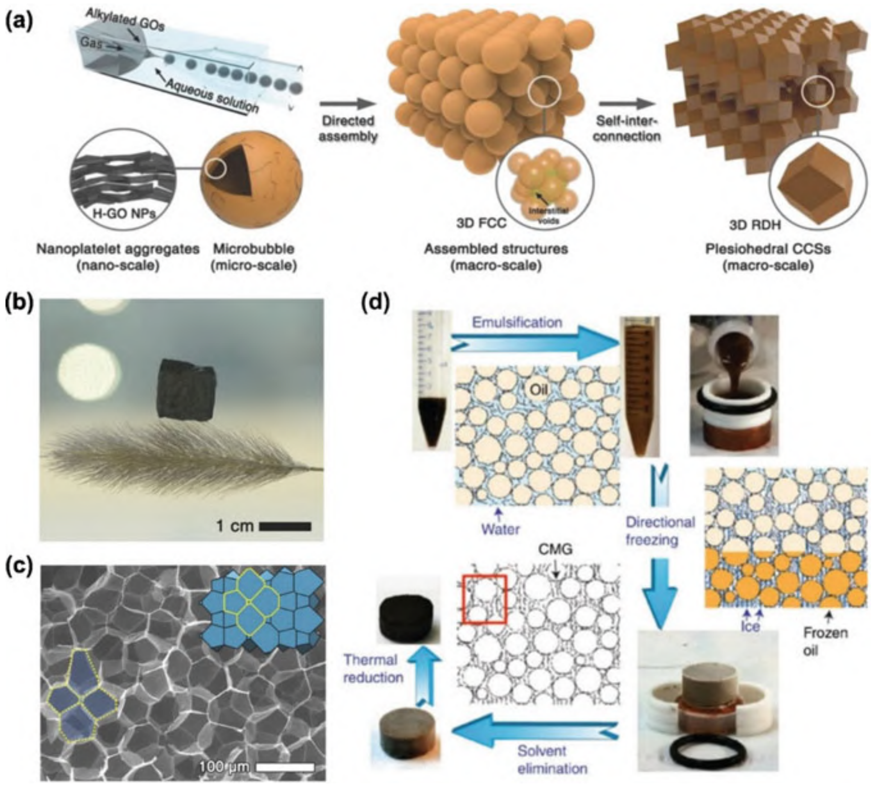

Fig. 4 **a** Soft template-assisted multiscale design of 3D graphene. **b** Photograph and **c** SEM image of the rhombic dodecahedral honeycomb 3D graphene. Adapted with permission [31]. Copyright (2018) John Wiley and Sons. **d** Assembly strategy of the 3D graphene structure using combined soft templating and ice templating techniques. Adapted with permission [32]. Copyright (2014) © The Authors, some rights reserved; exclusive licensee Springer Nature. Distributed under a Creative Commons Attribution License 4.0 (CC BY)

soft templating with ice templating, and the resulting graphene structure illustrated outstanding morphological properties (Fig. 4d) [32].

2.2 *Template-Free Synthesis Methods*

2.2.1 Crosslinking

3D graphene structures can be synthesized by crosslinking GO sheets using numerous gelling agents. GO hydrogels are formed during the crosslinking of GO sheets, and after reduction and freeze-drying, the 3D graphene structure can be obtained.

Polyvinyl alcohol (PVA), polyaniline, poly (N-isopropyl acrylamide), sodium alginate, cyclodextrin, metal ions (Mg^{2+}, Fe^{3+}, and Ni^{2+}), and chitosan-like crosslinkers have been widely used to make 3D graphene structures [12, 33, 34]. PVA is the first crosslinker used in 3D graphene synthesis [35]. The hydrogen bonds formed between PVA and functional groups (hydroxyl, epoxy, and carboxyl) of GO sheets cause gelation during hydrogel formation. Remarkably, this crosslinked hydrogel formation is pH dependent, as at high pH levels the hydrogel remains in aqueous form while at acidic pH levels, it gels. Moreover, the hydrogels formed with acidic conditions are strong because of π–π stacking between graphene sheets.

It is reported that the crosslinking mechanisms depend on the type of crosslinkers used in the hydrogel formations. For example, it is a nucleophilic addition mechanism when GO is reduced with chitosan, where epoxy groups in GO react with the amino groups of chitosan [36]. Another benefit of this 3D graphene synthesis method is its flexibility, which enables the fabrication of flexible structures such as beads. These beads are formed by injecting GO drops and crosslinkers into a gelling agent followed by washing and removing excess chemicals [37]. Further, additional properties like magnetic properties can be included in these materials by adding Fe^{+3} ions.

2.2.2 Assembly of GO by Reduction

GO is an amphiphilic 2D material. Hence, preparing GO dispersions using solvents like water is relatively easy due to the formation of H-bonds between water molecules and functional groups of GO sheets. However, when these interactions are unstabilized via GO reduction techniques, GO sheets coagulate and form hydrogels, after freeze-drying these hydrogels, free-standing 3D graphene structures can be obtained. Acids, hydrazine, metals, metal oxides, and reducing salts have been used as reducing agents [38]. The nature of the reducing agent affects the 3D graphene's properties (to produce uniform structures of 3D graphene mild reducing agents have been used). Furthermore, during GO reduction, the mixture should not be stirred, as it disturbs the stacking of graphene into 3D structures. In addition, plant derivatives such as extracts of tea leaves, roselle flowers, and spinach leaves have also been found as effective reducing agents [39–41].

Hydrothermal reduction of GO sheets has also been identified as a template-free approach to synthesizing 3D graphene. Here, a GO solution in a Teflon-lined hydrothermal reactor is heated under pressure to enable the construction of 3D graphene hydrogels. Zhuang and co-workers designed a reduced GO nanofiltration membrane using the hydrothermal method [42]. The resultant membrane exhibited excellent water purification performance, rejecting ~100% organic dye at 53 L m^{-2} h^{-1} water flux (Fig. 5a). In another study, Wasalathilake et al. fabricated 3D graphene structures with various pore sizes using a pH-assisted hydrothermal process [43]. They found that the 3D graphene structures with small pores and thick walls exhibit the best mechanical properties. Besides, 3D graphene structure with small pores has the highest electrical conductivity owing to the highly interconnected structure. Meanwhile, the hydrothermal process can be converted into a solvothermal process by changing the dispersion medium of water with a solvent [44]. Moreover, the ability of these hydrothermal and solvothermal techniques to surface functionalize 3D graphene structures with diverse end groups is an added benefit.

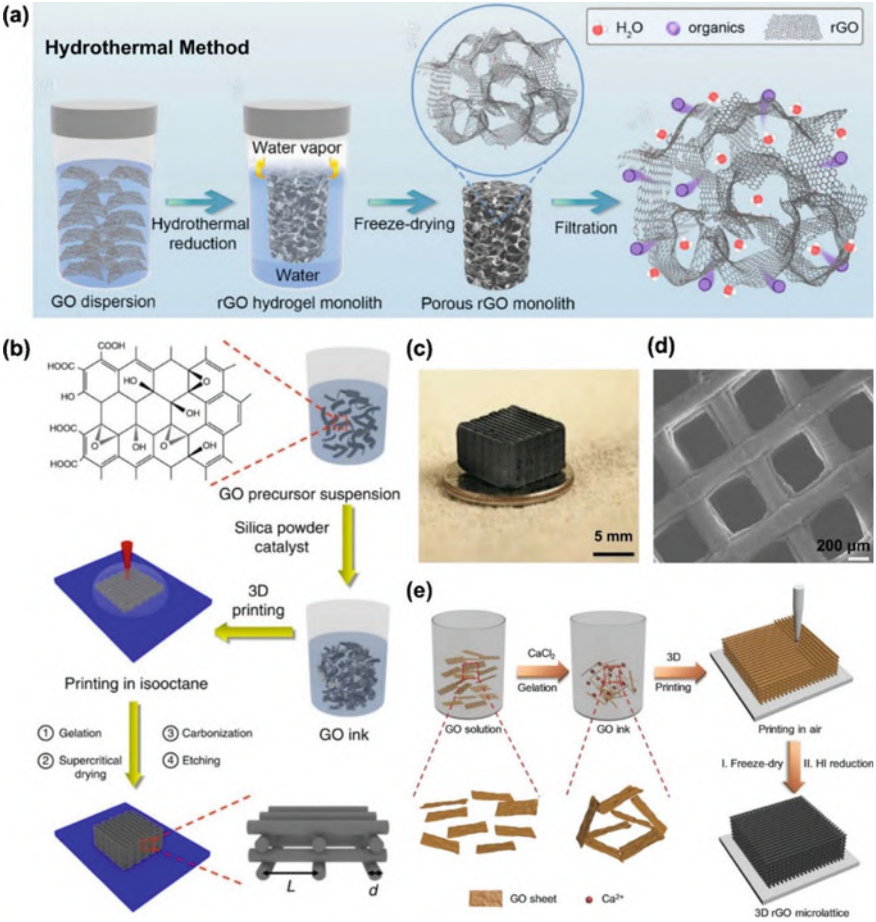

Fig. 5 **a** Synthesis of 3D graphene using hydrothermal method. Adapted with permission [42]. Copyright (2021) © The Authors, some rights reserved; exclusive licensee American Chemical Society. Distributed under a Creative Commons Attribution License 4.0 (CC BY) **b** 3D printing of graphene structures using silica/GO ink. **c** Photograph and **d** SEM image of the 3D-printed graphene structure. Adapted with permission [47]. Copyright (2015) © The Authors, some rights reserved; exclusive licensee Springer Nature. Distributed under a Creative Commons Attribution License 4.0 (CC BY) **e** 3D printing of graphene structures using GO/Ca^{+2} ink. Adapted with permission [48]. Copyright (2018) John Wiley and Sons

2.2.3 3D Printing

3D printing is a manufacturing technique that constructs 3D objects using computer-aided designed (CAD) models. Numerous materials, including polymers, metals, and ceramics, can be used as precursors in 3D printing. Recently, manufacturing of 3D graphene structures using the 3D printing method has attracted a lot of attention owing to the advantages like low cost, short design-manufacturing cycle, scalability, and the possibility to design complex 3D objects in large quantities [45, 46]. For instance, Zhu et al. fabricated a lightweight and highly conductive graphene aerogel using a 3D printing method called direct ink writing [47]. Here, the 3D printing ink was synthesized by mixing silica powder with a GO solution, which improved the viscosity of the ink. After printing, the 3D structure was freeze-dried and carbonized. Finally, the silica filler was etched to produce the 3D graphene framework (Fig. 5b). The 3D-printed graphene structure demonstrated 90% compressive strain, high surface area (~1000 m^2 g^{-1}), and large mesopores (3 $cm^3 g^{-1}$) (Fig. 5c, d). In a similar study, Jiang et al. 3D-printed a graphene structure using GO/Ca^{+2} ink [48]. After printing, the free-standing 3D graphene structure was obtained via freeze-drying and hydroiodic acid (HI) reduction (Fig. 5e). To demonstrate the potential applications, this 3D graphene structure was employed as supercapacitor electrodes and exhibited outstanding gravimetric capacitance (213 F g^{-1}) and cyclic performance (50 000 cycles).

2.2.4 Sugar Blowing Technique

Sugar-blown 3D graphene foams can be developed using a glucose and ammonium chloride mixture followed by heating at 1350 °C [12, 49]. Here, a mixture of glucose with ammonium chloride at a 1:1 ratio was heated for 3 h at a heating rate of 4 °C min^{-1} under Ar atmosphere in a tube furnace (Fig. 6a). In principle, the molten glucose syrup was formed by the decomposition products of the ammonium mixture to produce graphene, while the subsequent heating forms the 3D graphene structure. The 3D graphene produced with this method was a pack of polyhedral bubbles with an average diameter of 186 μm.

2.3 Scalable Production of 3D Graphene

Despite extensive research into various 3D graphene production techniques, scaling up the processes to produce high-quality 3D graphene structures has proven to be a persistent obstacle. The goal of 3D graphene synthesis on a large scale is to provide 3D graphene for real-world applications. The requirement to accomplish this goal is a low production cost. Generally, the prices of 3D graphene structures produced using Ni foams are very high (~$100–600/1 cm^3) when compared with similar commercial products. To reduce the production cost of 3D graphene, the development of simple

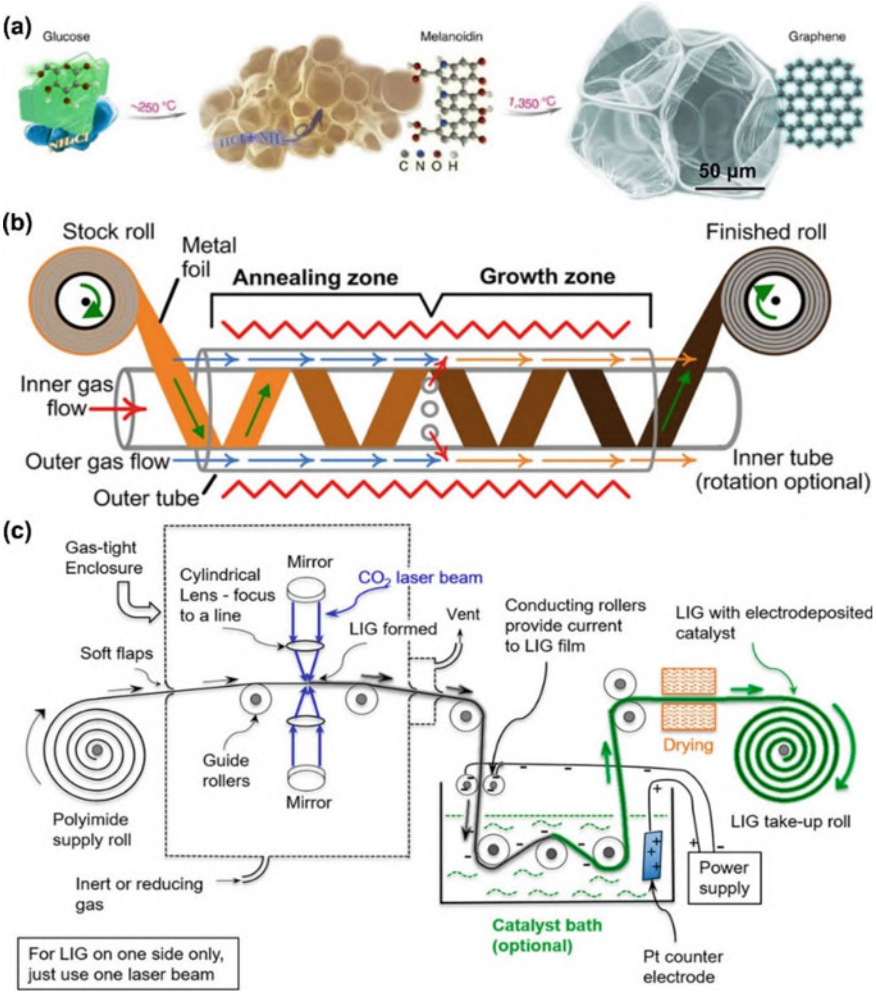

Fig. 6 **a** Growth of 3D graphene using sugar-blown technique. Adapted with permission [49]. Copyright (2013) Springer Nature. **b** R2R manufacturing of 2D graphene. Adapted with permission [50]. Copyright (2015) © The Authors, some rights reserved; exclusive licensee Springer Nature. Distributed under a Creative Commons Attribution License 4.0 (CC BY) **c** R2R manufacturing of laser-induced 3D graphene films. Adapted with permission [51]. Copyright (2018) American Chemical Society

and large-scale processes is critically important. Therefore, in this section, recent advances in the mass production of 3D graphene structures are discussed.

It is possible to scale up the CVD synthesis of 2D graphene using Cu or Ni metal foils as templates. This novel technique is called R2R manufacturing of 2D graphene [50]. As illustrated in Fig. 6b, this process contains a concentric tube reactor which continuously deposits graphene on a metal foil. In this system, a ribbon of metal foil is fed through from one end of the reactor and graphene sheets are grown on this foil using C_2H_4 and H_2 gases. Subsequently, graphene-deposited metal foil exists from the reactor and is rolled up for further processing. Here, the R2R manufacturing technique has only been used for the large-scale synthesis of 2D graphene. However, this technique can be applied to the mass production of 3D graphene by substituting the metal foils with thin and flexible metal foams.

Meanwhile, 3D graphene films can be produced by utilizing the laser-induced on-site polymerization method. This technique has many advantages such as low manufacturing time, availability of many substrates, and mild reaction conditions. Furthermore, these 3D graphene films can be directly applied as electrode materials for energy storage, sensors, flexible wearable devices, adsorbents, etc. As shown in Fig. 6c, Ye et al. reported the R2R manufacturing of 3D laser-induced 3D graphene films [51]. In this manufacturing process, the laser source is fixed, and the laser beam is focused on a line to maximize efficiency. Then, the polymer substrate (polyimide) is constantly fed into the laser chamber and subjected to the laser to form 3D graphene films. Afterward, this film is immersed in a catalyst bath to obtain hybrid structures. Finally, the film is dried and collected by a roller.

2.4 Conclusion and Outlook

Graphene with sp^2-hybridized carbon atoms arranged into a 2D honeycomb-like structure has attracted a lot of research interest owing to its outstanding electrical, thermal, and mechanical properties. However, restacking and high contact resistance of graphene sheets have hindered its practical applications, especially at a large scale. These challenges can be largely overcome by assembling graphene or its derivatives into 3D structures. Typically, 3D graphene structures can be synthesized using two techniques: template-assisted synthesis and template-free synthesis. For the template-assisted approach, a template is used to assemble the 3D graphene structure. Then, the template can be removed via chemical etching or thermal decomposition. With the template-free method, graphene or its derivatives are assembled into 3D graphene structures by altering their interfacial properties. Despite recent advances, numerous challenges remain in the development of 3D graphene structures with unique properties, which include

- Each 3D graphene structure exhibits distinctive features based on its unique structure. Therefore, to establish a structure–property relationship in 3D graphene structures, comprehensive and standardized characterization methodologies need to be developed.
- Less focus is given to analyzing the effects of internal and external defects in 3D graphene structures. Hence, understanding the role of defects in the overall performance of 3D graphene structures is required.
- Only a few studies have focused on the industry-scale fabrication of 3D graphene. So, more attention should be given to upgrading the lab-scale processes to

industry-scale technologies. Also, optimizing the process window against cost, property, and environmental considerations should be prioritized.

- Future research can be focused on multifunctional 3D graphene structures by coupling graphene with other functional materials like CNTs, MXenes, TMDs, and functional polymers.

References

1. Novoselov, K.S., Fal′ko, V.I., Colombo, L., Gellert, P.R., Schwab, M.G., Kim, K.: A roadmap for graphene. Nature **490**, 192–200 (2012)
2. Lee, C., Wei, X., Kysar, J.W., Hone, J.: Measurement of the elastic properties and intrinsic strength of monolayer graphene. Science **321**(80), 385–388 (2008)
3. Sun, Z., Fang, S., Hu, Y.H.: 3D graphene materials: from understanding to design and synthesis control. Chem. Rev. **120**, 10336–10453 (2020)
4. Han, J., Johnson, I., Chen, M.: 3D continuously porous graphene for energy applications. Adv. Mater. **34**, e2108750 (2022)
5. Yun, Q., Ge, Y., Chen, B., Li, L., Wa, Q., Long, H., Zhang, H.: Hybridization of 2D nanomaterials with 3D graphene architectures for electrochemical energy storage and conversion. Adv. Funct. Mater., 32 (2022)
6. Zhao, H.Y., Yu, M.Y., Liu, J., Li, X., Min, P., Yu, Z.Z.: Efficient Preconstruction of Three-Dimensional Graphene Networks for Thermally Conductive Polymer Composites. Springer Nature Singapore (2022)
7. Zhi, D., Li, T., Li, J., Ren, H., Meng, F.: A review of three-dimensional graphene-based aerogels: synthesis, structure and application for microwave absorption. Compos. Part B Eng. **211**, 108642 (2021)
8. Xiao, W., Li, B., Yan, J., Wang, L., Huang, X., Gao, J.: Three dimensional graphene composites: preparation, morphology and their multi-functional applications. Compos. Part A Appl. Sci. Manuf. **165**, 107335 (2023)
9. Sun, H., Lin, Y., Takeshi, H., Wang, X., Wu, D., Tian, Y.: Synthesis of 3D graphene-based materials and their applications for removing dyes and heavy metals. Environ. Sci. Pollut. Res. **28**, 52625–52650 (2021)
10. Shi, Q., Cha, Y., Song, Y., Lee, J.I., Zhu, C., Li, X., Song, M.K., Du, D., Lin, Y.: 3D graphene-based hybrid materials: Synthesis and applications in energy storage and conversion. Nanoscale **8**, 15414–15447 (2016)
11. Bano, Z., Mazari, S.A., Saeed, R.M.Y., Majeed, M.A., Xia, M., Memon, A.Q., Abro, R., Wang, F.: Water decontamination by 3D graphene based materials: a review. J. Water Process Eng. **36**, 101404 (2020)
12. Hiew, B.Y.Z., Lee, L.Y., Lee, X.J., Thangalazhy-Gopakumar, S., Gan, S., Lim, S.S., Pan, G.T., Yang, T.C.K., Chiu, W.S., Khiew, P.S.: Review on synthesis of 3D graphene-based configurations and their adsorption performance for hazardous water pollutants. Process Saf. Environ. Prot. **116**, 262–286 (2018)
13. Fang, Q., Shen, Y., Chen, B.: Synthesis, decoration and properties of three-dimensional graphene-based macrostructures: a review. Chem. Eng. J. **264**, 753–771 (2015)
14. Zeng, J., Xu, C., Gao, T., Jiang, X., Bin Wang, X.: Porous monoliths of 3D graphene for electric double-layer supercapacitors. Carbon Energy **3**, 193–224 (2021)
15. Chen, Z., Ren, W., Gao, L., Liu, B., Pei, S., Cheng, H.M.: Three-dimensional flexible and conductive interconnected graphene networks grown by chemical vapour deposition. Nat. Mater. **10**, 424–428 (2011)

16. Ito, Y., Tanabe, Y., Qiu, H.-J., Sugawara, K., Heguri, S., Tu, N.H., Huynh, K.K., Fujita, T., Takahashi, T., Tanigaki, K., Chen, M.: High-quality three-dimensional nanoporous graphene. Angew. Chemie Int. Ed. **53**, 4822–4826 (2014)
17. Han, J., Guo, X., Ito, Y., Liu, P., Hojo, D., Aida, T., Hirata, A., Fujita, T., Adschiri, T., Zhou, H., Chen, M.: Effect of chemical doping on cathodic performance of bicontinuous nanoporous graphene for Li-O2 batteries. Adv. Energy Mater. **6**, 1–9 (2016)
18. Kashani, H., Ito, Y., Han, J., Liu, P., Chen, M.: Extraordinary tensile strength and ductility of scalable nanoporous graphene. Sci. Adv. **5**, 1–7 (2019)
19. Chen, K., Li, C., Shi, L., Gao, T., Song, X., Bachmatiuk, A., Zou, Z., Deng, B., Ji, Q., Ma, D., Peng, H., Du, Z., Rümmeli, M.H., Zhang, Y., Liu, Z.: Growing three-dimensional biomorphic graphene powders using naturally abundant diatomite templates towards high solution processability. Nat. Commun. **7**, 13440 (2016)
20. Han, G.F., Chen, Z.W., Jeon, J.P., Kim, S.J., Noh, H.J., Shi, X.M., Li, F., Jiang, Q., Baek, J.B.: Low-temperature conversion of alcohols into bulky nanoporous graphene and pure hydrogen with robust selectivity on CaO. Adv. Mater. **31**, 1–7 (2019)
21. Nishihara, H., Simura, T., Kobayashi, S., Nomura, K., Berenguer, R., Ito, M., Uchimura, M., Iden, H., Arihara, K., Ohma, A., Hayasaka, Y., Kyotani, T.: Oxidation-resistant and elastic mesoporous carbon with single-layer graphene walls. Adv. Funct. Mater. **26**, 6418–6427 (2016)
22. Sunahiro, S., Nomura, K., Goto, S., Kanamaru, K., Tang, R., Yamamoto, M., Yoshii, T., Kondo, J.N., Zhao, Q., Ghulam Nabi, A., Crespo-Otero, R., Di Tommaso, D., Kyotani, T., Nishihara, H.: Synthesis of graphene mesosponge via catalytic methane decomposition on magnesium oxide. J. Mater. Chem. A **9**, 14296–14308 (2021)
23. Su, H., Yin, S., Yang, J., Wu, Y., Shi, C., Sun, H., Wang, G.: In situ monitoring of circulating tumor cell adhered on three-dimensional graphene/ZnO macroporous structure by resistance change and electrochemical impedance spectroscopy. Electrochim. Acta. **393**, 139093 (2021)
24. Yang, Z.-Y., Jin, L.-J., Lu, G.-Q., Xiao, Q.-Q., Zhang, Y.-X., Jing, L., Zhang, X.-X., Yan, Y.-M., Sun, K.-N.: Sponge-templated preparation of high surface area graphene with ultrahigh capacitive deionization performance. Adv. Funct. Mater. **24**, 3917–3925 (2014)
25. Shao, G., Hanaor, D.A.H., Shen, X., Gurlo, A.: Freeze casting: from low-dimensional building blocks to aligned porous structures—a review of novel materials. Methods Appl. Adv. Mater., 32 (2020)
26. Shahbazi, M.A., Ghalkhani, M., Maleki, H.: directional freeze-casting: a bioinspired method to assemble multifunctional aligned porous structures for advanced applications. Adv. Eng. Mater., 22 (2020)
27. Zhang, P., Li, J., Lv, L., Zhao, Y., Qu, L.: Vertically aligned graphene sheets membrane for highly efficient solar thermal generation of clean water. ACS Nano **11**, 5087–5093 (2017)
28. Wu, X., Tang, L., Zheng, S., Huang, Y., Yang, J., Liu, Z., Yang, W., Yang, M.: Hierarchical unidirectional graphene aerogel/polyaniline composite for high performance supercapacitors. J. Power Sources **397**, 189–195 (2018)
29. Zhang, R., Hu, R., Li, X., Zhen, Z., Xu, Z., Li, N., He, L., Zhu, H.: A bubble-derived strategy to prepare multiple graphene-based porous materials. Adv. Funct. Mater., 28 (2018)
30. Huang, X., Sun, B., Su, D., Zhao, D., Wang, G.: Soft-template synthesis of 3D porous graphene foams with tunable architectures for lithium-O2 batteries and oil adsorption applications. J. Mater. Chem. A. **2**, 7973–7979 (2014)
31. Yeo, S.J., Oh, M.J., Jun, H.M., Lee, M., Bae, J.G., Kim, Y., Park, K.J., Lee, S., Lee, D., Weon, B.M., Lee, W.B., Kwon, S.J., Yoo, P.J.: A Plesiohedral cellular network of graphene bubbles for ultralight, strong, and superelastic materials. Adv. Mater. **30**, 1–7 (2018)
32. Barg, S., Perez, F.M., Ni, N., Do Vale Pereira, P., Maher, R.C., Garcia-Tuñon, E., Eslava, S., Agnoli, S., Mattevi, C., Saiz, E.: Mesoscale assembly of chemically modified graphene into complex cellular networks. Nat. Commun., 5 (2014)
33. Venkateshalu, S., Grace, A.N.: Review—Heterogeneous 3D graphene derivatives for supercapacitors. J. Electrochem. Soc. **167**, 050509 (2020)
34. Moussa, M., Zhao, Z., El-, M.F., Liu, H., Michelmore, A., Kawashima, N., Majewski, P., Ma, J.: Free-standing composite hydrogel films for superior volumetric capacitance. J. Mater. Chem. A. **3**, 15668–15674 (2015)

35. Bai, H., Li, C., Wang, X., Shi, G.: A pH-sensitive graphene oxide composite hydrogel. Chem. Commun. **46**, 2376 (2010)
36. Shao, L., Chang, X., Zhang, Y., Huang, Y., Yao, Y., Guo, Z.: Graphene oxide cross-linked chitosan nanocomposite membrane. Appl. Surf. Sci. **280**, 989–992 (2013)
37. Rasoulzadeh, M., Namazi, H.: Carboxymethyl cellulose/graphene oxide bio-nanocomposite hydrogel beads as anticancer drug carrier agent. Carbohydr. Polym. **168**, 320–326 (2017)
38. Ma, Y., Chen, Y.: Three-dimensional graphene networks: synthesis, properties and applications. Natl. Sci. Rev. **2**, 40–53 (2015)
39. De Silva, K.K.H., Huang, H.H., Joshi, R.K., Yoshimura, M.: Chemical reduction of graphene oxide using green reductants. Carbon N. Y. **119**, 190–199 (2017)
40. Chu, H.J., Lee, C.Y., Tai, N.H.: Green reduction of graphene oxide by Hibiscus sabdariffa L. to fabricate flexible graphene electrode. Carbon N. Y. **80**, 725–733 (2014)
41. Wang, J., Salihi, E.C., Šiller, L.: Green reduction of graphene oxide using alanine. Mater. Sci. Eng. C. **72**, 1–6 (2017)
42. Zhuang, P., Guo, Z., Wang, S., Zhang, Q., Zhang, M., Fu, L., Min, H., Li, B., Zhang, K.: Interfacial hydrothermal assembly of three-dimensional lamellar reduced graphene oxide aerogel membranes for water self-purification. ACS Omega **6**, 30656–30665 (2021)
43. Wasalathilake, K.C., Galpaya, D.G.D., Ayoko, G.A., Yan, C.: Understanding the structure-property relationships in hydrothermally reduced graphene oxide hydrogels. Carbon N. Y. **137**, 282–290 (2018)
44. Liu, X., Shen, L., Hu, Y.: Preparation of TiO_2-graphene composite by a two-step solvothermal method and its adsorption-photocatalysis property. Water, Air, Soil Pollut. **227**, 141 (2016)
45. Wu, X., Mu, F., Lin, Z.: Three-dimensional printing of graphene-based materials and the application in energy storage. Mater. Today Adv., 11 (2021)
46. Yao, B., Chandrasekaran, S., Zhang, H., Ma, A., Kang, J., Zhang, L., Lu, X., Qian, F., Zhu, C., Duoss, E.B., Spadaccini, C.M., Worsley, M.A., Li, Y.: 3D-printed structure boosts the kinetics and intrinsic capacitance of pseudocapacitive graphene aerogels. Adv. Mater., 32 (2020)
47. Zhu, C., Han, T.Y.J., Duoss, E.B., Golobic, A.M., Kuntz, J.D., Spadaccini, C.M., Worsley, M.A.: Highly compressible 3D periodic graphene aerogel microlattices. Nat. Commun. **6**, 1–8 (2015)
48. Jiang, Y., Xu, Z., Huang, T., Liu, Y., Guo, F., Xi, J., Gao, W., Gao, C.: Direct 3D printing of ultralight graphene oxide aerogel microlattices. Adv. Funct. Mater., 28 (2018)
49. Wang, X., Zhang, Y., Zhi, C., Wang, X., Tang, D., Xu, Y., Weng, Q., Jiang, X., Mitome, M., Golberg, D., Bando, Y.:Three-dimensional strutted graphene grown by substrate-free sugar blowing for high-power-density supercapacitors. Nat. Commun., 4 (2013)
50. Polsen, E.S., McNerny, D.Q., Viswanath, B.: Pattinson, S.W., John Hart, A.: High-speed roll-to-roll manufacturing of graphene using a concentric tube CVD reactor. Sci. Rep., 5, 1–12 (2015)
51. Ye, R., James, D.K., Tour, J.M.: Laser-induced graphene. Acc. Chem. Res. **51**, 1609–1620 (2018)

Architectural and Chemical Aspects of 3D Graphene for Emerging Applications

Juan Bai and Jun Mei

Abstract As one of the versatile and intensively studied functional materials, three-dimensional (3D) graphene has shown great potential in a wide range of emerging applications, particularly in energy and environment fields. To well meet practical requirements, different 3D graphene nano architectures, such as gels, sponges, and membranes, with various structural features have been designed and synthesized, aiming to improve physical, chemical, mechanical, thermal, and biological properties. In this chapter, the design principles of different architectures of 3D graphene are first summarized. Subsequently, some chemical aspects associated with surfaces, interfaces, defects, pores, and functional groups are well analyzed to explore the cost-effective goal for a specific application. Finally, a brief summary of the current challenges is concluded to provide some useful insights on the future design of 3D graphene for emerging applications.

Keywords Graphene · Three-dimensional · Surface chemistry · Environmental · Energy

1 Introduction

Since the successful exfoliation of graphene from layered graphite, two-dimensional (2D) graphene has received unprecedented attention [1]. It is a honeycomb-like planar structure that is arranged by sp^2 hybridized carbon atoms. Due to the ultra-thin and long-range $\pi-\pi$ conjugated links, 2D graphene possesses fascinating chemical and physical properties in terms of surface area, carrier mobility, thermal conductivity, chemical stability, mechanical properties, and so on [2]. However, until now, achieving large-scale production of single-layer and defect-free high-quality 2D

J. Bai · J. Mei (✉)
School of Chemistry and Physics, Queensland University of Technology, 2 George Street, Brisbane, QLD 4000, Australia
e-mail: j2.mei@qut.edu.au

Centre for Materials Science, Queensland University of Technology, 2 George Street, Brisbane, QLD 4000, Australia

© The Author(s), under exclusive license to Springer Nature Switzerland AG 2023

R. K. Gupta (ed.), *3D Graphene*, Carbon Nanostructures,
https://doi.org/10.1007/978-3-031-36249-1_4

graphene is still challenging, which is limited by high-cost manufacturing technology and high-demanding conditions for long-term storage. Another major issue for graphene is the serious restack of 2D nanosheets at the post-processing stage, such as drying and modifications, leading to performance decay in practical applications [3].

To well address these issues, one of the effective solutions is to explore 2D graphene unit-based three-dimensional (3D) structures. The assembly of 2D graphene into a well-organized and interconnected 3D structure can not only retain the primary characteristics of 2D nanosheets, but also maintain the interconnected porous structures, endowing 3D graphene with abundant exposed surfaces, high-rate diffusion channels, and active chemical reactivity [4]. There are many types of 3D graphene that have been successfully synthesized, including hydrogel, aerogel, foam, sponge, and membrane, and some other 3D networks with a flower-like, coral-like, or honeycomb-like framework [5]. With aspect to synthetic methods of 3D graphene, the assembly step and the reduction process are generally involved in a separate or simultaneous way. For example, one of the simple and commonly used approaches is the hydrothermal reaction conducted in aqueous solutions at elevated temperatures by using graphene oxide (GO) as the starting material. Compared to relatively unstable 2D structure, the massive production and storage of 3D graphene, and the quality control are readily achieved, resulting in much wider applications, particularly in batteries, supercapacitors, electrocatalysis, sensors, solar-thermal devices, and environmental adsorption field [6, 7].

In this chapter, the design principles on different architectures of 3D graphene, such as gels, sponges, and membranes, are briefly reviewed, and then some chemical aspects associated with surfaces, interfaces, defects, pores, and functional groups are well analyzed. Subsequently, a summary on the emerging energy and environment-related applications by using 3D graphene is given. Finally, the current challenges and the possible solutions are critically analyzed, which provides some insights and ideas on future studies.

2 Typical Architectures of 3D Graphene

2.1 3D Graphene Gels

As a typical 3D structure, graphene hydrogel is composed of loose and porous network with multi-dimensional molecular, ion, or electron transport and diffusion properties, so it is widely used in electrochemical materials, catalysis, sensors, and industrial wastewater treatment fields. Generally, the preparation methods of 3D graphene hydrogel include self-assembly, mixed solution, and in situ polymerization. In 2010, Xu et al. prepared the self-assembled 3D graphene hydrogels with the assistance of a facile hydrothermal method, in which the resultant graphene hydrogel was composed of ~2.6% graphene and ~97.4% water, and a typical interconnected

3D porous framework was identified after freeze drying (Fig. 1a, b, c, d). Moreover, the 3D graphene hydrogel delivered a measured conductivity of 5×10^{-3} S cm^{-1} and good thermal stability in the temperature between 25 and 100 °C [8]. If some functionalized molecules are introduced during reduction processes, the functionalized 3D graphene hydrogels can be obtained for specific applications. For example, the chemical reduction conducted at 100° C for 12 h of GO in the presence of hydroquinone as the reducing and functionalizing molecule could produce 3D functionalized graphene hydrogels, which could be used as binder-free supercapacitor electrodes with a specific capacitance of 441 F g^{-1} at a rate of 1.0 A g^{-1} in the acidic electrolyte, much higher than that of the unfunctionalized graphene hydrogels (211 F g^{-1}) [10].

In contrast to 2D unit-based uniform films, 3D aerogel frameworks are assembled based on interconnected micro-/nano-size sheets and hierarchical pores at a wide scale ranging from micropore, mesopore, to macropore. The unique porous structure and the 2D morphology of individual graphene units contribute to high-percentage exposed surfaces of 3D aerogels. More importantly, 3D graphene aerogels possess quite low density and excellent flexibility, leading to superior mechanical stability and high bending strength. Compared to the dispersed graphene sheets, 3D graphene aerogels exhibit much higher conductivity. Besides, 3D graphene aerogels are light, even lighter than air in some cases, which is proposed as an alternative candidate to

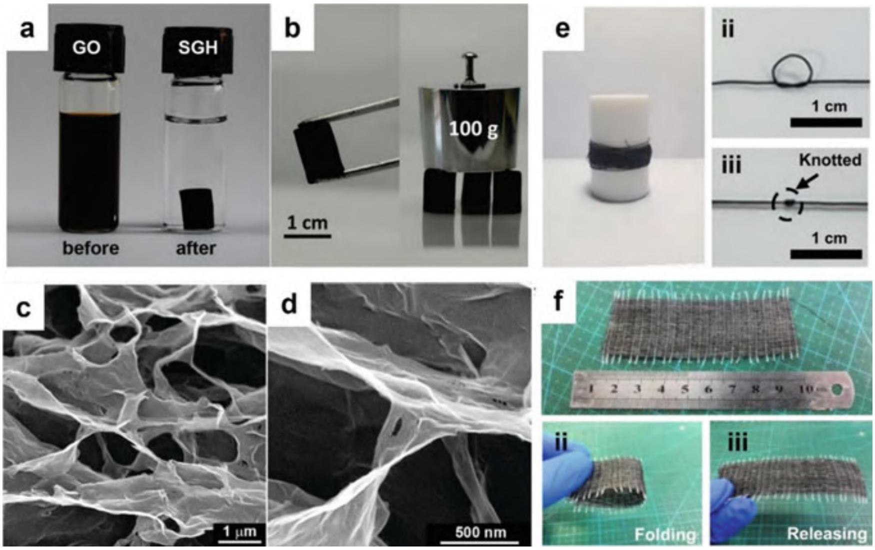

Fig. 1 **a** Photographs of a GO aqueous dispersion before and after hydrothermal reduction and **b** the resultant self-assembled graphene hydrogel (SGH), and **c**, **d** SEM images of SGH. Adapted with permission [8]. Copyright (2010) American Chemical Society. **e**, **f** Photographs of **e** knotted holey-graphene aerogel fibers (HGAFs) and **f** flexible HGAF-derived textiles. Adapted with permission [9]. Copyright (2022) Copyright The Authors, some rights reserved; exclusive licensee Springer Nature. Distributed under a Creative Commons Attribution License 4.0 (CC BY)

the relatively rare helium gas [11]. 3D graphene aerogels are generally synthesized from molecular precursors via sol–gel methods, in which the solvent is removed by freezing or supercritical drying and replaced by air. Some reported preparation methods include chemical reduction, hydrothermal reduction, and 3D printing [4]. Due to the high porosity, the low refractive index, and the high conductivity, 3D graphene aerogels have been widely used in capacitors, catalysis, photo-thermal processes, and electronic devices.

3D graphene aerogels with superhydrophobic surfaces exhibit sensitive responses to some external stimuli, such as electric, light, and thermal fields, and can be used as porous hosts to incorporate the second responsive phase. Hou et al. fabricated hygroscopic porous graphene aerogel fibers (LiCl@HGAFs) and explored their moisture capture, heat distribution, and microwave absorption properties [9]. Based on the synthetic design, the holey GO was first prepared by etching GO in H_2O_2 at 100 °C, and the LiCl@HGAFs were fabricated by wet-spinning, reducing, supercritical drying, and then LiCl-filling. Morphological characterization results indicated that the holey-graphene sheets were assembled in a long-range order and subsequently the uniform deposition of the hygroscopic LiCl was achieved with the assistance of a liquid impregnation strategy. Also, the obtained HGAFs manifested a hierarchical structure and could be knotted or woven into a textile, demonstrating excellent flexibility (Fig. 1e, f).

2.2 3D Graphene Foams/Sponges

Graphene foams are composed of a 3D macroscopic graphene and a continuous network of interconnected graphene sheets with pore sizes ranging from submicron to several microns. 3D graphene foams are advantageous in terms of high specific surface area and pore volume, good structural integrity, integrated conductive network, and superior adsorption capacity, which is suitable for energy storage, biomedicine, electronics, and environment remediations. With respect to the synthetic approaches of 3D graphene foam, the commonly used ones mainly include templates, metal ion-induced self-assembly, (electro)chemical reduction, chemical vapor deposition (CVD), and 3D printing. Chen et al. developed an effective strategy for the synthesis of 3D graphene foams by using template-directed CVD [12]. Figure 2a demonstrates a large piece of free-standing graphene foam with an area of 170×220 mm^2 that is produced by using a CVD furnace coupled with a 71-mm-in-diameter quartz tube. Unlike the structures formed from chemically derivatized small graphene sheets, the graphene foams produced by this method are integral to a 3D network (Fig. 2b), which could facilitate the fast transport of charge carriers for achieving high conductivity. Even with a low loading of ~0:5 wt% graphene foam, the resultant graphene/poly(dimethyl siloxane) composites manifested a high electrical conductivity of approximately 10 S cm^{-1} [12].

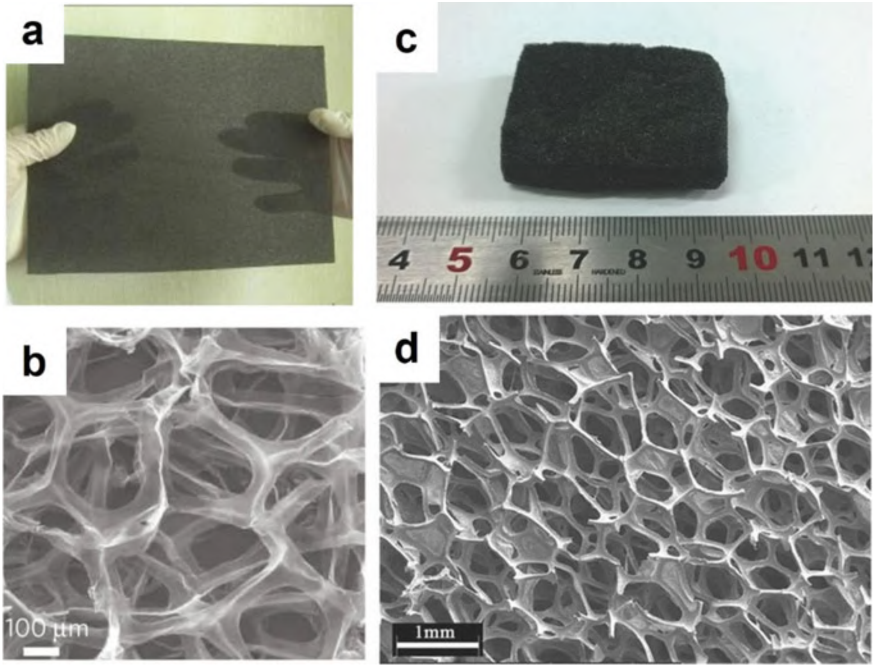

Fig. 2 **a** Photograph of a free-standing graphene foam and **b** SEM image. Adapted with permission from [12]. Copyright (2011) Springer Nature. **c** Photograph of 3D graphene network and **d** SEM images. Adapted with permission from [13]. Copyright (2015) Wiley

Graphene sponges, as expressed in their names, possess 3D sponge-like structures and similar functional characteristics, such as efficient and recyclable absorption properties. Li et al. developed a template-induced fabrication of 3D graphene sponges, in which GO nanosheets were first hydrothermally distributed on the skeleton of a commercialized sponge, followed by a heat reduction process under argon atmosphere [13]. The obtained 3D graphene sponges delivered ultra-thin graphene walls and a low density of 1.6 mg L^{-1} (Fig. 2c, d). Furthermore, to generate 3D graphene foam–silicon networks, a silica layer was grown onto the skeleton of GO sponges, which were subsequently reduced into silicon and graphene with the assistance of a magnesium thermal reaction. When employed as an anode material for Li-ion batteries, the optimal graphene–silicon networks presented a high capacity over 2050 mAh g^{-1} after 200 cycles [13].

2.3 3D Graphene Membranes

Graphene membranes are another important family of 3D graphene networks, which can be fabricated through spray coating, layer-by-layer assembly, and filter-based assembly. Shao et al. developed an integrated approach for synthesizing 3D porous graphene films by using freeze-casting and filtration assembly [14]. Figure 3a shows a typical cross-section SEM image of a 3D porous graphene film (Fig. 3b), delivering a continuous open and porous framework. Due to the presence of ice crystals during freeze, the honeycomb-like structures were finally formed, in which a wide pore size distribution ranging from nanoscales to several micrometers was identified (Fig. 3c, d). This scalable synthetic approach could be applied for the synthesis of various 3D porous films by assembling the corresponding 2D units. Recently, inspired by multilevel natural bamboo-membrane (Fig. 3e) with the unique function for rapid water and electrolyte transport, Mei et al. synthesized a multilevel graphene-based membrane consisting of 2D graphene and 2D cobalt oxide nanosheets and the resultant membrane manifested a multilevel interlayer spacing distribution and a gradient interlayer channel, which could facilitate ultrafast Li-ion transport [15]. Specifically, the inner layers are closely packed with sub-nanosized spacing for confined ion transport, and the outer layers are loosely stacked with micro-sized open channels for rapid wetting of liquid electrolytes, which is much favorable to significantly increasing volumetric capacity as free-standing electrodes for rechargeable Li-ions batteries.

3 Surface Chemistry of 3D Graphene

As known, the pristine graphene possesses a zero-bandgap, and it is also a chemically inert 2D material. To open its intrinsic bandgap and expand its application fields, a series of effective strategies, such as doping (e.g. N, P, B, and S), defects (e.g. point defects, topological defects, vacancy defects, and edge defects), pores (e.g. micropores, mesopores and macropores) and functionalization (e.g. functional groups and crosslinking), have been applied to modulate surface chemistry of 3D graphene networks.

3.1 Doping Chemistry

Doping 3D graphene with heteroatoms (Fig. 4a), such as N, B, S, and P, can significantly change the intrinsically inertness of graphene and thus induce excellent catalytic and chemical properties of 3D graphene [16]. This is mainly caused by the differences on the electronegativity and the atomic size between these introduced heteroatoms and carbon in graphene, which can break the electroneutrality and meanwhile introduce strain/stress on the graphene planes [17]. Furthermore, the integration of different heteroatoms into 3D graphene can result in desirable charge polarization and spin density, endowing 3D graphene with new physicochemical properties. For the synthesis of doped graphene, the heteroatom-containing precursors are generally required, and the doping reactions are often proceeded via a wet-chemical reaction

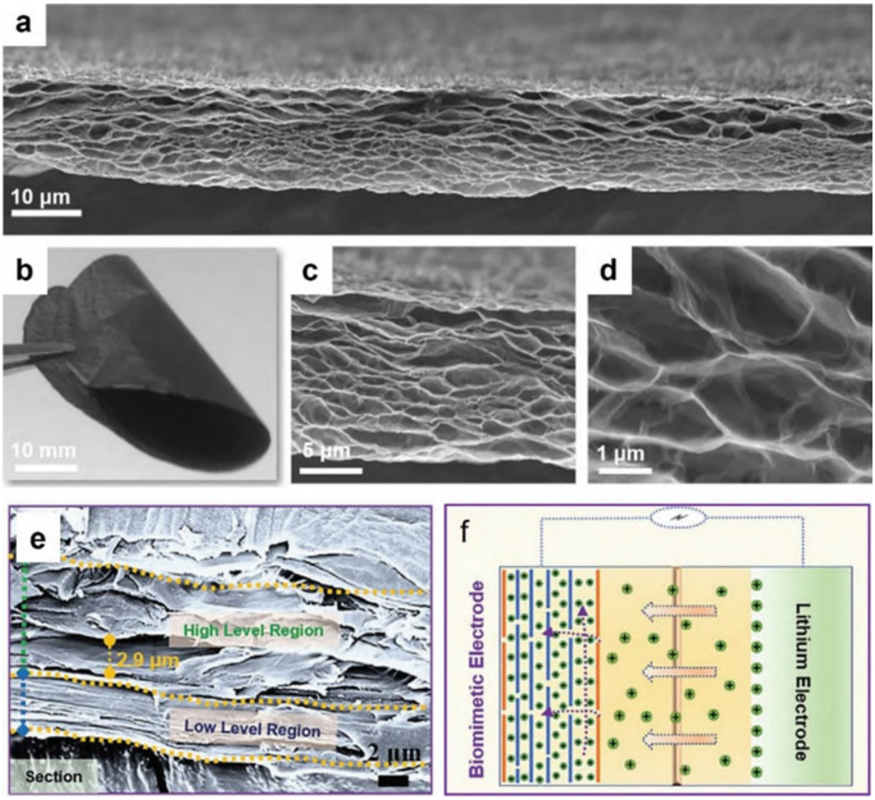

Fig. 3 **a** Cross-section SEM image of a 3D porous reduced GO film; **b** photograph of a 3D folded film, and **c**, **d** the corresponding SEM images. Adapted with permission [14]. Copyright (2016) Wiley. **e** SEM image of the natural bamboo membrane, and **f** schematic illustration of graphene-based multilevel membranes for ion transport in batteries. Adapted with permission [15]. Copyright (2021) Wiley

or a thermal impregnation technique. However, the high-concentration doping is still challenging. Mei et al. proposed a self-sacrificing strategy to achieve ultrahigh-level P-doped 3D graphene hydrogels by using 2D black phosphorus nanosheets as the precursor. As a result, the P-doping concentration in the obtained 3D graphene hydrogel reached 4.84 at%, accompanied by the formation of adjustable pore sizes in the range of 1.7−17.5 nm. Through reaction kinetic analysis on electrochemical Li-ions storage, the P-doped 3D graphene hydrogel presented a favorable capacitive-controlled characteristic, as evidenced by a high specific Li-ions storage capacity of 1,000 mA h g^{-1} after 1,700 discharging/charging cycles, outperforming the undoped 3D graphene hydrogel [19].

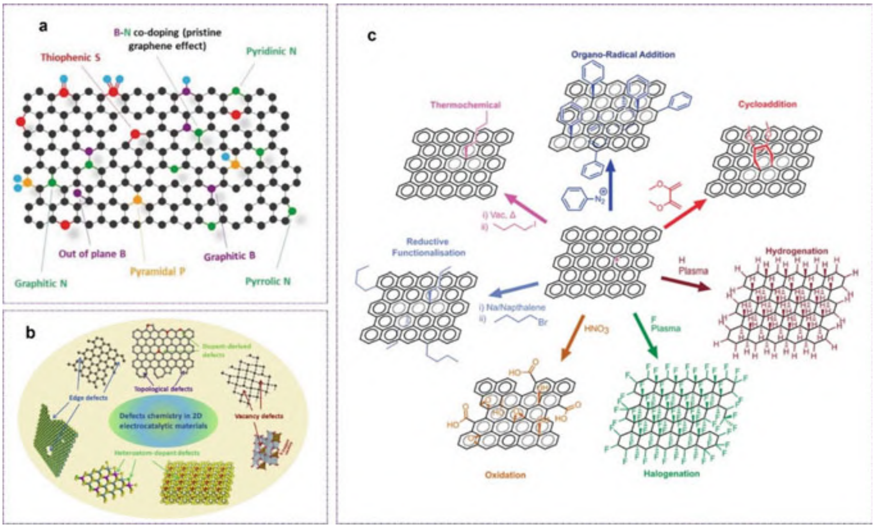

Fig. 4 **a** Schematical illustration of various doping configurations on graphene. Adapted with permission [16]. Copyright (2019) Wiley. **b** Schematical illustration of various defects on graphene. Adapted with permission [17]. Copyright (2019) Elsevier. **c** Schematical illustration of various functionalization reactions on graphene. Adapted with permission [18]. Copyright (2020) Royal Society of Chemistry

3.2 Defect Chemistry

Defective 3D graphene networks have been intensively studied for energy conversion and storage applications, which is primarily due to their active reactivities at defective sites and the optimal electronic structures. There are various levels of defects in nanomaterials, including point-level, line-level, plane-level, and volume-level defects. Based on specific locations and compositions, point-level defects can be further classified into heteroatom dopants, vacancies, interstitial atoms, and impurities [20]. The inherent defects of 3D graphene networks mainly include edge and lattice/topological defects (Fig. 4b), which usually originates from the assembly and/or the reduction process of 3D graphene. If the reduction of GO networks is employed to produce 3D graphene networks, the defect levels are largely associated with the GO precursors and the reducing agents. Generally, more oxygen-containing groups in the GO precursors may induce more defects in the reduced 3D graphene networks. It should be noteworthy that defects are not always static, which may further migrate upon reduction. At present, different effective methods have been developed for generating various defects on the surfaces of graphene, mainly including thermal annealing, particle irradiation, and chemical treatment, and these defects act as crucial roles in some applications such as catalysis [21]. For example, it was concluded that electrocatalytic performance is highly related to the edge sites of 3D graphene networks. 3D graphene with high-density edge sites could efficiently catalyze H_2 evolution, as verified by a low onset potential of ~18 mV and a Tafel slope of ~64 mV dec^{-1} [22].

3.3 Pore Chemistry

As mentioned above, one obvious feature of 3D graphene networks is porosity, so the modulation on the pore chemistry is significant for adapting the practical applications. For example, 3D hierarchical and macro-porous graphene foam assembled from graphene mesh with in-plane nanopores presented a hierarchical pore arrangement, which is much more favorable for mass transport and edge exposure for developing functional materials for energy applications [23]. After further doping with N, the resultant 3D graphene delivered a uniform pore size of 2–50 nm, a specific surface area of 362 $m^2\ g^{-1}$, a high nanohole density of ~5.0×10^9 holes per cm^2, a high porosity of ~99.79%, and an interpore distance up to ~100 nm [23]. Choi et al. prepared a 3D macro-porous graphene structure with the assistance of polystyrene colloidal particles as the sacrificial template [24]. This porous 3D graphene with a surface area of 194.20 $m^2\ g^{-1}$ and an electrical conductivity of 1204 S m^{-1} could facilitate rapid ion transport for energy storage devices and it could be a suitable candidate as for hosting metal oxides that are active for electrochemical reactions, such as the widely used MnO_2 in supercapacitors, to enhance electrochemical performance [24].

3.4 Functionalization

Generally, the functionalization strategy of graphene can be achieved through a covalent or noncovalent bonding reaction. Due to the stronger chemical bonding capability for robust interfaces, covalent modification on graphene is a widely used approach. The covalent functionalization motivations of graphene are largely dependent on the existing chemistry, particularly at these defect or edge sites (Fig. 4c). In the synthesis of 3D graphene networks, GO is often used as the starting material. GO surfaces contain many oxygen-containing groups, such as hydroxyl, carboxyl, carbonyl, and epoxy, leading to a serious conductivity decay. Hence, the reduction is highly required for partial or complete removal of oxygen species on graphene surfaces. Currently, the reduction methods used during the synthesis of 3d graphene mainly include high-temperature treatment, chemical reduction, electrochemical reduction, hydrothermal or solvothermal reduction, and photon-induced reduction. In most cases, after reduction under thermal or (electro)chemical treatment, most of the unstable oxygen species are removed, leaving a small amount of O−H, C−O, and C=O on the surfaces. This existing oxygen chemistry environment is crucial for the further covalent functionalization of 3D graphene and offers many new possibilities for structural modifications. Besides, if highly reactive species are introduced with the assistance of plasmas (e.g. H, F, and Cl), the π-bonded network on the basal plane of graphene will be directly destroyed and meanwhile the functionalization of reactive species on graphene is achieved [18].

Another intensively studied and versatile functionalization approach for 3D graphene is to design graphene-based composites. Depending on the synergistic effects in graphene-based composites, the functionalization of 3D graphene by the combination with other counterpart materials is a powerful approach. Specifically, this strategy can make use of the advantages of graphene and overcome the intrinsic weakness of graphene by coupling with these materials with complementary structures and/or functions [25]. Moreover, the rational integration of graphene and other functional materials could bring about some new physicochemical properties, such as increasing catalytic sites and improving reaction kinetics for electrocatalysis via the functionalization of 3D graphene with the incorporation of highly reactive metal sites. For example, the advantages of the combination of 3D graphene and noble-metal nanoparticles for catalysis can be summarized as follows: (i) an integrated conductive framework can be formed; (ii) the serious agglomeration of nano-sized graphene sheets can be overcome; (iii) the dispersion degree of metal nanoparticles can be increased as exposed active sites; (iv) the strong metal–carbon coupling may exist for robust interfaces; (v) the consumption of expensive noble metals can be reduced; (vi) the structural stability and durability can be improved to accommodate the practical conditions; (vii) the reaction mechanisms may be rationally modulated for favorable kinetics and increased activities; (viii) the operation process and the manufacture technology is promising for large-scale applications.

4 3D Graphene for Emerging Applications

3D graphene networks have been widely applied in various fields across physics, chemistry, biology, nanotechnology, and engineering [26, 27]. In this part, as summarized in Fig. 5, we mainly focus on the emerging energy and environment-associated applications of 3D graphene, such as batteries, capacitors, solar cells, electrocatalysis, sensors, and environmental adsorption.

4.1 Energy Storage

Owing to the ever-increasing demands for portable electronics and electric vehicles in our daily life, the innovation of energy storage devices with high power density and high energy density, such as batteries and capacitors, is becoming urgent. Currently, one major concern for achieving performance enhancement is highly associated with electrode materials. For example, as one of the important energy storage devices, supercapacitors possess high capacity, high rate, and long cycle life, however, the cost-effective electrode materials are still lacking. Graphene

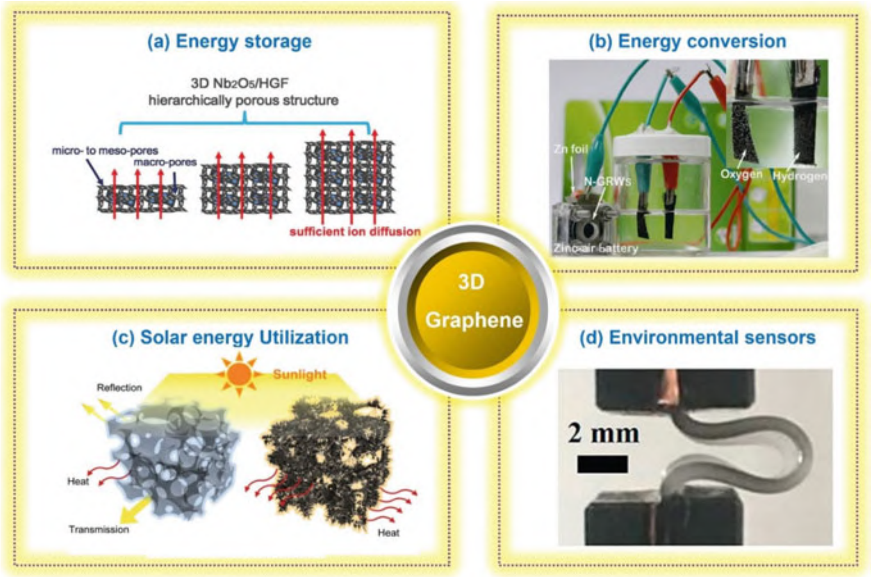

Fig. 5 Summary of emerging energy and environment-related applications of 3D graphene. **a** Adapted with permission [28]. Copyright (2017) American Association for the Advancement of Science. **b** Adapted with permission [29]. Copyright (2016) Copyright The Authors, some rights reserved; exclusive licensee Springer Nature. Distributed under a Creative Commons Attribution License 4.0 (CC BY). **c** Adapted with permission [30]. Copyright (2017) Wiley. **d** Adapted with permission [31]. Copyright (2018) Wiley

has been regarded as one of the potential electrode materials for supercapacitors, and 3D graphene networks could maximize the exposed active area and accelerate electrons/ions transfer, resulting in superior electrochemical performance [24]. To date. different types of 3D graphene networks have been designed and synthesized for high-performance energy storage devices. Wang et al. proposed a 3D graphene bubble network, which was fabricated by using a sugar-blowing approach, and this network was composed of continuous graphitic membranes tightly scaffolded by graphitic struts. Such intimate topological configuration is beneficial to increasing power and energy densities for electrochemical capacitors [32].

Besides, 3D graphene networks and their derived composite electrodes have been intensively used in rechargeable batteries, such as anodes in Li/Na/K-ion batteries and cathodes in metal-air/sulfur batteries [33, 34]. In 2017, a 3D holey-graphene/niobia (Nb_2O_5) composite was reported for high-rate energy storage at a mass loading above 10 mg cm^{-2}. Within the designed composite electrode, the interconnected graphene network facilitates electron transport while the hierarchical porous framework favors ion transport. As a result, the optimal electrode presented a capacity of 139 mAh g^{-1} with a high loading of 11 mg cm^{-2}, and a stable cycle life with 90% capacity retention after 10,000 cycles at a rate of 10C [28].

4.2 Energy Conversion

As one of the essential reactions for energy conversion, electrocatalysis aims to converting renewable resources (e.g. CO_2 or biomass), to valuable chemicals, fuels, and electrical energy with the assistance of highly active catalyst materials [35]. An ideal electrocatalyst should possess high conductivity, abundant active sites, good mass transfer capability, suitable structural stability and durability, and earth abundant. Except for the structural merits of 3D graphene associated with surface area and porous framework, the modulation of surface chemistry is crucial for electrocatalysis. To increase the reactivity of graphene units, doping, defects, and functionalization are often adopted for 3D graphene for tuning electronic structures and optimizing reaction pathways, and thus improving catalytic activities. 3D graphene networks have been explored for various electrocatalytic reactions, such as oxygen evolution reaction (OER), oxygen reduction reaction (ORR), hydrogen evolution reaction (HER), and carbon dioxide reduction reaction (CO_2RR) [36]. For example, Yang et al. synthesized N-doped graphene nanoribbons with interconnected 3D architectures, exhibiting excellent electrocatalytic activity for both ORR and OER. It was revealed that the ORR activity originated from the electron-donating quaternary N sites and the OER activity was determined by the electron-withdrawing pyridinic N moieties. When used as rechargeable Zn-air batteries in a two-electrode configuration, an open-circuit voltage of 1.46 V, a specific capacity of 873 mAh g^{-1}, and a peak power density of 65 mW cm^{-2}, and a stable cycle over 150 cycles at a rate of 2 mA cm^{-2} [29].

Graphene materials are also used as a promising substitution for noble-metal electrodes in fuel cells. For ORR occurred at cathodes in fuel cells, the dominant catalysts are Pt-based metals, however, the limited reservation and high price of Pt metal inhibited their practical applications. Perfect graphene is chemically inert toward ORR, so structural modifications are required for graphene materials. Heteroatom-doped 3D graphene has been evidenced as one of the promising metal-free catalysts with high electrochemical activities. Foreign atoms, such as N, P, B, and S, can change the distribution states of local electrons within graphene lattices and enhance reaction kinetics. Among them, N-doped graphene catalysts are commonly studied for ORR, which is largely due to the favorable charge redistribution and the decreased energy barrier for ORR [37].

4.3 Solar Energy Utilization

3D graphene networks deliver a wide range of light absorption properties and tuneable thermal conductivity, endowing them promising for photovoltaic solar cells and solar-thermal energy conversion systems. Solar-thermal energy conversion is a continuous process for solar energy harvest by collecting the steam generated by the heat of localized sunlight. 3D graphene has good light absorption effect, low thermal conductivity and excellent wettability, and efficient light-to-heat conversion rate [30, 38]. It should be noteworthy that the hierarchical pores in 3D graphene networks are significant for steam generation. Specifically, the small pores can promote the high light absorption while the micropores can induce the capillary effect of water [5]. Ren et al. reported a hierarchical porous graphene foam, in which graphene arrays were grown on 3D foam skeleton by using plasma-enhanced chemical vapor deposition, manifested attractive broadband and omnidirectional absorption capability, resulting in a solar-thermal energy conversion efficiency of ~93.4% when utilized as a heating material [30].

4.4 Environmental Sensors and Remediation

Sensors are a large family of functional devices that demonstrate the immediate response to environmental varieties, such as temperature, humidity, pressure, and chemicals, which can be easily found in industrials and residential communities. 3D graphene materials have been widely used in various sensors, including strain sensors, gas sensors, and (electro)chemical sensors [31, 39]. Particularly, gas sensors are mainly used to detect low-concentration gases (e.g. O_2, CO_x, NO_x, Cl_2, SO_2, H_2S, NH_3, and CH_4) and volatile organic compounds (e.g. acetone, alcohol, aromatics, and hydrazine) [40]. Based on the adsorption mechanism, the target gas can be adsorbed onto 3D graphene skeletons with the assistance of interaction drivers such as van der Waals force or covalent bonding, and then the gas concentration can be reflected by the conductance changes of 3D graphene. For example, Wu et al. designed a NO_2 gas sensor based on 3D graphene flowers grown on a Ni foam skeleton, which presented a high sensitivity of 133.2 ppm^{-1}, a high response of 1411% to 10 ppm, a low theoretical detection limit of 785 ppt, and an ultrafast signal recovery of 2 s [41].

3D porous graphene networks can be also employed in environment remediation fields in terms of pollutant control and toxicant adsorption. 3D graphene materials have been investigated for the effective adsorption of various pollutants, such as harmful gas (e.g. SO_2, H_2S, and CO_2) and impurities in solutions (e.g. dyes, oils, organic solvents, and heavy metals) [42–44]. Generally, the adsorption capability of 3D graphene networks for environmental purification is closely associated with surface area, pore size and distribution density, and surface chemistry. A high surface area with high porosity is essential for achieving efficient adsorption of 3D graphene for most adsorbates, however, the adsorbed types depend on surface chemistry. A hydrophobic surface facilitates the adsorption of organic compounds, and the adsorption in aqueous solutions depends on the interaction between adsorbates and adsorbents, including electrostatic force, hydrogen bonding, and $\pi-\pi$ bonding.

5 Summary

In this chapter, some typical architectures of 3D graphene networks, such as gels, foams, sponges, and membranes, are briefly discussed. However, one of the major challenges is the large-scale production of 3D graphene materials. There are many factors, including concentrations, temperatures, reaction time, reactors, and costs, which require to be considered. Also, there is a large gap between laboratory synthesis and industrial massive production, in which the accurately control on the interconnected porous structures at a large scale is more difficult. Therefore, it is still essential to design and develop new synthetic methods for 3D graphene networks. Surface chemistry acts as a crucial role for structural modifications on 3D graphene. By adjusting surface chemistry, 3D graphene networks have been widely used in the emerging energy storage and conversion and environmental remediation fields. Further understanding and modulating surface chemistry on 3D graphene networks can bring about some customed properties to well meet the practical requirements and can intrigue more new applications. The regulation on the macroscopic morphology, the specific surface area, the pore distribution, the surface wettability state, the electronic structures, the thermal conductivity, the mechanical flexibility, and the electrical conductivity, have been investigated for 3D graphene networks. To further improve the performance of 3D graphene and to widen the application scope, a variety of 3D graphene-based composites have been fabricated by coupling with the structure- or function-complementary counterparts. It is expected that these research outputs on the synthesis and the optimization strategies of 3D graphene by controlling surface chemistry can offer some scientific evidence for constructing 3D graphene-based devices for addressing the current energy and environmental issues.

References

1. Hernandez, Y., Nicolosi, V., Lotya, M., Blighe, F.M., Sun, Z., De, S., McGovern, I.T., Holland, B., Byrne, M., Gun'Ko, Y.K.: High-yield production of graphene by liquid-phase exfoliation of graphite. Nat. Nanotechnol. **3**(9), 563–568 (2008)
2. Lee, C., Wei, X., Kysar, J.W., Hone, J.: Measurement of the elastic properties and intrinsic strength of monolayer graphene. Science **321**(5887), 385–388 (2008)
3. Li, D., Müller, M.B., Gilje, S., Kaner, R.B., Wallace, G.G.: Processable aqueous dispersions of graphene nanosheets. Nat. Nanotechnol. **3**(2), 101–105 (2008)
4. Zhu, C., Han, T., Duoss, E.B., Golobic, A.M., Kuntz, J.D., Spadaccini, C.M., Worsley, M.A.: Highly compressible 3D periodic graphene aerogel microlattices. Nat. Commun. **6**, 6962 (2015)
5. Sun, Z., Fang, S., Hu, Y.H.: 3D graphene materials: from understanding to design and synthesis control. Chem. Rev. **120**(18), 10336–10453 (2020)
6. Yousefi, N., Lu, X., Elimelech, M., Tufenkji, N.: Environmental performance of graphene-based 3D macrostructures. Nat. Nanotechnol. **14**(2), 107–119 (2019)
7. Xu, X., Zhang, Q., Yu, Y., Chen, W., Hu, H., Li, H.: Naturally dried graphene aerogels with superelasticity and tunable Poisson's ratio. Adv. Mater. **28**(41), 9223–9230 (2016)
8. Xu, Y., Sheng, K., Li, C., Shi, G.: Self-assembled graphene hydrogel via a one-step hydrothermal process. ACS Nano **4**(7), 4324–4330 (2010)

9. Hou, Y., Sheng, Z., Fu, C., Kong, J., Zhang, X.: Hygroscopic holey graphene aerogel fibers enable highly efficient moisture capture, heat allocation and microwave absorption. Nat. Commun. **13**, 1227 (2022)
10. Xu, Y., Lin, Z., Huang, X., Wang, Y., Huang, Y., Duan, X.: Functionalized graphene hydrogel-based high-performance supercapacitors. Adv. Mater. **25**(40), 5779–5784 (2013)
11. Gorgolis, G., Galiotis, C.: Graphene aerogels: a review. 2D Materials **4**(3), 032001 (2017)
12. Chen, Z., Ren, W., Gao, L., Liu, B., Pei, S., Cheng, H.-M.: Three-dimensional flexible and conductive interconnected graphene networks grown by chemical vapour deposition. Nat. Mater. **10**(6), 424–428 (2011)
13. Li, B., Yang, S., Li, S., Wang, B., Liu, J.: From commercial sponge toward 3D graphene–silicon networks for superior lithium storage. Adv. Energy Mater. **5**(15), 1500289 (2015)
14. Shao, Y., El-, M.F., Lin, C.W., Zhu, G., Marsh, K.L., Hwang, J.Y., Zhang, Q., Li, Y., Wang, H., Kaner, R.B.: 3D freeze-casting of cellular graphene films for ultrahigh-power-density supercapacitors. Adv. Mater. **28**(31), 6719–6726 (2016)
15. Mei, J., Peng, X., Zhang, Q., Zhang, X., Liao, T., Mitic, V., Sun, Z.: Bamboo-membrane inspired multilevel ultrafast interlayer ion transport for superior volumetric energy storage. Adv. Func. Mater. **31**(31), 2100299 (2021)
16. Ullah, S., Hasan, M., Ta, H.Q., Zhao, L., Shi, Q., Fu, L., Choi, J., Yang, R., Liu, Z., Rümmeli, M.H.: Synthesis of doped porous 3D graphene structures by chemical vapor deposition and its applications. Adv. Func. Mater. **29**(48), 1904457 (2019)
17. Sun, T., Zhang, G., Xu, D., Lian, X., Li, H., Chen, W., Su, C.: Defect chemistry in 2D materials for electrocatalysis. Materials Today Energy **12**, 215–238 (2019)
18. Clancy, A.J., Au, H., Rubio, N., Coulter, G.O., Shaffer, M.S.: Understanding and controlling the covalent functionalisation of graphene. Dalton Trans. **49**(30), 10308–10318 (2020)
19. Mei, J., He, T., Zhang, Q., Liao, T., Du, A., Ayoko, G.A., Sun, Z.: Carbon–phosphorus bonds-enriched 3D graphene by self-sacrificing black phosphorus nanosheets for elevating capacitive lithium storage. ACS Appl. Mater. Interfaces. **12**(19), 21720–21729 (2020)
20. Yan, D., Li, Y., Huo, J., Chen, R., Dai, L., Wang, S.: Defect chemistry of nonprecious-metal electrocatalysts for oxygen reactions. Adv. Mater. **29**(48), 1606459 (2017)
21. Liu, L., Qing, M., Wang, Y., Chen, S.: Defects in graphene: generation, healing, and their effects on the properties of graphene: a review. J. Mater. Sci. Technol. **31**(6), 599–606 (2015)
22. Wang, H., Li, X.B., Gao, L., Wu, H.L., Yang, J., Cai, L., Ma, T.B., Tung, C.H., Wu, L.Z., Yu, G.: Three-dimensional graphene networks with abundant sharp edge sites for efficient electrocatalytic hydrogen evolution. Angew. Chem. **130**(1), 198–203 (2018)
23. Zhao, Y., Hu, C., Song, L., Wang, L., Shi, G., Dai, L., Qu, L.: Functional graphene nanomesh foam. Energy Environ. Sci. **7**(6), 1913–1918 (2014)
24. Choi, B.G., Yang, M., Hong, W.H., Choi, J.W., Huh, Y.S.: 3D macroporous graphene frameworks for supercapacitors with high energy and power densities. ACS Nano **6**(5), 4020–4028 (2012)
25. Wang, M., Duan, X., Xu, Y., Duan, X.: Functional three-dimensional graphene/polymer composites. ACS Nano **10**(8), 7231–7247 (2016)
26. El-, M.F., Shao, Y., Kaner, R.B.: Graphene for batteries, supercapacitors and beyond. Nat. Rev. Mater. **1**(7), 1–14 (2016)
27. Bonaccorso, F., Colombo, L., Yu, G., Stoller, M., Tozzini, V., Ferrari, A.C., Ruoff, R.S., Pellegrini, V.: Graphene, related two-dimensional crystals, and hybrid systems for energy conversion and storage. Science **347**(6217), 1246501 (2015)
28. Sun, H., Mei, L., Liang, J., Zhao, Z., Lee, C., Fei, H., Ding, M., Lau, J., Li, M., Wang, C.: Three-dimensional holey-graphene/niobia composite architectures for ultrahigh-rate energy storage. Science **356**(6338), 599–604 (2017)
29. Yang, H.B., Miao, J., Hung, S.-F., Chen, J., Tao, H.B., Wang, X., Zhang, L., Chen, R., Gao, J., Chen, H.M.: Identification of catalytic sites for oxygen reduction and oxygen evolution in N-doped graphene materials: Development of highly efficient metal-free bifunctional electrocatalyst. Sci. Adv. **2**(4), e1501122 (2016)

30. Ren, H., Tang, M., Guan, B., Wang, K., Yang, J., Wang, F., Wang, M., Shan, J., Chen, Z., Wei, D.: Hierarchical graphene foam for efficient omnidirectional solar–thermal energy conversion. Adv. Mater. **29**(38), 1702590 (2017)
31. Pan, F., Chen, S.M., Li, Y., Tao, Z., Ye, J., Ni, K., Yu, H., Xiang, B., Ren, Y., Qin, F.: 3D graphene films enable simultaneously high sensitivity and large stretchability for strain sensors. Adv. Func. Mater. **28**(40), 1803221 (2018)
32. Wang, X., Zhang, Y., Zhi, C., Wang, X., Tang, D., Xu, Y., Weng, Q., Jiang, X., Mitome, M., Golberg, D.: Three-dimensional strutted graphene grown by substrate-free sugar blowing for high-power-density supercapacitors. Nat. Commun. **4**, 2905 (2013)
33. Wang, Z., Gao, H., Zhang, Q., Liu, Y., Chen, J., Guo, Z.: Recent advances in 3D graphene architectures and their composites for energy storage applications. Small **15**(3), 1803858 (2019)
34. Mei, J., Zhang, Y., Liao, T., Peng, X., Ayoko, G.A., Sun, Z.: Black phosphorus nanosheets promoted 2D-TiO_2-2D heterostructured anode for high-performance lithium storage. Energy Storage Materials **19**, 424–431 (2019)
35. Mistry, H., Varela, A.S., Kühl, S., Strasser, P., Cuenya, B.R.: Nanostructured electrocatalysts with tunable activity and selectivity. Nat. Rev. Mater. **1**, 16009 (2016)
36. Cui, H., Guo, Y., Zhou, Z.: Three-dimensional graphene-based macrostructures for electrocatalysis. Small **17**(22), 2005255 (2021)
37. Wu, Z.-S., Yang, S., Sun, Y., Parvez, K., Feng, X., Müllen, K.: 3D nitrogen-doped graphene aerogel-supported Fe_3O_4 nanoparticles as efficient electrocatalysts for the oxygen reduction reaction. J. Am. Chem. Soc. **134**(22), 9082–9085 (2012)
38. Ito, Y., Tanabe, Y., Han, J., Fujita, T., Tanigaki, K., Chen, M.: Multifunctional porous graphene for high-efficiency steam generation by heat localization. Adv. Mater. **27**(29), 4302–4307 (2015)
39. Wu, S., He, Q., Tan, C., Wang, Y., Zhang, H.: Graphene-based electrochemical sensors. Small **9**(8), 1160–1172 (2013)
40. Wang, T., Huang, D., Yang, Z., Xu, S., He, G., Li, X., Hu, N., Yin, G., He, D., Zhang, L.: A review on graphene-based gas/vapor sensors with unique properties and potential applications. Nano-Micro Letters **8**(2), 95–119 (2016)
41. Wu, J., Feng, S., Wei, X., Shen, J., Lu, W., Shi, H., Tao, K., Lu, S., Sun, T., Yu, L.: Facile synthesis of 3D graphene flowers for ultrasensitive and highly reversible gas sensing. Adv. Func. Mater. **26**(41), 7462–7469 (2016)
42. Wu, Y., Yi, N., Huang, L., Zhang, T., Fang, S., Chang, H., Li, N., Oh, J., Lee, J.A., Kozlov, M.: Three-dimensionally bonded spongy graphene material with super compressive elasticity and near-zero Poisson's ratio. Nat. Commun. **6**, 6141 (2015)
43. He, K., Chen, G., Zeng, G., Chen, A., Huang, Z., Shi, J., Huang, T., Peng, M., Hu, L.: Three-dimensional graphene supported catalysts for organic dyes degradation. Appl. Catal. B **228**, 19–28 (2018)
44. Shi, L., Chen, K., Du, R., Bachmatiuk, A., Rümmeli, M.H., Xie, K., Huang, Y., Zhang, Y., Liu, Z.: Scalable seashell-based chemical vapor deposition growth of three-dimensional graphene foams for oil–water separation. J. Am. Chem. Soc. **138**(20), 6360–6363 (2016)

Recent Advancements in 3D Graphene for Electrochemical Sensors

Hamide Ehtesabi and Seyed-Omid Kalji

Abstract Graphene, a new class of carbon nanostructures, has recently garnered much attention and is a quickly growing field. It exhibits a wide range of features, including thermal conductivity, charge carrier mobility, electrical and mechanical characteristics, magnetism, and more. These characteristics, along with a large surface area, are essential in electrochemical, optoelectronic, and medicinal applications. However, some features have restricted its applicability, including poor light absorption, low capacitance, ease of stacking and agglomeration in a solvent, and its zero-gap semi-metal nature. In response to these limitations, there has been a rising effort to alter the graphene surface and create three-dimensional (3D) graphene arrangements to broaden its applicability in various industries. Due to their high efficiency, simple operation, as well as modularity in chemical, physical, and biological features, electrochemical sensors have developed over time. With outstanding qualities, such as a high surface area, abundant pores, and free binder, 3D graphene with a porous structure is a suitable electrode for electrochemical sensors. The most current developments in 3D graphene-based electrochemical sensing for various analytes are covered in this chapter.

Keywords Graphene Oxide · Three-dimensional · Electrode · Sensing · Detection · Nanoparticle

1 Introduction

Graphene is a two-dimensional (2D) layer of carbon atoms with a lattice of hexagonal structures. Owing to its high surface area, remarkable electrical conductivity, and appropriate charge carrier mobility, graphene is widely used in various applications,

---

H. Ehtesabi (✉)
Faculty of Life Sciences and Biotechnology, Shahid Beheshti University, Tehran, Iran
e-mail: h_ehtesabi@sbu.ac.ir

S.-O. Kalji
Faculty of Biological Sciences, Tarbiat Modares University, Tehran, Iran

© The Author(s), under exclusive license to Springer Nature Switzerland AG 2023

R. K. Gupta (ed.), *3D Graphene*, Carbon Nanostructures,
https://doi.org/10.1007/978-3-031-36249-1_5

including sensors, supercapacitors, catalysis, bio-fuel cells, and chromatography analysis [1–3]. Despite high structural stability, via the π–π interactions and strong Van der Waals forces, the 2D plane of graphene sheets can stack together irreversibly and create graphitic form. Graphene loses its particular properties after these stacking interactions. Preparing a 3D graphene structure prevents the stacking and agglomeration of 2D nanosheets. Currently, 3D graphene constructions come in various forms, including hydrogel, aerogel, foam, sponge, and others [4, 5]. These 3D materials have an ordered and interconnected framework, and they have the distinct advantages of a greater surface area, abundant pores, and a free binder. Therefore, 3D graphene could be promising material in various problematic applications [6, 7]. Because of its advanced surface area and electron transport capacity, 3D graphene shows a specific ability as an electrode material. Its porous structure is also applicable as a supporting substrate for various materials, catalysts, and enzymes for the designation and fabrication of desired systems such as electrochemical sensors [8]. However, these new 3D graphene-based sensors suffer from low selectivity, sensitivity, repeatability, and a slow dynamic response against the analyte changes. Accordingly, searching for a novel approach to achieving proportional 3D graphene-based nanocomposites and hybrids is required to overcome the sensing and detection limitations of electrochemical sensors and improve their robustness and reusability [1].

Herein, we review the latest advancements in 3D graphene-based electrochemical sensors. First, a basic explanation of 3D graphene and the processes used for its fabrication is given. The electrochemical sensing of numerous analytes, including heavy metals, pesticides, phenolic compounds, drugs, chiral materials, dopamine, glucose, free radicals, ions, and hydrogen peroxide (H_2O_2), is then presented using 3D graphene. The chapter concludes with a consideration of current issues and prospects.

2 Definition of 3D Graphene Materials

3D graphene materials currently do not have a clear definition. The goal of developing 3D graphene frameworks is to achieve a stable graphene material with high performance through a 3D organization of layers instead of graphite-like ordering, which dramatically reduces the surface area and other unique features of graphene. Because of this, it is obvious that non-graphite 3D structured graphene materials are named 3D graphene materials. Fewer than ten layers of graphene should form the walls of a 3D graphene material while maintaining the fundamental properties of graphene materials. Figure 1 illustrates the connections of graphite, graphene, 2D and 3D graphene materials [9].

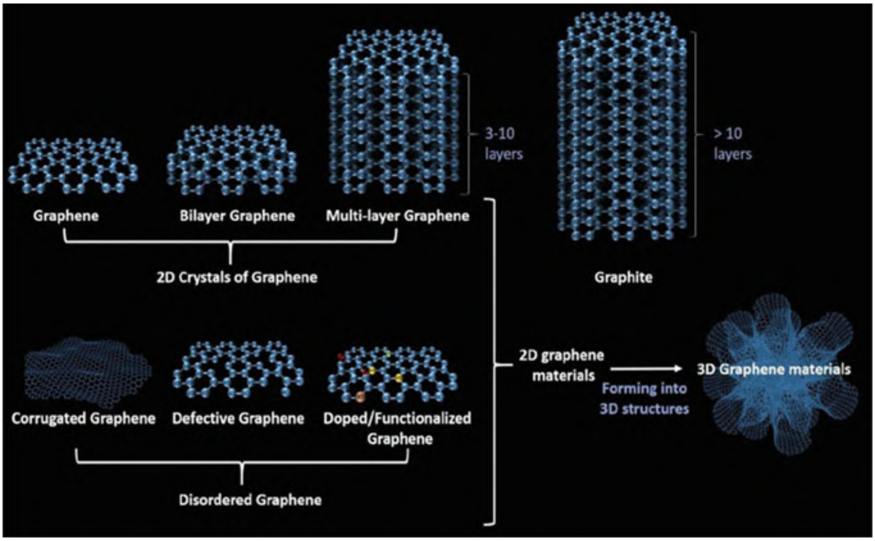

Fig. 1 Diagram showing the connections between graphite, 2D and 3D graphene, and graphene materials. Adapted with permission [9]. Copyright (2020) Copyright The Authors, some rights reserved; exclusive licensee American Chemical Society. Distributed under a Creative Commons Attribution License 4.0 (CC BY)

3 Synthesis Methods of 3D Graphene

In recent years, numerous techniques for creating 3D graphene have been done in order to give it different morphologies, structures, and characteristics. The key methods that have been developed are the hydro/solvothermal approach, chemical vapor deposition (CVD), template-assisted assembly, chemical reduction self-assembly, 3D printing, etc., [10–13]. These techniques can generally be split into template free and template-based methods (Fig. 2). While the template-based approach can precisely regulate the production of a desired pore size, shape, and density, the template free approach offers the benefits of self-assembly but cannot manage the pore structure. The dependent (hydrogel, aerogel) and independent (foam, sponge) 3D graphene on the substrate can be produced using a single preparation process or a mixture of several procedures to fulfill various needs [1].

4 Electrochemical Sensing of Different Analytes

Because different compounds can be oxidized or reduced at various potentials, electrochemical detection is very sensitive to electroactive compounds and enables detection selectivity. Because of their high surface renewable potential, low residual current, and broad potential window, carbon materials (such as graphene, graphite,

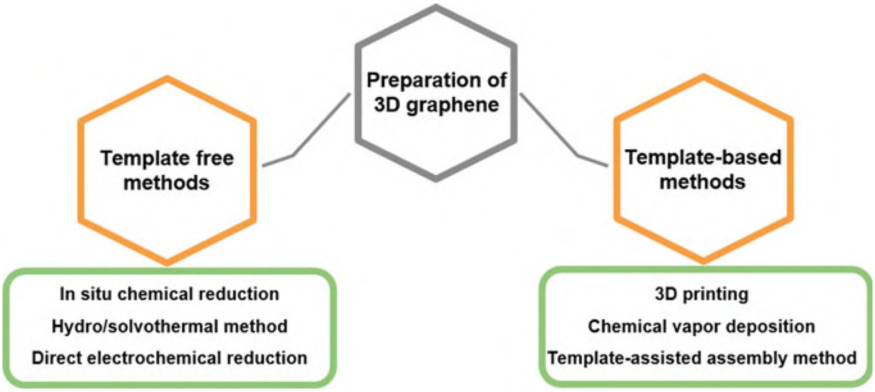

Fig. 2 Synthesis methods of 3D graphene materials. Adapted with permission [1]. Copyright (2020) Elsevier

carbon nanotube (CNT), and fullerene) are frequently utilized in electrochemistry. Electron transfer from multiple active sites to biospecies is provided by the overpotential for O_2 reduction and H_2 density of the edge-plane defect site on them [14, 15]. The use of 2D and 3D graphene and their composites as sensing materials for the electrochemical monitoring of various analytes is widespread. In contrast to a flat graphene film, 2D porous graphene has a higher surface area and additional exposed active sites because of its distinctive structural design. Due to the extra channels, it has improved electrochemical performance in terms of ion and mass transport (e.g., sensing, energy storage, catalytic ability, etc.). A 3D graphene has a similar distinctive structure of constantly interconnected networks, with a sizable accessible surface area and a significant pore volume. Additionally, it improves mechanical strength, flexibility, and stability [16]. In this section, a few illustrative examples of 3D graphene-based electrochemical sensing are presented.

4.1 Heavy Metal

It is crucial to create rapid, sensitive, and precise methods for identifying toxic heavy metal ions because they pose a serious threat to human life and the environment. Owing to its great sensitivity, outstanding selectivity, simplicity, low-cost, and good portability, electrochemical detection has become one of the most popular techniques. In one study, pyrrole (Py) was added to 3D graphene aerogels to control their structures and properties. These aerogels were then used as electrode materials to study the unique function of Py for sensing metal ions. Py can act as a reductant and a regulator to change the composition and structure of graphene aerogels, significantly affecting their electrochemical performance for sensing cadmium (Cd^{2+}). Py also functions as a nitrogen source to provide active metal ion binding sites. The effectiveness of Py is greatly influenced by the reaction ratio between Py and graphene oxide (GO). The 3D-GO-Py modified electrode can successfully determine Cd^{2+} in aqueous solutions using the square wave anodic stripping voltammetry method [17].

4.2 *Pesticide*

Many crops and vegetables are protected against pests by applying organophosphate pesticides (OPs) [18]. OPs, however, have several detrimental consequences on humans and animals due to their excessive use. Therefore, it is critical to make a rapid, precise, sensitive, and trustworthy analytical approach for OPs detection [19]. Due to their straightforward preparation processes, high sensitivity, and excellent selectivity, acetylcholinesterase (AChE)-based electrochemical biosensors have recently become recognized as viable alternatives to traditional approaches for pesticide residues. Enzymatic-based biosensors, however, have certain drawbacks that limit their uses, including high price, poor stability, and low repeatability. Nonenzymatic sensors appear to be a promising solution in this situation. 3D graphene was used to prepare a copper oxide nanoparticle (CuO-NPs/3DG) electrocatalyst that was used as a nonenzymatic sensing platform for malathion detection (Fig. 3a). A 3D graphene framework offered a great surface area for excellent dispersion of CuO-NPs. Given that the resulting CuO-NPs/3DG nanocomposite has a high affinity for malathion, CuO's redox reaction may be constrained. Under ideal circumstances, measurements of the suppressed signal allowed the CuO-NPs/3DG modified electrode to detect malathion at concentrations as low as 0.01 nmol/L. The 3D graphene has a high surface area to anchor CuO-NPs and promote electron transfer, contributing to the high sensitivity. The sensor also revealed good recovery, stability, and selectivity for recognizing malathion in real samples [20].

4.3 *Phenolic Compound*

Applications for electrochemical sensors in the monitoring of dangerous compounds may benefit from graphene's special electrical characteristics. A significant and often utilized chemical feedstock, 4-nitrophenol (4-NP), is typically found in wastewater. Unfortunately, it is a stable compound with a high level of carcinogenicity and is listed as one of the most important pollutants [21]. Therefore, it is crucial to detect 4-NP effectively in the environment. In a study, it was suggested to manufacture nitrogen-doped 3D graphene with manganese-doped Fe_3O_4-NPs loaded on the surface (Mn–Fe_3O_4/3DG) using a straightforward urushiol templated solvothermal technique (Fig. 3b) accompanied with calcination. The as-prepared Mn-Fe_3O_4/3DG sensor demonstrated great activity in detecting 4-NP, which is much better than the control unmodified samples due to the wide active surface area, porous channel, and high

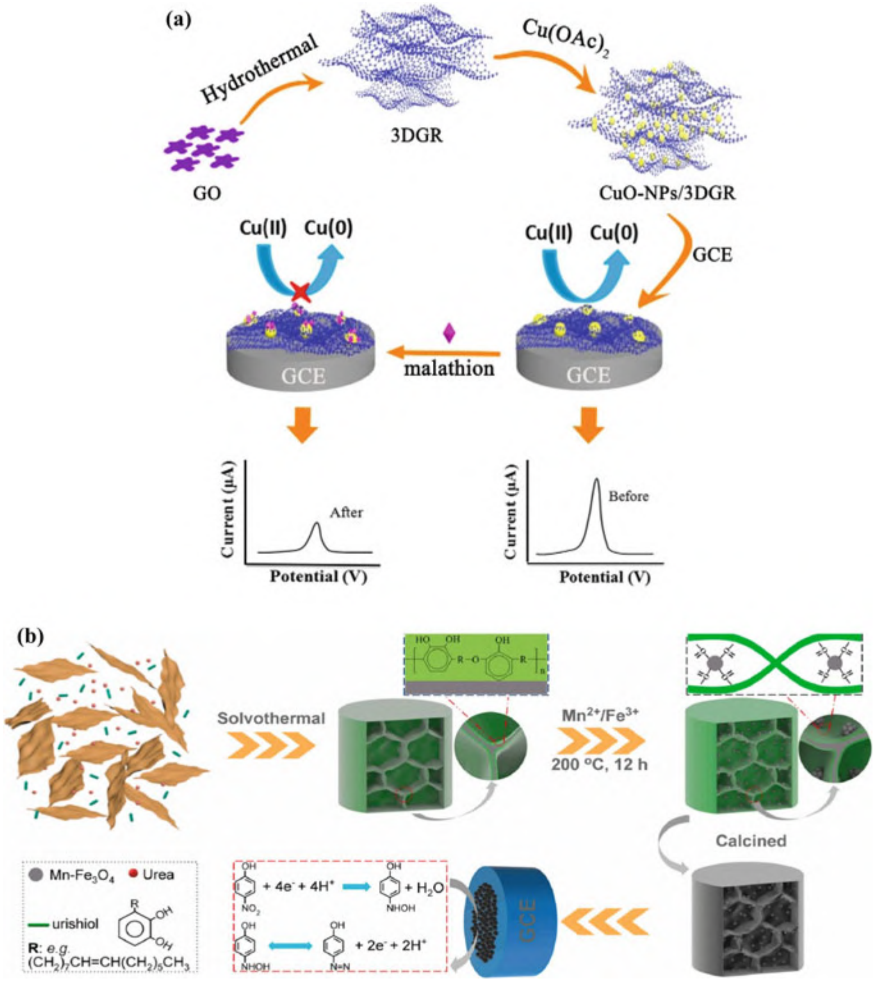

Fig. 3 **a** Diagram showing the creation of CuO-NPs/3DGR/glassy carbon electrode (GCE) and the electrochemical sensing of malathion. Adapted with permission [20]. Copyright (2018) Copyright The Authors, some rights reserved; exclusive licensee Elsevier. Distributed under a Creative Commons Attribution License 4.0 (CC BY) **b** Diagram showing how electrode materials are made for 4-NP detection. Adapted with permission [22]. Copyright (2021) Copyright The Authors, some rights reserved; exclusive licensee Elsevier. Distributed under a Creative Commons Attribution License 4.0 (CC BY)

loading ratio of Mn–Fe_3O_4–NPs. The Mn-Fe_3O_4/3DG electrode may be used in practical applications due to its broad linear range (5–100 µmol/L), low LOD (19 nmol/L), and acceptable recovery of 4-NP in a variety of water samples [22].

4.4 Biomarker Detection

4.4.1 Cancer

For the recognition of tumor markers, electrochemical aptasensors using an aptamer as a probe have obtained a lot of consideration because of their exceptional qualities, which include good selectivity, cost-effectiveness, high stability, a widespread target range, and the simplicity of synthesizing and modifying methods. A study creates an electrochemical aptasensor for the simultaneous measurement of carcinoembryonic antigen (CEA) and cancer antigen 15–3 (CA 15–3), which are two critical biomarkers of breast cancer. The biosensing substrate was a nanocomposite made of 3D graphene hydrogel with gold NPs (Au-NPs/3DGH). Aptamers of CEA and CA 15–3 were connected to graphene nanocomposite-redox probe-Au-NPs as biosensing probes. Hemin (the redox agent of CEA) and ferrocene (the redox agent of CA 15–3) provided electrochemical signals to detect dual biomarkers. The aptamers CEA and CA 15–3 were immobilized on Au-NPs/3DGH. The current and potential of peaks in the differential pulse voltammograms provided information about the nature and concentration of the biomarkers (Fig. 4a). The LOD for CEA and CA 15–3 were 11.2 pg/mL and 11.2×10^{-2} U/mL, respectively. The analysis of clinical serum samples was also done with the duplexed aptasensor. The results showed good compliance with the enzyme-linked immunosorbent assay (ELISA) method, proving the aptasensor's high validity [23].

Circulating tumor DNA (ct-DNA) is a reliable biomarker for predicting treatment effects and is critical for the early detection of many cancers. One of the best advantages of the ct-DNA detection method is its non-invasive nature, but the low abundance in peripheral blood and the large background of wild-type DNA hamper the exact and specific detection of ct-DNA. For the efficient detection of ct-DNA, a team created a 3D graphene/Au-platinum-palladium nanoflower sensing platform (3DGR/Au-Pt–Pd) based on the CRISPR/Cas9 cleavage-triggered entropy-driven strand displacement reaction (ESDR). This technique allows for the detection of low quantities of ct-DNA. Their approach produced excellent specificity for distinguishing single nucleotide mismatches by the rapid amplification of ESDR and the site-specific cleavage of Cas9/sgRNA. The 3DGR/Au-Pt–Pd biosensor in human serum tests showed high specificity and acceptable performance [24].

4.4.2 Osteoblast Activity

An important biomarker for osteoblast activity and skeletal growth is alkaline phosphatase (ALP). Methods for effective ALP detection are crucial for clinical diagnosis and medication development. An electrochemical sensor based on in situ generated 3D graphene networks (3DGN) was designed to measure ALP activity. The sensor uses ALP to convert a non-electroactive substrate into a product with electroactivity; finally, the activity of ALP is shown as an electrochemical signal (Fig. 4b). The

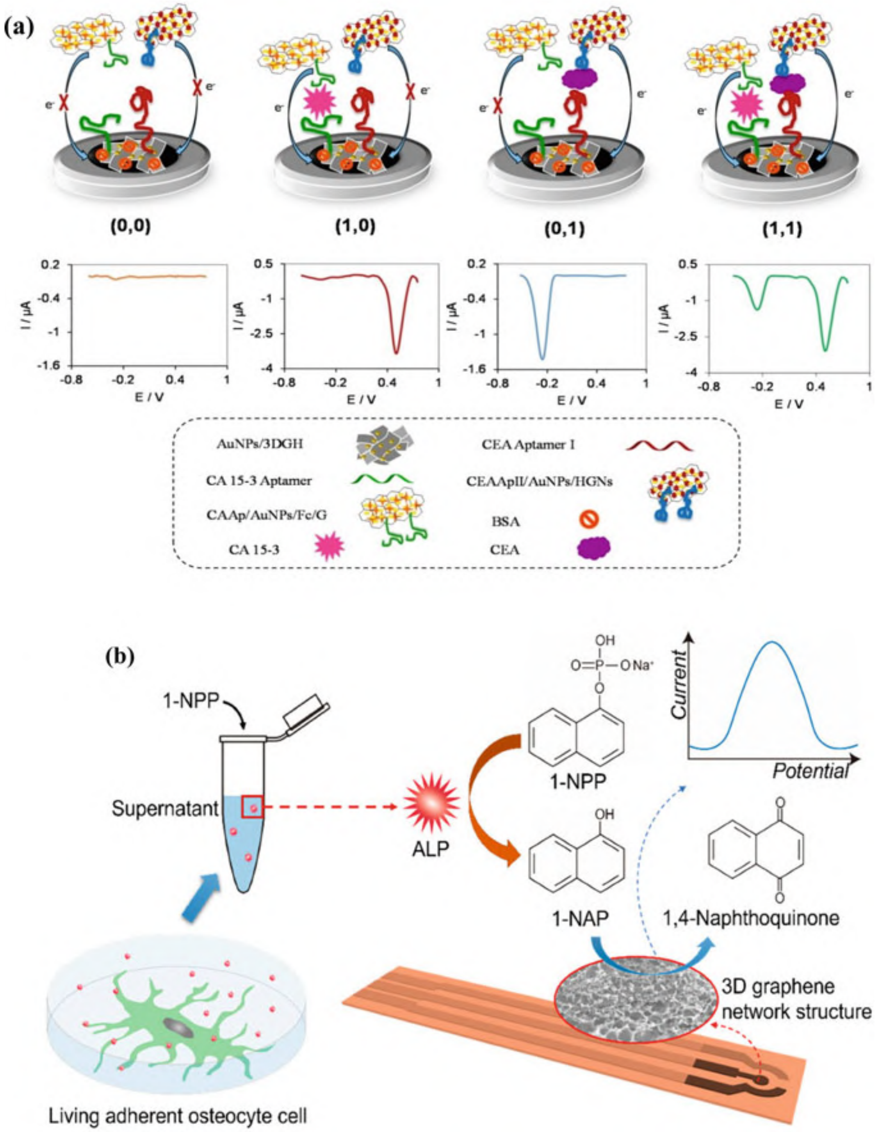

Fig. 4 **a** Schematic illustrating the simultaneous detection of the biomarkers CEA and CA 15–3. Adapted with permission [23]. Copyright (2021) Copyright The Authors, some rights reserved; exclusive licensee Elsevier. Distributed under a Creative Commons Attribution License 4.0 (CC BY). **b** Using a 3DGNs modified sensor, the ALP activity of adhering osteocyte cells is detected. Adapted with permission [25]. Copyright (2022) Copyright The Authors, some rights reserved; exclusive licensee Multidisciplinary Digital Publishing Institute. Distributed under a Creative Commons Attribution License 3.0 (CC BY)

sensor detects ALP activity in a wide range (10–10,000 U/L) and a LOD of 5.70 U/L with 5μL sample volume and a 2 min incubation time when 3DGN catalyzes the process and amplifies the signal. This sensor shows good performance in various biological systems and serum samples. It offers a rapid response, economical, and nondestructive technique for tracking living adherent osteoblast cell activity [25].

4.4.3 Acute Kidney Injury

Compared to conventional biomarkers such as creatinine, neutrophil genatase-associated lipocalin (NGAL) responds significantly faster to acute kidney injury (AKI). For the detection of NGAL, a 3D graphene nickel (Ni) foam (GF) electrochemical sensor covered with Au-NPs was created. It achieved a low LOD (42 pg/mL) and a linear range of 0.05–210 ng/mL. In order to facilitate antibody binding on Au-NPs, self-assembled monolayers, and 11-mercaptoundecanoic acid were used. Utilizing cyclic voltammetry and chronoamperometry on ferri/ferrocyanide redox measurements, NGAL was electrochemically determined. The ability to detect NGAL in the presence of uric acid (UA) and creatinine was examined. Large surface areas of GF and Au-NPs, and the role of the graphene/Ni/Au electric dipole in the enhanced electron transport from the analyte may be responsible for the achieved performances [26].

4.5 Drug

Drug monitoring is very important in the field of drug safety. By electropolymerization imprinting on 3D Au–Pd–NPs-ionic liquid (IL) functionalized graphene-CNTs nanocomposite (Au–Pd/GN-CNTs-IL) modified GCE, a novel paracetamol (PCM) sensor was created. In addition to promoting the construction of Au–Pd alloy NPs, IL (1-hydroxyethyl-3-methylimidazolium bis(trifluoromethyl sulfonyl) imide) served as a “spacer” to avoid the $\pi-\pi$ stacking and aggregation of graphene sheets and CNTs during the preparation of the GN-CNTs that supported Au–Pd alloy NPs. The resultant composite has significant electrocatalysis and a large surface area. The imprinted position of PCM on poly(carbazole)-co-Poly(Py) demonstrated good PCM detection and showed excellent stability. Using 3D Au–Pd/GN-CNTs-IL nanocomposite and PCM imprinted position on copolymer, an electrochemical sensor was developed. Having a LOD of 50 nmol/L, it displayed an excellent linear range of 0.10–10 μmol/L. The sensor’s recoveries are adequate for PCM detection in biological samples. Additionally, it successfully monitored the level of PCM in a patient’s urine with a fever cold [27]. A straightforward approach for anchoring silver NPs (Ag-NPs) onto 3D reduced GO (3D-rGO) has been described in another work for the detection of rifampicin (Ag-NPs/3D-rGO). Due to its substantial electrochemically active surface area and superior electron transport capabilities, the modified electrode demonstrated effective electrical activity to measure rifampicin. With a LOD of 0.810 nmol/L, the sensor showed an excellent linear range (0.01 nmol/L–45 μmol/L). Notably, the created sensor was used to evaluate rifampicin in samples of human blood, drugs, and aquatic products [28].

4.6 Chiral Material

In biochemical analysis, enantioselective recognition is crucial. Therefore, separating amino acid enantiomers using diverse methods is critical for biochemistry, pharmaceutical science, and medical systems. The creation of practical and effective methods for chiral discrimination is still regarded as a difficult problem. Due to their straightforward equipment, low-cost, fast, and effective detection, chiral electrochemical sensors have generated a great deal of attention. A group described how to recognize L and D tryptophan (Trp) using a chiral sensor. The sensor consists of self-assembly between Cu^{2+}/β-cyclodextrin with carboxymethyl cellulose (CD-Cu-CMC) as a chiral selector, N-doped rGO as substrate, and differential pulse voltammetry for enantiomer recognition. rGO and Py were used as the initial components to create the 3D N-rGO. The carboxy groups of CMC and Cu^{2+} in Cu-CD interact electrostatically. The CD-Cu-CMC was able to be immobilized owing to the 3D N-rGO, which also enhances the active regions. N-rGO/CD-Cu-CMC was used to modify a GCE, which then demonstrated a larger electrochemical signal for L than for the D isomer, typically at a working potential of about 0.78 V. It was demonstrated by UV–visible spectroscopy that CD-Cu-CMC has a stronger affinity for the D isomer. D-Trp has a 4.72 enantioselectivity over L-Trp. The modified electrode had a linear detection range of 0.01–5 mmol/L and a LOD of 0.063 and 0.003 μmol/L for L and D isomers, respectively. Trp (D or L) was found using the sensor in samples of human serum protein and spiked real human urine [29].

4.7 Dopamine

The cardiovascular, central neurological, renal, and hormonal systems all depend on the neurotransmitter dopamine (DA). Regular assessment of DA levels in patients' bodies is necessary because excess or insufficient concentrations of DA in neurological systems can cause schizophrenia, Parkinson's disease, hyperactivity disorder, and other conditions. As a result, it is particularly important for developing a sensitive and reliable test for DA molecule detection in the medical and biological fields. To monitor the electrochemical behavior of DA, a 3D-rGO with CD-modified GCE was created (Fig. 5a). The CD was effectively modified on 3D porous graphene. By using cyclic voltammetry and electrochemical impedance spectroscopy to examine the electrochemical characteristics of various modified electrodes, it was determined that the 3D-rGO/CD-modified electrode had the highest electron transfer rate. Scan rate, pH, enrichment time, and layer thickness were among the experimental parameters that were optimized. A wide linear range of 0.5–100 μmol/L and the LOD of 0.013 μmol/L were achieved by differential pulse voltammetry by 3D-rGO/CD/GCE under the best experimental conditions for DA detection [30]. A rapid and easy method for creating 3D graphene nanomesh (3D-GNM) with electrocatalytic property has been demonstrated. The initial electrode is made of monolithic and macroporous 3D graphene foam (Fig. 5b). Simple electrochemical polarization of 3D graphene, which involves oxidation of the anode and subsequent reduction of the cathode, makes it simple to create 3D-GNM. The entire process takes only 10 min. The peaks of DA, UA, and ascorbic acid (AA) in 3D-GNM are clearly distinct. Selective detection of DA, UA, and AA in triplex mixtures or serum samples is accomplished with the LOD of 0.26 μmol/L, 6.0 nmol/L, and 3.1 μmol/L, respectively [31].

4.8 Glucose

Due to their remarkable advantages of simplicity and ease of use, electrochemical sensors are greatly desired for the detection of glucose in diabetes prevention, diagnosis, and treatment. Creating a 3D sensing interface with an immobilized electrochemical probe and nonenzymatic recognition groups is still difficult. By adding functional nanostructure to 3D graphene, a new nonenzymatic electrochemical sensor was created for glucose. The electrode scaffold was a 3D graphene foam created by CVD. 3D graphene was first electrodeposited with Prussian blue (PB) and Au-NPs (3DG/PB-Au-NPs) as an immobilized signal indicator and electron conductor. A simple self-polymerization of DA was used to add a layer of polydopamine (PDA) to 3DG/PB-Au-NPs for stabilizing of internal PB probe and providing chemical reducibility. After that, in situ formation of a second layer of Au-NPs was done for recognition ligand placement, i.e., mercaptobenzoboric acid. The nonenzymatic sensor could detect glucose without reagent with good selectivity, a wide linear range (5–65 μmol/L), and a low LOD (1.5 μmol/L) because of the PB stability and good affinity between mercaptobenzoboric acid and glucose. Additionally, the sensor has been used to measure glucose in human serum samples [32].

4.9 Free Radicals

The measurement of nitric oxide released by living cells helps to understand the pathological and physiological processes of the human body and related disorders [33]. In a research, a new sensor called COF-366-Fe/GA was developed by growing COF-366-Fe electrocatalyst on 3D porous graphene aerogel (GA) for nitric oxide detection (Fig. 6a). The constructed biosensor exhibits a sensitive response in the wide range of 0.18–400 μmol/L with a LOD of 30 nmol/L. Furthermore, after the release of nitric oxide by HUVEC cells (human umbilical vein endothelial cells), the

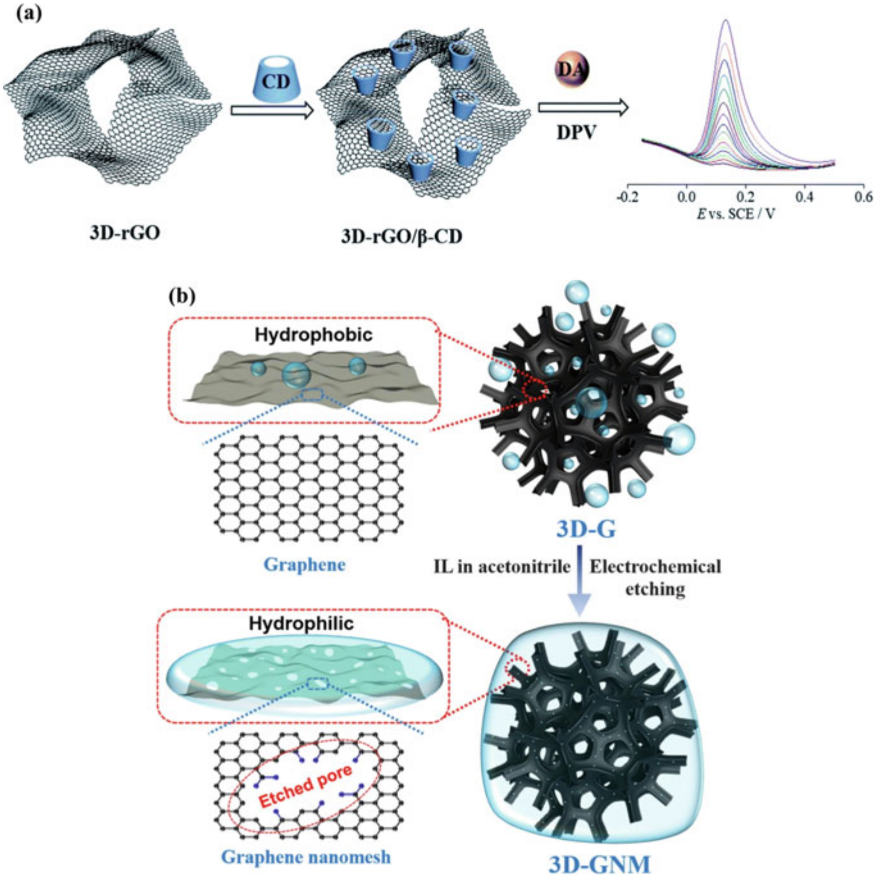

Fig. 5 **a** Electrochemical detection of DA by prepared 3D-rGO/CD. Adapted with permission [30]. Copyright (2021) Copyright The Authors, some rights reserved; exclusive licensee Royal Society of Chemistry. Distributed under a Creative Commons Attribution License 3.0 (CC BY) h. **b** The preparation of 3D-GNM for detecting DA, UA, and AA. Adapted with permission [31]. Copyright (2022) Copyright The Authors, some rights reserved; exclusive licensee [Elsevier]. Distributed under a Creative Commons Attribution License 3.0 (CC BY)

constructed device was able to capture the molecular signals rapidly. According to these findings, this biosensor solves the problem of random organization of active sites for nitrogen-coordinated electrocatalysts because its active sites are adjustable and also have the 3D porous structure of graphene [34].

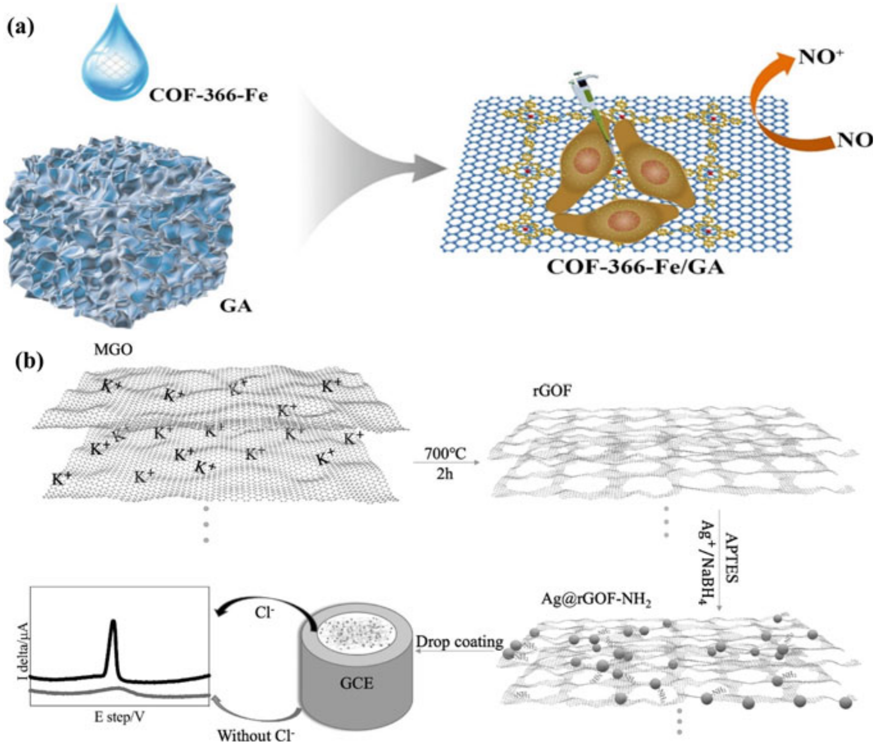

Fig. 6 **a** Nitric oxide detection using COF-366-Fe/GA. Adapted with permission [34]. Copyright (2021) Copyright The Authors, some rights reserved; exclusive licensee Elsevier. Distributed under a Creative Commons Attribution License 4.0 (CC BY), **b** Fabrication of an $Ag@rGOF-NH_2$/GCE sensor for Cl^- detection. Adapted with permission [35]. Copyright (2021) Copyright The Authors, some rights reserved; exclusive licensee Elsevier. Distributed under a Creative Commons Attribution License 4.0 (CC BY)

4.10 Ion

Cl^- is extensively dispersed in nature, and specific concentration ranges are needed for agricultural production, concrete engineering, and the medical and health industries. Therefore, quick detection of Cl^- concentrations in the environment has significant applicability. A study showed the direct usage of multilayer GO to synthesize mesoporous 3D-rGO framework (rGOF) (Fig. 6b). This work used a KOH activation procedure that relies on the adsorption and fixation of the proper amount of K^+ by utilizing the interlayer space of multilayer GO and freeze-drying crystallization technology. Additionally, they found that the structure of rGOF is consistent with the usual 3D structure. Moreover, rGOF has a unique 3D structure and rGO characteristics, making it an excellent platform for functionalized modifications. The prepared Ag@rGOF-NH_2/GCE sensor detects Cl^- over a broad linear range of 5–10 μmol/L, with a LOD of 0.1 μmol/L. This study demonstrates the effectiveness of rGOF as a platform with modification by amine and loading of Ag-NPs [35].

4.11 H_2O_2

H_2O_2 is a crucial component of biological, medical, food, and environmental activities and is a signaling molecule involved in cell growth, cell death, and intracellular signaling transduction. Studies show that improper management of H_2O_2 in cells leads to some diseases, from cancer to neurological diseases [36]. Therefore, H_2O_2 must be detected accurately and reliably. Hydrothermal reduction, freeze-drying, and high-temperature annealing were proposed as synthesis methods for graphene foam that was functionalized with taurine (a-NSGF). The increased temperature during annealing made it possible for taurine's N/S atoms to reach the graphene lattice, considerably enhancing its electrocatalytic activity. The 3D layers of graphene modified with taurine make up the a-NSGF that quickly responds to $H_2O_{2.}$ Owing to the stable 3D structure and superior electrical conductivity of a-NSGF, the modified electrode with a-NSGF exhibits excellent sensitivity and stability to the concentration change of H_2O_2. From 1.5–300 μmol/L, there is a linear relationship between the H_2O_2 concentration and the electrochemical signal, with a $R^2 = 0.99$. The modified electrode was used to measure H_2O_2 in rain samples, and the outcomes were compared to those obtained using the standard method. The recoveries vary between 94.6 and 106.7% [37].

5 Conclusion, Challenges, and Future Perspective

This chapter highlights recent advancements and successes in 3D graphene for electrochemical sensing. 3D graphene is an amazing electrode substance, and there are many prospects to study its application in electrochemical sensors. Its properties make it incredibly competitive in comparison to traditional electrodes. High electrochemical activity, simplicity of surface functionalization, and outstanding electron transport capabilities are just a few of the exceptional properties of 3D graphene that have made it possible to employ it to detect analytes with better sensitivity and selectivity. We concentrated on using 3D graphene related materials as sensors for detecting dopamine, glucose, free radicals, ions, pesticides, phenolic compounds, biomarkers of disease, drugs, and H_2O_2.

While 3D graphene production, functionalization, and applications have come a long way, there are still plenty of obstacles to overcome. For instance, new methods for 3D graphene synthesis need to be developed. These procedures must have the benefits of speed, economy, simplicity, and a high potential for 3D graphene mass production. Additionally, 3D graphene's exceptional properties depend solely on the material's successful creation. The material's porosity has not been accurately regulated up to this moment, and the distribution of pore sizes is between nm and µm. In addition, many architectural defects are created during preparation, negatively affecting how well they work in electrochemical sensing. The mechanical stability still needs to be improved to make the 3D network of graphene a useful sensing instrument. Additionally, there is a need to pay more attention to identifying material defects during construction and figuring out how to fix them. This will benefit the 3D graphene electrodes' mechanical stability and electrochemical activity. To get the best synergistic impact for selective and sensitive sensing of the analytes, more theoretical and experimental investigation of 3D graphene with other nanocomposites is needed. In conclusion, to create sensitive and affordable sensors for electrochemical sensing, 3D graphene has great potential.

References

1. Hou, X., Xu, H., Zhen, T., Wu, W.: Recent developments in three-dimensional graphene-based electrochemical sensors for food analysis. Trends Food Sci. Technol. **105**, 76–92 (2020)
2. Kalji, O., Sefidbakht, Y., Nesterenko, A.M., Uskoković, V., Ranaei-Siadat, S.-O.: Colloidal graphene oxide enhances the activity of a lipase and protects it from oxidative damage: Insights from physicochemical and molecular dynamics investigations. J. Colloid Interface Sci. **567**, 285–299 (2020)
3. Ehtesabi, H., Gupta, R.K.: Flexible and Wearable Sensors, Flexible and Wearable Sensors for Biomedical Applications. CRC Press (2023)
4. Haque, E., Yamauchi, Y., Malgras, V., Reddy, K.R., Yi, J.W., Hossain, M.S.A., Kim, J.: Nanoarchitectured graphene-organic frameworks (GOFs): synthetic strategies, properties, and applications. Chem. Asian J. **13**, 3561–3574 (2018)
5. Idowu, A., Boesl, B., Agarwal, A.: 3D graphene foam-reinforced polymer composites–a review. Carbon **135**, 52–71 (2018)
6. Wu, Y., Zhu, J., Huang, L.: A review of three-dimensional graphene-based materials: synthesis and applications to energy conversion/storage and environment. Carbon **143**, 610–640 (2019)
7. Yousefi, N., Lu, X., Elimelech, M., Tufenkji, N.: Environmental performance of graphene-based 3D macrostructures. Nat. Nanotechnol. **14**, 107–119 (2019)
8. Owusu-, S., Tripp, C.P.: Controlled growth of layer-by-layer assembled polyelectrolyte multilayer films under high electric fields. J. Colloid Interface Sci. **541**, 322–328 (2019)
9. Sun, Z., Fang, S., Hu, Y.H.: 3D graphene materials: from understanding to design and synthesis control. Chem. Rev. **120**, 10336–10453 (2020)
10. Dong, S., Xia, L., Guo, T., Zhang, F., Cui, L., Su, X., Wang, D., Guo, W., Sun, J.: Controlled synthesis of flexible graphene aerogels macroscopic monolith as versatile agents for wastewater treatment. Appl. Surf. Sci. **445**, 30–38 (2018)
11. Lai, K.C., Lee, L.Y., Hiew, B.Y.Z., Thangalazhy-Gopakumar, S., Gan, S.: Environmental application of three-dimensional graphene materials as adsorbents for dyes and heavy metals: Review on ice-templating method and adsorption mechanisms. J. Environ. Sci. **79**, 174–199 (2019)
12. Tang, X., Zhou, H., Cai, Z., Cheng, D., He, P., Xie, P., Zhang, D., Fan, T.: Generalized 3D printing of graphene-based mixed-dimensional hybrid aerogels. ACS Nano **12**, 3502–3511 (2018)
13. Li, F., Yu, Z., Han, X., Lai, R.Y.: Electrochemical aptamer-based sensors for food and water analysis: A review. Anal. Chim. Acta **1051**, 1–23 (2019)

14. Shao, Y., Wang, J., Wu, H., Liu, J., Aksay, I.A., Lin, Y.: Graphene based electrochemical sensors and biosensors: a review. Electroanal. Int. J. Devoted Fund. Practical Aspects Electroanal. **22**, 1027–1036 (2010)
15. Lawal, A.T.: Synthesis and utilisation of graphene for fabrication of electrochemical sensors. Talanta **131**, 424–443 (2015)
16. Zhang, Y., Wan, Q., Yang, N.: Recent advances of porous graphene: synthesis, functionalization, and electrochemical applications. Small **15**, 1903780 (2019)
17. Guo, X., Cui, R., Huang, H., Li, Y., Liu, B., Wang, J., Zhao, D., Dong, J., Sun, B.: Insights into the role of pyrrole doped in three-dimensional graphene aerogels for electrochemical sensing Cd (II). J. Electroanal. Chem. **871**, 114323 (2020)
18. Derbalah, A., Ismail, A., Shaheen, S.: Monitoring of organophosphorus pesticides and remediation technologies of the frequently detected compound (chlorpyrifos) in drinking water. Polish J. Chem. Technol. **15**, 25–34 (2013)
19. Zheng, Q., Chen, Y., Fan, K., Wu, J., Ying, Y.: Exploring pralidoxime chloride as a universal electrochemical probe for organophosphorus pesticides detection. Anal. Chim. Acta **982**, 78–83 (2017)
20. Xie, Y., Yu, Y., Lu, L., Ma, X., Gong, L., Huang, X., Liu, G., Yu, Y.: CuO nanoparticles decorated 3D graphene nanocomposite as non-enzymatic electrochemical sensing platform for malathion detection. J. Electroanal. Chem. **812**, 82–89 (2018)
21. Hu, L., Peng, F., Xia, D., He, H., He, C., Fang, Z., Yang, J., Tian, S., Sharma, V.K., Shu, D.: Carbohydrates-derived nitrogen-doped hierarchical porous carbon for ultrasensitive detection of 4-nitrophenol. ACS Sustain. Chem. Eng. **6**, 17391–17401 (2018)
22. Su, Y., Zheng, X., Cheng, H., Rao, M., Chen, K., Xia, J., Lin, L., Zhu, H.: Mn-Fe3O4 nanoparticles anchored on the urushiol functionalized 3D-graphene for the electrochemical detection of 4-nitrophenol. J. Hazard. Mater. **409**, 124926 (2021)
23. Shekari, Z., Zare, H.R., Falahati, A.: Dual assaying of breast cancer biomarkers by using a sandwich–type electrochemical aptasensor based on a gold nanoparticles–3D graphene hydrogel nanocomposite and redox probes labeled aptamers. Sens. Actuators, B Chem. **332**, 129515 (2021)
24. Chen, M., Wu, D., Tu, S., Yang, C., Chen, D., Xu, Y.: CRISPR/Cas9 cleavage triggered ESDR for circulating tumor DNA detection based on a 3D graphene/AuPtPd nanoflower biosensor. Biosens. Bioelectron. **173**, 112821 (2021)
25. Zhao, N., Shi, J., Li, M., Xu, P., Wang, X., Li, X.: Alkaline phosphatase electrochemical microsensor based on 3D graphene networks for the monitoring of osteoblast activity. Biosensors **12**, 406 (2022)
26. Danvirutai, P., Ekpanyapong, M., Tuantranont, A., Bohez, E., Anutrakulchai, S., Wisitsoraat, A., Srichan, C.: Ultra-sensitive and label-free neutrophil gelatinase-associated lipocalin electrochemical sensor using gold nanoparticles decorated 3D Graphene foam towards acute kidney injury detection. Sens. Bio-Sens. Res. **30**, 100380 (2020)
27. Yang, L., Zhang, B., Xu, B., Zhao, F., Zeng, B.: Ionic liquid functionalized 3D graphene-carbon nanotubes-AuPd nanoparticles-molecularly imprinted copolymer based paracetamol electrochemical sensor: Preparation, characterization and application. Talanta **224**, 121845 (2021)
28. Zhang, Q., Ma, S., Zhuo, X., Wang, C., Wang, H., Xing, Y., Xue, Q., Zhang, K.: An ultrasensitive electrochemical sensing platform based on silver nanoparticle-anchored 3D reduced graphene oxide for rifampicin detection. Analyst **147**, 2156–2163 (2022)
29. Niu, X., Yang, X., Mo, Z., Liu, N., Guo, R., Pan, Z., Liu, Z.: Electrochemical chiral sensing of tryptophan enantiomers by using 3D nitrogen-doped reduced graphene oxide and self-assembled polysaccharides. Microchim. Acta **186**, 1–12 (2019)
30. Chen, X., Li, N., Rong, Y., Hou, Y., Huang, Y., Liang, W.: β-Cyclodextrin functionalized 3D reduced graphene oxide composite-based electrochemical sensor for the sensitive detection of dopamine. RSC Adv. **11**, 28052–28060 (2021)
31. Gong, J., Tang, H., Wang, M., Lin, X., Wang, K., Liu, J.: Novel three-dimensional graphene nanomesh prepared by facile electro-etching for improved electroanalytical performance for small biomolecules. Mater. Des. **215**, 110506 (2022)

32. Liu, Q., Zhong, H., Chen, M., Zhao, C., Liu, Y., Xi, F., Luo, T.: Functional nanostructure-loaded three-dimensional graphene foam as a non-enzymatic electrochemical sensor for reagentless glucose detection. RSC Adv. **10**, 33739–33746 (2020)
33. Privett, B.J., Shin, J.H., Schoenfisch, M.H.: Electrochemical nitric oxide sensors for physiological measurements. Chem. Soc. Rev. **39**, 1925–1935 (2010)
34. Zhu, P., Li, S., Zhou, S., Ren, N., Ge, S., Zhang, Y., Wang, Y., Yu, J.: In situ grown COFs on 3D strutted graphene aerogel for electrochemical detection of NO released from living cells. Chem. Eng. J. **420**, 127559 (2021)
35. Dai, J., Meng, L., Rong, S., Gao, H., Zhang, Z., Zhang, Y., Qiu, R., Wang, Y., Chang, D., Ding, P.: Facile preparation of 3D graphene frameworks as functional modification platform for sensitive electrochemical detection of chloride ions. J. Electroanal. Chem. **887**, 115155 (2021)
36. Zhao, Y., Hu, Y., Hou, J., Jia, Z., Zhong, D., Zhou, S., Huo, D., Yang, M., Hou, C.: Electrochemical biointerface based on electrodeposition AuNPs on 3D graphene aerogel: direct electron transfer of Cytochrome c and hydrogen peroxide sensing. J. Electroanal. Chem. **842**, 16–23 (2019)
37. Guo, Z.-Y., Feng, Y.-F., Chen, Y.-Y., Yao, Q.-H., Luo, H.-Z., Chen, X.: A taurine-functionalized 3D graphene-based foam for electrochemical determination of hydrogen peroxide. Talanta **208**, 120356 (2020)

3D Graphene-Based Biosensors

Mert Akin Insel, Sena Nur Karabekiroglu, and Selcan Karakuş

Abstract In the last 30 years, there have been increasingly developments in the fabrication, properties, and applications of graphene-based three-dimensional (3D) materials with their excellent performances of high mechanical strength, excellent surface area, high electrical conductivity, and thermal stability. Over the last century, the number of various applications of 3D graphene has increased dramatically in areas such as sensors, batteries, separation, aerospace, catalysis, and thermal management. In this chapter, all aspects of fabrication strategies, characterization, and biosensing mechanisms of 3D graphene-based biosensors are reviewed. In addition, there is a great deal of interest in a variety of 3D graphene-based sensor systems, such as gas sensors, health monitoring, wearable temperature sensors, electrochemical food sensors, and environmental pollutant sensors. Consequently, a comprehensive understanding of the unique performance, current limitations, and outlook of 3D graphene-based biosensors was highlighted.

Keywords 3D graphene · Sensing systems · Biosensors · Fabrication strategy

1 3D Material-Based Sensing Systems

Detection systems detect physical quantities such as temperature, light, sound, or motion, make the desired measurements, and convert the data into electrical signals that a device can read and interpret. The design and stability of the sensor are critical, as they affect measurement performance and the quality of system performance [1].

The single layer of graphite termed "graphene," which has 2D arrays of sp2 hybrid carbon atoms, is an excellent structure with exceptional qualities, including

---

M. A. Insel · S. N. Karabekiroglu
Faculty of Chemical-Metallurgical Engineering, Department of Chemical Engineering, Yıldız Technical University, Istanbul, 34210, Turkey

S. Karakuş (✉)
Faculty of Engineering, Department of Chemistry, Istanbul University-Cerrahpaşa, 34320 Istanbul, Turkey
e-mail: selcan@iuc.edu.tr

© The Author(s), under exclusive license to Springer Nature Switzerland AG 2023

R. K. Gupta (ed.), *3D Graphene*, Carbon Nanostructures,
https://doi.org/10.1007/978-3-031-36249-1_6

high chemical resistance, high surface area, and high conductivity. Graphene materials have unique properties such as a high optical transmittance of 98%, charge-carrier mobility of 2×10^5 $cm^2/(Vs)$, high mechanical strength of 125 GPa, high surface area of 2600 m^2/g, and excellent thermal conductivity of 5000 W/(mK) [2]. It enables significant new advancements in a variety of sectors, including chemical sensors, biosensors, field-effect transistors, conversion technology, energy storage systems, etc. Although typically found as powders, graphene is not flexible enough. Many studies have focused on developing porous, three-dimensional (3D)-structured graphene materials with superior mechanical strength, outstanding photothermal conversion, electrochemical properties, and high electrical conductivity to solve this problem. There have been reports of graphene-derived sponges, graphene-based foams, graphene-based hydrogels, and graphene-based aerogels. These 3D graphene-based structures have been manufactured using a variety of techniques, including direct fabrication techniques as a solution-based method and chemical vapor deposition, hydrothermal methods, solvothermal treatments, and freeze-drying methods. Different components, such as inorganic materials, activated carbon, conducting polymers, sulfur compounds, are combined into 3D graphene to form nanosized composites, further increasing their performance and broadening their application areas. 3D graphene-based nanomaterials show promising possibilities in the sectors of sensors, energy, water treatment, medicine, etc. 3D graphene-based nanomaterials offer promising therapeutic applications in the areas of biosensing, physical sensors, drug delivery systems, gene delivery systems, bone tissue engineering, etc. by taking advantage of intriguing features such as high specific surface area, nanoscale size, excellent morphology, high antibacterial activity, high antifungal activity, high anticancer activity, and excellent photoluminescence. There are several types of 3D materials that can be used in sensing systems, including metals, semiconductors, polymers, and ceramics. Some of the most common examples of 3D materials used in sensing systems with superior properties are gold nanoparticles (GNP), zinc oxide (ZnO) nanowires, polymer nanofibers, and graphene.

1.1 Gold Nanoparticles

Gold nanostructures are small particles of gold that have dimensions on the nanoscale. Gold has a very stable structure and is preferred because it has biologically inert and plasmonic properties. The surface of GNP reacts spontaneously with amine, sulfur, and carboxyl groups. Therefore, it is known that GNPs are conjugated with target molecules such as nucleic acids, carbohydrates, enzymes, DNA, RNA, and peptides, which are important building blocks in all living systems and play an important role in biosensing and bioactive nanomaterials. One of the key properties of gold nanostructures that makes them useful for sensing applications is their ability to exhibit surface-enhanced Raman scattering (SERS) [3]. SERS is a phenomenon in which the Raman scattering signal of a molecule is significantly enhanced when the molecule is adsorbed onto the surface of a metal nanoparticle with high plasmonic properties [4, 5]. In addition, the functional groups play an important role in the determination of the target molecule. Composite materials containing metals/metal oxides are used to further increase the sensitivity, selectivity, and accuracy of the sensor. Graphene-based nanostructures containing metal NPs show great potential for high-performance electrochemical sensors as they conduct electrons very well.

This enhancement can be used to detect specific biomolecules, such as proteins and DNA, with high sensitivity and selectivity [6, 7]. GNPs have been used to detect different structures, including target biomolecules, harmful gases, and environmental pollutants. In addition, they have a wide range of uses in the field of health, such as the detection of cancer biomarkers in blood samples, the detection of oxygen saturation, the assessment of cardiovascular activity, and the detection of heart rate. Overall, gold nanoparticles are a promising material for use in sensing systems (especially calorimetric sensors) due to their excellent optical, chemical, and electronic properties and their ability to exhibit SERS [6, 7].

1.2 Zinc Oxide Nanowires

ZnO nanowires are thin zinc oxide wires with a high surface-to-volume ratio and nanoscale dimensions [8]. ZnO nanowires have many advantages, such as optical transparency, biocompatibility, good chemical stability, ease of fabrication, the ability to be converted into 3D structures, and a well-known synthesis method (Lupan et al. 2017). In addition, the detection of gases (such as CO_2, NO_2, and so on), proteins, biological molecules such as DNA, and the development of sensors for environmental monitoring and medical diagnosis is in high demand [8, 9].

1.3 Polymer Nanofibers

Polymer nanofibers are nanoscale polymer material fibers with larger surface areas per unit mass. Polymer nanofibers are utilized as filters, tissue engineering scaffolds, protective clothing, reinforcements, and sensors in composite materials. In general, polymer nanofibers are widely used in sensing systems due to their unique properties, good chemical stability that makes them resistant to degradation, and their ability to be converted into a wide variety of 3D structures [10]. They can be produced into a wide variety of 3D structures, such as mats, films, bars, aerogels, and coatings [11].

1.4 Graphene

Graphene is a form of carbon that exists as a two-dimensional (2D), atomic-scale lattice. Because of its extremely thin and flat structure, it is considered a 2D material. It is known as a nanomaterial with superior properties consisting of a perfect arrangement of carbon molecules linked by covalent bonds with a hexagonal structure [12, 13]. Although graphene is typically synthesized as a 2D material, 3D structures can be created using layering, folding, wrapping, or 3D printing methods [14]. The differences among graphene, graphite, 2D graphene-based formulations, 3D graphene-based nanomaterials, are illustrated in Fig. 1.

The trend in the latest literature is toward sensitive and accurate detection of traditional food contaminants, predominately bacteria, agrochemicals, and toxic metabolites with nanotechnological solutions. In truth, really novel graphene-based biosensor solutions are lacking, and the latest published advances are frequently based on tried-and-true methods with the application of graphene nanostructures or nanosized blends to produce highly sensitive detectors. Due to its numerous special qualities, graphene has the potential to be useful in a variety of applications. The most prevalent superior characteristics of graphene are listed below [13];

- high surface area
- superior thermal conductivity
- excellent electron mobility
- stronger than steel, more durable than a diamond

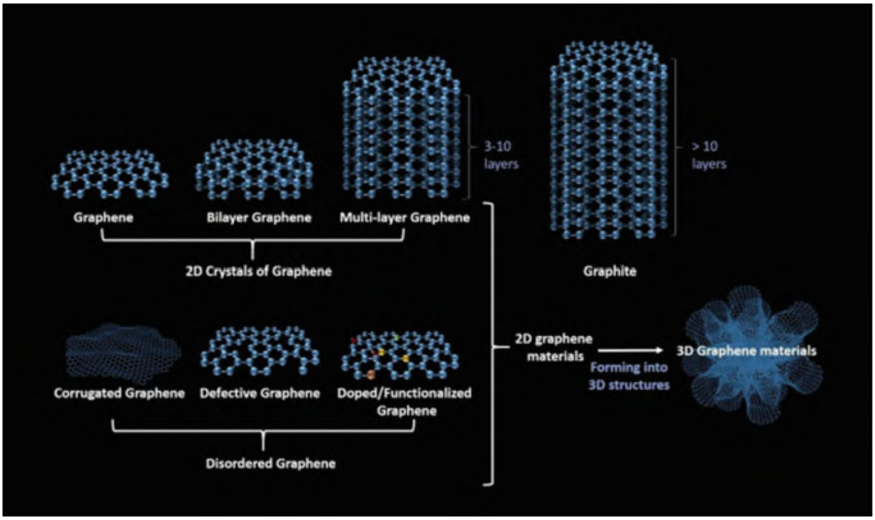

Fig. 1 American Chemical Society. The differences among graphene, graphite, 2D graphene-based formulations, 3D graphene-based nanomaterials. Adapted with permission [12]. Copyright (2020), American Chemical Society.

- flexibility up to 20%
- high thermal conductivity
- high current carrying capacity $>10^2$
- very high intrinsic mobility provides outstanding electronic characteristics.
- very high critical properties.

Thanks to these superior properties, graphene is used in many application areas. These include transparent electrodes, biosensors, field-effect transistors, clean energy storage systems, nanostructures, and organic photovoltaic platforms. It is also used as a conductive material in a number of sensitive electronic/optoelectronic systems, such as thin-film photovoltaic touch screens, light-emitting diodes (LEDs), and transparent electrodes [15]. Recent studies also focus on enabling the fabrication of graphene in numerous applications, including supercapacitors, batteries, and fuel [12].

2 Fabrication of 3D Graphene-Based Biosensors

Graphene can be fabricated using various methods such as micromechanical separation of graphite layers (exfoliation), chemical vapor deposition (CVD), electrodeposition, 3D graphene-based printing, and the folded graphene method [12].

- ***3D printing systems***: Utilization of a 3D printer to create the sensor structure by depositing layers of graphene in the desired shape.
- ***Exfoliation***: The process of obtaining a single or few layers of material from a bulk sample. This process is used to obtain a single layer or a few layers of graphene from bulk graphite.
- ***Chemical vapor deposition (CVD)***: Growing of graphene on a material using the chemical process and then etching away the substrate to create a free-standing graphene structure.
- ***Electrodeposition***: Deposition of layers of graphene onto a substrate using an electric current.
- ***Folded graphene***: Folding of a sheet of graphene into a 3D structure that can be used as a sensor.
- ***Directed Assembly***: The self-assembly of graphene layers into 3D morphologies using various techniques such as capillary forces, mechanical folding, and electrostatic interactions.

After the 3D graphene structure is developed, functionalization of biomolecules for biosensor fabrication may be possible. Numerous methods, such as covalent bonding, physical adsorption, and chemical modification, can be used for this purpose [12]. The identification and recognition of specific biomolecules form the basis for the modifications of 3D graphene-based biosensors. With this purpose, a functionalized 3D structure can be fabricated using various fabrication techniques. One of the most widely used processes for creating 3D graphene structures is electrospinning. According to this method, a polymer solution or a graphene-containing melt is spun to produce highly porous and conductive 3D graphene fibers. Other methods include 3D printing, self-assembly, and template creation. These methods are ideal for fabricating high-precision and complex 3D graphene structures for difficult-to-control systems [13, 15].

2.1 3D Printing

One of the most promising applications for developing micro or nanomaterials with specific multifunctional characteristics and design flexibility is 3D printing, which aims to address the growing demand for such materials. This process, which also plays an active role in the production of graphene or its derivatives, is preferred in most cases for the fabrication of complex 3D structures, as it offers significantly better properties, shorter processing time, and lower printing costs [16].

2.2 Exfoliation

Graphite is a form of packaged graphene sheet bonded together by van der Wall ties. For this reason, graphene can be obtained from the graphite raw material by breaking the weak bonds (a repeated peeling process) using high-purity graphite [15].

Mechanical exfoliation: In this technique, tiny layers of graphene are peeled off from a bulk sample of graphite using adhesive tape or a sharp object (such as pencil lead). This process works well for manufacturing tiny quantities of high-quality graphene, but it is unsuitable for fabrication on a large scale. Although this approach is more scalable and less complicated than others, it enables the creation of graphene of inferior quality.

Electrochemical exfoliation: This method involves suspending graphite flakes in a liquid electrolyte and applying an electric current to exfoliate the flakes into individual graphene layers. This method is relatively simple and scalable, but it allows the production of lower-quality graphene compared to other methods.

Novoselov et al. investigated the ability of highly oriented pyrolytic graphite and adhesive tape to block monocrystalline graphite films between the tape [17]. The resulting structure was metallic, only a few atoms thick, and of extremely high quality. It was also stable under ambient settings. In this work, they produced graphene as thin as a few atoms by repeatedly manipulating the separated blocks. This method has proven useful for producing small quantities of high-quality graphene; however, due to its labor-intensive and time-consuming structure, it is not suitable for large-scale productions [12].

2.3 Chemical Vapor Deposition

CVS is a technique for depositing material from the vapor phase onto a substrate to form thin films and coats [18]. CVD is known as an inexpensive, efficient, high quality, and reproducible production method [15]. In the context of graphene production, CVD involves heating a substrate (such as copper or silicon) to a high temperature (typically around 1000–1500 °C) and introducing a hydrocarbon gas (such as methane or ethylene) into the chamber. The hydrocarbon gas decomposes on the substrate and the carbon atoms rearrange themselves into a monolayer graphene sheet. Graphene grows layer by layer on the substrate, and the thickness of the graphene can be controlled by adjusting the growth time [12]. Transition metals such as nickel, palladium, iridium, and copper are used as catalysts in this effective method [18, 19].

The basic principle of electrochemical biosensors is based on the change in some parameters (impedance, current, or potential) when a reaction occurs on an electrode surface. Following this approach, graphene-based biosensors are primarily preferred as they are effective in DNA and miRNA bioassays with their unique properties such as ultra-high sensitivity, high selectivity, and the lowest limit of detection (LOD) values [19].

In producing 3D graphene biosensors, the CVD method offers many advantages, including:

- The capacity to develop graphene on a number of different substrates, generate high-quality graphene films with few problems, and manufacture reproducible and scalable graphene are all advantages of the CVD approach.
- It promotes the growth of high-quality graphene films with good coverage and few defects. This property is important for biosensors that rely on graphene's electrical conductivity and stability to function properly.
- It allows graphene to grow on various surfaces (silicon and glass) in biosensor devices.
- It can be used to grow graphene in a controlled and uniform manner, which is important for producing reproducible biosensor devices.
- It can be used to deposit graphene over large areas, making it suitable for the fabrication of scalable biosensor devices [15, 19, 20].

2.4 Electrodeposition

Electrodeposition is a process in which reduced metal ions are used to form a solid metal residue on a substrate. The process typically involves the use of an ionic solution containing metal ions and an electric current to drive the reduction reaction. The electrodeposition method is widely used to prepare high-quality and low-cost graphene films and is an advanced technique for the production of large-scale graphene [20]. In the electrodeposition method, an ultrathin layer of graphene is deposited on the surface by applying an electric current in a precursor solution containing carbon ions. The substrate is typically used as the cathode in the electrodeposition process. Excellent properties of 3D graphene can be controlled by changing the electrodeposition conditions, such as the applied voltage and the precursor solution [20, 21]. Electrodeposition is the process of the electrochemical interaction of a thin layer of conductive material (metals or conductive polymers) with the target analyte on the surface of biosensors using an electric current from a solution. An increase in contact area is given by the change of metal nanostructures in the cathode, which are most typically formed from gold. For enzymes, this typically encourages electron transfer directly between the surface of the metal and the active catalytic site. The functionalized biosensor can be used in various fields, such as medical diagnostics, oxygen saturation level, glucose monitoring, pulse rate, daily physical activity, food safety, food quality, environmental analysis, and many other fields. This method has been used since 1980 to improve the properties of sensors and biosensors. The three most important reasons for choosing this method are (i) precision, (ii) selectivity, and (iii) consistency [12, 21].

2.5 Folded Graphene

Folded graphene is a term used to describe a sheet of graphene that has been folded or bent into a specific shape. The double fold can form a tri-layer region with highly curved fold edges embedded in the endless single layer [22]. It was showed using potential density functional theory calculations that bi-folding alters the electronic band structure of 3D graphene and that localized electronic states can form in the folded regions. This can be achieved by various methods such as mechanical folding, electrostatic folding, or chemical folding [15, 22]. Folded graphene has gained attention in recent years as it has excellent electronic, chemical, mechanical, and thermal properties that can be used for various applications such as energy storage devices, sensors, and electronics. It has been shown that folded graphene can exhibit unique electronic properties compared to plain graphene. For example, it has been found that folded graphene can exhibit a bandgap not found in plain graphene [23].

Folded graphene-based material is preferred in sensor applications due to its unique electronic and mechanical properties. Particularly, folded graphene can be used as a conductive layer in a field-effect transistor (FET) sensor and mechanical sensing elements. The greatest bindings in scientific knowledge are the two-dimensional, carbon/carbon bindings found in monolayer graphene. These connections give graphene-based biosensors with its extraordinary mechanical strength, flexibility, and toughness. Folded graphene can also be used in biosensor applications by functionalizing the graphene with biological recognition elements such as enzymes, DNA, RNA, proteins, and antibodies that can bind to specific target molecules [13, 23].

2.6 Directed Assembly

In the innovation of 3D graphene-based materials with hierarchical morphologies, oriented assembly uses the remarkable and adaptable building blocks of 3D structure graphene and its functionalized derivatives. Due to the combination of the 3D graphene structure and the extraordinary fundamental characteristics of the layered structure, 3D formulations show 3D graphene's large specific surface areas, small sizes, unique electron transport, shape, and high mechanical properties. 3D architectures produced by this method exhibit graphene materials with small dimensions, large specific surface areas, unique shapes, and high mechanical properties due to the interaction of the 3D graphene structure and the extraordinary fundamental properties of the layered structure. Here are a few methods that can be used for the directed assembly of 3D graphene-based systems:

Self-assembly: This method involves using chemical or physical interactions between graphene building blocks to drive the assembly process. For example, the researchers used self-assembly to create 3D graphene structures by stacking graphene sheets together using Van der Waals interactions [24].

Template creation: This method involves using a template, such as formwork or scaffolding, to guide the assembly of the graphene building blocks. For example, the researchers used templating to create 3D graphene structures by growing graphene on a stencil patterned with a specific 3D shape. Directed assembly by using external fields, and directed assembly by using DNA or proteins as scaffolds are also less common methods.

3 Application and Characterization of 3D Graphene-Based Biosensors

3D graphene-based biosensors are widely preferred in the field of health. Examples of these are COVID-19 detection, advanced health technology applications, and individualized medical applications. 3D graphene-based nanomaterial-based biosensors are typically needed in the medical field, which is still in its infancy. The development, extraordinary capabilities, and applications of next-generation 3D graphene-based biosensors with smart and in situ modules are in high demand. The structural characteristics of 3D graphene can be correlated with the crystal structure and the number of layers of graphene in the 3D graphene. The crystal structure of graphene can be either hexagonal (also known as "few-layer graphene") or turbostratic (also known as "disordered graphene"). Hexagonal graphene has a regular arrangement of carbon atoms while turbostratic graphene has a disordered arrangement of carbon atoms. The number of layers of graphene in a 3D structure may also vary, with some structures having single layers of graphene and others having multiple layers [13, 14]. In fact, the unique morphological and structural features of 3D graphene can have an important effect on the development of the material and support its potential applications. For example, structures with small, uniform particles may have better mechanical properties and be more suitable for use in energy storage applications while structures with large particles may be more suitable for use in filtration and separation applications. Similarly, structures with a high number of layers may show better electrical performances and be more suitable for use in electronic applications while structures with a low number of layers could be more suitable for use in biomedical applications [12]. 3D graphene, a carbon molecule with layers of single carbon atoms arranged in a hexagonal shape, has the function to detect bioactive molecules and their composites. The 3D graphene layer's special physical and chemical features, such as superior thermal and electrical conductivity, optical transmittance, highly chemically sensitive surface area, biocompatibility, and increased mechanical resistance, make it an ideal solution for cancer biomarker detection. Graphene is able to achieve the experimental goal of any biosensing, which is to generate more portable and compact point-of-care equipment for early cancer diagnosis, pH, and temperature. Graphene-based biosensors may detect a broad range of illnesses, their metabolites, and infections in addition to detecting cancers. The effectiveness of nanoparticles in detecting the majority of biochemical markers has been demonstrated by numerous impressive recent studies [23, 25, 26].

Biosensors can be prepared of 3D graphene-based materials that appeal to a variety of applications due to their distinctive features. The following are some of the crucial traits of 3D graphene-based biosensors [15, 22]:

- ***High sensitivity***: 3D graphene-based biosensors have an ultra-high sensitivity, allowing for the detection of low concentrations of biomolecules.
- ***High selectivity***: 3D graphene-based biosensors have a high selectivity, allowing them to distinguish between different types of biomolecules.
- ***Fast response time***: 3D graphene-based biosensors have a fast response time, allowing for rapid detection of biomolecules.
- ***High stability***: 3D graphene-based biosensors have a high stability, allowing them to maintain their performance over a long period of time.
- ***Biocompatibility***: Graphene is considered biocompatible, and 3D graphene-based biosensors can also be biocompatible. It makes them suitable for use in biomedical applications such as drug efficacy monitoring, disease diagnosis, and environmental pollutant detection.
- ***Easy to fabricate***: 3D graphene-based biosensors can be fabricated by growing graphene on a substrate or assembling graphene nanoparticles into a 3D structure, making them easy to produce and scale up.
- ***Low cost***: 3D graphene-based biosensors can be made at low cost by using a simple fabrication process, and the material is relatively inexpensive.
- ***High conductivity***: Due to the high conductivity and transparency of 3D graphene-based materials, CVD-graphene is an excellent choice for manufacturing flexible electrodes used in optoelectronic applications [28].

In point-of-care (POC) systems, 3D graphene-based biosensors are frequently low cost and simple to operate. Point-of-care systems could result from virtual and real-time mobile medical screening using sensor technologies. Due to their potential to identify patterns of indicator organisms and provide experimental data on their existence in biological fluids, which enables correct assessment, 3D graphene-based biosensors have been the center of significant research in recent years. Future point-of-care 3D graphene-based biosensors will be limited in the types of biosensors they can use because of requirements like rapid label-free detection, small sensor size, and mobility with artificial intelligence approaches. It's worth mentioning that the properties of 3D graphene-based biosensors can vary depending on the specific design and fabrication method. Therefore, to understand the properties and potential sensor applications of biosensors, it is important to comprehensively characterize them[12]. Some of the application areas of 3D graphene biosensors are [25]:

Medical Diagnostics

Because of its outstanding qualities in nano additive manufacturing, 3D graphene as a filler has recently attracted a lot of study attention. 3D graphene biosensors can be used to detect biomolecules such as proteins, DNA, and enzymes in the blood, urine, and other body fluids. This type of early diagnosis is of great importance in the prevention of diseases. The integration of all the applied studies into a single frame and their relationship to global applications are two limitations that this research is currently subject to. These 3D graphene-based biosensors, however, represent the next generation of portable, adaptable, small, energy-efficient, and reasonably priced medical technology that has the potential to reach even the most distant regions of the globe. Additionally, making education and healthcare services available to everyone, will contribute to the sustainable performance targets of human health and well-being. As a result, hospital-in-chip biosensors have the ability to turn the current health insurance system into a small-scale method of reducing future fatalities and the severity of infectious and potentially lethal diseases. With this approach, Chen et al. [28] prepared a novel 3D graphene-silver nanoparticle-based DNA biosensor for the detection of the CYFRA21-1 DNA lung cancer biomarker. Experimental results presented that the prepared DNA biosensor had good sensitivity (1.0×10^{-14} M) in the range of 1.0×10^{-14} M–1.0×10^{-7} M. According to their research, this 3D graphene-silver nanoparticle-based DNA biosensor has the ability to play a role in the early detection of lung cancer.

Environmental applications

To present, a number of hybrid adsorbents based on graphene, GO, and rGO have been studied for the excellent removal of inorganic and organic contaminants from water, including chemicals that affect health. The preservation of water quality has been one of the most urgent issues in the modern world. Recent years have seen an increase in the number of dangerous pollutants in the environment, including, explosive materials, heavy metals, organophosphate pesticides, hydrocarbons, phenolic acids, and other pollutants. This is due to the quick advancements in market and agriculture as well as the widespread use of pharmaceutical chemicals in the ordinary routine.

A very minimal percentage of these carcinogenic compounds is dangerous, directly enter the ecosystem, and can be extremely harmful to both the ecosystem and public health. Thus, it is vital to develop acute, economic sensors that can quickly and accurately identify these important chemicals. While GO has a variety of oxygen-containing functional molecules on its surface, it has low binding interactions for ions with negative charges and molecules due to strong electrostatic interactions between them. Moreover, additional pollutants are produced by the problem of desorbing and removing 3D graphene and its derivatives from tap wastewater following adsorption. The modification of graphene, GO, and rGO with other chemicals through covalent or ionic bonding has been carried out to produce composite materials having the extraordinary features of all the adsorbates. It was done to overcome these shortcomings.

Alves et al. [29] developed a novel reduced graphene oxide (rGO)-modified glassy carbon sensor for the amperometric sensing of diuron (DIU) herbicide in real water and food samples. According to the experimental results, they found that the sensor had a low detection limit of 0.36 μmol L^{-1} in the range of 5 μmol L^{-1}–50 μmol L^{-1} and a high recovery of 81%–106%. In this regard, the proposed methodology demonstrates that it can be used as an experimental platform for use in the examination of food and environmental real samples. In another study, Srivastava et al. [30] prepared a graphene-based sensor for sensing different heavy metals such as cadmium (Cd), arsenic (As), mercury (Hg), chromium (Cr), and lead (Pb). Experimental data; confirmed that graphene, As, and Cr exhibited chemisorption interaction, while Pb exhibited physisorption interaction. In addition, graphene has proven to have a high detection capacity against heavy metals in threshold voltage.

Food applications

Food pollutants have received attention because they can appear at any step of food manufacturing. Due to its detrimental impact on human health, a quick, selective, flexible, sensitive, and robust method is required to analyze the unwanted substances in food. Several scientists are currently taking a greater interest in the electrochemical sensor technology utilized in food analysis. Jiang et al. [31] prepared a novel electrochemical 3D graphene foam-based sensor for the determination of uric acid and dopamine. They showed that the sensor had high sensitivities to uric acid (1.27 μM) and dopamine (0.21 μM) in real samples. In this study, the electrochemical performance of 3D graphene is confirmed to be high due to its outstanding physical and chemical properties, such as its interesting electronic conductivity and large specific surface area. The success of highly sensitive and precise uric acid and dopamine evaluation in real samples was demonstrated in relation to 3D graphene's large specific surface areas.

4 Comparative Sensing Performance of 3D Graphene-Based Biosensors

Graphene is a two-dimensional substance comprised of carbon atoms arranged in a hexagonal shape. One type of biosensor that uses graphene is called a 3D graphene-based biosensor. They are compared with other reported biosensors in terms of their sensitivity, specificity, cost, electrical conductivity, biocompatibility, stability, and potential applications [27, 32]. These structures can include things like microfabricated scaffolds, hydrogels, and other materials that can be used to develop a 3D environment for the biological components of the biosensor [14]. There are many different types of biosensors, each with its own unique characteristics and various applications such as antibody-based biosensors, enzyme-based biosensors, cell-based biosensors, optical sensors, and electrochemical sensors [32, 33].

Graphene has been used in transparent electrodes, field-effect transistors (FETs), energy harvesting and storage, and many electronic applications with its superior electronic and chemical properties. Furthermore, the small thickness of graphene allows all carbon atoms to interact directly with the analyte. It means that it gives more sensitive results in sensor applications compared to one-dimensional Si nanowires (1D SiNWs) and carbon nanotubes [27, 34].

"Optical biosensors" are a type of sensor that uses light to detect changes in the biological components of the sensor and has highly sensitive and specific properties. Optical biosensors have been used in various sensor applications, such as the detection of biological components, enzymes, nucleic acids, proteins, and cells, and can be used in various types of samples such as urine, blood, and saliva samples. 3D graphene-based biosensors detect minor changes in biological components compared to optical biosensors; they are preferred due to their high sensitivity, high specificity, high surface area, and low cost [35]. He et al. investigated a 3D graphene foam with several layers of graphene grown by the CVD method that can detect NO_2 gas at much lower concentrations compared to the commercially produced polypyrrole sensor [27]. 3D graphene-based biosensors are biocompatible, meaning they can be used without damaging living cells if they come into contact with them. They also have a very stable structure and are highly resistant to harsh environments. In this way, they are preferred in biosensors that need to be used in harsh conditions [32].

5 Future Outlook of 3D Graphene-Based Biosensors

3D graphene-based materials have garnered a lot of attention in recent years due to their exceptional qualities, including strong electrical conductivity, a very high surface area, stability and flexibility. The preparation of 3D graphene with a special porosity structure is given a lot of attention because of the issues it encounters, like its ease of aggregation. Nanomaterials are frequently created by combining nanosized materials with 3D graphene to enhance their overall performance and their applications.

One of the most promising applications of nanomaterials and 3D graphene-based material is in energy storage fields. Graphene-based materials have a high electrical conductivity and a high surface area, making them ideal for use in batteries applications and supercapacitors studies. Researchers continue to explore the use of graphene in lithium-ion batteries, where it can be used as a conductive material to improve the performance of electrodes. The fabrication of graphene-based supercapacitors, which have the potential to charge and discharge much faster than conventional batteries and have a longer life, is also one of the promising applications. These energy storage systems will have an important place in electric vehicles, in the production of portable electronics, and in many other areas of the renewable energy system [36].

Graphene's superior properties, such as its large surface area, high conductivity, biocompatibility, make it highly suitable for general consumer applications and multi-purpose use when making measurements such as strain, pressure, or magnetic field using a single sensor. The large surface area, low pollution levels, and easy functionalization make graphene suitable for further use in biosensing applications. However, more work is needed to select a reliable, robust, environmentally sound, and financially viable production method for such applications. In addition, excellent properties of graphene make it a potential candidate for detecting and monitoring cardiovascular and neurodegenerative diseases For example, previous studies showed that graphene can be used to scavenge amyloid monomers, which are associated with the development of neurodegenerative diseases such as Alzheimer's.

Due to their unique morphology, 3D graphene-based materials have recently been investigated for gas sensing applications since they provide a larger area of contact and holes large enough in gas diffusion than their 2D materials. The 3D graphene-system increases the sensor devices' robustness and stability in addition to their sensitivity and repeatability to gas molecules. According to numerous experts, graphene-based sensors also offer effective H_2 detection sensing capabilities. There have been a few previous study of ultrasensitive H_2 gas sensors composed of 3D graphenes, but their use has been limiting due to their slow response and recovery times. In comparison to traditional 2D graphene sensors, the findings on 3D graphene-based sensors showed tremendous potential for its usage in a successful comprehension in sensing performance. In comparison to pure graphene, the addition of functional groups provides the 3D graphene surface more sensitive to target molecules. The degree of control of the binding sites may significantly improve the improved electrochemical and optical performance of 3D graphene-based sensors and enable ongoing research in gas sensing systems. The modification of graphene-based materials, synthesis method, control of the functional groups, and development of composite materials are some effective techniques to enhance 3D graphene-based sensor's sensing capacity.

New types of molecular-scale bioelectronic systems based on graphene contribute to the development of engineered tissues with biosensors closely integrated into natural tissues, in addition to the improvement of in vitro formulations for nanomaterials' close association with cells and tissues, fundamental research or biomedical applications. Such laboratory-on-a-chip systems enable, for example, the testing of candidate bio-therapeutic molecules. In addition, graphene-based biosensors have begun to be produced for the early detection and continuous monitoring of the progression of some common cancer diseases [37]. Unfortunately, these studies are very limited. Many studies need to be expanded to be used more effectively for the production of biosensors in the health field. While research in this area is still in its infancy, the potential for graphene to impact the medical field in such a significant way is certainly worth further exploration. The use of 3D graphene-based biosensors in point-of-care diagnostics and personalized medicine is also seen as a promising area of research [38, 39].

In the future studies, 3D graphene-based biosensors are expected to have improved sensitivity, selectivity, and affordability in the field of sensors. Wide-ranging fields, particularly in catalysis, energy, and smart drug systems, could benefit from the improved electrochemical property of 3D graphene mixed with polymers, inorganic compounds, and other biomaterials. The exploration of wearable, flexible, portable, and economical electrochemical sensors based on 3D graphene nanomaterials will undoubtedly receive increasing attention. Finally, the use of 3D graphene-based biosensors in point-of-care diagnostics and personalized medicine is also seen as a promising area of research [13, 39].

References

1. Pallas-Areny, R., Webster, J.G.: kupdf.net_pallas-areny-r-jg-webster-sensors-and-signal-conditioning-wiley-1991 (1991)
2. Ikram, M., Bari, M.A., Bilal, M., Jamal, F., Nabgan, W., Haider, J., et al.: Innovations in the synthesis of graphene nanostructures for bio and gas sensors. Biomater. Adv. **145**, 213234 (2023)
3. Hegde, M., Pai, P., Gangadhar Shetty, M., Sundara Babitha, K.: Gold nanoparticle based biosensors for rapid pathogen detection: a review. Environ. Nanotechnol. Monitoring Manag., 100756 (2022)
4. Liu, C., Xu, D., Dong, X., Huang, Q.: A review: research progress of SERS-based sensors for agricultural applications. Trends Food Sci. Technol. **128**, 90–101 (2022)
5. Gupta, Y., Ghrera, A.S.: Recent advances in gold nanoparticle-based lateral flow immunoassay for the detection of bacterial infection. Arch. Microbiol. **203**(7), 3767–3784 (2021)
6. Sadsri, V., Trakulsujaritchok, T., Tangwattanachuleeporn, M., Hoven, V.P., Na, P.: Simple colorimetric assay for vibrio parahaemolyticus detection using aptamer-functionalized nanoparticles. ACS Omega **5**(34), 21437–21442 (2020)
7. Ahmadi, S., Kamaladini, H., Haddadi, F., Sharifmoghadam, M.R.: Thiol-capped gold nanoparticle biosensors for rapid and sensitive visual colorimetric detection of Klebsiella pneumoniae. J. Fluoresc. **28**(4), 987–998 (2018)
8. Tonezzer, M., Lacerda, R.G.: Zinc oxide nanowires on carbon microfiber as flexible gas sensor. Physica E **44**(6), 1098–1102 (2012)
9. Lupan, O., Schütt, F., Postica, V., Smazna, D., Mishra, Y.K., Adelung, R.: Sensing performances of pure and hybridized carbon nanotubes-ZnO nanowire networks: a detailed study. Scientific Reports **7**(1) (2017)
10. Vasita, R., Katti, D.S.: Nanofibers and their applications in tissue engineering. Int. J. Nanomed. **1**(1), 15–30 (2006)

11. Cheng, Y., Xiong, Y., Pan, M., Li, L., Dong, L.: A flexible, sensitive and stable humidity sensor based on an all-polymer nanofiber film. Mater. Lett. 330 (2023)
12. Sun, Z., Fang, S., Hu, Y.H.: 3D Graphene materials: from understanding to design and synthesis control. Chem. Rev. **120**(18), 10336–10453 (2020)
13. Moldovan, O., Iñiguez, B., Deen, M.J., Marsal, L.F.: Graphene electronic sensors—review of recent developments and future challenges. IET Circuits Dev. Syst. **9**(6), 446–453 (2015)
14. Bianco, A., Cheng, H.-M., Enoki, T., Gogotsi, Y., Hurt, R.H., Koratkar, N., et al.: All in the graphene family-a recommended nomenclature for two-dimensional carbon materials (2013)
15. Bedeloğlu, A., Taş, M.: Graphene and its production methods. Afyon Kocatepe Univ. J. Sci Eng. **16**(3), 544–554 (2016)
16. Ponnamma, D., Yin, Y., Salim, N., Parameswaranpillai, J., Thomas, S., Hameed, N.: Recent progress and multifunctional applications of 3D printed graphene nanocomposites. Compos. Part B: Eng., 204 (2021)
17. Novoselov, K.S., Geim, A.K., Morozov, S.V., Jiang, D., Zhang, Y., Dubonos, S.V. et al.: Electric Field Effect in Atomically Thin Carbon Films (n.d.)
18. Bahri, M., Gebre, S.H., Elaguech, M.A., Dajan, F.T., Sendeku, M.G., Tlili, C. et al.: Recent advances in chemical vapour deposition techniques for graphene-based nanoarchitectures: from synthesis to contemporary applications. Coordination Chem. Rev., 475 (2023)
19. Mattevi, C., Kim, H., Chhowalla, M.: A review of chemical vapour deposition of graphene on copper. J. Mater. Chem. **21**(10), 3324–3334 (2011)
20. Biswal, H.J., Vundavilli, P.R., Gupta, A.: Perspective—electrodeposition of graphene reinforced metal matrix composites for enhanced mechanical and physical properties: a review. J. Electrochem. Soc. **167**(14), 146501 (2020)
21. Stine, K.J.: Biosensor applications of electrodeposited nanostructures. Appl. Sci. (Switzerland) **9**(4) (2019)
22. Kim, K., Lee, Z., Malone, B.D., Chan, K.T., Alemán, B., Regan, W. et al.: Multiply folded graphene. Phys. Rev. B Condensed Matter Mater. Phys., 83 (24) (2011)
23. Zhang, C., Li, Z., Jiang, S.Z., Li, C.H., Xu, S.C., Yu, J., et al.: U-bent fiber optic SPR sensor based on graphene/AgNPs. Sens. Actuators B Chem. **251**, 127–133 (2017)
24. Cao, X., Yin, Z., Zhang, H.: Three-dimensional graphene materials: preparation, structures and application in supercapacitors. Energy Environ. Sci. **7**(6), 1850–1865 (2014)
25. Lei, H., Mi, L., Zhou, X., Chen, J., Hu, J., Guo, S., et al.: Adsorption of double-stranded DNA to graphene oxide preventing enzymatic digestion. Nanoscale **3**(9), 3888–3892 (2011)
26. Schedin1, F., Geim1, A.K., Morozov2, S.V., Hill1, E.W., Blake1, P., Katsnelson3, M.I. et al.: Detection of Individual Gas Molecules Adsorbed on Graphene (n.d.)
27. He, Q., Wu, S., Yin, Z., Zhang, H.: Graphene-based electronic sensors. Chem. Sci. **3**(6), 1764–1772 (2012)
28. Chen, M., Wang, Y., Su, H., Mao, L., Jiang, X., Zhang, T., et al.: Three-dimensional electrochemical DNA biosensor based on 3D graphene-Ag nanoparticles for sensitive detection of CYFRA21-1 in non-small cell lung cancer. Sens. Actuators B Chem. **255**, 2910–2918 (2018)
29. Alves, G.F., de Faria, L.V., Lisboa, T.P., Matos, M.A.C., Muñoz, R.A.A., Matos, R.C.: Simple and fast batch injection analysis method for monitoring diuron herbicide residues in juice and tap water samples using reduced graphene oxide sensor. J. Food Compos. Anal. **106**, 104284 (2022)
30. Srivastava, M., Srivastava, A., Pandey, S.K.: Suitability of graphene monolayer as sensor for carcinogenic heavy metals in water: a DFT investigation. Appl. Surf. Sci. **517**, 146021 (2020)
31. Jiang, J., Wang, J., Wang, P., Lin, X., Diao, G.: Three-dimensional graphene foams with two hierarchical pore structures for metal-free electrochemical assays of dopamine and uric acid from high concentration of ascorbic acid. J. Electroanal. Chem. **928**, 117056 (2023)
32. Liu, Y., Dong, X., Chen, P.: Biological and chemical sensors based on graphene materials. Chem. Soc. Rev. **41**(6), 2283–2307 (2012)
33. Xie, Y., Xie, G., Yuan, J., Zhang, J., Yang, Y., Yao, Y., et al.: A novel fluorescence biosensor based on double-stranded DNA branch migration-induced HCR and DNAzyme feedback circuit for sensitive detection of Pseudomonas aeruginosa (clean version). Analytica Chimica Acta, 1232 (2022)

34. Wang, F., Liu, L., Li, W.J.: Graphene-based glucose sensors: a brief review. İn: IEEE Trans Nanobioscience, Institute of Electrical and Electronics Engineers Inc., pp. 818–834 (2015)
35. Cao, X., Shi, Y., Shi, W., Lu, G., Huang, X., Yan, Q., et al.: Preparation of novel 3D graphene networks for supercapacitor applications. Small **7**(22), 3163–3168 (2011)
36. Gao, X., Li, J., Xie, Y., Guan, D., Yuan, C.: A multilayered silicon-reduced graphene oxide electrode for high performance lithium-ion batteries. ACS Appl. Mater. Interfaces. **7**(15), 7855–7862 (2015)
37. Goenka, S., Sant, V., Sant, S.: Graphene-based nanomaterials for drug delivery and tissue engineering. J. Control. Release **173**(1), 75–88 (2014)
38. Cohen-, T., Langer, R., Kohane, D.S.: The smartest materials: the future of nanoelectronics in medicine. ACS Nano **6**(8), 6541–6545 (2012)
39. Celik, N., Balachandran, W., Manivannan, N.: Graphene-based biosensors: methods, analysis and future perspectives. IET Circuits Dev. Syst. **9**(6), 434–445 (2015)

3D Graphene-Based Optical Sensors

Amrit Kumar, V. Manjuladevi, and Raj Kumar Gupta

Abstract 3D graphene (3DG) has been utilized as a functional material for the development of gas and chemical sensors. The sensor based on optical phenomena such as surface plasmon resonance (SPR) offers label-free measurements at a very high resolution and sensitivity. It is essential for any sensor to exhibit a very high analyte adsorption capability and good perceptibility to measure changes in electrical and optical properties due to such adsorption. Although SPR is extremely sensitive, 3DG is one of the potential functional materials which can exhibit a high analyte adsorption capability. Therefore, the use of 3DG as a functional layer in SPR devices can ensure a next-generation sensor. The Kretschmann configuration in angular interrogation-based SPR sensors may offer a sensitivity of the order of 10^{-8} RIU. In the SPR sensor, the extent of the plasmonic field over the metallic surface is limited to a few hundred nanometres. The excellent adsorption capability of 3D graphene can be employed for bio-sensing applications. However, due to the bulk nature of 3DG, the plasmonic field during SPR-based sensing decays rapidly into the porous structure of the 3DG, and therefore, the measurement becomes unresponsive even after the efficient adsorption of the analytes. Therefore, the layer of 3D graphene can be grown over the gold surface by some bottom-up deposition mechanism with control over the thickness. The bottom-up deposition mechanism may yield monolayer, bilayer, and twisted bilayer graphene which also exhibit excellent bio-sensing merits.

Keywords 3D graphene · Surface plasmon resonance · Biosensing · Monolayer · Bilayer graphene · Twisted bilayer graphene

---

A. Kumar · V. Manjuladevi · R. K. Gupta (✉)
Department of Physics, Birla Institute of Technology and Science Pilani, (BITS Pilani), Pilani 333031, Rajasthan, India
e-mail: raj@pilani.bits-pilani.ac.in

© The Author(s), under exclusive license to Springer Nature Switzerland AG 2023

R. K. Gupta (ed.), *3D Graphene*, Carbon Nanostructures,
https://doi.org/10.1007/978-3-031-36249-1_7

1 Introduction

Since its discovery in 2004, graphene has been considered one of the most widely used nanomaterials in diverse applications. This 2D hexagonal crystalline arrangement of carbon atoms has inducted a great deal of interest in the fields of sensors, biomedicals, composite materials, and microelectronics. Graphene has sp^2 hybridized carbon atoms arranged in a honeycomb-like network on a single plane. It is the thinnest material with an unusually large specific surface area. Graphene has many unique properties due to its long-range π–π conjugation including high chemical stability, excellent mechanical strength, enormous electron mobility, and outstanding thermal conductivity at room temperature. It also demonstrates excellent optical properties including wideband optical absorption in the near-infrared and visible range. The nonlinear optical feature such as saturation absorption is also observed for graphene and its derivatives. Moreover, graphene systems have a unique band structure. The Fermi surface is located at the junction of the completely filled valence band and the empty conduction band, and in the middle of the band formed by p-orbitals [1]. The electrons in the valence band of graphene have very high mobility and are also known as massless Dirac Fermions. Due to the linear distribution of the Dirac electrons, a single layer of graphene absorbs 2.3% of the incident light from the visible to the terahertz band [2]. Thus, even though single-layer graphene has a thickness of 3.35 Å, its absorbance is predominately very high. These fast Dirac Fermions have a linear energy–momentum dispersion ratio around the Dirac point, allowing for an ultra-wide frequency range resonant optical response to input photons. Thus, due to its unique optical and electrical characteristics, graphene has been employed in various optical devices such as polarizers, modulators, ultrafast lasers, sensors, photodetectors, and light-emitting diodes. The excellent physicochemical properties of graphene play a vital role in various sensing applications. These sensors are based on the electrical, electrochemical, or optical properties of graphene.

Despite of many promising applications of 3D graphene, the drawbacks in the scalable production of high-quality graphene with minimal defects have prevented its prevalent use in physical devices. This, on the other hand, has propelled the growth of graphene-based chemistry research, where many novel ways to synthesize graphene materials with different functionality and w application of graphene materials have been projected.

2 3D Graphene

One way to overcome the drawbacks is to build 3D structures of the 2D interconnected graphene layers. These 3D structures can maintain the extraordinary qualities of 2D graphene materials while also being easily used without the issue of restacking. The interconnected graphene sheets form a highly 3D conductive network with ultrahigh porosity, extremely low density, high surface area, and exceptional electrical, optical, and mechanical properties. Thus, the capabilities and potential uses of graphene are significantly increased through the assembly and integration of the 2D graphene sheets into 3D form. 3DG materials are explicitly characterized as nongraphite 3D structured graphene materials. 3DG walls may have less than ten graphene layers which retain the typical features of graphene materials.

In general, 3D graphene structures can be divided into two groups: (1) microscopic 3D graphene materials which are less than 100 μm along all dimensions, and (2) macroscale 3D graphene materials, which are greater than 100 μm in one or more dimensions. These 3D graphene structures are widely regarded as 3D graphene monoliths (foams/sponges/aerogels), films, fibers, and milli spheres.

Recently, substantial progress has been achieved in the production of 3D graphene (3DG) with ultralow density and customizable optical properties, which may open the way for graphene to be used as an ultralight, wideband, and wide-angle terahertz absorber [3]. In comparison to conventional 2D graphene and functionalized graphene networks, 3DG with an extremely porous structure has higher absorption intensity, a wider qualifying bandwidth, and a significantly lower density. The porous structure and long-range conductive network of 3DG are responsible for its excellent optical efficiency and broadband absorption performance. The effective dielectric constants of 3DG may match the dielectric constants of air. Thus, the design of a highly porous structure becomes critical in reducing surface reflection in comparison to other graphene systems [4]. Because of their finite (micrometer) thickness, 3DG samples have virtually constant minimal transmittance, corresponding to 99% extinction of incident light in the near-infrared and visible spectrum [5]. It shows excellent absorption of the electromagnetic (EM) wave in the frequency range from 0.1 to 1.2 THz due to low surface reflection and high internal absorption. The absorbance can be modified by changing the physical parameters such as pore size, annealing temperature, and the angle of incidence of the external electromagnetic field [4]. It also exhibits high-frequency pass-filter behavior with a sharp rise in transmittance from THz to mid-Infrared. The transmittance achieves a saturation value of about 13% in this range. For the lower frequency (below 1THz), the transmittance converges to a minimum value [6]. The observed broadband transmittance behavior implies that due to their nano and micro spatial morphology light-matter interaction is dominated by scattering processes. This exhibits that the optical properties of 3D graphene samples are directed by scattering, rather than the usual intrinsic absorption that occurs in the graphene layers. This is further supported by the absence of absorptive characteristics in the UV spectral region, which predicts the interband electronic transitions in graphene. The absence of such absorptive characteristics is due to the higher intrinsic roughness (>100 nm) related to interconnected graphene layers which are similar in nanoporous metal frameworks [7]. The 3DG architectures are effective absorbers in the microwave frequency range (i.e., 2 GHz–110 GHz). The frequency range is engaged for many critical applications, including radar-centered detections, satellite communications, and remote sensing [3]. It's interesting to note that 3DG structures with a nonporous structure display exceptional photosensitivity for increased light absorption and photo carrier transfer. Ito et al. [8] have reported that optimized 3DG exhibits a ~40-times higher light absorption than monolayer graphene materials. The photodetector based on 3D graphene validates extraordinary photo response of 3.10 × 10^4 A/W at room temperature and retains an excellent external quantum efficiency of 1.04 × 10^7%, which is higher than that of commercial silicon photodetector (~6.5 × 10^5%).

To improve the physicochemical properties of 3D graphene-based materials, nanocomposites of 3D graphene with technologically important materials can be developed. The 3D nanocomposite structures of graphene can offer objective-driven physicochemical properties. It can also exhibit high porosity, a large surface-to-volume ratio, and excellent electron and mass transfer materials during device operation. Polymers, metal, and metal oxides can easily be incorporated during the fabrication of the nanostructure of 3D graphene [9]. These nanocomposites promise wider applications such as energy storage, sensors, water treatment, catalysts, and electromagnetic interference (EMI) shielding. The EMI shielding materials are essential to address the EM pollution in our daily life. The shielding materials protects not only the electrical devices, but also the health of human being due to prolonged exposure to non-avoidable EM radiations. EM shielding is required for defense-related equipment seeking stealth technology. In general, EM shielding can be obtained using a conductor such as metal. The present state of the art requires the EM shielding material not only to be good in thermal and electrical conduction, but also flexible and lightweight. The research in this field employs composites of epoxy resin as EMI shielding materials as it offers good flexibility, thermal and electrical properties, easy processibility, and low cost. However, the shielding effectiveness (SE) needs tremendous improvement due to advancements in technology causing EM pollution and defense threat with rapid development. The shielding material can be improvised by adding nanofillers in epoxy resin. There are several works where the nanocomposites of epoxy resin with carbon nanotubes and graphene have been utilized. However, the improvement in SE was found to be minuscule. 3D graphene can be a suitable material due to its excellent electrical and thermal behavior, porous structure, and easy dispersibility in solvents. The 3D graphene can act as a template for developing polymer nanocomposite for EMI shielding applications. Wan et al. [10] have developed a 3 mm thick graphene aerogel-epoxy composite layer for an EMI shield. They reported the best SE to be around 30 dB. The low performance is due to poor conducting networks in such composites. In an interesting article by Liang et al. [11], a template method was reported for the fabrication of 3D graphene nanoplatelets/reduced graphene oxide foam/epoxy (GNPs/rGO/EP). The 3D framework enhances the EMI shielding remarkably with an SE value ~51 dB. The porous 3D structures exhibited excellent electrical conductivity (Fig. 1) and can entrap the EM waves by absorption and internal scattering in the nanocomposites. This ensures a very high degree of EMI shielding performance by the 3D graphene nanocomposites.

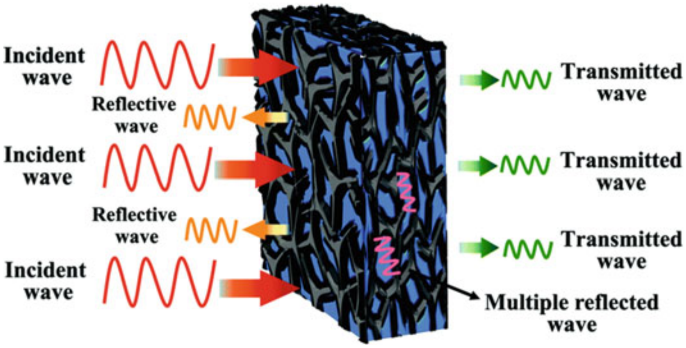

Fig. 1 Schematic of 3D graphene nanocomposites for electromagnetic shielding application. Adapted with permission [11], Copyright (2019), Royal Society of Chemistry

3 3D Graphene-Based Sensors

Due to its interesting physical properties, 3DG may offer a variety of sensing applications. It offers high electroactive surface area, good inner and outer surface contact with the analyte, ease of loading with (bio)catalysts, and strong electrochemical sensitivity. The 3D linked network provides many electron routes, allowing for quick and sensitive analyte detection. The interconnected open porosity of the 3D graphene may facilitate the kinetic diffusion and mass transfer of macromolecules. The porous network allows efficient absorption of small biomolecules as well as micromolecules. The high surface-to-volume ratio and the porous structure of the 3D graphene network amplify the interaction between gas molecules and the 3D network of sp^2 hybridized carbon atoms. Xing et al. [12] enhanced the sensitivity of a graphene-based optical fiber humidity sensor by employing a 3D graphene network as a cladding material. They observed enhancement in the response time and sensitivity compared to the conventional graphene cladding optical fiber-based humidity sensor. At present, 3D graphene is predominantly studied for gas sensing, biofuel cells, energy storage supercapacitors, electrochemical sensing, and battery applications [13]. It is a potential material for the electrochemical sensing of toxic heavy metals [14]. In terms of gases, 3D graphene is very sensitive to gases such as NO_2 and NH_3. The adsorption and desorption of the analyte gases on 3D graphene need to be accelerated to reduce the response and recovery times of the sensor [15]. Figure 2 shows the normalized change in electrical resistance ($\Delta R/R$) during the sensing of NH_3 and NO_2 at different concentrations. The recovery of the sensor is completely achieved by the Joule heating ~400 K [16].

Compared to the different graphene-based biosensors, 3D graphene exhibits the highest affinity for redox species mass transfer. 3D graphene has a larger surface area than its 2D equivalents. Thus, more enzymatic, and catalytic activities can take place at the surface of the materials. As a result, it is an excellent option for photoelectrochemical sensors for various bio-analytes and enzymes. Wang et al. [17] have

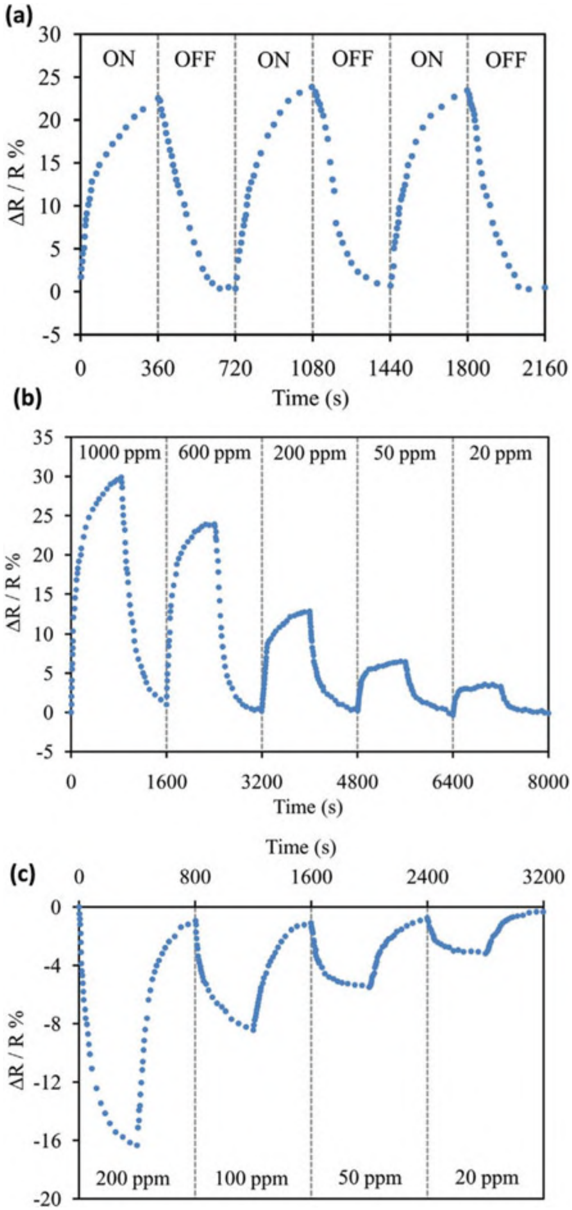

Fig. 2 **a** Normalized change in electrical resistance (ΔR/R) as a function of time for three cycles at a concentration of 1000 ppm of NH_3. **b**, **c** Sensing cycles for NH_3 and NO_2, respectively. Adapted with permission [16], Copyright (2011), Nature

developed a photo-electrochemical biosensor for studying the enzymatic activity of lipase. The immobilization of glycerol dehydrogenase on the photoelectrode was found to be easier due to the huge specific surface area of 3D graphene. The sensor showed outstanding optoelectronic characteristics and clear signal amplification. The photoelectric response of the sensor in the presence of glycerol was activated by a redox interaction between the enzyme and the substrate that results in an electron transfer under the influence of light. The photocurrent was linearly associated with the lipase activity throughout the 0.1–6 U/mL range of enzyme activity, proving the utility of the biosensor with a detection limit as low as 0.069 U/mL. The above result indicates that the 3D graphene is highly responsive toward the external incident light. Therefore, the application of 3D graphene structures for optical and optoelectronic sensing is clearly foreseen.

The 3D nanoarchitecture of graphene is also being efficiently employed for Surface Enhanced Raman Spectroscopy (SERS). In 3D graphene, high-intensity hot spots magnify the SERS signals remarkably. These high-intensity hot spots are formed due to broad plasmonic peaks from 550–850 nm. The plasmonic peak broadening signifies the aggregation of nanomaterials; these aggregations are very conducive to the formation of amplified Raman signals. Thus, the 3D graphene nano architectures have the potential to be employed in the SERS of different bio conjugates and analytes in future research. Fan et al. [18] developed a chemically modified 3D plasmonic graphene architecture to employ as a selective sensor for rotavirus using SERS. They observed that extremely selective and sensitive virus detection is conceivable due to the presence of broad plasmonic peaks and high-intensity hot spots in the magneto-plasmonic 3D graphene configuration system.

The SERS substrate should be stimulated at its localized surface plasmon resonance (LSPR) peak for the most effective surface-enhanced Raman scattering. In the conventional SERS platforms, metal nanoparticles are employed for the sensitive detection of analytes. In recent years, it has been observed that the practice of graphene/metal hybrid structure gives a much higher field enhancement. This enhancement ascends due to the strong coupling between the metallic nanoparticles and the graphene layer. The 3D graphene structures, due to their large specific surface area and improved optical scattering, are being employed for SERS-based chemical sensing. The dispersed light from many metallic nanoparticles located on multi-layer graphene sheets in 3D graphene is incorporated cumulatively, leading to a greater Raman enhancement factor. Srichan et al. [19] studied the field enhancement in silver/3D graphene foam composite SERS platform and compared the results with the conventional silver/graphene and silver/silicon substrates. They observed approximately 10^4 times Raman signal enhancement compared to the other SERS substrate. They further employed the fabricated substrate for low-level detection of methylene blue. For sensing studies, the sensitivity of the silver/3D graphene foam composite offered the highest sensitivity and best lower-level detection.

Due to the absence of a bandgap in graphene, fluorescence has not yet been seen in pristine two-dimensional (2D) or three-dimensional (3D) graphene. However, creating fluorescent-labeled graphene by noncovalent or covalent alteration is one of the best techniques to adjust the optical characteristics of graphene. It has been observed, most organic compounds have a limited lifespan, and more significantly, when adsorbed on graphene sheets, their fluorescence is quickly satiated because of photoinduced electron transfer or energy transfer to graphene. Therefore, to encourage fluorescence, 2D graphene is doped with some rare earth elements. Rare earth elements such as lanthanides ion compounds have been one of the finest families of inorganic luminous metals. They attracted attention due to their high quantum yields, extended luminescence durations, considerable stokes shifts, and outstanding chemical stabilities. Therefore, to study the photoluminescence of 3D graphene, Wang et al. [20] have presented a one-step hydrothermal method for preparing trivalent Europium (Eu)-complexed graphene in a 3D self-assembled architecture. In addition to altering the inherent structure of 3D self-assembled graphene and adding active emission sites, complexing it with Eu-ions results in unique phenomena and abilities. The outcomes show that doping Eu-ion is a feasible method to enhance graphene's photoluminescence performance. Its potential use in optoelectronics and bio-sensing is indicated by its dual optical activities, such as self-luminescence and quenching of organic dye fluorescence.

The existence of intrinsic 2D Dirac plasmons in 3D graphene shows strong and tuneable plasmonic absorption from terahertz to mid-infrared through appropriate doping and pore size control. Thus, the nonporous 3D graphene can be used to develop plasmonic-based sensors. Plasmonic sensing is based on the interaction of light with free electrons in the graphene lattice. Because of its large surface area, 3D graphene is the potential candidate to be engaged as a substrate for plasmonic sensing [5]. This can improve the interaction between light and the graphene surface. The plasmonic behaviors of graphene are similar to those generated at the metal–dielectric interface. Additionally, the plasmonic waves on graphene exhibit low losses in a range of frequencies and better mechanical flexibility. Graphene shows a better light–matter interaction. These attributes make graphene suitable for nanophotonic and waveguide applications. Several 3D graphene structures have been proposed with the possibility of better waveguide applications. In an interesting article [21], a 3D graphene structure has been reported to generate transverse electric and transverse magnetic graphene plasmon polaritons. The proposed structure can be used for the detection of electromagnetic wave detection. The plasmon polaritons are found to be stable under temperature variation. Such structure can be used for photonic devices operating in extreme environments. The excellent optical properties of 3DG in addition to the superior analyte adsorption capabilities can ensure that it is a wonderful functional material for sensing applications through the efficient SPR optical phenomenon. The Kretschmann configuration in an angular interrogation-based SPR sensor consists of a functional layer deposited over the gold surface. The selectivity and sensitivity of the sensor depend on the nature of the functional layer. At the resonance, the plasmonic field generated in the gold film gets perturbed due to the interaction of the analytes with that of the functional layer. Such interaction may change the refractive index which can be measured at a very high resolution using the SPR phenomenon. The extent of the plasmonic field in the sensing medium decays rapidly, and therefore, the thickness of the functional layer should be optimal for perception by the SPR sensing instrument. Although 3DG can be an ideal functional layer for analyte adsorption capability and exceptional electrical and optical properties, the bulk nature of the 3DG can reduce the SPR perception even due to the adsorption of the analytes. It is, therefore, essential to deposit the 3DG over the gold film through a bottom-up mechanism that ensures good control over the thickness. Some of the bottom-up deposition techniques are Langmuir–Blodgett and chemical vapor deposition mechanisms. Using the bottom-up deposition techniques often a functionalized film of the monolayer, bilayer, and twisted bilayer graphene is obtained. These films of graphene can be considered as a 2D layer that exhibits physicochemical properties similar to 2D graphene. It is, therefore, essential to understand the bio-sensing performance of the graphene in its fundamental geometrical states, i.e., 2D graphene in monolayer and bilayer graphene (MLG) states. Additionally, the electrical and optical properties of the BLG system are found to be dependent on the in-plane twist angle between the individual layers. The understanding of such a graphene system may enable us to develop the next-generation SPR biosensors using 3GD as the functional materials. Hence, further discussion follows some preliminary studies on bio-sensing using 2D graphene as the functional material.

2D Graphene: The superior optical properties of graphene are due to its unique two-dimensional band structure. Its exceptional optical features such as tuneable broadband absorption, saturation absorption, polarization-dependent effects, and fluorescence have drawn scientific attention. It shows a resonant optical response to photons at any frequency in the broadband spectrum [22]. The linear optical characterization shows that it has high absorbance in the incident visible light [23]. The reflectance and absorption of graphene monolayer depend on Drude–Boltzmann conductivity for infrared incidence and interband absorption for lower wavelength. The absorption spectra for the monolayer graphene show three major peaks as shown in Fig. 3. The low energy peaks (2.62 eV and 4.45 eV) are attributed to the π–$\pi*$ transition and the high energy peak (14 eV) is attributed to σ–$\sigma*$ interband transitions. The corresponding variation in the real (n) and imaginary (γ) parts of the refractive index is consistent with Lorentz's electron model of the origin of the refractive index (RI).

The broadened spectra of $\boldsymbol{n}$ shown in Fig. 3 are caused by an empty conduction band and a completely filled valence band in monolayer graphene, which generates free electron–hole pairs that are ready to be stimulated by incoming photons. The optical characteristics of graphene are also dependent on its structure. It varies with the number of graphene layers due to stacking. The bilayer graphene has different optical properties based on the type of stacking. For instance, AA-type stacking exhibits nearly monolayer type of behavior whereas AB-stacked bilayer has different behavior as compared to that of monolayer graphene. This variation in properties is due to the difference in the band structure of AA and AB stacking of the bilayer graphene. In AA stacking, the band structure shows two identical copies of monolayer bands that are vertically offset from each other, with Dirac cones located at the edge of the Brillouin zone. On the other hand, the band structure in AB stacking appears as a pair of intersecting parabolic bands, with additional parabolic bands located further away from these intersecting bands. Further, the band structure gets more complex if the bilayer system contains an additional relative in-plane twist between the layers. The optical properties are also altered due to such twists. The development of the Moiré pattern because of the application of relative in-plane twist in the bilayer graphene suggests that the optical and electrical characteristics can be altered as a function of the twist angle. If a relative in-plane twist is applied

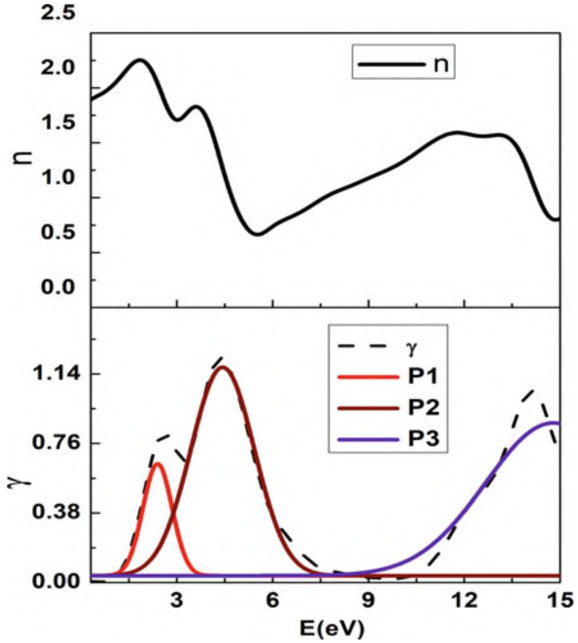

Fig. 3 Real index of refraction (n) and absorption spectra (γ) of monolayer graphene, where the refractive index ($r = n + i\gamma$). Adapted with permission [24], Copyright (2022), IOP

in the AA-type of stacked bilayer graphene, it shows a dominant dielectric material type behavior for a wide range of incident wavelengths, whereas in AB, it has semi-metallic and metallic behavior depending on the twist angle [24]. Thus, depending on the relative in-plane twist angle, twisted bilayer graphene exhibits either a semi-metallic, dielectric, metallic, or semiconducting behavior, over a range of incident energy photons. Such flexibility in bilayer graphene promises a range of innovative applications including waveguides, sensors, and modulators.

Monolayer and bilayer graphene-based optical sensors: Optical sensors based on graphene exploit its excellent optical properties which are generally designed to analyze the energy transfer mechanism between the source and the material. Graphene has ultrahigh luminescence quenching efficacy, a large planar surface that permits simultaneous adsorption of multiple analytes to achieve detection in the same solution. Graphene possesses excellent capabilities for the adsorption of biomolecules due to the π–π stacking and hydrophobic interactions. The three primary types of graphene-based optical sensors available are surface plasmon resonance (SPR) sensors [25], graphene-based photoluminescence sensors [26], and graphene-based spatial light sensors [27]. The SPR sensor is highly sensitive, label-free, and capable of real-time measurement. SPR sensors can be used for real-time monitoring, rapid detection, high sensitivity, tracking and observing ligand stability, maintaining reaction equilibrium, and a variety of other applications. In a conventional SPR system, a metallic layer (preferably Au or Ag) of optimal thickness is coupled with a high-index glass prism. Surface plasmon (SP) waves are generated at the metal–dielectric interface due to the incident EM radiation. These SP waves are due to the collective oscillations of free charges at the metallic surface. When the wavevector of the incident radiation and the SP waves exhibit a matching condition, a resonance is established. At resonance, the maximum energy is transferred from the incident wave to the SP wave, leading to the extinction of the unique incident electromagnetic wave from the spectrum. The conventional Kretschmann configuration of SPR involves using a p-polarized monochromatic electromagnetic wave to probe the metal–dielectric interface via a coupling medium, with angular interrogation being the typical approach. The SPR effect is determined by changing the angle of incidence and measuring the reflected light intensity. The reflected intensity reduces to zero at the point of resonance, which is recorded as the resonance angle (RA). The resonance angle is unique to the individual metal-dielectric interaction. During sensing, analyte adsorption on the metal surface causes a change in the dielectric property. A change in the dielectric property is observed as a result of the analyte adsorption on the metal surface during sensing. Such changes can shift the resonance angle (RA) accordingly. The change in RA is used to compute the change in RI due to the adsorption of the analyte using Fresnel's equations [28]. Therefore, a RI vs concentration of the analyte calibration curve can be obtained. The interaction of the analyte at the interface plays an important role in the sensing performance of SPR instruments. In the conventional metal and dielectric-based SPR, gold is most recurrently preferred as the plasmonic material for the generation of SP waves. It has several advantages over other materials, such as chemical inertness, ease of functionalization, and high stability in aqueous media. However, gold possesses a very low affinity toward many analytes. Thus, to increase the analyte affinity, the gold surface can be functionalized with a suitable layer. Recently, it has been studied that graphene may be employed as a biomolecular recognition element (BRE) to functionalize the metal film. Graphene has a high surface-to-volume ratio and a rich π electron conjugation. It enhances the binding affinity of bio-analytes through π-π interaction. Thus, graphene is largely employed as a functionalized layer over the metal film for sensitivity enhancement. There are many advantages of using graphene-functionalized gold surfaces during sensing measurements, they are:

1. In contrast to gold, graphene has a very high surface-to-volume ratio, which is anticipated to be advantageous for the effective adsorption of biomolecules.
2. The carbon-based ring structures in organic and biomolecules might enable efficient π stacking interaction with hexagonal graphene.
3. The control over the number of graphene layers transferred to the metal interface enables control of the SPR response and its sensitivity.

Thus, the employment of graphene as the functionalized layers seem to be appropriate for SPR sensing applications [25, 29]. In 2010, Wu et al. [30] investigated the effect of graphene layers on sensitivity enhancement in the gold-prism-based SPR. They presented that graphene monolayer-coated over gold surface-based bio-sensing chip had a larger SPR angle shift than traditional gold chips for the same refractive index variation ($n = 0.005$). The calculation also shows that the graphene on gold SPR biosensors exhibits $(1 + 0.025\ L) \times t$ times more sensitivity than standard gold

SPR biosensors (where t > 1, L-number of graphene layer). He et al. [29] proposed a point-of-care device employing graphene-coated SPR chips to detect folic acid protein (FAP). By utilizing the exceptional properties of graphene, a highly selective and sensitive SPR device was observed for the detection of serum folate biomarkers. The interaction due to π-stacking on the graphene-coated SPR chip and analyte in serum allowed femtomolar (fM) detection of albumin mixtures. Thus, the detection of very low concentrations is also possible using graphene-functionalized gold chips. It is rational to presume that increasing the number of graphene layers might increase the sensitivity. However, the SPR curve broadens as we increase the number of graphene layers which makes it difficult to measure the resonant angle/wavelength. Also, one of the most important parameters in SP generations is the strength of the evanescent waves at the metal–dielectric interface and the decay length of these evanescent waves in the sensing medium. If the decay length is small, the detection in the RI change due to the adsorption of the analyte will not be observable. If the decay length is smaller than the thickness of the functionalized layer, the evanescent waves will not be perturbed by the adsorption of the analyte. Therefore, if the sensing layer has a large thickness even in the case of stacked graphene, the sensitivity of the SPR sensor would tend to decrease. Therefore, stacking a few layers of graphene may boost sensitivity, however, using bulk or macroscopic structures will reduce the effectiveness of the sensor. The bulk behavior of 3DG would limit the perception of the interaction of evanescent waves with the analytes at the interface. Therefore, there will be minuscule responses that cannot be measured even with SPR technology.

Although, graphene-coated gold chips can enhance the adsorption affinity of the analytes. However, sensitivity and figure-of-merit (FOM) decrease in the aqueous medium when graphene is coupled with a gold chip [31, 32]. Therefore, for the fabrication of a highly sensitive device, if the plasmonic field can be itself generated in the graphene layer system, it can operate both as a plasmonic material and BRE through π-π interaction.

Plasmons generation in graphene

Due to the two-dimensional (2D) character of graphene, surface plasmons excited in graphene are much more strongly confined than those in traditional noble metals because of the collective excitations. The plasmons generated in graphene are confined to a volume million times smaller than the diffraction limit. This strong confinement facilitates efficient light–matter interaction and offers minimal losses and effective wave localization up to mid-infrared frequencies [33]. Since the carrier densities in graphene can also be adjusted by electrical gating and doping, the tunability of surface plasmons would be the most significant benefit of graphene [34]. Inspired by these findings, a few research groups [35–37] have performed SPR-based sensing using graphene as the plasmonic material. Maleki et al. [35] have deposited a double-layer graphene nanograting on a dielectric substrate as the basis of the gas sensor. They were able to monitor the sensitivity of 430 nm/RIU over incident radiation of 1–2 μm. Wu et al. [36] have proposed an SPR sensor that uses an array of graphene nanoribbons over a SiO_2 substrate operating in the infrared range. They recorded a sensitivity of 4720 nm/RIU and a FOM of 5.43. Kumar et al.

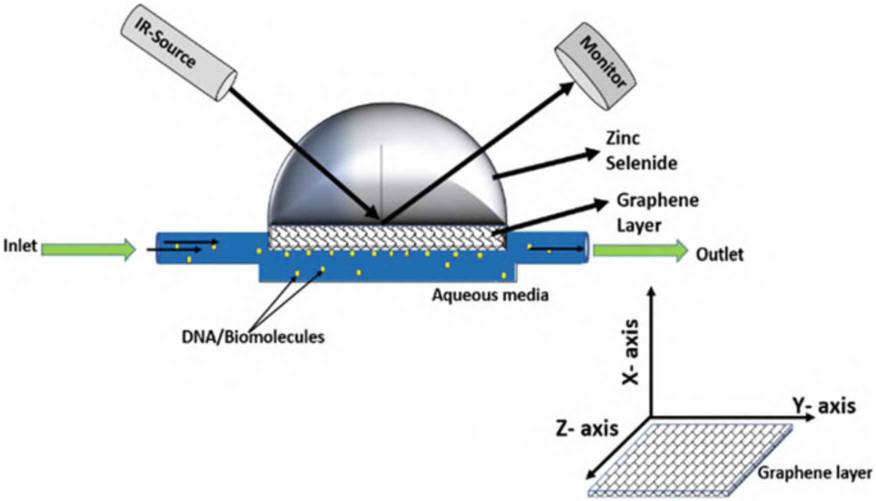

Fig. 4 A schematic diagram showing the SPR sensor where ZnSe is employed as the coupling prism. Graphene as both plasmonic and biorecognition element, incident electromagnetic infrared source, detector, and flow cell. Inset shows the geometry, viz. XY as the plane of incidence, and YZ as the surface plane of the graphene layer. The analytes are dispersed through the flow cell. Adapted with permission [37], Copyright (2022), Springer

[37] have proposed a novel and highly sensitive graphene-ZnSe-based SPR sensor for biomolecule detection (Fig. 4). They measured the sensitivity of 20,000 nm/RIU for monolayer graphene, which is the highest in the class of graphene-based SPR sensors available in the literature. They observed the FOM of 15 for the wavelength interrogation Kretschmann configuration of the SPR device operating in an aqueous medium.

Figure 5 shows the observed spectrum for the proposed graphene-based SPR configuration [37]. The resonant wavelength is observed at 13.7 μm. The two-dimensional surface field profile at resonance also shows anisotropic behavior which is consistent with the conventional gold-based SPR system [38].

Therefore, the graphene monolayer itself over a semiconducting substrate can be employed for plasmon generation. Additionally, the BRE features for attracting bio-analytes have made it a more suitable functional material for bio-sensing using the SPR technology. This may not only reduce device size, but also the fabrication complexity. The number of layers can be increased optimally to enhance the sensing performance. The bilayer graphene (BLG) and twisted–BLG (TBLG) exhibit interesting physicochemical properties which can be altered as a function of in-plane twist angle. Such a BLG system can lead to the development of next-generation sensors. Kumar et al. [37] have proposed a bilayer graphene-based SPR sensor. They observed that bilayer graphene does not show any drastic change in the sensitivity irrespective of the type of stacking (Bernal or non-Bernal). Thus, to alter the sensing characteristics, a relative in-plane twist can be added between the two graphene layers of the

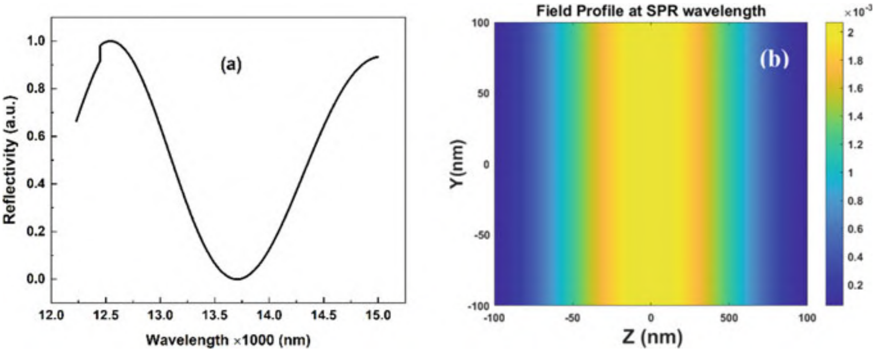

Fig. 5 **a** SPR spectrum for the proposed graphene-based SPR configuration and **b** two-dimensional surface EM field profile over the graphene monolayer surface measured at resonance. Reprinted with permission [37], Copyright (2022), Springer

BLG system. In the case of non-Bernal stacking, the optical property of the graphene system does not change drastically due to the relative in-plane twist. However, in the case of Bernal stacking, the in-plane twist plays a major role in altering its optical properties. A phase diagram depicting the different optical characteristics of both stacking with varied relative in-plane twists (θ) is shown in Fig. 6 [24].

From Fig. 6, it is evident that for non-Bernal stacking, the BLG system exhibits mostly dielectric behavior, irrespective of in-plane twist and incident photon energy. But, in Bernal stacking, the material property varies. It showed semi-metallic behavior between 13–14 μm of incident wavelength. This range of incident photon energy also corresponds to the SPR wavelength for the monolayer and BLG system. Thus, it will be interesting to probe the system in this range for studying SPR sensing. Thus, for different in-plane twists, Kumar et al. [37] studied the sensitivity of SPR-based sensors where the twisted graphene system was employed both as BRE and plasmonic material. They proposed that for Bernal stacked twisted bilayer graphene, the sensitivity near the magic angle (1°) is maximum. They observed a sensitivity of 29,120 nm/RIU sensitivity with 23.5 FOM which is much higher than the monolayer/bilayer graphene system. The collective oscillations of plasmons near the magic angle is maximum. Also, near the magic angle, the time-periodic electric field causes electrons to vibrate around their equilibrium positions, resulting in an interband transition. So, the oscillating electrons create a strong electric field at resonance, allowing the oscillation to continue for a longer period. This resonant action produces collective modes known as interband plasmons [39]. Therefore, the interaction with the adjacent dielectric is amplified due to this strong collective mode oscillation. A comparative data for the sensitivity for various twists (θ) is shown in Fig. 7. It is observed that the sensitivity for smaller in-plane twists is comparatively higher than the sensitivity for larger in-plane twists.

The decrease in sensitivity for larger in-plane twists is due to the decrease in the oscillation of the collective mode and the dominant metallic behavior as shown in Fig. 6.

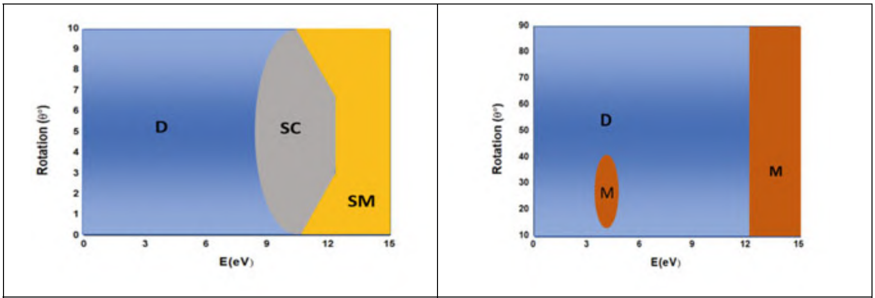

(a) Non-Bernal (AA) stacking with small in plane twist

(b) Non-Bernal (AA) stacking with large in-plane twist

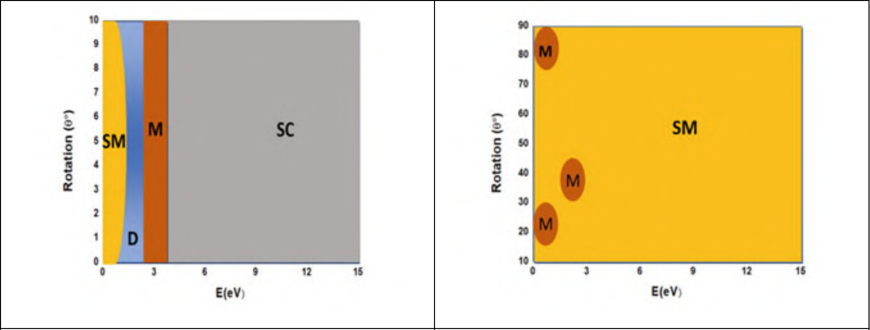

(c) Bernal (AB) stacking with small in-plane twist

(d) Bernal (AB) stacking with large in-plane twist

Fig. 6 A phase diagram representation of diverse material properties observed for different in-plane twists (θ) in Bernal and non-Bernal stacking. (D = Dielectric, M = Metallic, SC = Semiconducting, and SM = Semi-metallic). Here *E* is the energy of the incident photons. Adapted with permission [24], Copyright (2022), IOP

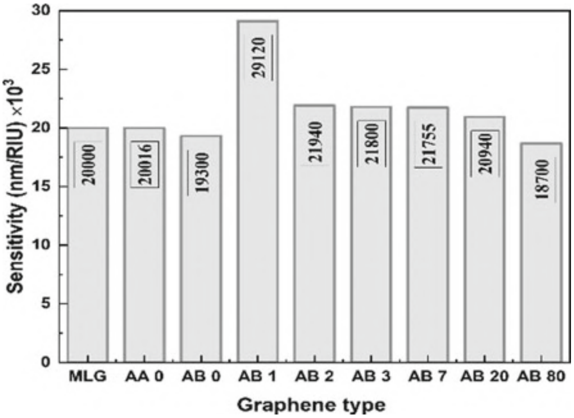

Fig. 7 Sensitivity of various graphene-based SPR systems. Corresponding values of sensitivity are as mentioned. The numeric value with the symbol AB represents the twist angle (θ) in degrees. Adapted with permission [37], Copyright (2022), Springer

Future Scope and Challenges: 3DG can be considered a remarkable material that can find numerous novel applications. The unique morphology, very high porosity, and excellent electrical, thermal, and optical properties of 3DG have ranked the material among the top for device fabrication. However, the vast surface area and high porosity of 3DG may enhance the possibility of non-specific binding of analytes, resulting in misleading positive or negative findings in sensing applications. Therefore, careful data analysis is required for isolating the signals for specific and non-specific interactions. Surface functionalization is frequently necessary to increase the sensitivity and selectivity of sensors. Still, the complex surface structure of 3DG may make it more challenging to get functionalized like any other material. Development of 3DG using the existing protocols can yield material with different porosity and the network which may alter the physical properties beyond the tolerance. 3DG is a relatively new and specialized material, which may make it more expensive than other materials typically used for SPR-based sensing applications. Therefore, the fabrication of 3GD from the bottom-up approach can provide a good level of confidence. 3DG can be fabricated through layer-by-layer assembly of graphene. Most of the reported studies on monolayer and BLG systems are based on theoretical calculations. The fabrication of devices based on monolayer, BLG, and TBLG is challenging and a good number of efforts are being invested in this direction. The monolayer and bilayer state of graphene can be controlled experimentally by a few advanced thin film fabrication techniques such as Langmuir–Blodgett (LB) deposition [40] and chemical vapor deposition [41, 42]. In-plane twisting of the graphene layers in BLG is another challenge in this field. The twists can be applied by the advanced LB or CVD technique. The SPR sensors employing the monolayer, BLG, or TBLG still require the immobilization of suitable ligands to make the sensing selective, rapid, and sensitive. A suitable protocol can be developed for the immobilization and stable sensing measurement using the SPR technology.

The fundamental studies on monolayer, BLG, and TBLG yield better scenarios for the development of the next-generation sensor. Although the 3DG is a random network of 2D graphene sheets, it will be very interesting to study 3D graphene with twisted bilayers at a magic angle. Such a state of graphene will be important not only for fundamental studies, but also for the development of efficient biosensors.

Acknowledgments The authors are thankful to the Physics Department, BITS Pilani, for supporting Lumerical software. AK is thankful to SERB for the fellowship (CRG/2018/000755).

References

1. Cao, M.-S., Wang, X.-X., Cao, W.-Q., Yuan, J.: Ultrathin graphene: electrical properties and highly efficient electromagnetic interference shielding. J. Mater Chem. C **3**, 6589 (2015). https://doi.org/10.1039/c5tc01354b
2. Mak, K.F., Ju, L., Wang, F., Heinz, T.F.: Optical spectroscopy of graphene: From the far infrared to the ultraviolet. Solid State Commun. **152**, 1341–1349 (2012). https://doi.org/10.1016/j.ssc.2012.04.064

3. Zhang, Y., Huang, Y., Zhang, T., et al.: Broadband and tunable high-performance microwave absorption of an ultralight and highly compressible graphene foam. Adv. Mater. **27**, 2049–2053 (2015). https://doi.org/10.1002/ADMA.201405788
4. Huang, Z., Chen, H., Huang, Y., et al.: Ultra-broadband wide-angle terahertz absorption properties of 3D graphene foam. Adv. Funct. Mater. **28**, 1–8 (2018). https://doi.org/10.1002/adfm.201704363
5. D'Apuzzo, F., Piacenti, A.R., Giorgianni, F., et al.: Terahertz and mid-infrared plasmons in three-dimensional nanoporous graphene. Nat Commun **8**, 1–7 (2017). https://doi.org/10.1038/ncomms14885
6. Tomarchio, L., Macis, S., D'Arco, A. et al.: Disordered photonics behavior from terahertz to ultraviolet of a three-dimensional graphene network. NPG Asia Mater., 13 (2021). https://doi.org/10.1038/s41427-021-00341-9
7. Ron, R., Haleva, E., Salomon, A.: Nanoporous metallic networks: fabrication, optical properties, and applications. Adv. Mater., 30 (2018). https://doi.org/10.1002/ADMA.201706755
8. Ito, Y., Zhang, W., Li, J., et al.: 3D Bicontinuous Nanoporous Reduced Graphene Oxide for Highly Sensitive Photodetectors (2015). https://doi.org/10.1002/adfm.201504146
9. Xiao, W., Li, B., Yan, J., et al.: Three dimensional graphene composites: preparation, morphology and their multi-functional applications. Compos. Part A Appl. Sci. Manuf. **165**, 107335 (2023). https://doi.org/10.1016/J.COMPOSITESA.2022.107335
10. Wan, Y.J., Yu, S.H., Yang, W.H., et al.: Tuneable cellular-structured 3D graphene aerogel and its effect on electromagnetic interference shielding performance and mechanical properties of epoxy composites. RSC Adv. **6**, 56589–56598 (2016). https://doi.org/10.1039/C6RA09459G
11. Liang, C., Qiu, H., Han, Y., et al.: Superior electromagnetic interference shielding 3D graphene nanoplatelets/reduced graphene oxide foam/epoxy nanocomposites with high thermal conductivity. J. Mater Chem. C Mater **7**, 2725–2733 (2019). https://doi.org/10.1039/C8TC05955A
12. Xing, Z., Zheng, Y., Yan, Z., et al.: High-sensitivity humidity sensing of microfiber coated with three-dimensional graphene network. Sens Actuators B Chem. **281**, 953–959 (2019). https://doi.org/10.1016/J.SNB.2018.11.057
13. Baig, N., Saleh, T.A.: Electrodes modified with 3D graphene composites: a review on methods for preparation, properties and sensing applications. Microchim. Acta, 185 (2018).https://doi.org/10.1007/s00604-018-2809-3
14. Yang, Y., Kang, M., Fang, S., et al.: Electrochemical biosensor based on three-dimensional reduced graphene oxide and polyaniline nanocomposite for selective detection of mercury ions. Sens Actuators B Chem. **214**, 63–69 (2015). https://doi.org/10.1016/j.snb.2015.02.127
15. Dong, Q., Xiao, M., Chu, Z. et al.: Recent progress of toxic gas sensors based on 3d graphene frameworks. Sensors, 21 (2021). https://doi.org/10.3390/s21103386
16. Yavari, F., Chen, Z., Thomas, A.V. et al.: High sensitivity gas detection using a macroscopic three-dimensional graphene foam network. Scientific Reports **1**:1 1:1–5 (2011). https://doi.org/10.1038/srep00166
17. Wang, L., Zhang, H., Li, Z., et al.: Development of a three-dimensional graphene-based photoelectrochemical biosensor and its use for monitoring lipase activity. LWT **170**, 114076 (2022). https://doi.org/10.1016/J.LWT.2022.114076
18. Fan, Z., Yust, B., Nellore, B.P.V., et al.: Accurate identification and selective removal of rotavirus using a plasmonic-magnetic 3D graphene oxide architecture. J. Phys. Chem. Lett. **5**, 3216–3221 (2014). https://doi.org/10.1021/JZ501402B/SUPPL_FILE/JZ501402B_SI_001.PDF
19. Srichan, C., Ekpanyapong, M., Horprathum, M. et al.: Highly-sensitive surface-enhanced Raman spectroscopy (SERS)-based chemical sensor using 3d graphene foam decorated with silver nanoparticles as SERS substrate. Scientific Reports **6**:1 6:1–9 (2016). https://doi.org/10.1038/srep23733
20. Wang, D., Gao, H., Roze, E., et al.: Synthesis and photoluminescence of three-dimensional europium-complexed graphene macroassembly. J. Mater Chem. C Mater **1**, 5772–5778 (2013). https://doi.org/10.1039/C3TC30732H

21. Zhang, L., Wang, L., Liu, D. et al.: Plasmon polaritons in 3D graphene periodic structure 42, 210–225 (2022). https://doi.org/10.1080/02726343.2022.2082099
22. Wang, F., Zhang, Y., Tian, C., et al.: (2008) Gate-variable optical transitions in graphene. Science **320**, 206–209 (1979). https://doi.org/10.1126/SCIENCE.1152793/SUPPL_FILE/WANG_SOM.PDF
23. Kumar, V.: Linear and nonlinear optical properties of graphene: a review. J. Electron. Mater **50**, 3773–3799 (2021). https://doi.org/10.1007/s11664-021-08904-w
24. Kumar, A., Manjuladevi, V., Gupta, R.K.: Refractive index of graphene AA and AB stacked bilayers under the influence of relative planar twisting. J. Phys. Condens. Matter **34**, 15302 (2022). https://doi.org/10.1088/1361-648X/ac2d5f
25. Szunerits, S., Maalouli, N., Wijaya, E., et al.: Recent advances in the development of graphene-based surface plasmon resonance (SPR) interfaces. Anal. Bioanal. Chem. **405**, 1435–1443 (2013). https://doi.org/10.1007/s00216-012-6624-0
26. Li, Z., He, M., Xu, D., Liu, Z.: Graphene materials-based energy acceptor systems and sensors. J. Photochem. Photobiol. C **18**, 1–17 (2014). https://doi.org/10.1016/J.JPHOTOCHEMREV.2013.10.002
27. de Sanctis de, A., Mehew, J.D., Craciun, M.F., Russo, S.: (2018) Graphene-based light sensing: fabrication, characterisation, physical properties and performance. Materials **11**, 1762 11 1762 (2018). https://doi.org/10.3390/MA11091762
28. Devanarayanan, V.P., Manjuladevi, V., Gupta, R.K.: Surface plasmon resonance sensor based on a new opto-mechanical scanning mechanism. Sens. Actuat. B Chem. **227**, 643–648 (2016). https://doi.org/10.1016/J.SNB.2016.01.027
29. He, L., Pagneux, Q., Larroulet, I., et al.: Label-free femtomolar cancer biomarker detection in human serum using graphene-coated surface plasmon resonance chips. Biosens. Bioelectron. **89**, 606–611 (2017). https://doi.org/10.1016/j.bios.2016.01.076
30. Wu, L., Chu, H.S., Koh, W.S. et al.: Highly sensitive graphene biosensors based on surface plasmon resonance. Opt. Express **18**(14), 14395–14400 (2010). https://doi.org/10.1364/OE.18.014395
31. Saeed, W., Abbasi, Z., Majeed, S., et al.: An insight into the binding behavior of graphene oxide and noble metal nanoparticles. J. Appl. Phys. **129**, 125302 (2021). https://doi.org/10.1063/5.0041894
32. Vanin, M., Mortensen, J.J., Kelkkanen, A.K., et al.: Graphene on metals: A Van Der Waals density functional study. Phys. Rev. B Condens. Matter Mater Phys. **81**, 1–4 (2010). https://doi.org/10.1103/PhysRevB.81.081408
33. Jablan, M., Buljan, H., Soljačić, M.: Plasmonics in graphene at infrared frequencies. Phys. Rev. B Condens. Matter Mater Phys. **80**, 245435 (2009). https://doi.org/10.1103/PHYSREVB.80.245435/FIGURES/5/MEDIUM
34. Koppens, F.H.L., Chang, D.E., García De Abajo, F.J.: Graphene plasmonics: a platform for strong light-matter interactions. Nano Lett. **11**, 3370–3377 (2011). https://doi.org/10.1021/NL201771H/SUPPL_FILE/NL201771H_SI_001.PDF
35. Mokhtari, A., Mehran, M., Maleki, M.: Design of a near-infrared plasmonic gas sensor based on graphene nanogratings. JOSA B **37**(11), 3478–3486 (2020). https://doi.org/10.1364/JOSAB.401589
36. Wu, J., Zhou, C., Yu, J., et al.: Design of infrared surface plasmon resonance sensors based on graphene ribbon arrays. Opt. Laser Technol. **59**, 99–103 (2014). https://doi.org/10.1016/J.OPTLASTEC.2013.12.019
37. Kumar, A., Gupta, V.M.: The effect of relative in-plane twisting in graphene bilayer on sensing using surface plasmon resonance Plasmonics **1**, 1–12 (2022).https://doi.org/10.1007/S11468-022-01760-2/TABLES/2
38. Kumar, A., Gupta, R.K., Manjuladevi, V., Joshi, A.: Surface plasmon resonance for in-plane birefringence measurement of anisotropic thin organic film. Plasmonics **16**, 1023–1028 (2021). https://doi.org/10.1007/s11468-021-01373-1
39. Stauber, T., Kohler, H.: Quasi-flat Plasmonic bands in twisted bilayer graphene. Nano Lett **16**, 6844–6849 (2016). https://doi.org/10.1021/acs.nanolett.6b02587

40. Poonia, M., Manjuladevi, V., Gupta, R.K.: Ultrathin film of carboxylated graphene at air-water and air-solid interfaces. Surfaces Interfaces **13**, 37–45 (2018). https://doi.org/10.1016/J.SURFIN.2018.07.007
41. Fu, Y., Hansson, J., Liu, Y. et al.: Graphene-based biosensors. 2d Mater **7**, 040401. https://doi.org/10.1088/2053-1583/ABA3BF
42. Kuila, T., Bose, S., Khanra, P., et al.: Recent advances in graphene-based biosensors. Biosens. Bioelectron. **26**, 4637–4648 (2011). https://doi.org/10.1016/j.bios.2011.05.039

3D Graphene for Flexible Sensors

Ahmad Hussain, Adeela Naz, Nawishta Jabeen, and Jazib Ali

Abstract Recently, the importance of research for graphene-based materials and their applications has risen especially for flexible and wearable sensors. There exist several features which make it a promising material for devices including lightweight, cost-effective fabrication, heat resistance, and flexibility. Graphene in the form of three-dimensional (3D) composites or hybrid materials is investigated as a useful material to be utilized in different types of sensors including flexible humidity, biological, piezoelectric, electronic, piezoresistive, and pressure sensors. But the fabrication of flexible, super-elastic, and stable 3D graphene-based designs is challenging to date owing to structural distortion or substantial plastic bending and deformation. Integration of various morphologies, modifications in the synthesis techniques, and dopants/additives are employed to surmount the fundamental effects of high deformation in graphene-based materials for the utilization of wearable and flexible sensors. In this chapter, the focus will lie to discuss the till date achievements and methodologies of 3D graphene-based flexible sensors, their synthesis, and their performances for various applications.

Keywords Graphene · Flexible · Piezoresistive · Strain · Humidity · Sensors

---

A. Hussain · A. Naz
Department of Physics, The University of Lahore, Sargodha Campus, Sargodha 40100, Pakistan

N. Jabeen
Department of Physics, Fatima Jinnah Women University Rawalpindi, Rawalpindi 46000, Pakistan

J. Ali (✉)
Center for Hybrid and Organic Solar Energy (CHOSE), University of Rome Tor Vergata, 00133 Rome, Italy
e-mail: jazibali028@gmail.com

© The Author(s), under exclusive license to Springer Nature Switzerland AG 2023

R. K. Gupta (ed.), *3D Graphene*, Carbon Nanostructures,
https://doi.org/10.1007/978-3-031-36249-1_8

1 Introduction

3D functional systems like sensors and actuators have attained rapid development in the past few decades because of their excessive utilization in robotics [1, 2], memory and logic devices, portable technology [3, 4], flexible medical equipment [5, 6], tissues manufacturing [7, 8], and energy storage/harvesting devices [9, 10]. Complex 3D structures are essential as the main building blocks of functioning systems or devices due to the advantages provided by their geometrical shapes. In line with this development, Andre and Konstantin at the University of Manchester focused their research on such materials and described the significance of graphene-based materials in 2004 [11]. Graphene has remained the subject of scientific speculation since the early twentieth century. The most recent discovery in carbon nanostructures is the graphene-based material as an allotropic form of carbon that takes the shape of a two-dimensional (2D) hexagon with one atom at each vertex. Graphene-based materials are renowned for their flexibility, strength, lightweight, and conductivity. Combining graphene with already-existing materials is one of the most efficient strategies to acquire the promising properties of this material. Graphene and its composite materials have shown magnificent characteristics in various applications, which have not only caused improvement in their performance, but also expanded the versatility in new generation applications.

There exist various synthesis techniques for graphene-based materials, including chemical vapor deposition (CVD) and wet-chemical techniques. No technique has been able to fabricate 2D graphene larger than a microscopic scale yet [12]. In many studies and publications, graphene has been fabricated as a 3D porous structure. The graphene structure may increase its surface area while retaining its exceptional mechanical characteristics and strong electrical conductivity. Figure 1 depicts the unit cell structural overview of graphene.

3D porous systems made on 2D graphene architectures have intrigued the sensing-related properties, which are capable to perform in sensing devices. There are many features present in 3D graphene-based structures, including a significant outer and inner surface area to contact with the analyte, a suitable electro-active surface area, the ability to easily load (bio)catalysts, and flexibility. It is even feasible to employ 3D freely standing graphene-based morphologies as an electrode for energy storage devices. An extensive section on fabrication techniques for 3D graphene is followed including the hydrothermal process, CVD, chemical deposition, electrochemical deposition method, and lithography. Figure 2 presents the specific reasons why 3D graphene-based morphologies are preferred for flexible sensors depending upon their unique characteristics. 3D graphene-based composites comprising carbon nanotubes decorated 3D graphene, organic polymers, and 3D graphene-based morphologies are significantly explored as electrode materials for energy storage applications. Evaluation of such potential materials as device-based applications is made possible by analyzing the potential directions and recent challenges [13].

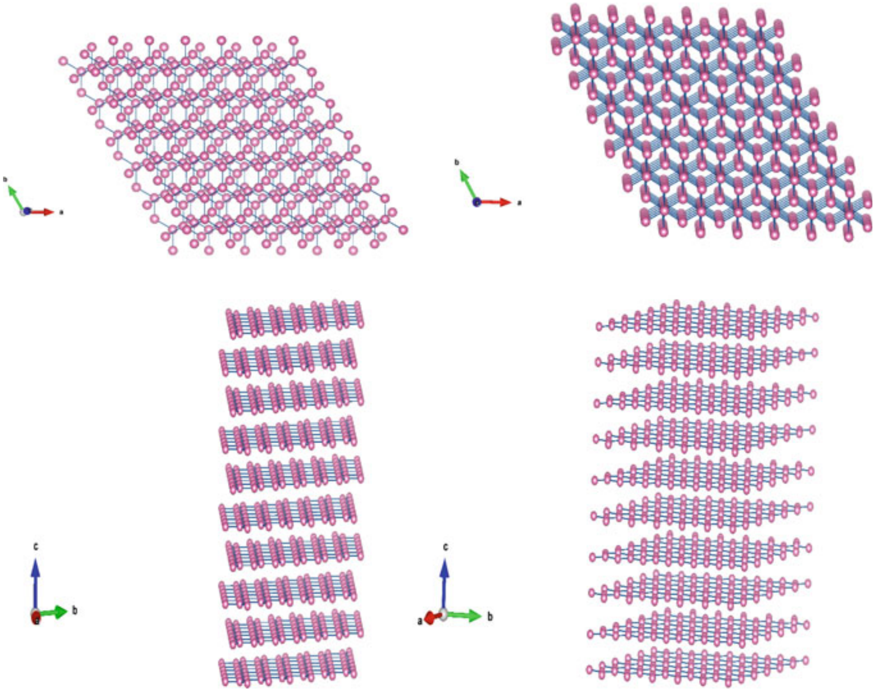

Fig. 1 The unit cell structure of 3D graphene

Fig. 2 Potential and best merits of 3D graphene-based composites for sensing devices [13]

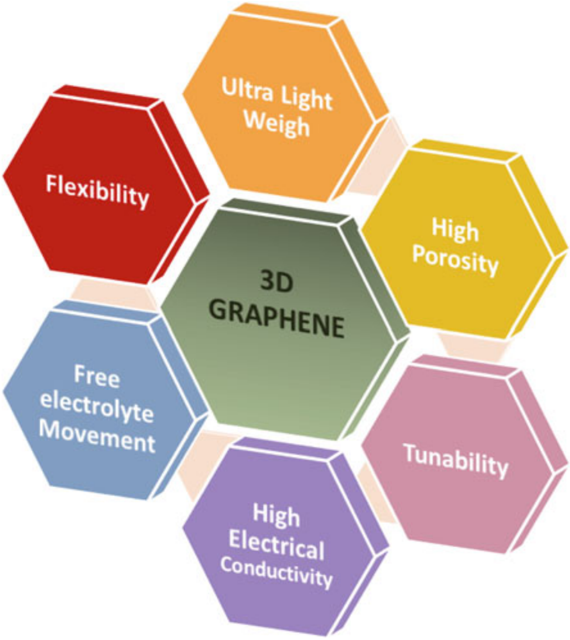

2 Sensors

Science and technology are always being improved by humanity, and they are always searching for new methods to raise standards of living. Humans created the computer and the internet as advanced technology, changing how people transmit information. Humans are now developing sensors to broaden their field of perception, and various sensors are used often in daily life and the workplace.

A sensor is a gadget that can gauge a certain quantity, such as pressure, temperature, and humidity, and then relay the data to other gadgets for processing. The measurement of an ideal sensor has two characteristics: first, it is unaffected by the measuring factor; and second, it does not alter the measuring factor. As sensors can compromise the information required to understand the instantaneous surroundings, they henceforward upkeep the decision-making ability. Nowadays, sensors have become an essential part of all sorts of vehicles [14]. This chapter describes each of these sensors' functions, benefits, and drawbacks, as well as how sensor fusion techniques might be applied to build a more ideal.

Flexible sensors possess basic construction, which is inexpensive in nature and can be utilized in wearable devices. Furthermore, flexible sensors need to be very sensitive and stretchable for various possible applications, including monitoring human health, robotics, wearable electronics, and artificial intelligence [15]. This study presents a summary of the most recent progress for flexible sensors. Moreover, the current status of flexible sensors, including the materials used, sensing mechanisms, manufacturing processes, and the most recent advancements in 3D graphene-based flexible sensors for utilization in soft robotics and healthiness nursing. Additionally, this chapter offers viewpoints on the difficulties facing this sector and the potential of flexible sensors.

3 3D Graphen-Based Flexible Sensors

The use of graphene in several electrical gadgets has increased in recent years. As a flexible material for piezoresistive, electrical, pressure, and humidity sensors, graphene has gained popularity. 3D graphene-based structures offer the potential to be utilized in gas sensors, oil absorption sensors, electrode material the s for supercapacitors and piezoresistive sensors owing to their electrical conductivity, mechanical toughness, and high porosity [16]. For sensors, graphene is the perfect material, as it can detect changes in its surroundings. The main purpose to idealize chemical sensors is to detect injurious materials. Graphene-based materials and composites have been developed to construct tiny sensors with molecular-level sensitivity. Figure 3 is representing the utilization of 3D graphene-based materials for various kinds of sensors.

With the era of advanced technology, crop monitoring graphene-based sensors have been developed, and moreover, improvement in efficiency is occurring in the

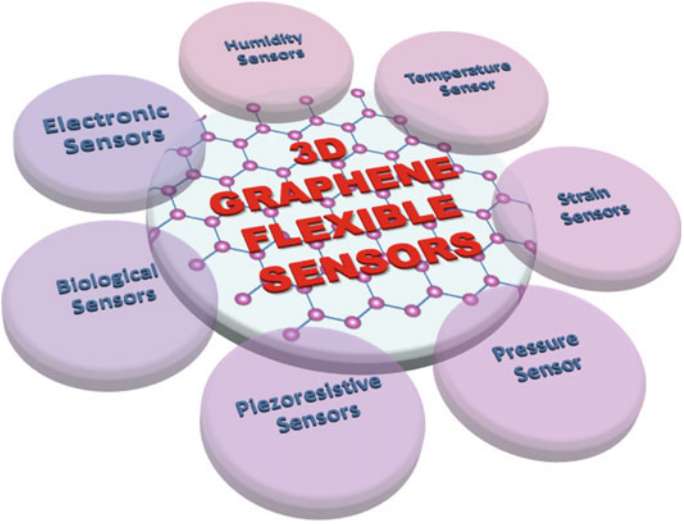

Fig. 3 3D graphene-based materials utilization for various flexible sensors

agricultural sector. With such developments, farmers will be able to explore and highlight the existence of any hazardous gases which might distress crop growth and they will be able to take appropriate actions on time without any significant damage. With the existence of the sensitivity property of graphene-based sensors, it is possible to locate the positions to cultivate specific crops based on environmental conditions.

3.1 Flexible Humidity Sensors

Porous 3D graphene-based structures have received notable consideration in the field of humidity sensing owing to their several reaction sites, and improved sensing properties [17]. The performance of the humidity sensor is totally dependent on the sensitivity of the employed material, which can be described as (Eq. (1))

$$S = \frac{I_{wet} - I_{dry}}{I_{dry} RH} \times 100 \tag{1}$$

Recently, Yu et al. reported the 3D Graphene foam humidity sensor. Implementation of such materials with strong characteristics, such as humidity sensors, have enabled electrical devices to transform the amount of water present in the environment into electronic signals. 3D graphene foam is synthesized by the CVD process on 3D metallic foam. Graphene-based foam can be utilized in humidity sensors, as this material is strongly conductive. Yu et al. demonstrated that 3D graphene foam with exceptional permeability for water allows the humidity sensors to display a wider relative humidity range (0%–85.9%), along with a quick reaction response of 89 ms and rapid recovery time of 189 ms. Moreover, the 3D graphene foam model was overstated with water molecules to compute the structural energy. The authors employed the software Materials Studio to explain the physical mechanism of electrical contribution due to chemically adsorbed water into a 3D graphene foam surface. Additionally, this gadget offered a user interface with unmatched performance for humidity-sensitive materials [18].

One of the lightest materials in the world is 3D graphene aerogel spheres (GASs), which possess the promising character to be utilized in high-performance thermal flexible sensors. Mao et al. fabricated the 3D graphene aerogel spheres through a unique spinning process, the material was capable to sense pressure, temperature, and material elasticity. Fabricated sensors demonstrated a temperature coefficient of resistance of 2.2% C^{-1}, five times greater compared to conventional resistance thermometers. The fabricated thermal humid sensor also demonstrated exceptional temperature-detecting capabilities. The 3D design of the graphene aerogel spheres allows the sensor to sense forces coming from all directions (360°). Because of the unique 3D special structures of graphene aerogel spheres, it exhibited improved sensitivity (0.15 kPa^{-1}) and rapid response and relaxation durations (~100 ms). Even after significant distortion, extraordinary cycle stability and lengthy operating life were observed for the sensor [19].

In comparison to the two sensors, the thermal humidity sensor is extremely unique. This sensor is frequently used to detect absolute humidity (AH). It consists of two thermistors, one of which is in touch with dry nitrogen, and the other is enclosed in the ambient air. Two thermistors' resistances can be measured. Humidity-sensing devices have been made using a variety of nanomaterials, including multi-wall carbon nanotubes. The shape and excellent electrical conductivity of 3D porous graphene make it a suitable material for a humidity sensor. The material's 3D structure and porous nature increase its surface area and improve its hygroscopicity, and its strong electrical conductivity might contribute to its high sensitivity to humidity [20].

3.2 Flexible Electronic Sensors

2D graphene-based structures are governing interest of researchers because of their exceptional features regarding electronic devices. The thickness of the graphene sheet makes it the best contender to be utilized in field effect transistors for electronic sensors since it is very sensitive to the changes in the surrounding environment. Here various types of graphene-based electronic sensors will be discussed, which are capable to detect numerous substances and biological materials. Firstly, the focus will lie on the types of graphene-based materials and then their utilization in electronic sensors, and finally in what way those materials impact the sensitivity of the resulting devices [21].

For the emerging field of flexible intelligent electronic stretchable sensors, flexibility and sensitivity play crucial roles. The sensitivity and stretchability of 3D graphene-based foams can be improved by modifying the specific surface area and mechanical strength. Yang et al. reported the stretchable electronic sensor applications by 3D graphene-based nickel particles peasecod foams. These foams were fabricated by stamp transfer and CVD techniques [22]. The nickel particles were proven to be beneficial for the construction of 3D nanostructures and remained isolated from one another to facilitate stretchy applications since they are coated by graphene layers. Such 3D graphene-based nickel particle foams were capable to show 80% stretchability. There exists a low limit of detection of <1%, as well as strong linearity (R^2) of ~0.997. Manjakkal reported the fabrication of a flexible 3D porous graphene-based foam supercapacitor to work as a chemo-resistive pH sensor. The 3D porous graphene-based foam supercapacitor demonstrated exceptional electrochemical and supercapacitive performance owing to its innovative layer structure of conductive nature. The 3D porous graphene-based foam supercapacitor exhibited better character for the areal capacitance of ~38 $mFcm^2$ which was around 3 times greater than reported flexible carbon-based supercapacitors at 0.67 mA cm^2 current density. The measured power and energy densities are 0.27 $mWcm^2$ and 3.4 $Whcm^2$, respectively. These values are higher than those reported carbon-based supercapacitors. The 3D porous graphene-based foam supercapacitor also demonstrated better cycling stability with capacitance retention of 68% even after 25,000 charge/discharge cycling examined under flexible circumstances [23].

Wearable electronics which are very sensitive and stretchable have become a promising topic of research for scientists with several applications, including e-skin and human motion sensing. Li et al. reported the 3D graphene-based structures for high-performance strain. In this study, the authors described a revolutionary 3D graphene-based structure as a flexible electronic sensor, which can self-heal. Furfuryl amine was employed as a reducing and modifying agent. The fabricated composite demonstrated high stretchability of ~200% and intrinsic conductivity with a little combination of graphene (~2 wt%), making it a suitable candidate for utilization in stretchable electronics for human motion detection [24].

Boxing et al. reported the successful fabrication of graphene aerogel endows with 3D deformation morphology and good flexibility to be utilized in wearable electronics as an electrical sensor. Printing of graphene patterns demonstrated high conductivity, and the 3D nano-structured graphene aerogel subsidizes multidimensional deformation responses, making them ideal for multi-recognition stretchable electric sensors. Moreover, fabricated electrical sensor devices with movement perception showed the ability to perform astonishingly well with gesture language analysis for a deaf-mute [25].

Zahed et al. fabricated the poly aziridine-encapsulated phosphorene-inserted flexible 3D porous graphene (PEP-3DPG) electrode via laser writing and drop-casting techniques. Due to the very stable PEP's superior electrochemical properties and surface functionality, the fabricated PEP/3DPG was considered a possible electrode in micro/nano supercapacitors, electrocardiogram recording, and immunosensing. The fabricated PEP/3DPG carcinoembryonic immune sensor demonstrated better linear ranges (0.1–700 pg mL^{-1} and 1–100 ng mL^{-1}) with a detection limit of 0.34 pg mL^{-1} operating under optimum circumstances. Moreover, signal to noise ratio of the constructed sensor was 13.5 dB equivalent to that of traditional electrodes Ag/AgCl, because the finger touch-based ECG sensor exhibits comparatively steady and low impedance at the skin–electrode interface. Additionally, the prepared micro supercapacitor exhibited an areal capacitance of 16.94 mF cm^2, six times more than a non-doped 3DPG-based micro supercapacitor. These findings show the potential of fabricated PEP/3DPG systems for multimodal applications [26].

Watthanawisuth et al. fabricated the 3D graphene foam sensors which were stretchable and wearable sensors employed for Internet of Things (IoT) technology. Herein, authors used the Wi-Fi to transfer the data from a sensor to the cloud by using of web-socket powered by Node.js. The authors fabricated the armband muscle to measure muscle expansion and stretch in real-time by utilizing 3D graphene foam sensors based on an IoT device. The data displayed the muscle's expansion on the website. These wearable flexible sensors are made up of 2–5 cm long strips of 3D graphene foam that were joined by conductive epoxy. The silver paste was applied to the sensor edge to achieve conductivity for better accuracy. As Intel Edison was used in the main CPU, connecting the sensor to the internet was made simpler. ADXL335 was selected along with the fabricated sensor as a three-axis accelerometer for monitoring gesticulations and fitness tracking applications. Intel Edison's main CPU board's lower side was equipped with an accelerometer, a battery, and an analog-to-digital conversion circuit [27].

3.3 Flexible Biological Sensors

Devices called biosensors combine biological and physical–chemical elements to detect analytes by creating a signal that can be measured. In many different domains, including the diagnosis of diseases and the bio-monitoring of contaminants, biosensors have a wide range of uses. Blood glucose biosensors are widely utilized devices in medical sciences. Antibodies, DNA probes, and cell receptors that interrelate with analytes can all be used as biological sensing materials. The transducer converts biological signals into optical and electrical impulses using materials that are optical, physicochemical, or piezoelectric [28].

It has been observed that H_2O_2 and glucose sensors are mostly used enzyme-based electrodes which possesses several drawbacks. Si et al. proposed a unique hierarchical composite-type material made of Mn_3O_4 that was fabricated at the top of 3D graphene foam (Mn_3O_4/3D GF). This fabricated composite-type material was flexible and free-standing biosensor, capable to detect nonenzymatic H_2O_2 and glucose for the applications of the medical industry and health care. Mn_3O_4/3D GF biosensor demonstrated a better sensitivity of 360 μA mM cm^{-2}, detection limit of 10 μM, and linear range of 0.1–8 mM. Synergistic effects among Mn_3O_4/3D GF-based biosensors exhibited the high electrocatalytic performance of the nano-structured Mn_3O_4 system with better conductance and improved surface area of 3D GF. Real-time detection of H_2O_2 and glucose in food and blood trials by the enzyme-less biosensor also showed good performance [29]. Xiao et al. fabricated the flexible electrochemical sensor by adding the high-density Pt nanoparticles on free-standing graphene oxide paper along with nanowires of MnO_2. This triple constituent system detected H_2O_2 from an alive cell with <5% amperometric response after 100 bending conditions [30]. Wang et al. fabricated the graphene with a conductive polymer, poly(3,4-ethylenedioxythiophene) (PEDOT), by galvanostatic electro-polymerization to achieve a G/PEDOT hybrid anode for biological fuel cell sensor. The fabricated device demonstrated the maximum 873 mW m^{-2} power output, presenting a 15-fold variation as compared to carbon paper bioanodes [31].

There are several applications of biosensors including environmental monitoring, illness diagnosis, drug development, food safety, biological research, etc. Collaboration of bio-molecular analytes with detecting constituents, device manufacturing and scheme, microfluidics, microchip technology, sample selection methods, etc., are just a few of the extremely particular properties that these devices rely on. An upcoming advanced generation of sensing technologies/science can be developed by incorporating nanoparticles into biosensors. On the other hand, nanoparticle-based biosensors have promising future applications in food analysis, process control, clinical diagnostics, and environmental monitoring.

3.4 Flexible Piezoresistive Sensors

For wearable piezoresistive sensors, 3D graphene-based materials are regarded as auspicious stretchable sensors because of their easy fabrication, straightforward understanding procedure, short power need, and simple gesture collection. In the last two decades, piezoresistive sensors are recognized as outstanding potential contenders in the field of human expression sensing, healthcare detecting, etc., that are now considered as being crucial in developing next-generation artificial intelligence classifications [32].

Graphene-based aerogels with their better porosity, high conductance, and good flexibility have become the ideal materials to be utilized in piezoresistive applications/sensors. But, achieving a successful synthesis along with excellent sensing abilities, electric, piezoelectric, and mechanical characteristics at the same time is a challenge. Following the above-mentioned fact, Cao et al. fabricated unique nanofiber-reinforced graphene-based aerogel that possessed a hierarchical 3D inter-connected micro-structure. This designed morphological structure demonstrated significant 43.50 kPa compressive stress and high 28.62 kPa^{-1} piezoresistive sensitivity along with a linear sensitivity range of 0–14 kPa. The piezoresistive sensor exhibited better resilience of compression at 3 Pa, fast response time (37 ms) and stability of the structure along with sensing ability remained significant even after 2600 cycles. At 20% compressive strain, assembled sensors exhibited a 91.57% value of the current signal of the initial value. Such stable, durable, and persistent current signal values correspond to the excellent features of assembled piezoresistive biosensor to monitor wrist pulse, real-time movement of the throat, knee joints, and finger impressions [33].

There are several excellent techniques to fabricate extremely well-ordered 3D porous graphene sponges (PGSs), and where emulsion process is one of them. Wang et al. demonstrated a well-organized ordered 3D PGSs-based wearable pressure sensor with great sensitivity and flexibility. High-performance piezoresistive sensors fabricated on 3D PGSs have evolved rapidly due to their effective performances, yet issues including low sensitivity, high cost, and restricted flexibility still exist. After the successful fabrication of well-organized ordered 3D PGSs by emulsion approach, a wearable pressure sensor at the device level was put together with an Au electrode and polydimethylsiloxane for dependable packaging. To achieve a stable emulsion, the pH values were carefully regulated. The ordered 3D PGSs demonstrated lower density, better conductance, and better porosity, proving a 0.79–1.46 gauge factor with a compression strain of 50% and excellent durability even after 500 cycles. The designed pressure sensor demonstrated improved sensing ability to distinguish hominoid activities such as human finger, wrist, palm, and elbow movements. Therefore, pressure sensors showed tremendous promise in the areas of human–computer interaction, e-skin, biomechanical systems, etc. [34].

Recently, Ma et al. fabricated 3D graphene-based flexible piezoresistive sensors with excellent stability and sensing abilities. Here, a unique surface-filled conductive layer of graphene nanosheets was created using fused deposition molding; 3D printing was performed to create a stable, highly sensitive 3D graphene-based flexible piezoresistive sensor. The device exhibited better flexibility of strain 1960%, 175.57 kPa^{-1} sensitivity at <300 Pa applied pressure, high 18.95–66.29 gauge factor (0–100% strain), exceptional stability even after >2000 compression/relaxing cycles, the 105 ms mechanical response time and 66 ms recovery time owing to the surface-filled graphene conductive layer. Such features of the device make it an ideal candidate to be utilized in practical applications to detect human behaviors [35].

Nowadays, researchers are focusing to adjust the high content of conductive nanocomposites into graphene to improve the detecting ability of flexible piezoresistive sensors. Ma et al. have utilized two carbon black (CB)/graphene nanosheet (GN) composite structures, which were employed to fabricate flexible piezoresistive 3D sensors. Three different styles of CB and GNs were adjusted to fabricate flexible piezoresistive sensors with nanocomposites and so much difference in their gauge factor and sensitivity was observed. The sensor with the composite construction was first coated with GNs and then filled with CB in a substrate. The sensor demonstrated the maximum 197.56 kPa^{-1} sensitivity below 300 Pa and 47.60 gauge factor. Moreover, it demonstrated better stability >2000 compression and relaxation cycles, with a quick response of 120 ms and rapid recovery of 63 ms. The sensor also showed the potential for speech and gesture monitoring. This study offers a method for making conductive nanocomposites into a highly sensitive piezoresistive sensor [36].

Sengupta et al. presented the 3D squeezable piezoresistive graphene polydimethylsiloxane foam sensor fabricated by incorporating multi-layered graphene nanoparticles in porous polydimethylsiloxane foam supported by a sugar scaffold. A 3D printing method was used to create cellular graphene/PDMS composites with controlled topologies. Under diverse loading scenarios, the resulting composite exhibited outstanding stretchability, toughness, and exceptionally stable temperature sensitivity. The resultant piezoresistive foam sensors underwent strain testing with two response areas and linearity of 2.87–8.77 gauge factor range throughout the 0–50% strain range. To measure the dynamic pressure, the dynamic-stimulus–response experiment also demonstrated the ability of sensors' capacity to accurately measure dynamic pressure up to a frequency of ~70 Hz. A high level of stability was also shown by the sensor during 36,000 compressing/relaxing cycles and 100 cycles of a whole human stride. By using simulated gait models and real-time gait classification trials, both have identified precise human gait monitoring by 3D sensing foams. The sensors' capacity to detect a variety of fundamental joint bending responses further demonstrated their applicability for individualized health-caring devices/applications [37].

Chen et al. have demonstrated a detailed description of the fabrication, importance, and utilization of graphene-based flexible piezoresistive sensors. One of the key elements of intelligent tactile skin, the piezoresistive sensor, is a widely used flexible pressure sensor with outstanding performance. Such sensors can be categorized methodically into different formations, such as 1D, 2D, and 3D foamed geometry, and can be utilized in various real-world devices, such as multifunctional sensing, health monitoring, system integration, and human motion sensing [38].

3.5 Flexible Pressure Sensor

Flexible pressure sensors possessing improved sensing abilities and extensive practical implementation range are widely used in wearable technology and biomimetic technology. In particular, the skin of the human fingertip may be a useful model to follow for very sensitive sensors since it has many epidermal ridges that enhance external stimulations. Xia et al. developed the flexible pressure sensing membrane (3D graphene films) via CVD and it displayed extraordinary 110 $(\text{kPa})^{-1}$ sensitivity at 0–0.2 kPa and up to 75 kPa an extensive workable pressure range. The pressure sensors' enhanced performance is also a result of the usage of hierarchically structured supporting elastic films (polydimethylsiloxane). This pressure sensor demonstrated stability for more than 10,000 compressing/relaxing cycles, with a 0.2 Pa low detection limit and 30 ms swift reaction time. The authors illustrated the potential uses of sensors for sensing small stuffs, human physical gestures, and sound [39].

Xu et al. fabricated the flexible force sensor with flexible polydimethylsiloxane and 3D graphene foam (GF/PDMS). The 3D GF/PDMS sensor demonstrated the ability to sense frequency response via a piezoelectric transducer and tuning fork tests. The sensor has clearly shown the audio frequency linear response with an ultrasound frequency range of up to 141 kHz, since the sensor's work on the principle of alteration in the electronic band structure. Such sensors are desirable for collaborative wearable sensor technology or simulated prostheses that can sense ultrasonic waves, seismic waves, transient pressures, and shock waves due to their

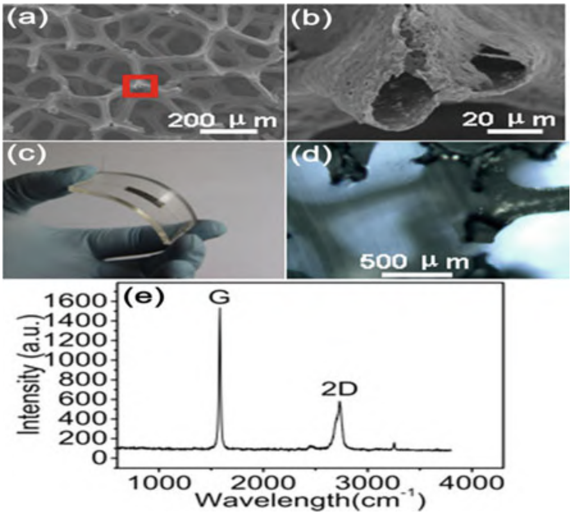

Fig. 4 **a** SEM micrographs of graphene foam (GF) illustration of morphology **b** High resolution SEM micrographs of GF to show its porous 3D structure, **c** Picture of the 3D GF/PDMS sensor shows bending ability, and **d** 3D GF/PDMS sensor's cross-sectional optical image **e** Raman spectra of GF [40]

excellent response and broad bandwidth [40]. SEM images, flexibility, and Raman spectra of the 3D graphene foam (GF/PDMS) sensor are presented in Fig. 4.

There are many ways to prepare graphene where intricate steps are involved in creating multilayer 3D graphene structures. Depending on the variation in the resistance offered by electrical signals of 3D graphene by the influence of sonic waves, the flexible acoustic pressure sensor has been created by Xu et al. The detector was synthesized by flexible 3D graphene foam and PDMS. Such sensors showed the ability in real time to delicately sense the distortion and the acoustic pressure; studies used human physiological data and a tuning fork. These findings are important for the creation of graphene-based applications/devices in the areas of transient pressure measurement, in-vitro-diagnostics, and improved therapeutics [41].

Zhu et al. employed the neoteric method to fabricate a 3D structure graphene-based pressure and strain sensor [42]. Ultrahigh sensitivity and significant hysteresis were exhibited by the 3D bubble-derived graphene-based porous sensor. Fang et al. followed the confined self-assembly methodology to fabricate a novel 3D porous network with the aligned graphene-based wall, that was treated with holey-reduced graphene oxide/lignin sulfonate (HrGO/Lig) composites and were oriented on the framework of the Lig/single-wall carbon nanotube (Lig/SWCNT) hydrogel by vacuum-assisted filtration. Achieved ultra-light Lig/SWCNT/HrGO$_{al}$ aerogel was employed as pressure sensor which demonstrated 2.28 kPa^{-1} high sensitivity and 0.27–14.1 kPa wide detection range. Moreover, the fabricated aerogel film showed the ability to perform in the symmetric supercapacitor and exhibited better energy storage performance even after 5000 fatigue bending cycles [43].

Baolin et al. discussed that bionic skin is a kind of scheme that has the ability to perform many simulations and also demonstrate several identifications of human skin. The authors fabricated the flexible graphene piezoresistive tactile sensor, which showed the ability to disclose the use of graphene's piezoresistive capabilities. The innovative tactile-pressure sensor was combined with a 2D graphene-based film tactile sensor along with a 3D graphene foam pressure sensor to concurrently quantify highly precise and extended range measurements simultaneously. The test findings demonstrated that this sensor's measuring range was split into two ranges: 0–2 N and 2–40 N. The 472.2 $\Omega(\text{kPa})^{-1}$ sensitivity, the 0.01 N force resolution, and less than 40 ms reaction time were observed for the 0–2 N measurement range. While 5.05 $\text{k}\Omega(\text{kPa})^{-1}$ sensitivity, the 1 N force resolution, and less than 20 ms reaction time were the observations for the 2–40 N measurement range. This sensor provided utilization for numerous applications like in biomedical devices and prosthetic limbs and also can be employed for highly precise and broad range force implemented calculations [44].

Flexible sensors are in great demand for research in many intelligence-based systems such as the Internet-of-Things (IoT). Wei et al. provided the easiest and most environmentally facile process for producing pressure sensors which were based on an aerogel composite made of bacterium cellulose and caffeic acid-reduced graphene oxide. The fabricated 3D graphene-based sensor showed a porosity of 98.9% and demonstrated the 13.89 kPa^{-1} high sensitivity, 47.2 Pa ultra-low detection limit, and 120 ms fast response time, clearly detecting subtle strain and monitoring human physical motions. Moreover, the aerogel demonstrated remarkable durability even after 1000 compressing/relaxing cycles, depicting the suitable performance of the material to be utilized in the area of flexible electronics [45].

3.6 Flexible Strain Sensors

Regarding flexible and stretchy strain sensors, various scholarly findings have recently been presented [46]. Pan et al. have discussed the ability to increase the stretchability of graphene-based materials by transforming the 2D membranes into 3D macroscopic structures. The authors used the porous copper foil as a template for atmospheric pressure to fabricate the 3D graphene films. Later, 3D graphene film (3D GF) was transferred to the PDMS membrane by treating the 3D GF at 1000 °C (3D GF-1000/PDMS). 3D GF-1000/PDMS hybrid film exhibited good flexibility, as evidenced by relatively low resistance changes (R/R_0), 2.67 and 0.36, under employing 50% tensile strain and 1.6 mm bending radius. Conversely, 3D GF-900/PDMS hybrid film demonstrates exceptional strain sensing capability with 187% practical strain range and 1500 gauge factor. Additionally, the 3D GF-900/PDMS exhibited astonishing strength in its resistance to repeatedly stretching-relaxing cycles of 5000. Kinetic investigations demonstrated that resistance changes dependence on strain was relying on graphitization, while the conductivity of 3D GF was sensitive to the temperature of the CVD process [47]. The core elements of smart and flexible electronics are pressure and strain sensors, which are a hot topic of research [48]. Flexible graphene-based pressure sensors possessing $PbTiO_3$ nanowires are renowned for their piezoelectric performance, reported by Xu et al. The material was employed to monitor healthcare and human gesture detection. The sensor exhibited 0 to 1400 Pa good linearity and 9.4×10^{-3} kPa^{-1} ultrahigh sensitivity [49].

Li et al. demonstrated the importance of graphene-based strain sensors as wearable strain sensors which can be utilized in biomechanical systems, human motion detection, and other applications. There are several examples where high-performance strain sensors have achieved the unique morphology of 3D graphene foam, although there are still issues with preparation costs, sensitivity, and stretchability. Li et al. presented a composite fabricated by 3D graphene foam and PDMS that showed extremely flexible behavior and showed a response to strain. The graphene foam was fabricated from graphene oxide using a simple technique and it demonstrated better mechanical properties which make it easier to incorporate PDMS into the graphene system. The fabricated sensor showed a gauge factor of 98.66 under applied strain 5%, and it may be extended up to 30% of its original length. Additionally, the strain sensor exhibited excellent durability after 200 stretching–relaxing cycles. When the elbow and finger bending monitoring device was used, it produced repeatability and a variety of reactions due to resistance variation [50].

Xiang et al. fabricated the strain sensor composed of the printed nanocomposite of carbon nanotube and thermoplastic polyurethane (CNT/TPU) via fused deposition modeling (FDM), and later 1-pyrenecarboxylic acid (PCA) was added non-covalently to alter the CNT and amplify polymer-nanofiller collaborations. The sensor exhibited the 117,213 gauge factor at 250% strain, high detectable 0–250% strain range, and better durability up to 10,000 loading–unloading cycles [51]. Xu et al. described that by incorporating PDMS into 3D graphene foam (GF), fabricated by CVD employing Ni foam as a template, a 3D GF-PDMS composite was investigated. In order to increase the sensitivity of the 3D GF-PDMS composite, a thin layer of poly(ethylene terephthalate) (PET) was added to work as substrate and designed the double-layer 3D GF-PDMS/PET composite. According to calculations made for resistance, there was variation in the composite's resistance after bending the edge side of PET, but it started to decrease when bent from the side of GF. In both instances, bending curvature increased the relative change in electrical resistance. More crucially, at the same bending curvature, the relative change in electrical resistance for double-layer 3D GF-PDMS/PET composite can be up to six times greater. Additionally, the 3D GF-PDMS/PET composite has demonstrated greater stability and flexibility [52].

Highly-flexible strain sensors with good multifunctional properties are required for significant developments in the field of flexible electronics. Xu et al. proposed a novel strain sensor based on Eco-flex rubbers, 3D graphene foams (GF), and altered silicone rubber in a straightforward and affordable production technique (MSR). Highly stretchable with tolerable 100% strain including pressure sensing, strain meditation, and strain-dependent heating, are all features of the device. The strain sensor demonstrated the broad sensing range of 100% strain and 66 kPa stress, high sensitivity with gauge factor 584.2 for strain range 80% to 100%, and sensitivity of 0.183 kPa^{-1} in 5–10 kPa. The sensor exhibited excellent durability life even above 10,000 compressing/relaxing cycles. The GF showed splendid electrical properties, and the MSR exhibited ideal mechanical properties. Under 5 V, the device's temperature may be raised by 35 °C in 5 min. As a result, the thermochromic MSR's color change rendered the deformation visible to the naked eye. The reversible and soft strain sensor has the potential to be utilized in the intelligent visual-touch panel and real-time detection of electrophysiological stimuli [53].

3.7 Flexible Temperature Sensor

Temperature sensors must be periodically calibrated to ensure accurate readings while in continuous operation. Wu et al. reported a self-calibrating thermistor, which was regarded as practical, economical, and quick self-calibration employing embedded microheaters to operate as a self-heating platform. Based on the n microheater platform, authors illustrated the sensing abilities of 3D reduced graphene oxide hydrogel (RGOH), for the first time. They reported the 3D sulfonated RGOH (S-RGOH) based thermistor, which demonstrated exceptional resolution (0.2 °C), high sensitivity 2.04% K^{-1}, and a wide detection range of 26–101 °C. By comparison, it was found that S-RGOH showed improved thermal sensitivity as compared to RGOH, which is dependent upon the chemical modification during varying temperature sensing. The microheaters were also employed for in situ thermal annealing of S-RGOH and assessed temperature-dependent characteristics in addition to self-calibration. Future wearable electronics will be able to use the flexible S-RGOH thermistor since it is mechanically flexible and has a variety of useful applications [54]. Figure 5 is not only representing the schematic illustration of 3D S-RGOH, but also demonstrates the SEM images, Raman, and FTIR spectra as well.

4 Conclusion

In this chapter, a comprehensive review of the 3D graphene-based flexible sensors has been presented. It is noticed that structural destruction or considerable plastic distortion are the causes of restrictions for developing flexible 3D graphene-based, super-elastic structures. Flexible sensors' specific uses are determined by performance factors including sensitivity, linearity, and stability. A detailed literature review regarding various types of 3D graphene-based flexible sensors is demonstrated. Understanding sensing processes and researching novel sensing mechanisms are equally elaborated. Future research on 3D graphene-based flexible sensors should focus on computational and machine learning techniques, as well as the chemistry, preparation, and characterization of polymer nanocomposites. Presented summarized work will be helpful for researchers to better understand the relationship between flexible sensors' process structure and performance to improve their structural designs in accordance with the applications. We can conclude that 3D graphene-based wearable/ flexible sensors illustrate the magnificent potential for multifunctional applications/ devices which should be further scrutinized.

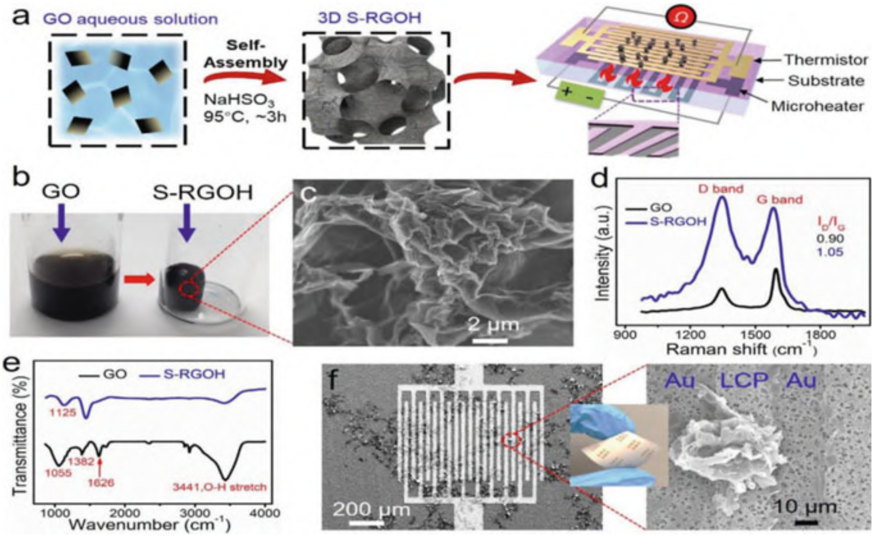

Fig. 5 **a** Schematic diagram for the 3D S-RGOH synthesis by one-pot self-assembly process and application for constructing a self-calibrated thermistor. **b** Picture of GO aqueous solution and resultant S-RGOH. **c** SEM micrographs of 3D porous S-RGOH. **d** Raman spectra of GO and S-RGOH. **e** FTIR spectra of GO and S-RGOH. **f** SEM micrograph of Au IEs patterned porous and flexible LCP substrate with 3D S-RGOH [54]

References

1. Guo, Y., Liu, L., Liu, Y., Leng, J.: Review of dielectric elastomer actuators and their applications in soft robots. Adv. Intell. Syst. **3**(10), 2000282 (2021)
2. Guan, Q., Sun, J., Liu, Y., Wereley, N.M., Leng, J.: Novel bending and helical extensile/contractile pneumatic artificial muscles inspired by elephant trunk. Soft Rob. **7**(5), 597–614 (2020)
3. Huang, Zhenlong, Hao, Y., Li, Y., Hu, H., Li1, W., Lei, Y., Kim, N., Wang, C., Zhang, L., Ward, J.W., Maralani, A., Li, X., Durstock, M.F., Pisano, A., Lin, Y., Xu, S.: Three-dimensional integrated stretchable electronics. Nat. Electron., 473–480 (2018)
4. Xue, Zhaoguo, Xu, M., Li, X., Wang, J., Jiang, X., Wei, X., Yu, L., Xu, J., Shi, Y., Chen, K., Cabarrocas, P.R.I.: Adv. Funct. Mater **26**, 5352–5359 (2016)
5. Lü, Chaofeng, Li, M., Xiao, J., Jung, I., Wu, J., Huang, Y., Hwang, K-C., Rogers, J.A.: Mechanics of tunable hemispherical electronic eye camera systems that combine rigid device elements with soft elastomers. J. Appl. Mech. **80**(6) (2013)
6. Yi, N., Gao, Y., Jr, A.L.V., Zhu, J., Erdely, D., Xue, C., Lavelle, R., Cheng, H.: Fabricating functional circuits on 3D freeform surfaces via intense pulsed light-induced zinc mass transfer. Mater. Today **50**, 24–34 (2021)
7. Zhao, W., Huang, Z., Liu, L., Wang, W., Leng, J., Liu, Y.: Porous bone tissue scaffold concept based on shape memory PLA/Fe_3O_4. Compos. Sci. Technol. **203**, 108563 (2021)
8. Lu, Haiqing, Zou, Z., Wu, X., Shi, C., Xiao, J.: Fabrication and characterization of highly deformable artificial muscle fibers based on liquid crystal elastomers. J. Appl. Mech. **88**(4) (2021)
9. Lan, Xin, Liu, L., Pan, C., Li, F., Liu, Z., Hou, G., Sun, J., et al.: Smart solar array consisting of shape-memory releasing mechanisms and deployable hinges. Aiaa J. **59**(6), 2200–2213 (2021)

10. Gao, H., Li, J., Liu, Y., Leng, J.: Shape memory polymer solar cells with active deformation. Adv. Compos. Hybrid Mater. **4**(4), 957–965 (2021)
11. Lin, Jian, Peng, Z., Liu, Y., Ruiz-Zepeda, F., Ye, R., Samuel, E.L.G., Yacaman, M.J., Yakobson, B.I., Tour, J.M.: Laser-induced porous graphene films from commercial polymers. Nature Commun. **5**(1), 1–8 (2014)
12. Wang, C., Vinodgopal, K., Dai, G.-P.: Large-area synthesis and growth mechanism of graphene by chemical vapor deposition. Chem. Vap. Depos. Nanotechnol **5**, 97–113 (2018)
13. Baig, N., Saleh, T.A.: Electrodes modified with 3D graphene composites: a review on methods for preparation, properties and sensing applications. Microchim. Acta **185**(6), 1–21 (2018)
14. Campbell, Sean, O'Mahony, N., Krpalcova, L., Riordan, D., Walsh, J., Murphy, A., Ryan, C.: Sensor technology in autonomous vehicles: a review. In: 2018 29th Irish Signals and Systems Conference (ISSC), pp. 1–4. IEEE (2018)
15. Zazoum, Bouchaib, Mujasam Batoo, K., Azhar Ali Khan, M.: Recent advances in flexible sensors and their applications. Sensors **22**(12), 4653 (2022)
16. Xu, Xiang, Hui, L., Zhang Q., Han, H., Zhao, Z., Li, J., Jingye, L., Qiao, Yu., Gogotsi, Y.: Self-sensing, ultralight, and conductive 3D graphene/iron oxide aerogel elastomer deformable in a magnetic field. ACS Nano **9**(4), 3969–3977 (2015)
17. Ding, Haojun, Wei Wei, Y., Wu, Z., Tao, K., Ding, M., Xi, X., Wu, J.: Recent advances in gas and humidity sensors based on 3D structured and porous graphene and its derivatives. ACS Mater. Lett. **2**(11), 1381–1411 (2020)
18. Yu, Yu, Zhang, Y., Jin, L., Chen, Z., Li, Y., Li, Q., Cao, M., Che, Y., Yang, J., Yao, J.: A fast response−recovery 3D graphene foam humidity sensor for user interaction. Sensors **18**(12), 4337 (2018)
19. Mao, Renwei, Yao, W., Qadir, A., Chen, W., Gao, W., Xu, Y., Hu, H.: 3-D graphene aerogel sphere-based flexible sensors for healthcare applications. Sens. Actuators A **312**, 112144 (2020)
20. Chen, W.-P., Zhao, Z.-G., Liu, X.-W., Zhang, Z.-X., Suo, C.-G.: A capacitive humidity sensor based on multi-wall carbon nanotubes (MWCNTs). Sensors **9**(9), 7431–7444 (2009)
21. He, Qiyuan, Wu, S., Yin, Z., Zhang, H.: Graphene-based electronic sensors. Chem. Sci. **3**(6), 1764–1772 (2012)
22. Yang, Cheng, Xu,Y., Man, P., Zhang, H., Huo, Y., Yang, C., Li, Z., Jiang, S., Man, B.: Formation of large-area stretchable 3D graphene–nickel particle foams and their sensor applications RSC. Adv. **7**(56), 35016–35026 (2017)
23. Manjakkal, Libu, Núñez, C.G., Dang, W., Dahiya, R.: Flexible self-charging supercapacitor based on graphene-Ag-3D graphene foam electrodes. Nano Energy **51,** 604–612 (2018)
24. Li, Jinhui, Liu, Q., Ho, D., Zhao, S., Wu, S., Ling, L., Han, F. et al.: Three-dimensional graphene structure for healable flexible electronics based on diels–alder chemistry. ACS Appl. Mater Interfaces **10**(11), 9727–9735 (2018)
25. An, Boxing, Ma, Y., Li, W., Su, M., Li, F., Song, Y.: Three-dimensional multi-recognition flexible wearable sensor via graphene aerogel printing. Chem. Commun. **52**(73), 10948–10951 (2016)
26. Zahed, Abu, Md., Barman, S.C., Sharifuzzaman, Md., Zhang, S., Yoon, H., Park, C., Yoon, S.H., Park, J.Y.,: Polyaziridine-encapsulated phosphorene-incorporated flexible 3D porous graphene for multimodal sensing and energy storage applications. Adv. Funct. Mater. **31**(25), 2009018 (2021)
27. Watthanawisuth, N., Maturos, T., Sappat, A., Tuantranont, A.: The IoT wearable stretch sensor using 3D-Graphene foam. In: 2015 IEEE SENSORS, pp. 1–4. IEEE (2015)
28. Nguyen, Hiep, H., Lee, S.H., Lee, U.J., Fermin, C.D., Kim, M.: Immobilized enzymes in biosensor applications. Materials **12**(1), 121 (2019)
29. Si, P., Dong, X.-C., Chen, P., Kim, D.-H.: A hierarchically structured composite of Mn 3 O 4/3D graphene foam for flexible nonenzymatic biosensors. J. Mater. Chem. B **1**(1), 110–115 (2013)
30. Xiao, Fei, Li, Y., Zan, X., Liao, K., Rong, X., Duan, H.: Growth of metal–metal oxide nanostructures on freestanding graphene paper for flexible biosensors. Adv. Func. Mater. **22**(12), 2487–2494 (2012)

31. Wang, Ying, Zhao, C.-E., Sun, D., Zhang, J.-R., Zhu, J.-J.: A graphene/poly (3, 4-ethylenedioxythiophene) hybrid as an anode for high-performance microbial fuel cells. ChemPlusChem **78**(8), 823–829 (2013)
32. Cao, Minghui, Su, J., Fan, S., Qiu, H., Dongliang, S., Li, L.: Wearable piezoresistive pressure sensors based on 3D graphene. Chem. Eng. J. **406**, 126777 (2021)
33. Cao, Xueyuan, Zhang, J., Chen, S., Varley, R.J., Pan, K.: 1D/2D nanomaterials synergistic, compressible, and response rapidly 3D graphene aerogel for piezoresistive sensor. Adv. Funct. Mater. **30**(35), 2003618 (2020)
34. Wang, Tao, Li, J., Zhang, Y., Liu, F., Zhang, B., Wang, Y., Jiang, R., Zhang, G., Sun, R., Wong, C.-P.: Highly ordered 3D porous graphene sponge for wearable piezoresistive pressure sensor applications. Chem. Europ. J. **25**(25), 6378–6384 (2019)
35. Ma, L., Lei, X., Li, S., Guo, S., Yuan, J., Li, X., Cheng, G.J., Liu, F.: A 3D flexible piezoresistive sensor based on surface-filled graphene nanosheets conductive layer. Sens. Actuators A **332**, 113144 (2021)
36. Ma, Lijun, Lei, X., Guo, X., Wang, L., Li, S., Shu, T., Cheng, G.J., Liu, F.: Carbon black/graphene nanosheet composites for three-dimensional flexible piezoresistive sensors. ACS Appl. Nano Mater. (2022)
37. Sengupta, D., Pei, Y., Kottapalli, A.G.P.: Ultralightweight and 3D squeezable graphene-polydimethylsiloxane composite foams as piezoresistive sensors. ACS Appl. Mater. Interfaces. **11**(38), 35201–35211 (2019)
38. Chen, Kai-Yue, Xu, Y.-T., Zhao, Y., Li, J.-K., Wang, X.-P., Qu, L.-T. Recent progress in graphene-based wearable piezoresistive sensors: From 1D to 3D device geometries. Nano Mater. Sci. (2022)
39. Xia, Kailun, Wang, C., Jian, M., Wang, Q., Zhang, Y.: CVD growth of fingerprint-like patterned 3D graphene film for an ultrasensitive pressure sensor. Nano Res. **11**(2), 1124–1134 (2018)
40. Xu, R., Zhang, H., Cai, Y., Ruan, J., Qu, K., Liu, E., Ni, X., Lu, M., Dong, X.: Flexible and wearable 3D graphene sensor with 141 KHz frequency signal response capability. Appl. Phys. Lett. **111**(10), 103501 (2017)
41. Xu, Rongqing, Wang, D., Zhang, H., Xie, N., Shan, L., Ke, Q.: Simultaneous detection of static and dynamic signals by a flexible sensor based on 3D graphene. Sensors **17**(5), 1069 (2017)
42. Zhang, Rujing, Hu, R., Li, X., Zhen, Z., Xu, Z., Na, L., He, L., Zhu, H.: A bubble-derived strategy to prepare multiple graphene-based porous materials. Adv. Func. Mater. **28**(23), 1705879 (2018)
43. Peng, Zhiyuan, Yu, C., Zhong, W.: Facile preparation of a 3D porous aligned graphene-based wall network architecture by confined self-assembly with shape memory for artificial muscle, pressure sensor, and flexible supercapacitor. ACS Appl. Mater. Interfaces. **14**(15), 17739–17753 (2022)
44. Sha, Baolin, Lü, X., Jiang, L.: High sensitivity and wide range biomimetic tactile-pressure sensor based on 2D graphene film and 3D graphene foam. Micromachines **13**(7), 1150 (2022)
45. Wei, S., Qiu, X., An, J., Chen, Z., Zhang, X.: Highly sensitive, flexible, green synthesized graphene/biomass aerogels for pressure sensing application. Compos. Sci. Technol. **207**, 108730 (2021)
46. Yan, T., Wang, Z., Pan, Z.-J.: Flexible strain sensors fabricated using carbon-based nanomaterials: a review. Curr. Opin. Solid State Mater. Sci. **22**(6), 213–228 (2018)
47. Pan, Fei, Chen, S.-M., Li, Y., Tao, Z., Ye, J., Ni, k., Yu, H. et al.: 3D graphene films enable simultaneously high sensitivity and large stretchability for strain sensors. Adv. Funct. Mater. **28**(40), 1803221 (2018)
48. Luo, Zewei, Hu, X., Tian, X., Luo, C., Xu, H., Li, Q., Li, Q. et al.: Structure-property relationships in graphene-based strain and pressure sensors for potential artificial intelligence applications. Sensors **19**(5), 1250 (2019)
49. Chen, Zefeng, Wang, Z., Li, X., Lin, Y., Luo, N., Long, M., Zhao, N., Xu., J.-B.: Flexible piezoelectric-induced pressure sensors for static measurements based on nanowires/graphene heterostructures. ACS Nano **11**(5), 4507–4513 (2017)

50. Li, J., Zhao, S., Zeng, X., Huang, W., Gong, Z., Zhang, G., Sun, R., Wong, C.-P.: Highly stretchable and sensitive strain sensor based on facilely prepared three-dimensional graphene foam composite. ACS Appl. Mater. Interfaces. **8**(29), 18954–18961 (2016)
51. Xiang, D., Zhang, X., Li, Y., Harkin-Jones, E., Zheng, Y., Wang, L., Zhao, C., Wang, P.: Enhanced performance of 3D printed highly elastic strain sensors of carbon nanotube/thermoplastic polyurethane nanocomposites via non-covalent interactions. Compos. B Eng. **176**, 107250 (2019)
52. Xu, Rongqing, Lu, Y., Jiang, C., Chen, J., Mao, P., Gao, G., Zhang, L., Wu, S.: Facile fabrication of three-dimensional graphene foam/poly (dimethylsiloxane) composites and their potential application as strain sensor. ACS Appl. Mater. Interfaces. **6**(16), 13455–13460 (2014)
53. Xu, M., Li, F., Zhang, Z., Shen, T., Zhang, Q., Qi, J.: Stretchable and multifunctional strain sensors based on 3D graphene foams for active and adaptive tactile imaging. Sci. China Mater. **62**(4), 555–565 (2019)
54. Wu, Jin, Huang, W., Liang, Y., Wu., Z., Zhong, B., Zhou, Z., Ye, J., Tao, K., Zhou, Y., Xie, X.: Self-calibrated, sensitive, and flexible temperature sensor based on 3D chemically modified graphene hydrogel. Adv. Electron. Mater. **7**(4), 2001084 (2021)

Graphene-Based Materials for the Remediation of Hydrogen Sulfide Gas

Nishesh Kumar Gupta, Kaptan Rajput, and Herlys Viltres

Abstract In the family of carbon allotropes, graphene oxide (GO) has shown tremendous potential in energy and the environment. Besides being developed for the remediation of water pollutants, these carbon nanostructures are highly effective for air purification applications. Air pollutants like hydrogen sulfide (H_2S) could lead to the acidification of ecosystems and a high human mortality rate. GO-based adsorbents with suitable structural and functional modifications have shown unprecedented performance for the capture and mineralization of H_2S in relevant experimental conditions. This chapter is focused on highlighting the potential of GO-based adsorbents in removing H_2S gas in ambient conditions. The chapter aims to present an in-depth explanation of the trend and mechanism, which is the driving force for future research.

Keywords Adsorption · Graphene oxide · Hydrogen sulfide · Mechanism

---

N. K. Gupta (✉)
Department of Environmental Research, University of Science
and Technology (UST), 217 Gajeong-Ro, Daejeon 34113, Republic of Korea
e-mail: guptan@kict.re.kr

Department of Environmental Research, Korea Institute of Civil Engineering and Building Technology (KICT), 283 Goyang-Daero 10223, Goyang-si, Republic of Korea

K. Rajput
Materials and Biophysics Group, Department of Applied Physics, Sardar Vallabhbhai National Institute of Technology, Ichchhanath Surat-Dumas, Surat 395007, India

School of Electrical Engineering, Korea Advanced Institute of Science and Technology (KAIST), 291 Daehak-Ro, Daejeon 34141, Republic of Korea

H. Viltres
School of Engineering Practice and Technology, McMaster University, 1280 Main Street, West Hamilton, ON L8S 4L8, Canada

© The Author(s), under exclusive license to Springer Nature Switzerland AG 2023
R. K. Gupta (ed.), *3D Graphene*, Carbon Nanostructures,
https://doi.org/10.1007/978-3-031-36249-1_9

1 Introduction

While graphene nanosheets have found numerous applications in energy and the environment, this sp^2 hybridized, covalently bonded chain of polycyclic aromatic hydrocarbons needs further modification for their compatibility in gas treatment applications. More often, graphene oxide (GO) or reduced graphene oxide (RGO) materials are explored for treating acidic gases in conjugation with an active adsorbent due to the poor acidic gas adsorption behavior of GO/RGO. Since RGO/GO is highly porous, they are used as a support for anchoring gas-binding functionalities and catalysts/adsorbents. Section 2 of this chapter has discussed some strategies adopted for developing novel GO-based materials.

Among numerous acidic gaseous pollutants, hydrogen sulfide (H_2S) stands out due to its ubiquitous presence in different ecosystems. Naturally, H_2S is released from the hydrolysis of volcanic rocks and the anaerobic respiration of sulfate-reducing bacteria. However, a large proportion of H_2S in the atmosphere is released from oil refineries and coal gasification units. Even the wastewater treatment facilities in our areas are a common source of H_2S gas. H_2S is a colorless, pungent-smelling, and flammable gas which tends to settle in poorly ventilated areas [1]. While inhaling a low concentration (1–5 ppm) of H_2S can irritate the eyes and throat, exposure to high concentrations (500–1000 ppm) could be fatal to humans [2]. Thus, it is necessary to develop techniques to eliminate H_2S gas from different sources.

RGO/GO-based materials could act as adsorbents/catalysts in eliminating a broad concentration of H_2S gas in different experimental conditions. As such, Sect. 3 of this chapter is focused on the performance of RGO/GO-based adsorbents for eliminating H_2S gas in ambient conditions. The section further aims to explore the role of GO and experimental conditions that affect uptake performance. The H_2S capture process over GO-based adsorbents is associated with H_2S dissociation, followed by its oxidation to sulfur byproducts like sulfur, sulfite, and sulfate. Understanding H_2S removal mechanisms are necessary to develop superior materials for their industrial applications. Section 4 has presented a detailed discussion of the H_2S removal mechanism with a particular interest in spectroscopic findings and theoretical calculations. This chapter provides brief and concise information on GO-based adsorbents for the remediation of H_2S gas from different contamination sources. Moreover, Sect. 5 provides the limitations and possible developments that could make these materials suitable for industrial purposes.

2 Synthesis of RGO/GO-Based Adsorbents

Since many of the chapters in this book have discussed the synthesis of graphene and GO in detail, this section provides a brief description of the conventional synthesis route adopted for graphene, GO, and RGO. The two-dimensional (2D) graphene describes a single layer of sp^2 hybridized aromatic carbon structure peeled off from a three-dimensional (3D) graphite block. The poor dispersion behavior of graphene sheets due to π–π interactions between the sheets limits their possible application in environmental decontamination. However, anchoring oxygen-rich functionalities like hydroxyl groups, epoxides, and carboxylic acid on the graphene sheets, termed GO, could improve its dispersion behavior without compromising the intrinsic properties of graphene. GO was produced in large quantities through the chemical exfoliation of graphite in a strong acidic oxidizing medium (Hummers' method). However, the method has seen numerous modifications in the last six decades to improve the physicochemical properties, yield, greenness, and affordability [3]. The thermal or chemical reduction of GO sheets yields RGO with graphene domains, defects, and residual O-functionalities on the surface of the sheets. Though RGO has a lower mechanical strength and conductivity than graphene sheets, these oxidation–reduction strategies have been employed for the large-scale synthesis of graphene-like materials [4].

For H_2S gas removal, RGO/GO is covalently modified with functional groups or integrated with metal oxides or other active adsorbents to form RGO/GO-based nanocomposites. Covalent modification of RGO/GO is a straightforward strategy as the O-functionalities could be used for supporting other functional groups [6]. Rahighi and coworkers reported a simple covalent modification of GO nanosheets with piperazine by refluxing in ethanol for 24 h at 100 ºC (Fig. 1a) [5]. The same group modified the RGO surface with amide functionality by amidation of acyl-chlorinated RGO in a multi-step approach [7]. Even waste ammonia gas could be used for the covalent functionalization of GO through high-temperature annealing in an inert atmosphere after ammonia gas adsorption [8].

Since GO-based nanocomposites are better-suited adsorbents for H_2S removal, the synthetic strategies adopted for their fabrication have been discussed here. The most common method adopted for synthesizing GO-based nanocomposites relies on the in situ growth of active adsorbent with the GO. For this, pre-synthesized GO is dispersed in the reactant medium before subjecting it to the regular route of active adsorbent synthesis. The in situ growth allows uniform distribution of active adsorbents over the GO surface on a nanoscale. In some cases, thermal annealing in an inert atmosphere to form active adsorbents could reduce the GO into RGO [9, 10]. When discussed in the context of MOF-GO composites, GO is dispersed in the metal-linker reactant solution before subjecting it to hydrothermal/solvothermal synthesis (Fig. 1b) [11]. However, some researchers have added additional functionalities to the composite by pre-modifying the GO surface. Karanikolos et al. have reported polyethyleneimine-GO/HKUST-1 composite for H_2S removal, where primary amine functionality was grafted on the GO surface before forming a composite with HKUST-1 [12]. Bandosz and coworkers have reported the pre-functionalization of GO with sulfanilic acid or 4-ammonium polystyrene sulfonate before composite formation with Cu-BTC [13]. Some researchers have reported the benefits of ternary composites with two active adsorbents distributed on the GO

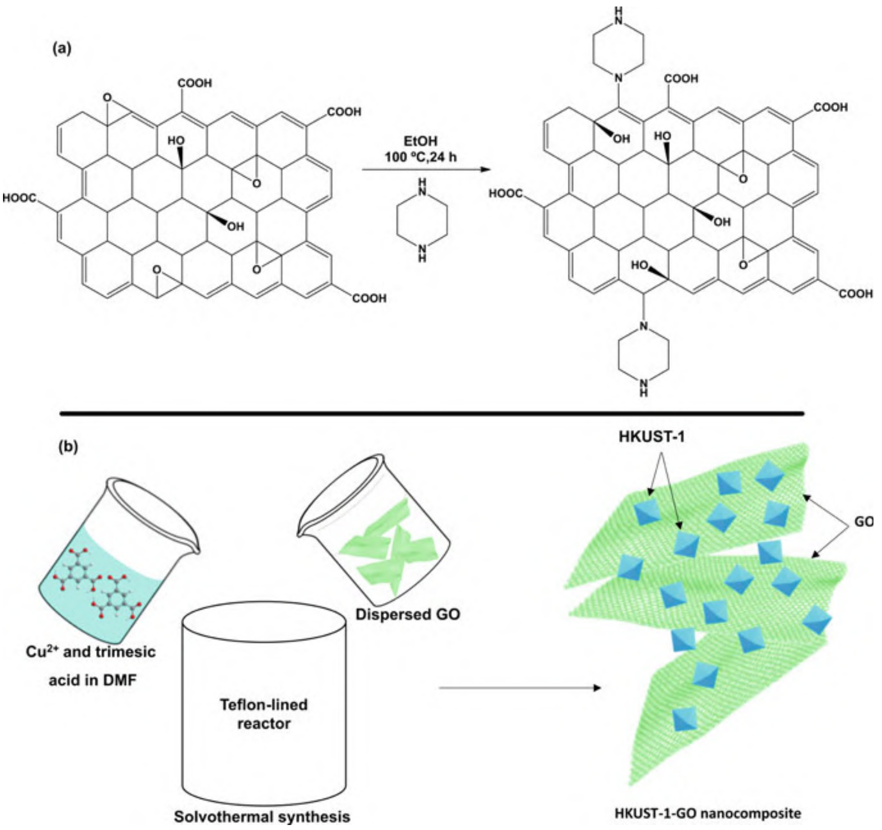

Fig. 1 **a** Covalent modification of GO with piperazine [5]; **b** in situ growth of HKUST-1 nanocrystals over GO surface

surface. In such a case, one active component is pre-synthesized and dispersed in the reaction medium like GO. For Au–$Zn(OH)_2$–GO composite, pre-synthesized Au nanoparticles were dispersed in $ZnCl_2$ solution along with GO to form the composite [14].

3 H_2S Removal Application

GO has limited H_2S uptake capacity (3 mg g^{-1}) [9], which makes it less relevant to the purpose in the raw form. However, anchoring suitable functional groups over the GO surface makes it an efficient adsorbent for H_2S gas removal. GO surface functionalization with amine-bearing or similar basic functional groups is an ideal strategy to improve the H_2S capture performance of GO-based materials. Though some studies have reported improvement in H_2S gas uptake after the surface modification with N-donor groups (amido and piperazine), the method adopted for functionalization is a multi-step approach, which severely limits the scale-up of materials [5, 7]. However, using a waste gas like NH_3 for GO surface modification with N-groups and subsequent utilization for H_2S capture could reduce the overall cost and improve the efficiency of GO materials. GO with a high NH_3 capacity of 90 mg g^{-1} was thermally treated in N_2 gas after NH_3 capture and used for H_2S adsorption (capacity ~30.5 mg g^{-1}) [8]. Unlike GO surface functionalization, GO-based composites are well-researched materials in the literature, where GO acts as a porous support for metal oxides, metal hydroxides, and metal–organic frameworks (MOFs). The subsequent section is dedicated to the discussion involving GO-based composites.

The main reason behind the use of GO-based composite is to improve the distribution of active adsorbent over a porous surface, which provides a better adsorbate–adsorbent (gas-active site) interaction. Moreover, GO in the nanocomposite opposed to graphene, provides a higher H_2S uptake capacity both in dry and moist conditions [18]. However, the implications of this approach on the surface and pore properties are highly related to the kind of active adsorbent, i.e., metal oxide, metal oxyhydroxide, or MOFs. For metal oxides like ZnO, GO acts as a highly porous support irrespective of the ZnO: GO composition ratio ZnO has a much lower surface area than GO (Fig. 2a). Though the increasing proportion of ZnO in the composite could lower the surface area and clog the pores, the H_2S adsorption capacity increased due to abundant ZnO active sites [9]. For some porous metal oxyhydroxides, the composite fabrication with GO could either lower the surface area, like in the case of CoOOH-GO (Fig. 2b) [15], or improve slightly with the increasing GO proportion, like in the case of FeOOH-GO (Fig. 2c) [16]. In such a case, the adsorption capacity is improved slightly or decreases to an extent, which makes the overall process of incorporating GO inconsequential. In the case of highly porous materials like MOFs, GO incorporation is beneficial as it improves the surface area and H_2S uptake capacity to a greater extent [17, 19, 20]. However, only a small fraction of GO could be incorporated into the MOF-GO composite. Beyond an optimum GO loading, both surface area and uptake capacity drop drastically due to the interference of GO in the MOF crystallization [19] or loss of microporosity and pore blocking [20]. For HKUST-1-GO nanocomposite, only a fraction of GO (~5%) was sufficient to double the H_2S adsorption capacity, and beyond, it declined rapidly and reached below HKUST-1's adsorption capacity (Fig. 2d). Thus, it is essential to understand the nature of active adsorbent before fabricating GO-adsorbent composites, and an optimum GO loading is required to have promising H_2S removal performance.

The synthesis method affects the composite physicochemical properties, and thus its H_2S adsorption capacity. In one such study involving the fabrication of ZnO-RGO through reflux and microwave methods, the ZnO-RGO synthesized by microwave heating had a superior H_2S removal capacity (120.6 mg g^{-1}) than the one synthesized by reflux method (50.2 mg g^{-1}). Besides being a faster synthetic route, the microwave method created smaller-size ZnO nanoparticles distributed uniformly over the RGO surface [10]. Other than the surface area of a composite, the synergy between the constituents [21] or the surface heterogeneity [13] could improve its H_2S adsorption

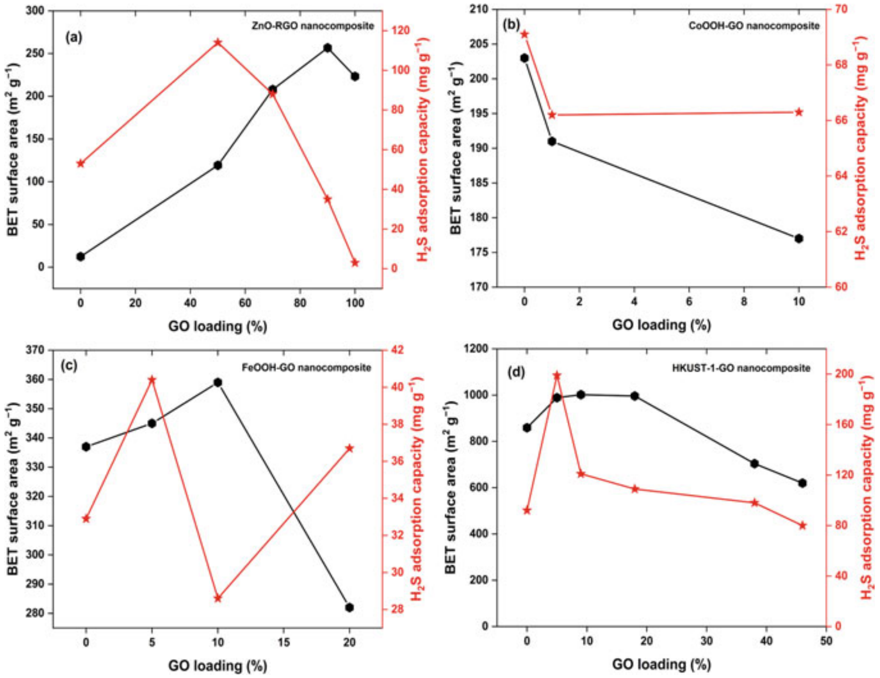

Fig. 2 Relationship between GO loading, surface area, and H_2S adsorption capacity of **a** ZnO-GO [9]; **b** CoOOH-GO [15]; **c** FeOOH-GO [16]; **d** HKUST-1-GO [17] nanocomposites

capacity. The increasing surface heterogeneity improves the H_2S removal performance, which was observed for a ternary Au–ZnO–GO composite. The ternary composite showed a higher H_2S uptake than the binary composites, even with a minor increment in its surface area. Au and GO in the nanocomposite provided a pathway for rapid electron transport, which benefitted the H_2S oxidation process. The surface heterogeneity could be further improved by introducing functional groups and active adsorbents over the GO layers as in Cu-BTC-sulfanilic acid-modified GO [13]. The functionalized MOF-GO composite has a higher H_2S adsorption capacity (241 mg g^{-1}) than the MOF-GO composite (130 mg g^{-1}), highlighting the importance of increasing surface heterogeneity.

In practice, these adsorbents are always tested for breakthrough studies in column configuration where experimental parameters like gas flow rate, adsorbent mass (bed height), gas concentration, and humidity play an important role in deciding the adsorption performance. However, the moisture content in the adsorbent has a striking effect on the H_2S adsorption capacity. The experimental and theoretical calculations predict a preferential interaction of H_2O with the carbonyl groups on the GO surface, which blocks the potential active sites for H_2S decomposition [22]. However, for metal oxides like ZnO, water molecules chemisorbed over the ZnO surface improve the hydroxyl density and provide an alternative reaction pathway for H_2S dissociation with lower activation energy [23]. Thus, the amount of water pre-adsorbed on the composite surface improves its H_2S adsorption capacity if GO loading is much lower than the active adsorbent.

The effect of moisture has been studied in detail in numerous reported studies. For many GO-based composites, there is a linear relationship between the amount of water pre-adsorbed and their H_2S adsorption capacity (Fig. 3a). Pre-adsorbed water on the composite surface creates a thin film, which dissolute and dissociates an H_2S molecule into $2H^+$ and S^{2-} ions. This proton release during the dissociation reaction is the reason behind an increase in the surface acidity of the composite, which rises further with the increasing amount of pre-adsorbed water [17]. The easy dissociation of H_2S molecules improves the adsorption capacity, and for this reason, a positive linear relationship has been witnessed for GO-based composites, even though H_2O and H_2S compete for the binding sites over the GO surface. The linear relationship could also be associated with the amount of GO in the composites. Since GO is a hydrophobic material, a higher proportion of it in the composite could lower the hydrophilicity of the composite, which reduces the amount of pre-adsorbed water and H_2S uptake capacity [17, 26]. Thus, the proportion of GO in the composite decides its adsorption capacity in dry and humid conditions. Unlike humidity, the effect of other experimental factors like gas flow rate, gas concentration, and adsorbent loading has been reported the least in these studies, which should be the focus of future studies to understand the column design parameters. Long et al. studied the effect of space velocity on H_2S adsorption capacity with MgO/RGO as the catalyst/adsorbent. The adsorption capacity decreased with the increasing space velocity due to the drop in gas retention time, which disfavored the interaction of H_2S molecules with the MgO/RGO surface [28].

Some studies have probed the role of visible light on the H_2S removal capacities of GO-based composites [18, 25, 27]. The sp^2 hybridized aromatic structure of GO provides a photoactive surface for electron–hole pair formation during radiation exposure and works as a conductive surface for a fast electron transfer. Besides, transition metal-containing active adsorbents are excellent absorbers of ultraviolet–visible radiation and generate electron–hole pairs. Thus, the GO-based adsorbents could also serve as photocatalysts for H_2S removal. The effect of ambient light exposure on the H_2S adsorption capacity of $Cd(OH)_2$-GO nanocomposite was reported in both the dry and moist conditions (Fig. 3b) [25]. For $Cd(OH)_2$-GO nanocomposite, the effect of visible light is more pronounced in dry conditions. In moist conditions, the favorable splitting of surface water molecules could lower the sensitivity of H_2S molecules. This negative effect of moisture on the gas uptake behavior of composite has been reported for $Zn(OH)_2$-GO, where the adsorption capacity of 155 mg g^{-1} in the dark condition dropped to 115 mg g^{-1} under ambient light [27]. In the dry condition, the increasing GO loading in the composite negatively impacted the composite's gas uptake behavior. However, this behavior reversed during the visible light exposure, as more GO in the composite provided efficient photoelectrons mobility, extended their lifetime, and restricted the electron–hole pair recombination process [25].

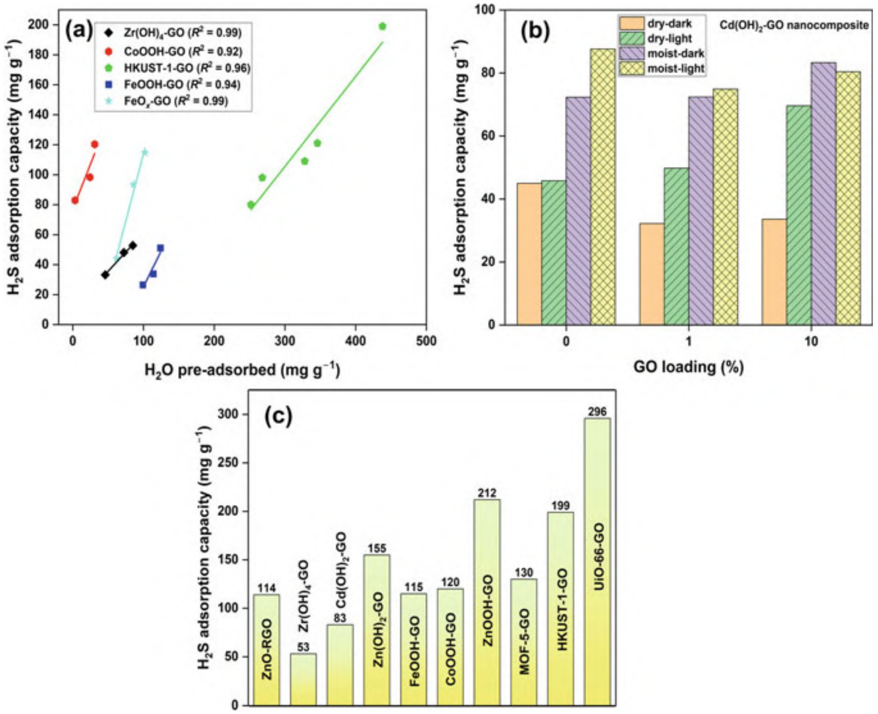

Fig. 3 **a** A linear relationship between the amount of water pre-adsorbed in the composites and their H_2S adsorption capacity [16, 17, 24]; **b** The H_2S adsorption capacity of $Cd(OH)_2$-GO nanocomposite in the absence and presence of ambient light in dry and moist conditions [25]; **c** The H_2S adsorption capacity of different GO composites with metal oxides, hydroxides, (oxy)hydroxides, and MOFs as active adsorbents [9, 15–20, 25–27]

GO-based composites for fuel and flue-gas desulfurization need to be non-toxic, high performing, and regenerable. Considering the high toxicity of cadmium, Cd-based materials for desulfurization application should be replaced with other transition metals like Zn, Fe, and Co [25]. Based on the adsorption performance of GO composites with Zn-based active adsorbents, ZnO, $Zn(OH)_2$, and ZnOOH are better choices than Zn-terephthalate MOF (MOF-5). Since MOF-5 fabrication needs toxic chemicals like N,N-dimethylformamide (DMF), chloroform, and an expensive terephthalic acid linker (\$85 kg^{-1}, Sigma Aldrich) [19, 29], the overall benefits of using MOF-5-GO composites are minimal. The only cost-cutting and environmentally benign solution is the use of polyethylene terephthalate (PET) bottle waste to fabricate MOF-5 [30]. Among MOFs, UiO-66 (Zr-terephthalate MOF) is a suitable candidate for GO composite formation due to its excellent H_2S uptake behavior and regenerability after heating in N_2 gas [20]. But considering the cost of Zr salts and organic linkers and the toxicity of organic solvents used in the MOF fabrication, the most suitable adsorbents are transition metal (oxy)hydroxides, which are porous materials with high hydroxyl density and H_2S removal capacity (Fig. 3c).

4 Removal Mechanism

Based on theoretical calculations, H_2S adsorption over pure graphene and hydrogenated graphene (graphane) nanosheets are governed by physical interaction, reflected by a lower adsorption energy and charge transfer in the range of -0.02–0.05 eV and 0.002–0.007e, respectively. However, when 3*d* transition metals like Fe, Co, and Cu are doped in the graphene nanosheets, it exhibits significantly higher adsorption energy of -0.93, -1.50, and -0.88 eV and charge transfer of 0.058, 0.170, and 0.302 e, respectively, which eventually leads to chemisorption [31]. Interactions with the graphene surface could be improved by modifying the surface with O-functionalities like epoxy and hydroxyl groups which enhanced the adsorption energy and charge transfer. The maximum change in these parameters is noticed for zigzag graphene nanoribbons as -0.0252 eV and -0.097e, respectively [32]. More detailed experimental and theoretical analyses have confirmed that H_2S molecules react with the carbonyl functional groups on the GO surface, which was also reflected in the population analysis of H_2S, where the functional group coverage increase from 10 to 30% led to an increment in the number of chemisorbed H_2S molecules. The population analysis spectra confirmed that water molecules could block these reactive sites and restrict the decomposition of H_2S molecules [22]. The introduction of transition metal (Cu) or metal oxide (CuO) in GO nanostructures could substantially improve the H_2S binding energy in the range of -1.33–-1.93 eV for Cu atom and -2.36–-2.95 eV for CuO at the top, hollow, and bridge binding sites compared to the pristine GO nanostructure [33]. Water over the surface of transition metal oxides could improve their H_2S removal capacity by lowering the energy barrier from 63.3 to 53.3 kJ mol^{-1} for newly formed hydroxyl groups, further confirmed for ZnO through spectroscopy and density functional theory calculations [23]. Thus, theoretical calculations have demonstrated that GO nanosheets decorated with transition metal oxides are highly effective in H_2S mineralization, which we have critically discussed here.

In dry conditions, the H_2S adsorption mechanism over a metal oxide such as ZnO is initiated with the dissociation of H_2S molecules to H^+ and HS^- ions, followed by diffusion of HS^- ions in the oxide lattice and migration of oxide and formed water molecules to the surface. Thus, the conversion of ZnO to ZnS is facilitated by protons transfers from H_2S to the surface-bound hydroxyl groups. Due to this direct acid–base reaction, ZnS as a byproduct could be traced in the X-ray diffraction pattern of spent ZnO samples [10, 34]. However, this is not the case with other studies dealing with H_2S adsorption due to the sulfidation of two to three oxide surface monolayers after H_2S saturation, and sophisticated techniques are required to deduce the mechanism [35, 36]. Since sulfide formation is a common occurrence in the H_2S adsorption process over transition metal oxide, X-ray photoelectron spectroscopy (XPS) is a standard analytical technique to conclude the adsorption mechanism. Due to the replacement of lattice O^{2-} with S^{2-} ions, there is a change in the electron density around transition metal ions, which causes a shift in the binding energy of metal ions [37]. Moreover, the sulfide ions could be detected in the high-resolution S2p spectrum, where a $2p_{3/2}$-$2p_{1/2}$ doublet is witnessed at 161–162 eV [38]. Other than sulfide, even sulfate ions could form in dry conditions. This acidic high-valent sulfur species could be identified in the S 2p spectrum as a $2p_{3/2}$-$2p_{1/2}$ doublet between 168–170 eV. The sulfate species generates through the oxidation of S^{2-} or HS^{-} by loosely bound oxygen species or adsorbed molecular oxygen [34].

In moist conditions, the H_2S adsorption mechanism has more complexities due to the involvement of chemically adsorbed water on the GO-based composite surface. As discussed earlier, moisture certainly restricts the interaction of H_2S with the GO surface due to the competitive nature of H_2O for the H_2S binding sites. However, chemisorbed H_2O plays a positive role in H_2S adsorption over the transition metal oxide surface. The chemisorbed water could dissociate on the transition metal oxide surface with alkaline nature to form additional hydroxyl groups, which promotes the reactive dissociation of H_2S by providing a low activation energy pathway [23, 28]. Thus, the role of water toward H_2S adsorption over RGO/GO-based composites is highly related to the active adsorbent of the composite. The H_2S adsorption-oxidation over metal oxide composite forms sulfide, sulfur, and sulfate species, which are distinguishable in the S 2p spectrum of the exhausted samples (Fig. 4a). The elemental sulfur formation is associated with the redox chemistry of transition metal ions, where high-valent cation reduces to a lower oxidation state by accepting electrons from the sulfide ions, which changes the sulfide into elemental sulfur.

A more recent investigation by Long et al. has provided better insight into the reaction byproducts of the H_2S adsorption-oxidation process. Three RGO/metal oxide composites with MgO, ZnO, and Fe_2O_3 were investigated for H_2S adsorption in humid conditions at room temperature. While sulfide, sulfur, and sulfate species were confirmed over ZnO/RGO and Fe_2O_3/RGO, sulfide formation was absent in MgO/RGO when experiments were performed with 1% O_2 in the carrier gas (Fig. 4a). Theoretical calculations and electron paramagnetic spectroscopy confirmed the formation of $O_2^{\cdot-}$ radicals in the O_2 flow, which were absent in the N_2 flow. These $O_2^{\cdot-}$ radicals were generated by the single-electron transfer from the RGO matrix, which catalytically oxidized S^{2-} and HS^{-} species to elemental sulfur. This radical-based oxidation ($\Delta G = -0.174$ eV) is preferred over acid–base neutralization of sulfides ($\Delta G = 0.853$ eV) in MgO/RGO, which resulted in a large proportion of elemental sulfur. However, for Fe_2O_3/RGO and ZnO/RGO, the calculations suggested that HS^{-} prefers reacting with ZnO ($\Delta G = -0.365$ eV) and Fe_2O_3 ($\Delta G = -0.771$ eV) to form ZnS and Fe_2S_3, respectively, rather than being oxidized by $O_2^{\cdot-}$ radicals. For this reason, a large proportion of formed sulfide remained metal-bound, and a small fraction oxidized to elemental sulfur and sulfate species (Fig. 4b, c) [28].

Even the physicochemical properties of active adsorbents play an important role in the adsorption mechanism and are responsible for the H_2S uptake capacity. Unlike metal oxides, where the role of hydroxyl groups in H_2S dissociation is limited due to the low hydroxyl group density, metal (oxy)hydroxides have a high hydroxyl group density. These hydroxyl groups are responsible for a high H_2S uptake capacity compared to metal oxides or hydroxides. For instance, CoOOH-GO with Co^{3+} ions has a higher oxidation ability than $Co(OH)_2$-GO with Co^{2+} ions, which makes CoOOH-GO a superior material for H_2S mineralization [15, 24]. In dry conditions,

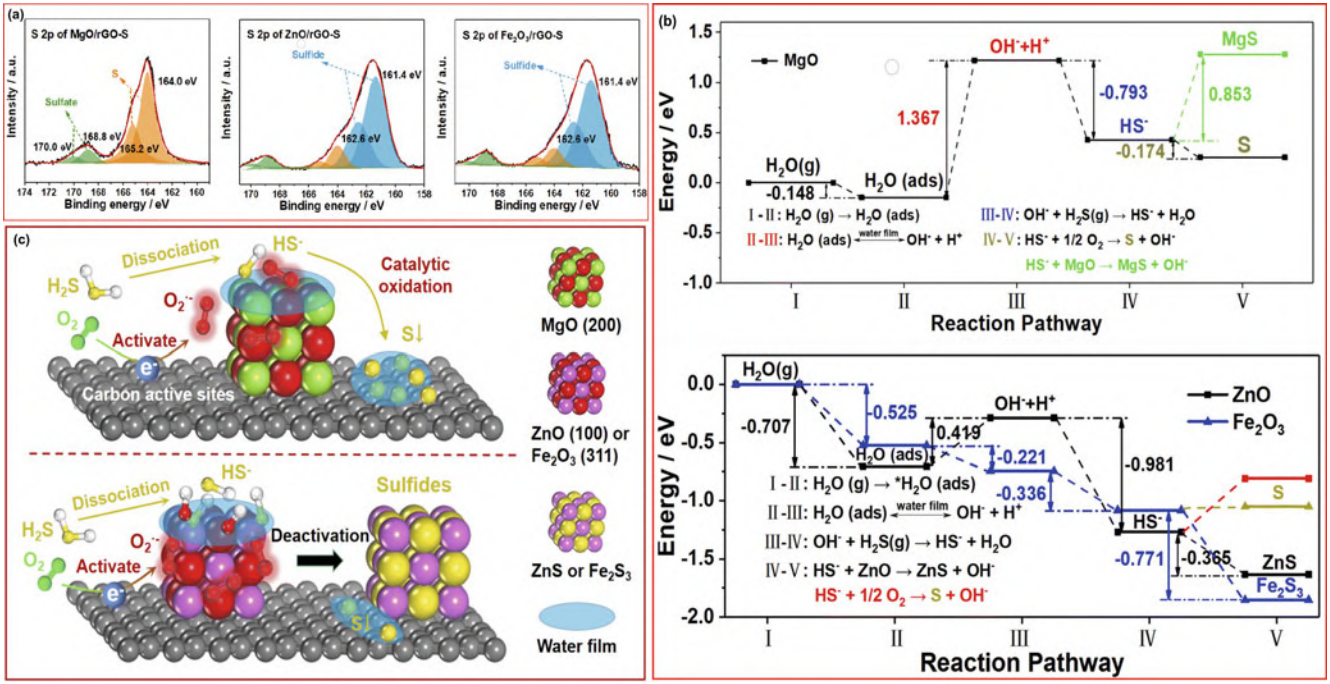

Fig. 4 **A** High-resolution S 2p spectra of MgO/rGO-S, ZnO/rGO-S, and Fe_2O_3/rGO-S; **b** The calculated free-energy changes of the H_2S catalytic oxidation reaction on the MgO (200), ZnO (100), and Fe_2O_3 (311); **c** Schematic illustrations of room-temperature H_2S removal over MgO/rGO, ZnO/rGO, or Fe_2O_3/rGO. Adapted with permission [28], Copyright (2022), The Royal Society of Chemistry

the high oxidation activity of CoOOH results in the minor evolution of SO_2 gas, which could be suppressed in moist conditions. The H_2S reaction chemistry over moist CoOOH involves multiple reaction pathways, forming several sulfurous byproducts, including metal sulfides and sulfates [15]. The same is true for other metal (oxy)hydroxides like FeOOH, where both the lattice oxygen and hydroxyl groups are crucial for H_2S oxidation (Fig. 5). The H_2S molecules dissociate in the water film to generate HS^- ions which replace the surface hydroxyl groups to form iron sulfide. The formed sulfide is oxidized to elemental sulfur by molecular oxygen and water to replenish the consumed hydroxyl groups. In another reaction pathway, H_2S molecules react with the lattice oxygen to form SO_2 molecules and reduced Fe^{2+} species. SO_2 could oxidize to SO_3 by molecular oxygen and form surface-bound SO_4^{2-} species by reacting with water. Furthermore, this molecular oxygen could oxidize Fe^{2+} to Fe^{3+} ions [16].

For MOFs-GO composite, the adsorption mechanism involves the reactive interaction of H_2S molecules with the open metal sites in the MOF framework. The open metal sites are highly active and accommodate the incoming H_2S molecules [17, 19]. However, this reactive dissociation of H_2S is accompanied by the release of H^+ ions, which dissociate the metal–carboxylate bonding and lowers the overall structural stability of the MOF (Fig. 6). Thus, despite having a large adsorption capacity,

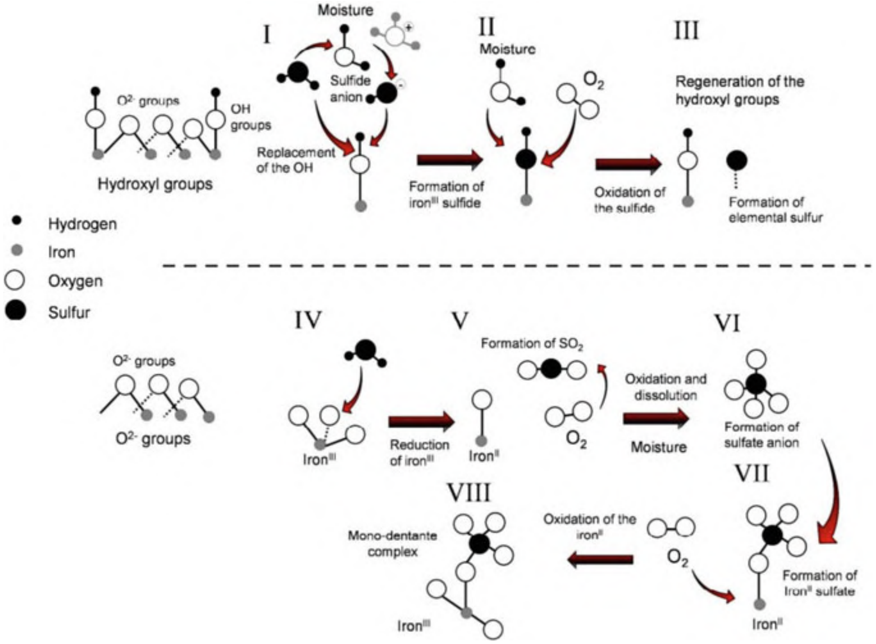

Fig. 5 Reactive adsorption mechanism of H_2S on the surface of FeOOH-GO composite. Adapted with permission [16], Copyright (2022), American Chemical Society

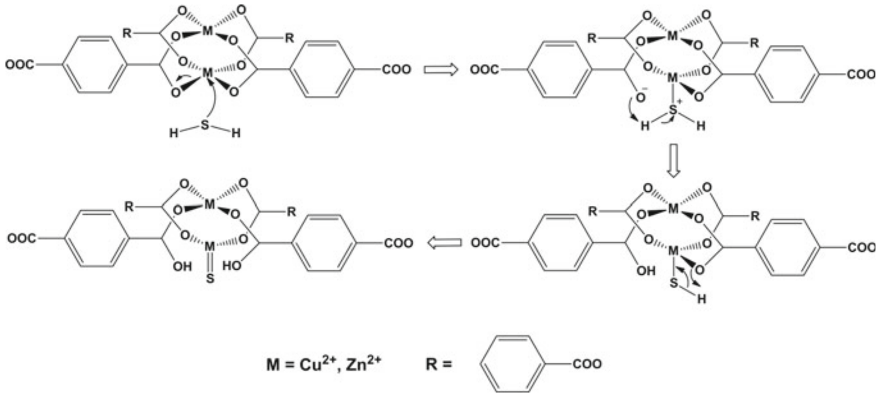

Fig. 6 H_2S adsorption mechanism over MOF-5-GO or HKUST-1-GO composites [17, 19]

MOF-GO composites of 3d transition metals like Cu and Zn are hard to regenerate with conventional regeneration techniques.

5 Challenges and Strategies

Though the research on the room-temperature desulfurization process has made significant progress toward developing outstanding GO-based adsorbents and understanding the mechanism driving the H_2S removal processes, these studies do not shed light on the regeneration capabilities of the composites. Regeneration is vital from economic and environmental perspectives as single-use adsorbents are misfit for achieving sustainable development goals. The researchers should focus on developing affordable and green regeneration strategies for commercialization with minimal labor and energy requirements [39]. Another major drawback of these studies is the lack of research data on operational parameters like gas concentration, flow rate, and adsorbent loading (bed height). These operation parameters should be systematically investigated in future studies for testing composite materials on an industrial scale. Besides optimizing the experimental parameters, the researchers should keenly seek pilot-scale studies and provide practical solutions for real-world problems like the desulfurization of biogas, fuel gas, and industrial flue gases.

As discussed earlier, the researchers have devoted efforts to developing GO-based composites using numerous active adsorbents, including metal oxides, hydroxides, oxyhydroxides, and MOFs. These materials have been judged for desulfurization applications solely based on their H_2S capture performance without considering the cost-to-performance ratio and the environmental impact of the overall gas cleaning process. Firstly, the researchers should look for green alternatives for the precursors and synthetic processes required for composite development. Instead of using the conventional Hummer's method for GO synthesis, which uses toxic oxidants and generates a large volume of wastewater, the researchers should follow water electrolytic oxidation of graphite that is safe, fast, and green and provides better control over the thickness and oxidation degree of GO [40]. Secondly, instead of using graphene as precursors for GO synthesis, the current focus should be on agro-waste for GO/RGO production [41, 42].

The choice of active adsorbent in the GO composite is hectic as there are numerous possibilities, and any of these adsorbents could be integrated with GO. However, the choice should not be merely influenced by the performance, but also by the non-toxicity and greenness of the overall synthesis process. Like in the case of MOFs, non-toxic and green solvents like water/ethanol should be adopted over DMF. HKUST-1, widely used in GO composite for H_2S adsorption [11–13, 17, 21], could be synthesized at room temperature in water on a commercial scale [43]. The alternative method over high-temperature solvothermal synthesis could reduce the environmental cost. Moreover, reliance on solvothermal synthesis could be ignored by adopting solvent-free synthesis routes, which are less expensive (\$13–36 kg^{-1}) than solvothermal synthesis (\$35–71 kg^{-1}) [44]. As such, even commercial organic linkers like terephthalic acid used in the synthesis of UiO-66(Zr) and MOF-5 could be replaced by extracting these linkers from PET bottle waste through mid-temperature acidic/alkaline hydrolysis [45] or directly using the crushed PET bottles [46]. This approach can further reduce the plastic burden on the planet and convert PET waste into value-added products, providing a win-win strategy required in the current research scenario.

6 Conclusion

In this chapter, we have highlighted the application of various RGO/GO-based composites for the room-temperature removal of H_2S gas. GO has been integrated with transition metal oxides, hydroxides, (oxy)hydroxides, and MOFs to construct porous nanocomposites with uniform distribution of active sites over the GO surface. In general, these composites have shown high H_2S adsorption capacity in moist conditions due to the dissociation and reactive dissolution of H_2S in surface water films. Moreover, the performances of these composites were primarily controlled by the nature of the active adsorbent, GO loading, and synthesis methods. Besides providing a large surface area, GO imparted heterogeneity to the surface, which was crucial in the reactive adsorption of H_2S. Some studies highlighted the role of visible light in improving the H_2S uptake performance in dry conditions by creating electron–hole pairs required during the oxidation of dissociated H_2S byproducts (like sulfide). The adsorption mechanism over these adsorbents involved the dissociation and oxidation of H_2S into sulfide, sulfur, and sulfates. In some cases, the reactive adsorbent oxidized H_2S into SO_2 gas in dry conditions. Though the literature has been saturated with numerous studies on GO/RGO-based composites for H_2S removal, their practical application is limited due to improper investigation of operational parameters and utilization of GO-adsorbent composites as aerogels and fabrics, which could be used directly in real-world applications.

References

1. Shah, M.S., Tsapatsis, M., Siepmann, J.I.: Hydrogen sulfide capture: from absorption in polar liquids to oxide, zeolite, and metal–organic framework adsorbents and membranes. Chem. Rev. **117**, 9755–9803 (2017)
2. Yalamanchili, C., Smith, M.D.: Acute hydrogen sulfide toxicity due to sewer gas exposure. Am. J. Emerg. Med. **26**(518), e5-518.e7 (2008)
3. Marcano, D.C., Kosynkin, D.V., Berlin, J.M., Sinitskii, A., Sun, Z., Slesarev, A., Alemany, L.B., Lu, W., Tour, J.M.: Improved synthesis of graphene oxide. ACS Nano **4**, 4806–4814 (2010)
4. Compton, O.C., Nguyen, S.T.: Graphene oxide, highly reduced graphene oxide, and graphene: versatile building blocks for carbon-based materials. Small **6**, 711–723 (2010)
5. Khaleghi Abbasabadi, M., Khodabakhshi, S., Esmaili Zand, H.R., Rashidi, A., Gholami, P., Sherafati, Z.: Covalent modification of reduced graphene oxide with piperazine as a novel nanoadsorbent for removal of H_2S gas. Res. Chem. Intermed. **46**, 4447–4463 (2020)
6. Georgakilas, V., Otyepka, M., Bourlinos, A.B., Chandra, V., Kim, N., Kemp, K.C., Hobza, P., Zboril, R., Kim, K.S.: Functionalization of graphene: Covalent and non-covalent approaches, derivatives and applications. Chem. Rev. **112**, 6156–6214 (2012)
7. Khaleghi Abbasabadi, M., Rashidi, A., Safaei-Ghomi, J., Khodabakhshi, S., Rahighi, R.: A new strategy for hydrogen sulfide removal by amido-functionalized reduced graphene oxide as a novel metal-free and highly efficient nanoadsorbent. J. Sulfur Chem. **36**, 660–671 (2016)
8. Seredych, M., Bandosz, T.J.: Adsorption of hydrogen sulfide on graphite derived materials modified by incorporation of nitrogen. Mater. Chem. Phys. **113**, 946–952 (2009)
9. Lonkar, S.P., Pillai, V., Abdala, A., Mittal, V.: In situ formed graphene/ZnO nanostructured composites for low temperature hydrogen sulfide removal from natural gas. RSC Adv. **6**, 81142–81150 (2016)
10. Song, H.S., Park, M.G., Kwon, S.J., Yi, K.B., Croiset, E., Chen, Z., Nam, S.C.: Hydrogen sulfide adsorption on nano-sized zinc oxide/reduced graphite oxide composite at ambient condition. Appl. Surf. Sci. **276**, 646–652 (2013)
11. Petit, C., Bandosz, T.J.: Exploring the coordination chemistry of MOF–graphite oxide composites and their applications as adsorbents. Dalton Trans. **41**, 4027–4035 (2012)
12. Bhoria, N., Basina, G., Pokhrel, J., Kumar Reddy, K.S., Anastasiou, S., Balasubramanian, V.V., AlWahedi, Y.F., Karanikolos, G.N.: Functionalization effects on HKUST-1 and HKUST-1/graphene oxide hybrid adsorbents for hydrogen sulfide removal. J. Hazard. Mater. **394**, 122565 (2020)
13. Ebrahim, A.M., Jagiello, J., Bandosz, T.J.: Enhanced reactive adsorption of H_2S on Cu–BTC/S- and N-doped GO composites. J. Mater. Chem. A **3**, 8194–8204 (2015)
14. Giannakoudakis, D.A., Bandosz, T.J.: Zinc (hydr)oxide/graphite oxide/AuNPs composites: role of surface features in H_2S reactive adsorption. J. Colloid Interface Sci. **436**, 296–305 (2014)
15. Florent, M., Bandosz, T.J.: Effects of surface heterogeneity of cobalt oxyhydroxide/graphite oxide composites on reactive adsorption of hydrogen sulfide. Microporous Mesoporous Mater. **204**, 8–14 (2015)
16. Arcibar, J.A., Wallace, R., Mitchell, J.K., Bandosz, T.J.: Role of surface chemistry and morphology in the reactive adsorption of H_2S on iron (hydr)oxide/graphite oxide composites. Langmuir **31**, 2730–2742 (2015)
17. Petit, C., Mendoza, B., Bandosz, T.J.: Hydrogen sulfide adsorption on MOFs and MOF/graphite oxide composites. ChemPhysChem **11**, 3678–3684 (2010)

18. Seredych, M., Mabayoje, O., Bandosz, T.J.: Visible-light-enhanced interactions of hydrogen sulfide with composites of zinc (oxy)hydroxide with graphite oxide and graphene. Langmuir **28**, 1337–1346 (2012)
19. Huang, Z.-H., Liu, G., Kang, F.: Glucose-promoted Zn-based metal–organic framework/ graphene oxide composites for hydrogen sulfide removal. ACS Appl. Mater. Interfaces **4**, 4942–4947 (2012)
20. Daraee, M., Ghasemy, E., Rashidi, A.: Synthesis of novel and engineered UiO-66/graphene oxide nanocomposite with enhanced H_2S adsorption capacity. J. Environ. Chem. Eng. **8**, 104351 (2020)
21. Petit, C., Levasseur, B., Mendoza, B., Bandosz, T.J.: Reactive adsorption of acidic gases on MOF/graphite oxide composites. Microporous Mesoporous Mater. **154**, 107–112 (2012)
22. Huang, L., Seredych, M., Bandosz, T.J., van Duin, A.C.T., Lu, X., Gubbins, K.E.: Controllable atomistic graphene oxide model and its application in hydrogen sulfide removal. J. Chem. Phys. **139**, 194707 (2013)
23. Zhao, Y., Zhang, Z., Yang, C., Fan, H., Wang, J., Tian, Z., Zhang, H.: Critical role of water on the surface of ZnO in H_2S removal at room temperature. Ind. Eng. Chem. Res. **57**, 15366–15374 (2018)
24. Mabayoje, O., Seredych, M., Bandosz, T.J.: Cobalt (hydr)oxide/graphite oxide composites: Importance of surface chemical heterogeneity for reactive adsorption of hydrogen sulfide. J. Colloid Interface Sci. **378**, 1–9 (2012)
25. Florent, M., Wallace, R., Bandosz, T.J.: Removal of hydrogen sulfide at ambient conditions on cadmium/GO-based composite adsorbents. J. Colloid Interface Sci. **448**, 573–581 (2015)
26. Seredych, M., Bandosz, T.J.: Reactive adsorption of hydrogen sulfide on graphite oxide/ $Zr(OH)_4$ composites. Chem. Eng. J. **166**, 1032–1038 (2011)
27. Mabayoje, O., Seredych, M., Bandosz, T.J.: Reactive adsorption of hydrogen sulfide on visible light photoactive zinc (hydr)oxide/graphite oxide and zinc (hydr)oxychloride/graphite oxide composites. Appl. Catal. B, 132–133, 321–331 (2013)
28. Xu, H., Pan, Y., Hu, F., Niu, B., Zhang, Y., Long, D.: Anti-corrosion MgO nanoparticle-equipped graphene oxide nanosheet for efficient room-temperature H_2S removal. J. Mater. Chem. A **10**, 18308–18321 (2022)
29. Kim, T.H., Kim, S.G.: Clinical outcomes of occupational exposure to N, N-dimethylformamide: Perspectives from experimental toxicology. Saf. Health Work **2**, 97–104 (2011)
30. Villarroel, D., Bernini, M.C., Arroyo-Gómez, J.J., Villarroel, J., Sapag, K.: Synthesis of MOF-5 using terephthalic acid as a ligand obtained from polyethylene terephthalate (PET) waste and its test in CO_2 adsorption. Braz. J. Chem. Eng. **39**, 949–959 (2022)
31. Zhou, Q., Su, X., Ju, W., Yong, Y., Li, X., Fu, Z., Wang, C.: Adsorption of H_2S on graphane decorated with Fe. Co and Cu: a DFT Study RSC Adv. **7**, 31457–31465 (2017)
32. Salih, E., Ayesh, A.I.: DFT investigation of H_2S adsorption on graphene nanosheets and nanoribbons: Comparative study. Superlattices Microstruct. **146**, 106650 (2020)
33. Jyoti, R., Deji, Choudhary, B.C., Sharma, R.K.: Graphene oxide nanoribbons decorated with Cu and CuO as H_2S gas sensor optimized with DFT. AIP Conf. Proc. **2369**, 020130 (2021)
34. Song, H.S., Park, M.G., Ahn, W., Lim, S.N., Yi, K.B., Croiset, E., Chen, Z., Nam, S.C.: Enhanced adsorption of hydrogen sulfide and regeneration ability on the composites of zinc oxide with reduced graphite oxide. Chem. Eng. J. **253**, 264–273 (2014)
35. Balsamo, M., Cimino, S., de Falco, G., Erto, A., Lisi, L.: ZnO-CuO supported on activated carbon for H_2S removal at room temperature. Chem. Eng. J. **304**, 399–407 (2016)
36. Galtayries, A., Bonnelle, J.-P.: XPS and ISS studies on the interaction of H_2S with polycrystalline Cu, Cu_2O and CuO surfaces. Surf. Interface Anal. **23**, 171–179 (1995)
37. Lee, S., Kim, D.: Enhanced adsorptive removal of hydrogen sulfide from gas stream with zinc-iron hydroxide at room temperature. Chem. Eng. J. **363**, 43–48 (2019)
38. Gupta, N.K., Bae, J., Kim, K.S.: Metal organic framework derived $NaCo_xO_y$ for room temperature hydrogen sulfide removal. Sci Rep. **11**, 14740 (2021)
39. Gupta, N.K., Vikrant, K., Kim, K.S., Kim, K.-H., Giannakoudakis, D.A.: Regeneration strategies for metal–organic frameworks post acidic gas capture. Coord. Chem. Rev. **467**, 214629 (2022)

40. Pei, S., Wei, Q., Huang, K., Cheng, H.-M., Ren, W.: Green synthesis of graphene oxide by seconds timescale water electrolytic oxidation. Nat. Commun. **9**, 145 (2018)
41. Tamilselvi, R., Ramesh, M., Lekshmi, G.S., Bazaka, O., Levchenko, I., Bazaka, K., Mandhakini, M.: Graphene oxide–based supercapacitors from agricultural wastes: a step to mass production of highly efficient electrodes for electrical transportation systems. Renew. Energy **151**, 731–739 (2020)
42. Debbarma, J., Naik, M.J.P., Saha, M.: From agrowaste to graphene nanosheets: chemistry and synthesis. Fullerenes, Nanotubes, Carbon Nanostruct. **27**, 482–485 (2019)
43. Huo, J., Brightwell, M., El Hankari, S., Garai, A., Bradshaw, D.: A versatile, industrially relevant, aqueous room temperature synthesis of HKUST-1 with high space-time yield. J. Mater. Chem. A **1**, 15220 (2013)
44. DeSantis, D., Mason, J.A., James, B.D., Houchins, C., Long, J.R., Veenstra, M.: Techno-economic analysis of metal–organic frameworks for hydrogen and natural gas storage. Energy Fuels **31**, 2024–2032 (2017)
45. Kaur, R., Marwaha, A., Chhabra, V.A., Kaushal, K., Kim, K.-H., Tripathi, S.K.: Facile synthesis of a Cu-based metal-organic framework from plastic waste and its application as a sensor for acetone. J. Cleaner Prod. **263**, 121492 (2020)
46. Deleu, W.P.R., Stassen, I., Jonckheere, D., Ameloot, R., De Vos, D.E.: Waste PET (bottles) as a resource or substrate for MOF synthesis. J. Mater. Chem. A **4**, 9519–9525 (2016)

3D Graphene for Removal of Inorganic Pollutants

**Iqra Fareed, Muhammad Danish Khan, Danish Rehman,
Masood ul Hassan Farooq, and Faheem K. Butt**

Abstract 3D Graphene (3DG) has attracted a lot of attention in recent years because of its unique features. The advancement in 3DG structures fundamentally makes it easier to use the material in practical applications while maintaining its beneficial features such as low density, large surface area, high porosity, outstanding mechanical properties, and rapid transport for mass and electron. 3DG has been investigated to remove inorganic pollutants, such as heavy metal ions (lead, arsenic, chromium, mercury), fluorides, nitrides, chlorides, phosphates, antimony, and radium, that mainly come from industrial litter, pharmaceutical waste, agricultural discharge, oil refineries, improper radioactive disposal, and natural seepage which seriously threaten the human health as well as aquatic flora and fauna. Environmental remediation using 3DG is still being explored. The progress that has been made thus far in this respect is summarized in the current chapter. Further research is required to focus on its development for real-world applications.

Keywords 3D Graphene · Adsorption · Heterostructures · Synergy · Inorganic pollutant

---

I. Fareed · M. D. Khan
Department of Physics, University of Engineering and Technology, G.T. Road, Lahore 54890, Pakistan

D. Rehman · F. K. Butt (✉)
Department of Physics, Division of Science and Technology, University of Education Lahore, Township, Lahore 54770, Pakistan
e-mail: faheemk.butt@ue.edu.pk

M. ul Hassan Farooq
Department of Natural Sciences and Humanities, University of Engineering and Technology (UET), New Campus (KSK), Lahore 54890, Pakistan

© The Author(s), under exclusive license to Springer Nature Switzerland AG 2023

R. K. Gupta (ed.), *3D Graphene*, Carbon Nanostructures,
https://doi.org/10.1007/978-3-031-36249-1_10

1 Introduction

Pollutants are known to have adverse effects on surrounding and are found as gases, aerosols, liquids, or solids that are either naturally occurring or produced by human activity [11]. Pollutants with non-biodegradable nature have a harmful impact on health even in minute quantities. These pollutants are generally caused by man-made activities including industrialization, urbanization, uncontrolled sewerage discharge, and so on in addition to naturally occurring activities [22]. They hail from chemicals that are being dumped out by industries and factories working in the field of engineering, papermaking, fine chemicals, dyes, paints, pharmaceuticals, and textiles [21]. They include trace elements, mineral acids, inorganic salts, metals that have formed complexes with organic compounds, sulfates, and cyanides, contaminating waters. These inorganic contaminants are persistent in the environment and are not biodegradable. Human health as well as flora and fauna are all negatively impacted by this inorganic pollution [43]. Drinking water that has inorganic pollutants dissolved in them has diverse effects on the human body because these materials are carcinogenic, teratogenic, and mutagenic with accumulative amplification effects [21].

The world health organization (WHO) has set standards for several inorganic pollutants, acceptable in drinking water. Many countries around the world have constructed models and adopted guidelines to reduce the number of inorganic pollutants in heavy water which is in support of WHO standards. The following Table 1 summarizes the limit of inorganic pollutants that are acceptable in drinking water and the diseases that may be caused in case of access amount.

Due to the cumulative long-term impacts on health, inorganic contamination in the environment is a serious health hazard all around the globe, even at low concentrations. Ingesting these hazardous substances through consumables not only affects

Table 1 Acceptable limit of inorganic pollutants. Adapted with permission [19], Copyright (2018), Elsevier

Heavy metals	WHO standards (mg/mL)
Cadmium (Cd)	0.003
Lead (Pb)	0.010
Chromium (Cr-III)	0.050
(Cr-VI)	0.010
Arsenic (As)	0.010
Nickel (Ni)	0.070
Manganese (Mn)	0.400
Zinc (Zn)	3.000
Tin (Sn)	–
Mercury (Hg)	0.006
Copper (Cu)	2.000
Iron (Fe)	0.300
Silver (Ag)	–

organs and body function, but also diminishes body immunity and causes growth retardation, poor mental development, bad psycho-social attitude, and a number of disorders in people. Radioactive elements such as Uranium (U), Radium (Ra), and others, if they are present in drinking water, can cause genetic damage and infertility and are carcinogenic which in low traces can cause changes in bone structure and nephritis [31]. Water pollution is bad for the environment and human health. Statistics showed that each year, 1 billion people are directly harmed by toxic pollutants in the water, and therefore, diseases and other health problems erupt. Inorganic pollutants can cause gastrointestinal distress, cirrhosis, necrosis, low blood pressure, hypertension, headaches, stomachaches, diarrhea, and vomiting [43]. Inorganic contaminants that accumulate in the food chain and harm human health are polluting the environment at a devastating rate. It has been discovered that both organic and inorganic substances can increase the generation of free radicals [30].

Rapid industrialization results in the discharge of significant inorganic pollutants that impact water and soil. Heavy metals, which are hazardous or deadly even at low concentrations, make up many inorganic contaminants [34]. Pesticides can be detrimental to human health when used carelessly and without discrimination. The sensitivity and toxicity of these pollutants to the organisms define their scope and adverse effects. But no inferences regarding the amounts of heavy metals could be made based only on an extensive evaluation of human impacts [30].

1.1 Categorizing Inorganic Pollutants

There are many inorganic pollutants that exist, but we mainly categorize them into metallic pollutants, sulfides, and fertilizers as illustrated in Fig. 1.

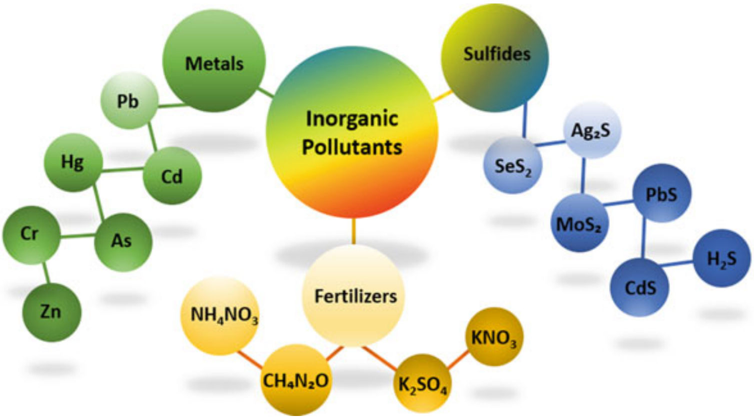

Fig. 1 Inorganic pollutants divided into three main categories

Aluminum (Al), Copper (Cu), Iron (Fe), Lead (Pb), and Zinc (Zn) are all present in drinking water. However, the naturally occurring materials that are the major cause of inorganic pollution include compounds of Boron (B), Arsenic (As), and Fluorides (F^-). These naturally occurring inorganic minerals typically contaminate surface water and groundwater as well as canals, ponds, lakes, distribution pipelines systems, and primarily, tap water. Other than that, heavy metals like Mercury (Hg), Cadmium (Cd), Chromium (Cr), Cyanides ($-CN$), etc. are also categorized as inorganic industrial waste. They can create health problems by entering the body through consumables [18]. The phylogenetic sources that are connected to the soil and plants discharge heavy metals, which have a negative influence on the environment. The resultant food insecurity causing health risks leads to a troubling situation with undeniable environmental distress [1].

From the deepest strata of the earth, heavy metals are excavated and released into the environment. On the other hand, mines, smelters, thermal power plants, metallurgical industries, electronics, textiles, phosphatic fertilizers, and municipal solid waste are also a few of the businesses and sources that give off heavy metals into the surroundings. The largest contributors to Cr, Hg, Nickel (Ni), Vanadium (V), and Selenium (Se) emissions were from stationary sources such as coal-fired power plants, while Pb emissions come from transportation, Cu production causing As, Cd, and Cu emissions, while Zn manufacturing leads to Zn emission. Trace metals after being released into the atmosphere are transported within air masses. A significant portion of these metals is deposited on the land mass, sometimes even covering national or continental boundaries [31].

Salt (primarily sodium chloride, NaCl) is majorly used in industries, particularly those related to the manufacturing of soap and detergent, glass, textiles, rubber, leather tanning, metal processing, and oil/gas drilling. Industrial effluents contain salt ions that are highly mobile in the soil and can seep through the soil profile, contaminating groundwater reservoirs when released into the environment. Agricultural land soils can become salinized (have access of NaCl) or sodic (have a large amount of sodium) when such salt-laden groundwater and surface water are utilized to irrigate crops. Na damages typical plant growth at greater concentrations and this damage is relative to high chloride and salt levels. As a result, harm brought on by excess Na and salinity occurs simultaneously. Reduced water availability rather than a specific harmful effect is typically blamed for growth inhibition brought on by high Na and salinity concentrations [31].

Obsolete inorganic-based pesticides have accumulated over the last few decades in practically every developing nation or emerging market. Given that many of the products are quite old and usually lack documentation, it is challenging to determine the precise number of obsolete pesticides. Insecticides containing organochlorines were initially used to manage parasites. Persistent and non-biodegradable pesticides have contaminated numerous elements of the soil, water, and air ecosystems. A number of factors, such as gene mutation, altered population growth rates, and an increase in population size in terms of generations, could be a consequence of the pest's adaptation to the new environment [30]. Heavy metals are poisonous to soil microorganisms; they have an impact on a number of important microbial-mediated soil processes in agriculture. Toxicity mostly manifests as inhibition of growth, morphology, and activity of various microorganisms, including symbiotic N_2 fixers. Nutrient cycling in soil involves biochemical, chemical, and physico-chemical reactions, with microorganisms primarily mediating biochemical processes. As the quantity of heavy metals in the soil grew, it was discovered that the activities of soil dehydrogenases, proteases, lipases, and esterases considerably decreased. Pb did not significantly alter the activity of acid phosphatases, while only Ni and Cr considerably reduced the activity of arylsulfatases [31]. Some of the most commonly reported inorganic pollutants in water are listed below:

Ammonia: Industrial, agricultural, and food processing waste are its main sources in water channels. Its overuse makes the body poisonous. The toxic gaseous content is produced when mixed with bleach [43].

Arsenic: Glass, pigments, and textiles are a few examples of industrial waste sources that contain As. As is found in materials like preservatives, paper, and metal adhesives. In the past, it was utilized in feed additives, medicines, and pesticides. It is a group-I carcinogen according to Organization for International Cancer Research [43]. If As becomes part of the body, it can cause gastronomical symptoms, melanosis, hepatomegaly, and in severe cases death [19].

Barium: Barium has the same adverse effects as As. It can result in heart abnormalities, tremors, weakness, shortness of breath, and paralysis if ingested in excess. It comes from the scrap metal industry [43].

Chloride: Manure, sewage effluent, salt storage waste, industrial waste, and drilling waste all contain chlorides. The widespread usage of water contaminated with chloride can result in toxicity above the allowable level of 250 mg/L [43].

Chrome: Cr waste is released by the dye, paints, and tanning of leather in industries. Total Cr in drinking water is permitted up to 0.1 mg/L. There are two oxidation states of Cr^{+3}, among them Cr^{+6} is notorious for having cancer-causing properties [43]. This also brews up diseases like genotoxic and alopecia [19].

Copper: Cu is released into water resources from the corrosion of water pipes. While 0.3 mg/L per day is required for metabolic processes, excessive ingestion can result in stomach pain and intestinal conditions [43], liver and kidney disease, cancer, and stomach irritation [19].

Mercury: Hg is an extremely hazardous inorganic element at ultra-trace concentrations. It enters aquatic bodies because of a number of activities, such as small-scale gold mining, the production of non-ferrous metals, and the burning of fossil fuels [43]. Symptoms of Hg poisoning include kidney disease, muscle impairment, and gum inflammation, and if left untreated can cause death [19].

Uranium: Uranium is discovered in water-polluting sources because of the extraction, processing, and disposal of radioactive waste. It might be detrimental to the heart, brain, kidney, liver, and other organ systems [43].

Zinc: In addition to other items, Zn is frequently used in dry-cell batteries, paints, dyes, plastics, wood preservatives, rubber, cosmetics, and coatings that resist corrosion. Rubber tires, waste incineration, metal manufacturing, and industrial coal combustion are further sources of Zn-contaminated waste [43]. Zn poisoning often causes dizziness [19].

Cadmium: Cd seeping in the water cycle also has adverse effects on human health. If unfiltered water is consumed by humans, this can irritate the eyes which can lead to retinal failure. It can also harmfully affect pregnant women and brew up birth defects. Other than that, this can cause anemia and is a carcinogen [19].

Lead: Excess consumption of Pb can lead to problems related to blood filtration and can cause kidney failure. This can also affect the motor nerves of the body leading to a lack of response in muscles [19].

Silver: Ag is considered a precious metal and is used in many industries, but it is not harmless. Indigestion of this element can cause argyria and argyrias, and if inhaled can cause respiratory damage [19].

Tin: Sn can cause metabolic disruption and its excess amount is carcinogenic [19].

Iron: Fe lies at the heart of the industrial revolution and is used in almost every household product. In places like steel mills, the concentration of Fe is too high and causes unrequired disruption in health. Indigestion of Fe can cause swear kidney damage and blood creatinine [19].

Nickel: Ni poisoning is caused when drinking water has an excess amount of Ni than the limit introduced by WHO, i.e., 0.070 mg/mL. In this case, diseases like anaphylaxis, lung cancer, loss of red blood cells, and nephrotoxic nature take place [19].

Manganese: Mn is an important part of the chemical industry. Production of goods leads to contamination of surface water. If the amount of this element exceeds 0.400 mg/mL, it can cause sleep dysfunction and is neurotoxic [19].

2 Conventional Remediation Techniques

There are several conventional methods to remove inorganic pollutants which can be classified into biological, chemical, and physical processes, as shown in Fig. 2.

2.1 Biological Processes

The reaction between microorganisms and pollutants is carried out for the decontamination of the environment. This cost-effective bioremediation extracts the pollutants

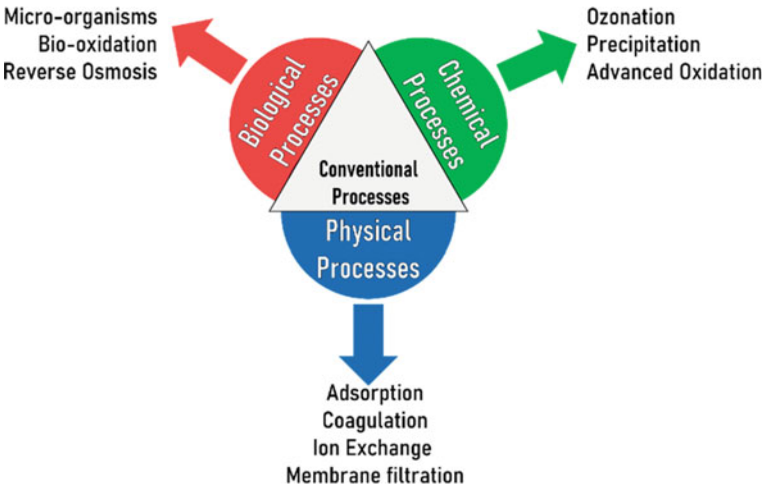

Fig. 2 Conventional methods to remove inorganic pollutants

with the help of microorganisms like algae, fungi, and bacteria using sunlight. But the process is quite slow and unable to remove all the contaminants. Enzymes being biological catalysts trigger biological oxidation in the aquatic environment. Nevertheless, bio-oxidation processes strongly depend on temperature and pH. In suspended growth, contaminants surround the free-floating microorganisms, forming biological flocs (larger size particles), providing low-concentration pollutant removal. But it suffers from the disadvantage of microorganism removal with the variable water flow. The attached growth is another resilient process in which bacteria are attached to immersed media (called a biofilm) for high-concentration pollutants treatment. The odor problem and inefficiency in cold weather conditions are causes of its limited use. The reverse osmosis procedure provides contaminant removal under high pressure using a semi-permeable membrane. However, it requires pre-treatment to avoid undesired depositions on the membrane surface or inside the membrane pores, resulting in a decrease in permeation flux and a reduced process efficiency [3, 23, 28].

2.2 Chemical Processes

In this process, certain chemicals are added to facilitate the separation of pollutants. Precipitation is performed by the deliberate addition of appropriate flocculants to remove dissolved pollutants. Nevertheless, it is specific to some pollutants, resulting in sludge with a large quantity of toxic compounds. Advance oxidation processes (AOPs) remove the inorganic pollutants by in situ formation of hydroxyl radicals via redox reactions. The fast reaction kinetics is involved at room temperature and atmospheric pressure with no footprints and sludge formation. Sometimes AOPs involve ultraviolet exposure on a catalyst, leading to high operating costs and inefficient use of reactive species. Ozonation, another AOP, removes inorganic contaminants by generating highly reactive free radicals during the reaction of ozone with water. The short life of ozone necessitates its on-site production, which raises the cost of treatment. Fenton's reagent, i.e., hydrogen peroxide and ferrous ion, provides the most efficient oxidation of pollutants. However, it produces acidic conditions that must be neutralized. Zeolites being aluminosilicate crystals with oxygen bridging provide the removal of pollutants with high sorption capacity through ion exchange. Nonetheless, zeolites require suspended matter and turbidity-free fluid to avoid clogging [32, 38, 41].

2.3 Physical Processes

The suspended or floating inorganic contaminants can be removed by settling and skimming from the top of the surface. Coagulation is a process that converts suspended, emulsified, unsettled, dissolved contaminants or slow-settling fine-sized particles into larger sizes by the addition of a coagulant in an aqueous medium. The larger size particles (flocs) are de-stabilized, weekly bound with water, and can be removed through filtration. Post-coagulation results in sludge that requires additional sedimentations for further filtration purposes. The ion-exchange process provides water treatment without the formation of sludge; nevertheless, it is specific to certain pollutants, resulting in salty water, chlorine, and/or bacterial contamination, as well as a high cost required for the replacement of the ion-exchanged resin over time. Membrane filtration is another simple and efficient separation technology used to remove contaminants with no secondary pollutant generation. However, its use is limited by the cause of severe fouling and high engineering costs. In another process, the solution with adsorbable solute is brought into contact with a porous structure called adsorbent (may be natural or synthetic). The intermolecular forces are responsible for the adsorption/deposition of impurities onto the adsorbent, which is retained at the adsorbent surface; the accumulation of targeted particles onto the adsorbent surface is known as adsorption. This is an effective method, employed for a long time to remove pollutants by absorbing the contaminants [2, 5, 40].

3 3DG Architecture

Since the discovery of graphene, it has been a material of interest because it exhibits sp^2 hybridization. The sp^2 hybridization of graphene is responsible for a honeycomb-like structure, and to date, it is the thinnest material known to man. Many defects can be created in graphene due to its pi-pi junction. Because of its fascinating properties, graphene can be found in zero-dimensional quantum dots, one-dimensional carbon nanotubes (CNT), two-dimensional graphene nanosheets, and 3D graphene-based macro and microstructures. 3DG owing to its outstanding characteristics, as exhibited in Fig. 3 is a very attractive material for researchers and is used in a variety of applications. However, there is one problem with graphene, i.e., restacking of layers during the performance that accompanies less yield as compared to theoretical calculations [36].

The study of graphene architecture in 3D structures has been greatly investigated after 2009. 3DG has a high specific area and does not restack itself when in use. If the structure of graphene has a size of 10 nm or greater, it is referred to as 3DG architecture. The 3D architecture of graphene includes macroscopic hydrogels, graphene forms, macroscopic graphene flowers, and porous graphene framework. The porosity of the 3DG-based materials depends upon the bending, wrinkling, and carving of graphene nanosheets. This induces a high specific area in the graphene architecture, and the average surface area of graphene ranges from 500 m^2/g to 1000 m^2/g [36].

The properties of graphene and the 3D architecture of graphene are highly dependent upon the synthesis process. The minor changes in the experimental conditions give unique and diverse graphene structures. The perfect graphene is a semiconductor with zero bandgaps. The bandgap is introduced to the material by producing topological defects, edge defects, disordered graphene, the substitution of functional groups, and doping of heterogeneous atoms [36].

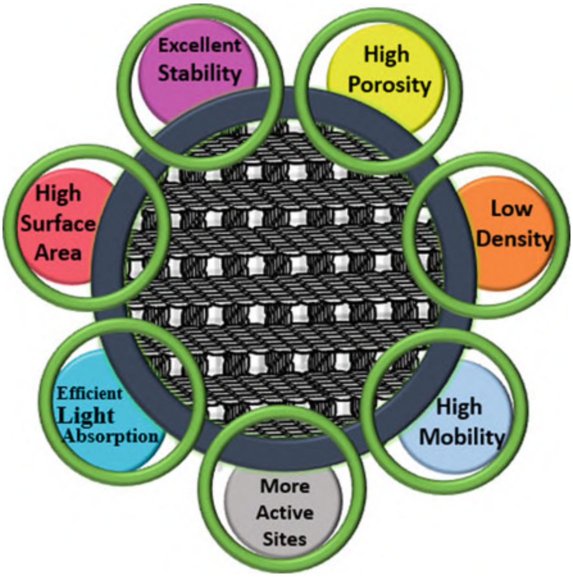

Fig. 3 Characteristics of 3DG

4 3DG for Removal of Inorganic Pollutants

Graphene has been studied a lot for the elimination of inorganic pollutants because of its efficient light absorption properties, superior charge transfer capabilities, thermal conductivity, and multidimensional electron transport channels. 3DG architecture exhibits high absorption, profound stability, high specific area, enhanced active sites, availability of oxygen, carboxyl, and hydroxyl functional groups and acts as a charge carrier mediator [48]. 3DG bestows excellent steadiness under acidic and salty conditions. Other than that, 3DG architectures are also stable in organic solvents such as dimethylformamide and cyclohexane [33]. 3DG architecture has been employed and reported for inorganic pollutant removal through the adsorption method, photocatalysis, and their synergistic outcomes [48].

4.1 3DG Adsorption Technology

The adsorption properties of graphene depend on the following factors.

4.1.1 Adsorption Sites

Graphene usually has three possible adsorption sites.

(a) Oxygen functional groups.
(b) π-electrons of carbon.
(c) Decorated nanoparticles.

Metal ions have a higher affinity toward oxygen atoms that are present in the graphene structure. The adsorption is performed by two types of interactions involving electrostatic interactions and coordination of oxygen and metal ions, especially in the carboxyl group. Heat treatment of the material can cause a decrease in oxygen functional groups, but the number of carboxyl group increases [4]. 3DG architecture has delocalized π-electrons which can react with inorganic impurity obeying the Lewis acid and base. In 3DG and metal ion interaction, 3DG act as Lewis's base while metal ion behaves like Lewis's acid, and upon interaction, complexes are formed [17]. Decorating the outer surface of 3DG architecture with different types of nanoparticles such as MnO_2, TiO_2, and ZnO increases the number of active sites of graphene, thus leading to enhanced adsorption [4].

4.1.2 Pore Structure

The adsorption capacity of graphene-based architecture depends upon the number of available pores and pore size. Ultrapure graphene has an immense specific area and zero porosity. To increase the porosity of 3DG, it is combined with other porous materials [4].

3DG when synthesized with natural acids, self-assembled themselves through π-π interaction. This material shows superhydrophobicity, high porosity, and low density, which proved itself efficient for fast adsorption [4]. CNT-Aerogel shows an adsorption rate of 230–451 μmol g^{-1} for Pb, which is better than pristine CNTs. The extent of adsorption depends upon the particle diffusion which is the rate-controlling step. The particle diffusion further depends upon the complexes in the medium and the ion exchange [33].

4.1.3 pH of the Solution

The pH of the polluted solution is of great importance and majorly affects the adsorption properties of 3DG. The pH of the solution provides a surface charge to the absorbing material and gives an ionization impact to the pollutants. In the case of 3DG, the effect of pH on adsorption is discussed by evaluating the pH at the point of zero charges pH_{PZC}. If $pH < pH_{PZC}$, 3DG is positively charged and attract negatively charged (anionic) inorganic pollutant. Conversely, for $pH > pH_{PZC}$, cationic inorganic pollutants are attracted by the negatively charged surface of 3DG architecture [4]. The ion-exchange method was much preferred for the adsorption of pollutants, but in 2012 electrostatic adsorption was introduced. 3DG macrostructures display good results in increasing pH values so that metal ions (cations) from the aqueous phase attracts negatively charged 3DG macrostructures. The temperature changes and co-existing ions can affect this phenomenon. Adsorption is an endothermic reaction so having a high temperature helps, and with electrostatic attraction, the removal of inorganic pollutants can be achieved with high efficiency [33].

4.1.4 Contact Time

The absorption properties of graphene are mainly influenced by the contact time between adsorbent and adsorbate. In case of graphene, the adsorption occurs on its planar surface, which then diffuses into the material through pores to get captured by carbon atoms [45]. By keeping the adsorption properties of 3DG in view, the pollutants are divided into anionic pollutants and cationic pollutants.

Anionic Pollutants:

Fluoride (F^-) is one of the main anionic inorganic species that pollutes the water. The toxicity of heavy metal-polluted water greatly depends upon the valence state of dissolved metal ions [48]. For example, As is found as arsenate (As-V) and arsenite (As-III). Surface water contains As-V in large quantities, while As-III is present in groundwater. Ar-III as a negative ion is $H_2AsO_3^-$ but As-V changes its anionic state based on pH, i.e., H_3AsO_4 at pH < 2.2, $H_2AsO_4^-$ at pH 2.2 to 6.98, $HAsO_4^{2-}$ at pH 6.98 to 11.5, and AsO_4^{3-} at pH > 11.5. Similarly, Cr originates in two oxidation states, Cr(III) and Cr(VI). At lower values of pH, Cr(VI) is found as $HCrO_4^-$ but as the increment in pH takes place, Cr changes its form to $Cr_2O_7^{2-}$ or CrO_4^{2-}. For the removal of anionic inorganic pollutants, low pH solutions are preferred because they give graphene a positive charge and promote electrostatic attraction [4].

Cationic Pollutants:

Wastewater contains many cationic pollutants; the most common are Pb^{+2}, Hg^{+2}, Cd^{+2}, Cu^{+2}, Ni^{+2}, Co^{+2}, and Zn^{+2}. For the adsorption of these cationic pollutants, three main adsorption mechanisms, electrostatic interactions, ion-exchange method, and complex formations are used. 3DG enriched with oxygen-containing functional groups have anchoring sites that secure the metal ions, either by electrostatic interaction, ion-exchange, or coordination method. A solution having a high pH also facilitates the adsorption process. This is because higher pH poses a negative charge on the surface of 3D graphene, which helps in attracting the metal ions, and adsorption efficiency increases as the consequence [4].

3DG macrostructures having many oxygen functional groups perform adsorption by π-cation interactions and form strong complexes with heavy metals, resulting in the successful removal of pollutants. The absorption rate of 3DG macrostructures is 434 mg/g for Cd^{2+}, 882 mg/g for Pb^{2+},1683 mg/g for Ni^{2+}, and 3820 mg/g for Cu^{2+}. The adsorption ability of graphene-based hydrogel is 139.2 mg/g for Cr(VI), 373.8 mg/g of Pb, and 15.6 mg/g for γ-iron oxide [33]. Other methods of adsorption of inorganic pollutants contain physio-sorption and hydrogen bonding interactions. Chromates $(Cr_2O_7)^{-2}$ adsorption by graphene hydrogel has been reported through physiochemical adsorption and hydrogen bonding, at the rate of 140 mg/g [33].

4.2 3DG with Synergistic Effects of Adsorption and Photocatalysis

The high porosity of the graphene material, the catalytic functional groups that are present in the 3DG architecture, the presence of micropores and mesopores that increase surface area, and the availability of active sites all contribute toward the increased synergistic effects of 3DG when combined with different photocatalysts. On the other hand, 3DG shows fantastic recyclability and can be used for several rounds. Owing to such fascinating properties, 3DG macrostructures have been used in multiple systems for the removal of Pb, Hg, Cd, cobalt (Co), and As [33]. 3DG architecture and 3DG-based microstructures provide a good number of binding sites which are favorable for the fabrication of heterojunctions. During the fabrication of different types of heterojunctions, the material can stick with graphene due to electrostatic interactions, hydrogen bonding, π -π interactions, and chelation [12]. 3DG and its heterojunctions with different materials have been reported for the removal of inorganic pollutants via the adsorption method, photocatalysis, or the synergistic effect of both, as displayed in Table 2.

Table 2 3DG structures for inorganic pollutant removal

Adsorbate	Adsorbent	Adsorption Rate (mg/g)	Method	References
Graphene Aerogel (GA)	Pb(II)	80	Adsorption	[14]
GA	Cu(II)	68.2	Adsorption	[29]
GA	Cd(II)	149.25	Adsorption	[37]
GA	U(VI)	238.67	Adsorption	[49]
3DG macroscopic gel modified with polydopamine and Fe_3O_4 nanoparticles	As(III)	172	Adsorption	[13]
	As(V)	217		
3DG Foam/MnO_2	Sr(II)	47	Adsorption	[20]
3DGA /TiO_2	U(VI)	441	Adsorption	[47]
Graphene Foam	As(V)	177	Adsorption	[6]
	Pb(II)	399	Adsorption	
Cyclodextrin functionalized 3D Graphene (CDGF)	Cr(VI)	107	Adsorption	[42]
Tetraethylenepentamine modified Graphene Foam (TEPA-GF)	Pb(II)	305	Adsorption	[15]
N,N,N’,N’-Tetraoctyldiglycolamide impregnated GA (GA-TODGA)	Th(IV)	67	Adsorption	[7]
GA /Fe_3O_4	As(V)	40.048	Adsorption	[46]
Graphene	Sb(III)	7.463	Adsorption	[24]
Amine functionalized GA	Cr(VI)	170	Adsorption	[35]
GA	Cr(VI)	Almost 100% removal in 5 h	Photocatalysis	[9]
g-C_3N_5/reduced Graphene Oxide Aerogel	U(VI)	94.9% removal	Photocatalysis	[44]
3D RGO/TiO_2 Aerogel	U(VI)	99% removal within 140–270 min under visible light	Photocatalysis	[10]
3D MXene-derived TiO_2(M)@reduced Graphene Oxide Aerogel	U(VI)	95.7% removal within 60 min under visible light	Photocatalysis	[8]
g-C_3N_4 integrated Cellulose/ Graphene Oxide Foams	Cr(VI)	98% removal within 3 h under visible light	Photocatalysis	[16]

(continued)

Table 2 (continued)

Adsorbate	Adsorbent	Adsorption Rate (mg/g)	Method	References
TiO_2-Graphene Hydrogel	Cr(VI)	100% removal in 30 min under UV irradiation	Synergy of adsorption and photocatalysis	[25]
$TiO_2/Zn_xCd_{1-x}S$/ GA	Cr(VI)	100% removal in 30 min under visible irradiation	Synergy of adsorption and photocatalysis	[26]
$Bi_2S_3/BiVO_4$/ GA	Cr(VI) Bisphenol A	100% removal after adsorption for 40 min and photocatalysis for 120 min under visible light	Synergy of adsorption and photocatalysis	[27]
g-C_3N_4/Graphene Hydrogel	Cr(VI)	80% absorption in 30 min and 100% removal in 120 min under visible light	Synergy of adsorption and photocatalysis	[39]

The presence of micropores in 3DG offers accessibility to the adsorption of pollutants. The increased surface area and many active sites provide the profound photocatalytic ability to 3DG macrostructures. Adsorption and photocatalysis can work together to remove inorganic pollutants more effectively. 3DG macrostructures and microstructures are used with different photocatalysts to take advantage of their synergistic effects. Based on this aspect, the removal of many metals such as antimony (Sb) and Cr(VI) has been reported [48]. 3DG has also been employed with different materials by fabricating binary and ternary heterojunctions to improve the removal efficiency because of synergism. The construction of heterojunction is also advantageous for graphene as it reduces the agglomeration of the particles, provides the material with a hydrophilic nature, and reduces the number of oxygen groups [12].

Li et al. [25] reported the 3D TiO_2/GA structure exhibiting 100% Cr(VI) removal from aqueous solution within 30 min upon UV light exposure, as illustrated in Fig. 4b. $\pi-\pi$ interaction of graphene caused enhanced adsorption while TiO_2 nanospheres facilitated the charge formation, transport, and separation. The removal efficacy of Cr(VI) is attributed to synergistic performance. Liang et al. [26] combined TiO_2 with $Zn_xCd_{1-x}S$ and GA to take the advantage of the synergistic effect of adsorption and photocatalysis to remove Cr(VI) from an aqueous environment. The graphene acted as a mediator to accelerate the electron transfer, Cr(VI) adsorbent and 100% removal of Cr(VI) occurred in 30 min of visible light irradiation, as shown in Fig. 4e. The toxic Cr(VI) removal was also tested by D. Hou et al. [16] using g-C_3N_4 integrated cellulose/graphene oxide foams as photocatalysts. The carboxylic group of cellulose/graphene oxide foams and amino group present in g-C_3N_4 made a strong contact at the interface and enhanced conductivity. 98% of Cr(VI) removal was demonstrated with excellent recyclability, as displayed in Fig. 4i. Liang et al. [27] constructed Z-scheme heterojunction Bi_2S_3/$BiVO_4$/GA to study Cr(VI) removal efficacy. Graphene significantly enhanced the removal efficiency by facilitating electron transport. 40 min of adsorption and 120 min of photocatalysis collectively provided the 100% removal of Cr(VI) from the aqueous environment, exhibited in Fig. 4k. X. Wang et al. [39] carried out g-C_3N_4/graphene hydrogel to explore the synergistic effect of adsorption and photocatalysis on Cr(VI) removal. The graphene sheets provided fast surface adsorption of Cr(VI) and promoted charge transfer. As a consequence, 100% Cr(VI) degradation was obtained in 120 min of visible light irradiation, which can be seen in Fig. 4n.

5 Conclusion

Different materials and methods in the past have been used to eliminate toxic inorganic pollutants that arise from various sources and pose the danger to living entities. But the advantageous traits of 3DG structures have attracted a lot of interest in recent years. 3DG owing to its outstanding characteristics such as large specific surface area, low density, increased porosity, small aggregation, more active sites, and high light adsorption capability has been widely investigated for the removal of inorganic pollutants. The mesoporous structure of 3DG favors the adsorption of inorganic pollutants while photocatalytic reaction degrades the harmful pollutants. The synergistic effect of adsorption and photocatalytic reaction provides efficient removal as compared to conventional methods. The excellent charge separation and migration ability of graphene enhance the rate of photocatalytic reaction. Furthermore, 3DG and its composites exhibit exceptional recyclability, allowing its repeated use. This chapter covers the current development made in removing hazardous inorganic pollutants from the environment.

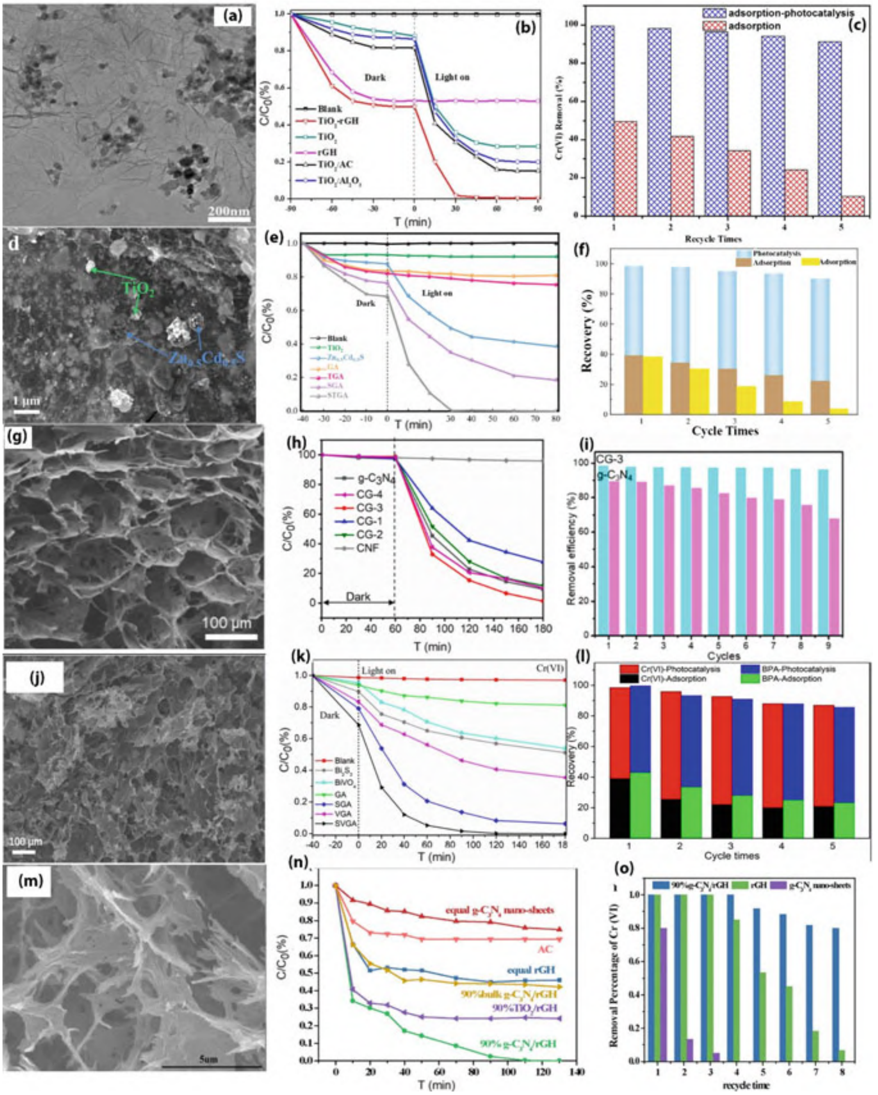

Fig. 4 **a** Transmission electron microscopy (TEM) micrograph of TiO_2-rGH highlighting enhanced porosity, **b** Cr(VI) removal by 3D TiO_2-rGH in 30 min, **c** TiO_2-rGH displaying exceptional cyclic stability over the course of 5 cycles. Adapted with permission [25], Copyright (2016), Elsevier. **d** SEM image of TiO_2-$Zn_xCd_{1-x}S$ graphene hydrogel heterojunction. **e** TiO_2-$Zn_xCd_{1-x}S$ graphene hydrogel shows enhanced results for the removal of Cr(VI) due to synergism. **f** Cyclic stability of TiO_2-$Zn_xCd_{1-x}S$ graphene hydrogel. Adapted with permission [26], Copyright (2023), Elsevier. **g** SEM micrograph of CNF foam. (h) Cr(VI) removal using CG-3 photocatalyst. **i** Cyclic stability test of CG-3 and g-C_3N_4. Adapted with permission [16], Copyright (2022), Elsevier. **j** SEM image of Bi_2S_3-$BiVO_4$ GA. **k** Cr(VI) removal tested for Bi_2S_3, $BiVO_4$, GA, Bi_2S_3/GA and $BiVO_4$/GA and Bi_2S_3-$BiVO_4$. **l** Cyclic stability test of Bi_2S_3-$BiVO_4$-GA. Adapted with permission [27], Copyright (2020), Elsevier. **m** SEM micrograph of g-C_3N_4/rGH. **n** Corresponding Cr(VI) removal ability and **o** cyclic stability. Adapted with permission [39], Copyright (2017), Elsevier

References

1. Akram, R., Turan, V., Hammad, H., Ahmad, S., Hussain, S., Hasnain, A., Maqbool, M., Rehmani, M., Rasool, A., Masood, N., Mahmood, F., Mubeen, M., Sultana, S., Fahad, S., Amanet, K., Saleem, M., Abbas, Y., Akhtar, H., Hussain, S., Waseem, F., Murtaza, R., Amin, A., Zahoor, S., Sami ul Din, M., Nasim, W.: Fate of organic and inorganic pollutants in paddy soils, 197–214 (2018)
2. Ambaye, T.G., Vaccari, M., van Hullebusch, E.D., Amrane, A., Rtimi, S.: Mechanisms and adsorption capacities of biochar for the removal of organic and inorganic pollutants from industrial wastewater. Int. J. Environ. Sci. Technol. **18**:10, 18, 10, 3273–3294 (2020)
3. Anna, I., Bartkowska, I., Biedka, P.: Treatment of young and stabilized landfill leachate by integrated sequencing batch reactor (SBR) and reverse osmosis (RO) process. Environ. Nanotechnol. Monitoring Manag. **16**, 100502 (2021)
4. Cao, Y., Li, X.: Adsorption of graphene for the removal of inorganic pollutants in water purification: a review. Adsorption **20**(5–6), 713–727 (2014)
5. Chadha, U., Selvaraj, S.K., Vishak Thanu, S., Cholapadath, V., Abraham, A.M., Zaiyan, M.M., Manoharan, M., Paramsivam, V.: A review of the function of using carbon nanomaterials in membrane filtration for contaminant removal from wastewater. Mater. Res. Express **9**(1), 012003 (2022)
6. Chen, G., Liu, Y., Liu, F., Zhang, X.: Fabrication of three-dimensional graphene foam with high electrical conductivity and large adsorption capability. Appl. Surf. Sci. **311**, 808–815 (2014)
7. Chen, M., Li, Z., Geng, Y., Zhao, H., He, S., Li, Q., Zhang, L.: Adsorption behavior of thorium on N, N, N′, N′-tetraoctyldiglycolamide (TODGA) impregnated graphene aerogel. Talanta **181**, 311–317 (2018)
8. Chen, T., He, P., Liu, T., Zhou, L., Li, M., Yu, K., Meng, Q., Lian, J., Zhu, W.: MXene-derived 3D defect-Rich TiO_2 @reduced graphene oxide aerogel with ultrafast carrier separation for photo-assisted uranium extraction: a combined batch, X-ray absorption spectroscopy, and density functional theory calculations. Inorg. Chem. **61**(32), 12759–12771 (2022)
9. Dong, S., Xia, L., Guo, T., Zhang, F., Cui, L., Su, X., Wang, D., Guo, W., Sun, J.: Controlled synthesis of flexible graphene aerogels macroscopic monolith as versatile agents for wastewater treatment. Appl. Surf. Sci. **445**, 30–38 (2018)
10. Dong, Z., Zhang, Z., Li, Z., Feng, Y., Dong, W., Wang, T., Cheng, Z., Wang, Y., Dai, Y., Cao, X., Liu, Y., Liu, Y.: 3D structure aerogels constructed by reduced graphene oxide and hollow TiO_2 spheres for efficient visible-light-driven photoreduction of U(vi) in air-equilibrated wastewater. Environ. Sci. Nano **8**(8), 2372–2385 (2021)
11. Fuller, R., Landrigan, P.J., Balakrishnan, K., Bathan, G., Bose-O'Reilly, S., Brauer, M., Caravanos, J., Chiles, T., Cohen, A., Corra, L., Cropper, M., Ferraro, G., Hanna, J., Hanrahan, D. et al.: Pollution and health: a progress update. Lancet Planetary Health **6**(6), e535–e547 (2022)
12. G.G., Sathish, A, Kumar, P.S., Nithya, K., Rangasamy, G.: A review on current progress of graphene-based ternary nanocomposites in the removal of anionic and cationic inorganic pollutants. Chemosphere **309**, 136617 (2022)
13. Guo, L., Ye, P., Wang, J., Fu, F., Wu, Z.: Three-dimensional Fe_3O_4-graphene macroscopic composites for arsenic and arsenate removal. J. Hazard. Mater. **298**, 28–35 (2015)
14. Han, Z., Tang, Z., Shen, S., Zhao, B., Zheng, G., Yang, J.: Strengthening of graphene aerogels with tunable density and high adsorption capacity towards Pb2+. Sci. Rep. **4**(1), 5025 (2014)
15. Han, Z., Tang, Z., Sun, Y., Yang, J., Zhi, L.: Controllable synthesis of tetraethylenepentamine modified graphene foam (TEPA-GF) for the removal of lead ions. Sci. Rep. **5**(1), 16730 (2015)
16. Hao, D., Liu, J., Sun, H., Fu, B., Liu, J., Zhou, J.: Integration of g-C3N4 into cellulose/graphene oxide foams for efficient photocatalytic Cr(VI) reduction. J. Phys. Chem. Solids **169**, 110813 (2022)
17. Hao, L., Song, H., Zhang, L., Wan, X., Tang, Y., Lv, Y.: SiO2/graphene composite for highly selective adsorption of Pb(II) ion. J. Colloid Interface Sci. **369**(1), 381–387 (2012)
18. Hayet, S., Sujan, K.M., Mustari, A., Miah, M.A.: Hemato-biochemical profile of turkey birds selected from Sherpur district of Bangladesh. Int. J. Adv. Res. Biol. Sci **8**(6), 1–5 (2021)

19. Hiew, B.Y.Z., Lee, L.Y., Lee, X.J., Thangalazhy-Gopakumar, S., Gan, S., Lim, S.S., Pan, G.T., Yang, T.C.K., Chiu, W.S., Khiew, P.S.: Review on synthesis of 3D graphene-based configurations and their adsorption performance for hazardous water pollutants. Process Saf. Environ. Prot. **116**, 262–286 (2018)
20. Kasap, S., Nostar, E., Öztürk, İ: Investigation of MnO2 nanoparticles-anchored 3D-graphene foam composites (3DGF-MnO2) as an adsorbent for strontium using the central composite design (CCD) method. New J. Chem. **43**(7), 2981–2989 (2019)
21. Kong, Q., Shi, X., Ma, W., Zhang, F., Yu, T., Zhao, F., Zhao, D., Wei, C.: Strategies to improve the adsorption properties of graphene-based adsorbent towards heavy metal ions and their compound pollutants: A review. J. Hazard. Mater. **415**, 125690 (2021)
22. Kumar, M., Borah, P., Devi, P.: Priority and emerging pollutants in water. Inorganic Pollut. Water, 33–49 (2020)
23. Lee, J., Ahn, W.Y., Lee, C.H.: Comparison of the filtration characteristics between attached and suspended growth microorganisms in submerged membrane bioreactor. Water Res. **35**(10), 2435–2445 (2001)
24. Leng, Y., Guo, W., Su, S., Yi, C., Xing, L.: Removal of antimony(III) from aqueous solution by graphene as an adsorbent. Chem. Eng. J. **211–212**, 406–411 (2012)
25. Li, Y., Cui, W., Liu, L., Zong, R., Yao, W., Liang, Y., Zhu, Y.: Removal of Cr(VI) by 3D TiO_2-graphene hydrogel via adsorption enriched with photocatalytic reduction. Appl. Catal. B **199**, 412–423 (2016)
26. Liang, Q., Chen, X., Liu, R., Xu, K., Luo, H.: Efficient removal of Cr(VI) by a 3D Z-scheme TiO2-Zn Cd1-S graphene aerogel via synergy of adsorption and photocatalysis under visible light. J. Environ. Sci. **124**, 360–370 (2023)
27. Liang, Q., Ploychompoo, S., Chen, J., Zhou, T., Luo, H.: Simultaneous Cr(VI) reduction and bisphenol A degradation by a 3D Z-scheme Bi2S3-BiVO4 graphene aerogel under visible light. Chem. Eng. J. **384**, 123256 (2020)
28. Mohammadi, S.A., Najafi, H., Zolgharnian, S., Sharifian, S., Asasian-Kolur, N.: Biological oxidation methods for the removal of organic and inorganic contaminants from wastewater: a comprehensive review. Sci. Total Environ. **843**, 157026 (2022)
29. Pan, M., Shan, C., Zhang, X., Zhang, Y., Zhu, C., Gao, G., Pan, B.: Environmentally friendly in situ regeneration of graphene aerogel as a model conductive adsorbent. Environ. Sci. Technol. **52**(2), 739–746 (2018)
30. Radwan, E.H., Saber, M.A.K., Saber, M.E.K., Fahmy, G.H.: The impact of some organic and inorganic pollutants on fresh water (Rashid, River Nile). Egypt. J. Adv. Biol. **10**(2), 2133–2145 (2017)
31. Saha, J.K., Selladurai, R., Coumar, M.V., Dotaniya, M.L., Kundu, S., Patra, A.K.: Major inorganic pollutants affecting soil and crop quality, 75–104 (2017)
32. Saleh, I.A., Zouari, N., Al-, M.A.: Removal of pesticides from water and wastewater: chemical, physical and biological treatment approaches. Environ. Technol. Innov. **19**, 101026 (2020)
33. Shen, Y., Fang, Q., Chen, B.: Environmental applications of three-dimensional graphene-based macrostructures: adsorption, transformation, and detection. Environ. Sci. Technol. **49**(1), 67–84 (2015)
34. Sidana, N., Kaur, H., Devi, P.: Organic linkers for colorimetric detection of inorganic water pollutants. Inorganic Pollut. Water, 135–152 (2020)
35. Singh, D.K., Kumar, V., Mohan, S., Hasan, S.H.: Polylysine functionalized graphene aerogel for the enhanced removal of Cr(VI) through adsorption: kinetic, isotherm, and thermodynamic modeling of the process. J. Chem. Eng. Data **62**(5), 1732–1742 (2017)
36. Sun, Z., Fang, S., Hu, Y.H.: 3D graphene materials: from understanding to design and synthesis control. Chem. Rev. **120**(18), 10336–10453 (2020)
37. Trinh, T.T.P.N.X., Quang, D.T., Tu, T.H., Dat, N.M., Linh, V.N.P., van Cuong, L., Nghia, L.T.T., Loan, T.T., Hang, P.T., Phuong, N.T.L., Phong, M.T., Nam, H.M., Hieu, N.H.: Fabrication, characterization, and adsorption capacity for cadmium ions of graphene aerogels. Synthetic Metals **247**, 116–123 (2019)

38. Vishnu, D., Dhandapani, B., Kannappan Panchamoorthy, G., Vo, D.V.N., Ramakrishnan, S.R.: Comparison of surface-engineered superparamagnetic nanosorbents with low-cost adsorbents of cellulose, zeolites and biochar for the removal of organic and inorganic pollutants: a review. Environ. Chem. Lett. **19**(4), 3181–3208 (2021)
39. Wang, X., Liang, Y., An, W., Hu, J., Zhu, Y., Cui, W.: Removal of chromium (VI) by a self-regenerating and metal free g-C3N4/graphene hydrogel system via the synergy of adsorption and photo-catalysis under visible light. Appl. Catal. B **219**, 53–62 (2017)
40. Wang, X., Xu, J., Xu, M., Zhou, B., Liang, J., Zhou, L.: High-efficient removal of arsenite by coagulation with titanium xerogel coagulant. Sep. Purif. Technol. **258**, 118047 (2021)
41. Wang, Y., Kuntke, P., Saakes, M., van der Weijden, R.D., Buisman, C.J.N., Lei, Y.: Electrochemically mediated precipitation of phosphate minerals for phosphorus removal and recovery: progress and perspective. Water Res. **209**, 117891 (2022)
42. Wang, Z., Lin, F., Huang, L., Chang, Z., Yang, B., Liu, S., Zheng, M., Lu, Y., Chen, J.: Cyclodextrin functionalized 3D-graphene for the removal of Cr(VI) with the easy and rapid separation strategy. Environ. Pollut., 254 (2019)
43. Wasewar, K.L., Singh, S., Kansal, S.K.: Process intensification of treatment of inorganic water pollutants. Inorganic Pollut. Water, 245–271 (2020)
44. Wu, L., Yang, X., Chen, T., Li, Y., Meng, Q., Zhu, L., Zhu, W., He, R., Duan, T.: Three-dimensional C3N5/RGO aerogels with enhanced visible-light response and electron-hole separation efficiency for photocatalytic uranium reduction. Chem. Eng. J. **427**, 131773 (2022)
45. Yagub, M.T., Sen, T.K., Afroze, S., Ang, H.M.: Dye and its removal from aqueous solution by adsorption: a review. Adv. Coll. Interface. Sci. **209**, 172–184 (2014)
46. Ye, Y., Yin, D., Wang, B., Zhang, Q.: Synthesis of three-dimensional Fe3O4/graphene aerogels for the removal of arsenic ions from water. J. Nanomater. **2015**, 1–6 (2015)
47. Yu, S., Wei, D., Shi, L., Ai, Y., Zhang, P., Wang, X.: Three-dimensional graphene/titanium dioxide composite for enhanced U(VI) capture: Insights from batch experiments, XPS spectroscopy and DFT calculation. Environ. Pollut. **251**, 975–983 (2019)
48. Zhang, F., Li, Y.H., Li, J.Y., Tang, Z.R., Xu, Y.J.: 3D graphene-based gel photocatalysts for environmental pollutants degradation. Environ. Pollut. **253**, 365–376 (2019)
49. Zhao, D., Wang, Y., Zhao, S., Wakeel, M., Wang, Z., Shaikh, R.S., Hayat, T., Chen, C.: A simple method for preparing ultra-light graphene aerogel for rapid removal of U(VI) from aqueous solution. Environ. Pollut. **251**, 547–554 (2019)

3D Graphene Structures for the Removal of Pharmaceutical Residues

Wan Ting Tee, Nicholas Yung Li Loh, Billie Yan Zhang Hiew, and Lai Yee Lee

Abstract Graphene nanomaterials have great potential applications in treating wastewater containing pharmaceutical residues due to their extraordinary physicochemical and adsorption properties. Despite being present in minute amounts in the aquatic environment, pharmaceutical residues can cause various health and environmental risks owing to their non-biodegradability, bioaccumulative and toxicity features. Hence, it is extremely vital to control the concentration of pharmaceutical residues in water resources. Notably, three-dimensional (3D) graphene structures have emerged as innovative adsorbents with fortified adsorption properties such as super-large theoretical surface area, abundant functional groups, and the capability to preserve the intrinsic properties of nanomaterials at a macroscopic level. In this chapter, the classification and main sources of pharmaceutical pollution are discussed. Thereafter, the principles and advantages of adsorption for pharmaceutical removal are covered. This chapter further evaluates the performance of primary 3D graphene structures, namely graphene aerogel, hydrogel, and beads, in relation to pharmaceutical adsorption. The synthesis methods and adsorption mechanisms of pharmaceutical residues by 3D graphene structures are assayed. Lastly, the challenges and outlook of 3D graphene structures in pharmaceutical adsorption are presented.

Keywords Graphene · 3D graphene structures · Pharmaceutical residues · Adsorption · Wastewater treatment

---

W. T. Tee · N. Y. L. Loh · L. Y. Lee (✉)
Department of Chemical and Environmental Engineering, University of Nottingham Malaysia, Jalan Broga, 43500 Semenyih, Selangor, Malaysia
e-mail: Lai-Yee.Lee@nottingham.edu.my

N. Y. L. Loh
Department of Chemical and Environmental Engineering, University of Nottingham Ningbo China, Ningbo 315100, China

B. Y. Z. Hiew
School of Engineering and Physical Sciences, Heriot-Watt University Malaysia, 62200 Putrajaya, Wilayah Persekutuan Putrajaya, Malaysia

© The Author(s), under exclusive license to Springer Nature Switzerland AG 2023

R. K. Gupta (ed.), *3D Graphene*, Carbon Nanostructures,
https://doi.org/10.1007/978-3-031-36249-1_11

1 Introduction

The detection of pharmaceutical residues in the aquatic environment is an emerging environmental issue owing to their high toxicity and detrimental effects on all lifeforms and the environment. Pharmaceuticals can be considered as chemical compounds produced to cure and control diseases to achieve desired therapeutic effects via biological activity. The market sales of global pharmaceutical industries reached USD 1.27 trillion in 2020, signifying an escalating demand for pharmaceutical products [1]. Nonetheless, the growing production and consumption of medicinal products are accompanied by the release of such compounds into the environment. In general, pharmaceutical residues are micropollutants as they are detected in very low concentrations, ranging from ng/dm^3 to μg/dm^3 [1]. Furthermore, the presence of pharmaceutical residues in the water body can lead to adverse effects, including anti-microbial resistance, endocrine disruption, and toxic metabolites discharge [2]. As such, it is crucial that these drug components are removed from the affected water effluent prior to release into the environment.

Conventional remediation technologies which include coagulation, flocculation, and biological treatment are ineffective in removing pharmaceutical-based pollutants and are also associated with other issues such as non-selectivity, low performance at trace concentrations, and generation of undesired by-products upon treatment [3]. Among the available technologies, adsorption offers a promising treatment solution for pharmaceutical residues. The performance of adsorption is highly influenced by the selection of adsorbing material. Ideally, adsorbents with high selectivity, efficiency, and renewability are favourable for use in wastewater treatment [4]. Despite their wide availability, commercial adsorbents such as activated carbon and zeolites are ineffective against pharmaceutical residues. They also pose potential sustainability problems, hindering their applications in pharmaceuticals removal. Hence, there is an urgent need to devise new and effective adsorbents capable of fully removing the pharmaceutical pollutants.

Recently, three-dimensional (3D) graphene structures have surfaced as the next generation of adsorbing materials for wastewater treatment. Notably, the unique characteristics of 3D graphene such as ultralight density, ease of functionalization, and high porosity have supported their role in remediating polluted aqueous systems. The porous framework of 3D graphene is one of the prominent features that can promote high selective affinity towards a wide range of pharmaceutical pollutants [5]. In comparison to nanometer-scale adsorbing particles, 3D graphene adsorbents offer merits in terms of reusability and regenerability, increasing their feasibility in industrial wastewater treatment [6]. From the current literature, various 3D graphene configurations with relatively high adsorption performance for different pharmaceutical residues have been constructed. For instance, a three-dimensional manganese dioxide-engrafted reduced graphene oxide (3D MnO_2/rGO) hybrid aerogel was reported to adsorb a higher amount of acetaminophen (252.87 mg/g) [7] as compared to spent tea leaves activated carbon (59.2 mg/g) [8]. In a separate study, Tee et al. [9] investigated the adsorptive removal of amitriptyline using a 3D boron-doped graphene oxide (3D-BGO) aerogel. The adsorbent achieved an amitriptyline adsorption capacity of 737.4 mg/g which was at least 4 times higher than commercial granular activated carbon [9]. A relatively high removal efficiency (89.31%) was achieved at 50 ppm amitriptyline solution concentration and 30 °C using 10 mg of the adsorbent, while the adsorption process reached equilibrium within 60 min across solution concentrations ranging from 10 to 300 ppm. These results suggested that the 3D-BGO aerogel was a superior adsorbent for amitriptyline removal [9]. The findings indicated the high potential utilization of 3D graphene structures for pharmaceuticals adsorption.

This chapter focuses on the application of 3D graphene structures for eliminating pharmaceutical residues from aqueous media. The background of pharmaceuticals and types of 3D graphene structures along with their respective adsorption performance are discussed. The challenges and possible improvements of 3D graphene structures for enhanced removal of pharmaceuticals are also addressed.

2 Pharmaceutical Pollution

More than 10,000 different types of pharmaceutical products have been produced for human and veterinary medications [10], resulting in the detection of numerous pharmaceutical residues in the aquatic ecology. It is essential to understand the properties of pharmaceuticals in order to devise appropriate treatment strategies for minimizing their adverse effects on the environment.

3 Classification and Harmful Effects of Pharmaceuticals

Generally, pharmaceuticals can be classified based on their therapeutic effects. Table 1 summarizes the key classes of medicinal products with their corresponding therapeutic effects and examples.

Despite having disease healing and control effects, the active ingredients of pharmaceuticals usually cannot be metabolized completely by consumers and the metabolite residuals can reach the environment, causing toxicity accumulation [11]. It was reported that the concentrations of pharmaceuticals exceeding 1–500 ng/L could harm the aquatic organisms [12]. Moreover, a prolong exposure to the medicinal pollutants can lead to different negative responses, highly influenced by the species' vulnerability and pharmaceutical type [13]. For instance, diclofenac drug caused mortality in pigeon and chicken at dosages of 0.25 and 2.5 mg/kg, respectively [14]. A post-mortem study detected the buildup of triclosan, triclocarban, and other drug residues in human tissues [15]. Hence, these revelations indicated that the uncontrolled discharge of medicinal products into the water body can impose significant impacts on the ecological systems.

Table 1 Classifications and examples of pharmaceuticals

Pharmaceutical class	Therapeutic effect	Examples
Antibiotics	Eliminate bacteria	Sulfamethoxazole Ofloxacin Tetracycline Ciprofloxacin Trimethoprim
Antifungal	Treat and prevent fungal infections	Triclosan
Anticonvulsants	Mood stabilizer, anti-seizure, and treat mood disorder	Carbamazepine Primidone Mephobarbital
Antidepressants	Treat major depression-related symptoms and relieve long term neuropathic pain	Diazepam Doxepin Amitriptyline
Beta blockers	Hormone/adrenaline/neurotransmitter inhibitor	Acebutolol Atenolol Satolol
Hormones	Regulate the metabolism rate, control sexual development, and maintain homeostasis	Estrone Estradiol Testosterone
Lipid regulators	Regulate triglycerides and cholesterol in blood stream	Clorfibric acid Gemfibrozil
Non-steroidal anti-inflammatory drugs	Pain reliever and reduce inflammation	Diclofenac Ibuprofen Acetaminophen Naproxen

4 Occurrence and Sources of Pharmaceuticals

Terrestrial and aquatic systems are the major sinks for pharmaceutical residues in the environment. The occurrence and major sources of pharmaceutical residue are illustrated in Fig. 1.

Both commercial (pharmaceutical manufacturers and wastewater treatment plants) and domestic (organisms' excreta and landfill) activities are the primary contributors of pharmaceutical residues in the environment. The effluent and solid disposals from clinical facilities such as hospitals and veterinary centers also contribute significantly to pharmaceutical water pollution [17]. Typically, the micropollutants enter the surface water through direct effluent discharge from identified sources. Thereafter, the pharmaceuticals infiltrate to the groundwater, eventually ending up in the wastewater treatment plants. Due to low efficiency of current treatment systems, the treatment effluent contains a variety of pharmaceutical residues. Some of the pharmaceutical residues may undergo rapid metabolism upon interaction with the biological treatment system and the unmetabolized active ingredients may cause toxicity accumulation [16]. In view of their harmful effects, it is desired

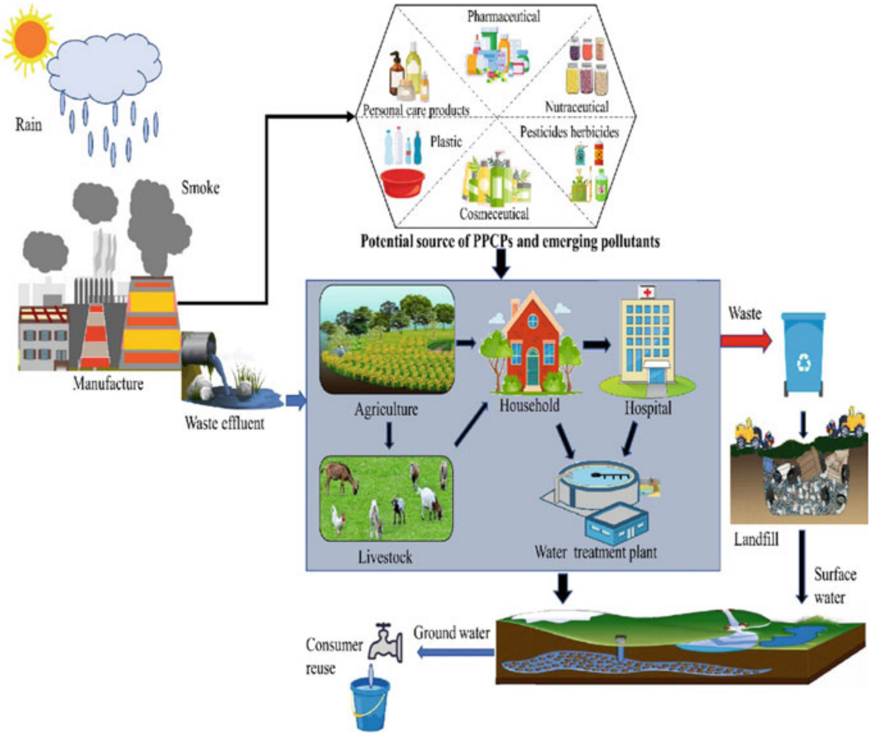

Fig. 1 Potential sources and pathway of pharmaceutical residues in the environment. Adapted with permission [16]. Copyright (2023) Elsevier

to develop alternative treatment systems to regulate the pharmaceutical levels in the environment.

5 Adsorption of Pharmaceuticals

Table 2 compiles the principal terminologies associated with adsorption technology. Generally, the term ‘adsorption’ is the enrichment of one or more components in the region between two bulk phases (interfacial layer or adsorption space). In the context of aqueous pharmaceutical adsorption, one of these phases is a solid while the other is a liquid.

Adsorption can be utilized for treating various pharmaceutical pollutants, whereby the pharmaceutical molecules or ions are removed from the aqueous media by attaching onto the solid surface of the adsorbent. Owing to its relatively low operating cost and simple operation, adsorption is a widely acceptable technique for treating pharmaceutical contaminated water [19]. Another highlight of this approach is the

Table 2 Terminology used in adsorption [18]

Term	Definition
Adsorption	Enrichment of one or more components in the vicinity of an interface
Adsorbate	Substance in the adsorbed state
Adsorptive	Adsorbable substance in fluid phase
Adsorbent	Solid material on which adsorption occurs
Chemisorption	Adsorption involving chemical bonding
Physisorption	Adsorption without chemical bonding
Monolayer capacity	Either chemisorbed amount required to occupy all surface sites or physisorbed amount required to cover the surface
Surface coverage	Ratio of amount of adsorbed substance to monolayer capacity

ability to perform regeneration on the adsorbent, specifically through manipulation of the aqueous phase conditions (temperature, pH, and concentration), which can prolong its lifespan for extended adsorption–desorption operations as well as reduce operating cost [20].

A vital adsorption parameter, namely the equilibrium adsorption capacity (q_e), is applied for gauging the adsorption efficiency or adsorbent performance. It is represented by Eq. (1):

$$q_e = \frac{(C_o - C_e)V}{m} \tag{1}$$

where C_o is the initial adsorbate concentration (mg/L), C_e is the equilibrium adsorbate concentration (mg/L), V is the volume of solution (L), and m is the mass of adsorbent (g). Typically, an adsorbent should possess features such as high adsorption capacity, adaptability to remove a wide range of pollutants, and high reusability, as well as low production cost [21]. The effectiveness of the adsorption process is influenced by various parameters such as adsorbent surface area, porosity, and surface chemistry [1]. Apart from that, the adsorbent should also be able to adsorb the pharmaceuticals rapidly and can be regenerated completely for reutilization [22].

Pharmaceutical adsorption can be influenced by various adsorption mechanisms. As depicted in Fig. 2, interactive mechanisms such as hydrophobic, hydrogen bonding, electron donor-acceptance, electrostatic, covalent bonding, and oxidative reactions are the dominant adsorption mechanisms for pharmaceuticals removal [2]. As indicated by the various literature, the characteristics of adsorbent and adsorbate could initiate different adsorption mechanisms to facilitate the sequestration of pharmaceuticals [7, 23]. Hence, a suitably designed adsorbent is crucial for the successful removal of pharmaceuticals from wastewater.

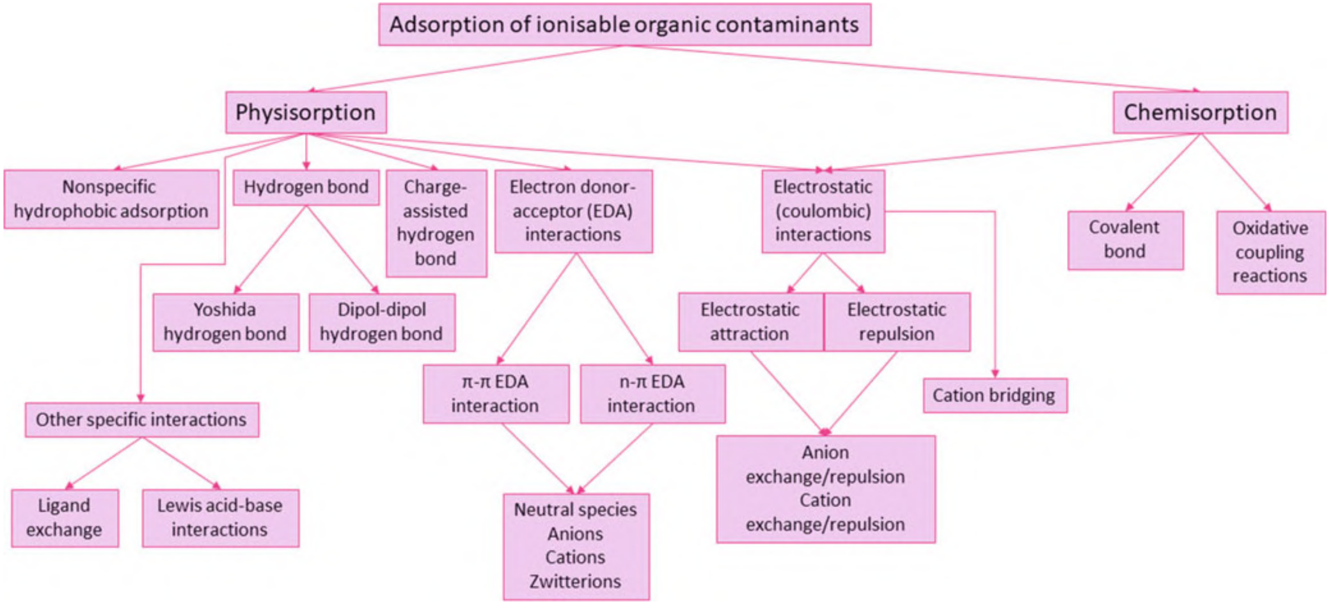

Fig. 2 An overview of adsorption mechanisms for pharmaceutical residues. Adapted with permission [2]. Copyright (2022) Elsevier

6 3D Graphene Structures for Pharmaceutical Adsorption

The assembly of nano-sized two-dimensional (2D) graphene into 3D graphene structures has been extensively explored in recent years. Synthesis of 3D graphene structures can be categorized into two main routes, namely direct synthesis and solution-based synthesis [24]. The construction of 3D graphene structures via interconnecting graphene nano-layers can form a highly porous network, favouring the mass transfer of pharmaceuticals in the water body. Several configurations of 3D graphene have been devised for removing the pharmaceuticals, and these include graphene aerogel [20], hydrogel [25], beads [26], and fibre [27]. Each configuration is further elaborated in the following section, together with the respective synthesis step and pharmaceutical removal performance.

7 Graphene Aerogel

Graphene aerogel is a 3D self-supporting solid network that resembles interconnected graphene sheets forming various pore structures. It is mostly filled with air (> 90%) while maintaining its nanoscale properties within the macroscale structure [28]. This structure presents attractive properties such as low apparent density, large specific surface area, and abundant pores, making it a potential adsorbent for pharmaceutical adsorption. Graphene aerogel has relatively high colloidal and chemical stabilities, as well as ease of modification compared to conventional adsorbents, hence making it the most assayed configuration of 3D graphene for wastewater treatment. Various synthesis methods for graphene aerogels have been reported in the literature and Fig. 3 depicts the schematics of different graphene aerogels preparation.

Among the reported methods, self-assembly coupled with freeze drying is the most widely investigated method in graphene aerogels preparation. This method is also known as solution-based synthesis, whereby graphene oxide (GO) is used as the precursor material. It involves the initial formation of graphene hydrogel through hydrothermal reduction of GO under the influence of a reducing agent. At this stage, the electrostatic repulsion among the GO sheets is reduced by the elimination of oxygen-rich functional groups, hence triggering the bridging of reduced GO sheets to form the 3D graphene hydrogel. The hydrogel is subsequently transformed into aerogel via freeze drying or supercritical fluid drying. The main benefit of this route is that functionalization and process scale-up are possible without the requirement of further processing steps [29].

The template assembly method is an alternative approach for the synthesis of graphene aerogel. This method is flexible, whereby a template is applied as the scaffold for shaping the 3D graphene. Furthermore, organic or inorganic polymers can be incorporated into the GO to construct the 3D structure through van der Waals force, hydrogen, and/or ionic bonding [29]. However, the aerogel constructed may experience stacking of GO sheets leading to the inconsistent internal structure of the

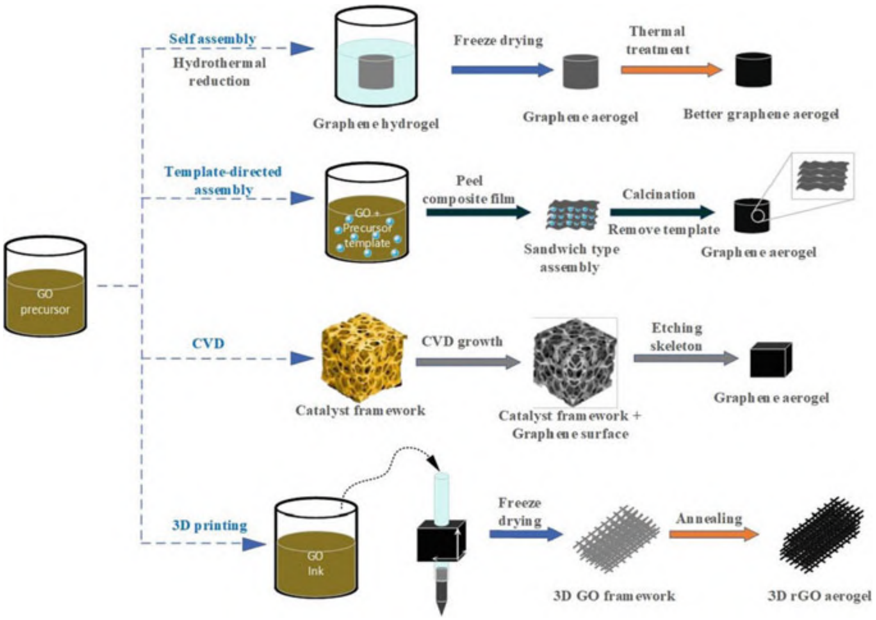

Fig. 3 Schematic diagram for graphene aerogels preparation. Adapted with permission [29]. Copyright (2023) Elsevier

aerogel. In contrast, chemical vapour deposition (CVD) can produce high-quality graphene aerogels. The CVD method requires a porous catalyst framework to initiate the growth of graphene layers from a gaseous carbon precursor. The graphene aerogel can be retrieved by etching the sacrificial template out from the graphene framework. Furthermore, this method enables tuning of pore size of the graphene aerogel through size adjustment of the catalytic template.

Graphene aerogel has been applied in the adsorption of various pharmaceutical residues. For instance, a novel graphene aerogel fabricated by integrating cellulose nanocrystalline with polyvinylamine and reduced GO (CNC-PVAm/rGO) exhibited a high adsorption capacity of 605.87 mg/g towards diclofenac [30]. One interesting finding from the study is the incorporation of PVAm and rGO had increased the adsorption capacity by 53 times as compared to bare CNC aerogel, which might be due to the presence of rGO in the aerogel [30]. According to X-ray photoelectron spectroscopy (XPS) analysis, the π–π groups of graphene were detected at a binding energy of 291.50 eV (C1s spectra) and the percentage of π–π groups decreased from 3.92 to 0.86%, confirming that π–π interaction was one of the adsorption mechanisms [30].

In addition, a graphene-boron nitride composite aerogel (GNP/BNA) was prepared via one-pot foam-gelcasting/nitridation route for ciprofloxacin removal [31]. The developed GNP/BNA possessed low density (28–34 mg/cm^3) as well as high porosity (~99%), compressive strength (40–52 kPa), and ciprofloxacin removal

(99%) [31]. Furthermore, the main adsorption mechanism of ciprofloxacin by the GNP/BNA aerogel was determined as synergistic interaction between graphene and boron nitride functional groups that resulted in the remarkable adsorption of 185 mg/g [31]. An impressive adsorption of tetracycline (1776.26 mg/g) was also achieved using the zeolitic-imidazolate framework-8@reduced graphene oxide (ZIF-8@rGO) aerogel [32]. The ZIF-8@rGO aerogel demonstrated interesting characteristics, where the ZIF-8 nanoparticles grown on the rGO aerogel acted like tentacles to attract tetracycline, while the rGO aerogel served as the storage sites to accommodate the pharmaceutical [32]. The adsorption mechanisms involved were largely linked to hydrogen bonding, π–π interaction, and electrostatic attraction [32].

8 Graphene Hydrogel

Graphene hydrogel is another 3D form developed for the adsorption of pharmaceutical residues in wastewater. In general, hydrogel is a polymeric material with capabilities to swell and retain large portions of water within its structure without collapsing when contacted with aqueous media [33]. Furthermore, the hydrogel has a strong hydrophilicity imparted by the hydrophilic functional groups (e.g., hydroxyl, carboxyl, and carbonyl) of graphene derivatives and polymer additives [34]. As such, the hydrogel can facilitate access and diffusion of aqueous pollutants through its porous channels.

Graphene hydrogels can be synthesized via facile hydrothermal reaction and graft polymerization technique. Nonetheless, the mechanical strength of hydrogel is comparatively poor as the internal structure tends to suffer from irreversible damage once it is broken under a high strain [35]. Therefore, many strategies have been used to strengthen the mechanical properties of hydrogel with crosslinking being the widely accepted approach. Crosslinkers can be incorporated into the graphene precursor to improve interactions between the precursor constituents and promote self-assembly. Crosslinkers such as metal ions, biomolecules, organic molecules, and polymer have been studied in the construction of 3D graphene hydrogels [36].

A yttrium-immobilized GO-alginate hydrogel (Y-GO-SA) with a high specific surface area (147 m^2/g) was developed for the adsorption of tetracycline [6]. The adsorbent contained -COO, -CH_2, and C–O–C groups as the key chemical functional groups [6]. It was reported that the tetracycline adsorption capacity was 477.9 mg/g and the prevailing adsorption mechanisms were hydrogen bonding, π–π interaction, and cation-bonding bridge effects [37]. Interestingly, the potential of Y-GO-SA hydrogel in arsenic adsorption was also investigated. According to the study, the arsenic removal by Y-GO-SA hydrogel was initiated with the formation of hydrogen bonding and ionic exchange mechanisms, resulting in the arsenic adsorption capacity of 273.4 mg/g [37]. In the binary adsorption study, the presence of tetracycline has competed with arsenic for the sorption sites, leading to a lower arsenic adsorption capacity. However, the presence of arsenic has a negligible effect on tetracycline adsorption due to the balance contributions from anion–π interaction and competitions from Y-ions [37].

An organic-crosslinked graphene hydrogel, namely β-cyclodextrin-immobilized rGO composite (β-CD/rGO), was constructed for the adsorption of naproxen [38]. The hydrogel exhibited a relatively large adsorption of naproxen (361.85 mg/g) through distinctive adsorption mechanisms including host–guest interaction, hydrogen bonding, and π–π interaction [38]. In this study, the 3D structure was constructed by crosslinking reaction through acetalization between the aldehyde groups of glutaraldehyde (crosslinker) and the hydroxyl groups of β-CD, and the rGO [38]. In addition, the saturated β-CD/rGO hydrogel was regenerated using ethanol. The adsorption capacity remained as 286.95 mg/g at minimum efficiency [38]. Hence, this finding recommended the graphene hydrogel as an effective and regenerable adsorbent for the pharmaceutical residue.

A continuous removal of chloroquine by an agar-GO hydrogel which was packed in a borosilicate glass column was investigated [39]. The pharmaceutical solution was pumped in an up-flow manner through the column. The breakthrough times for chloroquine at flowrates of 2 and 4 mL/min were 91 and 21 min, respectively [39]. The results showed a decreasing trend of breakthrough time with flowrate, proposing pore diffusion as the limiting step in the pharmaceutical adsorption [39].

9 Graphene Beads

Graphene beads are spherically shaped 3D graphene structures which have attracted much attention owing to their relatively small macro-size with a shorter diffusional pathway for micropollutants to reach the sorption sites [40]. Graphene beads can be synthesized through crosslinking between the GO/polymer matrix and the crosslinking agent (calcium chloride, glutaraldehyde, sodium hydroxide, etc.) with the assistance of freeze drying or supercritical fluid drying [40].

The adsorption of bilirubin onto macro-mesoporous reduced GO aerogel beads was investigated by Li et al. [41]. The graphene beads were synthesized via self-assembly of GO in the presence of a crosslinking agent (calcium ions) and reducing chemical (ascorbic acid), followed by freeze drying [41]. The graphene beads shown in Fig. 4 possessed a spherical shape and a specific surface area of 287.5 m^2/g. It was reported that the size of the graphene beads could be customized by adjusting the needle size during the synthesis stage, and the beads structure became more regular at higher GO concentrations [41].

From the results of scanning electron microscopy (SEM), the graphene beads had a 3D interconnected porous network with randomly distributed pore sizes from 1 to 10 μm, and these might have served as the binding sites for bilirubin. Furthermore, π–π interaction between the graphene sheets provided a high mechanical strength for the beads, where they could support a mass of 202 g, which was 101,000 times more

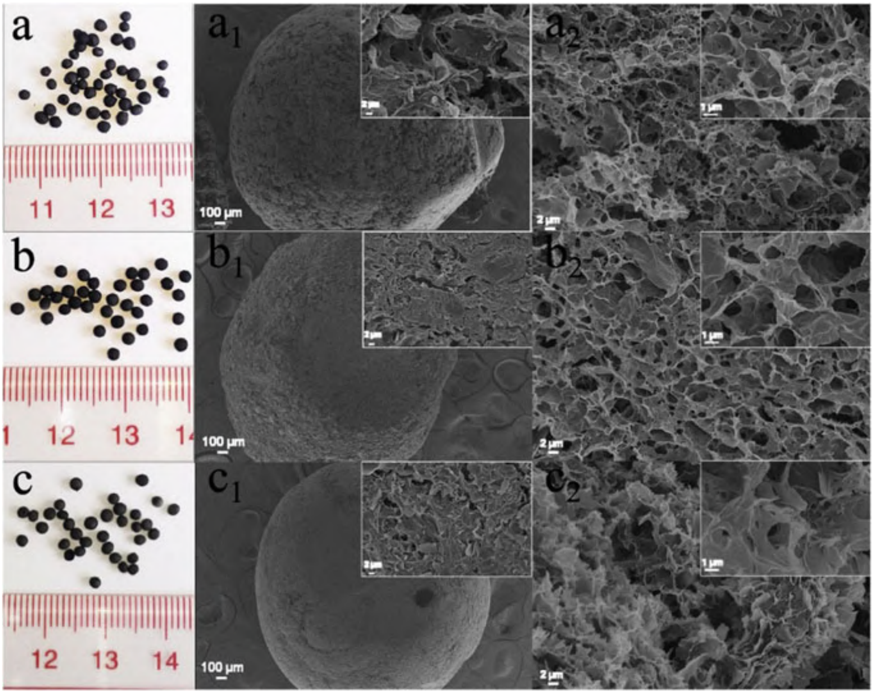

Fig. 4 Optical photograph of rGOn beads (**a**: rGO_8, **b**: rGO_{12}, **c**: rGO_{16}). The SEM morphologies of rGOn beads (a1: rGO_8, b1: rGO_{12}, c1: rGO_{16}) and internal structure of rGOn beads (a2: rGO_8, b2: rGO_{12}, c2: rGO_{16}). Adapted with permission [41]. Copyright (2020) Elsevier

than the original weight of the beads [41]. Such attractive features have resulted in a remarkable bilirubin adsorption capacity of 649 mg/g, further supporting the application of 3D graphene beads in wastewater treatment.

In a separate study, Yang et al. [42] have successfully synthesized GO modified κ-carrageenan/sodium alginate (GO-κ-car/SA) double network hydrogel beads for the removal of different antibiotics (ciprofloxacin and ofloxacin). An interesting highlight from this study is the double network strategy to enhance the mechanical strength of the beads. In this work, sodium alginate (with high content of carboxyl group) and carrageenan (with high content of hydroxyl group) were bonded via hydrogen bonding and ionic interactions [42]. The crosslinked network not only retained the shape of the beads, but also decreased the intermolecular spacing between the sodium alginate and the carrageenan, thereby creating more compact graphene beads. Notably, the addition of GO further enhanced the elastic modulus of the beads from 2.1 MPa (without GO) to 4.5 MPa [42]. Hydrogen bonding and electrostatic interaction were the primary adsorption mechanisms for ciprofloxacin removal (272 mg/g) [42]. Additionally, the continuous removal of ofloxacin by GO-κ-car/SA double network graphene beads was investigated in a fixed-bed operation. The study revealed that the developed adsorbent was reliable for practical applications as supported by the extended breakthrough time of 4 h and bed sorption capacity of 84.43 mg/g [41]. Notably, the GO-κ-car/SA double network beads demonstrated excellent mechanical properties and could withstand high-pressure operation as they did not show any sign of deformation and breakage during the fixed-bed operation.

10 Other Structures

Owing to the ease of modification of graphene materials, there are other configurations of 3D graphene that can be synthesized for pharmaceutical adsorption. Contrarily to aerogel, graphene xerogel can be formed through the sol–gel technique. However, the developed xerogel may experience shrinkage due to capillary collapse of liquid inside the pores of the hydrogel network during the drying stage [43]. As a result, graphene xerogel tends to be denser than aerogels and has a smaller surface area and a lower porosity. A carbon xerogel/graphene hybrid adsorbent was developed to adsorb metronidazole antibiotic. The addition of GO increased the specific surface area of the adsorbent from 648 to 816 m^2/g as the GO content was increased from 0.62 to 1.87 g [44]. Furthermore, the metronidazole adsorption capacity was also increased from 116.86 to 172.59 mg/g as the GO content was increased [44]. The addition of GO was reported to promote $\pi-\pi$ interactions between the adsorbent and metronidazole species along with other mechanisms such as electrostatic attraction and hydrogen bonding [44].

Fibrous structure is also another configuration of 3D graphene adsorbent. The 3D graphene fibre can be prepared through electrospinning, crosslinking, and wet coating. A work was conducted to study the adsorption of trimethoprim by GO-carboxymethylcellulose film coated on polyethylene terephthalate (PET) support [45]. The addition of GO film content demonstrated an increase in trimethoprim adsorption capacity from 2.15 to 39.43 mg/g when the GO film was increased by 20 %(w/w) [45]. This was due to the increase in active sites availability at higher GO film content. However, the adsorption capacity was not significantly increase when the GO film content exceeded 20 % due probably to the aggregation of GO has led to a reduction in surface area and active sites for adsorption [45].

The fibrous structure can be applied in membrane operation to adsorb pharmaceutical residues. For instance, a GO-polysulfone hollow fibre membrane (PSU-GO HFs) was developed to synergize ultrafiltration and adsorption mechanisms for enhanced ciprofloxacin removal [46]. The effect of GO loading on the development of PSU-GO HFs was investigated (Fig. 5) [46].

It was revealed that the optimum removal of ciprofloxacin was achieved at a loading of 3.5% GO, but loadings above 3.5% did not show any significant improvements. This observation was due to the reduction in surface area caused by GO aggregation at higher GO loading [46]. Another highlight of this study is the pilot-test investigation using 100 L tap water with 1 mg/L ciprofloxacin concentration. The initial ciprofloxacin removal was around 65% and decreased to 30% after treating 40

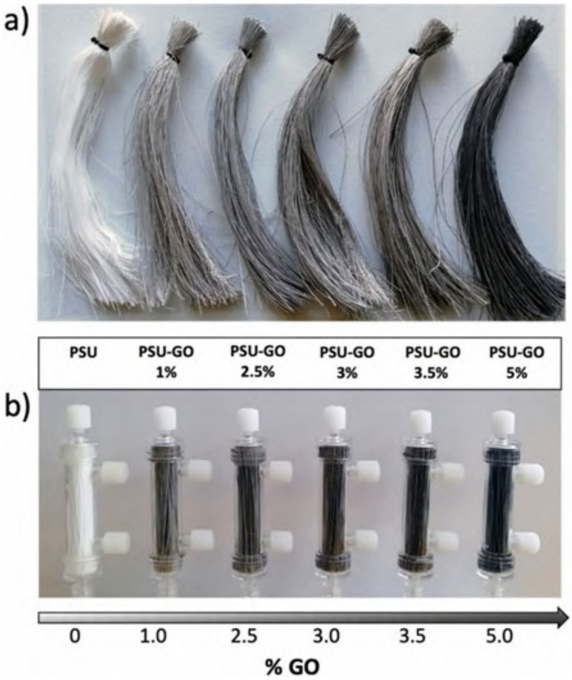

Fig. 5 **a** PSU HFs and **b** filtration modules, with different amounts of GO (w/w). From left to right: pristine PSU; PSU-GO 1%; PSU-GO 2.5%; PSU-GO 3%; PSU-GO 3.5%; PSU-GO 5%. Adapted with permission [46]. Copyright (2022) Elsevier

L of ciprofloxacin-spiked tap water and the adsorption capacity was approximately 110 mg/g [46].

11 Conclusion and Outlook

3D graphene structures development for environmental pollution control has attracted great interest lately. The 3D hierarchical network of graphene has showcased superior adsorption capacities towards numerous pharmaceuticals. The construction of 3D graphene has introduced additional adsorption functionalities from the chemical additives while maintaining the intrinsic properties of the nanomaterial in the bulk structure, thus making it a favourable adsorbent. Presently, the most developed 3D graphene structures are aerogel, hydrogel, and spherical beads as they offer practical structures to remove pharmaceutical residues. The primary binding mechanisms involved in the adsorption of pharmaceuticals are π–π interaction, hydrogen bonding, and electrostatic interaction.

The application of 3D graphene structure for industrial-scale removal of pharmaceutical has not been realized yet. The graphene structures previously discussed were mostly prepared at a laboratory scale and may not be sufficiently robust to withstand the harsh flow conditions of industrial wastewater treatment. To improve the mechanical strength of 3D graphene, it is crucial to optimize the formulation of the graphene from the aspects of crosslinker choice, chemical functionalities, crosslinking conditions, and post-treatment processes. Additionally, most of the studied pharmaceutical residues were under the classes of antibiotic and non-steroidal anti-inflammatory drugs, but studies on other classes of medicines such as antidepressant, hormones, and beta-blocker remain scarce. Therefore, comprehensive research on these drugs is necessary to understand the adsorption affinity of 3D graphene structures towards the persistent pharmaceutical pollutants.

Moreover, the simultaneous adsorption of multi-pollutants, continuous adsorption via fixed-bed column, and pilot-scale adsorber design are still lacking in the literature. Hence, it is highly recommended to conduct such studies to increase the feasibility of commercialization of 3D graphene structures for pharmaceutical wastewater treatment. In addition, most research works mainly focussed on the development and assessment of the 3D graphene structures in pharmaceuticals removal, but the sustainability of using these structures is unclear. As such, life cycle analysis, techno-economic analysis, and density functional theory should be applied to determine the viability of 3D graphene structures in large-scale wastewater remediation.

Acknowledgements The authors gratefully acknowledge the financial support provided by the Ministry of Higher Education (MOHE), Malaysia, under the Fundamental Research Grant Scheme, FRGS/1/2020/STG05/UNIM/02/2.

References

1. Kujawska, A., Kiełkowska, U., Atisha, A., Yanful, E., Kujawski, W.: Comparative analysis of separation methods used for the elimination of pharmaceuticals and personal care products (PPCPs) from water—a critical review. Sep. Purif. Technol. **290**, 120797 (2022)
2. Shearer, L., Pap, S., Gibb, S.W.: Removal of pharmaceuticals from wastewater: a review of adsorptive approaches, modelling and mechanisms for metformin and macrolides. J. Environ. Chem. Eng. **10**(4), 108106 (2022)
3. Alnajjar, M., Hethnawi, A., Nafie, G., Hassan, A., Vitale, G., Nassar, N.N.: Silica-alumina composite as an effective adsorbent for the removal of metformin from water. J. Environ. Chem. Eng. **7**(3), 102994 (2019)
4. Quesada, H.B., Baptista, A.T.A., Cusioli, L.F., Seibert, D., de Oliveira Bezerra, C., Bergamasco, R.: Surface water pollution by pharmaceuticals and an alternative of removal by low-cost adsorbents: a review. Chemosphere **222**, 766–780 (2019)
5. Liu, Y.-P., Lv, Y.-T., Guan, J.-F., Khoso, F.M., Jiang, X.-Y., Chen, J., Li, W.-J., Yu, J.-G.: Rational design of three-dimensional graphene/graphene oxide-based architectures for the efficient adsorption of contaminants from aqueous solutions. J. Mol. Liq. **343**, 117709 (2021)
6. He, J., Cui, A., Ni, F., Deng, S., Shen, F., Yang, G.: A novel 3D yttrium based-graphene oxide-sodium alginate hydrogel for remarkable adsorption of fluoride from water. J. Colloid Interface Sci. **531**, 37–46 (2018)
7. Hiew, B.Y.Z., Tee, W.T., Loh, N.Y.L., Lai, K.C., Hanson, S., Gan, S., Thangalazhy-Gopakumar, S., Lee, L.Y.: Synthesis of a highly recoverable 3D MnO2/rGO hybrid aerogel for efficient adsorptive separation of pharmaceutical residue. J. Environ. Sci. **118**, 194–203 (2022)

8. Wong, S., Lim, Y., Ngadi, N., Mat, R., Hassan, O., Inuwa, I.M., Mohamed, N.B., Low, J.H.: Removal of acetaminophen by activated carbon synthesized from spent tea leaves: equilibrium, kinetics and thermodynamics studies. Powder Technol. **338**, 878–886 (2018)
9. Tee, W.T., Loh, N.Y.L., Hiew, B.Y.Z., Show, P.L., Hanson, S., Gan, S., Lee, L.Y.: Evaluation of adsorption performance and mechanisms of a highly effective 3D boron-doped graphene composite for amitriptyline pharmaceutical removal. J. Environ. Manage. **344**, 118363 (2023)
10. Iqbal, J., Shah, N.S., Khan, Z.U.H., Rizwan, M., Murtaza, B., Jamil, F., Shah, A., Ullah, A., Nazzal, Y., Howari, F.: Visible light driven doped CeO2 for the treatment of pharmaceuticals in wastewater: a review. J. Water Process Eng. **49**, 103130 (2022)
11. Al Falahi, O.A., Abdullah, S.R.S., Hasan, H.A., Othman, A.R., Ewadh, H.M., Kurniawan, S.B., Imron, M.F.: Occurrence of pharmaceuticals and personal care products in domestic wastewater, available treatment technologies, and potential treatment using constructed wetland: a review. Process Saf. Environ. Protect. **168**, 1067–1088 (2022)
12. Mackuľak, T., Černanský, S., Fehér, M., Birošová, L., Gál, M.: Pharmaceuticals, drugs, and resistant microorganisms—environmental impact on population health. Curr. Opin. Environ. Sci. Health **9**, 40–48 (2019)
13. Ramírez-Durán, N., Moreno-Pérez, P.A., Sandoval-Trujillo, A.H.: Bacterial treatment of pharmaceutical industry effluents. Ecopharmacovigilance 175–187 (2017)
14. Hussain, I., Khan, M.Z., Khan, A., Javed, I., Saleemi, M.K.: Toxicological effects of diclofenac in four avian species. Avian Pathol. **37**(3), 315–321 (2008)
15. Van der Meer, T.P., Artacho-Cordón, F., Swaab, D.F., Struik, D., Makris, K.C., Wolffenbuttel, B.H.R., Frederiksen, H., Van Vliet-Ostaptchouk, J.V.: Distribution of non-persistent endocrine disruptors in two different regions of the human brain. Int. J. Environ. Res. Public Health (2017)
16. Kumar, M., Sridharan, S., Sawarkar, A.D., Shakeel, A., Anerao, P., Mannina, G., Sharma, P., Pandey, A.: Current research trends on emerging contaminants pharmaceutical and personal care products (PPCPs): a comprehensive review. Sci. Total Environ. **859**, 160031 (2023)
17. Madikizela, L.M., Ncube, S., Chimuka, L.: Uptake of pharmaceuticals by plants grown under hydroponic conditions and natural occurring plant species: a review. Sci. Total Environ. **636**, 477–486 (2018)
18. Rouquerol, F., Rouquerol, J., Sing, K.S.W., Maurin, G., Llewellyn, P.: 1 - Introduction. In: Rouquerol, F., Rouquerol, J., Sing, K.S.W., Llewellyn, P., Maurin, G. (eds.) Adsorption by Powders and Porous Solids (Second Edition), pp. 1–24. Academic Press, Oxford (2014)
19. Chen, M., Yan, Z., Luan, J., Sun, X., Liu, W., Ke, X.: π-π electron-donor-acceptor (EDA) interaction enhancing adsorption of tetracycline on 3D PPY/CMC aerogels. Chem. Eng. J. **454**, 140300 (2023)
20. Pinelli, F., Piras, C., Rossi, F.: A perspective on graphene based aerogels and their environmental applications. FlatChem **36**, 100449 (2022)
21. Gang, D., Uddin Ahmad, Z., Lian, Q., Yao, L., Zappi, M.E.: A review of adsorptive remediation of environmental pollutants from aqueous phase by ordered mesoporous carbon. Chem. Eng. J. **403**, 126286 (2021)
22. Ateia, M., Helbling, D.E., Dichtel, W.R.: Best practices for evaluating new materials as adsorbents for water treatment. ACS Mater. Lett. **2**(11), 1532–1544 (2020)
23. Liu, H., Qiu, H.: Recent advances of 3D graphene-based adsorbents for sample preparation of water pollutants: a review. Chem. Eng. J. **393**, 124691 (2020)
24. Hiew, B.Y.Z., Lee, L.Y., Lee, X.J., Thangalazhy-Gopakumar, S., Gan, S., Lim, S.S., Pan, G.-T., Yang, T.C.-K., Chiu, W.S., Khiew, P.S.: Review on synthesis of 3D graphene-based configurations and their adsorption performance for hazardous water pollutants. Process Saf. Environ. Prot. **116**, 262–286 (2018)
25. Zhuang, Y., Yu, F., Ma, J., Chen, J.: Enhanced adsorption removal of antibiotics from aqueous solutions by modified alginate/graphene double network porous hydrogel. J. Colloid Interface Sci. **507**, 250–259 (2017)
26. Ma, J., Jiang, Z., Cao, J., Yu, F.: Enhanced adsorption for the removal of antibiotics by carbon nanotubes/graphene oxide/sodium alginate triple-network nanocomposite hydrogels in aqueous solutions. Chemosphere **242**, 125188 (2020)

27. Zhang, P., Yin, L., Yang, X., Wang, J., Chi, M., Qiu, J.: Cotton-derived 3D carbon fiber aerogel to in situ support Bi2O3 nanoparticles as a separation-free photocatalyst for antibiotic removal. Carbon **201**, 110–119 (2023)
28. Jiang, X., Du, R., Hübner, R., Hu, Y., Eychmüller, A.: A roadmap for 3D metal aerogels: materials design and application attempts. Matter **4**(1), 54–94 (2021)
29. Wu, W., Du, M., Shi, H., Zheng, Q., Bai, Z.: Application of graphene aerogels in oil spill recovery: a review. Sci. Total Environ. **856**, 159107 (2023)
30. Lv, Y., Liang, Z., Li, Y., Chen, Y., Liu, K., Yang, G., Liu, Y., Lin, C., Ye, X., Shi, Y., Liu, M.: Efficient adsorption of diclofenac sodium in water by a novel functionalized cellulose aerogel. Environ. Res. **194**, 110652 (2021)
31. Han, L., Khalil, A.M.E., Wang, J., Chen, Y., Li, F., Chang, H., Zhang, H., Liu, X., Li, G., Jia, Q., Zhang, S.: Graphene-boron nitride composite aerogel: a high efficiency adsorbent for ciprofloxacin removal from water. Sep. Purif. Technol. **278**, 119605 (2021)
32. Liu, Y., Fu, J., He, J., Wang, B., He, Y., Luo, L., Wang, L., Chen, C., Shen, F., Zhang, Y.: Synthesis of a superhydrophilic coral-like reduced graphene oxide aerogel and its application to pollutant capture in wastewater treatment. Chem. Eng. Sci. **260**, 117860 (2022)
33. Yu, F., Yang, P., Yang, Z., Zhang, X., Ma, J.: Double-network hydrogel adsorbents for environmental applications. Chem. Eng. J. **426**, 131900 (2021)
34. Guo, Y., Bae, J., Fang, Z., Li, P., Zhao, F., Yu, G.: Hydrogels and hydrogel-derived materials for energy and water sustainability. Chem. Rev. **120**(15), 7642–7707 (2020)
35. Wang, X.-H., Song, F., Qian, D., He, Y.-D., Nie, W.-C., Wang, X.-L., Wang, Y.-Z.: Strong and tough fully physically crosslinked double network hydrogels with tunable mechanics and high self-healing performance. Chem. Eng. J. **349**, 588–594 (2018)
36. Wu, Y., Zhu, J., Huang, L.: A review of three-dimensional graphene-based materials: synthesis and applications to energy conversion/storage and environment. Carbon **143**, 610–640 (2019)
37. He, J., Ni, F., Cui, A., Chen, X., Deng, S., Shen, F., Huang, C., Yang, G., Song, C., Zhang, J., Tian, D., Long, L., Zhu, Y., Luo, L.: New insight into adsorption and co-adsorption of arsenic and tetracycline using a Y-immobilized graphene oxide-alginate hydrogel: adsorption behaviours and mechanisms. Sci. Total Environ. **701**, 134363 (2020)
38. Feng, X., Qiu, B., Dang, Y., Sun, D.: Enhanced adsorption of naproxen from aquatic environments by β-cyclodextrin-immobilized reduced graphene oxide. Chem. Eng. J. **412**, 128710 (2021)
39. Bezerra de Araujo, C.M., Wernke, G., Ghislandi, M.G., Diório, A., Vieira, M.F., Bergamasco, R., Alves da Motta Sobrinho, M., Rodrigues, A.E.: Continuous removal of pharmaceutical drug chloroquine and Safranin-O dye from water using agar-graphene oxide hydrogel: selective adsorption in batch and fixed-bed experiments. Environ. Res. **216**, 114425 (2023)
40. Liu, H., Tian, X., Xiang, X., Chen, S.: Preparation of carboxymethyl cellulose/graphene composite aerogel beads and their adsorption for methylene blue. Int. J. Biol. Macromol. **202**, 632–643 (2022)
41. Li, Z., Huang, X., Wu, K., Jiao, Y., Zhou, C.: Fabrication of regular macro-mesoporous reduced graphene aerogel beads with ultra-high mechanical property for efficient bilirubin adsorption. Mater. Sci. Eng., C **106**, 110282 (2020)
42. Yang, P., Yu, F., Yang, Z., Zhang, X., Ma, J.: Graphene oxide modified κ-carrageenan/sodium alginate double-network hydrogel for effective adsorption of antibiotics in a batch and fixed-bed column system. Sci. Total Environ. **837**, 155662 (2022)
43. Bratovcic, A., Petrinic, I.: Carbon based aerogels and xerogels for removing of toxic organic compounds. In: International Conference "New Technologies, Development and Applications", Springer, pp. 743–749 (2020)
44. Segovia-Sandoval, S.J., Pastrana-Martínez, L.M., Ocampo-Pérez, R., Morales-Torres, S., Berber-Mendoza, M.S., Carrasco-Marín, F.: Synthesis and characterization of carbon xerogel/graphene hybrids as adsorbents for metronidazole pharmaceutical removal: effect of operating parameters. Sep. Purif. Technol. **237**, 116341 (2020)

45. Juengchareonpoon, K., Wanichpongpan, P., Boonamnuayvitaya, V.: Trimethoprim adsorption using graphene oxide-carboxymethylcellulose film coated on polyethylene terephthalate as a supporter. Chem. Eng. Process.—Process Intensification **169**, 108641 (2021)
46. Zambianchi, M., Khaliha, S., Bianchi, A., Tunioli, F., Kovtun, A., Navacchia, M.L., Salatino, A., Xia, Z., Briñas, E., Vázquez, E., Paci, D., Palermo, V., Bocchi, L., Casentini, B., Melucci, M.: Graphene oxide-polysulfone hollow fibers membranes with synergic ultrafiltration and adsorption for enhanced drinking water treatment. J. Membr. Sci. **658**, 120707 (2022)

3D Graphene for Metal-Ion Batteries

Jin Kwei Koh and Chin Wei Lai

Abstract A metal-ion battery is a rechargeable secondary battery. Lithium-ion was the first metal-ion battery introduced in the 1980s. Various metal-ion batteries have then emerged in the last few decades. However, each has limitations in terms of cost and availability. Several recent inventions employ three-dimensional (3D) graphene oxide to advance the electrochemical performance of metal-ion batteries. This chapter discusses the type of metal-ion batteries, followed by an overview of 3D graphene, including its fabrication method and structure. Various structures of 3D graphene material in metal-ion batteries are discussed, including foam, aerogels, microsphere, ball, vertical sheet, and others. Each structure of modified 3D graphene has been outlined with its detailed fabrication process. Additionally, the recent development regarding 3D graphene in metal-ion batteries is also discussed detailed. This review concludes that most studies exhibited good electrochemical performance using modified 3D graphene materials in a metal-ion battery. In the future, there is a need to seek alternatives for metal ions or graphene resources as they suffer from a few limitations, such as the depletion of metal ions and the cost and fabrication of graphene.

Keywords 3D graphene · Metal-ion battery system · Electrochemical · Fabrication methods

1 Introduction

A metal-ion battery is a rechargeable battery with two electrodes (cathode and anode), a separator membrane, an electrolyte, and an external electronic circuit. There is various type of metal-ion batteries. The lithium-ion battery is the most common electrochemical technology and is convenient in numerous industries, such as communications, transportation, and others. The primary functioning mechanism of all metal-ion batteries is the discharge and charge process (Fig. 1). Energy is

---

J. K. Koh · C. W. Lai (✉)
Nanotechnology and Catalysis Research Centre (NANOCAT), Institute for Advanced Studies, Universiti Malaya, Level 3, Block A, 50603 Kuala Lumpur, Malaysia
e-mail: cwlai@um.edu.my

© The Author(s), under exclusive license to Springer Nature Switzerland AG 2023

R. K. Gupta (ed.), *3D Graphene*, Carbon Nanostructures,
https://doi.org/10.1007/978-3-031-36249-1_12

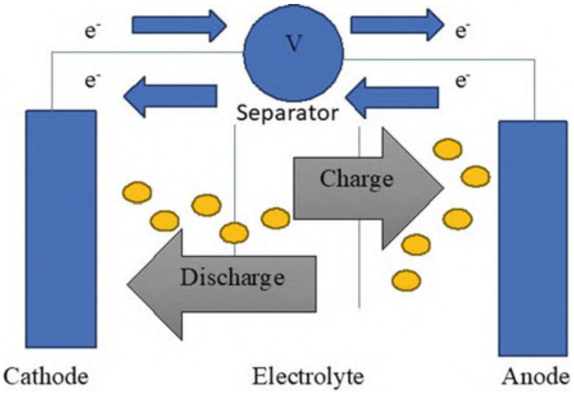

Fig. 1 Schematic of metal-ion battery structure

generally stored in the form of electrons in the lithium ions within the anode for the discharge process. The anode initiates an oxidation process, which causes lithium ions to exit the anode and move to the cathode. The electrons that have been stored are released to produce the electric current. The charging mechanism can be explained as the electrons from the power source charging the battery attaching with the lithium ions in the cathode during the charging phase, during which the ions pass through the electrolyte and the separator to the anode [1, 2].

The concept of the lithium-ion battery was introduced in the late 1970s. Armand proposed a lithium-ion battery, using two different intercalation materials for anodes and cathodes. Meanwhile, the lithium-ion battery was named a "rocking-chair battery" because its charge–discharge mechanism shuttles the ions from one electrode to another. Subsequently, Lazzari and Scrosati demonstrated the concept of lithium-ion batteries in 1980. The sodium-ion battery also was introduced in the 1980s. Over that decade, the research and development of metal-ion batteries were mainly focused on lithium-ion batteries. The lithium-ion battery was also commercialised by Sony in 1991, while sodium-ion batteries received less attention in the market. Due to the cost-efficiency of materials, other types of metal-ion batteries have emerged, such as aluminium and potassium-ion batteries [1–3]. Due to concerns about the efficiency of battery technology, the charging and discharging capacity with the cycling performance are the main criteria to improve the metal-ion batteries. There have been many advancements in all metal-ion batteries, including existing lithium and sodium-ion batteries. The advancement of all metal-ion batteries is focused on modifying electrodes using nanomaterial. Currently, 3D graphene has garnered attention in the electrochemical battery industry as its nanostructure contributes to the higher theoretical capacity, large surface area contact for charging and discharging process, and others. This chapter summarises the recent development of 3D graphene in the metal-ion battery and their achievement of electrochemical properties. This chapter then outlines the future challenges and opportunities of this 3D graphene in metal-ion batteries.

2 Overview of the Types of Metal-Ion Battery

Metal-ion battery is mainly made up of four basic functional components, which are the anode, cathode, electrolyte, and current collector. There are various types of metal-ion batteries, such as lithium-ion, magnesium-ion, aluminium-ion, sodium-ion, potassium-ion, and others. The type of metal in the metal-ion battery can be classified based on the inclusion of alkaline metal, alkaline earth metal, or other transition metal.

2.1 Alkaline Metal-Ion Battery

According to the periodic table, lithium and sodium are the most frequently studied in the metal-ion battery systems. The lithium-ion battery is one of the most successful commercialised in the electrochemistry and power field. This is due to the high energy and power density supply in that system. It has been utilised in electric vehicles since the 1990s. Normally, lithium-ion acts as a cathode, while the anode is made of lithium metal. The lithium-ion battery has been used in various applications, such as electronic communications gadgets, transportation, and others in this era of technology. However, it has a short lifespan and there are safety concerns in the practical application of lithium-ion batteries [3–6].

Due to these concerns, abundant resources on Earth, such as sodium and potassium, are emerging in battery systems, since they are alkali metals with similar physicochemical properties to lithium. Further, both are inexpensive and can be utilised in large-scale electric storage. However, both have large radii, which can influence metal-ion batteries' discharge and charge capacity [7, 8].

2.2 Alkali Earth Metal

Due to the high cost of lithium-based batteries, safety concerns, and the scarcity of lithium elements in nature, there is an urgent need to develop alternatives in the battery system. Hence, alkali earth metals also have been giving rise to battery research, such as magnesium and aluminium. For instance, magnesium ions in battery systems can be more economical and eco-friendly in electric vehicles. Magnesium can act as both an anode and cathode for the intercalation or deintercalation of magnesium ions. Hence, it is a potential candidate in the metal-ion battery system.

An aluminium ion is another metal earth metal that can flow from anode to cathode in an electro-battery system. It can exchange three electrons for every ion and has three times the energy density of a lithium-ion battery system. It is a low-cost and high-abundance material, but it has operation issues at high temperatures [9].

3 Overview of 3D Graphene Material with Its Fabrication Method and Structure in the Current Metal-Ion Battery Technology

Graphene is known as a two-dimensional (2D) and was discovered in 2000. Normally, this material is called "graphene" and is rarely specifically named "2D graphene". Graphene garners attention with the remarkable improvement of advanced science and technology to date. This is due to its unique structural configuration, which consists of a single layer of honeycomb configuration with sp^2 hybridised carbon atoms. Its intrinsic features have been broadened in various research fields, providing insights into cutting-edge nanomaterials. 3D graphene materials are considered an advanced technology because the 3D features of graphene oxide are conducive to various applications. Theoretically, 3D graphene material is formed from unstacked 2D graphene. Graphene material is conventionally synthesised via two distinct approaches, namely bottom-up and top-down approaches. Chemical vapour deposition (CVD), pyrolysis, and epitaxial growth are examples of bottom-up approaches, whereas chemical synthesis, chemical exfoliation, and mechanical exfoliation are examples of top-down approaches.

CVD, synthesis of carbon, and other bottom-up approaches are unfavourable in the massive production of graphene due to several concerns, including cost, product purity, scalability, and yield. For instance, Table 1 shows CVD having low crystallinity with controlled layers and sizes, which is convenient in graphene synthesis and boosts graphene-based energy devices' performance. However, it is costly and available on a limited scale [10, 11]. However, liquid phase exfoliation and reduction of graphene oxide are favourable in the massive production of graphene, because of their cost-effectiveness and high scalability for bulk production [10, 12]. Technically, pristine graphite is used as starting material to undergo pre-treatment, such as thermal treatment, mechanical milling, or Hummers' oxidation, followed by exfoliation by ultra-sonification. Besides, the pristine graphite also can undergo direct exfoliation in the liquid phase. After exfoliation, the treated and exfoliated sources are converted to reduced graphene oxide or graphene oxide-based compounds by chemical, thermal, and electrochemical reactions.

Although 2D graphene has outstanding performance with its extraordinary properties, the agglomeration effects of 2D graphene-based materials are the main problem of dispersive behaviour, which is caused by its morphology structure. Hence, 3D graphene materials have been advocated for nanotechnology emerging in the past few years. Although the fabrication of 3D graphene materials is almost similar to the fabrication of the graphene materials that is aforementioned, there is a difference in terms of crystallinity, purity, cost, and scalability between 2 and 3D graphene materials, as shown in Table 1 [13]. As electrical battery technology is sensitive to conductivity, the powder form is more favourable than bulk materials. Therefore, there are challenges faced in 3D graphene material synthesis. This is attributed to the high crystallinity in most approaches, such as micromechanical exfoliation, reduction of graphene oxide, and liquid phase exfoliation, which contribute to bulk material

Table 1 The comparison of 2D graphene and 3D graphene in terms of crystallinity, purity, layer number controllability, cost aspect, and scalability for each process. Adapted with permission [13], copyright (2018), chemical society reviews

Graphene types	Method of fabrication	Crystallinity	Purity	Layer number controllability	Cost aspect	Scalability
2D	Chemical vapour deposition	Low	High	High	High	Medium
	Micromechanical exfoliation	High	High	Medium	Low	Low
3D	Chemical vapour deposition	Medium	High	High	Medium	High
	Reduction of graphene oxide	High	Low	Low	Low	High
	Liquid phase exfoliation	High	Medium	Low	Low	High

production. The fabrication of 3D graphene materials in powder form is thus more attractive in battery design [14].

3D graphene can be prepared using several methods with different morphology structures. In battery technology, the typical structural design of 3D graphene composite can be encapsulated in a ball, mixed, anchored, and layered form, according to Chang et al. [12]. In the following, the previous studies regarding the fabrication of 3D graphene material on the electrochemical battery are discussed in terms of the process, structure, precursors, template, and temperature required, as summarised in Table 2.

3.1 Cvd

In 2006, CVD was launched. This is fabricated with a planar few-layer graphene structure. Up to now, there have been various studies on the fabrication of graphene via CVD. This process requires the precursor for the fabrication of the graphene material, which can be applied in various forms. Methane gas is the most common carbon source for the production of graphene materials [14–19]. For the growth of graphene, nickel is usually used as the template. The operation temperature is in the range of 790–1050 °C. The samples are always treated in a hydrogen or Argon atmosphere. Certain researchers have utilised CVD process initially for the synthesis of 2D graphene material and then further with other processes such as hydrothermal, calcination, annealing, and others. However, CVD also can be used to produce 3D graphene materials further. For instance, Guo et al. [15] and Son et al. [16] synthesised graphene foam and graphene balls using methane gas as a carbon source via CVD process. They also utilised 3D graphene material fabricated from CVD process, further hybridising with the functionalised materials in their metal

Table 2 Previous studies of metal-ion batteries with their process details

Method of fabrication	Product structure	Precursor	Template	Operating condition	Author
CVD, etching	Graphene hollow structure (hybrid with ZnO and $Mg(OH)_2$ intermediate nanostructure layer)	Methane (CVD), Nitric acid (etching)	Nickel foam	790 Pa and 1000 °C (CVD)	Guo et al. [15]
CVD	Graphene ball: hybrid silica with graphene in popcorn structure	Methane, hydrogen	Silica	Atm pressure and 900–1050 °C	Son et al. [16]
CVD, plasma etching, annealing	Graphene-nanoribbon on the surface of highly porous 3D graphene	Methane, hydrogen, Argon (CVD) Ar^+ ion (plasma etching) Argon and hydrogen (annealing)	nickel (CVD)	Ambient pressure and 1000 °C (CVD), 110 °C (plasma etching), 650 (Annealing)	Yu et al. [19]
CVD, hydrothermal	Multilayer 3D graphene foam: hybrid with sulphur-based material	Methane, soybean oil (CVD) Carbon Sulphide (hydrothermal)	Nickel foam (CVD)	800 °C (CVD), 155 °C (hydrothermal)	Choi et al. [23]
	D graphene foam: hybrid with sulphur-based material 3	Hydrogen, argon, methane (CVD) Sulphur, argon (hydrothermal)	nickel foam (CVD)	1000 °C (CVD), 155 °C (hydrothermal)	He et al. [18]
CVD, hydrothermal	Graphene foam: hybrid with carbon nanotube and MoS_2 nanoparticles	Methane (CVD) Argon (hydrothermal)	Nickel	1000 °C (CVD, 200 °C (hydrothermal)	Ren et al. [17]
Thermal CVD	Vertical graphene sheets on carbon black	Methane, hydrogen	NA	Ar atmosphere and 1100 °C	Ji et al. [14]
Modified Hummer's method, Hydrothermal and freeze-drying and calcination	Crystal Microstructure of antimony/graphene composite	GO powder and potassium antimony tartrate (hydrothermal) Argon (calcination)	NA	180 °C (hydrothermal), −56 °C (freeze-drying), 850 °C (calcination)	Li et al. [22]

(continued)

Table 2 (continued)

Method of fabrication	Product structure	Precursor	Template	Operating condition	Author
	Mesoporous amorphous $FePO_4$ nanoparticles cross-linked with 3D holey graphene framework	Graphene nanosheet, $(NH_4)_2Fe(SO_4)_2$ and $NH_4H_2PO_4$	CTAB, n-hexane, n-butanol	180 °C (hydrothermal), 400 (calcination)	Mo et al. [24]
Modified Hummer's method, hydrothermal, freeze-drying and annealing	Hybrids of 3D graphene with Fe_3O	Graphene oxide, ferric citrate (hydrothermal), nitrogen (annealing)	NA	180 °C (hydrothermal), 500 °C (annealing)	Liu et al. [25]
	SnO_2-GA 3D porous aerogels	SnO_2, graphene oxide	NA	75 °C (hydrothermal), 600 (annealing)	Chen et al. [27]
Modified Hummer's, hydrothermal and calcination	3D graphene-encapsulated nearly monodisperse Fe_3O_4 (3D Fe_3O_4@rGO) composite	$FeSO_4.7H_2O$, lysine (hydrothermal) argon (calcination)	Graphene oxide	180 °C (hydrothermal), 600 °C (calcination)	Li et al. [21]
Hummer's method, Reflux, annealing and freeze-drying	Nano $FeSb_2S_4$ in CNT/graphene 3D porous network	$SbCl_2$, $FeCl_2$, S (hydrothermal) argon (annealing) carbon nanotubes (mixed before freeze-drying)	NA	180 °C (Reflux), 450 °C (annealing), –50 °C (freeze-drying)	Zeng et al. [28]
Hydrothermal process and roasting process	Microsphere: crystal carbon shell-coated graphene sheets	Sucrose (hydrothermal process), argon (roasting process)	Aluminium nitrate nonahydrate	200 °C (hydrothermal), 2000 °C (roasting process)	Liu et al. [26]
Solvothermal and 2-step annealing	Oxygen-rich graphene is vertically grown on 3D N-doped carbon foam composite	Graphene oxide, alcohol (solvothermal) argon (annealing)	Melamine (solvothermal)	180 °C (solvothermal), 800 °C (1st calcination), and 325 °C (2nd calcination)	Ma et al. [30]

(continued)

Table 2 (continued)

Method of fabrication	Product structure	Precursor	Template	Operating condition	Author
Facile spray drying, ball milling, calcination	3D graphene decorated iron-based mixed-polyanion compound $Na_4Fe_3(PO_4)_2(P_2O_7)$ microspheres	$Fe(NO_3)_3 \cdot 9H_2O$, $NaH_2PO_4 \cdot 2H_2O$ and $C_6H_8O_7 \cdot H_2O$, GO (spray drying) argon (calcination)	NA	500 °C (spray drying), 900 °C (calcination)	Yuan et al., [29]
Modified Hummer's, Freeze-drying and thermal reduction	Ultrathin MoS_2 nanosheet/ graphene hybrid aerogels	Ammonium tetrathiomolybdate, graphene oxide (freeze-drying) argon and hydrogen (for thermal use)	Carbon fibre paper	800 °C	Yuan et al. [8]
Pyrolysis	Porous monolith of graphene (also known as zinc-guided 3D graphene)	Glucose	Zinc	1000 °C	Wang et al. [7]
Modified Hummer's, pyrolysis	3D wrinkled N, S co-doped multilayer graphene sheets embedding with SiOx microparticles	Thiourea, SiO_x	NA	800 °C	Shi et al. [31]

battery studies, as explained in Table 2. This indicates the broader use of graphene-based composite, promoting the integration of 3D graphene materials with other functionalised materials. A CVD-based process that is applied at high temperatures for the reduction and decomposition of atoms in the synthesis of nanomaterial is known as a thermal CVD. Ji et al. [14] produced a novel 3D graphene powder via thermal CVD. This study revealed that the specific surface area of powder substrate led to higher yield production. Therefore, the carbon black utilised in this study was 34 nm, contributing to a kilogram yield of 3D graphene powder through thermal CVD.

3.2 Hummer's Method and Modified Hummer's Method

Hummer's method is an older method that is a form of oxidative exfoliation. This method has been replaced by Brodie's method, as it offers several advantages, such as safety concerns in Brodie's method in the past. However, there is an environmental problem related to toxic waste removal associated with Nitrogen dioxide (NO_2) and Dinitrogen tetroxide (N_2O_4) during the fabrication of graphite material via Hummer's method. Therefore, several researchers have modified this method in various ways, such as the exclusion of the consumption of sodium nitrate ($NaNO_3$), an incline of the potassium permanganate ($KMnO_4$) usage, and others [20]. For instance, Li et al. [21] worked with the modified method by excluding $NaNO_3$. However, Li et al. [22] reported the fabrication of graphene using a $KMnO_4$: $NaNO_3$ ratio of 6:1 for modified Hummer's method. Concerning 3D graphene-based battery technology, several studies have also reported on this modified method in the fabrication of graphene oxide. Therefore, the precursors of reduced graphene material and 3D graphene-based materials are initiated by this modified method before further undergoing other processes (hydrothermal, calcination, annealing, etc.) in the fabrication of 3D graphene-based materials. Related studies are shown in Table 2.

3.3 Hydrothermal

Hydrothermal process is generally utilised for the thermal reduction of graphene oxide which has been synthesised from the modified Hummer's method or any initial pre-treatment. It emerged in the late nineteenth century. Several studies have been performed with this step for the reduction of graphene oxide in metal-ion battery technology. For instance, Choi et al. [23] and He et al. [18] performed a hydrothermal process at 155 °C for 12 h after CVD process, which involvedsulphur-based material in the hydrothermal process. Their finalised product is graphene foam hybridising with sulphur-based material.

Further, several researchers have reported on the operation temperature of the hydrothermal process at 180 °C with various precursors with graphene material. The precursors depend on hybridised organic or inorganic material in the battery studies. For instance, Li et al. [22] fabricated a crystal antimony/graphene composite for a metal-ion battery. The hydrothermal process involved graphene oxide with potassium antimony tartrate at 180 °C for 24 h. Mo et al. [24] developed a holey 3D graphene cross-linked with mesoporous amorphous Iron (III) Phosphate ($FePO_4$) nanoparticles using graphene nanosheet, Ammonium Iron (II) Sulphate ($(NH_4)_2Fe(SO_4)_2$), Ammonium dihydrogen Phosphate ($NH_4H_2PO_4$), Centrimonium Bromide (CTAB), n-hexane, and n-butanol at 180 °C for 10 h. Additionally, Li et al. [21] fabricated a 3D graphene-encapsulated nearly monodisperse Iron (II, III) Oxide (Fe_3O_4) composite using lysine and Iron(II) Sulphate Heptahydrate ($FeSO_4.7H_2O$) in the thermostatic oven at 180 °C for 12 h. Similarly, Liu et al. [25] also performed 12 h of hydrothermal process at 180 °C to fabricate 3D graphene hybridising with the ferric citrate. Liu et al. [26] synthesised a 3D graphene microsphere using the hydrothermal process at 200 °C for 12 h. Hence, the typical hydrothermal process is 180 °C or more than 180 °C, according to Chen et al. [27]. Apparently, the period of the hydrothermal process is 10–24 h. However, Chen et al. [27] reported that the hydrothermal process for the fabrication of 3D graphene aerogels was at 75 °C for 4 h. They proposed this operating parameter to save on industrial production cost.

3.4 *Freeze-Drying*

Freeze-drying is a process of freezing a sample under a vacuum at a low temperature for dehydration. The pore structure on the sample can be observed when the sublimation of the ice developed itself during vacuum freeze-drying, which was studied by Zeng et al. [28]. The result revealed that a macrospore structure was formed after freeze-drying at −50 °C. This method can maintain the integral structure for battery assembly, and the macropore can facilitate the mass transfer of the electrolyte channel. Li et al. [22] also performed a freeze-drying process at −50 °C for 72 h for the precipitated sample from the hydrothermal process, which obtained an antimony/graphene composite after further calcination. Mo et al. [24] performed a similar method for 48 h to synthesise mesoporous amorphous $FePO_4$ nanoparticles cross-linked with a 3D holey graphene framework. Similarly, Chen et al. [27] utilised this method to maintain the shape and size of graphene aerogels. Apparently, this method is always performed after the hydrothermal process and before further calcination. However, Liu et al. [25] performed this method before further annealing treatment for the synthesis of 3D graphene-Fe_3O_4. In short, freeze-drying is a step that maintains the structure and size of a sample.

3.5 Calcination

Calcination is a high-temperature process that happens normally in an inert atmosphere. This method is used for the removal of the volatile component, oxidation of the organic or inorganic precursor, and crystallisation of the final product. Hence, it is always considered the last step in the synthesis of the crystal structure of nanomaterials; sometimes, it can be considered a purification process. In the fabrication of 3D graphene-based material for battery technology, several researchers have reported this step as the last step after undergoing several processes, including Hummer's method, hydrothermal, freeze-drying, and others. For instance, Li et al. [22] prepared an Sb/graphene composite using potassium antimony tartrate and graphene oxide via the hydrothermal method, followed by high-temperature calcination at 850 °C for 8 h. The operations are performed in an argon atmosphere. However, Mo et al. [24] spent 1 day in the calcination process at 400 °C to fabricate 3D holey graphene frameworks cross-linked with encapsulated mesoporous amorphous $FePO_4$ nanoparticles. Further, Li et al. [21] used a shorter calcination period of 2 h to fabricate 3D graphene-encapsulated nearly monodisperse Fe_3O_4, performed at 600 °C. An oxidation process is involved in the calcination process, which can be observed in the study of Yuan et al. [29]. This study revealed that the oxidation of Ferum (III) ion into Ferum (II) and the transformation of pyrophosphate ion from phosphate ion, which cause the formation of reduced graphene oxide (rGO) confined iron-based mixed-polyanion compound $Na_4Fe_3(PO_4)_2(P_2O_7)$. Its calcination process was performed at 900 °C for 6 h in an air atmosphere. Apparently, the operation temperature is interrelated with the operation period. A higher calcination temperature requires a shorter period.

3.6 Annealing

Annealing is a process of sample heating at a high temperature and cooling down naturally. It is similar to calcination in heat treatment, but does not involve phase or chemical changes, such as oxidation and decomposition. This process minimises crystal defects, which can alter microstructure properties, such as hardness, ductility, and strength. Yu et al. [19] studied a graphene nanoribbon on the surface of 3D graphene. The last step of the product preparation process in this study is annealing in argon/hydrogen (80 sccm) at 600 °C for 2 h. Similarly, Liu et al. [25] experimentally determined the finalised powder (hybrids of 3D Graphene with Iron (II, III) oxide, Fe_3O_4) obtained from hydrothermal with a freeze-drying process was heated at 500 °C for 2 h in the nitrogen atmosphere. Further, Chen et al. [27] also performed the annealing process as the last step for fabricating Tin Oxide-3D graphene aerogels (SnO_2-GA). This study showed the formation of Sn–C–O bonds between Tin Oxide (SnO_2) and reduced graphene sheets after annealing at 600 °C for 30 min under the nitrogen atmosphere. In short, annealing conditions are usually in the range of 500 to 600 °C under an ambient atmosphere.

3.7 Solvothermal

The solvothermal process is a process similar to the hydrothermal process in terms of operation parameters, but its precursor is usually a non-aqueous solvent such as alcohol. For instance, Ma et al. [30] utilised alcohol suspension mixed with dilute alcohol and exfoliated graphene oxide suspension for soaking cleaned melamine foam, which was subsequently heated at 180 °C for 10 h.

3.8 Pyrolysis

Pyrolysis is a process that produces carbon components. Normally, this method requires heat energy to decompose the organic compounds. A few researchers have reported that the process of fabrication on 3D graphene material can be initiated by pyrolysis. For instance, Wang et al. [7] use sugar to produce porous monolithic graphene as the sugar consists of glucose, which is a carbon source for fabricating graphene materials. They used zinc as a template for pyrolysis in the tubular furnace at 1000 °C for 2 h in the atmosphere of ammonia/nitrogen. Additionally, Shi et al. [31] utilised thiourea and SiO_x as a precursor in the pyrolysis process at 800 °C for 2 h for the fabrication of 3D wrinkled N,S co-doped multilayer graphene sheets embedded with SiOx microparticles.

3.9 Facile Spray Drying

Spray drying is a technique that is widely used in the food and chemical industry, owing to the simple setup and scale-up with low cost for massive production. In spray drying, the particle size can achieve nano or microstructure of bulk particles. For instance, one study showed that the reduced graphene oxide confined iron-based mixed-polyanion compound was obtained in 60 nm of particle size [29].

3.9.1 Ball Milling

Ball milling is a liquid phase exfoliation of bulk materials into powder form. Yuan et al. [29] utilised this method at 300 rpm for 3 h in a planetary mill to obtain powder from bulk particles. The bulk particles are from reduced graphene oxide confined iron-based mixed-polyanion compound, which is obtained from spray drying. The ball mill method in this study involved the bulk particles, Sodium Carbonate (Na_2CO_3), Nickel (II) Oxide (NiO), and Manganese (III) Oxide (Mn_2O_3).

3.9.2 Etching

The etching step is the process that removes the intermediate substance by using acid or solvent. Guo et al. [15] designed a 3D graphene hollow structure using an etching step to remove the intermediate Magnesium oxide (MgO) and Zinc oxide (ZnO) that developed from CVD of graphene foam. Similarly, Yu et al. [19] induced the defect on the graphene foam into nanoribbon via plasma etching, using a power of 40 W for 5 to 20 min.

4 Recent Research Regarding 3D Graphene in Metal-Ion Batteries—in Terms of Performance

3D graphene material is considered a potential energy conservation material in various metal-ion battery systems. The previous section describes the process involved in the fabrication of 3D graphene materials in metal-ion batteries. Subsequently, this section further discusses the achievement of the recent research regarding 3D graphene material in the metal-ion battery system according to the type of battery, as summarised in Table 3.

4.1 Lithium-Ion Batteries

Several researchers have investigated the improvement of a lithium-ion battery system by using graphene materials because it has high conductivity, chemical stability, low lithium reaction, and volume change during lithium intercalation. However, there are a few limitations of simple graphene applied in the lithium-ion battery system, such as the weak capacity of graphene in lithium adsorption and the interaction of lithium in the surface unit area. Therefore, Guo et al. [15] fabricated 3D graphene materials by developing an enhanced defect derivative graphene and incorporating zinc oxide and magnesium hydroxide as the intermediate nanostructure layer. The result revealed an improvement in the electrochemical performance of graphene hollow structure from ~382 mAh g^{-1} to ~2204 mAh g^{-1} at 0.5 A g^{-1}. Further, the initial electrochemical capacity in this study achieved 10,009 mAh g^{-1} with 83% of retention at 4A g-1 for 500 cycles. The high-rate characterisation at a rate of 20 A g^{-1} was ~330 mAh g^{-1}.

Cyclability and fast charging function are concerns in this study. Several researchers have modified the design of cathode and anode with various inventions. For instance, Son et al. [16] developed a graphene ball in popcorn structure (Fig. 2) applied as anode and coating on the cathode, demonstrating a high specific capacity of anode material (716.2 mAh g^{-1}), and an incline of capacity at 0.33 Cycle by 27.6% from 49.67 to 63.40 Ah. The commercial cell settling reached 800Wh L^{-1} in

Table 3 Previous studies with their achievements

Method of fabrication	Product structure	Battery	Achievement	Author
CVD	Graphene hollow structure (hybrid with ZnO and $Mg(OH)_2$ intermediate nanostructure layer)	Lithium	– Improvement of electrochemical performance from ~382 mAh g^{-1} to ~2204 mAh g^{-1} at 0.5 A g^{-1} – Improvement of electrochemical initial capacity at 4A g^{-1}:10,009 mAh g^{-1} with 83% of retention after 500 cycles – Improvement of high-rate characterisation at the rate of 20 A g^{-1}: ~330 mAh g^{-1}	Guo et al. [15]
	Graphene ball: Hybrid silica with graphene in popcorn structure	Lithium	– High specific capacity of anode material: 716.2 mAh g^{-1} – Incline of capacity at 0.33 Cycle: 27.6% from 49.67 to 63.40 Ah, which is potentially reaching 800Wh L^{-1} in a commercial cell setting – High cyclability of capacity retention after 500 cycles: 78.6% at 5 Cycle and 60 °C	Son et al. [16]
CVD, plasma etching, annealing	Graphene-nanoribbon on surface of highly porous 3D graphene	Aluminium	– Improvement in low charge voltage – High capacity of freestanding and flexible hybridised graphene foam-based pouch cell: 123 mA hg^{-1} at 5000 mA g^{-1} – Excellent cycling ability after 10 000 cycles, which contribute the fast charging (80 s) and slow discharged (more than 3100 s)	Yu et al. [19]
CVD, hydrothermal	Multilayer 3D graphene foam: hybrid with sulphur-based material and coated with the tungsten oxide	lithium-sulphur	– Initial discharge capacity with the cycling performance of lithium/sulphur with 3D graphene oxide after 200 cycles: ~1300 mAh/g at 0.8 A/g with approximately ~80% capacity retention – Improvement on the initial capacity with the cycling performance of Lithium/Sulphur with the coating of tungsten oxide on the 3D graphene oxide after 500 cycles: 1425 mAh/g with approximately 95% capacity retention	Choi et al. [23]
	3D graphene foam: hybrid with sulphur-based material	Lithium-Sulphur	– Improvement of areal capacity (10.9 $mAhr/cm^2$) when applied over sulphur loading (10.4 mg/cm^2) and its content (86.9 wt%)	He et al. [18]

(continued)

Table 3 (continued)

Method of fabrication	Product structure	Battery	Achievement	Author
	Graphene foam: hybrid with carbon nanotube and MoS_2 nanoparticles	Lithium-sulphur	– High specific capacity of MoS_2 as outer layer of electrode, high conductivity of carbon nanotubes as middle layer of electrode, and large electrode/electrolyte contact with short diffusion distance of lithium ions – Achieved a specific capacity of 935 mAh g^{-1} at a current density of 0.1 A g^{-1}, high reversible capacity of 606 mAh g^{-1} after 200 cycles at 0.2 A g^{-1} in the modified 3D graphene foam electrode	Ren et al. [17]
Thermal CVD	Vertical graphene sheets on carbon black	Lithium	– High specific capacity of $LiFePO_4$ electrode with 3D graphene material at 1C: 150 mAh g^{-1} with an 88.9% retention even after 1000 cycles – Achieved 542.8 mAh with 93.3% retention after 400 cycles at 0.2 C by using 1.3 wt % of modified 3D graphene material assembled with the $LiFePO_4$ electrode and graphite electrode	Ji et al. [14]
Modified Hummer's method, hydrothermal and freeze-drying and calcination	Crystal microstructure of antimony/graphene composite	Potassium	– High charge capacity (601.4 mAh g^{-1} at 100 mA g^{-1}), better cycle performance (345.3 mAh g^{-1} at 100 mA g^{-1} after 100 cycles), and rate capability (255.9 mAh g^{-1} at 800 mA g^{-1})	Li et al. [22]
	Mesoporous amorphous $FePO_4$ nanoparticles cross-linked with 3D holey graphene framework	Lithium	– Achieved a high-mass-loading electrodes with high reversible capacity (156 mA h g^{-1} under 0.5C), ultra-high-rate capability (76 mA h g^{-1} under 50C), and outstanding cycle stability (>95% reversible capacity retention over 500 cycles)	Mo et al. [24]
Modified Hummer's method, hydrothermal, freeze-drying and annealing	Hybrids of 3D graphene with Fe_3O_4	Sodium	– Achieved ultra-high sodium storage capacity (525 mAh g^{-1} at 30 mA g^{-1}), outstanding cycling stability (312 mAh g^{-1} after 200 cycles at 50 mA g^{-1}), and superior rate performance (56 mAh g^{-1} at 10 A g^{-1})	Liu et al. [25]
	SnO_2-GA 3D porous aerogels	Lithium	– A synergistic effect between flexible graphene layers and nano-sized SnO_2 improves the capacity and cyclic stability	Chen et al. [27]

(continued)

Table 3 (continued)

Method of fabrication	Product structure	Battery	Achievement	Author
Modified Hummer's, hydrothermal and calcination	3D graphene-encapsulated nearly monodisperse Fe_3O_4	Lithium	– Discharge-specific capacity and capacity retention of 3D graphene composite at a current density of 400 mA g^{-1}: 1139mAh g^{-1} and 85% capacity retention after 100 cycles – A good cycling stability and high capacity of 3D graphene composite on electrode even at 1000 mA g^{-1}: 665 mA h g^{-1} after 200 cycles	Li et al. [21]
Hummer's method, reflux, annealing and freeze-drying	Disc shape: nano $FeSb_2S_4$ in CNT/ graphene 3D porous network	Sodium	– Achieved a mass capacity of 391.7 mAh g^{-1} under 0.1 A g^{-1}, corresponding to 3.11 mAh cm^{-2} of area-capacity and 57.64 mAh cm^{-3} of volume-capacity	Zeng et al. [28]
Hydrothermal process and roasting process	Microsphere: crystal carbon shell-coated Graphene sheets	Potassium and aluminium	– Achievement of Potassium-ion battery electrode in a half-cell: – Initial capacity with coulumbic efficiency: 297.89 mAh g^{-1}, 99% after 1250 cycles – Achievement of the cathode for an aluminium battery – Reversible specific capacity at 1000 mA g^{-1}: 99.1 mAh g^{-1} – Retention capacity at 4000 mA g^{-1}: ~100% after 10 000 cycles	Liu et al. [26]
Solvothermal and 2-step annealing	Oxygen-rich graphene vertically grown on 3D N-doped carbon foam composite	sodium	– Reversible capability at 0.1 A g^{-1}: 508.6 mAh g^{-1} – Superior rate performance at 5.0 A g^{-1}: 113.3 mAh g^{-1} remarkable cycle stability at 1.0 A g^{-1}: 329.3 mAh g^{-1} over 1000 cycles	Ma et al. [30]

(continued)

Table 3 (continued)

Method of fabrication	Product structure	Battery	Achievement	Author
Facile spray drying, ball milling, calcination	3D graphene decorated iron-based mixed-polyanion compound $Na_4Fe_3(PO_4)2(P_2O_7)$ microspheres	sodium	– Reversible capacity at 0.1 C: 128 mAh g^{-1} – Superior rate capability at 200 C: 35 mAh g^{-1} – Long cycling life at 10 C: 62.3% capacity retention over 6000 cycles	Yuan et al. [29]
Modified Hummer's, freeze-drying and thermal reduction	Ultrathin MoS_2 nanosheet/graphene hybrid aerogels	Lithium and sodium	– Specific capacities and superior cyclic stability – Lithium at 0.2 A g^{-1}: 1526 mAh g^{-1} after 100 cycles – Sodium at 0.1 A g^{-1}: 850 mAh g^{-1} after 100 cycles – Notable rate performance at 1 A g^{-1} – Lithium: 865 mAh g^{-1}; Sodium: 462 mAh g^{-1}	Yuan et al. [8]
Pyrolysis	Porous monolith of graphene (also known as zinc-guided 3D graphene)	Potassium	– Capacity at a current density of 10 A g^{-1}: 180 mAh g^{-1} – Cycling capability at 1 A g^{-1}: 4000 cycles	Wang et al. [7]
Modified Hummer's, pyrolysis	3D wrinkled N, S co-doped multilayer graphene sheets embedding with SiOx microparticles	Lithium	– Reversible capacity: 1150 mA h g^{-1} after 500 cycles – high reversible capacity and superior energy density: 151 mA h g^{-1} and 501 W h kg^{-1} after 330 cycles	Shi et al. [31]

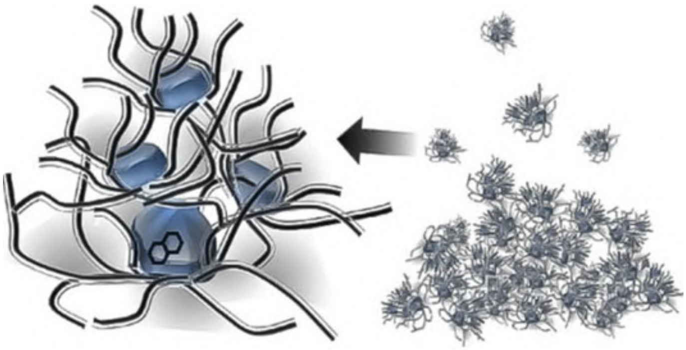

Fig. 2 Graphene ball in popcorn structure developed by Son et al. [16] in lithium-ion battery. Adapted from [16]. Copyright The Authors, some rights reserved; exclusive licensee springer nature limited. distributed under a creative commons attribution license 3.0 (CCB BY)

this study. That study achieved 78.6% of high cyclability of capacity retention after 500 cycles at 5 Columb (C) and 60 °C.

Similarly, a vertical graphene sheet growth on carbon black in a lithium-ion battery was studied by Ji et al. [14], who demonstrated a specific capacity of 150 mAh g^{-1} with an 88.9% retention at 1C even after 1000 cycles in a lithium iron phosphate ($LiFePO_4$) electrode. Further, there is an achievement in 542.8 mAh with 93.3% retention after 400 cycles at 0.2 C when the soft pack full cell was designed with 1.3 wt % of modified 3D graphene material assembled with an $LiFePO_4$ and graphite electrode. Mo et al. [24] achieved a high-mass-loading electrode with high reversible capacity in a lithium-ion battery, at 156 mA h g^{-1} under 0.5 C using a 3D holey graphene frameworks cross-linked with encapsulated mesoporous amorphous $FePO_4$ nanoparticles. Further, this result also achieved ultra-high-rate capability (76 mA h g^{-1} under 50 C) and outstanding cycle stability (>95% reversible capacity retention over 500 cycles).

A 3D graphene aerogel was modified with the nano-sized Tin Oxide (SnO_2) to enhance the capacity and cyclic stability, which exhibited the synergistic effect between the flexible layer of graphene and nano SnO_2 particles involved in the lithium-ion battery [27]. Similarly, Yuan et al. [8] developed an anchor 3D few-layered molybdenum sulphide (MoS_2) hybridised with graphene aerogels in the lithium-ion battery, which achieved 1526 mAh g^{-1} of specific capacities after 100 cycles. This study revealed the notable electrochemical performance of 865 mAh g^{-1} at 1 A g^{-1}. Another researcher reported that 3D graphene could be encapsulated with monodisperse Fe_3O_4 nanoparticles for lithium-ion battery systems, which achieved 1139 mAh g^{-1} of discharge capacity and 85% capacity retention at 400 mA g^{-1} after 100 cycles. Further, this study also achieved good cycling and high capacity (665 mA h g^{-1}) at 1000 mA g^{-1} after 200 cycles when a 3D graphene composite was applied to the electrode [21]. Additionally, Shi et al. [31] fabricated a novel silicon oxides (SiO_x) hybridised into 3D wrinkled multilayer graphene sheets, contributing 1150 mA h g^{-1} of reversible capacity after 500 cycles, along with high reversible capacity (151 mA h g^{-1}) and superior energy density (501 W h kg^{-1}) after 330 cycles.

4.2 Lithium Ion-Sulphur

Although lithium-ion batteries have been improved for cathode materials, there is a limitation in the theoretical capacity of transition metal oxides cathode (150–170 mAh/g^2) in commercial lithium-ion batteries. To improve the theoretical capacity of the cathode, sulphur has been introduced as a commercial cathode material. However, a few difficulties are related to the use of sulphur as commercial cathode material, such as polysulphide dissolution in the electrolyte, the poor electrical and ionic conductivity properties of sulphur, and the changes of charging with discharging volume. For instance, the polysulphide dissolution phenomenon is significantly found in 3D graphene materials involved in lithium-sulphur battery, as investigated by Choi et al. [23]. Owing to the amelioration of tungsten oxide on the polysulphide and shuttling effect, this study also further investigated the coating of tungsten oxide on 3D graphene oxide. An improvement of the initial capacity with the cycling performance of Lithium/Sulphur has been demonstrated with the coating of tungsten oxide on 3D graphene after 500 cycles (1425 mAh/g with approximately 95% capacity retention) when compared to the initial discharge capacity with the cycling performance of lithium/sulphur with 3D graphene after 200 cycles (~1300 mAh/g at 0.8 A/g with approximately ~80% capacity retention).

Further, He et al. [18] developed a 3D graphene foam material with the hybridisation of cobalt sulphide and sulphur (Fig. 3) as a cathode in lithium-sulphur batteries, which achieved a higher areal capacity (10.9 mAhr/cm^2) when applied over sulphur loading (10.4 mg/cm^2) and sulphur content (86.9 wt%). Additionally, the strong chemical entrapment of sulphur in lithium-ion batteries system is promoted by the synergistic effect of 3D graphene materials and cobalt sulphide.

Similarly, Ren et al. [17] fabricated a 3D graphene foam hybridised with carbon nanotube as the middle layer and MoS_2 as the outer layer in an electrode for the

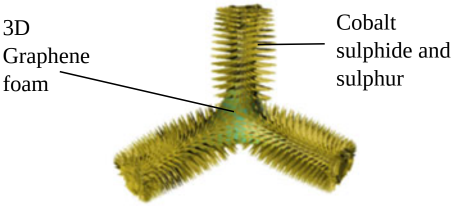

Fig. 3 3D graphene foam hybridised with cobalt sulphide in lithium ion-sulphur battery. Adapted with permission [18], copyright (2018), elsevier

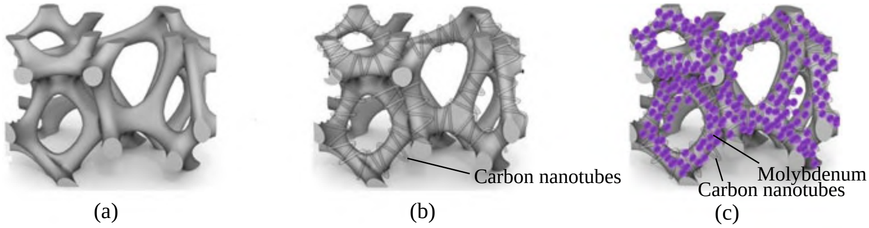

Fig. 4 **a** 3D graphene foam, **b** 3D graphene foam hybridised with carbon nanotube, and **c** 3D graphene foam hybridised with carbon nanotube and molybdenum sulphide. Adapted with permission [17], copyright (2018), elsevier

improvement of lithium-ion battery, as shown in Fig. 4. Due to the high specific capacity of MoS_2, high conductivity of carbon nanotubes, and large electrode/electrolyte contact with short diffusion distance of lithium ions, the electrochemical performance of this study achieved a specific capacity of 935 mAh g^{-1} at a current density of 0.1 A g^{-1}, a high reversible capacity of 606 mAh g^{-1} after 200 cycles at 0.2 A g^{-1} in the modified 3D graphene foam electrode.

4.3 Aluminium Batteries

Aluminium-ion batteries conventionally offer low discharge voltage and short cycle life. In order to achieve cutting edge of batteries performance with high power and energy density, safety, and long cycle life, Yu et al. [19] investigated the plasma etching of graphene nanoribbons on porous 3D graphene as a cathode in aluminium-ion batteries. The study revealed that the low charge voltage was improved with a high capacity of freestanding and flexible hybridised graphene foam-based pouch cell: 123 mA hg^{-1} at 5000 mA g^{-1}. It also demonstrated excellent cycling ability after 10 000 cycles, contributing to 80 s of fast charging and more than 3100 s of slow discharge rate in the aluminium-ion battery system. Liu et al. [26] also improved the aluminium-ion battery using a microsphere which is armoured graphene wrapped by a crystal carbon shell as illustrated in Fig. 5, which obtained a 99.1 mAh g^{-1} of reversible specific capacity at 1000 mA g^{-1} and ~ 100% retention capacity at 4000 mA g^{-1} after 10 000 cycles.

4.4 Potassium Batteries

Due to the abundance of potassium elements and low electrode potential of potassium-ion/potassium atom (K^+/K) couple, the electrochemical industry recently garnered attention on potassium-ion batteries. Although potassium-ion battery is

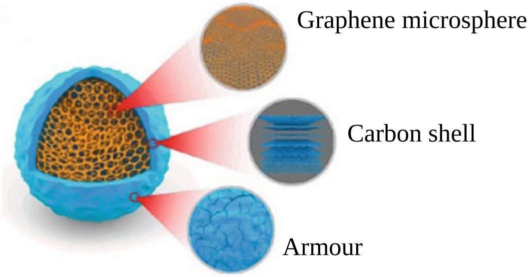

Fig. 5 Microsphere of 3D graphene, showing graphene wrapped by a crystal carbon shell. Adapted with permission [26], copyright (2019), American chemical society

inexpensive and has high energy density, its ionic radius is larger, which is unfeasible in its rapid transport and degradation of potassium storage. To mitigate this issue, a graphene material, with 279mAhg^{-1} of theoretical capacity, can be used as anode material for potassium-ion batteries because it has a larger surface of the interlayer, notable electron mobility, and mechanical properties. For the advancement of graphene materials, antimony can be used to incorporate graphene materials as its theoretical capacity is 660 mAh g^{-1}. This can enhance the electrochemical properties of potassium-ion battery. For instance, a study revealed that the antimony/graphene with a crystal microstructure exhibited a high charge capacity (601.4 mAh g^{-1} at 100 mA g^{-1}), better cycle performance (345.3 mAh g^{-1} at 100 mA g^{-1} after 100 cycles), and rate capability (255.9 mAh g^{-1} at 800 mA g^{-1}) [22].

Further, Liu et al. [26] synthesised a microsphere of crystal carbon shell wrapped with a graphene sheet, which obtained an initial capacity with a Coulombic efficiency (297.89 mAh g^{-1}, 99%) after 1250 cycles. Wang et al. [32] fabricated a porous monolith of graphene as the binder-free anode, which contributed a 180 mAh g^{-1} of capacity at a current density of 10 A g^{-1} and 4000 cycles of cycling capability at 1 A g^{-1}.

4.5 Sodium-Ion Battery

Sodium-ion batteries have garnered attention in the electrochemical industry because their theoretical interlinkage and technical inheritance are similar to the lithium-ion battery, such as inert materials used in the electrode (graphite anodes). However, Silicon (Si) anode in sodium-ion battery demonstrated lower electrochemical performance than Si anode in the lithium-ion battery. Hence, the anode in sodium-ion battery can be replaced by various materials such as Sodium Chromite ($NaCrO_2$), Sodium Vanadium Phosphate ($Na_3V_2(PO_4)_3$), and Maricite ($NaFePO_4$). Metal sulphides are alternatives to anode materials that may offer better electrochemical properties than monometallic sulphide. In the electrochemical industry, 3D graphene material is usually incorporated with the novel binary metal sulphide, which can demonstrate high mass capacity and remarkable cyclability. For instance, Zeng et al.

Fig. 6 Disc shape of anode that consists of carbon nanotubes/graphene 3D porous network hybridised with binary metal sulphide ($FeSb_2S_4$). Adapted with permission [28], copyright (2021), elsevier

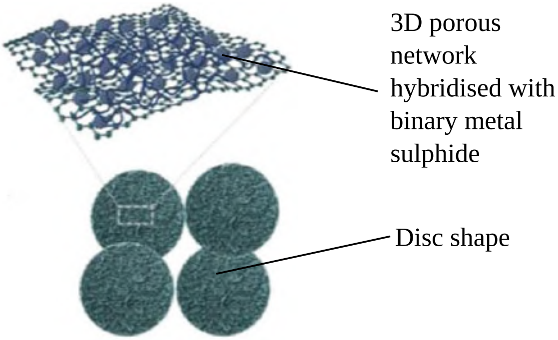

[28] developed a disc shape material that consists of high theoretical binary metal sulphide (Berthierite, $FeSb_2S_4$) hybridised in 3D graphene as an anode (Fig. 6), which achieved a mass capacity of 391.7 mAh g^{-1} under 0.1 A g^{-1}, corresponding to 3.11 mAh cm^{-2} of area-capacity and 57.64 mAh cm^{-3} of volume-capacity.

In addition, 3D graphene was introduced in carbon foam for an electrode in sodium-ion battery, reaching a reversible capability at 0.1 A g^{-1} (508.6 mAh g^{-1}), superior rate performance at 5.0 A g^{-1} (113.3 mAh g^{-1}), and remarkable cycle stability at 1.0 A g^{-1} (329.3 mAh g^{-1} over 1000 cycles), according to Ma et al. [30]. Yuan et al. [29] fabricated 3D graphene microsphere hybridised with $Na_4Fe_3(PO_4)_2(P_2O_7)$ in sodium-ion batteries, which contributed reversible capacity (128 mAh g^{-1}) at 0.1 C, superior rate capability (35 mAh g^{-1}) at 200 C, and long cycling life (62.3% capacity retention over 6000 cycles) at 10 C. Similarly, Yuan et al. [8] developed an anchor 3D few-layered MoS_2 hybridised with graphene aerogels in the sodium-ion battery, which achieved 850 mAh g^{-1} of specific capacities after 100 cycles. This study revealed notable electrochemical performance of 462 mAh g^{-1} at 1 A g^{-1}.

5 Conclusion, Challenges, and Future Prospects

This chapter discussed the modified 3D graphene in the electrode for each metal-ion battery. Owing to the superior characteristic of graphene, several research studies have reported 3D graphene material applied in the metal-ion batteries by hybridising with additives such as metal oxide, carbon nanotube, sulphur-based materials, and others involved in metal-ion batteries. Various fabrication processes in graphene material and its 3D graphene material incorporation method are discussed in this chapter. After being incorporated with the modified 3D graphene oxide in metal-ion batteries, most studies reported good electrochemical properties in terms of capacity, discharge and charging capacity, cycling rate, and reversible capacity. Although 3D graphene material is a promising dopant in various applications, there are a few challenges in terms of economics. The main challenge in this study is the production of 3D graphene, including the several processes involved in the synthesis of 3D graphene. Subsequently, the cost of production increases. Further, the cost of graphene also depends on the purity and crystallinity of graphene. For 3D graphene material involved in metal-ion batteries, the other concerns include product cost and portability, and the battery design's size since it is still not commercialised in the market.

Although most metal-ion batteries performed good electrochemical properties using modified 3D graphene material for sustainable energy, the metal-ion resources could be depleted, especially lithium-ion. Further, there are the difficulties aforementioned regarding the graphene material in the market. Owing to this issue, there are a few suggestions required to implement in the future as follows:

(a) Recycle metal ions if possible.
(b) Seek for alternatives of metal ion for the design of a dischargeable battery.
(c) Continue investigation on alternatives for graphene material as it is costly.
(d) Investigate sustainable resources for metal-ion batteries.

In short, this review has provided the overview of types of metal-ion batteries, the fabrication of 3D graphene material, and the recent development of 3D graphene material involved in metal-ion batteries.

References

1. Liu, Y., Holze, R.: Metal-ion batteries. Encyclopedia **2**(3), 1611–1623 (2022)
2. Hou, D., Xia, D., Gabriel, E., Russell, J.A., Graff, K., Ren, Y., Sun, C.J., Lin, F., Liu, Y., Xiong, H.: Spatial and temporal analysis of sodium-ion batteries. ACS Energy Lett. **6**(11), 4023–4054 (2021)
3. Li, Y., Lu, Y., Adelhelm, P., Titirici, M.M., Hu, Y.S.: Intercalation chemistry of graphite: alkali metal ions and beyond. Chem. Soc. Rev. **48**(17), 4655–4687 (2019)
4. Zhan, C., Wu, T., Lu, J., Amine, K.: Dissolution, migration, and deposition of transition metal ions in Li-ion batteries exemplified by Mn-based cathodes-a critical review. Energy Environ. Sci. **11**(2), 243–257 (2018)
5. Zhang, X.Q., Wang, X.M., Li, B.Q., Shi, P., Huang, J.Q., Chen, A., Zhang, Q.: Crosstalk shielding of transition metal ions for long cycling lithium-metal batteries. J. Mater. Chem. A **8**(8), 4283–4289 (2020)
6. Husmann, S., Zarbin, A.J.G.: Cation effect on the structure and properties of hexacyanometallates-based nanocomposites: improving cathode performance in aqueous metal-ions batteries. Electrochim. Acta **283**(2018), 1339–1350 (2018)
7. Wang, Q., Wang, Y., Zeng, J., Zhang, C., Liu, P., Hao, T., Ding, R., Jiang, X., Zhang, Y., Da, B., Liu, J., Hong, G., Xu, W., Meng, Z., Wang, X.B.: Zinc-guided 3D graphene bulk materials for high-performance binder-free anodes of potassium-ion batteries. J. Power Sources **540**(2022), 231613 (2022)
8. Yuan, J., Zhu, J., Wang, R., Deng, Y., Zhang, S., Yao, C., Li, Y., Li, X., Xu, C.: 3D few-layered MoS_2/graphene hybrid aerogels on carbon fiber papers: a free-standing electrode for high-performance lithium/sodium-ion batteries. Chem. Eng. J. **398**(2020), 125592 (2020)
9. Verma, J., Kumar, D.: Metal-ion batteries for electric vehicles: current state of the technology, issues and future perspectives. Nanoscale Adv. **3**(12), 3384–3394 (2021)

10. Ali, A., Liang, F., Zhu, J., Shen, P.K.: The role of graphene in rechargeable lithium batteries: synthesis, functionalisation, and perspectives. Nano Mater. Sci. **2022**, 2–19 (2022)
11. Ma, J., Yang, C., Ma, X., Liu, S., Yang, J., Xu, L., Gao, J., Quhe, R., Sun, X., Yang, J., Pan, F., Yang, X., Lu, J.: Improvement of alkali metal ion batteries: via interlayer engineering of anodes: from graphite to graphene. Nanoscale **13**(29), 12521–12533 (2021)
12. Chang, H.-H., Ho, T.-H., Su, Y.-S.: Graphene-enhanced battery components in rechargeable lithium-ion and lithium metal batteries. J. Carbon Res. **7**(65), 1–28 (2021)
13. Chen, K., Shi, L., Zhang, Y., Liu, Z.: Scalable chemical-vapour-deposition growth of three-dimensional graphene materials towards energy-related applications. Chem. Soc. Rev. **47**(9), 3018–3036 (2018)
14. Ji, X., Mu, Y., Liang, J., Jiang, T., Zeng, J., Lin, Z., Lin, Y., Yu, J.: High yield production of 3D graphene powders by thermal chemical vapor deposition and application as highly efficient conductive additive of lithium ion battery electrodes. Carbon **176**(2021), 21–30 (2021)
15. Guo, H., Long, D., Zheng, Z., Chen, X., Ng, A.M.C., Lu, M.: Defect-enhanced performance of a 3D graphene anode in a lithium-ion battery. Nanotechnology **28**(2017), 505402 (2017)
16. Son, I.H., Park, J.H., Park, S., Park, K., Han, S., Shin, J., Doo, S.G., Hwang, Y., Chang, H., Choi, J.W.: Graphene balls for lithium rechargeable batteries with fast charging and high volumetric energy densities. Nat. Commun. **8**(1561), 1–10 (2017)
17. Ren, J., Ren, R.P., Lv, Y.K.: A flexible 3D graphene@CNT@MoS_2 hybrid foam anode for high-performance lithium-ion battery. Chem. Eng. J. **353**(2018), 419–424 (2018)
18. He, J., Chen, Y., Manthiram, A.: MOF-derived cobalt sulfide grown on 3D graphene foam as an efficient sulfur host for long-life lithium-sulfur batteries. IScience **4**, 36–43 (2018)
19. Yu, X., Wang, B., Gong, D., Xu, Z., Lu, B.: Graphene nanoribbons on highly porous 3D graphene for high-capacity and ultrastable Al-Ion batteries. Adv. Mater. **29**(4), 1604118 (2017)
20. Paramasivan, T., Sivarajasekar, N., Muthusaravanan, S., Subashini, R., Prakashmaran, J., Sivamani, S., Koya, P.A.: Chapter 13: gaphene family materials for the removal of peticides from water. In: Naushad, M. (ed.) A New Generation Material Graphene: Applications in Water Technology. Springer International Publishing, Switzerland (2018)
21. Li, L., Wang, H., Xie, Z., An, C., Jiang, G., Wang, Y.: 3D graphene-encapsulated nearly monodisperse Fe_3O_4 nanoparticles as high-performance lithium-ion battery anodes. J. Alloy. Compd. **815**(2020), 152337 (2020)
22. Li, W., Gao, N., Li, H., Sun, R., Wu, J., Chen, Q.: A novel method to prepare Sb/graphene composite with high capacity for potassium-ion batteries. Mater. Lett. **319**(2022), 132259 (2022)
23. Choi, S., Seo, D.H., Kaiser, M.R., Zhang, C., Van Der Laan, T., Han, Z.J., Bendavid, A., Guo, X., Yick, S., Murdock, A.T., Su, D., Lee, B.R., Du, A., Dou, S.X., Wang, G.: WO_3 nanolayer coated 3D-graphene/sulfur composites for high performance lithium/sulfur batteries. J. Mater. Chem. A **7**(9), 4596–4603 (2019)
24. Mo, R., Rooney, D., Sun, K., Wang, J.N.: 3D holey-graphene frameworks cross-linked with encapsulated mesoporous amorphous $FePO_4$ nanoparticles for high-power lithium-ion batteries. Chem. Eng. J. **417**(2021), 128475 (2021)
25. Liu, H., Jia, M., Zhu, Q., Cao, B., Chen, R., Wang, Y., Wu, F., Xu, B.: 3D–0D graphene-Fe_3O_4 quantum dot hybrids as high-performance anode materials for sodium-ion batteries. ACS Appl. Mater. Interfaces **8**(40), 26878–26885 (2016)
26. Liu, Z., Wang, J., Jia, X., Li, W., Zhang, Q., Fan, L., Ding, H., Yang, H., Yu, X., Li, X., Lu, B.: Graphene armored with a crystal carbon shell for ultrahigh-performance potassium ion batteries and aluminum batteries. ACS Nano **13**(9), 10631–10642 (2019)
27. Chen, Z., Li, H., Tian, R., Duan, H., Guo, Y., Chen, Y., Zhou, J., Zhang, C., Dugnani, R., Liu, H.: Three dimensional Graphene aerogels as binder-less, freestanding, elastic and high-performance electrodes for lithium-ion batteries. Sci. Rep. **6**(2016), 27365 (2016)
28. Zeng, T., Li, Z., Feng, D., Zhu, Y.: Confining nano $FeSb_2S_4$ in carbon nanotube/oxide graphene 3D porous networks for high-capacity sodium ion battery anode. J. Alloy. Compd. **884**(2021), 161116 (2021)

29. Yuan, T., Wang, Y., Zhang, J., Pu, X., Ai, X., Chen, Z., Yang, H., Cao, Y.: 3D graphene decorated Na4Fe3(PO4)2(P2O7) microspheres as low-cost and high-performance cathode materials for sodium-ion batteries. Nano Energy **56**(2018), 160–168 (2019)
30. Ma, X., Ji, C., Liu, Y., Yu, X., Xiong, X.: Oxygen-rich graphene vertically grown on 3D N-doped carbon foam for high-performance sodium ion batteries. J. Power Sources **530**(2021), 231292 (2022)
31. Shi, L., Li, Y., Xing, Y., Lin, R., Cheng, G., Ding, J., Lam, K.H.: SiOx microparticles embedded into 3D wrinkled N, S co-doped multilayer graphene sheets as a high-performance anode for long-life full lithium-ion batteries. Electrochim. Acta **390**(2021), 138841 (2021)

3D Graphene for Metal–Air Batteries

Runwei Mo and Yuan An

Abstract In recent years, metal–air batteries have attracted extensive research owing to their extremely high theoretical energy density. However, the bottleneck problem of current metal–air batteries is the slow kinetics of oxygen reduction reaction catalysts. Recently, graphene has been widely used in metal–air batteries owing to its many active sites, excellent electrical conductivity, and large specific surface area. To meet the requirements of practical applications, three-dimensional (3D) graphene structures are prepared from two-dimensional graphene nanosheets through various assembly methods, which can tune their mechanical stability, electrochemical properties, and catalytic performance. 3D graphene can act as a catalyst carrier in metal–air batteries, which can not only improve its long-term stability and catalytic activity but also reduce the amount of active components. It is worth noting that the properties of 3D graphene can be further optimized by functionally modifying the surface of graphene. In this chapter, we describe the synthesis techniques of 3D graphene and summarize the properties and functional modifications of 3D graphene. Then we focus on the latest research progress and status of 3D graphene in metal–air batteries. Finally, future directions for enhancing the electrochemical properties of 3D graphene-based metal–air batteries prospect.

Keywords Graphene · Metal–air battery · Structural design · Oxygen reduction reaction · Catalyst

1 Introduction

With the rapid development of society, the sustainable development of energy has an increasingly important impact on the survival and development of human beings. Due to the non-renewable nature of the traditional energy structure dominated by fossil fuels, it is necessary to urgently develop new energy conversion and storage

---

R. Mo (✉) · Y. An
School of Mechanical and Power Engineering, East China University of Science and Technology, Shanghai, China
e-mail: rwmo@ecust.edu.cn

© The Author(s), under exclusive license to Springer Nature Switzerland AG 2023

R. K. Gupta (ed.), *3D Graphene*, Carbon Nanostructures,
https://doi.org/10.1007/978-3-031-36249-1_13

systems with sustainable development. As a representative energy storage device in the field of new energy, secondary batteries are more and more widely used in mobile electronic equipment, electric vehicles, and other fields. Among them, metal–air batteries (MABs) have attracted extensive attention owing to their ultra-high theoretical energy density, which makes them promising candidates for vehicle power sources or large-scale energy storage stations [1–3].

As one of the representatives of high energy density energy storage and conversion systems, MABs use metals with negative electrode potential, such as zinc, iron, magnesium, aluminum, and mercury, and the gas in the air is used as the active material of the positive electrode. Generally speaking, the main components of MABs are divided into air cathode, metal anode, current collector, electrolyte with separator, and gas diffusion layer. Different from the fully closed system of metal–ion batteries, the cathode reactant in MABs is the gas component in the air, which leads to the characteristics of the semi-open system of the battery [4, 5]. It is worth noting that the current cathodes of MABs containing alkali metals are usually studied in the environment of pure O_2, which is mainly attributed to the fact that various components in the air can easily make the reaction mechanism difficult to distinguish, and even some components can cause undesirable side reactions [6, 7].

MABs are classified in a number of different ways. According to the different types of electrolytes, MABs can be classified into four types: non-aqueous, aqueous, solid-state, and mixed-mode. In addition, according to the different types of anode metals, MABs can also be divided into the following types: zinc—air batteries, lithium–air batteries, magnesium or aluminum–air batteries, sodium or potassium–air batteries, etc. It is worth noting that different kinds of MABs have their own unique advantages. Compared with aqueous MABs, non-aqueous MABs tend to have the advantages of higher discharge platforms, wider electrochemical windows, and higher energy densities. Compared with non-aqueous MABs, aqueous MABs generally have the advantages of lower fabrication costs, more environmental protection, and faster mass transfer rates. Furthermore, solid MABs tend to have a more pronounced advantage in preventing fire risks and liquid leakage compared to liquid electrolytes. Different kinds of MABs have similar problems, which are mainly attributed to their similar working principles and electrode reaction pairs. The main factors hindering the improvement of the electrochemical properties of MABs are the slow kinetics of the oxygen evolution reaction (OER) and oxygen reduction reaction (ORR). In order to solve the above problems, the development of cathode materials with large specific surface area, high electronic conductivity, sufficient active sites, and hierarchical pore structure is an effective way to further enhance the electrochemical properties of MABs [8–10].

Recently, graphene has been widely used in MABs due to its many active sites, excellent electrical conductivity, and large specific surface area. As we all know, graphene was successfully prepared for the first time in 2004 and has attracted extensive research interest in many fields owing to its outstanding chemical and physical properties [11–13]. More importantly, the electrochemical properties, mechanical stability, and catalytic performance can be regulated by functional modification of the graphene surface, such as porous structure design, heteroatom doping, and defect fabrication [14–20]. On the one hand, more active sites can be provided by the design of porous structures. On the other hand, the kinetics of ORR and OER can be enhanced by heteroatom doping and defect fabrication. In order to meet the requirements of practical applications, three-dimensional (3D) graphene structures are prepared from two-dimensional (2D) graphene nanosheets through various assembly methods. It is worth noting here that 3D graphene is considered an ideal cathode material for MABs due to its abundant defects, hierarchical pore structure, and selective doping of atoms. Equally important, 3D graphene has a unique three-dimensional connected conductive network structure, which can provide an efficient transport path for metal ions and gas molecules, low charge transfer resistance, and can be used for the storage space of solid discharge products on the air electrode side. In this chapter, the latest research results of 3D graphene as a key material in the field of MABs are summarized. Based on an in-depth understanding of the reaction mechanism of ORR and OER, the synthesis strategies of 3D graphene are mainly introduced, and the properties and functional modifications of 3D graphene are summarized. In addition, the latest research results of 3D graphene as cathode materials in the field of MABs are summarized. Finally, future directions for enhancing the electrochemical properties of 3D graphene-based MABs prospect.

2 Synthesis of 3D Graphene

2.1 Chemical Reduction Self-Assembly Method

Chemical reductive self-assembly is a common method for preparing 3D graphene-based materials. The basic principle is that the raw graphene oxide (GO) is first reduced to reduced graphene oxide (rGO) by using a reducing agent (such as $NaHSO_3$, sodium ascorbate, vitamin C, Na_2S, etc.) under low-temperature heating conditions, and then its self-assembly is controlled to form a 3D graphene. Sheng et al. successfully prepared 3D graphene hydrogels by chemical reduction self-assembly method [21]. The specific steps are to use sodium ascorbate as the reducing agent and GO as the precursor. The homogeneous suspension was obtained by ultrasonic treatment first, and then the self-assembly process was carried out at a certain reaction temperature. The results showed that the optimum concentration of GO suspension was 2.0 $mg{\cdot}mL^{-1}$, and the optimum reaction temperature and time were 90 °C and 1.5 h, respectively. The chemical reduction treatment reduces the oxygen-containing functional groups of GO and restores the conjugated structure. On the one hand, it leads to a large number of π–π bonding sites and strong mutual adsorption force on the rGO surface, and on the other hand, it enhances the hydrophobicity of the rGO sheet. The synergistic effect of the above two aspects promotes the self-assembly of rGO sheets to form 3D graphene hydrogels. The chemical reduction self-assembly method to prepare 3D graphene-based materials has the advantages of a simple process and no harsh preparation conditions such as high temperature and high pressure. The self-assembly process and morphology of the product rGO can be precisely regulated by controlling the concentration of the raw GO suspension, the amount of the reducing agent, the reaction time, and other process conditions. The three-dimensional graphene-based material prepared by this method has outstanding mechanical properties and electrical conductivity, but its surface oxygen-containing functional groups are difficult to be completely removed, resulting in its electrical conductivity failing to reach the theoretical value.

2.2 Hydrothermal Reduction Self-Assembly Method

The hydrothermal reduction self-assembly method is mainly used to prepare 3D graphene materials with a three-dimensional network structure. The preparation principle of this method is to first place a suspension of GO or rGO in a sealed autoclave. Then, by controlling the pressure, temperature, time, and concentration of reactants in the hydrothermal process, GO or rGO was self-assembled to form a three-dimensional graphene material. Xu et al. successfully prepared three-dimensional graphene by hydrothermal reduction self-assembly method [22]. Specifically, the GO suspensions with concentrations of 0.5, 1.0, and 2.0 $\mathrm{mg \cdot mL^{-1}}$ were heated to 180 °C in the reactor and kept for 1 to 12 h. In this process, the hydrothermal reduction conditions, on the one hand, are the introduction of interlayer conjugated structures and high-density bonding (π-stacking) sites into the graphene sheets, thereby improving the π–π bonding force between graphene sheets and the structural stability of the product. On the other hand, the oxygen-containing functional groups on the GO sheets were reduced to exhibit hydrophobic properties. Under the synergistic effect of hydrophobicity and π–π bonds, the GO nanosheets self-assembled to form a 3D graphene hydrogel with a cross-linked structure. Its strength and conductivity increased with the increase of the concentration of the raw GO suspension and the reaction time. It is worth noting that the storage modulus of the material is as high as 490 kPa, and the corresponding conductivity is as high as 0.5 $\mathrm{S \cdot m^{-1}}$. Overall, the process of preparing 3D graphene materials by hydrothermal reduction self-assembly is relatively simple. However, this method requires harsh preparation conditions such as high pressure, high temperature, and long incubation time and requires the concentration of GO suspension to be higher than 2.0 $\mathrm{mg \cdot mL^{-1}}$. More importantly, the self-assembly process of this method is realized by physical binding force, which is often prone to the problem of poor structural stability.

2.3 Freeze-Drying Self-Assembly Method

The basic principle of the freeze-drying self-assembly method is to freeze the GO suspension or rGO after self-assembly to promote the formation of solid organic molecules or the growth of ice crystals. Then, the ice or solid organic molecules are sublimated and escaped by vacuum drying, thereby obtaining three-dimensional graphene with a porous structure. Jung et al. successfully prepared 3D graphene materials with hierarchical pore structures by freeze-drying self-assembly method [23]. Specifically, a suspension of sheet-like graphene was first prepared by an electrochemical exfoliation method and then self-assembled to form a 3D graphene hydrogel by a sol–gel method. Finally, 3D graphene can be obtained by freeze-drying. The results show that the pore structure and size distribution of the product 3D graphene can be effectively controlled by adjusting the aspect ratio of the exfoliated graphene sheets and the temperature of the freeze-drying treatment. The three-dimensional graphene aerogel prepared by this method has the advantages of high porosity, low density, large specific surface area, and high electrical conductivity, which is beneficial to the high-speed diffusion of electrolyte ions and the rapid transport of electrons.

In addition, this method can also be used to prepare 3D graphene-based composites. Xie et al. successfully prepared platinum or platinum–carbon-supported 3D graphene composites by freeze-drying self-assembly method [24]. Specifically, GO, carbon black, potassium tetrachloroplatinate, and ascorbic acid were used as raw materials, which were sequentially subjected to heat treatment at 90 °C for 3 h and rapid freeze-drying treatment to finally obtain 3D graphene-based composites. In the above-mentioned platinum–carbon/3D graphene composite formation process, the presence of carbon black effectively separates the clusters formed by graphene and platinum nanoparticles, thereby helping to improve platinum atom utilization and catalytic graphitization effect. In addition, the wrinkled graphene structure in the platinum–carbon/3D graphene composite increases the specific surface area and the density of active sites, which is beneficial to improve the electrocatalytic activity of platinum for reactions such as methanol oxidation. Although the freeze-drying self-assembly method has certain requirements in the vacuum environment, the 3D graphene-based materials prepared by this method generally have the characteristics of high porosity, high specific surface area, tunable pore size distribution, and high electrical conductivity.

2.4 Template Self-Assembly Method

Template self-assembly is an effective method to prepare 3D graphene materials with regular pore structures. For example, polystyrene colloid or silica colloid is used as the sacrificial template, and potassium hydroxide, hydrofluoric acid, or tetrahydrofuran are used as the corresponding template etchant, respectively [25–28]. Huang et al. successfully synthesized 3D graphene foams with porous nanostructures using a template self-assembly method [25]. Specifically, silica nanoparticles with methyl groups were used as templates, which were sequentially soaked in GO suspension and heat-treated at 900 °C for 5 h under an argon atmosphere. Then, the 3D graphene material was collected by hydrofluoric acid etching treatment. Among them, silica nanoparticles modified by methyl groups with hydrophobic properties can not only serve as templates for the preparation of graphene foams but also interact with hydrophobic GO nanosheets. Therefore, the modified silica nanoparticles can inhibit the agglomeration of GO nanosheets and promote the formation of porous nanostructures. The research results show that the pore size range of the 3D graphene foams prepared by this method is 30–90 nm, and the pore density and specific surface area are as high as 4.3 $cm^3 \cdot g^{-1}$ and 851 $m^2 \cdot g^{-1}$, respectively.

In addition, Kim et al. also successfully prepared 3D graphene foams using a similar method [27]. Specifically, GO-coated silica nanomaterials with a core–shell structure were prepared by utilizing the interaction between the amphiphilicity of GO and the hydrophobicity of methyl groups on the template surface. Then, the 3D graphene foams with porous nanostructures were obtained by successive treatments such as centrifugal collection, condensation, and hydrofluoric acid etching. The process of preparing 3D graphene materials using silica as a sacrificial template is relatively simple. It is worth noting that the pore structure, pore order, and pore size of the product can be effectively regulated by controlling the size of the template. However, the main disadvantage of this method is that the sacrificial template is difficult to be completely removed, and the prepared 3D graphene is prone to plastic cracking.

2.5 3D Printing Method

3D printing is an additive manufacturing method that prints raw materials into materials with specific shapes and sizes based on three-dimensional digital models [29]. Zhu et al. successfully synthesized 3D graphene-based composites through 3D printing. [30] Specifically, a mixed solution of 12.5 wt.% graphene nanosheets (GN), 3.3 wt.% GO, 4.2 wt.% SiO_2, and resorcinol–formaldehyde (R-F) were used as the printing ink, which was successively formed by direct writing, gelation, supercritical drying, carbonization, and etching to obtain GO/GN composite aerogels. It is worth noting that pre-soaking the printing ink in isooctane solution helps the ink to remain wet during the gelation and printing process, which avoids the deformation or cracking of the printing material during the freeze-drying process. The results show that the addition of SiO_2 and GN can synergistically improve the yield strength and storage modulus of printing ink. The electrical resistance of the GO/GN composite aerogel prepared by this method is only 0.96 $\Omega \cdot sq^{-1}$ and the specific surface area is as high as 418 $m^2 \cdot g^{-1}$. The results show that the material has the characteristics of a large specific surface area, low density, and high electrical conductivity and has application prospects in many fields. The direct writing molding method has the characteristics of a wide selection of raw materials, low cost, high preparation efficiency, and good shape controllability of the product. However, there are problems such as strict requirements on the rheological properties of the ink and subsequent heat treatment of the printing materials. The quality of printing ink (including core evaluation indicators such as rheological properties and solid content) is the key to determining the performance of direct-write molding products. By increasing the solid content of the ink, that is, the concentration of the GO suspension, not only the rheological properties of the ink can be enhanced, but also the volume and shape changes of the printed material during post-processing can be effectively reduced. The 3D graphene-based composites prepared by direct writing generally have outstanding mechanical properties and electrical conductivity.

3 Properties of 3D Graphene

The 3D graphene prepared by the above various self-assembly methods exhibits excellent properties, including large surface area and pore volume, high electrical conductivity, low density, and good mechanical properties. Compared with 3D graphene assembled by physical bonding, 3D graphene assembled by chemical bonding exhibits better properties, such as higher electrical conductivity, lower contact resistance, and better mechanical stability. The analytical reason is that cross-linking easily occurs between the functional groups on the edge and the GO surface during the self-assembly process through chemical bonding. In addition, the process of preparing 3D graphene by the self-assembly method is very versatile, and the microstructure and macrostructure can be regulated by changing the experimental conditions [31]. For example, the porosity and pore size of 3D graphene can be tuned by changing the size of the template. The number of graphene layers and the solution concentration also have a great influence on the density of 3D graphene. Higher graphene solution concentrations lead to an increase in the density of 3D graphene, which results in larger changes in the density, mechanical strength, and electrical conductivity of 3D graphene.

The microstructure and properties of 3D graphene can be optimized by changing the preparation conditions. For example, in the process of preparing 3D graphene by freeze-drying self-assembly, the freezing temperature plays an important role in the microstructure and properties of 3D graphene [32]. The results show that when the freezing temperature is decreased from -10 to -170 °C, the pore wall thickness and pore diameter decrease by 4000 times and 80 times, respectively. The water absorption properties of 3D graphene largely depend on its average pore size. Generally, the water absorption property of 3D graphene requires its pore size to be less than 150 μm, while the waterproof property of 3D graphene requires its pore size to be larger than 300 μm. To achieve water absorption in the central region of 3D graphene and water resistance in the edge region of 3D graphene, it is necessary to control the pore size between 150 and 300 μm. The regulation of the water-absorbing and waterproof properties of 3D graphene can expand the application of graphene materials in other fields. Furthermore, the pore morphology is also greatly altered, enabling a transition from an anisotropic layered architecture to a homogeneous cellular architecture. By manipulating the 3D graphene microstructure, Young's modulus was increased from 13.7 kPa to 204.4 kPa. In a word, the properties of 3D graphene can be adjusted in various ways, which can meet the requirements of graphene materials in different application fields.

4 Functional Modifications

It is well known that graphene generally exhibits poor catalytic activity, which is mainly attributed to its intrinsic structure. To effectively improve its catalytic activity, it is necessary to optimize the surface chemistry and atomic composition of graphene through functional modification. The electron density polarization at this carbon-heteroatom bond can be constructed by heteroatom doping of the graphene honeycomb lattice. More importantly, the sp^2 bond state can be effectively reconstructed by heteroatom doping treatment and the intrinsic electronic structure can be optimized, which is beneficial to provide more active sites [33]. On the one hand, functional modification of graphene can tune its interface and surface behavior. On the other hand, new functions can also be induced through the synergistic effect between multiple species. Therefore, functional modification plays an important role in optimizing the properties and functions of 3D graphene.

4.1 Heteroatom Doping

The electronic structure and properties of graphene can be optimized by doping its crystal structure with heteroatoms, which can effectively improve its electrochemical activity. In recent years, researchers have carried out a series of research work on the heteroatom doping of 3D graphene, such as N, B, S, P, and other element doping [34–36]. In order to perform heteroatom doping in 3D graphene, the corresponding precursors are usually introduced during the preparation of 3D graphene. For example, Mei et al. successfully prepared ultra-high-level P-doped 3D graphene materials. [34] The principle of this doping method is to sacrifice the heterostructured 2D black phosphorus on graphene to achieve P doping with a P content of 4.84%. The whole preparation process is mainly divided into three parts, the first part is the liquid exfoliation of GO and black phosphorus bulk. The second part is the construction of 2D-2D BPN/GO heterostructures. The third part is the formation of ultra-high-level P-doped 3D graphene materials by sacrificing BPNs to GO under hydrothermal reaction conditions. It is worth noting that the reason for the preparation of high-level P-doped 3D graphene materials is the stable and abundant C-P bonds.

In addition, to achieve the purpose of co-doping, it is necessary to introduce precursors containing a variety of different heteroatoms during the preparation of 3D graphene [37]. The results show that the co-doping treatment of 3D graphene significantly improves its electrochemical performance, which is mainly attributed to the synergistic effect between different heteroatoms. Recently, Yu et al. successfully synthesized P and S co-doped 3D graphene using thioglycolic acid and phytic acid as heteroatom precursors [38]. Specifically, the researchers used HI chemical reduction to synthesize modified 3D graphene under hydrothermal reaction and freeze-drying conditions. Then, co-doping of S and P was achieved in 3D graphene under thermal treatment conditions. In addition to the above metal-free heteroatom co-doping, researchers also successfully synthesized non-metal and metal co-doped 3D graphene using corresponding precursors [39]. Qiu et al. successfully achieved Ni and N co-doping in graphene [39]. The results showed that the loading of Ni was as high as 23 wt%, which was mainly attributed to the promotion of Ni doping by the pre-doping of N.

4.2 Single Dispersion of Metal Atoms

In order to achieve maximum atom utilization efficiency, single-atom catalysts in which metal atoms are dispersed on a substrate have attracted extensive attention in recent years [40]. 3D graphene is an ideal substrate for the synthesis of single-atom catalysts due to its unique three-dimensional continuous network structure. On the one hand, 3D graphene as a substrate can provide a large specific surface area to expose more active metal sites. On the other hand, 3D graphene as a substrate can provide heteroatom centers to anchor metal atoms. Mou et al. successfully synthesized Ni-based single-atom catalysts on N-doped 3D graphene substrates using an impregnation-pyrolysis strategy [41]. In this synthetic strategy, 3D graphene was prepared using 3D porous melamine foam as a template. During the pyrolysis process, highly dispersed Ni single atoms were successfully loaded on N-doped 3D graphene substrates through the combined action of nitrogen anchoring and atomic trapping. Hu et al. also successfully loaded a single iron atom into 3D N,S co-doped graphene through a similar strategy [42]. Notably, the as-prepared 3D graphene-based single-atom catalysts were used as electrode materials for Li-CO_2 batteries, which exhibited excellent electrochemical performance. The results show that the potential gap of this electrode material is only 1.17 V under a current density of 100 mA g^{-1}. More importantly, when the current density is increased to 1 A g^{-1}, the charge–discharge cycles of the electrode material can still reach 200 times. The electrode material exhibits excellent electrochemical properties, which is mainly attributed to the synergistic effect between the presence of “Fe-N4” moieties in the 3D graphene substrate and the spin and charge redistribution generated by N,S co-doping.

4.3 Compositing with Other Active Species

Besides the two strategies mentioned above, constructing 3D graphene-based composites by combining the advantages of multiple components is another effective strategy to significantly enhance their performance. The 3D graphene has a hierarchical pore structure and good electrical conductivity, which makes it a support material that can significantly improve electron mobility and ion diffusion rates. In recent years, researchers have carried out a lot of work on 3D graphene-based composites, such as polymers, metals, and their compounds, and MXenes [43–47]. Sun et al. innovatively designed a two-step process to successfully synthesize 3D graphene/niobium pentoxide composites [43]. The research results show that the composite material exhibits excellent fast-charging characteristics. The reason for the analysis is that the hierarchical porous structure and 3D graphene network structure in this composite provide fast ion diffusion channels and electron transport channels, respectively. Zhong et al. innovatively designed a hydrazine hydrate vapor reduction strategy to successfully synthesize polyurethane/rGO composite foam [44]. The composite material exhibits the function of a micro switch, which realizes the regulation of the number and contact area of its equivalent circuit. An in-depth analysis of the reason for this revealed that the composite had a unique wrinkle and burr structure. The composite exhibits excellent performance as a flexible piezoresistive sensor, such as high sensitivity, fast response, wide sensitive pressure range, and excellent durability. Chen et al. innovatively proposed a GO-assisted self-convergence method to successfully prepare the composite structure of $Ti_3C_2T_x$/3D graphene [45]. During the self-assembly process, GO was partially reduced by $Ti_3C_2T_x$, which facilitated the self-assembly of 2D graphene nanosheets to form a 3D connected network architecture. Furthermore, the interfacial interaction occurred between GO and $Ti_3C_2T_x$ during the self-assembly process, which also facilitated the uniform loading of $Ti_3C_2T_x$ in the 3D graphene structure. To further improve its performance, 3D graphene can also be treated with heteroatom doping, which can exploit the synergistic effect between active species and heteroatoms. Recently, Zhou et al. successfully supported Pt nanoparticles on 3D nitrogen-doped graphene by electrochemical deposition. The composite exhibits excellent electrochemical performance, which is mainly attributed to the synergistic effect between Pt nanoparticles and nitrogen atoms [46].

5 Recent Developments in Metal–Air Batteries

MABs play an important role in next-generation energy conversion and storage systems owing to their ultra-high theoretical energy density. For example, when lithium metal is used as the metal electrode, the energy density of the battery is even comparable to that of petroleum, and its theoretical energy density can be as high as 11,680 W h kg^{-1}. The electrochemical properties of the air battery system with lithium metal as the metal electrode is largely dependent on the cathode material. After many charge–discharge cycles in this battery system, the cathode material is prone to the problem of accumulation of a large number of discharge by-products. This not only reduces the gas transport efficiency of the cathode material but also causes passivation of the electrode, which greatly reduces the electrochemical properties of the battery. In order to solve the above problems, it is urgent to develop suitable cathode materials, which are of great significance for the development of high-performance lithium–air batteries. 3D graphene has the characteristics of hierarchical pore architecture, high electrical conductivity, large specific surface area, and interconnected network structure, which make it an ideal catalyst substrate for lithium–air batteries. In recent years, Wu et al. innovatively designed a 3D graphene-based N-doped carbon nitride composite and tested it as a cathode material for lithium–air batteries. [48] The results show that the composite material exhibits excellent electrochemical performance. In particular, the overpotential and reversible capacities of the composite are 430 mV and 8892 mA h g^{-1}, respectively, under the test conditions of a current density of 1000 mA g^{-1}. An in-depth analysis of the reasons found that there are mainly two factors. On the one hand, the introduction of N atoms in the composite increases the number of active sites, which is beneficial to promote the kinetic rate of the electrochemical reaction. On the other hand, the 3D graphene in the composite has a unique connected network structure, which provides sufficient reaction space for active substances.

In addition to MABs based on organic electrolyte systems, MABs based on aqueous electrolyte systems have attracted widespread attention in recent years owing to their high safety and low cost. Among them, the air battery system based on the aqueous electrolyte with zinc metal as the metal electrode has the characteristics of high safety, high theoretical energy density (1086 W h kg^{-1}), and low cost, which makes it a research hotspot in the field of MABs. After years of research, zinc–air battery technology has been greatly developed. However, Zinc–air batteries still have some key problems that need to be solved. For example, cathode materials still have disadvantages such as poor cycle stability and low catalytic activity. Designing single-atom catalysts in cathode materials through surface/interface engineering principles is an effective strategy to solve the above problems. It is worth noting that 3D graphene can be used as an efficient support for single-atom catalysts owing to its large surface area and unique network structure. Fu et al. successfully fabricated a Ni–MnO/3D rGO composite using a hydrogel strategy and tested it as a cathode material in a zinc–air battery [49]. In this composite, Ni–MnO is uniformly dispersed in 3D rGO. The results show that the composite material exhibits outstanding electrochemical performance. It is even close to commercial Pt/C in some metrics, such as the half-wave unit and onset of this composite are 0.78 V and 0.94 V, respectively. Through the innovative design of the composite structure, the composite material exhibits excellent electrochemical performance, which is mainly attributed to the good electrical conductivity, connected network structure, and stable active sites of the composite material. It is worth noting that other types of MABs have similar problems. Therefore, this strategy provides an efficient way to realize high-performance MABs.

6 Conclusions and Perspectives

As a new energy storage technology, MABs show high energy density and good application prospects. However, to realize the power of MABs, there are still a lot of scientific and technological problems that need to be solved urgently. Among them, the development of cost-effective oxygen reduction catalysts is particularly critical. In recent years, with the development of graphene application research, it has been found that 3D graphene can be used as an excellent oxygen reduction catalyst support. The doped graphene can be directly applied as an oxygen reduction catalyst and shows excellent catalytic activity for oxygen reduction. Therefore, 3D graphene-based oxygen reduction catalysts have become a research hotspot in this field and have received more and more attention from researchers. According to the research and development progress and status quo in 3D graphene-based oxygen reduction catalysts, this chapter divides them into three categories. The first category is the application of graphene as an oxygen reduction catalyst support. The second category is the direct application of doped graphene as an oxygen reduction catalyst. The third category is the formation of composite oxygen reduction catalysts by doped graphene and other types of catalysts. The following conclusions can be drawn from this chapter.

(i) Due to the special pore structure, ultra-high specific surface area, and corrosion resistance of 3D graphene, it is applied as a support for noble metal catalysts or transition metal oxide catalysts. On the one hand, 3D graphene can improve its catalytic activity for oxygen reduction. On the other hand, it can effectively inhibit the agglomeration and dissolution of catalyst active substances and greatly improve their long-term stability.
(ii) The heteroatom-doped graphene provides many "active centers" for the oxygen reduction catalytic reaction, thereby exhibiting good oxygen reduction catalytic activity and long-term stability. However, the catalytic mechanism of oxygen reduction in heteroatom-doped 3D graphene is still controversial and needs further research.
(iii) Combining heteroatom-doped graphene with other catalysts can obtain oxygen reduction catalysts with better performance. The catalytic activity of this composite catalyst is much higher than that of its single component, which is attributed to the strong interaction between heteroatom-doped graphene and other types of catalysts.

In recent years, a lot of research work has been carried out on the application of 3D graphene in MABs, and it has shown good prospects. However, research in this field is still at an early stage, and extensive and in-depth scientific work is still needed to realize the successful application of 3D graphene-based oxygen reduction catalysts in MABs. The author believes that the focus of future work can be summarized as the following aspects.

(i) Mechanism research and exploration

In order to design high-performance catalysts more rationally, it is necessary to further study and explore the catalytic mechanism of oxygen reduction of heteroatom-doped graphene and the interaction mechanism of heteroatom-co-doped graphene and other types of oxygen reduction catalysts. More importantly, it will also help to deeply understand the catalytic behavior of oxygen reduction of the catalysts in this system.

(ii) Material design and preparation

In order to better construct the relationship between 3D graphene microstructure and electrochemical performance, it is necessary to control and optimize the structure, morphology, composition, and preparation process of 3D graphene-based oxygen reduction catalyst in detail. In addition, it is also beneficial to obtain more cost-effective 3D graphene-based oxygen reduction catalysts.

(iii) Scale production technology

At present, the research on 3D graphene-based oxygen reduction catalysts is still in the laboratory stage. To ensure the repeatability and stability of the process and performance in the large-scale and batch preparation stages, a lot of work still needs to be done to develop the technology and process.

References

1. Cheng, F., Chen, J.: Metal–air batteries: from oxygen reduction electrochemistry to cathode catalysts. Chem. Soc. Rev. **41**, 2172–2192 (2012)
2. Zhang, T., Tao, Z., Chen, J.: Magnesium–air batteries: from principle to application. Mater. Horizons. **1**, 196–206 (2014)
3. Lee, J.S., Kim, S.T., Cao, R., Choi, N.S., Liu, M., Lee, K.T., Cho, J.: Metal–air batteries with high energy density: Li–air versus Zn–air. Adv. Energy Mater. **1**, 34–50 (2011)
4. Tan, P., Chen, B., Xu, H., Zhang, H., Cai, W., Ni, M., Liu, M., Shao, Z.: Flexible Zn– and Li–air batteries: recent advances, challenges, and future perspectives. Energy Environ. Sci. **10**, 2056–2080 (2017)
5. Feng Lu, X., Lin Zhang, S., Shangguan, E., Zhang, P., Gao, S., Lou, X.W.: Nitrogen-doped cobalt pyrite yolk–shell hollow spheres for long-life rechargeable Zn–air batteries. Adv. Sci. **7**, 2001178 (2020)
6. Chen, K., Huang, G., Ma, J.L., Wang, J., Yang, D.Y., Yang, X.Y., Yu, Y., Zhang, X.B.: The stabilization effect of CO_2 in lithium–oxygen/CO_2 batteries. Angew. Chem. Int. Ed. **59**, 16661–16667 (2020)
7. Zhang, Z., Zhang, Q., Anan Chen, Y., Bao, J., Zhou, X., Xie, Z., Wei, J., Zhou, Z.: The first introduction of graphene to rechargeable Li–CO_2 batteries. Angew. Chem. Int. Ed. **127**, 6650–6653 (2015)
8. Wang, P., Wan, L., Lin, Y., Wang, B.: Construction of mass-transfer channel in air electrode with bifunctional catalyst for rechargeable zinc-air battery. Electrochim. Acta. **320**, 134564 (2019)
9. Han, X., Li, X., White, J., Zhong, C., Deng, Y., Hu, W., Ma, T.: Metal–air batteries: from static to flow system. Adv. Energy Mater. **8**, 1801396 (2018)
10. Gao, Y., Xiao, Z., Kong, D., Iqbal, R., Yang, Q.H., Zhi, L.: N, P co-doped hollow carbon nanofiber membranes with superior mass transfer property for trifunctional metal-free electrocatalysis. Nano Energy **64**, 103879 (2019)
11. Novoselov, K.S., Geim, A.K., Morozov, S.V., Jiang, D., Zhang, Y., Dubonos, S.V., Grigorieva, I.V., Firsov, A.A.: Electric field in atomically thin carbon films. Science **306**, 666–669 (2004)
12. Novoselov, K.S., Geim, A.K., Morozov, S.V., Jiang, D., Katsnelson, M.I., Grigorieva, I.V., Dubonos, S.V., Firsov, A.A.: Two-dimensional gas of massless Dirac fermions in graphene. Nature **438**, 197–200 (2005)
13. Kucinskis, G., Bajars, G., Kleperis, J.: Graphene in lithium ion battery cathode materials: a review. J. Power Sources **240**, 66–79 (2013)

14. Cui, H., Guo, Y., Zhou, Z., Cui, H.J., Guo, Y.B., Zhou, Z.: Three-dimensional graphene-based macrostructures for electrocatalysis. Small **17**, 2005255 (2021)
15. Hou, S., Kluge, R.M., Haid, R.W., Gubanova, E.L., Watzele, S.A., Bandarenka, A.S., Garlyyev, B.: A review on experimental identification of active sites in model bifunctional electrocatalytic systems for oxygen reduction and evolution reactions. ChemElectroChem **8**, 3433–3456 (2021)
16. Quílez-Bermejo, J., Morallón, E., Cazorla-Amorós, D.: Metal-free heteroatom-doped carbon-based catalysts for ORR: a critical assessment about the role of heteroatoms. Carbon **165**, 434–454 (2020)
17. Fu, J., Liang, R., Liu, G., Yu, A., Bai, Z., Yang, L., Chen, Z.: Recent progress in electrically rechargeable zinc–air batteries. Adv. Mater. **31**, 1805230 (2019)
18. Zhu, J., Yang, D., Yin, Z., Yan, Q., Zhang, H.: Graphene and graphene-based materials for energy storage applications. Small **10**, 3480–3498 (2014)
19. Arafat, Y., Azhar, M.R., Zhong, Y., Tadé, M.O., Shao, Z.: Metal-free carbon based air electrodes for Zn-air batteries: recent advances and perspective. Mater. Res. Bull. **140**, 111315 (2021)
20. Liu, Q., Pan, Z., Wang, E., An, L., Sun, G.: Aqueous metal-air batteries: fundamentals and applications. Energy Storage Mater. **27**, 478–505 (2020)
21. Sheng, K.X., Xu, Y.X., Li, C., Shi, G.Q.: High-performance self-assembled graphene hydrogels prepared by chemical reduction of graphene oxide. New Carbon Mater. **26**, 9–15 (2011)
22. Xu, Y., Sheng, K., Li, C., Shi, G.: Self-assembled graphene hydrogel via a one-step hydrothermal process. ACS Nano **4**, 4324–4330 (2010)
23. Jung, S.M., Mafra, D.L., Te Lin, C., Jung, H.Y., Kong, J.: Controlled porous structures of graphene aerogels and their effect on supercapacitor performance. Nanoscale **7**, 4386–4393 (2015)
24. Xie, Y., Li, Z., Wang, Y., Xu, S., Lin, S.: Freezing synthesis of Pt/3D GNs (C) composites as efficient electrocatalysts for methanol oxidation. J. Appl. Electrochem. **48**, 355–364 (2018)
25. Huang, X., Qian, K., Yang, J., Zhang, J., Li, L., Yu, C., Zhao, D.: Functional nanoporous graphene foams with controlled pore sizes. Adv. Mater. **24**, 4419–4423 (2012)
26. Yu, P., Zhao, X., Li, Y., Zhang, Q.: Controllable growth of polyaniline nanowire arrays on hierarchical macro/mesoporous graphene foams for high-performance flexible supercapacitors. Appl. Surf. Sci. **393**, 37–45 (2017)
27. Kim, F., Luo, J., Cruz-Silva, R., Cote, L.J., Sohn, K., Huang, J.: Self-propagating domino-like reactions in oxidized graphite. Adv. Funct. Mater. **20**, 2867–2873 (2010)
28. Choi, B.G., Yang, M., Hong, W.H., Choi, J.W., Huh, Y.S.: 3D macroporous graphene frameworks for supercapacitors with high energy and power densities. ACS Nano **6**, 4020–4028 (2012)
29. Lee, J.Y., An, J., Chua, C.K.: Fundamentals and applications of 3D printing for novel materials. Appl. Mater. Today **7**, 120–133 (2017)
30. Zhu, C., Liu, T., Qian, F., Han, T.Y.J., Duoss, E.B., Kuntz, J.D., Spadaccini, C.M., Worsley, M.A., Li, Y.: Supercapacitors based on three-dimensional hierarchical graphene aerogels with periodic macropores. Nano Lett. **16**, 3448–3456 (2016)
31. Chen, Z., Ren, W., Gao, L., Liu, B., Pei, S., Cheng, H.M.: Three-dimensional flexible and conductive interconnected graphene networks grown by chemical vapour deposition. Nat. Mater. **10**, 424–428 (2011)
32. Xie, X., Zhou, Y., Bi, H., Yin, K., Wan, S., Sun, L.: Large-range control of the microstructures and properties of three-dimensional porous graphene. Sci. Rep. **3**, 2117 (2013)
33. Cheng, H., Huang, Y., Shi, G., Jiang, L., Qu, L.: Graphene-based functional architectures: sheets regulation and macrostructure construction toward actuators and power generators. Acc. Chem. Res. **50**, 1663–1671 (2017)
34. Mei, J., He, T., Zhang, Q., Liao, T., Du, A., Ayoko, G.A., Sun, Z.: Carbon-phosphorus bonds-enriched 3D graphene by self-sacrificing black phosphorus nanosheets for elevating capacitive lithium storage. ACS Appl. Mater. Interfaces **12**, 21720–21729 (2020)
35. Qi, Y., Cao, Y., Meng, X., Cao, J., Li, X., Hao, Q., Lei, W., Li, Q., Li, J., Si, W.: Facile synthesis of 3D sulfur/nitrogen co-doped graphene derived from graphene oxide hydrogel and the simultaneous determination of hydroquinone and catechol. Sens. Actuators B Chem. **279**, 170–176 (2019)

36. Ge, L., Wang, D., Yang, P., Xu, H., Xiao, L., Zhang, G.X., Lu, X., Duan, Z., Meng, F., Zhang, J., An, M.: Graphite N-C–P dominated three-dimensional nitrogen and phosphorus co-doped holey graphene foams as high-efficiency electrocatalysts for Zn–air batteries. Nanoscale **11**, 17010–17017 (2019)
37. Cheng, H., Yi, F., Gao, A., Liang, H., Shu, D., Zhou, X., He, C., Zhu, Z.: Supermolecule self-assembly promoted porous N, P Co-doped reduced graphene oxide for high energy density supercapacitors. ACS Appl. Energy Mater. **2**, 4084–4091 (2019)
38. Yu, X., Kang, Y., Park, H.S.: Sulfur and phosphorus co-doping of hierarchically porous graphene aerogels for enhancing supercapacitor performance. Carbon **101**, 49–56 (2016)
39. Qiu, H.-J., Du, P., Hu, K., Gao, J., Li, H., Liu, P., Ina, T., Ohara, K., Ito, Y., Chen, M.: Metal and nonmetal codoped 3D nanoporous graphene for efficient bifunctional electrocatalysis and rechargeable Zn–air batteries. Adv. Mater. **31**, 1900843 (2019)
40. Peng, Y., Lu, B., Chen, S., Peng, Y., Lu, B.Z., Chen, S.W.: Carbon-supported single atom catalysts for electrochemical energy conversion and storage. Adv. Mater. **30**, 1801995 (2018)
41. Mou, K., Chen, Z., Zhang, X., Jiao, M., Zhang, X., Ge, X., Zhang, W., Liu, L.: Highly efficient electroreduction of CO_2 on nickel single-atom catalysts: atom trapping and nitrogen anchoring. Small **15**, 1903668 (2019)
42. Hu, C., Gong, L., Xiao, Y., Yuan, Y., Bedford, N.M., Xia, Z., Ma, L., Wu, T., Lin, Y., Connell, J.W., Shahbazian-Yassar, R., Lu, J., Amine, K., Dai, L.: High-performance, long-life, rechargeable Li–CO_2 batteries based on a 3D holey graphene cathode implanted with single iron atoms. Adv. Mater. **32**, 1907436 (2020)
43. Sun, H., Mei, L., Liang, J., Zhao, Z., Lee, C., Fei, H., Ding, M., Lau, J., Li, M., Wang, C., Xu, X., Hao, G., Papandrea, B., Shakir, I., Dunn, B., Huang, Y., Duan, X.: Three-dimensional holey-graphene/niobia composite architectures for ultrahigh-rate energy storage. Science **356**, 599–604 (2017)
44. Zhong, W., Ding, X., Li, W., Shen, C., Yadav, A., Chen, Y., Bao, M., Jiang, H., Wang, D.: Facile fabrication of conductive graphene/polyurethane foam composite and its application on flexible piezo-resistive sensors. Polymers **11**, 1289 (2019)
45. Chen, Y., Xie, X., Xin, X., Tang, Z.R., Xu, Y.J.: $Ti_3C_2T_x$-based three-dimensional hydrogel by a graphene oxide-assisted self-convergence process for enhanced photoredox catalysis. ACS Nano **13**, 295–304 (2019)
46. Zhou, Y., Zhang, G., Yu, M., Wang, X., Lv, J., Yang, F.: Free-standing 3D porous N-doped graphene aerogel supported platinum nanocluster for efficient hydrogen production from ammonia electrolysis. ACS Sustain. Chem. Eng. **6**, 8437–8446 (2018)
47. Hu, X., Huang, T., Tang, Y., Fu, G., Lee, J.M.: Three-dimensional graphene-supported Ni_3Fe/Co_9S_8 composites: rational design and active for oxygen reversible electrocatalysis. ACS Appl. Mater. Interfaces **11**, 4028–4036 (2019)
48. Wu, A., Shen, S., Yan, X., Xia, G., Zhang, Y., Zhu, F., Zhang, J.: C_xN_y particles@N-doped porous graphene: a novel cathode catalyst with a remarkable cyclability for Li–O_2 batteries. Nanoscale **10**, 12763–12770 (2018)
49. Fu, G., Yan, X., Chen, Y., Xu, L., Sun, D., Lee, J.-M., Tang, Y.: Boosting bifunctional oxygen electrocatalysis with 3D graphene aerogel-supported Ni/MnO particles. Adv. Mater. **30**, 1704609 (2018)

3D Graphene for Flexible Batteries

Demet Ozer

Abstract The rapid advancement and widespread usage of flexible electronic devices need the development of flexible batteries, which depend on the use of flexible electrodes. The special electrical conductivity, mechanical stability, and switchable surface characteristics of graphene make it a great choice. Flexible batteries have recently seen a dramatic increase in the use of electrodes made of graphene. This chapter examines the usage of 3D graphene electrodes (based on hydrogels, aerogels, sponges, and foams) in flexible lithium-ion, metal-air, and metal-ion batteries. It appears to have unique qualities like a three-dimensional structure, a large surface area, and high porosity that increase active sites, allow for the doping of active substances, increase the mobility and effectiveness of electrolytes, and boost efficiency in both applications and devices. The challenges and expectations for the use and advancement of flexible batteries are addressed in the final stage.

Keywords 3D graphene · Battery · Graphene composites · Flexible electrodes

1 Introduction

The necessity of "green" energy conversion/storage systems is increasing continuously because of global warming, the rapid depletion of fossil fuels, and the rise in carbon dioxide emissions. In addition to its benefits, the rapidly changing and developing technology and the Internet of Things (IoT) creates the need for research and development about new generation energy systems. Flexible energy storage materials must be developed to accommodate flexible electronic devices such as wearable computers, touch screens, robotics, and portable medical equipment. Secondary batteries possess a high energy density and a long cycle life, making them appealing technologies. Since Sony first made lithium-ion batteries available for purchase in 1991, they have dominated the market for portable gadgets like laptops, tablets, and smartphones. Personal clothes, tents, packaging, and other items can all be powered

---

D. Ozer (✉)
Department of Chemistry, Hacettepe University, Beytepe, Ankara 06800, Turkey
e-mail: demetbaykan@hacettepe.edu.tr

© The Author(s), under exclusive license to Springer Nature Switzerland AG 2023

R. K. Gupta (ed.), *3D Graphene*, Carbon Nanostructures,
https://doi.org/10.1007/978-3-031-36249-1_14

by flexible batteries with good deformability and impact resistance. Flexibility, great speed capability, better stability under deformations, and the ability to be customized to operating circumstances are all benefits of flexible batteries. The same parts found in conventional rigid batteries, such as cathode/anode electrodes and electrolytes, are also present in flexible batteries. To take advantage of high-performance flexible batteries, flexible electrode materials need to be developed and made commercially available. The electrodes specify the capacity, energy, and power density of batteries because they supply ions and electrons and conduct electricity. High mechanical flexibility, great electrical conductivity, and structural strength to endure repeated deformations are all qualities that a flexible battery electrode should possess [1]. Conducting polymers, carbon cloth (CC), carbon fibers, and nanomaterials (carbon nanotubes, graphenes, and MXenes) are the most often employed materials as an electrode for flexible batteries.

The graphene-based materials are great alternatives choices for energy storage applications due to their high energy density, quick charging, and long-lasting performance. Large surface area and high porosity are two distinguishing features of the 3D structure, which enhance the active sites, improve the doping of active chemicals, and promote accessibility and mobility of electrolytes as well as efficiency. This section examines the preparation of 3D graphene electrodes and their uses as flexible electrodes for a variety of flexible batteries, including metal-ion, lithium-sulfide, and metal-air batteries. The difficulties with flexible batteries are also discussed, along with a preview of upcoming research.

2 Preparation of 3D Graphene Electrodes

The use of graphene in electrochemical applications has become widespread because of its exceptional electrical conductivity, mechanical toughness, and lightweight. Graphene and derivatives (graphene oxide and reduced graphene oxide) outperform other electrodes in terms of weight, cost, and energy density without the use of extra parts like conductive carbons and binders, as well as external heavy metal current collectors. Electron transport can be facilitated by conductive graphene structures by altering the kinetics of electrochemical reactions. Graphene has a large surface area, making it perfect for active agent doping and active agent dispersion. This reduces the van der Waals forces between layers, prevents the formation of graphene clumps, and gives graphene sheets structural stability with open channels for surface and ion migration and charge. Elastic graphene layers might lessen active material volume fluctuations during alloying or transformation events, improving the electrodes' integrity. The growing demand for flexible and portable electronic devices presents an incredible advantage for flexible graphene because of its strong mechanical resilience and conductivity [2].

Graphene is produced from graphite. It can be prepared as one-dimensional fibers and nanotubes, two-dimensional films and nanosheets, and three-dimensional networks as effective electrode material. The 1D graphene fibers can adapt to severe deformations in the length direction. The 2D films have excellent flexibility under different bending states without structural damage. The 3D offers special qualities including a wide surface area and high porosity that enhance the active sites, improve the doping of active chemicals, increase the accessibility and mobility of electrolytes, and improve the effectiveness of different applications and production tools. Agglomeration and subsequent deposition of graphene can be avoided by converting a 2D structure into a 3D one. The advantages of employing 3D graphene-based materials for energy storage purposes include: (1) Since the majority of the electrons in the honeycomb pattern are sp^2 hybrid electrons, the remaining electrons in the p-orbit are well suited for forming strong bonds that are flexible enough to support electron transmission. (2) A 3D cross-linking channel for ion/molecule diffusion is created by sequential pores. (3) The enhanced adsorption/desorption capability encourages mass transfer. (4) It is more suitable for usage in energy storage systems because of its amazing versatility in terms of structural traits, hydrophilicity, and electrical conductivity. (5) Excellent mechanical and chemical stability may be found in very stable energy storage systems [3].

The two main categories of 3D graphene materials are shown in Fig. 1 as follows: (1) macroscopic materials (>100 m in one or more dimensions), such as macro 3D graphene monoliths (foams/sponges/aerogels), films, fibers, and spheres; and (2) microscopic materials (100 m in all dimensions). Depending on the applied synthesis technique, the type of 3D graphene can be altered. In general, self-assembly techniques including reduction, cross-linking, sol–gel, and hydrothermal procedures, template techniques like template-directed chemical vapor deposition and assembly synthesis, laser casting, 3D printing, and electrothermal expansion have been used [4]. The 3D graphene hydrogel was prepared through the hydrothermal method using a Teflon autoclave at 180 °C for 12 h [5]. The obtained graphene hydrogel has high electrical conductivity (5×10^{-3} S/cm), strong mechanical strength, high thermal stability, high specific capacity (175 F/g at 10 mV/s scan rate), and is biocompatible. These characteristics make it useful in biotechnology and electrochemistry applications such as supercapacitors, tissue engineering, drug delivery, and biomaterials. The three-step sol–gel process was used to create the 3D aerogel graphene. In the first step, monolithic solids are prepared from single-layered graphene oxide suspensions, in the second step the obtained gels are dried in a supercritical environment, and finally, graphene aerogels are formed by thermal reduction. These graphene aerogels have two times higher electrical conductivity (87 S/m) compared to graphene with physical crosslinks alone. Graphene aerogels can be used effectively in energy storage, catalysis, and sensing applications due to their large surface areas (584 m^2/g), pore volumes (2.96 cm^3/g), and ultra-low densities (10 mg/cm^3) [6]. Three-dimensional (3D) graphene foam (GF) was created by chemical vapor deposition (CVD) using nickel foam as a template. Poly-(dimethylsiloxane) (PDMS) was then infused into the 3D GF. Investigation of the GF/PDMS composite's electrical characteristics under bending stress revealed that the resistance of the material increased with the curvature of the bend. It is more adaptable and environmentally stable, and it may be used as a strain sensor with high sensitivity for crucial real-time monitoring applications for buildings like bridges, dams, and high-speed railroads [7]. By using the ice template

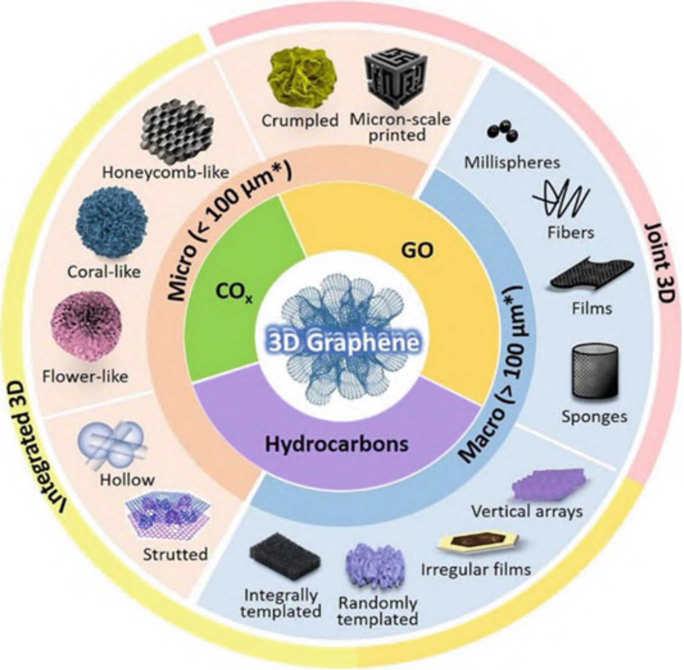

Fig. 1 The types of 3D graphenes. Reprinted with permission [4], copyright (2020) American chemical society

approach, which is often employed to create hierarchical microstructure for nanoparticles, the flexible macroporous 3D graphene sponge was created. A macroporous graphene sponge was created after freeze-drying the as-formed ice crystals, which rebuilt the inner walls of the graphene hydrogel into a hierarch macroporous structure at a gradual cooling rate. A microbial fuel cell made with a graphene sponge as the anode material had a power density of 427.0 W.m^{-3}, which was higher than an MFC made with carbon felt as the anode material [8].

3 Design of Flexible Batteries

The development of flexible electronics, which can fit complex curved surfaces with superior fatigue resistance and safety, has gradually advanced the requirement for flexibility. Flexible batteries consist of three main components: substrates, electrolytes, and electrodes (anode and cathode), along with a current collector and battery shell (Fig. 2a, b). Active materials are supported as they are utilized to create batteries by **current collectors**, which also serve as substrates for the collection and transit of electrons from active materials and external circuits. Because of their

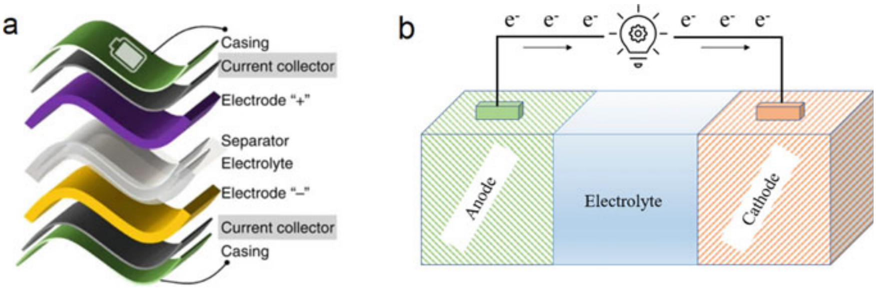

Fig. 2 **a** The representation of a flexible battery cell. Reproduced from [11], copyright 2016, springer nature, **b** schematic illustration of batteries

outstanding electrochemical durability against oxidation and reduction, low price, and exceptional electrical conductivity, Al and Cu are used as the cathode and anode current collectors in industrial Li-ion batteries, respectively. Additionally, enhanced current collector and electrode material adhesion as well as mechanical stability under deformation are required for flexible batteries. Battery performance degradation and thermal runaway are caused by the constant stretching of operational batteries, which leads to the failure of current collectors and active components. Flexible Cu and Al current collectors need to be made with a thickness that allows the tensile stress to be much lower than the yield stress and tensile breaking stress, or the metal foils need to be porous to lessen the stress. Flexibility improves with an increase in structural porosity. However, the current collectors' electrical conductivity is harmed by the porous structure. Flexible current collectors based on Cu and Al foils must therefore appropriately consider mechanical stress, thickness, porosity, and conductivity to build superior flexible batteries [9]. The **electrolyte**, which functions as both an ionic conductor and an electronic insulator, is an essential component to maintain simple ion movement and little self-discharge. A suitable electrolyte is required to produce functional batteries. Liquid electrolytes are frequently used for flexible Li-ion batteries because of their straightforward percolation, quick ion mobility, robust wetting ability, and stable solid electrolyte interphase features. Among the issues that need fixing are the safety issues with liquid electrolytes as well as the shortening of battery life brought on by the growth of lithium dendrites and electrolyte leaks. Alternative solid-state electrolytes to liquid electrolytes have recently shown promise as charge carriers when combined with lithium metal anodes to create flexible batteries that are both safe and highly energetic. Inert components to facilitate high voltage cathode requests, low electrolyte leakage to prevent cell failure or fire, a large electrochemical window, strong Young's modulus to prevent lithium dendrites, and straightforward cell modeling to reduce production costs have all benefited solid electrolytes. **Separators** are placed between the cathode and the anode and assist in the transport of ions. It also prevents electrons from migrating into internal circuits. The performance, dependability, and safety of batteries are primarily affected by the mesh structure, material structure, and processing technique of the separators.

Typically, separators made of 20–40 μm thick mixes of polyethylene, polypropylene (PP), and other microporous polyolefin membranes are utilized. However, polyolefin membranes are notorious for having poor electrolyte wettability and low heat stability. Therefore, it's critical to use separator materials in flexible batteries that have improved thermal stability, wettability, and fire resistance.

The other crucial part of flexible batteries is the electrodes (anodes and cathodes). It is substantial to enhance the properties of **electrode materials** like high specific capacity, better cycle life, mechanical stability, and rapid ion diffusion. Electrons are released during chemical processes between the anode and the cathode. The intercalation and deintercalation of the metal-ion take place between the anode and the cathode. Cell architecture is as important factor as electrode materials for developing a fully flexible battery. To increase the flexibility of the battery, each component must be portable, bendable, twistable, stretchable, ultrathin, and wearable [10]. The 3D graphene-based electrodes have successfully applied as both anode and cathode for various types of batteries like lithium-ion, sodium-ion, other ions, lithium-sulfide, and metal-air batteries.

4 3D Graphene Electrodes for Flexible Metal-Ion Batteries

Metal-ion batteries are applied as a reliable form of energy storage due to their high energy density, extended cycle life, and high energy conversion efficiency. The development of flexible rechargeable batteries is highlighted by the rising demand for flexible electronics of the future, including wearable electronics, portable electronics, and implanted biomedical technologies. The anode and cathode materials for 3D graphene-based electrodes have been effectively used in a majority of lithium-ion, sodium-ion, and other ion batteries.

4.1 3D Graphene Electrodes for Flexible Lithium-Ion Batteries

In mobile electronic devices like electric cars, laptop computers, and phones, lithium-ion batteries are among the metal-ion batteries that work well. Due to its high energy density and operating voltage, the lithium-ion battery (LIB) is evolving into a crucial energy storage technology. Lithium-ion batteries are sold in solid squares or cylinders that are brittle when deformed. Active materials and collectors have poor adherence when metallic aluminum and copper foils are utilized as current stabilizers. The active components tend to slip out of the current collectors when the electrodes are repeatedly deformed, which causes irreversible reductions in the device's energy density and cycle life. A good solution to these issues is flexible lithium-ion batteries with flexible electrodes. For instance, the hydrothermal approach was used after chemical vapor deposition to generate the 3D nitrogen-doped graphene foam containing encapsulated germanium quantum dots. The resultant electrode is extremely flexible and may be twisted in any direction without suffering any damage. The porous graphene foam facilitated the access of the electrolyte while suppressing the volume change of the germanium. It showed that flexible lithium-ion batteries could have a high specific capacity (1220 mAh g^{-1} at 1C), ultra-high speed performance (800 mAh g^{-1} at 40C), and a long life cycle (1000 cycles) [12]. Three-dimensional (3D) graphene foams (GF) were produced via chemical vapor deposition on nickel foam. After that, GF was covered in MoS_2 nanosheets that resembled flowers thanks to a microwave-assisted hydrothermal process. Due to its highly conductive network and linked channel, the flexible MoS_2@GF electrode demonstrates exceptional electrochemical performance for lithium-ion batteries (LIBs) and sodium-ion batteries (SIBs). At a current rate of 100 mA g^{-1}, MoS_2@GF's specific capacity for LIBs can reach up to 1400 mAh g^{-1}, and after 100 cycles, the high specific capacity (1127 mAh g^{-1}) can be attained at a rate of 250 mA g^{-1}. Additionally, at a rate of 100 mA g, the obtained specific capacity for SIBs after 50 cycles is 290 mAh g^{-1}. Fast electron transport, more effective electrolyte penetration, and shorter ion diffusion time for high conductivity, stable 3D structures are all credited with the flexible MoS_2@GF electrode's good performance [13]. Using ferrous sulfate as the iron supply and lysine as the precipitator, simple hydrothermal synthesis has been used to produce 3D graphene-encapsulated, essentially monodisperse Fe_3O_4 composites. The 3D Fe_3O_4@rGO composite has consistent Fe_3O_4 particle size, according to SEM and TEM characterizations. In addition to reducing volume changes and enhancing electric connection, the unique 3D graphene-encapsulated Fe_3O_4 structure can also prevent the aggregation of Fe_3O_4 NPs during repeated charge/discharge cycles. The 3D Fe_3O_4@rGO exhibits good electrochemical characteristics when used as an anode in LIBs. Electrochemical experiments show that the as-synthesized Fe_3O_4@rGO has an excellent rate capability and an improved discharge capacity (1139 mAh g^{-1} at 400 mA g^{-1} after 100 charge/discharge cycles) [14]. By calcining a 3D graphene/metal–organic framework in one step with selenium powder under an Ar/H_2 flow for two hours at 600 °C, Xu and colleagues created Fe_7Se_8@C core–shell nanoparticles enclosed within a 3D graphene aerogel composite as a flexible anode. In tests between 0.01 and 3.00 V, the 3DG/Fe_7Se_8@C composite showed exceptional rate performance and a high reversible capacity of 884.1 mAh g^{-1} at 0.1 A g^{-1} after 120 cycles and 815.2 mAh g^{-1} at 1 A g^{-1} after 250 cycles [15].

4.2 3D Graphene Electrodes for Flexible Sodium-Ion Batteries

The need for alternatives has arisen as a result of the challenges that lithium-ion batteries confront, particularly their inadequate energy/power density, safety concerns, durability, and particularly their limited supply, and expensive raw ingredients (cobalt and lithium). Due to the extensive accessibility of natural sodium sources including Na_2CO_3, Na_2SO_4, and NaCl as well as their affordability, sodium-ion batteries are of interest. The battery performance is influenced by low ion–solvent interaction energy and high Na^+ diffusion rate. Additionally, as cobalt is not necessary for the production of SIB cathodes, increasing the market share of SIB can lower the risk of cobalt supply for LIB [2].

A host must have lots of active sites for adsorption/chemisorption, large interlayer spacing, and long-range organized graphitic sheets for electron transport to store Na^+. These elements combine to create a host that has a large capacity, rapid charging, and stable cycling. Graphite shows limited capacity, low-velocity capacity, and a short life cycle due to its inability to adapt to sodium addition. Besides, the large atomic radius of sodium ions causes low conductivity and structural instability in sodiation and desodiation. While graphene oxide with adjustable d-spacing and flaws perform better, pure graphene is not the best material for holding sodium. As efficient anode materials for SIBs, metal oxides, which have the benefit of large theoretical capacity, are of great interest. When SIBs are charged or discharged, their low conductivity and significant volumetric shift cause these materials to typically have low cycle stability and capacitance ratios. The use of graphene to support metal oxides is effective in SIBs. A novel flexible electrode for sodium-ion batteries has been created by Chen et al. utilizing hydrothermal and CVD techniques. It is composed of 2D arrays of ultrathin SnO nanoflakes supporting a 3D substrate made of graphene foam and carbon nanotubes as the anode (Fig. 3a–c). In contrast, the large surface area 3D GF/CNTs@SnO electrode, high porosity, and strong permeability have improved the Na^+ diffusion and charge transfer kinetics due to their ultra-fine shape (Fig. 3d–f) of well-separated SnO nanoflakes (Fig. 3g). Figure 3h, i, j, and l demonstrate how the final 3D GF/CNTs@SnO electrode outperformed the competition in terms of high-rate capability and cycle stability in SIBs. It is possible to see a decrease in the GF/CNTs@SnO electrode's specific capacity from 584 to 390 mAh g^{-1} and an increment in the current density from 0.1 to 1 A g^{-1}. It's impressive that the higher speeds were able to achieve higher high-speed capabilities, providing 302 mAh g^{-1} at 2 A g^{-1} and 170 mAh g^{-1} at 10 A g^{-1}, respectively. After 600 charge/discharge cycles at 0.1 A g^{-1}, the initial capacity of 584 mAh g^{-1} was reduced to 540 mAh g^{-1} with only 91% retention. Two additional charge storage mechanisms in the 3D GF/CNTs@SnO electrode include diffusion-controlled faradaic doping from the alloying reaction and capacitive additive from charge transfer with surface/subsurface atoms. A qualitative analysis of the capacitance effect against diffusion behavior is possible. The results demonstrate that the capacitive contribution makes up roughly 46% of the overall sodium load, as shown by the relationship between current I and scan rate (v) as determined by the CV curves (Fig. 3k). According to the Nyquist plots, the GF/CNTs/SnO electrode has a lower overall ohmic resistance of the solution and electrodes than the GF@SnO electrode (Fig. 3m). Furthermore, there is less charge transfer resistance. The good conductivity of CNTs arrays as a component of electron and ion transportation networks, which results in faster reaction kinetics and greater capacity, is primarily responsible for the fast charge transfer and low

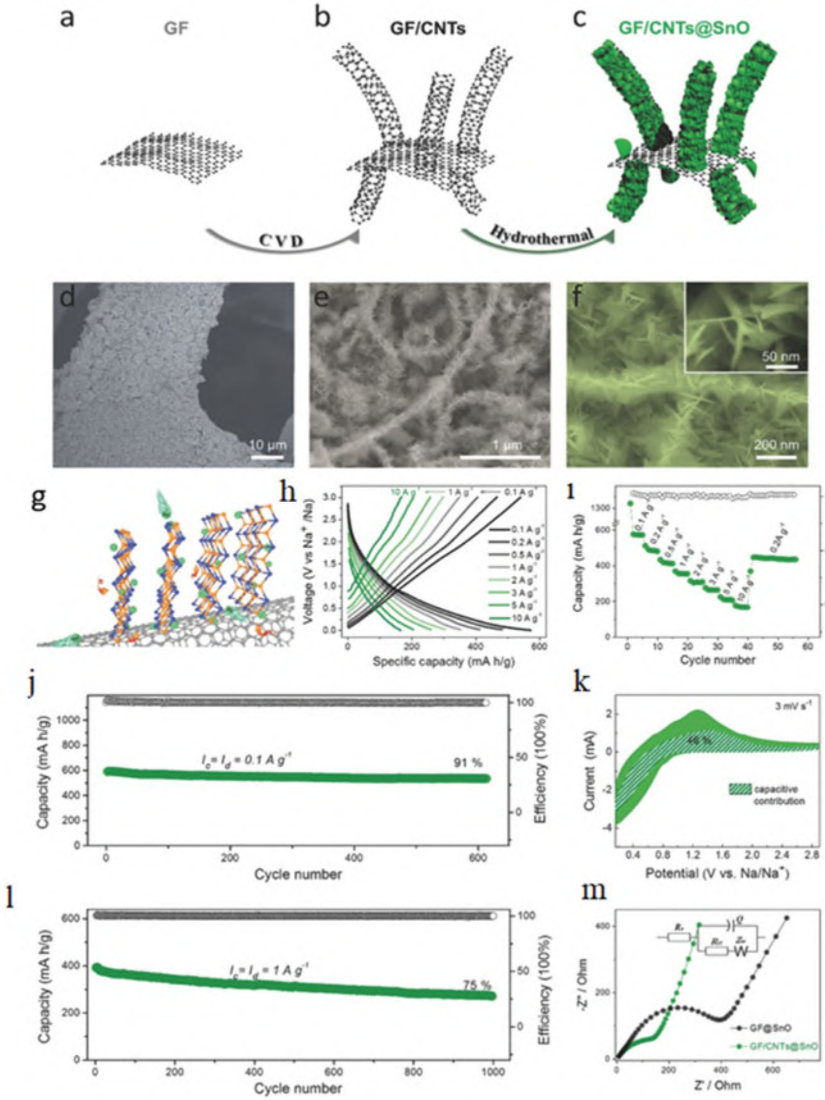

Fig. 3 Schematic representation of composite preparation **a** graphene foam; **b** GF/CNTs; **c** GF/CNTs@SnO; **d–f** SEM images of composite; **g** Schematic illustration of the GF/CNTs@SnO electrode; **h** Charge/discharge curves at various current densities; **ı** Rate capability; **j**, **l** Low and high-rate cycle life; **k** at 3 mV s^{-1}; **m** Nyquist plots of GF@SnO and GF/CNTs@SnO. Adapted with permission [16] copyright (2017) john wiley & sons

resistance in GF/CNTs/SnO. Quantitative analysis showed that the ultrathin GF/CNTs@SnO electrode's extraordinarily quick Na+ kinetics considerably increased the surfactant sites. The high surface area, porosity, and superior permeability of GF/CNT foam enable a 3D porous design for Na+ diffusion and transport. CNTs with an entangled 3D conductive structure are crucial for the dispersion of SnO nanoflakes [16].

Sun and colleagues developed the hydrothermal and freeze-drying method to prepare the 3D nitrogen-doped graphene (3DNG) frameworks doped Bi_2S_3 nanorods, which will serve as the anode material for a flexible sodium-ion battery. With a high reversible capacity (649 mAh g^{-1} at 62.5 mA g^{-1}), and excellent durability, the Bi_2S_3/3DNG composites displayed remarkable Na storing behavior (307 and 200 mAh g^{-1} after 100 cycles at 125 and 312.5 mA g^{-1}, respectively) [17]. $Na_3V_2O_2(PO_4)_2F$ (NVOPF), with its high operating voltage and theoretical capacity, is a potential cathode material for sodium-ion batteries (SIBs). Its weak intrinsic electrical conductivity significantly impairs its electrochemical performance. To get around this, NVOPF is combined with very flexible graphene sheets using the spray drying technique. The highly electrically conductive graphene framework contains uniformly dispersed NVOPF nanocrystal particles. The durable NVOPF/rGO microsphere composite performs admirably as a cathode for SIBs thanks to its high specific capacity (127.2 mAh g^{-1}), long-term cycle stability (83.4% capacity retention at 30 °C after 2000 cycles), and exceptional high-speed performance (70.3 mAh g^{-1} at 100 °C). For enhanced energy storage applications, the electrochemical characteristics of electrode materials seem to be improved by the graphene skeleton, which also functions as a high-throughput electronic conduction matrix [18].

4.3 3D Graphene Electrodes for Flexible Other Metal-Ion Batteries

Similar to how there is an abundance of Na (2.3 wt%), there is also a plenty of K (1.5 wt%) in the Earth's crust, and K raw materials like K_2CO_3 are widely available, which helps keep potassium-ion battery prices stable. Creating a 3D porous framework is a successful way to improve surface adsorption/desorption of potassium-ion saving. The one-pot hydrothermal synthesis of N/P dual-doped 3D graphene aerogels with hierarchical pores increased interlayer distance and high doping level results in materials with exceptional potassium-ion battery electrochemical performance. The products that were produced with the help of potassium bis(fluoro sulfonyl)imide (KFSI) in an EC/DEC electrolyte showed good rate capability (185 mAh g^{-1} at 5 A g^{-1}) and high reversible capacity (507 mAh g^{-1} at 100 mA g^{-1} after 100 cycles) [19].

Multivalent metal ions technologies, like those utilizing Mg^{2+}, Zn^{2+}, Ca^{2+}, and Al^{3+}, are being researched more and more as low-cost alternatives to lithium-ion batteries in recent years. Zinc-ion batteries have drawn a lot of interest because of their advantages in two-electron redox, high level of security, and simplicity in scaling. Additionally, because of the sluggish diffusion of divalent cations at the cathode, the speed performance of the majority of ZIBs is still insufficient. To produce high-rate ZIBs, Fan et al. produced a flexible graphene-based ZIB. On flexible graphene foam, a fresh layer of zinc orthovanadate was created and employed as a cathode. The Zn array anode was also supported by porous graphene foam. Since no active material peeled off the graphene substrate after periodic bending, it was found that both the graphene-based cathode and anode had exceptional mechanical stability and flexibility. An ultra-high-rate performance of 50C (discharge in 60 s) was demonstrated by the resulting flexible Zn-ion battery [20]. The cost-benefit of aluminum ion batteries outweighs the benefit of aluminum's inherent abundance. Aluminum metal has a large volumetric and gravimetric capacity (2980 mAh g^{-1} and 8034 mAh mL^{-1}). Aluminum is stable in air and may be used without the use of inert gases because of its outer oxide film. This improves the aluminum battery's safety throughout production and use. As an illustration, the 3D graphene mesh network was successfully designed and built using the folded Ni mesh-aided CVD technique. Ni was electroplated onto the surface of the Ni mesh before it was folded and attached. With a capacity retention rate of 96.5% after 200 cycles, this 3D graphene mesh network offers a high capacity of 57 mAh g^{-1} in an Al-ion battery at an extremely high rate of 40C. The cathode of an ultrafast Al-ion battery that has a similar gravimetric capacity but a substantially higher volumetric capacity can be made using this high-density 3D graphene mesh network [21].

5 3D Graphene Electrodes for Flexible Lithium-Sulfur Batteries

One of the best lithium-ion battery substitutes is lithium-sulfur technology. The most significant advantages include high theoretical specific capacities (1672 mAh g^{-1}), high energy densities (2600 Wh kg^{-1}), natural abundance of the sulfur cathode, low cost, and non-toxicity. In addition to the advantages, some disadvantages are still seeking solutions. One of these is sulfur's low electrical conductivity. Another is that the reaction's discharge products (Li_2S or Li_2S_2) are essentially insulating, which can significantly raise the cell's internal resistance. Volume expansion is another drawback. Li_2S and sulfur have different densities, and when sulfur is changed into Li_2S, the volume of the electrode rises by around 80%. When the electrode's volume increases, the structural degradation of the electrode causes the capacity to drop off quickly, creating a risk for injury. The shuttle effect, which occurs when polysulfide generated during charge and discharge dissolves in the electrolyte, is the final drawback. The polysulfide formed at the cathode dissolves in the electrolyte, advances to the lithium anode with the help of the separator comes into direct contact with lithium, and results in irreversible side reactions that cause loss of active substance from the cell. Low active material consumption has negative effects on coulomb efficiency and cycle performance. The flexibility of the electrodes and leakage of electrolyte place further limitations on the design of flexible lithium-sulfur batteries. If the electrode cannot withstand mechanical deformation under bending and folding, the electrode surface may crack and break, creating a safety hazard. Novel materials for Li anodes, functionalized solid-state electrolytes, functionalized separators, and sulfur cathodes could be developed to address these shortcomings [22].

Flexible sulfur cathodes differ from conventional cathodes in that a portion of the cathode becomes independent, the amount of sulfur in the electrode's total mass increases, increasing the battery's energy density in turn, the cathode is resistant to volume widening during charging, and discharging, and the amount of sulfur is improved by using 3D structures. The 3D graphene-based materials have been obtained and successfully applied as cathode material for flexible lithium-sulfide batteries. The 3D graphene sponge with sulfur nanoparticles was prepared through the facile reduction method and freeze-drying. The resulting composite was applied as a cathode material and provided fast Li^+ conduction, superior absorption, and effective electrochemical redox effects of sulfur with continuous conductivity, superior structural integrity, and flexibility. It has a high reversible capacity of 580 mA h g^{-1} over 500 cycles with a high-capacity retention of 78.4% and a low decay rate of 0.043% per cycle [23]. Zhou and coworkers prepared 3D graphene foam which provides a highly electrically conductive network, robust mechanical support, and sufficient space for a high sulfur loading as a sulfur cathode host. Figure 4a depicts a schematic representation of the cathode's synthesis. The process involved chemically depositing graphene on nickel (Ni) foam, coating the foam with poly(dimethylsiloxane), and then etching away the nickel and infiltrating it with a thoroughly mixed sulfur slurry. The PDMS/GF is very flexible and may be bent in any direction without breaking (Fig. 4b, c). Even after being loaded with a significant amount of sulfur, the flexible S-PDMS/GF electrode maintains its flexibility while the linked graphene network is kept intact during electrode construction (Fig. 4d, e). The sulfur loading was improved by the graphene foam's rich porosity, which allowed for significant amounts of sulfur to be accommodated. The structural variations between the flexible electrode based on GF and the electrode incorporating sulfur coating on an Al foil current collector are shown in Fig. 4g, h. The active components are principally supported by the current collector, which also offers a continuous conductive path. The foam structure produced interconnected conductive networks that aided in the rapid transport of ions and electrons. The flexible cathode's mechanical stability was improved by the thin PDMS covering, which also reinforced the topology of the conducting network. A 20% elastic strain flexible cathode that was created kept its conductivity through 22,000 bending tests. The electrodes exhibited no evidence of cracking after being bent. This demonstrates that the electrode is strong and flexible even when bent. After 1000 cycles with a constant cycling mechanism and a deterioration rate of 0.07%, this flexible cathode showed a reversible capacity of 450 mAh/g at 3.5C (Fig. 4f–i) [24].

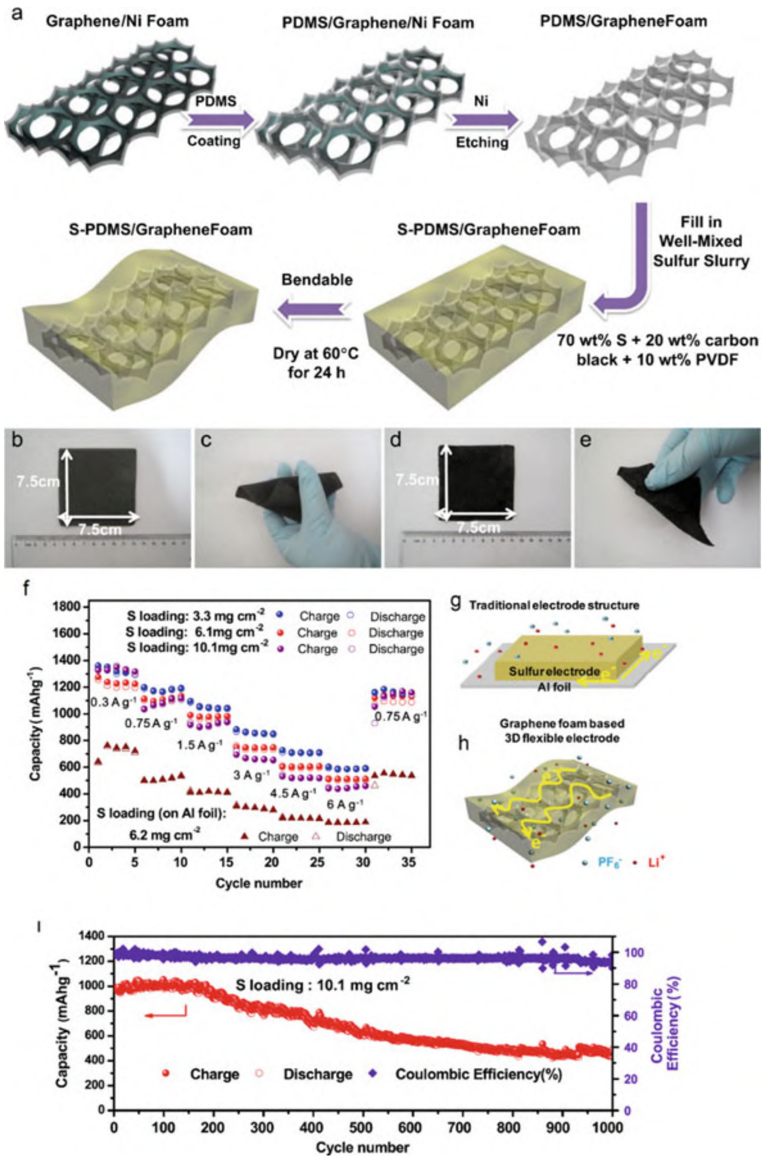

Fig. 4 **a** The schematic illustration of the synthesis of the cathode; **b**, **c** Photographs of a PDMS/GF; **d**, **e** Photographs of S-PDMS/GF electrode with sulfur; **f** Rate performance of S-PDMS/GF electrodes with various sulfur loadings and the electrode with sulfur deposited on an Al foil; **g**, **h** Comparison of a flexible electrode based on GF and an electrode design with sulfur coated on an Al foil; **i** Cycling performance and Coulombic efficiency of the S-PDMS/GF electrode. Adapted with permission of [24], copyright (2015) Elsevier

6 3D Graphene Electrodes for Flexible Metal-Air Batteries

For the future generation of EVs, metal-air batteries including lithium, zinc, magnesium, and aluminum show promise. They reduce the weight of the battery and increase the amount of space available for energy storage by using oxygen from the air as one of the battery's primary reactants. The lithium-air battery exhibits the highest potential energy density among all these metal-air batteries. Despite this, the practical energy density of commercial lithium-air batteries is still insufficient for high-power applications, and they have short lives. Including other metal-air batteries like zinc-air, aluminum-air, and magnesium-air batteries, the present lithium-air battery is not resistant to atmospheric moisture. Compared to magnesium-air, aluminum-air, and zinc-air batteries, it is more expensive to produce. While aluminum-air batteries cannot be recharged, lithium-air batteries have superior reversibility than zinc-air and magnesium-air batteries [25].

Electrodes made of graphene have recently been used as effective electrodes for metal-air batteries. To produce a moisture-resistant cathode for high-performance Li-air batteries, Duan et al. developed a three-dimensional (3D) hydrophobic graphene membrane without the need for a binder. The 3D graphene membranes have a porous nature for effective oxygen and electrolyte ion diffusion, an interconnected graphene network for efficient charge transfer, a large specific surface area for high-capacity storage of the insulating discharge product, and hydrophobic channels for O_2/H_2O selectivity. It promotes O_2 ingress, delays moisture diffusion, and offers outstanding charge/discharge cycle stability under ambient settings. It has a maximal cathode capacity of over 5,700 mAh/g and great recharge cycle behavior (> 2,000 cycles at 140 mAh/g and >100 cycles at 1,400 mAh/g), making it a strong Li-air membrane with exceptional performance. can make the batteries work. Unlike a standard lithium-ion battery cathode, the graphene membrane air cathode has a lifetime capacity of 100,000–300,000 mAh/g. Future mobile power supply might find the stable operation of Li-air batteries to be a desirable high energy density storage alternative thanks to their greatly improved single-charge capacities and lifetime capacities comparable to Li-ion batteries. These batteries can offer much lower charging frequency and much longer battery life [26]. CeO_2 microsphere doped 3D graphene foam was prepared by the hydrothermal method as a flexible cathode material for the lithium-air battery. The obtained cathode exhibits a high discharge capacity of roughly 3250 $mAhg^{-1}$ at a current density of 200 mAg^{-1} with high flexibility and good reversibility due to the synergetic effect of hollow graphene foam and ceria microsphere [27]. For zinc-air batteries, Qiu and colleagues used chemical vapor deposition and chemical etching to create 3D nanoporous graphene with nitrogen and nickel. To build the battery, co-doped graphene is employed as a flexible and free-standing air–cathode, PVA gel serves as the electrolyte, and Zn foil serves as the anode. Due to the high bifunctional activities, electrical conductivity, and improved mass movement, the produced battery demonstrated 83.8 mW cm^{-2} power density after a 48-h testing period. It can continue to work reliably for a long time and even in a variety of bending situations [28]. In another study, the ultrathin Co_3O_4 nanosheet clusters embedded onto nitrogen-doped carbon nanotubes/3D graphene (NCNTs/3D graphene) composite on top of a nickel foam substrate were made using chemical vapor deposition (CVD) and heat treatments. When the obtained composite is applied as the cathode in an aluminum-air battery, it exhibits higher open circuit voltages, specific capacities, and maximum power densities than Co_3O_4/3D graphene and Pt/C. It has a specific capacity of 482.80 mAh g^{-1} at a discharge current density of 1.0 mA cm^{-2} and a maximum power density of 4.88 mW cm^{-2} [29].

7 Challenges and Perspectives for Future Research

The environmental crisis is made worse by the increasing consumption of fossil fuels as a result of rising energy demand. Due to intense pressure from the energy and environmental sectors, researchers are looking for effective and renewable energy storage and transformation solutions. Flexible batteries as energy storage devices have a wide range of potential applications since they provide flexible displays, flexible sensors, and other components a consistent and dependable power source. The flexible electrode plays a crucial role in flexible batteries by carrying out a variety of functions such as facilitating electron transport, providing interfaces for electrode reactions, supporting battery architectures, and implementing flexible features. The flexible electrode material has a considerable impact on the energy density, rate performance, and flexibility of the battery. The development of flexible structures is essential for enhancing the mechanical characteristics of flexible batteries and broadening their scope of use. The advancement of flexible electronics and the expansion of its useful application fields will be aided by research on flexible battery electrodes.

The flexible electrodes made of carbon-based materials have special benefits when they used in flexible batteries. (1) Carbon materials with pores and a large amount of surface area provide a strong and conductive cross-linked framework for strong adhesion of active materials. The carbon structure enhances electrochemical kinetics by allowing both ion and electron transport and can tolerate repetitive deformation. (2) The positive traits of carbon materials, such as their lightweight nature, low interface resistance, and abundance of active sites, tend to boost FLIBs’ energy density. (3) The excellent electrochemical stability of carbon materials enhances the electrodes for FLIBs’ speed capability and favorable cyclic reversibility. The excellent conductivity and electrochemical activity of the graphene-based electrodes have allowed them to be successfully used as anodes and cathodes. Aside from these benefits, 3D graphene also has a large theoretical specific surface area (approximately 2630 m^2/g), outstanding mechanical flexibility, strong electrical conductivity, high thermal conductivity, superb chemical stability, and minimal installation cost. As a conductive additive to enhance kinetics and as a buffer to support the structural integrity of electrodes, graphene is utilized actively in electrochemical reactions. Due to the low theoretical capacity, enormous initial irreversible capacity, and rapid capacity loss during the cycling of graphene-based anodes, the incorporation of high-capacitance inorganic active materials atop the flexible graphene matrix is necessary.

Given the advancements in structure design technology and materials synthesis engineering, FLIBs, which combine exceptional mechanical flexibility and electrochemical performance, will help to significantly advance energy storage technology in the future. Additionally, the development and commercialization of portable and flexible electronics will spread quickly.

References

1. Dai, C., Sun, G., Hu, L., Xiao, Y., Zhang, Z., Qu, L.: Recent progress in graphene-based electrodes for flexible batteries. InfoMat **2**(3), 509–526 (2020)
2. Xu, H., Chen, H., Gao, C.: Advanced graphene materials for sodium/potassium/aluminum-ion batteries. ACS Mater. Lett. **3**(8), 1221–1237 (2021)
3. Ma, Y., Chen, J., Hu, Y., Zhang, Y., Zhang, Z., Zhan, J., Chen, A., Peng, Q.: Synthesis of three-dimensional graphene-based materials for applications in energy storage. Jom **72**, 2445–2459 (2020)
4. Sun, Z., Fang, S., Hu, Y.H.: 3D graphene materials: from understanding to design and synthesis control. Chem. Rev. **120**(18), 10336–10453 (2020)
5. Xu, Y., Sheng, K., Li, C., Shi, G.: Self-assembled graphene hydrogel via a one-step hydrothermal process. ACS Nano **4**(7), 4324–4330 (2010)
6. Worsley, M.A., Pauzauskie, P.J., Olson, T.Y., Biener, J., Satcher, J.H., Jr., Baumann, T.F.: Synthesis of graphene aerogel with high electrical conductivity. J. Am. Chem. Soc. **132**(40), 14067–14069 (2010)
7. Xu, R., Lu, Y., Jiang, C., Chen, J., Mao, P., Gao, G., Zhang, L., Wu, S.: Facile fabrication of three-dimensional graphene foam/poly (dimethylsiloxane) composites and their potential application as strain sensor. ACS Appl. Mater. Interfaces **6**(16), 13455–13460 (2014)
8. Chen, W., Huang, Y.-X., Li, D.-B., Yu, H.-Q., Yan, L.: Preparation of a macroporous flexible three dimensional graphene sponge using an ice-template as the anode material for microbial fuel cells. RSC Adv. **4**(41), 21619–21624 (2014)
9. Kong, L., Tang, C., Peng, H.J., Huang, J.Q., Zhang, Q.: Advanced energy materials for flexible batteries in energy storage: a review. SmartMat **1**(1) (2020)
10. Ozer, D., Ertekin, Z.: Nanocomposites of 2D materials for flexible Li-ion batteries. In: Energy Applications of 2D Nanomaterials, pp. 301–318. CRC Press (2022)
11. Lukatskaya, M.R., Dunn, B., Gogotsi, Y.: Multidimensional materials and device architectures for future hybrid energy storage. Nat. Commun. **7**(1), 1–13 (2016)
12. Mo, R., Rooney, D., Sun, K., Yang, H.Y.: 3D nitrogen-doped graphene foam with encapsulated germanium/nitrogen-doped graphene yolk-shell nanoarchitecture for high-performance flexible Li-ion battery. Nat. Commun. **8**(1), 13949 (2017)
13. Xiang, J., Dong, D., Wen, F., Zhao, J., Zhang, X., Wang, L., Liu, Z.: Microwave synthesized self-standing electrode of MoS2 nanosheets assembled on graphene foam for high-performance Li-Ion and Na-Ion batteries. J. Alloy. Compd. **660**, 11–16 (2016)
14. Li, L., Wang, H., Xie, Z., An, C., Jiang, G., Wang, Y.: 3D graphene-encapsulated nearly monodisperse Fe3O4 nanoparticles as high-performance lithium-ion battery anodes. J. Alloy. Compd. **815**, 152337 (2020)
15. Jiang, T., Bu, F., Liu, B., Hao, G., Xu, Y.: Fe 7 Se 8@ C core–shell nanoparticles encapsulated within a three-dimensional graphene composite as a high-performance flexible anode for lithium-ion batteries. New J. Chem. **41**(12), 5121–5124 (2017)
16. Chen, M., Chao, D., Liu, J., Yan, J., Zhang, B., Huang, Y., Lin, J., Shen, Z.X.: Rapid pseudocapacitive sodium-ion response induced by 2D ultrathin tin monoxide nanoarrays. Adv. Func. Mater. **27**(12), 1606232 (2017)

17. Lu, C., Li, Z., Yu, L., Zhang, L., Xia, Z., Jiang, T., Yin, W., Dou, S., Liu, Z., Sun, J.: Nanostructured Bi 2 S 3 encapsulated within three-dimensional N-doped graphene as active and flexible anodes for sodium-ion batteries. Nano Res. **11**, 4614–4626 (2018)
18. Yin, Y., Xiong, F., Pei, C., Xu, Y., An, Q., Tan, S., Zhuang, Z., Sheng, J., Li, Q., Mai, L.: Robust three-dimensional graphene skeleton encapsulated Na3V2O2 (PO4) 2F nanoparticles as a high-rate and long-life cathode of sodium-ion batteries. Nano Energy **41**, 452–459 (2017)
19. Gao, X., Dong, X., Xing, Z., Nie, C., Zheng, G., Ju, Z.: Electrolyte salt chemistry enables 3D nitrogen and phosphorus dual-doped graphene aerogels for high-performance potassium-ion batteries. Adv. Mater. Technol. **6**(8), 2100207 (2021)
20. Chao, D., Zhu, C., Song, M., Liang, P., Zhang, X., Tiep, N.H., Zhao, H., Wang, J., Wang, R., Zhang, H.: A high-rate and stable quasi-solid-state zinc-ion battery with novel 2D layered zinc orthovanadate array. Adv. Mater. **30**(32), 1803181 (2018)
21. Yang, G., Chen, L., Jiang, P., Guo, Z., Wang, W., Liu, Z.: Fabrication of tunable 3D graphene mesh network with enhanced electrical and thermal properties for high-rate aluminum-ion battery application. RSC Adv. **6**(53), 47655–47660 (2016)
22. He, Y., Bi, S., Jiang, C., Song, J.: Recent progress of sulfur cathodes and other components for flexible lithium-sulfur batteries. Mater. Today Sustain. 100181 (2022)
23. Lin, C., Niu, C., Xu, X., Li, K., Cai, Z., Zhang, Y., Wang, X., Qu, L., Xu, Y., Mai, L.: A facile synthesis of three dimensional graphene sponge composited with sulfur nanoparticles for flexible Li–S cathodes. Phys. Chem. Chem. Phys. **18**(32), 22146–22153 (2016)
24. Zhou, G., Li, L., Ma, C., Wang, S., Shi, Y., Koratkar, N., Ren, W., Li, F., Cheng, H.-M.: A graphene foam electrode with high sulfur loading for flexible and high energy Li-S batteries. Nano Energy **11**, 356–365 (2015)
25. Rahman, M.A., Wang, X., Wen, C.: High energy density metal-air batteries: a review. J. Electrochem. Soc. **160**(10), A1759 (2013)
26. Zhong, X., Papandrea, B., Xu, Y., Lin, Z., Zhang, H., Liu, Y., Huang, Y., Duan, X.: Three-dimensional graphene membrane cathode for high energy density rechargeable lithium-air batteries in ambient conditions. Nano Res. **10**, 472–482 (2017)
27. Jiang, Y., Cheng, J., Zou, L., Li, X., Huang, Y., Jia, L., Chi, B., Pu, J., Li, J.: Graphene foam decorated with ceria microspheres as a flexible cathode for foldable lithium-air batteries. ChemCatChem **9**(22), 4231–4237 (2017)
28. Qiu, H.J., Du, P., Hu, K., Gao, J., Li, H., Liu, P., Ina, T., Ohara, K., Ito, Y., Chen, M.: Metal and nonmetal codoped 3D nanoporous graphene for efficient bifunctional electrocatalysis and rechargeable Zn–air batteries. Adv. Mater. **31**(19), 1900843 (2019)
29. Liu, Y., Yang, L., Xie, B., Zhao, N., Yang, L., Zhan, F., Pan, Q., Han, J., Wang, X., Liu, J.: Ultrathin Co3O4 nanosheet clusters anchored on nitrogen doped carbon nanotubes/3D graphene as binder-free cathodes for Al-air battery. Chem. Eng. J. **381**, 122681 (2020)

Recent Development in 3D Graphene for Wearable and Flexible Batteries

Wei Ni and Ling-Ying Shi

Abstract 3D graphene-based flexible materials have attracted ever-increasing attention due to the fantastic intrinsic merits of graphene and its assemblies with high surface area, lightweight, superior electronic conductivity, and outstanding mechanical properties. Thus, 3D graphene-based wearable and flexible materials have been extensively investigated for various promising applications including advanced energy storage and conversion. In this chapter, we conducted a focused review of the recent progress in the design, synthesis, and engineering of 3D graphene materials/architectures as well as their specific applications for advanced wearable and flexible batteries. The major challenges, strategies, and prospects are also discussed for further development of 3D graphene materials for wearable and flexible batteries toward ultimate practical application.

Keywords 3D graphene · Batteries · Flexible · Wearable

1 Introduction

Flexible and wearable electrochemical energy storage devices (EESDs) have attracted tremendous attention as promising adaptive power sources for the fast-growing flexible and wearable smart electronic products market [1–3]. Carbon-based nanomaterials, especially graphene and its derivatives, have aroused intense interest as a vital component for flexible batteries for wearable electronics [4–7]. As a new generation of a special member of the graphene family, 3D graphene materials have been receiving considerable attention over the past decade [8]. Graphene-based 3D

W. Ni (✉)
State Key Laboratory of Vanadium and Titanium Resources Comprehensive Utilization, ANSTEEL Research Institute of Vanadium and Titanium (Iron and Steel), Chengdu 610031, China
e-mail: niwei@iccas.ac.cn; max.ni@hotmail.com

L.-Y. Shi
College of Polymer Science and Engineering, Sichuan University, Chengdu 610065, China

© The Author(s), under exclusive license to Springer Nature Switzerland AG 2023
R. K. Gupta (ed.), *3D Graphene*, Carbon Nanostructures,
https://doi.org/10.1007/978-3-031-36249-1_15

materials have exceptional conductivity, superior surface area, lightweight, favorable mechanical strength, and flexibility, as well as interconnected structures for high mass loading and superior charge transfer, thus for advanced flexible/wearable batteries with both high energy and power densities. 3D graphene materials have recently been exploited for potential applications including but not limited to flexible and wearable IoT stretch sensors (e.g., for real-time armband muscle measurement), (all-solid-state) electrochemical capacitors, alkali-metal–ion batteries, Li–S batteries, Zn–ion and Zn–air batteries, as well as other batteries (e.g., Ni–Fe batteries, Ni–Bi batteries).

2 Structures, Properties, and Methods

3D graphene may be classified into two distinct categories, i.e., macroscopic 3D graphene architecture and microscopic 3D graphene structure; although different from the appearance (e.g., adsorbent materials emphasizing more on macroscopic structure, compared to granular graphene materials emphasizing on microscopic 3D graphene structure to eliminate property changes), they are closely relative and are aiming at avoiding the restacking of 2D graphene layers in practical application [8]. 3D graphene materials inherit the astonishingly synergistic merits of 3D porous structures and exceptional intrinsic characteristics of graphene, thus endowing them with high specific surface area, large pore volume, enhanced mechanical strength, fast electron/ion transfer as ideal candidates for emerging wearable and flexible energy storage and conversion devices.

Graphene plays a vital role of framework, substrate, or modifier in the classic composite/hybrid structures as electrodes for energy storage and conversion [9]. For 3D graphene, the framework structures are usually fabricated by hydrothermal/chemical/electrochemical reduction, freeze drying [10, 11], 3D printing (or direct ink writing, DIW) [12–15], assembly, wet-spinning, (vacuum) filtration [16, 17], template-assisted chemical vapor deposition (CVD), or integrated techniques [18–20]. The as-prepared typical 3D graphene-based electrode materials for wearable or flexible batteries by these techniques include fiber-shaped rGO composites (rGO: reduced graphene oxide) [21], rGO/MnO_2-rGO-CNT nanocomposite membrane (CNT: carbon nanotube) [16], rGO-wrapped CNT/rGO@MnO_2 porous film [10], 3D porous MXene/rGO hybrid film [22], sandwich-structured graphene/NASICON/graphene hybrid film [23], rGO/2D materials (e.g., MoS_2) flexible free-standing porous film [18], rGO/TMOs hybrid paper or film (e.g., NiO microflowers) [17], graphene-regulated carbon cloth [24], graphene-modified SiOC ceramic cloth [11], and graphene aerogel-based composite (e.g., with ultrasmall Co_3O_4, Bi_2S_3 nanorods, MXene/Zn) [19, 20, 25].

It should be noted that some other carbonaceous materials including carbon nanotubes are often incorporated into graphene systems for microstructure adjustment and performance improvement thereof [10, 26]. Some other carbon-based 3D hierarchical electrodes such as carbon nanofiber/$Na_3V_2(PO_4)_3$ freestanding composite, polymer foam/sponge (e.g., melamine foam, MF)-derived flexible freestanding graphene-like carbon foam/paper and its composites [27, 28], or 3D graphene-like porous carbon nanosheets pyrolyzed from hydrocarbons [29] are not mentioned in this specific chapter.

3 Applications

3D graphene can endow the electrodes with high electric/ionic conductivity, flexible merits, and avoid using additional metal current collectors in the conventional battery design; also the lightweight 3D porous graphene framework with interconnected channels lowers the percolation threshold compared to other conductive adhesives (e.g., carbon black particles, 1D carbon nanotubes/nanofibers). In the following paragraphs, we highlighted the most promising rechargeable batteries based on 3D graphene including alkali-metal–ion batteries (Li–ion, Na–ion batteries), Li–S batteries, Zn–ion batteries, Zn–air batteries, and other batteries.

3.1 Li–Ion Batteries

Li–ion batteries (LIBs) hold substantial promise for current and next-generation power devices; 3D graphene provides promising pathways for the development of high power/energy density LIBs via improving the ion/electron transfer, accommodating the volume change and eliminating the conventional nonactive but heavy metal current collectors. For example, a flexible freestanding rGO-wrapped CNT/rGO@MnO_2 porous (GCMP) film with 3D multilevel conductive architecture as anode for LIBs demonstrates an increasing capacity of up to 1344 mAh g^{-1} at a constant current density of 2 A g^{-1} after 630 repeated cycles, as well as a superior rate performance and a prolonged cycling life (609 mAh g^{-1} at 7.5 A g^{-1} after 1000 cycles) [10]. Compared to traditional vacuum filtration method [16], the as-prepared composite film electrode showed enhanced long-term cycling performances; however, the relatively high average potential plateau (e.g., delithiation potential) as well as the lower initial capacity followed by gradual increase with activation may somewhat deteriorate the potential for practical application as advanced anode of high-performance LIBs. Cong et al. designed a soft-packed flexible LIBs by using ultrasmall Co_3O_4/ionic liquid-modified N-doped graphene aerogel (Co_3O_4-GA-IL) [19]. The flexible freestanding 3D porous electrode material could deliver a superior capacity of 1304 mAh g^{-1} at a rate of 0.5C, with an outstanding capacity retention of 98.4% after long-term cycle (500 cycles, 0.003% capacity loss per cycle), as well as an enhanced rate capability of 715 mAh g^{-1} at 5C. The 3D graphene framework with high conductivity and ultrasmall Co_3O_4 with shortened ion diffusion length synergistically improved the overall performance.

MoS_2 is a kind of classic 2D or layered material with significantly higher theoretical capacity (670 mAh g^{-1}) compared with commercial graphite, which simultaneously allows higher rate performance [18, 30]. For example, neuron-like few-layered MoS_2 could be incorporated into the N-doped graphene foam (derived from a GO-modified melamine sponge) to form a freestanding and binder-free anode for high-performance LIBs [30]. The polymer sponge/graphene composite precursor-derived graphene foam showed enhanced mechanical performances and improved charge transfer properties, and thus are showing advantages as freestanding electrodes for flexible soft-package batteries (SPB). For the as-assembled SPB, the freestanding composite electrode demonstrated an excellent specific capacity of 713 mAh g^{-1} at 0.5 A g^{-1} after 200 cycles with an average coulombic efficiency (CE) of 99.5%. It should also be mentioned that MoS_2 usually has a relatively high lithium extraction potential (i.e., delithiation potential) compared with commercial graphite, thus resulting in a lower voltage output for a full cell, although the lithium dendrites are avoided and high-power LIBs can be achieved.

Si-based materials possess much lower potential plateaus compared to conventional transition-metal oxides (TMOs) and thus more suitable for application as anode materials for high-energy-density LIBs. Cai et al. fabricated a nano-Si encapsulated rGO hybrid film as binder-free anode for flexible high-energy-density LIBs [31]. The silicon nanoparticles are confined in multilayered rGO film via zinc-induced redox layer-by-layer assembly followed by freeze drying. With commercial $LiCoO_2$ as cathode, the flexible full cell could deliver a high average voltage of 3.9 V (discharge) along with an initial coulombic efficiency (ICE) of 87.8% and around 97–100% afterward. The high reversible capacity of anode (667 mAh g^{-1} at 0.287 A g^{-1} and 713 mAh g^{-1} at 0.2 A g^{-1}, respectively, after 200 cycles) and low cut-off voltage (0–1.2 V) enhanced the energy density of flexible LIBs. Sang et al. fabricated a graphene-modified SiOC ceramic fiber cloth (3D-GNS/$SiOC_f$) for high-performance flexible LIBs [11]. The incorporation of graphene into the electrospun SiOC fibers enhances the electron transfer and assures the robust lithium storage. As a freestanding anode for LIBs, it demonstrated a high capacity of 924 mAh g^{-1} at 0.1 A g^{-1}, a good rate capacity of 330 mAh g^{-1} at 2 A g^{-1}, and an impressive cycle stability with stable capacity of 686 mAh g^{-1} at 0.5 A g^{-1} over 500 cycles. When configured with $LiFePO_4$ cathode for full-cell test the 3D-GNS/$SiOC_f$ anode exhibited a good electrochemical performance (with a high capacity of 703 mAh g^{-1} at 0.1 A g^{-1} after 100 cycles, and acceptable rate capacities) along with favorable flexible features, which could shed light on the design and engineering of general electrospun flexible devices. However, for these flexible electrodes, the simultaneous realization of high strength, high active material loading, and high cycling stability is still a challenge for competitive real-world application.

Mo et al. designed a 3D N-doped graphene composite foam comprised of Ge/graphene yolk–shell nanostructures (Ge-QD@NG/NGF) for high-performance flexible LIBs [32]. The N-doped graphene foam framework was first fabricated by a classic CVD method using a commercial porous nickel foam template and the common N,C-containing precursors (e.g., pyridine), followed by incorporating Ge quantum dots into the framework and removing the template. The interspace between yolks (quantum dots) and shell (N-doped graphene) could be tuned by the mediation of an etchable electroplating deposition layer (Fig. 1 a–e). As a highly conductive 3D interconnected porous N-doped graphene composite anode for LIBs, it demonstrated a superior specific capacity of 1220 mAh g^{-1} at 1C (here 1C = 1600 mAh g^{-1}), long-term cycle stability (with capacity retention of >96% from 2 to 1000 cycle, and an average CE of ~99.7%), excellent rate performance (1001 and 801 mAh g^{-1} at 10 and 40 C, respectively), and negligible overpotential and capacity loss (<2%) under bend state (Fig. 1f–h). The nickel foam-derived flexible 3D graphene anode with incorporated alloying materials (e.g., Si, Ge, Sn) paves a way for the development of flexible high-specific-capacity electrode systems, especially for those active materials with huge volume expansion. However, it should be noted that these Ni or Cu foam-derived lightweight 3D graphene frameworks may show uncompetitive volumetric capacity due to their lower tap density.

For the 3D printable LIBs, the graphene nanoplatelets may serve as conductive components for the preparation of printable electrode filaments as primary materials of 3D-printed electrodes, i.e., the classic and low-cost fused filament fabrication (FFF) or DIW [12, 15]. However, the content of active materials is low in the polymer-based filaments and higher energy densities are required for competitive applications. Active conductive fillers such as functional graphene may be a new class of promising alternative nanomaterials for 3D-printed electrodes and the full cells thereof. Furthermore, the 3D printing technique may be exploited for advanced batteries in arbitrary geometry to fulfill a customized product design with integrated batteries, which could simultaneously serve as a structural component in the wearable electronic devices.

3.2 Na-Ion Batteries

The most significant advantage of Na–ion batteries (SIBs) comes from the abundance of sodium in the Earth's crust as well as the low cost compared to lithium. SIBs are emerging as one kind of the most cost-effective rechargeable batteries and are getting more competitive and poised for rapid growth as an alternative to LIBs. To date, most flexible SIBs are based on graphene and carbon nanotubes, some electrospun carbon nanofibers are also referred to. Fiber battery is another kind of the most promising wearable devices, featured by their flexibility and knittability/weavability. However, the sluggish ion transport kinetics, owing to the limited interfacial intimacy and lowered conductivity of solid/gel-type electrolytes, have hindered their practical application. 3D graphene frameworks with interconnected tunnel could provide exclusive fast ion transport along with intrinsic electron conductivity. Wang et al. fabricated a wet-spun fibrous, 3D porous cathode comprised of 2D tungstate nanosheets and graphene nanosheets both with rigid and open lattice structures as well as molecular/atomic thickness and large lateral size (Fig. 2a–f) [21]. When configured with sodium or lithium metal fiber anode, the as-assembled fiber-shaped SIB and LIB

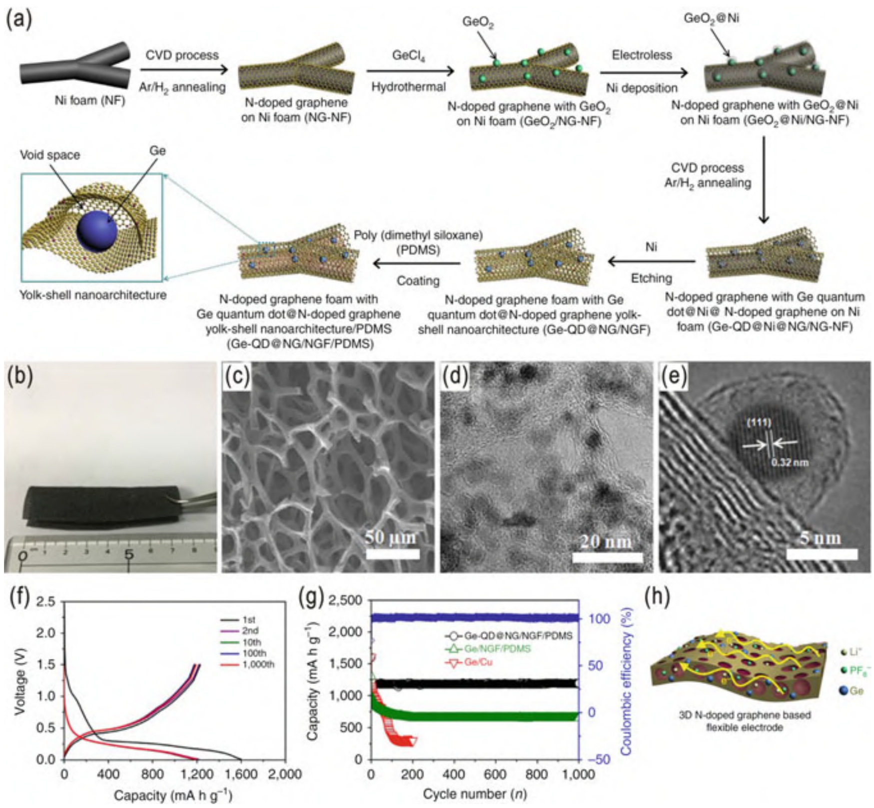

Fig. 1 **a** Schematic illustration of the preparation process of 3D N-doped graphene foam with encapsulated Ge-quantum-dot@N-doped graphene yolk–shell (denoted as Ge-QD@NG/NGF/PDMS) nanoarchitectures. PDMS: polydimethylsiloxane. **b** Photograph of the as-prepared flexible Ge-QD@NG/NGF electrode (size of 7 × 4 cm), and **c**–**e** the corresponding SEM and TEM images. **f** Galvanostatic charge–discharge (GCD) profiles in the potential window of 0.01–1.5 V (vs. Li/Li$^+$) at 1C rate, and **g** the cycling performance and CE of the Ge-QD@NG/NGF/PDMS electrode, compared to Ge/NGF/PDMS and Ge/Cu electrodes (1C, 1000 cycles). **h** Schematic illustration showing the advantages of the NGF-based flexible electrode structure. Adapted from reference [32]. Copyright The Authors, some rights reserved; exclusive licensee Springer Nature. Distributed under a Creative Commons Attribution License 4.0 (CC BY) https://creativecommons.org/licenses/by/4.0/

showed superior capacities (178 mAh g^{-1} for SIB and 206 mAh g^{-1} for LIB, respectively), outstanding rate performance, long-term cycle stability (up to 1000 cycles), and excellent flexibility (up to 200 bending cycles). Besides the structural advantages, the high-proportion pseudocapacitive charge storage contributes greatly to the enhanced capacities (Fig. 2g–i). The 3D graphene fiber-based electrodes provide new insight into the elegant engineering of fiber electrodes and the resultant fiber energy storage devices including fiber batteries; however, the strength of the fiber electrodes and the batteries thereof as well as the safety of the alkali-metal-based batteries needs to be further enhanced for actual wearable applications.

NASICON-type materials such as $NaTi_2(PO_4)_3$ with open 3D framework as well as the high thermal stability and superior Na^+ conductivity are another kind of promising anode materials for SIBs [33, 34]. $NaTi_2(PO_4)_3$ can be combined with graphene to form flexible freestanding electrode, e.g., sandwich-like GN/$NaTi_2(PO_4)_3$/GN film [23]. It can deliver a high specific capacity of 137 mAh g^{-1} at a current density of 0.1 A g^{-1} and a high rate capacity of 93 mAh g^{-1} at 1 A g^{-1}, as well as an excellent cycle stability with 92% capacity retention at 0.5 A g^{-1} after 1000 cycles. When configured with a typical cathode material, $Na_{0.44}MnO_2$, the full cell (voltage window of 4–2 V) demonstrated a high initial

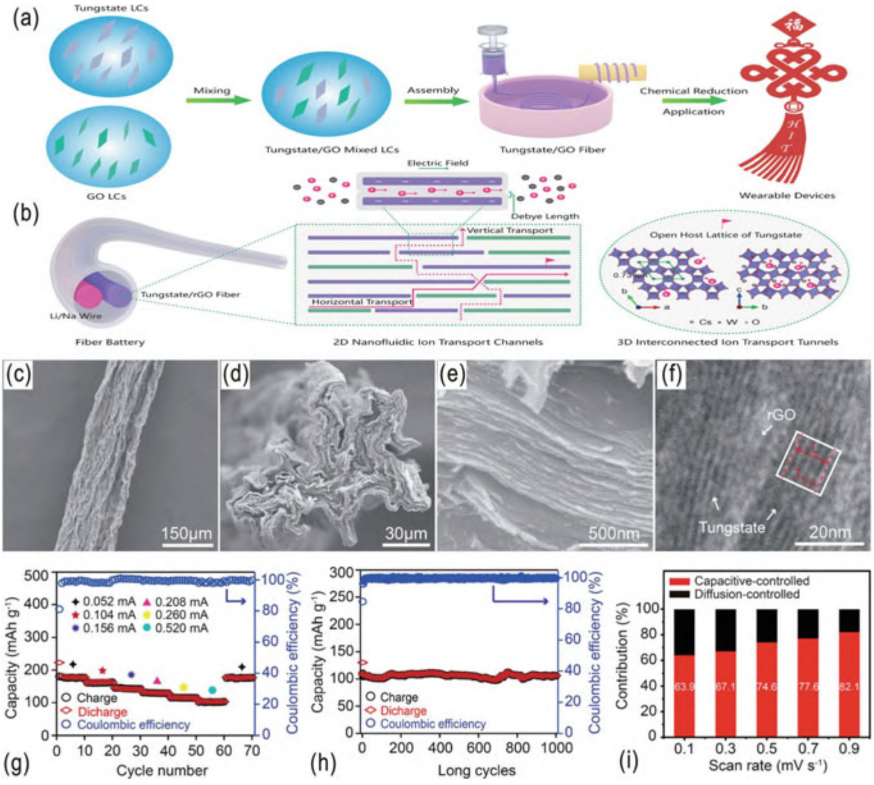

Fig. 2 **a** and **b** Schematic illustration of the preparation procedure of fiber electrode from 2D tungstate nanosheets, and the ion transport inside the fiber electrode. **c**–**e** SEM images of the tungstate/rGO fiber at different magnifications, and **f** the corresponding cross-sectional HRTEM image (HRTEM: high-resolution transmission electron microscopy). **g** rate performance of the fiber battery at different current densities (0.052–0.520 mA), and **h** the cycle performance and corresponding CE at 0.520 mA. **i** contribution ratio of capacitive-controlled (red color) and diffusion-controlled (black color) capacities at various scan rates. Adapted with permission [21], copyright (2020), the royal society of chemistry

capacity of 114 mAh g^{-1} (discharge at 0.1 mA g^{-1}, based on anode mass) and a high ICE of 82.3%. However, it should be noted that these NASICON-type high potential negative electrode materials somewhat deteriorate the voltage output and energy density of the full cell compared to Na metal anode, although theoretically and ideally the Na metal and its hybrids/composites are most eagerly anticipated for flexible SIBs.

Some other transition-metal chalcogenides (TMCs) were also applied as flexible anode materials for SIBs, e.g., graphene paper hybrids with CuS nanoflowers (flower-like microspheres) [35] and SnSe nanosheets [36] fabricated by a facile vacuum filtration approach. However, for transition-metal sulfides (TMSs) the low ICE should be paid particular attention for appropriate solutions. Compared to sulfides, the selenides possess lower Na–ion insertion/extraction potential and enhanced conductivity [37], thus for a battery with higher output voltage and enhanced rate performance. The annealing and presodiation of GO or rGO are effective strategies to improve the ICE.

3.3 Li–S Batteries

Due to the high mechanical flexibility and superior charge transfer merits, 3D graphene with multiscale structures holds great promise for energy storage; by incorporation of lithium–sulfur batteries (LSBs) featured by high theoretical energy density (2600 Wh kg^{-1}) and low cost, the 3D graphene-based flexible lithium–sulfur batteries (FLSBs) may demonstrate synergistic effects to overcome some of the critical obstacles faced by traditional LSBs and realize the simultaneous achievement of good flexibility, high energy density, and long cycle life [9, 38]. For example, Ni et al. designed a honeycomb-like graphene/sulfur composite film with multi-scale sulfur particles confined in the ultrathin but robust freestanding electrode via a facile vacuum filtration method (Fig. 3a–c) [39]. The as-prepared flexible composite cathode of Li–S batteries shows an enhanced specific capacity of 823 mAh g^{-1} at 0.5C after 100 cycles. The adoption of biosurfactant tuned the dimensions of the sulfur particles and increased the interfacial adhesion, thus for an enhancement of the flexibility and strength of the thin freestanding electrode in addition to the increased utilization of sulfur. These freestanding/flexible graphene/sulfur cathodes can be further incorporated with specific multifunctional separators/interlayers (e.g., polysulfone-functionalized separators, boron nitride–graphene interlayers) or advanced Li-metal-hosting anodes (e.g., 3D nanostructured lithium cloth or other carbon-based lithium hosts [40] with the adoption of Li metal anode but suppressed formation of Li dendrites) for high-performance flexible Li–S batteries with high energy density, long cycle life, and enhanced safety (Fig. 3d) [41, 42].

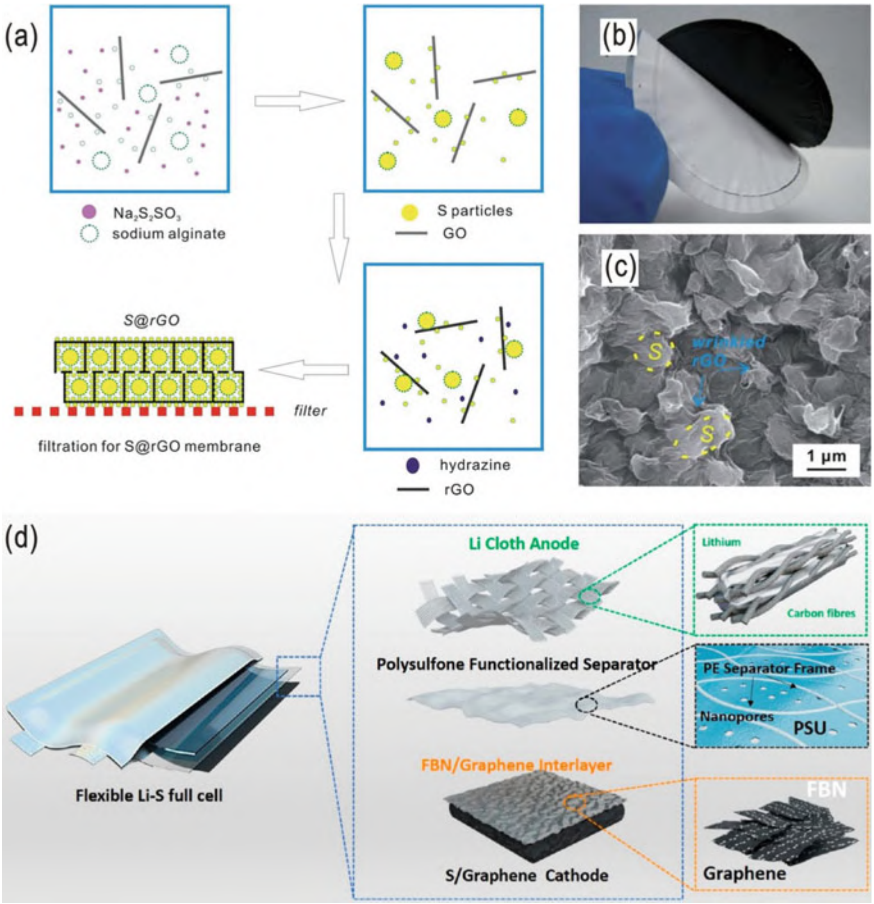

Fig. 3 **a** Schematic illustration of the synthesis procedure for the honeycomb-like S@rGO ultrathin nanocomposite membrane, and **b** and **c** the corresponding digital photo and SEM image of the upper surface of nanocomposite membrane. Adapted with permission [39], copyright (2016), the royal society of chemistry. **d** schematic illustration of a typical flexible soft-packed Li–S full cell, configured by lithium cloth anode, PSU-Celgard separator, and FBN/G interlayer protected free-standing graphene/sulfur cathode. PSU: polysulfone; FBN: functionalized boron nitride nanosheets. Adapted with permission [41], copyright (2020), American chemical society

The addition of graphene to other 3D matrices (e.g., MXene, cellulose nanofiber) can also improve the conductivity and enhance the immobilization/conversion of polysulfides. The incorporation of nanofillers such as cellulose nanocrystalline/nanofiber could improve the mechanical properties [43]. For more information on graphene/sulfur nanocomposites as cathode/anode materials and separators/interlayers for Li–S batteries, one may refer to some recent critical reviews [9, 42].

3.4 Zn-Ion and Zn–Air Batteries

Aqueous rechargeable Zn–ion batteries (ZIBs) with intrinsic safety and low cost have been revived due to the growing popular demand for wearable and portable electronics; however, the dendrite and low flexibility of zinc metal anode are hampering their practical application. 3D carbon frameworks, especially 3D graphene, are ideal materials for the construction of flexible freestanding anode as well as cathode [44]. Cao et al. fabricated a robust and dendrite-free electrodeposited Zn anode by in situ growth of 3D N-doped vertical graphene nanosheets on the carbon cloth (N-VG@CC, PECVD method) for uniform Zn nucleation (Fig. 4a–c) [24]. The N-containing groups (zincophilic) in the framework lowered the Zn nucleation overpotential due to the enhanced interaction between Zn^{2+} and N-VG, thus for uniform distribution of Zn nuclei; together with the synergistic effect of 3D graphene with homogenized electric distribution for optimized Zn deposition process, it suppressed the dendrite growth and significantly improved the Zn plating/stripping process (more reversible and higher CE) (Fig. 4d). When configured with elaborately fabricated cathode, MnO_2@N-VG@CC (similar structure with anode), the flexible ZIBs (quasi-solid-state) showed superior cycling performance with a high capacity retention of 80% over 300 cycles as well as excellent mechanical flexibility (Fig. 4e–g). The robust 3D graphene@CC framework could be a promising candidate for ultimate application of portable/wearable electronics [24, 45]. Some graphene-based aerogel hybrid with encapsulated Zn for foldable ZIB are also explored, these hybrid aerogels featured by abundant zincophilic micropores are showing even higher performances; however, additional current collector (e.g., Ti foil) is used, and further critical investigation is needed for real-world application as wearable/flexible batteries [25].

Rechargeable Zn–air batteries (ZABs) are another kind of promising energy storage device for flexible and wearable electronics, due to the high theoretical energy density (1086 Wh kg^{-1}), cost-effectiveness, inherent safety, and environmental friendliness [46]. 3D graphene with favorable honeycomb nanostructures (i.e., macroporous channels) could also be applied as efficient frameworks/skeletons of cathode in flexible/wearable rechargeable ZABs owing to the enhanced air/electrolyte permeability and efficient air diffusion compared to carbon membrane or carbon cloth. For example, Wu et al. fabricated an iron-decorated carbon aerogel (FeP/Fe_2O_3@N,P-doped rGO/CNF, abbr. FeP/Fe_2O_3@NPCA; CNF: cellulose nanofibril) with high ORR and OER catalysis activities (ORR, oxygen reduction reaction; OER, oxygen evolution reaction) via freeze-drying and pyrolysis (Fig. 5a–d) [46]. The as-obtained freestanding FeP/Fe_2O_3@NPCA air cathode for flexible solid-state ZAB (with classic alkaline PVA gel electrolyte) showed high mechanical stability (especially compressibility), an excellent specific capacity of 676 mAh g^{-1} and energy density of 517 Wh kg^{-1} (at 20 mA cm^{-2}), as well as small overpotential, distinct flexibility, and good cycling stability (Fig. 5e–g). It offers an alternative strategy for the design and preparation of competitive bifunctional air cathodes of ZABs. Some similar works by adhering/pressing the functional graphene (e.g., via CVD) to glassy carbon or carbon cloth also showed comparable performances [47].

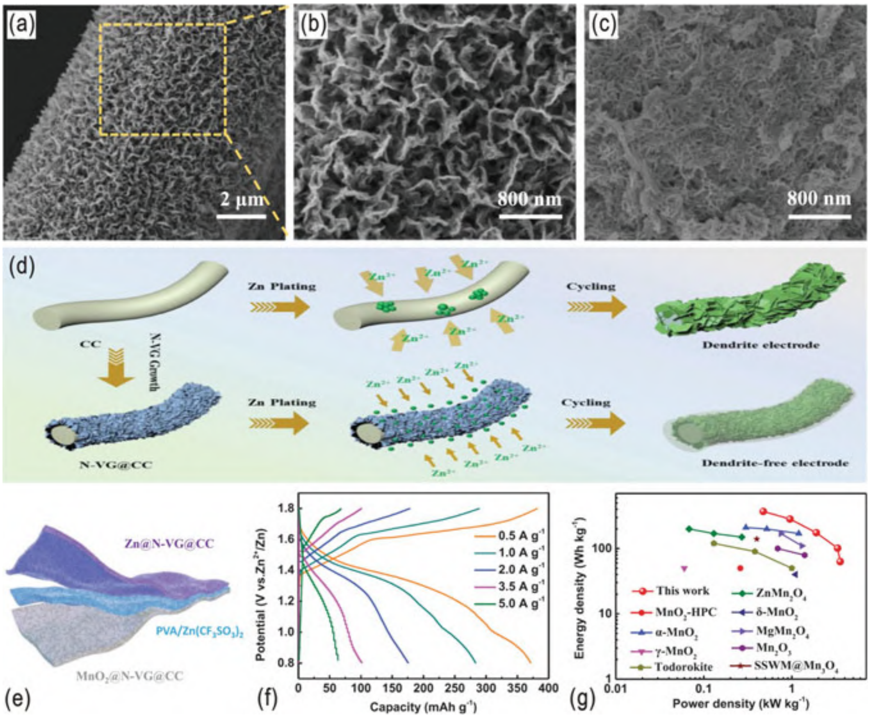

Fig. 4 SEM images of **a** and **b** the intermediate N-VG@CC at different magnifications and **c** the resultant Zn@N-VG@CC anode. **d** schematic illustration of Zn plating on CC and N-VG@CC electrodes, showing the effect of N-VG on Zn deposition. **e** schematic illustration of the construction of the flexible quasi-solid-state ZIB. **f** GCD curves of the as-designed ZIB at various current densities, and **g** the corresponding Ragone plot, compared with other reported energy storage devices. Adapted with permission [24], Copyright (2021) Wiley–VCH GmbH

Some researches also referred to rGO/MXene-coated nickel foam as air cathodes for flexible ZABs.

3.5 *Other Batteries*

Some other kinds of flexible or compressible quasi-solid-state batteries such as Ni–Fe batteries (QSS-NFB), Ni–Bi batteries have also been fabricated for flexible or compression-tolerant electronics. However, for these nickel-based aqueous batteries, self-discharge rate and power/energy density should be further improved. Kong et al. 3D-printed a series of freestanding electrodes with diverse structural configurations for Ni–Fe batteries [48]. The hierarchically porous rGO/CNTs composite electrodes were fabricated by the classic extrusion-based 3D printing technology, with embedded ultrathin $Ni(OH)_2$ nanosheet array serving as cathode, and with holey

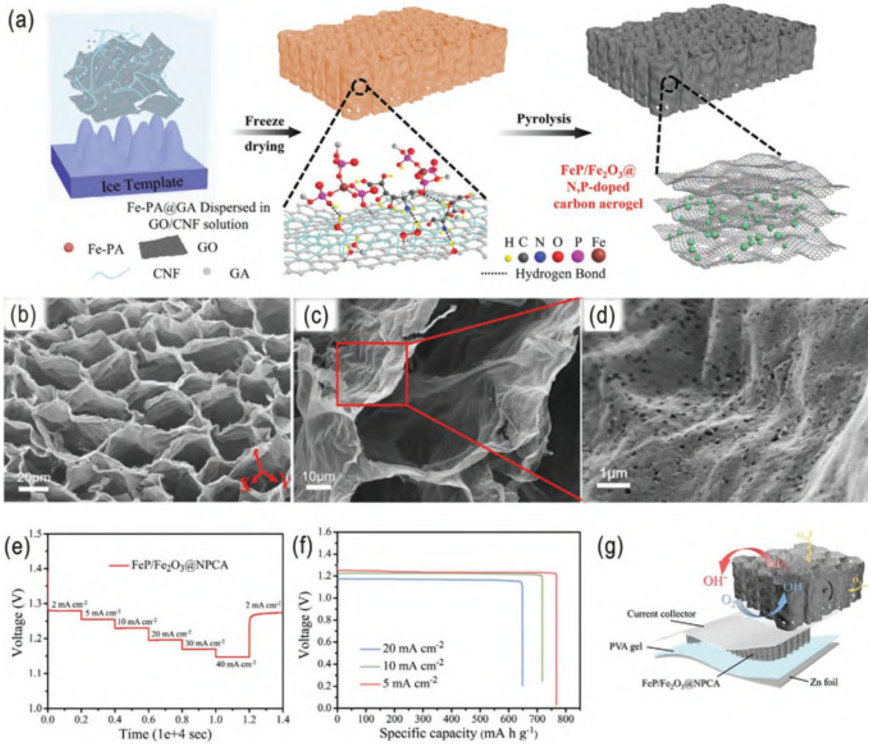

Fig. 5 **a** Schematic illustration of the fabrication of FeP/Fe_2O_3@NPCA air cathode of Zn–air battery (ZAB). **b–d** SEM images of FeP/Fe_2O_3@NPCA at different magnifications. **e** and **f** Rate performance (discharge) of FeP/Fe_2O_3@NPCA-based ZAB and the corresponding discharge curves (galvanostatic) at varied current densities (with specific capacity normalized by consumed Zn mass). **g** Schematic illustration of the solid-state ZAB with FeP/Fe_2O_3@NPCA working as freestanding air cathode. Adapted with permission [46], Copyright (2020), WILEY–VCH Verlag GmbH & Co. KGaA, Weinheim

Fe_2O_3 nanorod array serving as anode, respectively (Fig. 6a). When configured as a full cell, the QSS-NFB showed an outstanding long-term cycling stability (with a capacity retention of 91.3% over 10,000 cycles), a superior energy density of 28.1 mWh cm^{-3} (at a power density of 10.6 mW cm^{-3}), as well as a high loading of active materials of over 130 mg cm^{-3} and favorable compressibility (up to 60%) (Fig. 6b–d). Wang et al. fabricated a fiber-shaped Ni–Bi battery via coaxial coating of CNT fibers with electrodeposited 3D honeycomb-like rGO. For the fibrous hierarchical electrodes, NiO/Ni-containing electrode is working as cathode and the Bi metal-containing electrode as anode [49]. The fiber-shaped Ni–Bi battery (rGO/Ni/NiO/CNT//rGO/Bi/CNT) could deliver a high capacity of 164 mAh g^{-1} at 5 A g^{-1}, enhanced by the incorporation of graphene, i.e., 187% increase compared to original Bi/CNT anode, as well as 115% increase by introducing rGO/NiO/Ni. Also it showed a high energy density of 43.4 Wh kg^{-1} (or 26.0 mWh cm^{-3}) and a high power

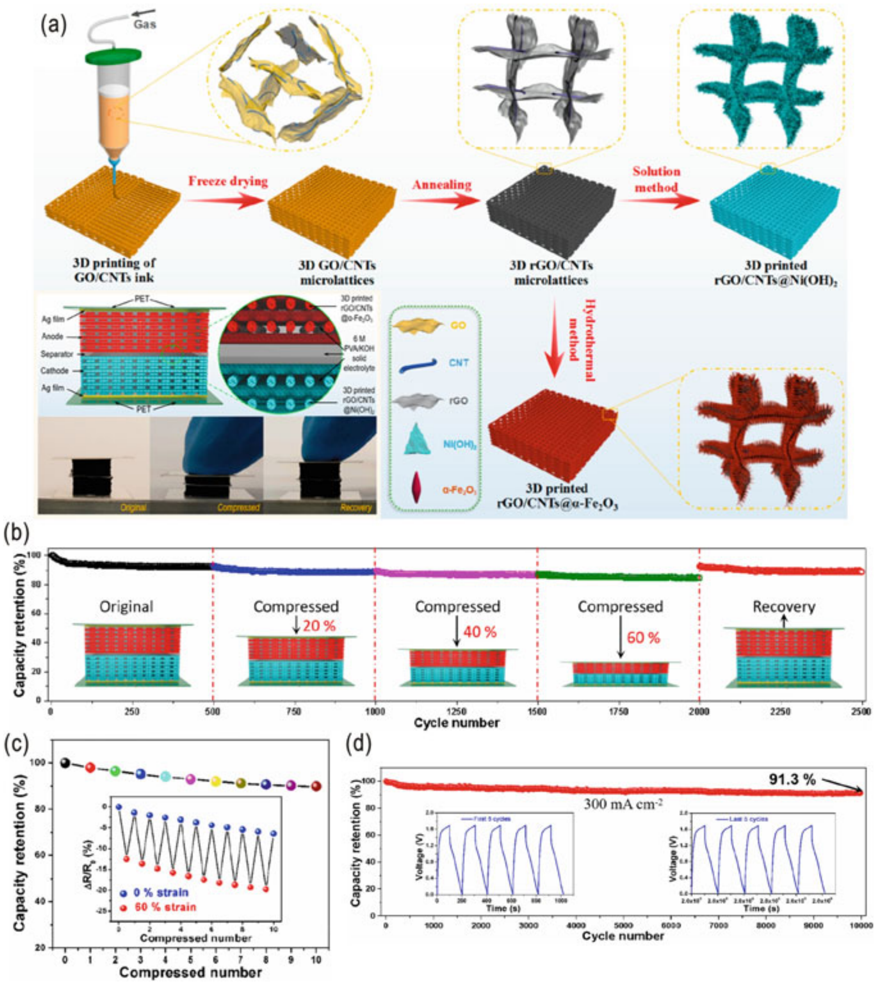

Fig. 6 **a** Schematic illustration of the preparation of rGO/CNTs@Ni$(OH)_2$ cathode and rGO/CNTs@α-Fe_2O_3 anode by 3D printing, and the corresponding configuration and compressibility of the as-prepared quasi-solid-state Ni–Fe battery (QSS-NFB). **b** cycle performance of the QSS-NFB at varied compression states at a constant current density of 200 mA cm^{-2}, and **c** the corresponding capacity retention of the QSS-NFB as a function of compression cycle number (inset: variation of electrical resistance with repeated compression up to 60% strain). **d** long-term cycling performance of the 3D-printed QSS-NFB (10,000 cycles at 300 mA cm^{-2}; insets: GCD curves for the initial 5 cycles and the last 5 cycles, respectively). Adapted with permission [48], copyright (2020) American chemical society

density of 6.6 kW kg^{-1} (or 4.0 W cm^{-3}), as well as an ultrahigh capacity retention of 96% after 10,000 cycles. Although the output voltage of Ni–Bi batteries is lower than that of Ni–Fe batteries, their high-rate performance demonstrates promising high-power applications. Some similar solid-state flexible/wearable batteries based on fiber-shaped electrodes are assembled to extend their practical application [50].

These abovementioned nickel-based batteries are beneficial addition to the family of flexible/wearable quasi-solid-state aqueous rechargeable batteries beyond alkali-metal–ion batteries and multivalent metal–ion batteries, and are showing great promise for safe, low-cost, and even large-scale electrochemical energy storage systems. Moreover, some novel batteries such as flexible H_2O_2 microfluidic fuel cell and dye-sensitized solar cell are also of research interest.

4 Challenges and Perspectives

3D graphene with specific structures possesses great advantages of integral conductivity of the electrodes, and the inherently soft framework with high surface area ensures the overall structural stability, high active material loading, and compatibility for advanced flexible/wearable rechargeable batteries. However, the simultaneous combination of electrochemical, mechanical properties, and cost performance index (CPI or price–performance ratio) is challenging, which may eventually determine its practical application and industrialization in wearable and flexible energy storage field.

(1) The microstructure control (e.g., for ordered structure) to rationally reduce the undesired defects could enhance the mechanical flexibility; some favorable defects may improve the electrochemical performances, thus, the physical/chemical defects should be weighed in the balance and an optimized synergy is favored.
(2) Carbon/graphite fibers and carbon cloth, as well as carbon nanotube foam, are versatile platforms for the fabrication of various robust flexible and wearable batteries, including rechargeable alkali-metal–ion batteries, Zn-ion and Zn–air batteries, Ni–Fe batteries, all-solid-state hybrid capacitors, etc. Some metal wires (such as stainless steel, copper) are often used as conductive backbone for flexible energy storage devices; however, these matrices/substrates may be relatively heavier and the reduced energy density limits its wide application.
(3) For some composite electrodes, suspending or thickening agents such as nanofibrillated cellulose (NFC) may be introduced to assist the preparation and/or performance of 3D graphene materials with enhanced structural uniformity and stability.
(4) The incorporation of high-energy-density materials and functional materials with 3D graphene such as sulfur for flexible Li–S batteries and electrocatalysts for metal–air or metal–CO_2 batteries is of great promise. Besides the promising

cathode materials, 3D graphene can also serve as efficient anode materials or (multi)functional components in advanced flexible/wearable batteries.

(5) More novel and compatible configuration designs of electrodes, electrolytes, and the energy storage devices should be explored for portable and wearable/flexible electronics. And general and consistent standards should be established for the evaluation of these unconventional energy storage devices regarding to their mechanical and electrochemical properties.

References

1. Fu, K.K., Cheng, J., Li, T., Hu, L.: Flexible batteries: from mechanics to devices. ACS Energy Lett. **1**, 1065–1079 (2016)
2. Xiang, F., Cheng, F., Sun, Y., Yang, X., Lu, W., Amal, R., Dai, L.: Recent advances in flexible batteries: from materials to applications. Nano Res. **16**, 4821–4854 (2023)
3. Nasreldin, M., de Mulatier, S., Delattre, R., Ramuz, M., Djenizian, T.: Flexible and stretchable microbatteries for wearable technologies. Adv. Mater. Technol. **5**, 2000412 (2020)
4. Wu, Z., Wang, Y., Liu, X., Lv, C., Li, Y., Wei, D., Liu, Z.: Carbon-nanomaterial-based flexible batteries for wearable electronics. Adv. Mater. **31**, 1800716 (2019)
5. Chen, K., Wang, Q., Niu, Z., Chen, J.: Graphene-based materials for flexible energy storage devices. J. Energy Chem. **27**, 12–24 (2018)
6. Kim, S.D., Sarkar, A., Ahn, J.-H.: Graphene-based nanomaterials for flexible and stretchable batteries. Small **17**, 2006262 (2021)
7. Dai, C., Sun, G., Hu, L., Xiao, Y., Zhang, Z., Qu, L.: Recent progress in graphene-based electrodes for flexible batteries. InfoMat **2**, 509–526 (2020)
8. Sun, Z., Fang, S., Hu, Y.H.: 3D graphene materials: from understanding to design and synthesis control. Chem. Rev. **120**, 10336–10453 (2020)
9. Yang, T., Xia, J., Piao, Z., Yang, L., Zhang, S., Xing, Y., Zhou, G.: Graphene-based materials for flexible lithium–sulfur batteries. ACS Nano **15**, 13901–13923 (2021)
10. Li, S., Zhao, Y., Liu, Z., Yang, L., Zhang, J., Wang, M., Che, R.: Flexible graphene-wrapped carbon nanotube/graphene@MnO_2 3D multilevel porous film for high-performance lithium-ion batteries. Small **14**, 1801007 (2018)
11. Sang, Z., Yan, X., Wen, L., Su, D., Zhao, Z., Liu, Y., Ji, H., Liang, J., Dou, S.X.: A graphene-modified flexible SiOC ceramic cloth for high-performance lithium storage. Energy Storage Mater. **25**, 876–884 (2020)
12. Reyes, C., Somogyi, R., Niu, S., Cruz, M.A., Yang, F., Catenacci, M.J., Rhodes, C.P., Wiley, B.J.: Three-dimensional printing of a complete lithium ion battery with fused filament fabrication. ACS Appl. Energy Mater. **1**, 5268–5279 (2018)
13. Zhang, Y., Shi, G., Qin, J., Lowe, S.E., Zhang, S., Zhao, H., Zhong, Y.L.: Recent progress of direct ink writing of electronic components for advanced wearable devices. ACS Appl. Electron. Mater. **1**, 1718–1734 (2019)
14. Zhang, S., Liu, Y.Q., Hao, J.N., Wallace, G.G., Beirne, S., Chen, J.: 3D-printed wearable electrochemical energy devices. Adv. Funct. Mater. **32**, 2103092 (2022)
15. Jiang, Y., Guo, F., Liu, Y., Xu, Z., Gao, C.: Three-dimensional printing of graphene-based materials for energy storage and conversion. SusMat **1**, 304–323 (2021)
16. Li, Y., Ye, D., Shi, B., Liu, W., Guo, R., Pei, H., Xie, J.: Free-standing reduced graphene oxide/MnO_2–reduced graphene oxide–carbon nanotube nanocomposite flexible membrane as an anode for improving lithium-ion batteries. Phys. Chem. Chem. Phys. **19**, 7498–7505 (2017)
17. Fu, J., Kang, W., Guo, X., Wen, H., Zeng, T., Yuan, R., Zhang, C.: 3D hierarchically porous NiO/Graphene hybrid paper anode for long-life and high rate cycling flexible Li-ion batteries. J. Energy Chem. **47**, 172–179 (2020)

18. Chao, Y., Jalili, R., Ge, Y., Wang, C., Zheng, T., Shu, K., Wallace, G.G.: Self-assembly of flexible free-standing 3D porous MoS_2-reduced graphene oxide structure for high-performance lithium-ion batteries. Adv. Funct. Mater. **27**, 1700234 (2017)
19. Cong, L., Zhang, S., Zhu, H., Chen, W., Huang, X., Xing, Y., Xia, J., Yang, P., Lu, X.: Structure-design and theoretical-calculation for ultrasmall Co_3O_4 anchored into ionic liquid modified graphene as anode of flexible lithium-ion batteries. Nano Res. **15**, 2104–2111 (2022)
20. Lu, C., Li, Z., Yu, L., Zhang, L., Xia, Z., Jiang, T., Yin, W., Dou, S., Liu, Z., Sun, J.: Nanostructured Bi_2S_3 encapsulated within three-dimensional N-doped graphene as active and flexible anodes for sodium-ion batteries. Nano Res. **11**, 4614–4626 (2018)
21. Wang, Y., Zheng, Y., Zhao, J., Li, Y.: Flexible fiber-shaped lithium and sodium-ion batteries with exclusive ion transport channels and superior pseudocapacitive charge storage. J. Mater. Chem. A **8**, 11155–11164 (2020)
22. Ma, Z., Zhou, X., Deng, W., Lei, D., Liu, Z.: 3D porous MXene (Ti_3C_2)/reduced graphene oxide hybrid films for advanced lithium storage. ACS Appl. Mater. Interfaces **10**, 3634–3643 (2018)
23. Guo, D., Qin, J., Zhang, C., Cao, M.: Constructing flexible and binder-free $NaTi_2(PO_4)_3$ film electrode with a sandwich structure by a two-step graphene hybridizing strategy as an ultrastable anode for long-life sodium-ion batteries. Cryst. Growth Des. **18**, 3291–3301 (2018)
24. Cao, Q.H., Gao, H., Gao, Y., Yang, J., Li, C., Pu, J., Du, J.J., Yang, J.Y., Cai, D.M., Pan, Z.H., Guan, C., Huang, W.: Regulating dendrite-free zinc deposition by 3D zincopilic nitrogen-doped vertical graphene for high-performance flexible Zn-ion batteries. Adv. Funct. Mater. **31**, 2103922 (2021)
25. Zhou, J., Xie, M., Wu, F., Mei, Y., Hao, Y., Li, L., Chen, R.: Encapsulation of metallic Zn in a hybrid MXene/graphene aerogel as a stable Zn anode for foldable Zn-ion batteries. Adv. Mater. **34**, 2106897 (2022)
26. Ni, W., Shi, L.: Layer-structured carbonaceous materials for advanced Li-ion and Na-ion batteries: beyond graphene. J. Vac. Sci. Technol. A **37**, 040803 (2019)
27. Wang, B., Yuan, W., Zhang, X., Xiang, M., Zhang, Y., Liu, H., Wu, H.: Sandwiching defect-rich $TiO_2-\delta$ nanocrystals into a three-dimensional flexible conformal carbon hybrid matrix for long-cycling and high-rate Li/Na-ion batteries. Inorg. Chem. **58**, 8841–8853 (2019)
28. Wang, Y., Kong, D., Huang, S., Shi, Y., Ding, M., Von Lim, Y., Xu, T., Chen, F., Li, X., Yang, H.Y.: 3D carbon foam-supported WS_2 nanosheets for cable-shaped flexible sodium ion batteries. J. Mater. Chem. A **6**, 10813–10824 (2018)
29. Wang, Y.S., Yang, J., Liu, S.Y., Che, X.G., He, S.J., Liu, Z.B., Wang, M., Wang, X.T., Qiu, J.S.: 3D graphene-like oxygen and sulfur-doped porous carbon nanosheets with multilevel ion channels for high-performance aqueous Zn-ion storage. Carbon **201**, 624–632 (2023)
30. Chen, F., Yuan, J., Zhou, M., Gui, H., Xiang, Y., Yang, J., Li, X., Xu, C., Wang, R.: Compressible neuron-like 3D few-layered MoS_2/N-doped graphene foam as freestanding and binder-free electrodes for high-performance lithium-ion batteries. ACS Appl. Energy Mater. **5**, 7249–7259 (2022)
31. Cai, X., Liu, W., Zhao, Z., Li, S., Yang, S., Zhang, S., Gao, Q., Yu, X., Wang, H., Fang, Y.: Simultaneous encapsulation of nano-Si in redox assembled rGO film as binder-free anode for flexible/bendable lithium-ion batteries. ACS Appl. Mater. Interfaces **11**, 3897–3908 (2019)
32. Mo, R., Rooney, D., Sun, K., Yang, H.Y.: 3D nitrogen-doped graphene foam with encapsulated germanium/nitrogen-doped graphene yolk-shell nanoarchitecture for high-performance flexible Li-ion battery. Nat. Commun. **8**, 13949 (2017)
33. Wu, M., Ni, W., Hu, J., Ma, J.: NASICON-structured $NaTi_2(PO_4)_3$ for sustainable energy storage. Nano-Micro Lett. **11**, 44 (2019)
34. Ni, W., Shi, L.: 2D and Layered Ti-based materials for supercapacitors and rechargeable batteries: synthesis, properties, and applications. Curr. Appl. Mater. **1**, e200521193451 (2022)
35. Liu, W., Shi, B., Wang, Y., Li, Y., Pei, H., Guo, R., Hou, X., Zhu, K., Xie, J.: A flexible, binder-free graphene oxide/copper sulfides film for high-performance sodium ion batteries. ChemistrySelect **3**, 5608–5613 (2018)

36. Kong, P., Zhu, L., Li, F., Xu, G.: Self-supporting electrode composed of SnSe nanosheets, thermally treated protein, and reduced graphene oxide with enhanced pseudocapacitance for advanced sodium-ion batteries. ChemElectroChem **6**, 5642–5650 (2019)
37. Wei, Z., Wang, L., Zhuo, M., Ni, W., Wang, H., Ma, J.: Layered tin sulfide and selenide anode materials for Li- and Na-ion batteries. J. Mater. Chem. A **6**, 12185–12214 (2018)
38. Zhang, Y., Gao, Z., Song, N., He, J., Li, X.: Graphene and its derivatives in lithium–sulfur batteries. Mater. Today Energy **9**, 319–335 (2018)
39. Ni, W., Cheng, J., Li, X., Guan, Q., Qu, G., Wang, Z., Wang, B.: Multiscale sulfur particles confined in honeycomb-like graphene with the assistance of bio-based adhesive for ultrathin and robust free-standing electrode of Li–S batteries with improved performance. RSC Adv. **6**, 9320–9327 (2016)
40. Chen, S., Chen, S., Han, D., Bielawski, C.W., Geng, J.: Carbon-based materials as lithium hosts for lithium batteries. Chem. Eur. J. **28**, e202201580 (2022)
41. Yu, B., Fan, Y., Mateti, S., Kim, D., Zhao, C., Lu, S., Liu, X., Rong, Q., Tao, T., Tanwar, K.K., Tan, X., Smith, S.C., Chen, Y.I.: An ultra-long-life flexible lithium–sulfur battery with lithium cloth anode and polysulfone-functionalized separator. ACS Nano **15**, 1358–1369 (2021)
42. Ni, W., Shi, L.-Y.: 14 - Graphene–sulfur nanocomposites as cathode materials and separators for lithium–sulfur batteries. In: Gupta, R.K., Nguyen, T.A., Song, H., Yasin, G. (eds.) Lithium-Sulfur Batteries, pp. 289–314. Elsevier (2022)
43. Luo, Y., Wan, Y., Huang, J., Li, B.: Nanofiber enhanced graphene–elastomer with unique biomimetic hierarchical structure for energy storage and pressure sensing. Mater. Des. **203**, 109612 (2021)
44. Wu, L.-S., Zhang, M.-H., Xu, W., Dong, Y.-F.: Recent advances in carbon materials for flexible zinc ion batteries. New Carbon Mater. **37**, 827–851 (2022)
45. Chen, J., Liang, J., Zhou, Y., Sha, Z., Lim, S., Huang, F., Han, Z., Brown, S.A., Cao, L., Wang, D.-W., Wang, C.H.: A vertical graphene enhanced Zn–MnO_2 flexible battery towards wearable electronic devices. J. Mater. Chem. A **9**, 575–584 (2021)
46. Wu, K., Zhang, L., Yuan, Y., Zhong, L., Chen, Z., Chi, X., Lu, H., Chen, Z., Zou, R., Li, T., Jiang, C., Chen, Y., Peng, X., Lu, J.: An iron-decorated carbon aerogel for rechargeable flow and flexible Zn–air batteries. Adv. Mater. **32**, 2002292 (2020)
47. Qiu, H.-J., Du, P., Hu, K., Gao, J., Li, H., Liu, P., Ina, T., Ohara, K., Ito, Y., Chen, M.: Metal and nonmetal codoped 3D nanoporous graphene for efficient bifunctional electrocatalysis and rechargeable Zn–air batteries. Adv. Mater. **31**, 1900843 (2019)
48. Kong, D.Z., Wang, Y., Huang, S.Z., Zhang, B., Lim, Y.V., Sim, G.J., Alvarado, P.V.Y., Ge, Q., Yang, H.Y.: 3D printed compressible quasi-solid-state nickel-iron battery. ACS Nano **14**, 9675–9686 (2020)
49. Wang, M., Xie, S., Tang, C., Zhao, Y., Liao, M., Ye, L., Wang, B., Peng, H.: Making fiber-shaped Ni//Bi battery simultaneously with high energy density, power density, and safety. Adv. Funct. Mater. **30**, 1905971 (2020)
50. Li, X., Gao, T., Liu, Q., Xu, Y., Li, J., Xiao, D.: Designing a high-performance anode composed of carbon nanotubes and Fe–Fe_3C nanoparticles for quasi-solid-state fibrous Ni/Fe batteries. Mater. Chem. Front. **5**, 3636–3645 (2021)

3D Graphene for High-Performance Supercapacitors

K. A. U. Madhushani and Ram K. Gupta

Abstract Over the past decades, the supercapacitor (SC) has received great attention as a developing energy storage device due to its unique characteristic features of high-power density and relatively high energy density. It is known that the properties of SC can be modified by tuning the electrode materials. Among those materials, graphene (GN) has great potential to transfer a higher amount of charge at a fast rate and store more energy in electrical double-layer capacitor-based supercapacitors. The properties of GN such as large specific area, porosity, higher specific capacitance, and higher electrical conductivity have led to novel routes for the modification of alternative materials. Although 2D structured GN was discovered earlier, it limited the performance of the devices due to the assembling of the sheets. As a result of the tremendous effort of many past studies, 3D-GN synthesized from the 2D-GN was able to overcome those limitations and become an effective electrode material compared to others. Some reports recorded that the strongness of 3D-GN is ten times greater than steel. Along with the changes in the morphological changes of the structure, some heterogeneous configurations of 3D-GN such as aerogel, sponge, film, fibers, foam, monolith, and spheres have been found for various purposes. This nanomaterial has already expanded in different fields including supercapacitors, batteries, fuel cells, sensors, flexible electronic devices, solar steam generation devices, catalysts , and absorbents. Although this material applies to various applications, this chapter focuses only on the contribution of 3D-GN to energy storage in SCs. Under this topic, various types of synthesis methods of 3D-GN with examples, the fundamental characteristics of three different SCs and the energy storage mechanism of each SC, and the electrochemical performances of both 3D-GN-based SCs and flexible SCs are discussed in detail.

Keywords 3D Graphene · Graphene synthesis · Energy storage devices · Supercapacitors · Flexible-supercapacitors

---

K. A. U. Madhushani · R. K. Gupta (✉)
Department of Chemistry, Pittsburg State University, Pittsburg, KS 66762, USA
e-mail: ramguptamsu@gmail.com

National Institute for Materials Advancement, Pittsburg, KS 66762, USA

© The Author(s), under exclusive license to Springer Nature Switzerland AG 2023

R. K. Gupta (ed.), *3D Graphene*, Carbon Nanostructures,
https://doi.org/10.1007/978-3-031-36249-1_16

1 Introduction

With the development of cutting-edge technology, the burning of fossil fuels as the main source of energy is increasing at an unprecedented rate. However, it has been recorded so many problems such as ozone layer depletion resulting in global warming, water, and air pollution because of the industrial revolution and globalization. Therefore, a leading solution should be essential to reduce these kinds of threats. Though renewable energy sources such as solar, wind tidal, and water can be used as eco-friendly energy sources, some problems such as their availability being limited to a certain region, time, and climate are being recorded. So, an efficient solution is essential to overcome these problems. Therefore, electrochemical energy storage devices (EESDs) are being invented to generate and store energy for future purposes. Depending on the utility, properties, processing costs, and long-term usage, these devices can be in a wide range. Some examples of EESDs are supercapacitors (SCs), fossil fuels, capacitors, and batteries. Among those, SCs are considered promising candidates due to their unique properties such as higher super capacitance, high-power density, fast charge–discharge rate, and excellent stability. The main issue with that is lower energy density. Therefore, a lot of research is being done to improve energy density.

The electrochemical performances of the devices mainly depend on two factors; electrode materials and the electrolyte, which are used for fabrication. Therefore, there should be much attention when selecting electrode materials that can be used for both energy transfer and storage. Among electrode materials, carbons have a greater potential in energy applications due to their surface characteristics. With the changes in the degrees of sp^2 hybridization, different types of carbon nanomaterials resulted. Based on the arrangement of the layers and coordination number, those carbon nanostructures can be classified as 0D (carbon dots), 1D (carbon nanotubes-CNT), 2D (graphene), and 3D (graphite) (Fig. 1). Zero-D materials, C_{60}, are composed of 60 carbon atoms with 12 pentagonal and 20 hexagonal rings. Two types of 1D carbons, single-walled and multi-walled carbon nanotubes (CNTs), were prepared by concentrically rolling one or more graphene (GN) sheets, respectively [1]. Some examples of each electrode material which are used for fabrication SCs are mentioned in Fig. 2.

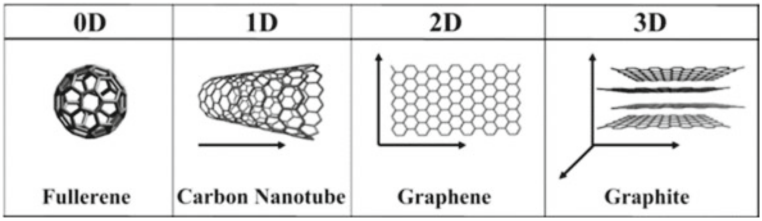

Fig. 1 Type of carbonaceous material based on layer arrangement. Adapted with permission [1], Copyright (2015), Springer Nature

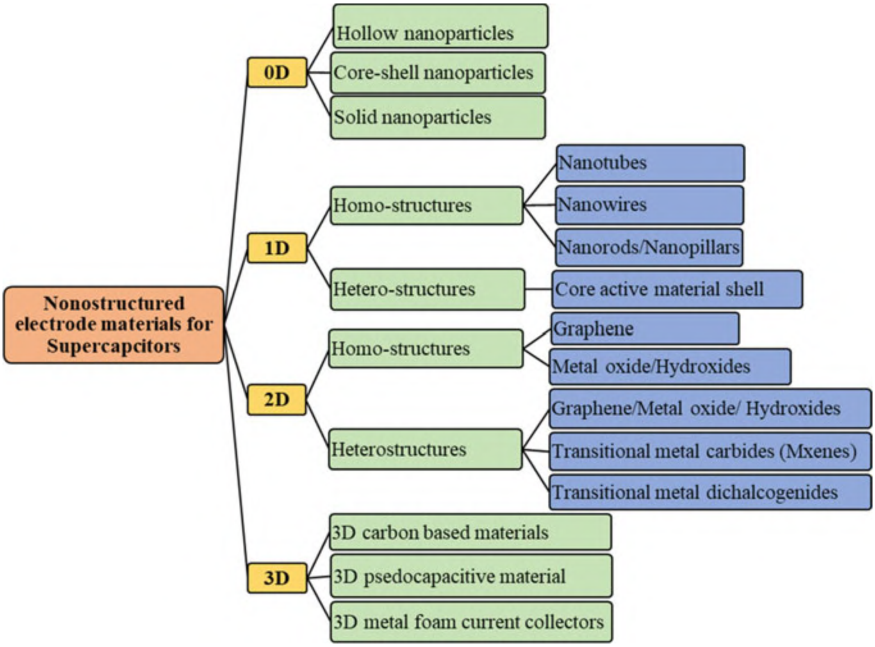

Fig. 2 Classification of nanostructured electrode materials used for fabrication of SCs

GN, the first synthesized 2D material in the world was discovered by Andre Geim and Konstantin Novoselov in 2004 [2]. This was a brilliant innovation that led to the award of the Nobel Prize in 2010. Due to the arrangement of the sp^2 carbon atoms, GN has the lowest thickness with a high surface area of ~2630 m^2/g. When considering the morphological features of 2D graphene, it has remarkable properties of carrier mobility (over 200,000 $cm^2/V.s$), high mechanical strength (Young modulus of ~1 TPa which is 300 times that of steel), excellent biocompatibility, high thermal conductivity (~5000 W/m.K), and magnetic properties. Although GN can act as an ideal electrode material for SCs, the material has some drawbacks. In that sense, due to the strong interlayer Van der Waals forces, GN sheets tend to assemble. Because of restacking, some properties such as lightness, porosity, and specific surface area are reduced, and this will end up in many defects. The problems arising in the synthesis of 2D-GN, and its structural limitations lead to an innovative new tunable structure with high properties. Thus, synthesizing a controllable design of 3D-GN from the 2D-GN would be an excellent approach to avoid the aggregation of GN sheets [3].

With the advance of 3D-GN in 2009, the demand for the GN has increased in the fabrication of different devices like sensors, catalysts, SCs, and batteries. Due to its unique characteristics and high porosity, this material shows better functional performance. To modify this material, the geometry of the GN is changed by applying mechanical strains, chemical functionalization, complex treatments for GN folding, etc. Typically, due to the multilayered structure or the morphology of the substrate, the folded GN has a high thickness. This can be controlled by changing the shapes like capsules, flowers, boxes, rings, etc. (Fig. 3). Experimentally, those configurations can be obtained with the changes in the temperature. Some research has confirmed that geometry is a considerable factor that decides the properties of the 3D-GN. This has two different structures, graphene foam and vertically aligned graphene (VAGN). Among them, VAGN is the most functioning electrode material due to its higher mass-transfer capability and fast rate of reaction [4].

3D-GNs possess a high surface area due to the presence of uniformly distributed, active porous sites. By combining this material with other effective functional groups, the volume change of this material can be reduced. And functionalization with different atoms gives an ultrathin, graded structure. Through these alternations, the properties of GN such as flexibility and mechanical strength can be enhanced. Further, the long-range π–π conjugation and hybridization allow transferring more electrons and ions rapidly resulting in high conductivity. In addition to the porosity and design, some aspects including the techniques used to produce nanocomposites, the relationship between GN and embedded atoms, and the arrangements of the sites within the material mainly affect the improvement of the electrochemical performances [5].

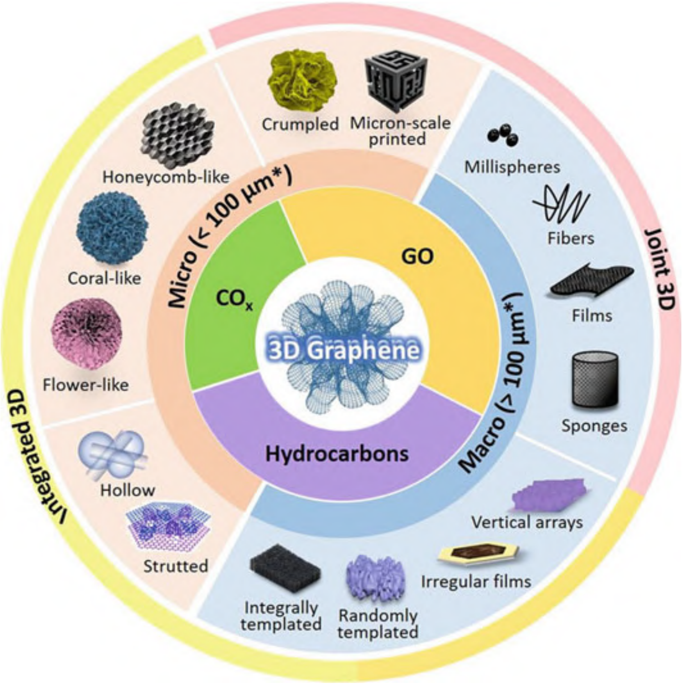

Fig. 3 Configuration of different 3D Graphene. Adapted with permission [3], Copyright (2020), American Chemical Society

2 3D Graphene: Synthesis and Functionalization

2.1 *Synthesis of 3D Graphene*

Over recent times, the demand for the 3D-GN has increased due to its unique electrochemical properties. Although the experimental higher values of specific capacitance, energy density, and conductivity bring good performance to the electrocatalysis processes, this material shows the contribution to energy storage applications. This issue can be recovered by composing 3D-GN with relevant materials such as metal oxides, and inorganic or organic materials. Over time, several methods such as hydrothermal methods, chemical vapor deposition (CVD), 3D printing, and self-assembly have been discovered for the fabrication of 3D-GN.

As a hydrothermal method, Li et al. produced 3D-GN monoliths from aqueous graphene oxide (GO) and hexane droplets [6]. In that sense, reduced GO was formed with the reduction of GO sheets, and they were bound around hexane droplets to produce 3D-GN which is called microporous graphene monolith (MGM). As a first step, an aqueous solution of GO and hexane were shaken to form MGMs. Then it was dipped in 80 °C de-ionized water to remove hexane. On the other hand, water was added to this to maintain the porosity of MGMs. Consequently, resulted from the product was freeze-dried and annealed at 40 °C under 100% moisture condition via the air-drying method (Fig. 4). The resulting 3D-GN is combined with the properties of pressure sensing, excellent electrical conductivity, low density, and high elasticity.

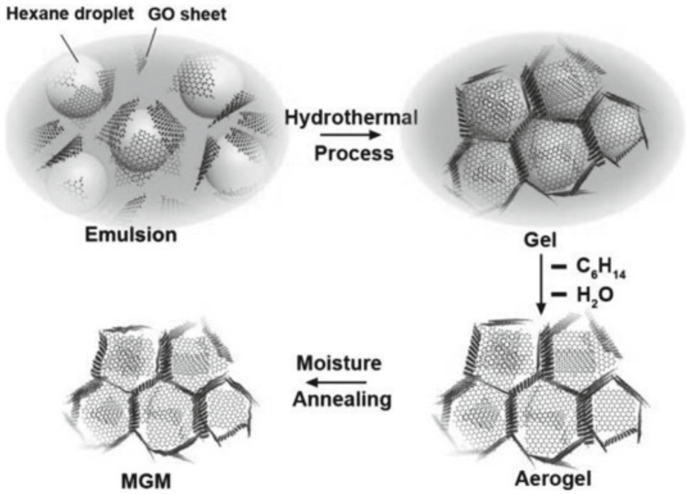

Fig. 4 Schematic illustration of 3D Graphene synthesized via hydrothermal method. Adapted with permission [6], Copyright (2014), John Wiley and Sons

In the synthesis of 3D-GN, the CVD process is the most popular technique that can be classified under a bottom-up method. The principle behind CVD is the transformation of gaseous carbon precursors into thin layers via chemical reactions under heating conditions. The product obtained through this has better properties like higher specific area, good quality, and uniform and thin layer structure. Generally, a high temperature of 500 to 1000 °C was applied for CVD, and the other significant factor is the carbon precursor that determines the structure of the GN formed afterward. Among those, methane which has robustness and high stability is considered a good precursor which can form uniform layers of GN. Although methane works at temperatures above 900 °C, some high carbon-contained materials can be operated at lower temperatures. The CVD process occurs inside a tube furnace, and it happens by completing five steps. As a first step, the carbon precursor is transferred into the CVD chamber. Then, a vapor-based product is obtained after several chemical reactions of gaseous carbon precursor. Later, the remaining carbon precursor with resulted carbon product is moved to the substrate via the process of surface adsorption. This is relatively the same as the latter after the decomposition and growth of the active sites are complete. Finally, the active material is formed with some physical actions of diffusion and collision. The most significant step in this CVD is to control the defects and the thickness of the obtained 3D-GN. Overall, a carbon precursor, a chamber, a substrate, and a heating system are needed to complete this process [5].

As a novel strategy, Zhu and his team produced graphene aerogels (GNA) through direct ink writing which is considered an extrusion-based 3D printing technique [7]. This 3D printed GN shows a high surface area, high compressibility, excellent conductivity, and lightweight. Herein, they faced two challenges in designing a printable GN-based ink and keeping the same intrinsic features of GN in the synthesized products. GO ink was prepared by applying both methods of addition of resorcinol and formaldehyde (R-F solution) with sodium carbonate as catalyst (sol–gel) and gelation to the highly concentrated GO suspension. Further, the viscosity of the ink can be increased with the concentration of GO solution resulting in good printability. Finally, hydrophilic fumed silica powder was added to the GO to enhance the viscosity with the increment of the yield stress and elastic modulus of the ink. This gives a highly viscous, homogenous ink. In 3D printing, this ink is loaded into the syringe barrel, and the 3D patterned GN structure is printed layer-by-layer with the extrusion of ink from the nozzle. As Fig. 5a, a simple cubic structured 3D-GN was designed via this method. During the process of converting aerogels from 3D printed GO structure, supercritical or freeze-drying steps are applied to remove the GO gel to maintain the porosity of the final product. Moreover, they analyzed the properties by comparing sol–gel and gelation separately. It is stated that the sol–gel method gives a less crosslinked more open network compared with gelation (without treating the R-F solution) Fig. 5b.

Most studies significantly stated that self-assembly via GO is very applicable in the large-scale preparation of 3D-GNs. Herein, 2D-GO sheets are gathered by dissolving GO in a solvent. These are bounded uniformly with the balanced interaction of Van der Waals and electrostatic repulsions. After adding cross-linking agent, the gelation process starts with the changes in the pH in the solution and its effects on the breakage

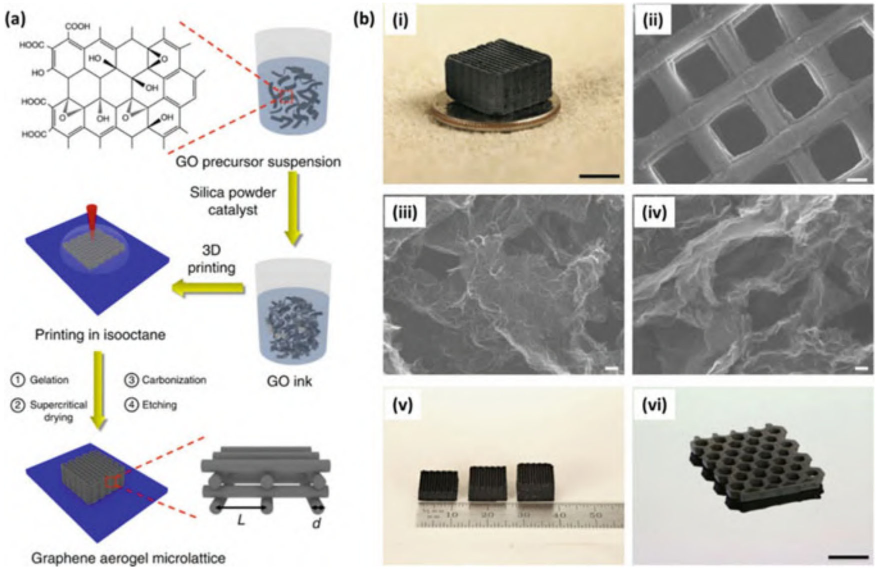

Fig. 5 **a** Steps in the 3D printing process of 3D-GNA. **b** Microstructure of 3D printed GNA (i) Optical image. SEM images of (ii) 3D-GNA and (iii) GNA without treating R-F. (iv) GNA after treating R-F. (v) GNAs at various thickness levels, (vi) honeycomb type 3D-GNA. Adapted with permission [7], Copyright (2015), Macmillan Publishers Limited. This is an open-access article distributed under the terms of the Creative Commons CC BY license

of the bonds. As a result of the chemical or physical assembling reactions, a 3D-GN network is formed, followed by the drying process which contributes to removing the excess water in this structure. For that, different types of drying methods, for instance, supercritical drying, freeze-drying, vacuum drying, and air-drying methods are used. In that process, the drying step is considered a significant factor that mainly affects the synthesis of porous materials [8, 9].

2.2 *Functionalization of 3D Graphene*

To improve some features of the 3D-GN in different applications, some issues arise, including variation in pore structure, high cost, and difficulty in controlling the structure while synthesizing only 3D-GN materials. Hence, it is necessary to develop this material by composing it with various functional groups/elements to enhance its functionality and manage the other expenses in large-scale production. Hetero atoms like nitrogen, boron, sulfur, and phosphorus doping can promote both interaction between inter-atoms, and the number of active sites and change the spreading pattern of the electron. After doping, this breaks the symmetrical structure of 3D-GN material and ended in a modified chemical design with improved conductivity properties.

With the changes in the valence electron numbers, the insertion of the hetero atoms into the lattice affects the changes in the position of carbon atoms. When considering the effectiveness of the atoms, nitrogen is the most popular dopant element compared with others. This is because its atomic diameter is very similar to that of the carbon atom, and the higher negativity of nitrogen compared to carbon can persuade the polarizability of carbon within the web and change the electronic configuration. The most important point is this has been able to improve the electronic properties without disturbing the structure of the carbon. Most research has been conducted related to N doping in 3D graphene lattices. For instance, Qiao and his team produced N-doped 3D bubble-like porous GN using melamine (as an N source) and polystyrene (as a skeleton) for the energy storage application [10]. Typically, porous GN can transfer ions/electrons rapidly resulting in fast charge/discharge cycles. Herein, melamine can influence the n-doing level, and this might contribute to greater electrochemical performances. In contrast, Wang et al.found that N-doped graphene can promote the catalytic properties of noble metal particles [11]. Further, they concluded that N-doped 3D-GN is an excellent catalytic carrier that can enhance the rate of the reaction. Due to the inability to recycle those materials, the N-dopped metal nanocomposites are rarely used as catalysts. In another recent study carried out by Yang et al., 3D nitrogen-doped graphene aerogel from the combination of graphitic carbon nitride (as N source) and graphene oxide (as template) with a higher surface area (536 m^2/g) and high photocatalytic performance was synthesized [12].

Apart from nitrogen, the atomic size and valency of boron are quite similar to that of carbon. When boron is incorporated with GN, it is considered a p-type dopant. Doping of this element can enhance the functionality of the 3D-GN. It has been proven by several recent pieces of research applied to various uses. For instance, boron-doped graphene aerogels via a simple hydrothermal method for the fabrication of electrodes in EESDs were synthesized by Li and his team [13]. Comparatively, boron can transfer more electrons than carbon, leading to high conductivity. Through this process, the capacitance of the devices can be improved instead of using a single 3D-GN.

Sulfur (S) and phosphorous (P) are also used as dopants with 3D-GN. Mostly, S-doped 3D-GN was used as both cathode and anode material for energy storage devices like metal-ion batteries, hybrid capacitors, etc. Due to the strong behavior of S in the GN structure, it is affected by the changes in carbon density while increasing the width of the band gap over N-doped GN. Li and co-workers discovered an S-doped 3D-GN with S composites as cathode material for Li–S batteries [14]. The design of the porous 3D-GN tends to incorporate hetero atoms doping due to having an open structure. Only S-doped carbonaceous material does not have high conductivity. Therefore, S-contained composites like polysulfide are combined with this to enhance properties. Compared with highly demanding N and S dopants, the large-sized P can modify the structure of 3D-GN very easily. P-doping can be showed higher electrochemical performances due to the presence of active P=O bonds. As a recent innovation, Mei et al. synthesized P-doped 3D-GN material as an anode material for Li-based devices [15]. They concluded that high P-doping to GN can be achieved to meet the requirements of industrial-scale production of EESDs.

Recently, doping of combined elements has become a very effective approach to achieve better performances of the EESDs. Xing-Quan et al. successfully designed a Co_9S_8- composed N, S, and P tertiary-doped 3D-GN electrode which has a catalytic property [16]. The composition of all the elements accelerates to the form of more sites and speeds up the reaction. Here, is just one example of the combination of the doping process discussed, many studies tend to explore it. Overall, the electrochemical and electronic performances of GN are increased through the technique of n-(electron) and p-(hole) doping into 3D-GN. This might be applicable in large-scale manufacturing processes. With the type of integrated element, the activity of the functional groups in the GN lattice might be changed. So, the behavior of the groups, either electron donating or withdrawing should be paid attention to while selecting dopants for GN [17].

3 Fundamentals of Supercapacitors

With the arising necessity for energy storage, different types of devices are invented based on their applications. Among those devices, SCs which are known as electrochemical capacitors, ultracapacitors have attracted attention due to their unique properties. When compared to other devices like batteries, capacitors, and fuel cells, this exhibited intermediate electrochemical performances. Most of the research has significantly proven that SCs have high-power density, fast charge–discharge density, superior specific capacitance, long cyclic stability, etc. Comparatively, batteries have high energy density while capacitors show low energy density. The variation in energy density and power density in different EESDs are shown in the Ragone plot. This provides a clear comparison of those two properties (Fig. 6). By putting all the properties together, SCs are lightweight, safe, portable, and flexible devices [18].

In general, SC consists of two electrodes, an electrolyte, and a separator that is permeable to ions. On the hand, the electrode is a decisive factor in electrochemical performance. Typically, a material that has high porosity and a high surface should be selected as an electrode. In SCs, energy storage occurs according to the charge–discharge (CD) principle at the interface of electrode and electrolyte. The CD process in SCs is relatively higher in speed. Based on the energy storage mechanism, there are three types of SCs such as electrical double-layer capacitors (EDLCs), pseudocapacitors (PCs), and hybrid capacitors (HCs) (Fig. 7).

3.1 Electrical Double-Layer Capacitors

As mentioned earlier, EDLCs, which is called an electrostatic capacitor, is one type of SCs. The surface of the electrode contributes to both the generation and storage of energy. Electrochemically inactive carbon-derived materials such as carbon, graphene, carbon aerogels, carbon nanotube, etc., are used for the fabrication of

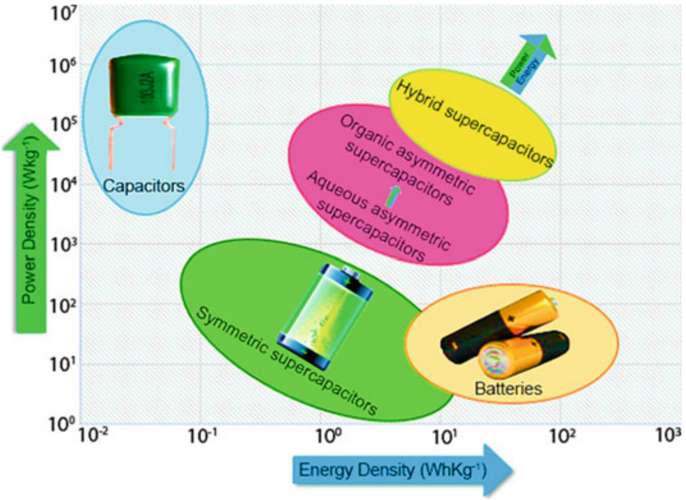

Fig. 6 Ragone plot which describes the power-energy density variation. Adapted with permission [18], Copyright (2020) by authors. Licensee MDPI, Basel, Switzerland. This article is an open-access article distributed under the terms and conditions of the Creative Commons Attribution (CC BY) license

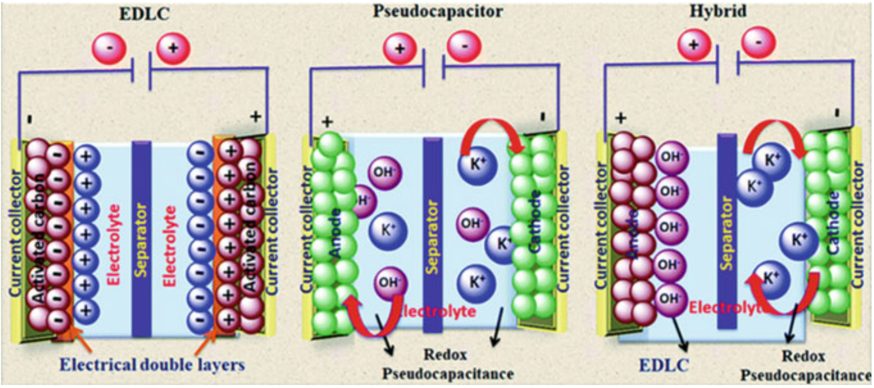

Fig. 7 Classification of three different SCs like EDLC, PC, and HC. Adapted with permission [19], Copyright (2019), The Royal Society of Chemistry. This article is an open-access article distributed under the terms and conditions of the Creative Commons Attribution (CC BY) license

electrodes of EDLCs. These materials do not involve any chemical reactions for energy storage and physical charge gathering contributes to this. It happens due to the ion adsorption from the electrolyte and the surface dissociation. The charge stores with the formation of the double layer. This originates on the external surface of the electrode due to the electroneutrality created from excess or deficit charges loaded on the electrode and the oppositely charged ion in the electrolytes. Here, this

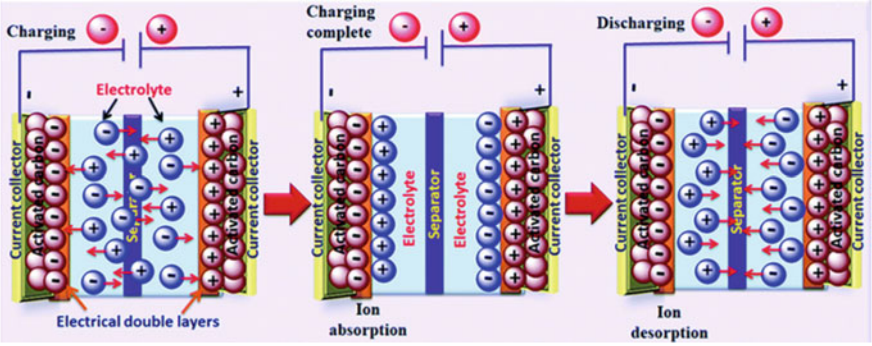

Fig. 8 Schematic illustration of charge–discharge mechanism in EDLC. Adapted with permission [19], Copyright (2019), The Royal Society of Chemistry. This article is an open-access article distributed under the terms and conditions of the Creative Commons Attribution (CC BY) license

scenario occurs within the CD period. During the charging process, the electrons in the negative electrode move to the positive electrode via the exterior circuit after supplying current. With that, anions and cations in the electrolyte start to migrate to negative and positive charged electrodes, respectively. After that, the reverse process is continued as discharging (Fig. 8). Shortage or excess electrons move through the external load. There is no ion/charge exchange between electrodes and electrolytes. Because of this circumstance, this kept a constant ion concentration within the CD process. The accumulated ions in the double-layer interface decide the amount of capacitance of EDLCs. When considering this mechanism, the surface characteristics of the electrode material are mainly affected by the electrochemical performance of EDLCs. Although carbons have excellent properties, their high availability and low cost lead to the development of novel innovations through modifications [19, 20].

3.2 *Pseudocapacitors*

PC, which is commonly known as redox or faradic capacitor, is also very popular as other SCs. The main difference between PCs compared to EDLC is that rapid, reversible redox reactions involve energy storage. Like EDLCs, energy stores with the formation of a double layer at the surface of the electrodes due to the CD process. Electrochemically active materials, which can provide redox reactions, for instance, transitional metal oxides/hydrides (TMOs/TMHs) and conducting polymers, are used for the fabrication of PCs. Herein, these materials exhibit three types of oxidation–reduction reactions such as the faradaic reaction of TMOs/TMHs, reversible adsorption, and electrochemical doping-de-doping reactions in CPs. Through these reactions, both energy density and specific capacitance can be enhanced. Because the rate of faradaic reaction is slower than that of non-faradaic ones, PCs show lower power density and reduced cyclic stability compared to EDLCs [21].

3.3 Hybrid Capacitors

With the modification of the electrode materials, each EDLC and PC show excellent unique electrochemical properties. As the best option to overcome the limitations related to each device, HC is made up of combining both devices. This illustrates an asymmetrical configuration because one electrode is made up of carbonaceous material, while the other one is composed of electrochemically active material. Based on the type of electrode materials, there are three categories of HC. The first group is based on composites of capacitive and pseudocapacitive materials. The other two are made with asymmetrical designs. One of them consists of an EDLC electrode and the other a PC electrode/battery-type electrode. The third one uses electrodes from PCs and rechargeable batteries. Here, non-faradaic electrodes provide high density and superior cyclic stability, while pseudocapacitive or battery-type ones have large energy densities. Therefore, it exhibits an improved electrochemical performance compared to the other SCs [22].

4 3D Graphene-Based Supercapacitors

It is significantly discovered that the features of the electrode material play a decisive role in the electrochemical performances of the SCs. Some factors like functional groups, surface, structural, and morphological characteristics are mainly affected by the changes in the properties of the electrode materials. Therefore, most research tends to innovate novel strategies to modify the features of the electrode materials. It is known that electrode material that has high porosity, high surface area, good mass-transfer efficiency, and an effective pathway for ion diffusion leads to good conductivity resulting in excellent behaviors in SCs. Although GN is richer in some properties compared to others, this can be improved through several modifications at the structural level. For example, 2D-GN, which has a less porous structure with limited surface area, was improved through the synthesis of 3D-GN from it to achieve better performance.

Mostly, GN-based carbon materials are used to fabricate the electrodes for EDLCs. In that sense, this shows the higher surface area in the range of 2630–3290 m^2/g and high specific capacitance of 135–205 F/g in aqueous electrolyte compared to other electrode materials (CNT, active carbon) applied for EDLCs. Zang and his team synthesized 3D-GN hydrogel via the one-step hydrothermal method (GN-H) which contributes to reaching the optimum properties of EDLC [23]. In this work, this device exhibited a high capacitance of 200 F/g at a low current density (0.3 A/g). At a high discharge rate, its capacitance is reduced due to a large amount of remaining oxygenated groups in the hydrogel, and its relatively low conductivity. Therefore, they treated this material with hydrazine (Hz)/HI to increase the capacitance by removing the residue and improving the conductivity. Compared to HI-reduced GN-H, Hz-reduced one shows better capacitive performances. This is because some nitrogen atoms were doped into GN-H while reducing with HZ and it enhances the wettability of the electrode that leads to excellent features. However, this showed higher stability, indicating capacitance retention of 92% over the 2000 cycles. These results were obtained because of the 3D microporous structures of GN-H. Overall, they observed that the power density and rate capability of this device are relatively higher than that of chemically treated GNs reported in previous research.

Most research considerably reported that doping heteroatoms into the GN lattice was a great strategy to improve the properties of the SCs. This is because these elements can impact the functional group of the GN surface. As discussed in Sect. 2, B or N is the best element that has similar characteristics to carbon for the fabrication of electrodes for SCs [13] For energy storage purposes, more benefits can be achieved through heteroatom-doping. Some of them are, that the spaces between the layers and the surface structure accelerate the rapid ion exchange, the number of active sites on the surface increases with defects, and the stability between the electrode and the electrolyte is enhanced by heteroatoms [15].

For instance, Wu et al. synthesized solid-state SCs using 3D-GN and boron co-doped monolithic GN aerogels (BN-GAs) [24]. As in Fig. 9, GO and ammonia boron trifluoride (NH_3BF_3) were used as precursors to synthesize BN-GAs through the combined processes of hydrothermal and freeze-drying. Here, GN behaves as the binder-free electrode, and polyvinyl alcohol (PVA)/H_2SO_4 was used as a gel electrolyte for the fabrication of SCs. Further, they produced nitrogen and boron-doped graphene aerogel (N-GAs and B-GAs) using dicyandiamide and boric acid as nitrogen and boron source, respectively. This is done to distinguish the electrochemical performance of the N-GAs, B-GAs, and BN-GAs. The size and shape of the GN aerogel monoliths can be adjusted with the changes in some factors including the concentration of GO, treated temperature, and time of the hydrothermal. They have experimentally found that BN-GAs showed higher specific capacitance, power density, and improved energy density with respect to N-GAs, and B-GAs.

Moreover, the preparation of nanomaterial by composting different elements gives better electrochemical performance rather than using a single type of electrode material. As an example, for this strategy, Sahoo et al. developed an effective multi-functional 3D-GN/Ag nanocomposite via the freeze-drying method for the fields of energy, catalysis, and medicine [25]. The main challenge in 3D-GN-based composite with noble metal elements processing is to improve its properties without harming the environment and keeping it cost-effective. Here, they synthesized the composite with different percentages (10, 20, and 40 wt. %) of Ag and in the presence of 0.625, 1.25, and 2.5 mg of $AgNO_3$, respectively. Among those, the 3D-GN/Ag (40%) nanocomposite exhibited the highest electrochemical performance due to the presence of a high amount of Ag particles. For example, this has more active sites, surface area, fast faradaic rate, and excellent conductivity resulting in the highest specific capacitance of 876 F/g at 1 A/g. And also, this showed great stability by giving capacitance

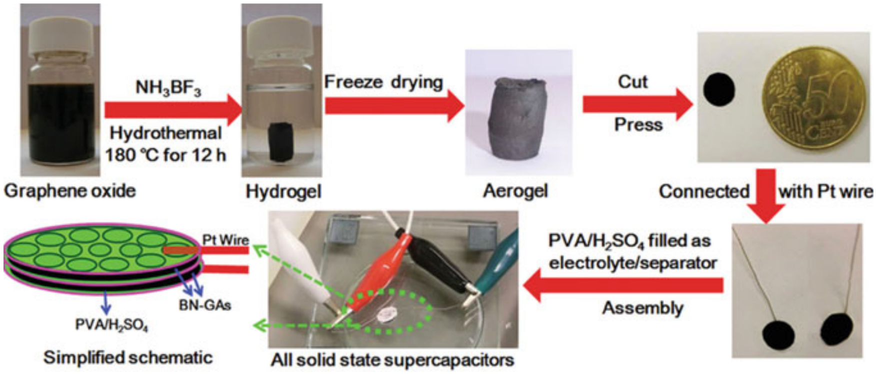

Fig. 9 The fabrication process of BN co-doped GN-based solid-state supercapacitor, Adapted with permission [24], Copyright (2012), John Wiley and Sons

retention of 97% after 1000 cycles. Further, they observed that Ag nanoparticles with an average particle size of 36 nm were uniformly arranged on the surface of the GN sheets without any collision. Even with a higher weight percentage of Ag molecules (40%), they are strongly bound together, proving that there is no separation even upon sonication for 10 min.

Recently, Kaner et al. used 3D-GN with covalently grafted aniline tetramer (TANI) material for the fabrication of a supercapacitor [26]. Here, they made this PANI/TANI-GN composite material using TANI which is the fundamental construction block of PANI onto 3D-GN through the single-step hydrothermal self-assembly process. Initially, GO and 4-azido-tetrafluoro benzoyl tetra-aniline (ATFB-TANI) were used for the formation of 3D-GN and after the one-step process, ATFB-TANI grafted 3D-GN (ATgGN) was obtained as electrode material for SCs. Herein, the symmetric SC was prepared using two similar ATgGN electrodes divided by an ion-permeable separator and $PVA/H_2SO_4/HQ$ gel electrolyte (Fig. 10a). In this 3D porous structure, both TANI and HQ are contributing to the faradaic processes leading to high super capacitance. The 3D porous ATgGN electrode materials used both mechanisms of ion adsorption–desorption (EDLC) and redox reaction to store more energy within this system. As demonstrated in Fig. 10b, c, this composite in HQ contained electrolyte shows excellent electrochemical performance compared to the regular electrolyte. According to Fig. 10d, the capacitance retention in PVA/H_2SO_4 electrolyte exhibits a higher value (87%) compared to that of HQ-contained solution. This is because of the incompletion of HQ redox reactions. However, specific and areal the capacitance of HQ contained device illustrated a high rate of 94 mF/cm^2 at 0.5 mA/cm^2 (Fig. 10e). The main challenge with PANI-based SC is poor cycling stability throughout the life cycle. But this synthesized composite material retained more than 85% of capacity after 30,000 charge–discharge cycles from this GN-TANI-based SC. Further, this value was maintained at about 82% even after 100,000 cycles using a redox-active electrolyte for this device.

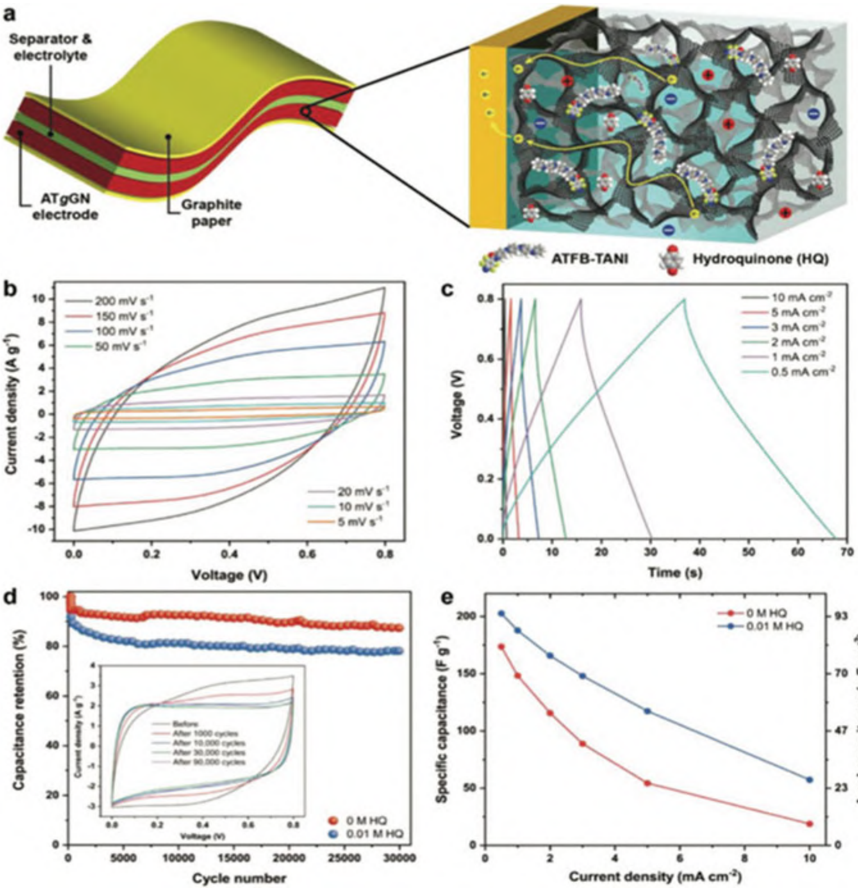

Fig. 10 **a** Schematic illustration of ATgGN symmetric supercapacitor, Characterization of HQ containing electrolyte and non-contained electrolyte (PVA/ H_2SO_4) **b** CV analysis at different scan rates, **c** GCD analysis at different densities, Comparison of (d) Stability and **e** capacitance with the presence of HQ in the electrolyte, Adapted with permission [26], Copyright (2021), John Wiley and Sons

5 3D Graphene-Based Flexible Supercapacitors

With the differentiation of the applications, the synthesis of the electrode material is changed according to their purposes of usage. fabricating 3D graphene having both high surface area and porosity brings significant value in practical applications, especially for energy storage purposes. It can be found that most wearable electronic devices are made up of electrode materials having flexible, stretchable, and folding properties. Based on past reports, only single material cannot achieve high flexibility for reaching its desired application. Therefore, most of them are synthesized by composing chemically treated materials together. In that sense, it can be seen that most electrodes in flexible SCs are coming from chemically derives 3D-GN-based composite materials. On the other hand, most current research has targeted the synthesis of 3D hybrid electrode materials for the fabrication of flexible devices using transitional metals (TMs) and carbon-based materials. But their electrochemical performance is comparatively very low. This happened because of their low conductivity and faults in reversible reactions. Some techniques including composing TMs on carbon materials, doping TMs with conductive polymers, etc., are used to avoid these errors. Therefore, it is an important task in the selection of doping material to synthesize a composite electrode that shows excellent electrochemical performance with flexibility. Here, some practices for the novel innovations of those are briefly discussed in this section.

As an example, Chen et al. developed a foam-typed macro-structured 3D-GN (GF) via the template-based CVD technique for the use of SCs [27]. Here, they followed the procedure where carbon was initiated into the nickel foam (NiF) through the decomposition of CH_4 at high temperature and ambient pressure and then GN films were dropped on the NiF. By changing the type of nickel foam, the macro/microstructure of GF can be adjusted and variations in the concentration of the CH_4 affect the surface area, density, and several layers of GF. The most significant fact is that this GF is composed of an internally connected flexible web of GN that acts as a carrier for the fast ion charge mobility resulting in high conductivity. As the final step, this GF was composed of poly (dimethyl siloxane) (PDMS) to gain high flexibility, twisting, and bending without breaking. The features of stretching and bending were tested using a homemade two-point bending device and a high-precision mechanical instrument. The structure of GF was not disturbed by incorporating PDMS and this was not affected by changes in the conductivity of GF. Because of the mechanical and electrical properties of this composite, this composite has great potential for application as a flexible conductor in EESDs. Even though conventional conductors like metallic foils provide better conductivity, those cannot apply for stretchable purposes. But this composite is the best combination for fabricating SCs with both high electrochemical performances and flexibility.

In another instance, Yu et al. invented a laser-induced 3D-GN (LIG)-based flexible solid-state micro-supercapacitor having ultra-thickness of 320 μm [28]. Herein, they have been discovered that porous 3D-GN can be synthesized with the conversion of commercial polyimide (PI) by the IR laser method in CO_2 air condition (Fig. 11a). The pores structure of this material proved a fast route for ion transportation. In electrochemical testing, LIG achieved a higher specific capacitance of 132.2 mF/cm^2 at 0.5 mA/cm^2 which is comparatively higher than that of GN electrodes. Further, they were able to improve the specific capacitance of this electrode material up to 2412.2 mF/cm^2 at 0.5 mA/cm^2 by composing it with pseudocapacitive polypyrrole (Ppy). This LIG/Ppy composite was prepared by the electrodeposition of Ppy on the porous 3D-LIG. The increased porosity of LIG allows more access to deposit more Ppy, leading to a higher loaded mass resulting in optimal properties (Fig. 11b). This composite, which achieved 325 μW/cm^2 of power density and 134.4 μWh/cm^2 of energy density, gives this device not only superior electrochemical performances, but also high flexibility.

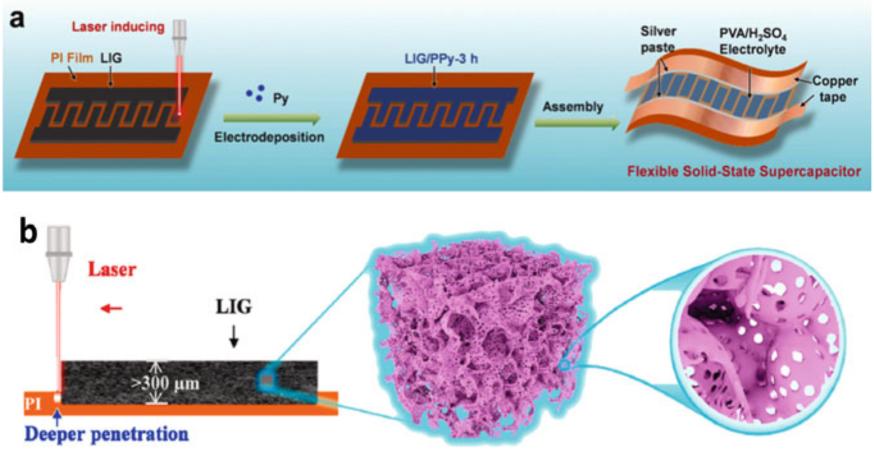

Fig. 11 **a** Preparation process of LIG/PPy electrode for the flexible solid-state supercapacitor **b** Pore structure of LIG, Adapted with permission [28], Copyright (2020), Elsevier

Recently, Chen et al. developed a lightweight flexible solid-state SC using the composite of GN, Fe, and $MnCo_2O_4$ targeting wearable applications [29]. Here, Fe was doped into $MnCo_2O_4$ to obtain the metallic properties of the compounds by maintaining electron density in the electrodes. After doping, the electron transfer rate and processing speed of $MnCo_2O_4$ enhanced resulting in good cyclic performance. In that case, 3DGN-PPy with a high surface area was used as a substrate to build the composite of $FeMnCo_2O_4$ nanowires while avoiding the production of adhesives and additional current collectors. This combination provides both low-weight and stretch characteristics for conductors. As experimental details, they prepared the 3D-GN on Ni foam via the CVD method. Then electrodeposition technique was used to deposit PPy on 3D-GN to synthesize the G-PPy composite. Later, through the process of the hydrothermal method, they made $MnCo_2O_4$ nanowire arrays. After doping Fe into that composite, it was grown on the substrate via a one-step hydrothermal method to finish the synthesis of the composite (Fig. 12). After all, symmetrical solid-state SC was fabricated by assembling 3DGN-PPy@$MnCo_2O_4$ electrodes. In this device, filter paper and PVA/KOH were used as a separator and gel electrolyte, respectively. However, 3D G-PPy@Fe- $MnCo_2O_4$-based SC exhibited 5136 mF/cm^2 at 2 mA/cm^2 of specific capacitance with long-term durability. The stability of this device was shown to be about 94.7% of capacitance retention after 7000 cycles. This study demonstrates that the 3D-GN can be applied to the production of wearable electronic devices by improving flexibility by changing the composition of the electrode materials.

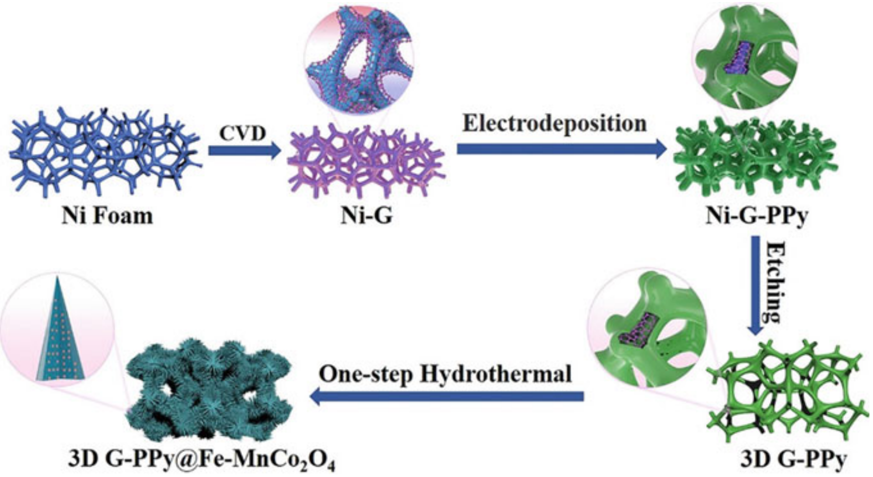

Fig. 12 Fabrication process of 3D G-PPy@Fe- MnCo$_2$O$_4$ electrode material for the flexible solid-state supercapacitor. Adapted with permission [29], Copyright (2022), American Chemical Society

6 Conclusion and Outlook

The demand for the usage of 3D-GN is increased because it can prevent the aggregation of GN sheets. Hydrogels, aerogels, foams, and monoliths which are the different formations of 3D-GN are widely used materials in recent studies. Depending on the application and material formation, the synthesis methods of 3D-Gn are varied. Some examples of strategies can be summarized as CVD, hydrothermal method, 3D printing, and self-assembly. Here, each method is briefly discussed with several examples in the above sections. Until today, there have been many findings on 3D-GN-based SCs because of their chemical, morphological, and electrochemical performances. The inherent features of 3D-GN including high surface area and porous structure that facilitate improved capacitance through fast ion transportation led to novel innovations. Considering all the properties, GN has become desired material for various applications not only for supercapacitors, but also in sensors, catalysts, adsorption of dyes and heavy metals, etc. Especially, the need for flexible GN-based SCs is enhanced in wearable electronic systems. In this review, the recent effort for the development of novel electrode materials by composing 3D-GN materials that are used for flexible SCs is discussed. It is noted that only 3D-GN does not have flexible properties, the composition of materials which has flexible, stretching, and bending properties can promote flexibility in 3D-GN.

When considering the industrial and practical applications, several challenges need to be developed in large-scale production. One of these is that most experiments regarding these 3D-GN materials are done on the laboratory scale, and because of its fragility, it is difficult to manipulate this material in a friendly manner. However, this can be overcome by combining different highly flexible materials to improve mechanical properties. But it should be more careful while integrating additives into 3D-GNs. Although some materials can improve the properties of 3D-GN, on the other hand, they can cause side effects to the primary materials. Therefore, it is necessary to study the characteristic features of each element before incorporating them into 3D-GN materials. An added solution for that issue is to adjust the cross-linking status. Another problem regarding 3D-GN production is that the size of this material cannot be controlled as much as desired. This should be done after a thorough analysis of structural characteristics. For future innovations, various structured 3D-GNs like scrolls, honeycombs, corals, and nano sacks are still to be studied for supercapacitor application.

References

1. Bergmann, C.P., Machado, F.M.: Carbon Nanomaterials as Adsorbents for Environmental and Biological Applications (2015). https://doi.org/10.1007/978-3-319-18875-1
2. Novoselov, K.S., Geim, A.K., Morozov, S.V., Jiang, D., Zhang, Y., Dubonos, S.V., Grigorieva, I.V., Firsov, A.A.: Electric field effect in atomically thin carbon films. Science **306**(2004), 666–669 (1979)
3. Sun, Z., Fang, S., Hu, Y.H.: 3D graphene materials: from understanding to design and synthesis control. Chem Rev. **120**, 10336–10453 (2020). https://doi.org/10.1021/acs.chemrev.0c00083
4. Song, J., Xia, X., Chen, J., Xia, D., Xue, Q., Li, Q., Dong, M.: Folding 2D Graphene Nanoribbons into 3D Nanocages Induced by Platinum Nanoclusters (2020). https://doi.org/10.1021/acs.jpcc.0c00463
5. Zaka, A., Hayat, K., Mittal, V.: Recent trends in the use of three-dimensional graphene structures for supercapacitors. ACS Appl. Electron. Mater. **3**, 574–596 (2021). https://doi.org/10.1021/acsaelm.0c00953
6. Li, Y., Chen, J., Huang, L., Li, C., Hong, J.D., Shi, G.: Highly compressible macroporous graphene monoliths via an improved hydrothermal process. Adv. Mater. **26**, 4789–4793 (2014). https://doi.org/10.1002/adma.201400657
7. Zhu, C., Han, T.Y.J., Duoss, E.B., Golobic, A.M., Kuntz, J.D., Spadaccini, C.M., Worsley, M.A.: Highly compressible 3D periodic graphene aerogel microlattices. Nat Commun. **6**, 1–8 (2015). https://doi.org/10.1038/ncomms7962
8. Ding, M., Li, C.: Recent advances in simple preparation of 3D graphene aerogels based on 2D graphene materials. Front Chem. **10**, 1–9 (2022). https://doi.org/10.3389/fchem.2022.815463
9. Lu, H., Li, C., Zhang, B., Qiao, X., Liu, C.Y.: Toward highly compressible graphene aerogels of enhanced mechanical performance with polymer. RSC Adv. **6**, 43007–43015 (2016). https://doi.org/10.1039/c6ra04995h
10. Qiao, Y., Cheng, X., Liu, Y., Han, R., Ma, M., Li, Q., Dong, H., Li, X., Yang, S.: Architecture design of nitrogen-doped 3D bubble-like porous graphene for high performance sodium ion batteries. Inorg Chem. Front. **4**, 2017–2023 (2017). https://doi.org/10.1039/c7qi00574a
11. Wei, Q., Liu, T., Wang, Y., Dai, L.: Three-dimensional N-doped graphene aerogel-supported Pd nanoparticles as efficient catalysts for solvent-free oxidation of benzyl alcohol. RSC Adv. **9**, 9620–9628 (2019). https://doi.org/10.1039/C9RA00230H
12. Maouche, C., Zhou, Y., Peng, J., Wang, S., Sun, X., Rahman, N., Yongphet, P., Liu, Q., Yang, J.: A 3D nitrogen-doped graphene aerogel for enhanced visible-light photocatalytic pollutant degradation and hydrogen evolution. RSC Adv. **10**, 12423–12431 (2020). https://doi.org/10.1039/d0ra01630f
13. Li, J., Li, X., Xiong, D., Wang, L., Li, D.: Enhanced capacitance of boron-doped graphene aerogels for aqueous symmetric supercapacitors. Appl. Surf. Sci. (2018). https://doi.org/10.1016/j.apsusc.2018.12.152

14. Li, N., Gan, F., Wang, P., Chen, K., Chen, S., He, X.: In situ synthesis of 3D sulfur-doped graphene/sulfur as a cathode material for lithium-sulfur batteries. J. Alloys Compd. **754**, 64–71 (2018). https://doi.org/10.1016/j.jallcom.2018.04.018
15. Mei, J., He, T., Zhang, Q., Liao, T., Du, A., Ayoko, G.A., Sun, Z.: Carbon-phosphorus bonds-enriched 3D graphene by self-sacrificing black phosphorus nanosheets for elevating capacitive lithium storage. ACS Appl. Mater Interfaces **12**, 21720–21729 (2020). https://doi.org/10.1021/acsami.0c03583
16. Ma, X.X., Dai, X.H., He, X.Q.: Co9S8-modified N, S, and P ternary-doped 3D graphene aerogels as a high-performance electrocatalyst for both the oxygen reduction reaction and oxygen evolution reaction. ACS Sustain. Chem. Eng. **5**, 9848–9857 (2017). https://doi.org/10.1021/acssuschemeng.7b01820
17. Pumera, M.: Heteroatom modified graphenes: electronic and electrochemical applications. J. Mater Chem. C Mater. **2**, 6454–6461 (2014). https://doi.org/10.1039/c4tc00336e
18. Forouzandeh, P., Kumaravel, V., Pillai, S.C.: Electrode materials for supercapacitors: a review of recent advances. Catalysts **10**, 1–73 (2020). https://doi.org/10.3390/catal10090969
19. Pal, B., Yang, S., Ramesh, S., Thangadurai, V., Jose, R.: Electrolyte selection for supercapacitive devices: a critical review. Nanoscale Adv. **1**, 3807–3835 (2019). https://doi.org/10.1039/c9na00374f
20. Soc, C., Wang, G., Zhang, J.: Chem. Soc. Rev. Critical Review A review of electrode materials for electrochemical supercapacitors, 797–828 (2012). https://doi.org/10.1039/c1cs15060j
21. Guan, M., Wang, Q., Zhang, X., Bao, J., Gong, X., Liu, Y.: Two-dimensional transition metal oxide and hydroxide-based hierarchical architectures for advanced supercapacitor materials. Front. Chem. **8**, 1–14 (2020). https://doi.org/10.3389/fchem.2020.00390
22. Zhong, C., Deng, Y., Hu, W., Qiao, J., Zhang, L., Zhang, J.: A review of electrolyte materials and compositions for electrochemical supercapacitors. Chem. Soc. Rev. **44**, 7484–7539 (2015). https://doi.org/10.1039/c5cs00303b
23. Zhang, L., Shi, G.: Preparation of highly conductive graphene hydrogels for fabricating supercapacitors with high rate capability. J. Phys. Chem. C **115**, 17206–17212 (2011). https://doi.org/10.1021/jp204036a
24. Wu, Z.S., Winter, A., Chen, L., Sun, Y., Turchanin, A., Feng, X., Müllen, K.: Three-dimensional nitrogen and boron co-doped graphene for high-performance all-solid-state supercapacitors. Adv. Mater. **24**, 5130–5135 (2012). https://doi.org/10.1002/adma.201201948
25. Sahoo, P.K., Kumar, N., Thiyagarajan, S., Thakur, D., Panda, H.S.: Freeze-casting of multifunctional cellular 3D-graphene/Ag nanocomposites: synergistically affect supercapacitor. Catalyt. Antibacterial Properties ACS Sustain. Chem. Eng. **6**, 7475–7487 (2018). https://doi.org/10.1021/acssuschemeng.8b00158
26. Chang, X., El-Kady, M.F., Huang, A., Lin, C.W., Aguilar, S., Anderson, M., Zhu, J.Z.J., Kaner, R.B.: 3D graphene network with covalently grafted aniline tetramer for ultralong-life supercapacitors. Adv. Funct. Mater., 31 (2021). https://doi.org/10.1002/adfm.202102397
27. Chen, Z., Ren, W., Gao, L., Liu, B., Pei, S., Cheng, H.M.: Three-dimensional flexible and conductive interconnected graphene networks grown by chemical vapour deposition. Nat Mater. **10**, 424–428 (2011). https://doi.org/10.1038/nmat3001
28. Yu, X., Li, N., Zhang, S., Liu, C., Chen, L., Han, S., Song, Y., Han, M., Wang, Z.: Ultra-thick 3D graphene frameworks with hierarchical pores for high-performance flexible micro-supercapacitors. J. Power Sources, 478 (2020). https://doi.org/10.1016/j.jpowsour.2020.229075
29. Chen, Z., Zu, X., Chen, L., Qi, Y., Jian, W., Wu, Y., Zhang, W., Lin, X., Yi, G., Liu, Q., Tang, Z., Wu, J., Dong, H., Qin, Y.: Flexible self-supporting 3D electrode based on 3D graphene-PPy@Fe-MnCo2O4Nanostructure arrays toward high-performance wearable supercapacitors. ACS Appl. Energy Mater (2012). https://doi.org/10.1021/acsaem.2c00311

3D Graphene for Photovoltaics

Alka Pareek and Sreekanth Mandati

Abstract Three-dimensional graphene (3D-G) is among the most interesting and emerging materials of the carbon clan due to its exemplary properties like high surface area, remarkable electrical properties, and exceptional mechanical characteristics that urged profound interest in various applications. Graphene sheets assembled into an ordered and internally connected three-dimensional network are a great solution to the problem of aggregation or overlaying that limits the active surface area and distinct characteristics of sheets. Furthermore, these structures possess interconnected porosity, larger specific surface area, and more integrality providing short ion diffusion length and additional active sites. 3D-G structures are widely used in various applications like supercapacitors, batteries, fuel cells, gas storage, biosensors, solar cells, and so on. In photovoltaics (PVs), the graphene-based materials appear very promising for (1) making cost-effective, lightweight, and flexible devices, (2) obtaining a wide range absorption window from UV to far IR regions, (3) improving charge transfer kinetics, and (4) high catalytic activities. Moreover, the optoelectronic and electrocatalytic activity of 3D-G structures can be altered through different ways of surface functionalization that expand the application in multiple PV devices like dye-sensitized, quantum dot-sensitized, and perovskite solar cells. This chapter highlights the recent research advancement and contribution of 3D-G structures and composites in PV applications while also discussing the limitations in achieving higher performance and directions for future development.

Keywords 3D graphene · Photovoltaics · Dye-sensitized solar cells · Quantum dot-sensitized solar cells · Perovskite solar cells

---

A. Pareek (✉) · S. Mandati
Laboratory of Thin Film Chemical Technologies, Department of Materials and Environmental Technology, School of Engineering, Tallinn University of Technology, Ehitajate Tee 5, 19086 Tallinn, Estonia
e-mail: alkapareek7@gmail.com

© The Author(s), under exclusive license to Springer Nature Switzerland AG 2023

R. K. Gupta (ed.), *3D Graphene*, Carbon Nanostructures,
https://doi.org/10.1007/978-3-031-36249-1_17

1 Introduction

Solar PV technologies that deal with the conversion of sunlight directly into electricity are sustainable, clean, and zero-emission energy production processes. In 1954, the first Si solar cell in crystalline form was invented in Bell Labs, after which PV research has seen a rapid increase in the next few decades with extensive studies dedicated to developing various absorber materials [1]. A variety of device configurations and architectures with different solar cell layers have been studied and several of them have seen industrial production. Solar cells are broadly divided into three categories according to the type of material and configuration: (1) The first generation solar cells are referred to as monocrystalline and polycrystalline silicon-based cells. Presently, Si solar cell technology covers 90% of the PV market and is considered the most mature PV technology. They have witnessed the best commercial success among all PV technologies on account of their higher output efficiencies and longer panel lifetime [2]. However, Si technology is still limited to meeting the global energy demand owing to the sophisticated and high-cost fabrication processes. (2) Solar cells based on thin film technologies are second generation wherein the absorbers are CdTe, copper-based chalcopyrite like CIGS, and GaAs. These absorbers possess direct bandgap and are advantageous for effective absorption of light even with very few microns thickness as compared to the indirect bandgap Si. (3) Third generation solar cells are constructed with recent structures and devices that can decrease the overall cost of devices. They include dye- and quantum dot- sensitized solar cells (DSSC and QDSC), and organic and perovskite solar cells (OSC and PSC). Low cost, abundance, flexibility, and simple production methods have paved the path for fast development and a rapid rise in interest in these devices. The performance of these devices is largely dependent on material aspects like the composition of the absorber layer, efficient charge transport layers, counter electrode, contact layer, and passivation layer. Extensive efforts are being dedicated to improving each of these areas to unveil a highly efficient and stable PV device that could meet the global energy demand.

Carbon-based materials and their numerous allotropes are among the most explored and indispensable parts of the current materials and energy industry. There are diverse nanostructures of carbon like zero-dimensional fullerenes, one-dimensional carbon nanotubes, and two-dimensional graphene materials, that have gathered huge interest and possess fascinating electrical, mechanical, and optical properties [3]. Among them, graphene is one of the most studied and appreciated thinnest materials with an exceptionally large specific surface area of 2630 m^2/g, electron mobility of 200 000 cm^2/Vs, high strength (Young's modulus of ~1 TPa), and thermal conductivity of 5000 W/mK. These properties make graphene apt for numerous applications like supercapacitors, batteries, fuel cells, gas storage, biosensors, and solar cells [4]. Although, graphene in its conventional two-dimensional form has significantly contributed to the performance enhancement of various PV and battery devices, it tends to agglomerate quickly countering its outstanding properties.

To combat this shortcoming, various strategies are employed to architect 2D layers into a 3D-G. The 3D-G architectures preserve most of the unique characteristics of individual layers without the issue of stacking. These architectures are basically non-graphitic 3D structured graphene material constituting not more than ten layers. The relationship between different graphene structures and transformation from one structure to another can easily be visualized as shown in Fig. 1a. Based on the morphology and dimensions, 3D-G structures are broadly classified into two categories as depicted in Fig. 1b [5]: (1) macrostructures or monoliths, such structures possess dimensions greater than 100 μm, for example, 3D-G foams, aerogels, sponges, films, fibres, and milli-spheres; (2) microscopic materials having dimensions smaller than 100 μm like micro-sized or nano-sized powdered 3D structures. Although dimensions are important in these structures, the type of connection between these graphene sheets is also crucial for the characteristics of 3D structures. Based on the type of connectivity, there are two types of structures: (1) Joint 3D structures in which individual graphene sheets are interlinked by weak Van der Waals forces; (2) Integrated graphene structures that possess strong chemical bonds among graphene sheets. Due to the strong chemical bonds, integrated structures display better electrical and mechanical properties. The precursor and synthesis methods of these structures are very essential in controlling the properties of these materials. For example, 3D-G architecture obtained from the hydrothermal method has depicted a very low conductivity of 0.5 S/m [6]. These structures are primarily produced using three types of precursors that include [3]: (1) direct assembly from rGO (reduced graphene oxide) sheets, (2) use of hydrocarbons, and (3) from inorganic chemicals such as CO, CS_2, and CO_2.

The exceptional properties of 3D-G like remarkably high transparency, high mobility, and superior electrical and thermal conductivity, have made it a great choice to be applied as counter electrodes, transparent electrodes, passivation/protective layer, and electron transport layer (ETL) or hole transport layer (HTL) in solar cells [7, 8]. Basically, these architectures are employed as conducting units to improve the charge transfer process in the solar cell and are required to possess long-term stability against moisture and air. It is pertinent to note that the conductivity of 3D-G plays an essential part in the successful establishment of these materials for power generation devices. The overall electrical conductivity is controlled by the quality of composing graphene sheets and the connection between them, which directly affects the charge transfer of electrons [9]. According to recent reports, conductivity of 3D-G varies between 100 000 to 1 S/m [10, 3]. The conductivity is generally measured by four-probe or two-probe methods, but the values may differ based on the position of detecting electrodes owing to the anisotropy of macro-monoliths of 3D-G [11]. The conductivity is also dependent on the mass density of the material, for example, a material having high density generally exhibits higher overall conductivity, and therefore, materials like 3D-G sponges with low mass density exhibit poor conductivities (0.7–110 S/m) [10, 11]. In addition to the mass density, as discussed earlier, the synthesis methods or reduction of graphene also impact the conductivity of this material. For instance, 3D-G produced by the hydrothermal reduction method with an exceptional density of 1600 mg/cm^3 has displayed limited conductivity (760 S/m) [12].

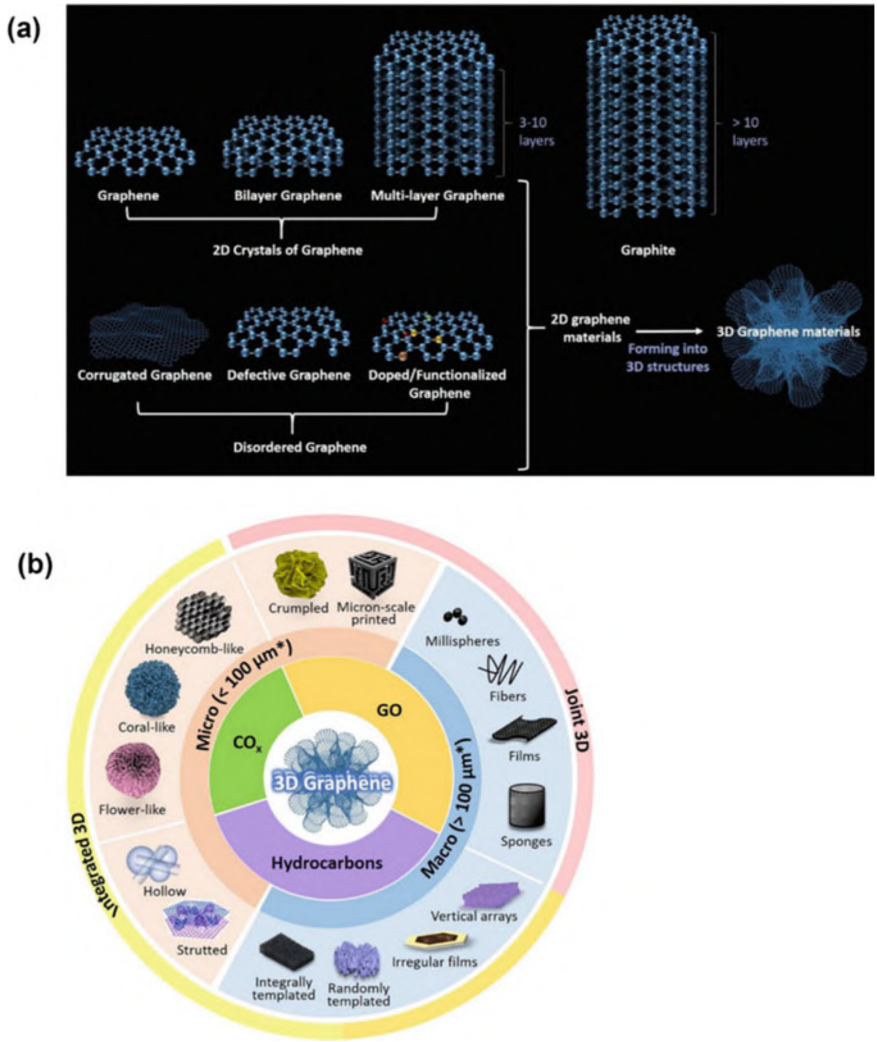

Fig. 1 Schematic diagram showing **a** different types of graphene-related materials and their formation **b** variety of microscopic 3D-G (<100 μm dimension) and macroscopic 3D-G materials (>100 μm dimension). Adapted with permission [3], Copyright (2020), American Chemical Society

While we are discussing the potential of 3D-G electrodes in PVs, it may be noted that the optical properties also play a vital role along with conductivity. Despite being just an atomic-layer thick, the graphene monolayers show absorption from the visible to infrared range [13]. Moreover, absorption of these structures can be further improved by mechanical compression or the introduction of surface defects and chemical functional groups on the surface of rGO [14]. Structural modification can also alter absorption phenomena like bi-continuous or nanoporous structures have displayed enhanced light absorption for visible light [15]. With further optimization of reduction degree, the 3D structure-based photodetector has shown 40 fold enhanced photon absorption than the single graphene layer that resulted in external quantum efficiency of $1.04 \times 10^7\%$ as compared to Si ($6.5 \times 10^5\%$) [15]. The preceding discussion emphasizes the scope of 3D-G structures in PV technologies. The output of PV devices is basically dependent on the open circuit potential and fill factor, which is correlated to the quasi-Fermi level splitting of the absorber. 3D-G with enhanced electrical and optical properties improves these two parameters, and hence boosts the overall performance of devices. In PV, 3D-G-based architectures are very appealing for making economic, lightweight, and flexible devices to obtain a wide range of absorption windows from UV to far IR region, to improve charge separation kinetics, and for high catalytic activity purposes. The optoelectronic and electrocatalytic characteristics of 3D-G could be suitably altered by surface functionalization. Based on these aspects, the use of 3D-G in different types of solar cells is discussed while focusing on the limitations in improving the performance and further directions for enhancement.

2 3D-G in DSSC

DSSC is among the promising alternative PV systems that offer reasonably high conversion efficiency, ease of fabrication, and integration into surfaces, while being a low-cost and environmentally friendly technology [16]. Typical construction of DSSC consists of a dye-adsorbed metal-oxide electrode, counter electrode, and an iodide electrolyte as shown in Fig. 2a [17]. Each component performs a significant part in improving the output performance of DSSC. Different types of dyes are explored such as black dye (N749), indoline, porphyrin, and phthalocyanine to enhance the optical properties of DSSC in the visible solar spectrum [18]. There have been numerous efforts to devise new photoanode to enhance the efficiency of existing metal-oxides like TiO_2 and ZnO [19]. While improving the properties of the photoanode is the widely studied aspect, the potential of the counter electrode to reduce the triiodide to iodide is also important for DSSC's performance. Pt is so far the most explored material as a counter electrode as a result of its high conductivity, remarkable stability, and exceptional electrocatalytic properties for the reduction of triiodide, but its high cost hinders the commercialization of the devices [20]. Carbon-based materials with robust catalytic activity, high conductivity, and superior chemical stability are considered a convincing substitute for Pt. There is a wide range of carbon materials like graphite, graphene, CNTs, and 3D-G that are studied in DSSC as both an efficient photoanode as well as the counter electrode.

3D-G is the emerging and the most promising material owing to its very porous, conductive, and flexible interconnected framework that provides an interconnected highway system for electron transfer. It also possesses defects and more enriched edges that act as catalytic active sites [21]. Moreover, due to its remarkably high electrical conductivity, desirable optoelectronic properties, and exceptionally large

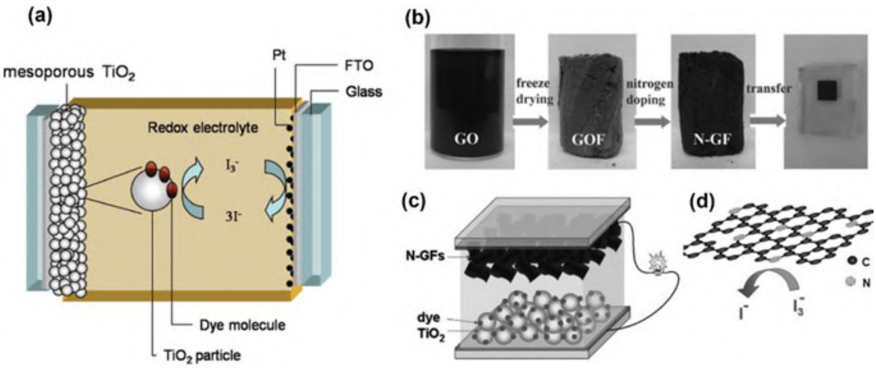

Fig. 2 **a** Schematic diagram showing the working principle of DSSC **b** Fabrication of N-doped graphene foam counter electrode (N-GF), **c** DSSC cell constituting N-GF as the counter electrode, and **d** electrolyte reduction on the counter electrode. Adapted with permission [17] and [31], respectively. Copyright (2012), WILEY–VCH Verlag GmbH & Co. KGaA, Weinheim. Copyright (2010), American Chemical Society

specific surface area, it is regarded as a convincing alternative for DSSC's working and counter electrodes [22]. Wang et al. have synthesized honeycomb structured 3D-G nanosheets that have exhibited a PCE of 7.8% which is equivalent to the DSSC with expensive platinum electrodes [23]. Tang et al. have adopted a chemical vapour deposition process to synthesize 3D-G with the nickel foam rod as a template which is then used as a photoanode. The electrode has demonstrated an efficiency enhancement of 32.7% as compared to pure P25 which could be attributed to the reduced contact resistance between the junction of graphene sheets forming the efficient channel for carrier transport [24]. Flexible DSSCs fabricated on plastic substrates often experience losses due to poor electron diffusion rates that could be correlated to the implausible situation of high-temperature sintering. Hence, the output efficiency of such devices is reported to be below 6%. Zhi et al. have fabricated flexible DSSCs on plastic substrates with improved performance by constructing a 3D-G decorated nanocrystalline TiO_2 electrode. The impact of the efficient charge transfer process and large surface area in 3D-G-based DSSC has assisted in exhibiting output efficiency of 6.41% (56% greater than DSSC without 3D-G). Yang et al. have synthesized Pt-free counter electrode by attaching Fe_2O_3 nanoparticles onto 3D-G frameworks, wherein Fe_2O_3 acts as a highly active site, and the 3D-G provides an internally connected electron transfer mechanism. The resulting system has demonstrated an improved PCE of 7.45% as compared to platinum electrodes (7.29%) [21]. He et al. have studied the effect of ZIF-8 and three-dimensional graphene network co-deposited TiO_2 electrode as photoanode in DSSC that has demonstrated superior PCE of 8.77% with 5 wt.% ZIF-8 loading. The combination of the large BET surface area of ZIF-8 and fast charge transport of 3D-G enhances the amount of dye loading and produces a high output current [25]. In a similar kind of study, Tang et al. have demonstrated RGO and 3D-G network co-deposited structures, wherein the 3D-G provides a fast charge transport network for electrons, while RGO nanosheets further accelerate the carrier transport at the interface between the graphene basal plane and TiO_2 [26]. Sun et al. have fabricated RGO and 3D-G-based two-layer constructed electrodes that have depicted a PCE of 8.87% as compared to the pristine P25-based DSSCs [27].

Chang et al. have fabricated a unique architecture of graphene nanosheets decorated with graphene foam that has shown a PCE of 7.70%. In this study, the group has explored the effect of big size graphene nanosheets and smaller size graphene quantum dots, produced by the reduction of GO using heat and laser, respectively. They have found that the quantum dots with a size of 100 nm or less provide a greater number of electroactive sites and edges and offer low charge transfer resistance. These novel structures utilize a fast electron transfer system using a graphene framework and smooth charge injection between the graphene nanosheets and the substrate [28]. In the quest for developing hierarchical structures, Yu et al. have contributed to synthesizing N-doped rGO to form a three-dimensional N-doped holey rGO framework (NHGF). The NHGF in the form of compressed paper possesses sufficient mechanical strength to be installed as free-standing counter electrodes and rGO nanosheets in 3D framework are interconnected and interlocked together to avoid restacking [29]. Zhu et al. have synthesized CuS nanocrystals modified 3D-G frameworks by in situ hydrothermal process and reported PCE of 7.07%. Figure 2b shows the complete process of electrode formation in DSSC using different methods. The 3D-G electrode in DSSC and a schematic diagram illustrating the reduction of triiodide electrolyte are shown in Fig. 2c, d. To further explore composite structures of 3D-G, Sun et al. have constructed 3D porous rGO/CoS containing spherical hierarchical (CSHPS-G) architectures as an effective counter electrode in DSSC by a simple hydrothermal method [30].

The porous structure of nanostructured electrode ensures a proficient electrolyte diffusion system and provides plenty of electrocatalytic sites. Consequently, CSHPS-G-based DSSC shows a remarkable PCE of 5.41% which is better than platinum-based DSSC. Roh et al. have fabricated 3D crumpled graphene (3D CGR)/GR sheets-based DSSC that has demonstrated a PCE of 7.2%, which is 56% greater than the conventional DSSC [32]. Lee et al. have studied 3D nano-foam graphene (3D-NFG) synthesized by CVD, where pyrolyzed carbonized-C and the nickel nano-frame are employed as carbon sources [33]. The study proves that the benefits of high surface area and electrical conductivity of 3D-NFG can be utilized to substitute expensive platinum as a counter electrode in DSSC. The 3D-NFG-based DSSC has exhibited a PCE of 5.2%. In one of the creative works, Wei et al. have reported 3D cauliflower-fungus-like graphene (3D CFG) from CO_2 and have employed it as an electrode in DSSC [34]. 3D-CFG-based DSSC has manifested maximum conversion efficiency of 8.1%, which is tenfold higher than the regular graphene counter electrode prepared through the graphite chemical exfoliation process (0.7%). The same group has also reported 3D crape myrtle flower-like graphene counter electrodes synthesized by the reaction of carbon dioxide and Na, and have obtained a high PCE of 10.1% [35].

Most of the studies discussed herein focus on the modification of working electrodes (generally TiO_2) with 3D-G where the dye adsorption capacity, charge transfer, and separation mechanisms depend on the properties of the working electrode. Loeblein et al. have utilized 3D-G as an independent working electrode by modifying it as an oxidized 3D-G (o-3D). By functionalizing oxygen groups over 3D-G, a bandgap of 0.2 eV is induced and a desirable electronic band structure is formed that could facilitate the interactions between p-p electron donors and acceptors, and induce the attraction between positive dye ions and negative adsorbents. [22]. Figure 3a shows the construction of DSSC with p-doped 3D-G nano-networks (3D-GN) as an electrode [36]. A comparative study is carried out between 3D-GN and platinum counter electrodes using photocurrent–voltage curves as depicted in Fig. 3b. The electrochemical impedance spectroscopy (EIS) and IPCE measurements are demonstrated in Fig. 3c and d, respectively. The 3D-GN nanostructure electrodes have exhibited a PCE of 8.46% as compared to Pt-based DSSC (6.01%) which is also evident from the IV and IPCE measurements. This detailed discussion on the reports constituting numerous studies clearly projects excellent performance of 3D-G-related materials as electrodes due to their large surface area and efficient charge transfer process.

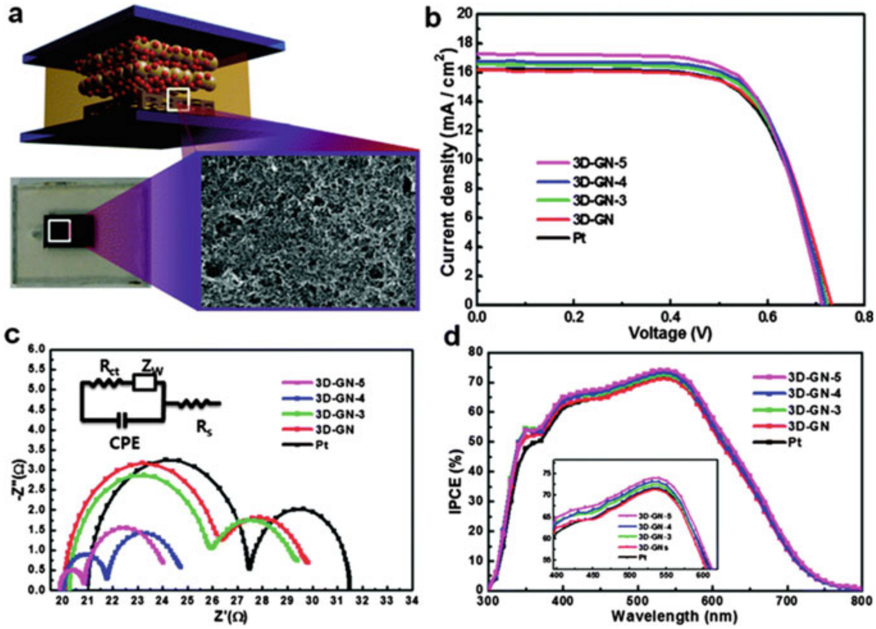

Fig. 3 **a** Schematic diagram showing DSSC with 3D-G electrode, PV performance of DSSC including **b** J–V, **c** EIS curves and **d** IPCE spectra using 3D graphene and platinum counter electrodes under the illumination of AM 1.5. Adapted with permission [36], Copyright (2014), The Royal Society of Chemistry

3 3D-G in QDSCs

QDSCs are the emerging third generation solar cells that are studied extensively owing to unique characteristics of quantum dots like easy tunability of band gap by altering size or composition, considerably high molar attenuation coefficient, large intrinsic dipole moments, and stability against photons, heat, and water as opposed to dye molecules and lead halide perovskite [37]. Moreover, the concept of multiple exciton generation provides the insights that QDSCs could break the Shockley–Quessier efficiency limit of 32.9% established for mono-junction solar cells. The concept of QDSC is like DSSC where a wide bandgap semiconductor is sensitized with a low bandgap material to harvest the light and produce charge carriers, though in QDSC, dye is replaced by quantum dots. Generally, QDSC consists of a quantum dot sensitized photoanode and counter electrode immersed in the electrolyte as displayed in Fig. 4a. The light absorption, charge carrier generation, and transfer processes are stepwise explained in Fig. 4b. When light is incident on the photoanode, quantum dots absorb it and produce electron in conduction band and hole in the valence band, respectively. Due to the favourable band edge alignment, the electrons from quantum dots are transferred to the conduction band of metal oxide (1) and then to counter electrode (2) via an external circuit, whereas holes travel from the valence band of quantum dots to electrolyte (3) where reduction of sulphides takes place (4). This leads to the efficient separation of charge carriers avoiding the charge recombination losses ((5) and (6)). The most employed metal-oxides in QDSC include TiO_2, ZnO, SnO_2, etc., while the most explored sensitizing quantum dots are Cd, Pb or multilayer chalcogenides. The performance of QDSC is limited by the losses due to the characteristic nature of electron transport throughout the quantum dots network [38]. The electron transfer in the network of quantum dots is through the hopping of electrons between orbitals of adjacent quantum dots, which is defined as a random walk. This process affects the electron collection at the photoanode as the electron must complete multiple hopping steps to reach the current-collecting substrate without unwanted processes like recombination or trapped-state termination. Not only the electron transfer kinetics is hindered, but also with an increase in quantum dots thickness or layering, quantum dots near metal oxide lack access to electrolytes, and hence regeneration of quantum dots is hindered. Utilizing graphene-related compounds improves this charge transfer phenomenon between different layers and provides efficient interface engineering by acting like an electron funnel.

In some reports, it has been established that incorporating graphene in quantum dots improved the collection and transport of photogenerated charge carriers. 3D-G possesses the potential to further improve the efficiency of these working electrodes by offering an efficient electron transfer mechanism through an interconnected electron transfer highway system, the presence of enriched edges and defects acting as electroactive sites, and a large surface area for electrolyte diffusion. Lightcap et al. constructed a unique structure of 3D QD-sensitized graphene photoelectrodes that provide a substantial solution to overcome the problem associated with a random walk and limited conductivity of quantum dot sensitizers [38]. In addition, the photocurrent

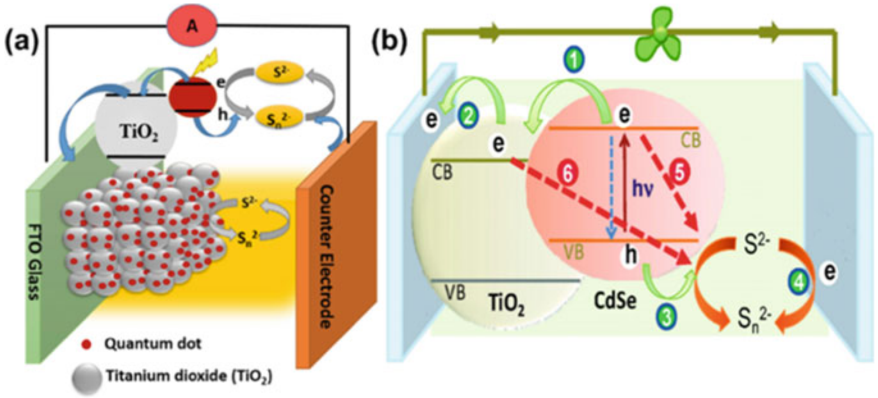

Fig. 4 Schematic diagram showing **a** typical construction of QDSSC **b** charge transfer processes in a QDSSC. Adapted with permission [39], Copyright (2016), Elsevier Ltd

response is improved by 150% as compared to QDSC without graphene. Tavakoli et al. have studied 3D-G networks (3DGNs)-based transparent electrodes to improve the output of lead sulphide-based QDSC [40]. The study has demonstrated that 3DGN electrodes improve the electron transfer process which leads to a 30% improvement in efficiency in comparison to the conventional DSSC. There are few reports where 3D-G is utilized as an efficient counter electrode owing to its extraordinary conductivity and large surface area. Zhu et al. have synthesized CuS nanocrystals loaded with 3D-G framework (GF) as a counter electrode in QDSC [41]. It is demonstrated that QDSC with GF counter electrode displays a PCE of 5.04% as compared to those of the traditional counter electrodes like platinum (3.18%), CuS (3.75%), and 2D graphene–CuS electrode (4.17%). The electron transport in 2D and 3D GF are explained in Fig. 5a, b. The GF–CuS electrode possessing an interconnected 3D conductive network structure facilitates the electron transfer via. "multi-channel transport pathways" and uniformly distributed copper sulphide nanoparticles provide numerous electrocatalytic sites, enhancing the electrical and catalytic properties of the composite electrode, as depicted in Fig. 5b. Superior performance of 3D-G-CuS-based counter electrodes as compared to platinum is quite evident by I-V plots in Fig. 5c. However, despite possessing the excellent potential to contribute to the significant improvement in the efficiency of QDSCs, as discussed already, the studies are yet limited and thus paves the way for researchers to explore this excellent material extensively to further enhance the performance of QDSCs.

3D-G in other solar cells

Research on perovskite solar cells (PSCs) is growing enormously and garnering attention due to their outstanding performance and cost-effective easy solution processability. PSCs have achieved higher performance in terms of conversion efficiency above 25% on par with monocrystalline, heterojunction Si [5], and higher than CIGS and CdTe solar cells (26.1, 26.7, 23.4, and 22.1%, respectively) in a quick

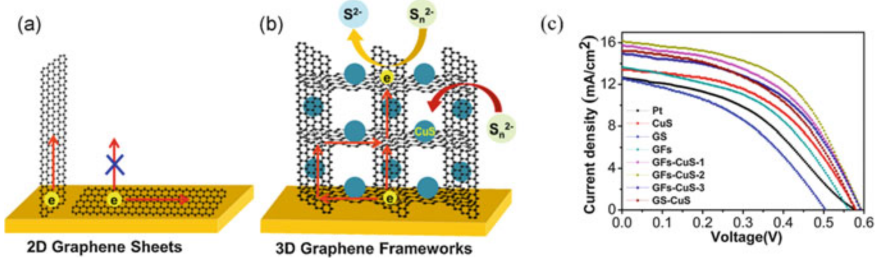

Fig. 5 Schematic diagram showing transfer of the electrons in **a** 2D graphene sheets, **b** 3D-G-CuS counter electrode for electrolyte reduction in QDSSC, and **c** I-V plots comparing the performance of various counter electrodes. Adapted with permission [41], Copyright (2016), Elsevier Ltd

time [42]. A typical PSC consists of three major layers classified based on their specific roles that control the performance and stability of devices like perovskite absorbers, ETLs, and HTLs. The hurdles in the commercialization of PSCs include instability of absorber and HTLs and the use of costly noble metal-based counter electrodes. It is reported that metal-free counter electrodes could contribute to the stability of PSCs [43]. Moreover, cost-effective counter electrodes also support in realization of achieving the ideal levelized cost of energy (LCOE) of PSC less than 5 US cents kWh^{-1} [5]. Carbon-based electrodes are a viable option to replace these costly metal-based counter electrodes as they are cheap, abundant, possess high chemical/electrochemical stability, large surface area, better electrical conductivity, and are eco-friendly. Recently, 3D-G is gaining attention as an efficient electrode material in PSC owing to its high surface area, remarkable electrical conductivity, and stability.

Wei et al. have studied the synthesis of a 3D honeycomb resembling graphene (3DHG) by a simple reaction of K and CO_2. They have utilized 3DHG as a counter electrode in PSC without any hole transport material (HTM) and have recorded a PCE of 10.06%. This study has embarked on a novel journey of material synthesis using chemistry related to potassium to produce electricity from solar light [44]. Similarly, Pandey et al. have fabricated 3D-G nanosheets (GNs) using plastic and have employed them in PSC without HTL. They have used a two-step pyrolysis technique in which a mesh of nickel (99.99%) is used as the template to synthesize 3D GNs without using any kind of acid in reaction. Figure 6a shows the cyclic voltammetry curves of 3D-GN which is used to determine the HOMO–LUMO of 3D-GN and compare with pristine graphene material (Fig. 6b). The device has resulted in a PCE of 12.40% as compared to the conventional device (11.04%) due to improved conductivity and lowered recombination process [5]. The reduced recombination is achieved owing to the fast charge transfer process as shown by bang edge positions in Fig. 6c where a desirable HOMO position of the 3D-GN can easily promote faster transfer of holes. Saheed et al. fabricated 3D-G foams that have improved the charge transport in ZnO ETL in PSCs. The 3D/ZnO architecture has not only improved PCE to 10.9% with respect to ZnO (4.2%), but has even enhanced the open circuit potential

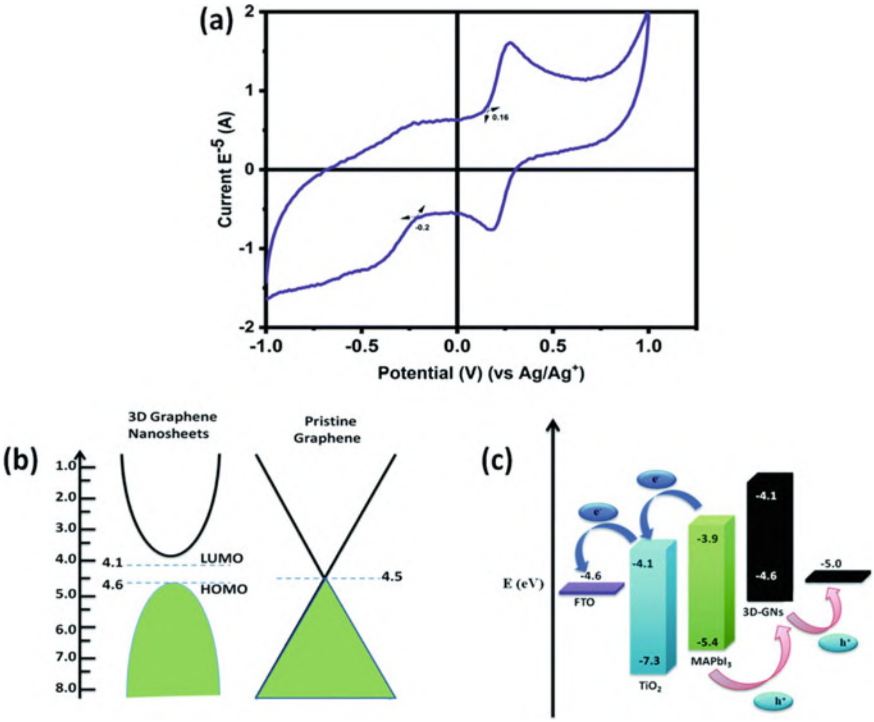

Fig. 6 **A** CV plots of 3DG nanosheets derived from waste, **b** HOMO–LUMO levels of 3DGNs and conventional graphene, and **c** band edge positions of 3DGN employed PSC. Adapted from reference [5]. Copyright The Authors, some rights reserved; exclusive licensee [The Royal Society of Chemistry 2021]. Distributed under a Creative Commons Attribution License 3.0 (CC BY) https://creativecommons.org/licenses/by/3.0/

of the device by two-fold. The improvement in the performance is attributed to the electron transporting highway system that leads to effective charge separation within the 3D-G framework [45]. 3D-G electrodes are also studied in other PV devices like CdTe solar cells. Bi et al. have carried out large-scale fabrication of 3D-G upon nickel foams using ambient pressure chemical vapour deposition (APCVD). The highly conductive films with a sheet resistance of ≈0.45 Ω/□ and a conductivity of ca 600 S/cm are explored in CdTe-based devices that have dramatically enhanced the PCE to 9.1% [46]. The above discussion clearly validates the fact that there are very few reports exploring 3D-G electrodes in PSC and other solar cells, and additional research efforts are required in order to utilize and realize the full potential of 3DG electrodes in PSC, CdTe, Si, organic, and other emerging solar cells.

4 Conclusions

The present chapter discusses the latest developments in the application of 3DG and its functional composites in PVs. These materials boost the PV performance of devices owing to their unique physical and chemical characteristics and remarkable properties like high carrier mobility, low resistivity, transmittance, and two-dimensional networks. There are pathbreaking evolutions happening in the field of 3DG synthesis, formation of composites, and its employment in various constituents of next generation solar cells. 3DG is being used as electrode material in liquid junction cells like DSSC and QDSC as well as solid junctions like organic PVs and PSCs, because of its minimal mass density, high specific surface area, remarkable electrocatalytic activity, stability, and excellent mechanical properties coupled with outstanding electrical and optical properties. Presently, most of the 3DG electrodes are used in conjunction with other semiconducting electrodes due to the absence of bandgap in these materials. Therefore, it is highly desirable to induce a bandgap in 3DG materials by implying some chemical modifications. Efforts should also be concentrated on developing 3DG-based functional and composite materials that could improve the interfacial charge transfer process across the electrode and electrolyte. This can be a significant step in replacing platinum as counter electrodes in QDSC since platinum causes a poisoning effect with polysulphide electrode. Defects in 3DG are favourable for catalytic properties but in some devices, controlled defects or high purity could be very beneficial. Achieving such purity depends on the method of reduction of GO explored in order to form 3DG structures. Utilizing CVD-based 3DG looks more promising for maintaining purity, innate 3D charge transport system, and superior electrical conductivity. Owing to these advantages, more studies should be concentrated on improving the CVD-3DG synthesis technique and making it industrially viable.

Moreover, attempts could be targeted to modify synthesis techniques in order to achieve precise control of surface properties like pore size and thickness. 3DG with a large pore size in the range from one hundred to several hundred micrometres decreases its mechanical properties, therefore, meso- or microporous features are highly desirable. In addition, there are only a few reports on the application of 3DG electrodes in PSC and other solid junction solar cells. There is wide scope to test this material and check its feasibility as a working or counter electrode, ETL or HTL, and passivation layers to enhance the performance and stability. Further, efforts are required in the field of interfacial engineering as it is very beneficial to control interfacial voltage drop and leakage current which plays an important part in enhancing the efficiency of PV devices. There is still huge scope to discover novel 3DG-based architectures that can be incorporated into numerous devices like multijunction or tandem solar cells to improve the output performance of these devices.

Acknowledgements The authors would like to acknowledge the project titled "Development of NiO_x Thin Films as Electrode Material for Semi-transparent Solar Cells" (SJD78) from the Estonian Research Council (ERC) granted to the Department of Materials and Environmental Technology, Tallinn University of Technology, Estonia. The authors wish to thank Prof. Ilona Oja Acik, Head of the Laboratory of Thin Film Chemical Technologies, Department of Materials and Environmental Technology, Tallinn University of Technology for her continuous support.

References

1. Chapin, D.M., Fuller, C.S., Pearson, G.L.: A new silicon p-n junction photocell for converting solar radiation into electrical power. J. Appl. Phys. **25**, 676 (1954)
2. Branker, K., Pathak, M.J.M., Pearce, J.M.: A review of solar photovoltaic levelized cost of electricity. Renew. Sustain. Energy Rev. **15**, 4470–4482 (2011)
3. Sun, Z., Fang, S., Hu, Y.H.: 3D graphene materials: from understanding to design and synthesis control. Chem. Rev. **120**, 10336–10453 (2020)
4. Novoselov, K.S., Fal, V.I., Colombo, L., Gellert, P.R., Schwab, M.G., Kim, K., Ko, V.I.F., Colombo, L., Gellert, P.R., Schwab, M.G., Kim, K.: A roadmap for graphene. Nature **490**, 192–200 (2012)
5. Pandey, S., Kumar, A., Karakoti, M., Garg, K.K., Rana, A., Tatrari, G., Bohra, B.S., Yadav, P., Singh, R.K., Sahoo, N.G.: 3D graphene nanosheets from plastic waste for highly efficient HTM free perovskite solar cells. Nanoscale Adv. **3**, 4726–4738 (2021)
6. Xu, Y., Sheng, K., Li, C., Shi, G.: Self-assembled graphene hydrogel via a one-step hydrothermal process. ACS Nano **4**, 4324–4330 (2010)
7. Yang, P., Hu, Z., Zhao, X., Chen, D., Lin, H., Lai, X., Yang, L.: Cesium-containing perovskite solar cell based on graphene/TiO_2 electron transport layer. ChemistrySelect **2**, 9433–9437 (2017)
8. Yan, K., Wei, Z., Li, J., Chen, H., Yi, Y., Zheng, X., Long, X., Wang, Z., Wang, J., Xu, J., Yang, S.: High-performance graphene-based hole conductor-free perovskite solar cells: schottky junction enhanced hole extraction and electron blocking. Small **11**, 2269–2274 (2015)
9. Pei, S., Cheng, H.: The reduction of graphene oxide. Carbon N. Y. **50**, 3210–3228 (2011)
10. García-TOn, E., Barg, S., Franco, J., Bell, R., Eslava, S., D'Elia, E., Maher, R.C., Guitian, F., Saiz, E.: Printing in three dimensions with Graphene. Adv. Mater. **27**, 1688–1693 (2015)
11. Qiu, L., Liu, J.Z., Chang, S.L.Y., Wu, Y., Li, D.: Biomimetic superelastic graphene-based cellular monoliths. Nat. Commun. **3**, 1–7 (2012)
12. Bi, H., Yin, K., Xie, X., Zhou, Y., Wan, N., Xu, F., Banhart, F., Sun, L., Ruoff, R.S.: Low temperature casting of graphene with high compressive strength. Adv. Mater. **24**, 5124–5129 (2012)
13. Nair, R.R., Blake, P., Grigorenko, A.N., Novoselov, K.S., Booth, T.J., Stauber, T., Peres, N.M.R., Geim, A.K.: Fine structure constant defines visual transparency of graphene. Science **320**, 1308 (2008)
14. Gao, H.L., Zhu, Y.B., Mao, L.B., Wang, F.C., Luo, X.S., Liu, Y.Y., Lu, Y., Pan, Z., Ge, J., Shen, W., Zheng, Y.R., Xu, L., Wang, L.J., Xu, W.H., Wu, H.A., Yu, S.H.: Super-elastic and fatigue resistant carbon material with lamellar multi-arch microstructure. Nat. Commun. **7**, 1–8 (2016)
15. Ito, Y., Zhang, W., Li, J., Chang, H., Liu, P., Fujita, T., Tan, Y., Yan, F., Chen, M.: 3D bicontinuous nanoporous reduced graphene oxide for highly sensitive photodetectors. Adv. Funct. Mater. **26**, 1271–1277 (2016)
16. Cells, P.D.S., Meyer, G.J.: The 2010 millennium technology grand, 4337–4343 (2010)
17. Hagfeldt, A., Boschloo, G., Sun, L., Kloo, L., Pettersson, H.: Dye-sensitized solar cells. Chem. Rev. **110**, 6595–6663 (2010)
18. Nazeeruddin, M.K., Péchy, P., Grätzel, M.: Efficient panchromatic sensitization of nanocrystalline TiO_2 films by a black dye based on a trithiocyanato-ruthenium complex. Chem. Commun., 1705–1706 (1997)
19. Grätzel*, M.: Solar energy conversion by dye-sensitized photovoltaic cells. Inorganic Chem. **44**, 6841–6851 (2005)

20. Yen, M.Y., Teng, C.C., Hsiao, M.C., Liu, P.I., Chuang, W.P., Ma, C.C.M., Hsieh, C.K., Tsai, M.C., Tsai, C.H.: Platinum nanoparticles/graphene composite catalyst as a novel composite counter electrode for high performance dye-sensitized solar cells. J. Mater. Chem. **21**, 12880–12888 (2011)
21. Yang, W., Xu, X., Li, Z., Yang, F., Zhang, L., Li, Y., Wang, A., Chen, S.: Construction of efficient counter electrodes for dye-sensitized solar cells: Fe2O3 nanoparticles anchored onto graphene frameworks. Carbon **96**, 947–954 (2016)
22. Loeblein, M., Bruno, A., Loh, G.C., Bolker, A., Saguy, C., Antila, L., Tsang, S.H., Teo, E.H.T.: Investigation of electronic band structure and charge transfer mechanism of oxidized three-dimensional graphene as metal-free anodes material for dye sensitized solar cell application. Chem. Phys. Lett. **685**, 442–450 (2017)
23. Wang, H., Sun, K., Tao, F., Stacchiola, D.J., Hu, Y.H.: 3D honeycomb-like structured graphene and its high efficiency as a counter-electrode catalyst for dye-sensitized solar cells. Angew. Chemie - Int. Ed. **52**, 9210–9214 (2013)
24. Tang, B., Hu, G., Gao, H., Shi, Z.: Three-dimensional graphene network assisted high performance dye sensitized solar cells. J. Power Sources. **234**, 60–68 (2013)
25. He, Y., Wang, W.: ZIF-8 and three-dimensional graphene network assisted DSSCs with high performances. J. Solid State Chem. **296**, 121992 (2021)
26. Tang, B., Ji, G., Wang, Z., Chen, H., Li, X., Yu, H., Li, S., Liu, H.: Three-dimensional graphene networks and reduced graphene oxide nanosheets co-modified dye-sensitized solar cells. RSC Adv. **7**, 45280–45286 (2017)
27. Sun, Y., Cao, Y., Huang, W., Zhu, Y., Heng, L., Tang, B.: High-performance photoanode for dye sensitized solar cells with graphene modified two-layer construction. Mater. Lett. **165**, 178–180 (2016)
28. Chang, Q., Huang, L., Wang, J., Ma, Z., Li, P., Yan, Y., Zhu, J., Xu, S., Shen, L., Chen, Q., Yu, Q., Shi, W.: Nanoarchitecture of variable sized graphene nanosheets incorporated into three-dimensional graphene network for dye sensitized solar cells. Carbon **85**, 185–193 (2015)
29. Yu, M., Zhang, J., Li, S., Meng, Y., Liu, J.: Three-dimensional nitrogen doped holey reduced graphene oxide framework as metal-free counter electrodes for high performance dye-sensitized solar cells. J. Power Sources. **308**, 44–51 (2016)
30. Sun, L., Lu, L., Bai, Y., Sun, K.: Three-dimensional porous reduced graphene oxide/sphere-like CoS hierarchical architecture composite as efficient counter electrodes for dye-sensitized solar cells. J. Alloys Compd. **654**, 196–201 (2016)
31. Xue, Y., Liu, J., Chen, H., Wang, R., Li, D., Qu, J., Dai, L.: Nitrogen-doped graphene foams as metal-free counter electrodes in high-performance dye-sensitized solar cells. Angew. Chemie Int. Ed. **51**, 12124–12127 (2012)
32. Roh, K.M., Kim, S.K., Choi, J.H., Jo, E.H., Chang, H., Jang, H.D.: Synergetic effect of graphene sheet and three-dimensional crumpled graphene on the performance of dye-sensitized solar cells. AIChE J. **62**, 574–579 (2016)
33. Lee, J.S., Ahn, H.J., Yoon, J.C., Jang, J.H.: Three-dimensional nano-foam of few-layer graphene grown by CVD for DSSC. Phys. Chem. Chem. Phys. **14**, 7938–7943 (2012)
34. Wei, W., Sun, K., Hu, Y.H.: Synthesis of 3D cauliflower-fungus-like graphene from CO_2 as a highly efficient counter electrode material for dye-sensitized solar cells. J. Mater. Chem. A. **2**, 16842–16846 (2014)
35. Wei, W., Sun, K., Hu, Y.H.: Direct conversion of CO2 to 3D graphene and its excellent performance for dye-sensitized solar cells with 10% efficiency. J. Mater. Chem. A. **4**, 12054–12057 (2016)
36. Ahn, H.J., Kim, I.H., Yoon, J.C., Kim, S.I., Jang, J.H.: p-Doped three-dimensional graphene nano-networks superior to platinum as a counter electrode for dye-sensitized solar cells. Chem. Commun. **50**, 2412–2415 (2014)
37. Pan, Z., Rao, H., Mora-Seró, I., Bisquert, J., Zhong, X.: Quantum dot-sensitized solar cells. Chem. Soc. Rev. **47**, 7659–7702 (2018)
38. Lightcap, I.V., Kamat, p.V.: Fortification of CdSe quantum dots with graphene oxide. Excited state interactions and light energy conversion. J. Am. Chem. Soc. **134**, 7109–7116 (2012)

39. Sun, J.K., Jiang, Y., Zhong, X., Hu, J.S., Wan, L.J.: Three-dimensional nanostructured electrodes for efficient quantum-dot-sensitized solar cells. Nano Energy **32**, 130–156 (2017)
40. Tavakoli, M.M., Simchi, A., Fan, Z., Aashuri, H.: Chemical processing of three-dimensional graphene networks on transparent conducting electrodes for depleted-heterojunction quantum dot solar cells. Chem. Commun. **52**, 323–326 (2016)
41. Zhu, Y., Cui, H., Jia, S., Zheng, J., Yang, P., Wang, Z., Zhu, Z.: 3D graphene frameworks with uniformly dispersed cus as an efficient catalytic electrode for quantum dot-sensitized solar cells. Electrochim. Acta. **208**, 288–295 (2016)
42. Muchuweni, E., Martincigh, B.S., Nyamori, V.O.: Perovskite solar cells: current trends in graphene-based materials for transparent conductive electrodes, active layers, charge transport layers, and encapsulation layers. Adv. Energy Sustain. Res. **2**, 2100050 (2021)
43. Mariani, P., Najafi, L., Bianca, G., Zappia, M.I., Gabatel, L., Agresti, A., Pescetelli, S., Di Carlo, A., Bellani, S., Bonaccorso, F.: Low-temperature graphene-based paste for large-area carbon perovskite solar cells. ACS Appl. Mater. Interfaces. **13**, 22368–22380 (2021)
44. Wei, W., Hu, B., Jin, F., Jing, Z., Li, Y., García Blanco, A.A., Stacchiola, D.J., Hu, Y.H.: Potassium-chemical synthesis of 3D graphene from CO2 and its excellent performance in HTM-free perovskite solar cells. J. Mater. Chem. A **5**, 7749–7752 (2017)
45. Mohamed Saheed, M.S., Mohamed, N.M., Mahinder Singh, B.S., Wali, Q., Saheed, M.S.M., Jose, R.: Foam-like 3D graphene as a charge transport modifier in zinc oxide electron transport material in perovskite solar cells. Photochem **1**, 523–536 (2021)
46. Bi, H., Huang, F., Liang, J., Tang, Y., Lü, X., Xie, X., Jiang, M.: Large-scale preparation of highly conductive three dimensional graphene and its applications in CdTe solar cells. J. Mater. Chem. **21**, 17366–17370 (2011)

3D Graphene for Fuel Cells

Norazuwana Shaari, Nik Farah Hanis Nik Zaiman, Siti Hasanah Osman, and Ajaz Ahmad Wani

Abstract Materials science technology and research are advancing all the time which has a direct impact on the large contribution of carbon-based materials. Carbon can be present in various allotropes including zero-dimensional Carbon-60 (0D C60) and one-dimensional (1D) carbon nanotubes, two-dimensional (2D) graphene materials, and many more with unique and excellent properties. However, the function of 2D graphene still needs to be improved to meet the needs of various applications such as electrochemical catalysis, environmental remediation, energy storage, and conversion. Modifications on 2D graphene have been done at various levels to obtain a material with more efficient properties, which is in the allotrope of three-dimensional (3D) graphene. This chapter focuses on the application of 3D graphene materials in fuel cell applications starting with the introduction of fuel cells, classification, and synthesis methods for 3D graphene. Then, the current study on aerogel, hydrogel, and foam-based graphene material for fuel cell application is discussed. Next, the challenge and future perspective as well as the conclusion are given to be a reference for the reader.

Keywords 3D Graphene · Aerogel · Hydrogel · Foam · Fuel cell

1 Introduction

A device called a fuel cell transforms the chemical energy from a fuel into electrical energy by engaging in a chemical reaction with an oxidizing agent. It operates similarly to a battery but requires a continuous source of fuel and air to sustain the reaction and produce electricity [1]. Fuel cells are highly efficient and emit very little pollution, making them a promising technology for use in clean energy systems, including

---

N. Shaari (✉) · N. F. H. N. Zaiman · S. H. Osman · A. A. Wani
Fuel Cell Institute, National University of Malaysia, 43650 Bangi, Selangor, Malaysia
e-mail: norazuwanashaari@ukm.edu.my

A. A. Wani
Department of Chemistry, Aligarh Muslim University, Aligarh, India

© The Author(s), under exclusive license to Springer Nature Switzerland AG 2023
R. K. Gupta (ed.), *3D Graphene*, Carbon Nanostructures,
https://doi.org/10.1007/978-3-031-36249-1_18

transportation and power generation [2]. Fuel cells have been a significant aspect of research due to their crucial role in various fields such as portable, stationary, transportation, engineering tissue, and medical. Despite rapid growth, some challenges need to be addressed to keep fuel cells making a positive impact, such as reducing costs and improving component durability. The most crucial component in a fuel cell in Fig. 1 illustrates a membrane electrode assembly (MEA), which includes a membrane and an electrocatalyst. The anode and cathode are key parts in determining the chemical reaction, and catalyst poisoning can occur due to ineffective oxidation. The reaction is also influenced by various factors like fuel concentration and process conditions [3].

The conventional catalyst commonly used in fuel cells is platinum supported by carbon black, known as Vulcan XC-72. This type of catalyst requires a large quantity of platinum which can lead to increased costs and stability problems, such as poisoning and sintering. There is a need for research to develop more affordable and efficient catalysts [4]. In order to attain optimal electrochemical performance, the catalyst layer should be manufactured. High reaction rates are achieved through a good catalyst's facilitation of electron, proton, and reactant transfers. It is vital for this to happen that the catalyst layer's structure and composition are optimized. Despite these promising characteristics and enhanced functionality, carbon-based nanostructured materials have been gaining favor as electrocatalysts [5].

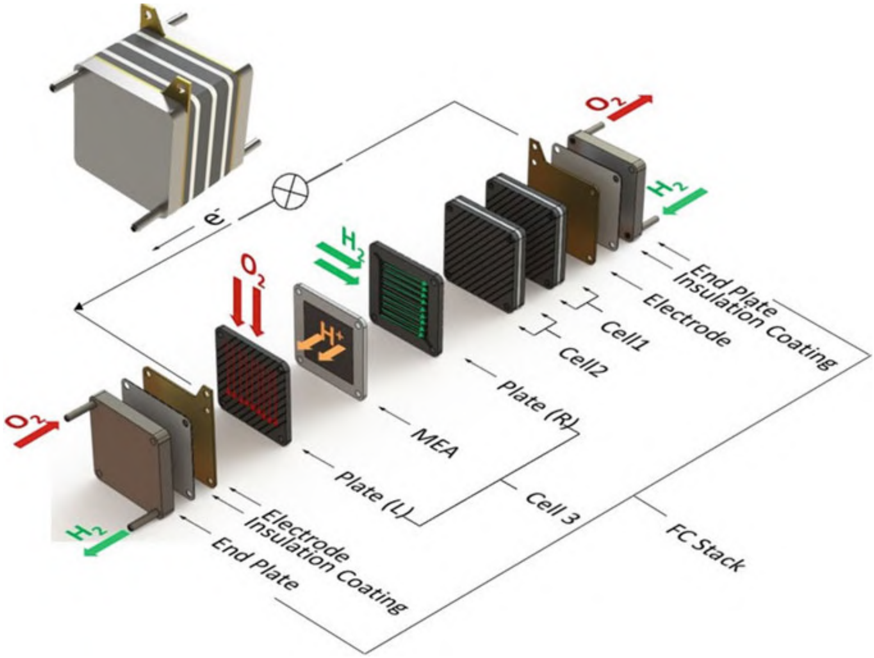

Fig. 1 Schematic of fuel cell component. Adapted with permission [14], copyright (2017), Elsevier

Paraknowitsch et al. [6] have conducted research on the use of advanced doped carbon-based catalysts in energy applications, including fuel cells. Examples of these materials include carbon and graphene in the structure of aerogels, xerogels, cryogels, hydrogels, and foam. The first carbon aerogels were created in the 1930s using the supercritical drying technique introduced by Kistler [7]. Additionally, the sol–gel polycondensation process of organic monomers such as resorcinol and formaldehyde can produce organic gels that can be transformed into carbon aerogels through carbonization, as demonstrated by the Pakalas method.

3D graphene-based materials have become highly popular for their various applications, such as in electrochemistry, fuel cells, photocatalysis, microelectronics, supercapacitors, oil clean-up sorbents, and lithium-ion batteries [8]. This is due to its unique properties, such as its high porosity, low thermal conductivity, large active surface area, and controlled pore size. It can be formed into different shapes, such as monoliths, thin films, and pellets. The structure of 3D graphene-based materials such as aerogel is composed of interconnected nano-sized particles, and it can be made with different textures like micropore, mesopore, and macropore [9]. As seen in Fig. 2, aerogel exists in a state between liquid and gas, and its texture can be fine-tuned to produce optimal catalyst support for fuel cell applications.

Recent research has shown that the gel made of 3D graphene can lower the mass transfer rate in the catalyst layer due to its distinctive pore structure. The surface chemistry of the 3D graphene-based materials gel can be altered through various methods, such as modifying the precursor used in the organic gel production stage or applying gas or liquid treatments during the final stages of gel production. These methods allow for the introduction of functional groups on the 3D graphene-based

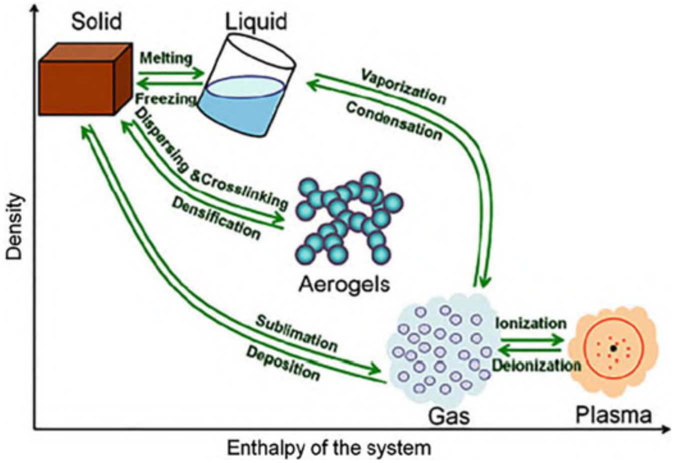

Fig. 2 The figure of "density" versus "enthalpy of the system" shows the distribution and transition of various states of matter. Adapted with permission [15], Copyright (2013) by the authors; licensee MDPI, Basel, Switzerland. This article is an open access article distributed under the terms and conditions of the Creative Commons Attribution License

materials support surface, which is crucial in preparing metal-supported catalysts and determining the loading, dispersion, oxidation conditions, and stability of the metal phase [8].

In the modern chemical industry, solid catalysts have gained prominence and 3D graphene-based materials structures have emerged as promising materials for heterogeneous catalysis and catalyst support. Kistler was the first researcher to explore the potential of aerogel as a catalyst, followed by further studies by researchers such as Baiker, Pajonk, Teichner, and other groups [10–13]. The development of 3D graphene-based materials for fuel cell applications, such as aerogel, hydrogel, and foam, is the main topic of this chapter. It also discusses the synthesis of catalysts and catalyst supports, as well as the materials' potential in fuel cells in terms of electrochemistry and power density. This chapter also nalyses how the design and operational parameters of fuel cells affect activity.

2 3D Graphene Based Aerogel Application in Fuel Cell

Nowadays, the use of nanomaterials produced by aerogel is of great importance in decreasing the reliance of fuel cells on pricey noble metals such as platinum and palladium that are used in the anode and cathode catalyst layers. The ultimate aim is to decrease the overall cost of the fuel cell system and boost its commercialization in the markets of both China and the United States. Aerogels' special qualities have the potential to increase fuel cells' effectiveness. The Proton Exchange Membrane Fuel Cell (PEMFC) stack is a widely utilized technology in various fields such as automotive, domestic, military, and small-scale applications. In order to function optimally, the PEMFC stack requires a certain amount of platinum, with a minimum requirement of 0.2 g per kilowatt, and a cell voltage of 0.65 V.

Despite this, the current PEMFC system needs to use a lot of platinum catalysts in order to achieve the desired power density of 1 kilowatt, ranging from 0.85 to 1.2 g per kilowatt. As a result, reaching the minimum level of platinum usage, which is five times less than what is currently being used, will be difficult for large-scale applications [4]. An intriguing fact is that graphene-based aerogel has the ability to stabilize on a leaf, and this material is noted for being exceptionally lightweight. Due to its appealing qualities like electrical conductivity, high mechanical strength, adsorption capacity, and thermal resistance, graphene aerogel has been reserved for a variety of applications as a special material. It also licenses names and shows to boost the characteristics and performance of catalysts in fuel cell applications. Recently, Guan and his co-worker [16] fabricated a new membrane electrode assembly (MEA), which involves placing a layer of graphene aerogel (GA) between the carbon powder microporous layer and the catalytic layer, has been developed to improve the output of direct methanol fuel cell (DMFC) at high methanol concentrations. This approach has been found to enhance the performance of DMFC significantly.

The maximal power density of the new MEA, which is 234% greater than that of the standard electrode, is reported in this study to be 27.4 mWcm^{-2} in an environment of 8 M methanol. According to the electrochemical impedance spectroscopy (EIS) test results, the novel MEA's internal resistance is not increased by the addition of GA, and the mass transfer resistance is noticeably lower at high concentrations. Çögenli et al. [17] work on graphene with carbon black heteroatoms Platinum nanoparticles supported by an aerogel hybrid served as Pt nanoparticles supported by three different hybrid carbons (50:50)—Pt/GA-C (Platinum/carbon black and graphene aerogel), Pt/NGA-C (Platinum/carbon black and nitrogen-doped graphene aerogel), and Pt/BGA-C (Platinum/carbon black and boron-doped graphene aerogel)—were used as electrocatalysts for the oxidation of methanol and formic acid that were made using the modified Hummers technique, hydrothermal procedure of the support materials, and microwave irradiation. In terms of methanol and formic acid oxidation, the Pt/BGA-C catalyst had the maximum catalytic activity.

Other than that, Guo and his colleague [18] performed the electrocatalyst support for methanol oxidation using nitrogen-doped graphene aerogel microspheres. This supported catalyst was produced by freeze-drying, thermal annealing, and electrospraying pyrrole and an oxidizing agent into a graphene oxide dispersion. The reported results show that Pt/N-doped graphene aerogel bulk (Pt/rGNAB), and Pt/N-doped graphene aerogel millimeter spheres (Pt/rGNAS) show that anode electrocatalysts achieve higher mass activity performance compared to Pt/C of 840.11 mA mg^{-1} for the electrooxidation of methanol. The Pt/rGNAMs additionally exhibit enhanced long-term electrocatalytic stability. Additionally, Sahoo et al. [19] consider 3D graphene supported by Palladium (Pd) as a possible electrocatalyst for alkaline direct methanol fuel cells. This study describes a straightforward, inexpensive, and environmentally friendly Pd supported on 3D graphene aerogel (Pd/GA) using a single freeze-casting process. According to this research, the Pd/GA catalyst outperforms standard Pd/carbon black (Vulcan XC-72R) with the same loading (20%) of Pd in electrocatalysis and exhibits abnormally high toxin tolerance and stability.

Interestingly in 2018, Selim Çögenli et al. [20] research on platinum nanoparticles for formic acid electrooxidation supported by graphene aerogel. Different support materials, such as commercial carbon black (C), produced graphene aerogel (GA), and their hybrids (GA/C), were used in this investigation. According to the research, commercially produced carbon-supported catalysts for the oxidation of formic acid did not perform as well as synthetic GA-supported catalysts did. Direct pathway dominated the electrooxidation of formic acid, and Pt/GA and Pt/GA/C(2) catalysts demonstrated improved tolerance against the CO poisoning effect. Since the study by Kwok and his team [21], graphene and carbon nanotube composites were used as catalyst supports for Ru at Pt catalyst to produce a high porosity anode for a flow-through direct methanol microfluidic fuel cell (MFC) application. The porosity size of the electrode and the size of the nanoparticles synthesized were in the range of 5 nm and 10 m, respectively. The conductivity had been enhanced due to the well-connected nature of the graphene sheets owing to the existence of carbon nanotubes (CNT).

In the presence of 1 M methanol and 1 M KOH, a catalyst with a maximum specific power of 13.1 mWmg^{-1} attained its highest performance in comparison to earlier research. Tsang et al. [22] studied a nickel foam plate covered with a bimetallic Pd/

Pt loaded GA that is free of a binder. The Pd/Pt/GA/NFP electrode is then put to the test in alkaline direct ethanol fuel cell (DEFC) applications, with the highest maximum power density achieved being 3.6 $\mathrm{mWcm^{-2}}$ at room temperature and a Pd/Pt ratio of 1:1. Besides, Zhou et al. [23], polyvinyl alcohol (PVA), which serves as an organic binder to be employed as an ultrafine Pt nanoparticle catalytic support, was used in the freeze-drying procedure to create 3D graphene/carbon nanotube (GRCNTs) aerogels. The good ant poisoning capability, high activity, and exceptional durability of this manufactured catalyst were indisputable great qualities. In addition, Kwok et al. [24] have successfully anchored the platinum nanoparticles on GA with a diameter of 1.5 nm for use in a direct methanol microfluidic fuel cell. Pt/GO aerogel has some reimbursements over commercial Pt/C electrodes, including a 358% increase in specific power, greater catalytic activity, and electroactive surface area. In applications involving direct glucose fuel cells (DGFC), Tsang and his team [22] search for alternate ways to generate binder-free electrocatalytic electrodes. Then, various Pd/Pt ratios on nickel foam plates without a binder were achieved by utilizing GA as catalyst support (1:2.32, 1:1.62, and 1:0.98). This innovative PdPt/GO/nickel form plate (NFP) composite was created using an environmentally friendly one-step mild reduction technique. The best performance was 1.25 $\mathrm{mWcm^{-2}}$ of maximal power density under ideal conditions (0.5 M glucose/3 M KOH as the anodic fuel and Pd1Pt0.98/GA/NFP as the catalyst).

Krittayavathananon and Sawangphruk [25] have successfully improved the performance of the Pd catalyst due to the high porosity of the graphene oxide aerogel paper support. They also conducted another study as a control and comparison, namely Pd coated on 3 other types of carbon materials including bare carbon fiber (CFP), and CFP modified with either 2D graphene oxide (GO) and 2D rGO nanosheets. It turns out that Pd supported RGO aerogel has higher performance than others. Based on the high porosity of 3D rGO support, the direct ethylene glycol fuel cell performs best when the catalyst is Pd/3D rGO aerogel. This Pd/3D rGO aerogel was capable of delivering a high anodic current density of 267.8 $\mathrm{mAcm^{-2}}$ at 3000 rpm. The distribution of pores and the shape of aerogel and aerogel composite are shown in Fig. 3.

Zhao et al. [26] used three straightforward combination techniques, including template removal process thermal treatment, and hydrothermal self-assembly to create 3D porous nitrogen-doped GA (3D NGA). The current-produced catalyst performs much better than Pt/G and Pt/3D-GA catalysts, especially when it comes to the electrooxidation of methanol. It has a high electrochemical active surface area (ECSA) of 90.7 $\mathrm{m^2g^{-1}}$, good stability, and greater catalytic activity. This exceptional performance was due to the well-connected 3D porous structure, high N doping level, and uniform Pt NP dispersion. Instead of that, Öztuna and his team [27] studied a supercritical deposition technique to create extremely tiny, thin, pyramidal mesoporous graphene aerogel (GA) supported Pt nanoparticles ($\mathrm{scCO_2}$). The conversion temperature (400 °C to 800 °C) and the typical particle size were the variables examined in this study (1.2 to 2.9 nm). The supercritical deposition (SCD) technique allows for the preservation of the original textural characteristics of GA even after the deposition of Pt nanoparticles. According to Fig. 4, the Pt/GA produced has a

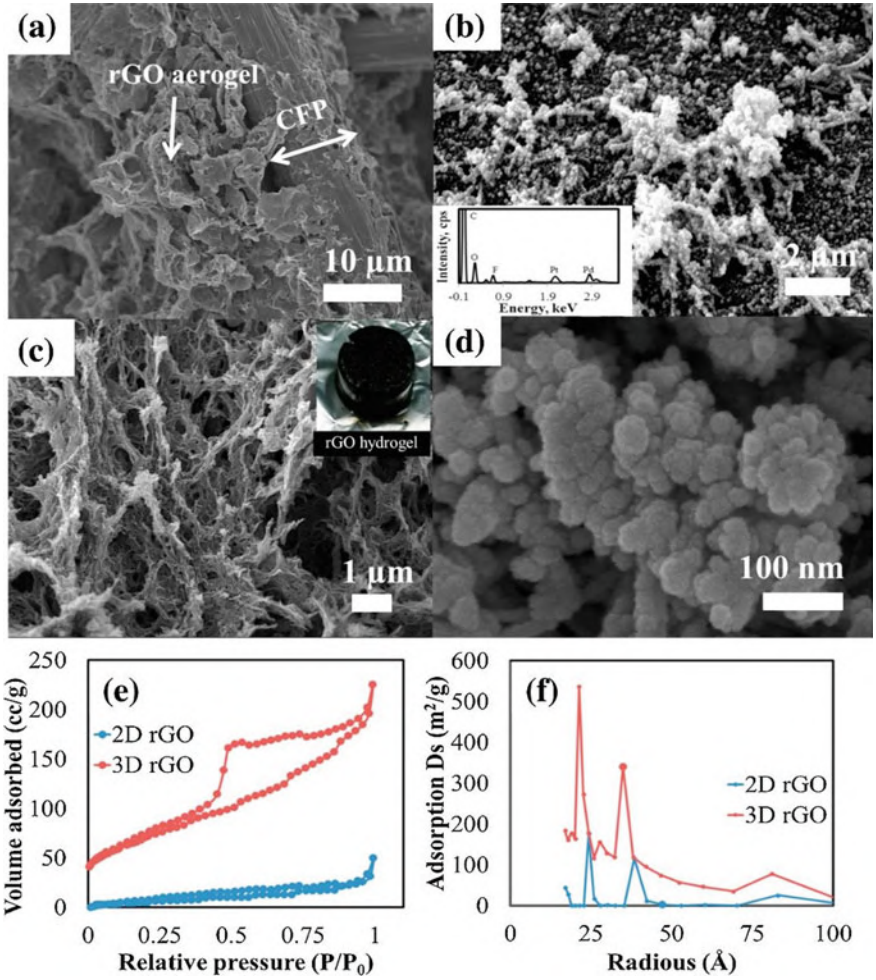

Fig. 3 SEM images at varying magnifications show the 3D rGO aerogel coated on CFP **a**, **c** and the Pd electrodeposition on the top layer of the 3D rGO/CFP **b**, **d**. Additionally, N_2 adsorption/desorption isotherms of the 3D rGO aerogel and 2D rGO sheets restacked (**e**), as well as the pore size distribution of these materials (**f**), are also presented. Adapted with permission [25], Copyright (2016), Elsevier

maximum mass activity of 30.6 $mAmg^{-1}$ Pt, which is significant when compared to the mass activity of the Pt/GA electrocatalyst produced using the traditional method. This makes the conversion temperature of 600 °C the most suitable. Furthermore, Huang and his collaborator [28] were employing 3D-GA as the support for the Pt catalyst, and Pt was subsequently added to 3D-GA using a straightforward process called the one-step co-reduction approach. The electrocatalyst of Pt/GA performed

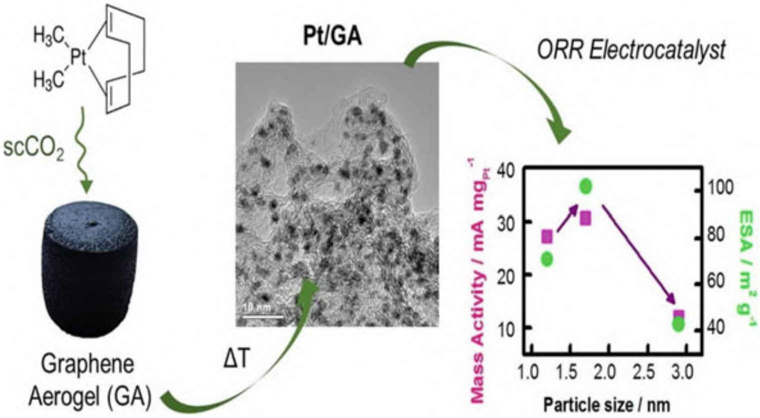

Fig. 4 Pt/GA, graphene aerogel morphology and electrochemistry behavior. Adapted with permission [27], Copyright (2017), Elsevier

well in terms of durability and electrocatalytic activity due to GA's unique 3D architecture structure, effective Pt deployment in GA spaces, and efficient interactions between Pt nanoparticles and GA.

Zhao et al. [29] used the quick and environmentally friendly hydrothermal technique in order to create a platinum, carbon, and graphene aerogel (Pt/C/GA) combined to form a highly stable hybrid electrocatalyst. The unusual 3D graphene framework structure of this electrocatalyst played a major role in its ability to accomplish substantial methanol electrooxidation without losing electrocatalytic activity. The Pt/C/GA is also more stable than Pt/C, whose mass activity remained relatively stable after 200 cycles of testing. Methanol electrooxidation's performance needs to be increased. Duan and team [30] synthesized graphene oxide aerogel (GOA) as a substitute for platinum as a catalyst. Pt/GOA has a large active surface area, which contributes to its excellent mass transfer process efficiency. In this research, a number of parameters that affected GA structures were found. One of them is the process used to make aerogel. The second is the temperature and time for drying the aerogel. The size of the pore, pore dispersion, and the networking established are all observed to be influenced by all of these factors and last is the usage of precursor materials.

3 3D Graphene-Based Hydrogel Application in Fuel Cell

Recently, Moradian and his team [31] studied the anode for effective microbial fuel cells powered by xylose using yeast-induced production of graphene hydrogels, as illustrated in Fig. 5. Yeast-based MFCs were developed employing an autonomously self-modified 3D reduced graphene oxide (rGO) hydrogel anode, which has a two-fold improvement in bioelectricity and biohydrogen production from xylose. Additional investigation revealed that the underlying reason for the enhancement of MFC performance was the 3D rGO hydrogel's ability to draw in more yeast cells and minimize the interfacial charge transfer resistance.

Additionally, Chen and his colleague [32] introduced an anode for microbial fuel cells that were constructed using a suggested 3D composite hydrogel made of reduced graphene oxide and polyacrylamide (rGO/PAM) and connected to a current collector graphite brush (GB). The in situ polymerization of acrylamide in a graphene oxide dispersion was used to create the rGO/PAM, which was then reduced with ascorbic acid. The resulting macro-porous scaffold had a high surface area and was biocompatible, which facilitated mass diffusion of the culture medium, microbial colonization, and electron mediators. The findings of this work show that at the stable stage of power generation, the maximal power density, and volumetric power density of the GB/rGO/PAM anode are impressively high 758 mWm^{-2} and 53 Wm^{-3}, respectively. The orientated rGO/PAM (O-rGO/PAM) with higher conductivity can significantly increase the greatest power density of MFCs and reach 782 mWm^{-2}.

Apparently, Kumar and his team [33] are emphasizing research on Carbonaceous nanocomposite hydrogels in their approach to the suspension polymerization Method used in anodes in microbial fuel cells (MFCs). In comparison to the empty hydrogel, (Poly N-Isopropylacrylamide) (PNIPAM) hydrogels loaded with electrically conductive carbonaceous nanoparticles have much greater MFC efficiency. Carbon nanotubes (CNTs) and graphene oxide (GO) are evenly dispersed throughout the PNIPAM matrix, as seen in the obtained morphological images. Remarkably, this work discovered that the synthesized PNIPAM-GO-CNT composite showed superior MFC performances with a durability of more than 300 h thanks to the combined efforts of high electrical conductivity and strong active carbon support. Hydrogel based structure material has several advantages that can potentially be used in MFC applications including low cost, a simple technique of manufacture, environmental friendliness, and outstanding electrocatalytic activity.

4 3D Graphene-Based Foam in Fuel Cell

In energy conversion and storage devices like fuel cells, oxygen evolution and reduction reactions (OER, ORR) are two vital electrochemical processes. Due to the slow nature of OER and ORR, commercial ruthenium and platinum-fabricated electrocatalysts as electrode materials are commonly employed to accelerate the reaction rates. However, the practical feasibility of these electrochemical applications is hampered by high noble metal cost, unavailability, and inadequate durability. Hence, significant efforts are being made to develop economic and sustainable electrocatalysts that replace costly noble metals in renewable energy technologies. Two-dimensional nanomaterials, specifically 2D graphene, are most commonly used in fuel cells owing to their remarkable electrical, optical, and mechanical properties. Strong interactions

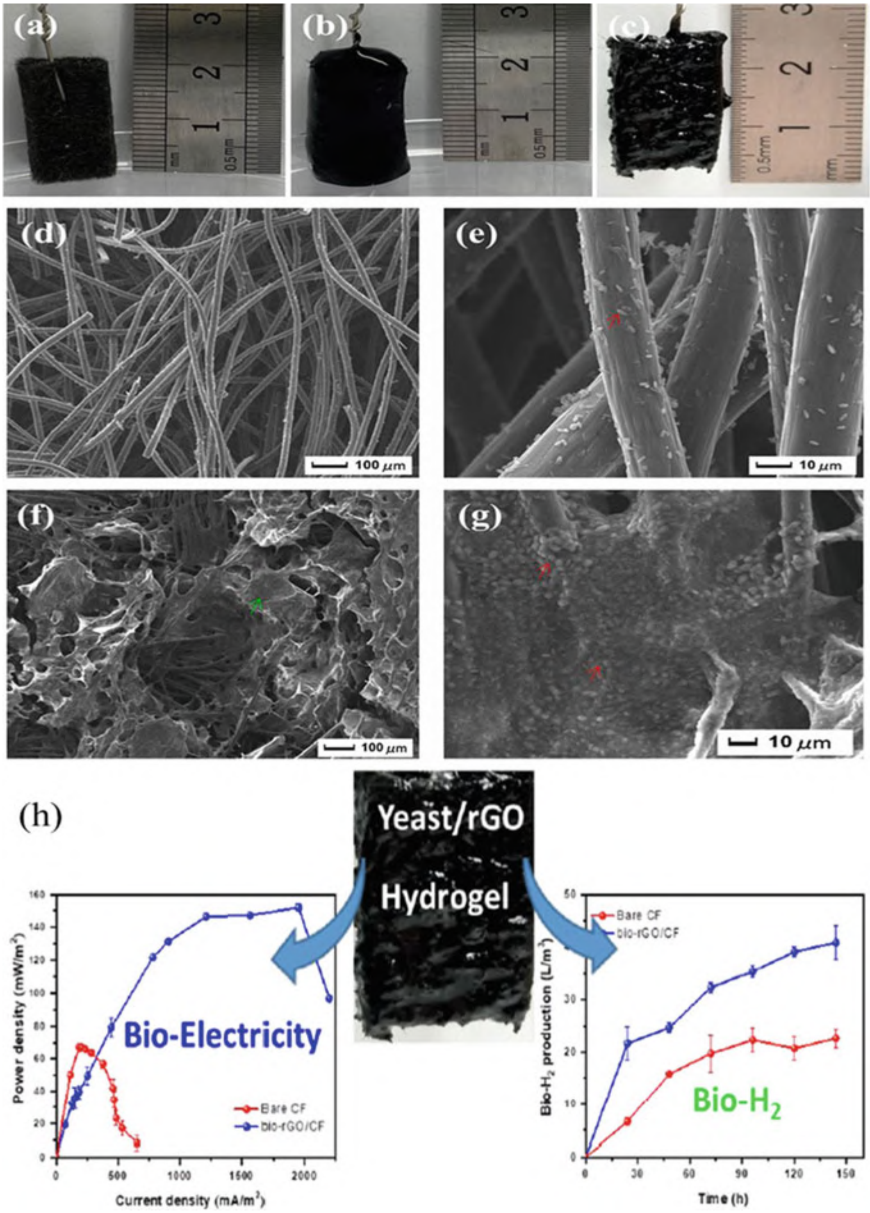

Fig. 5 **a** photograph of a bare CF electrode, while **b**, **c** CF electrodes with GO adsorption and yeast-induced bio-rGO/CF hydrogel, respectively. SEM images of **d**, **e** show the bare CF electrode, and **f**, **g** bio-rGO/CF electrode after discharge in MFC, with yeast cells indicated by red arrows and rGO nanosheets indicated by blue arrows which different magnifications used in the SEM images and **h** performance of yeast-induced formation of graphene hydrogels in MFC. Adapted with permission [31], Copyright (2022), Elsevier

between graphene sheets, aggregation, and stacking lower graphene nanosheets' conductivity and specific surface area.

One of the most efficient approaches to solving these drawbacks is to develop three-dimensional (3D) nanostructures. Graphene foam (GF) with a 3D structure, interconnected macropores, and high surface area has been effectively designed using different approaches [34]. These superior qualities make 3D graphene foam a potentially useful catalyst in fuel cells. Heteroatoms (like S, P, and N) and transition metals (like Ni, Co, and Fe) supported on 3D graphene foam appropriately are better alternatives to Ru/Pt-based electrocatalysts owing to their availability, cheap cost, and high stability. Highly efficient electrocatalysts, such as those that catalyze both the ORR and OER, hold great promise as a potential replacement for fossil fuels in the generation of usable energy in the future. The expensive noble metal electrocatalysts are consistently replaced by developing economic nanohybrid materials.

In Jeong et al. [35] studies, CoFe nanoparticles, and an N-doped carbon shell were integrated on three-dimensional (3D) mesoporous N-doped graphene foam (CoFe@N–C/MNGF). This CoFe@N–C/MNGF nanohybrid has shown excellent electron transfer efficiency with better OER activity in alkaline electrolytes and a lower overpotential of 330 mV. Due to high ORR activity (stability, electron transfer, catalytic activity, etc.), it may be a good replacement for noble-metal-based ORR materials in alkaline fuel cells as the cathode electrode. In an alkaline electrolyte, the nanohybrid displays a potential of 0.87 V and a low Tafel plot of 71.7 mV dec-1 at 5 mA cm^{-2}, with an estimated electron transfer number (n) of 2.1–3.61 at 0.15 to 0.35 V. The findings of this research provide novel perspectives on developing a low-cost, bi-functional electrocatalyst that does not require expensive noble metal catalysts. In Li et al. [36] study, 3D reduced graphene oxide (rGO) was synthesized and fabricated with Co nanosheets and Au nanoparticles for the electrooxidation of sodium borohydride (NaBH4) in an alkaline medium. The as-prepared 3D rGO foam shows a good current collector, and the composite material CoAu/rGO foam is used in a direct borohydride-hydrogen peroxide fuel cell (DBHPFC), as the anode electrode. The structural features of 3D rGO foam provide low electrochemical impedance, large electrochemical surface area (390 m^2 g^{-1}), and high efficiency for $NaBH_4$ oxidation. The electrode kinetics of CoAu/rGO foam suggests 6.9 electron transfer and first-order kinetics for the oxidation of $NaBH_4$.

Optimizing the efficiency of polymer electrolyte membrane fuel cells requires combining a gas diffusion layer with a flow field. This is accomplished by combining the gas diffusion layer with the flow field to reduce the thickness of the membrane electrode assembly (MEA) and reactant pathway, hence decreasing electron-mass transport resistance. In Park et al's. [37] study, graphene foam serves as a flow field as well as a gas diffusion layer as part of a unified MEA. A reduction in thickness of 82% allows for an increase in the projected volume power density. When compared to a conventional MEA, the unified membrane electrode performs better in the area of high current density due to a larger pressure drop, which is also confirmed by structural and design simulation data analysis. As a three-dimensional material consisting of interconnecting macropores, graphene foam combines the benefits of graphene with the morphological features of metal foam. The enhanced porosity of metal foams has led to their development as a flow field since it can be used to disperse reactants evenly over a large surface area and drain off any water that is generated during the process. However, these metal foams are highly susceptible to the corrosion process, which limits their practical applications during the working of polymer-electrolyte-membrane fuel cells. 3D graphene foam has been employed as a flow field to analyze its characteristic features toward the mass transfer of substrate and products [38]. The efficiency of 3D graphene foam has been enhanced at high current densities owing to its improved mass transfer properties in a single-cell test. The detailed electrochemical analysis, including the simulation, oxygen gain, and electrochemical impedance results, reveals that the 3D graphene foam-based electrode assembly offers lower mass transport resistance than conventional electrode assembly. These improved results displayed by 3D graphene foam are assumed due to the 3D graphene foam and interconnected macropores.

During the electrooxidation of NaBH4, the catalytic efficiency and the use of NaBH4 are of paramount importance. Ultra-thin CoNi nanosheets fabricated with innovative 3D reduced graphene oxide foam are developed as an effective anode catalyst to enhance the efficiency of NaBH4 oxidation in Li et al.'s [39] study. The electrooxidation of NaBH4 has been studied by developing ultrathin transition metal nanosheets on a 3D rGO anode catalyst (CoNi-NS/rGO foam). CoNi-NS fabricated on 3D rGO foam has been employed in a three-electrode system to determine its potential in an alkaline medium toward the oxidation of NaBH4. The as-prepared CoNi-NS/rGO foam exhibits low electrochemical impedance, high electrochemical surface area, and low activation energy (8.29 $\text{kJ}\cdot\text{mol}^{-1}$). The oxidation of NaBH4 on the fabricated electrode follows first-order kinetics, as confirmed by LSV studies. The as-prepared catalyst has been used in DBHPFC, and the results suggest excellent efficiency toward NaBH4 oxidation. Zhou et al. have synthesized transition metal-fabricated hierarchical porous N-doped graphene foams (HPGFs) that are supported by silica nanoparticles [40]. The transition metal and silica NPs provide excess surface active sites and high surface area (918.7 $\text{m}^2\ \text{g}^{-1}$). The ORR catalytic activity of HPGFs is tuned by employing different nitrogen precursors (urea, melamine, and cyanamide). HPGF displays better ORR activity than commercial Pt/C electrode materials. Furthermore, HPGF shows enhanced electrochemical performance in an acidic medium when compared to an alkaline medium. HPGF exhibits long-term stability (5000 cycles) and high resistance to methanol in both acidic and alkaline solutions. The HPGF-1 electrocatalyst has been integrated into the zinc-air battery for electrochemical energy conversion systems.

Platinum ruthenium (PtRu) NPs were successfully deposited on 3D graphene foam (PtRu/3D GF) to develop a hierarchical novel composite material in Kung et al. [41]. This PtRu/3D GF has been used as a nanocatalyst for methanol and ethanol oxidation. PtRu/3D GF has displayed better electrochemical efficiency toward oxidation of methanol and ethanol, along with high resistance to CO poisoning than PtRu, PtRu/C, and PtRu/graphene (commercial graphene). The methanol and ethanol oxidation is nearly doubled by PtRu/3D GF than PtRu/graphene, which is assumed due to the reduced crystal size of PtRu (3.5 nm) and enhanced surface area (186.2 $\text{m}^2\ \text{g}^{-1}$) provided by 3D graphene foam. A facile, economic, and single-step pyrolysis method is used in Shi et al. [42] study to prepare 3D FeNi-functionalized N, P doped graphene foam (FeNi@NP-GF) electrocatalyst for DMFCs. The FeNi@NP-GF exhibits high limiting current density and positive half-wave potential as compared to its precursors, which is due to the combined interaction of Fe/Ni-N_x with Fe/Ni and N groups and high surface active sites of 3D graphene foam. It also exhibits significant resistance in an alkaline medium for methanol crossover and a four-electron transfer mechanism. In addition, FeNi@NP-GF served as a reliable platform for Pt nanoparticles (NPs). The as-synthesized electrocatalyst showed excellent activity, for methanol electrooxidation in an acid medium.

The superior features of metal oxide nanostructures make them a competitive material for energy storage, conversion, and other green energy applications. In Kumar et al. [43] work, an asymmetric supercapacitor with a cathode electrode made of ZnO@stainless steel (SS) nano cauliflower and an anode electrode made of reduced graphene oxide (rGO) on nickel (Ni) has been successfully developed (rGO@Ni/ZnO@SS). ZnO thin film electrode is produced by reactive DC magnetron sputtering, and the rGO electrode by electrodeposition. In addition, the kinetics of thin film electrodes were studied in an alkaline electrolyte solution and the capacitance performance of this unique supercapacitor, rGO@Ni/ZnO@SS, exceeds that of conventional nanostructured metal oxides. The as-prepared ASCs show enhanced capacitance values (0–1.4 V), excellent electrochemical efficiency, and extended stability (89.5% after 5000 cycles). The ASC performs better than the previously reported ASCs, with an energy density of 23 Whkg^{-1} and an optimal power density of 156 Wkg^{-1} in alkaline aqueous electrolyte solutions. Because of their high performance, there is tremendous potential for using nanostructured rGO@Ni/ZnO@SS in portable electronic devices.

The hydrogen evolution process (HER) in alkaline electrolytes has seen the development of several catalysts, although its conversion efficiency has remained poor. Niobium disulfide (NbS2) heterostructures and graphene foam were grown on nickel foam to develop a mixed-dimensional structure (NbS2-Gr-NF) successfully synthesized by Aslam et al. [44] as shown in Fig. 6. The strong synergistic interaction between NbS2-Gr and NF activates the NbS2 surface active sites, enhances the surface area, and improves conductivity. As a consequence, NbS2-Gr-NF heterostructures result in a high current density of 500 mA cm^{-2} at a low overpotential of 306 mV in 1 M KOH solution, and the current density is further increased upto 914 mA cm^{-2} by an insignificant increase in overpotential (32 mV). Fast reaction kinetics, where the Volmer step is primarily responsible for controlling the reaction, have been confirmed by a Tafel value of 72 mV dec-1 for the prepared heterostructure. NbS2-Gr-NF is promising for water-splitting, particularly in alkaline electrolytes, because of their ability to achieve high current density at a rapid pace while maintaining high stability.

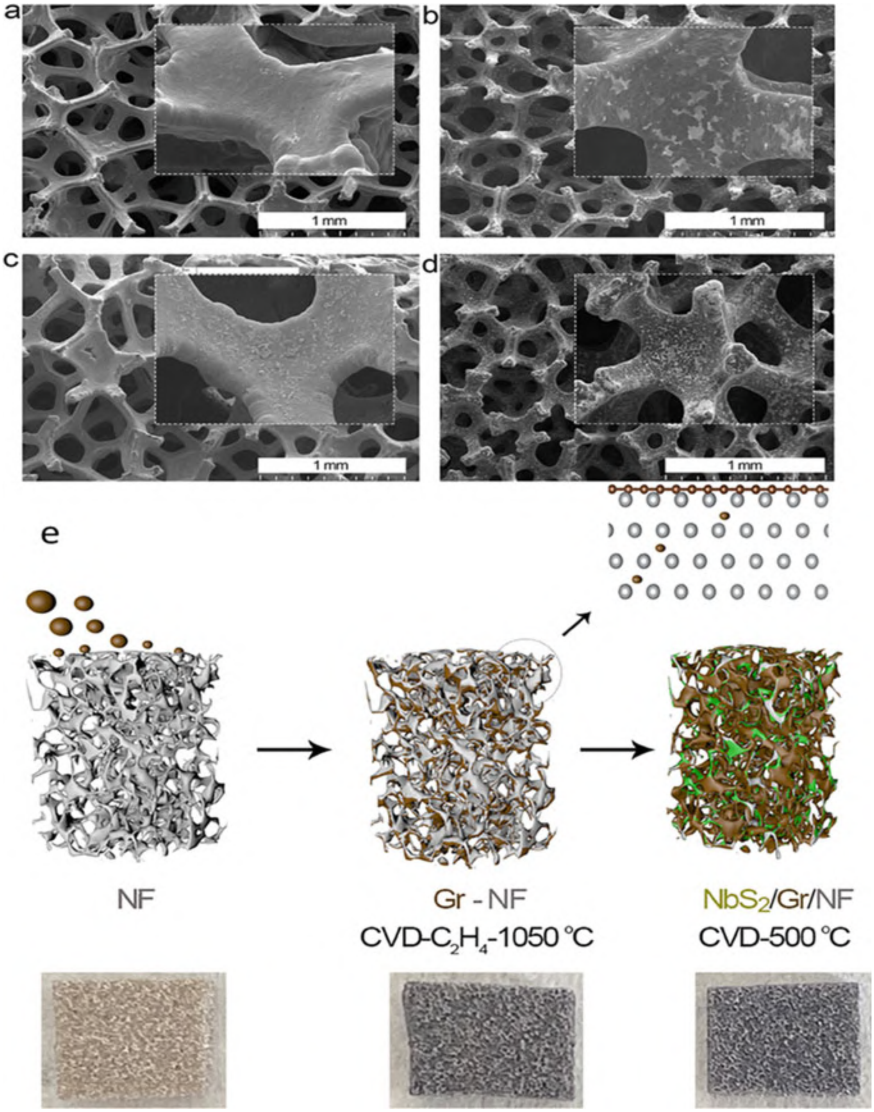

Fig. 6 SEM pictures of **a** NF, **b** NbS2 deposited on NF, **c** graphene foam deposited on NF, **d** NbS2-Gr-NF, and **e** a schematic showing the growth of graphene foam on nickel foam and the movement of carbon atoms within nickel. Adapted with permission [44], copyright (2021), Elsevier

5 Challenges and Future Perspectives

The use of 3D graphene-based materials such as aerogel structures has expanded into a variety of applications due to their unique chemical properties and their ability to form wet gels. The high pore volume and high surface area contribute to its versatility, making it one of the lightest and most adaptable materials. While thermal insulation remains the most widely used application, 3Dgraphene-based materials have also been utilized in fields such as electrochemistry (supercapacitors, fuel cells), as a carrier of catalysts and active agents, as filling materials, and in tissue engineering. In the fuel cell industry, 3D graphene-based materials have shown great potential as a catalyst or as part of a catalyst due to their high pore volume, high surface area, well-connected structure, and flexibility, performing better than commercial catalyst support like Pt/C. There are still many aspects that can be explored for the properties of 3D graphene-based materials to increase their potential and development in various applications including:

1. Flexibility in design. The flexibility of 3D graphene-based materials design such as aerogel is another advantage in its development. The 3D graphene-based aerogel structure can be easily modified and optimized to meet the desired specifications. For example, the surface area and pore size can be adjusted to meet the needs of the application. In fuel cell applications, the properties of 3D graphene-based materials structures can be tailored to maximize electrocatalytic performance.
2. Cost-effectiveness. Despite being a relatively new material, 3D graphene-based materials structures are cost-effective compared to traditional materials. For example, the cost of producing 3D-graphene-based materials structures for fuel cell applications is relatively low compared to other materials such as platinum. This makes 3D graphene-based materials a potential alternative to traditional catalysts, making them more accessible for commercial use.
3. Green synthesis. 3D graphene-based materials structures can be synthesized using environmentally friendly methods, which is an important factor in the development of sustainable technology. For example, the 3D graphene-based materials aerogel can be synthesized using a sol–gel process using natural materials such as resorcinol and formaldehyde. This green synthesis method makes aerogel an attractive option for environmentally conscious consumers.
4. Additionally, the low cost of these raw materials compared to other materials used in the catalyst industry makes 3D graphene-based materials a more attractive option for catalyst support. The availability of raw materials also allows for the large-scale production of 3D graphene-based materials, making them more accessible for various applications.

The 3D graphene-based materials structure still faces a few obstacles that limit its application possibilities and delay commercialization, including the following:

i. Cost and high production time. The production time of 3D graphene-based materials is still long and the cost is still high compared to other materials.

This is because the production process is still not efficient and requires high energy consumption. To achieve commercial success, it is important to find more efficient and cost-effective production methods.

ii. Handling and storage. Handling and storage of 3D graphene-based materials such as aerogel is also a challenge due to its lightweight and brittle nature. This requires special handling and storage facilities, which can increase the cost of aerogel use.

iii. Commercialization. Finally, the commercialization of 3D graphene-based materials is still limited due to limited applications and a lack of understanding of the properties and capabilities of 3D graphene-based materials among industries. This requires further research and development to explore the full potential of 3D graphene-based materials and to increase their commercialization in various fields.

In summary, further steps need to be taken to fully realize the potential of 3D graphene-based materials and their commercialization. This includes exploring alternative raw materials for 3D graphene-based materials production, innovating production methods to increase efficiency and scale, and standardizing 3D graphene-based materials characterization techniques. By addressing these challenges, the potential for 3D graphene-based materials in various applications can be further realized.

6 Conclusions

In conclusion, 3D graphene-based materials have a lot of potential to be used in various applications due to their high pore volume, high surface area, and lightweight properties. However, there are still challenges that need to be addressed such as the production process, regulation in characterization methods, and transformation from lab-scale to industrial-scale production. Further studies are needed to explore the diverse raw materials for 3D graphene-based materials fabrication, hybrid composite potentials, and regulations for comparison and standardization. With more research and development, 3D graphene-based materials have the potential to continue to penetrate new application areas in the future, particularly in the fields of environmental and electrochemistry.

Acknowledgments The authors would like to express their gratitude to Universiti Kebangsaan Malaysia (UKM) and the Ministry of Higher Education for providing financial assistance through a Fundamental Research Grant Scheme FRGS/1/2021/STG05/UKM/02/10.

References

1. Yusoff, Y.N., Shaari, N.: An overview on the development of nanofiber-based polymer electrolyte membrane and electrocatalyst in fuel cell application. Int. J. Energy Res. **45**(13), 18441–18472 (2021)
2. Shaari, N., Zakaria, Z., Kamarudin, S.K.: The optimization performance of cross-linked sodium alginate polymer electrolyte bio-membranes in passive direct methanol/ethanol fuel cells. Int. J. Energy Res. **43**(14), 8275–8285 (2019)
3. Sajid, A., Pervaiz, E., Ali, H., Noor, T., Baig, M.M.: A perspective on development of fuel cell materials: electrodes and electrolyte. Int. J. Energy Res. **46**(6), 6953–6988 (2022)
4. Ramli, Z.A.C., Shaari, N., Saharuddin, T.S.T.: Progress and major BARRIERS of nanocatalyst development in direct methanol fuel cell: a review. Int. J. Hydrogen Energy (2022)
5. Zaman, S., Wang, M., Liu, H., Sun, F., Yu, Y., Shui, J., ... & Wang, H.: Carbon-based catalyst supports for oxygen reduction in proton-exchange membrane fuel cells. Trends Chem. (2022)
6. Paraknowitsch, J.P., Thomas, A.: Doping carbons beyond nitrogen: an overview of advanced heteroatom doped carbons with boron, sulphur and phosphorus for energy applications. Energy Environ. Sci. **6**(10), 2839–2855 (2013)
7. Kistler, S.S.: Coherent expanded-aerogels. J. Phys. Chem. **36**(1), 52–64 (2002)
8. Sun, Z., Fang, S., Hu, Y.H.: 3D graphene materials: from understanding to design and synthesis control. Chem. Rev. **120**(18), 10336–10453 (2020)
9. Yu, X., Wang, B., Gong, D., Xu, Z., Lu, B.: Graphene nanoribbons on highly porous 3D graphene for high-capacity and ultrastable Al-ion batteries. Adv. Mater. **29**(4), 1604118 (2017)
10. Ng, S., Jelle, B.P., Sandberg, L.I.C., Gao, T., Wallevik, Ó.H.: Experimental investigations of aerogel-incorporated ultra-high performance concrete. Constr. Build. Mater. **77**, 307–316 (2015)
11. Moreno-Castilla, C., Maldonado-, F.: Carbon aerogels for catalysis applications: an overview. Carbon **43**(3), 455–465 (2005)
12. Tleimat-Manzalji, R., Manzalji, T., Pajonk, G.: Aerogels and xerogels for catalytic applications. J. Non-Cryst. Solids **147**, 744–747 (1992)
13. Schneider, M., Baiker, A.: Aerogels in catalysis. Catalysis Rev. **37**(4), 515–556 (1995)
14. Sutharssan, T., Montalvao, D., Chen, Y.K., Wang, W.C., Pisac, C., Elemara, H.: A review on prognostics and health monitoring of proton exchange membrane fuel cell. Renew. Sustain. Energy Rev. **75**, 440–450 (2017)
15. Du, A., Zhou, B., Zhang, Z., Shen, J.: A special material or a new state of matter: a review and reconsideration of the aerogel. Materials **6**(3), 941–968 (2013)
16. Guan, L., Balakrishnan, P., Liu, H., Zhang, W., Deng, Y., Su, H., Xing, L., Penga, Ž, Xu, Q.: A tortuosity engineered dual-microporous layer electrode including graphene aerogel enabling largely improved direct methanol fuel cell performance with high-concentration fuel. Energies **15**(24), 9388 (2022)
17. Çögenli, M.S., Bayrakçeken Yurtcan, A.: Carbon black-heteroatom-doped graphene aerogel hybrid supported platinum nanoparticles as electrocatalysts for oxidation of methanol and formic acid. Int. J. Energy Res. **46**(15), 24130–24147 (2022)
18. Guo, Q., Lu, X., Fei, G., Wang, Z., Xia, H.: Nitrogen-doped graphene aerogel microspheres used as electrocatalyst supports for methanol oxidation. Ind. Eng. Chem. Res. **61**(3), 1398–1407 (2022)
19. Sahoo, B.B., Biswal, K., Jena, A., Naik, B., Nayak, N.C., Dash, B.P., Mahanto, B.S., Soam, A., Sahoo, P.K.: Pd supported on 3D graphene aerogel as potential electrocatalyst for alkaline direct methanol fuel cells. Mater. Today Proc. **41**, 150–155 (2021)
20. Çögenli, M.S., Ayşe, B.Y.: Graphene aerogel supported platinum nanoparticles for formic acid electro-oxidation. Mater. Res. Express **5**(7), 075513 (2018)
21. Kwok, Y.H., Wang, Y.F., Tsang, A.C., Leung, D.Y.: Graphene-carbon nanotube composite aerogel with Ru@ Pt nanoparticle as a porous electrode for direct methanol microfluidic fuel cell. Appl. Energy **217**, 258–265 (2018)

22. Tsang, C.H.A., Leung, D.: Use of Pd-Pt loaded graphene aerogel on nickel foam in direct ethanol fuel cell. Solid State Sci. **75**, 21–26 (2018)
23. Zhou, Y., Hu, X., Guo, S., Yu, C., Zhong, S., Liu, X.: Multi-functional graphene/carbon nanotube aerogels for its applications in supercapacitor and direct methanol fuel cell. Electrochim. Acta **264**, 12–19 (2018)
24. Kwok, Y.H., Tsang, A.C., Wang, Y., Leung, D.Y.: Ultra-fine Pt nanoparticles on graphene aerogel as a porous electrode with high stability for microfluidic methanol fuel cell. J. Power Sources **349**, 75–83 (2017)
25. Krittayavathananon, A., Sawangphruk, M.: Electrocatalytic oxidation of ethylene glycol on palladium coated on 3D reduced graphene oxide aerogel paper in alkali media: effects of carbon supports and hydrodynamic diffusion. Electrochim. Acta **212**, 237–246 (2016)
26. Zhao, L., Sui, X.L., Li, J.L., Zhang, J.J., Zhang, L.M., Wang, Z.B.: Ultra-fine Pt nanoparticles supported on 3D porous N-doped graphene aerogel as a promising electro-catalyst for methanol electrooxidation. Catal. Commun. **86**, 46–50 (2016)
27. Oztuna, F.E.S., Barim, S.B., Bozbag, S.E., Yu, H., Aindow, M., Unal, U., Erkey, C.: Graphene aerogel supported Pt electrocatalysts for oxygen reduction reaction by supercritical deposition. Electrochim. Acta **250**, 174–184 (2017)
28. Huang, Q., Tao, F., Zou, L., Yuan, T., Zou, Z., Zhang, H., Zhang, X., Yang, H.: One-step synthesis of Pt nanoparticles highly loaded on graphene aerogel as durable oxygen reduction electrocatalyst. Electrochim. Acta **152**, 140–145 (2015)
29. Zhao, L., Wang, Z.B., Li, J.L., Zhang, J.J., Sui, X.L., Zhang, L.M.: Hybrid of carbon-supported Pt nanoparticles and three dimensional graphene aerogel as high stable electrocatalyst for methanol electrooxidation. Electrochim. Acta **189**, 175–183 (2016)
30. Duan, J., Zhang, X., Yuan, W., Chen, H., Jiang, S., Liu, X., Zhang, Y., Chang, L., Sun, Z., Du, J.: Graphene oxide aerogel-supported Pt electrocatalysts for methanol oxidation. J. Power Sources **285**, 76–79 (2015)
31. Moradian, J.M., Mi, J.L., Dai, X., Sun, G.F., Du, J., Ye, X.M., Yong, Y.C.: Yeast-induced formation of graphene hydrogels anode for efficient xylose-fueled microbial fuel cells. Chemosphere **291**, 132963 (2022)
32. Chen, J.Y., Xie, P., Zhang, Z.P.: Reduced graphene oxide/polyacrylamide composite hydrogel scaffold as biocompatible anode for microbial fuel cell. Chem. Eng. J. **361**, 615–624 (2019)
33. Kumar, G.G., Hashmi, S., Karthikeyan, C., GhavamiNejad, A., Vatankhah-Varnoosfaderani, M., Stadler, F.J.: Graphene oxide/carbon nanotube composite hydrogels—versatile materials for microbial fuel cell applications. Macromol. Rapid Commun. **35**(21), 1861–1865 (2014)
34. Liu, Z., Shen, D., Yu, J., Dai, W., Li, C., Du, S., Jiang, N., Li, H., Lin, C.T.: Exceptionally high thermal and electrical conductivity of three-dimensional graphene-foam-based polymer composites. RSC Adv. **6**(27), 22364–22369 (2016)
35. Jeong, D.I., Choi, H.W., Woo, S., Yoo, J.H., Kumar, M., Song, Y.H., Lim, B., Koo, B.K., Kang, B.K., Yoon, D.H.: Complementary performance improved crystalline N-doped carbon encapsulated CoFe/mesoporous N-doped graphene foam as bifunctional catalyst. Appl. Surf. Sci. **559**, 149077 (2021)
36. Li, B., Song, C., Zhang, D., Ye, K., Cheng, K., Zhu, K., Yan, J., Cao, D., Wang, G.: Novel self-supported reduced graphene oxide foam-based CoAu electrode: an original anode catalyst for electrooxidation of borohydride in borohydride fuel cell. Carbon **152**, 77–88 (2019)
37. Park, J.E., Lim, J., Lim, M.S., Kim, S., Kim, O.H., Lee, D.W., Lee, J.H., Cho, Y.H., Sung, Y.E.: Gas diffusion layer/flow-field unified membrane-electrode assembly in fuel cell using graphene foam. Electrochim. Acta **323**, 134808 (2019)
38. Park, J.E., Lim, J., Kim, S., Choi, I., Ahn, C.Y., Hwang, W., Lim, M.S., Cho, Y.H., Sung, Y.E.: Enhancement of mass transport in fuel cells using three-dimensional graphene foam as flow field. Electrochim. Acta **265**, 488–496 (2018)
39. Li, B., Yan, Q., Song, C., Yan, P., Ye, K., Cheng, K., Zhu, K., Yan, J., Cao, D., Wang, G.: Reduced graphene oxide foam supported CoNi nanosheets as an efficient anode catalyst for direct borohydride hydrogen peroxide fuel cell. Appl. Surf. Sci. **491**, 659–669 (2019)

40. Zhou, X., Tang, S., Yin, Y., Sun, S., Qiao, J.: Hierarchical porous N-doped graphene foams with superior oxygen reduction reactivity for polymer electrolyte membrane fuel cells. Appl. Energy **175**, 459–467 (2016)
41. Kung, C.C., Lin, P.Y., Xue, Y., Akolkar, R., Dai, L., Yu, X., Liu, C.C.: Three dimensional graphene foam supported platinum–ruthenium bimetallic nanocatalysts for direct methanol and direct ethanol fuel cell applications. J. Power Sources **256**, 329–335 (2014)
42. Shi, C., Maimaitiyiming, X.: FeNi-functionalized 3D N, P doped graphene foam as a noble metal-free bifunctional electrocatalyst for direct methanol fuel cells. J. Alloy. Compd. **867**, 158732 (2021)
43. Kumar, A., Adalati, R., Sharma, M., Choudhary, N., Kumar, K.S., Hurtado, L., Jung, Y., Kumar, Y., Thomas, J. and Chandra, R.: Self-assembled zinc oxide nanocauliflower and reduced graphene oxide nickle-foam based Noval asymmetric supercapacitor for energy storage applications. Materials Today Commun., 105362 (2023)
44. Aslam, S., Sagar, R.U.R., Ali, R., Gbadamasi, S., Khan, K., Butt, S., Xian, J., Mahmood, N., Qiu, Y.: Mixed-dimensional niobium disulfide-graphene foam heterostructures as an efficient catalyst for hydrogen production. Int. J. Hydrogen Energy **46**(68), 33679–33688 (2021)

3D Graphene as Electrocatalysts for Water Splitting

Farkhondeh Khodabandeh and Mohammad Reza Golobostanfard

Abstract Considering the rapidly growing Earth pollution and energy crisis in the last several decades, the development of renewable energy sources has been at the forefront of research trends. Hydrogen production and storage through electrochemical water splitting holds great promise for the future green energy system. From the commercial side of the spectrum, higher reaction kinetics is required for these devices to meet industry demands. Graphene with a 3D hierarchical network has represented a great progress in water electrolysis both as an electrocatalyst and a support for other active materials owing to its distinctive properties such as large surface area, chemical robustness, and exceptional conductivity. This chapter provides a comprehensive review of the latest advances in 3D graphene-based electrocatalysts for water splitting techniques. In this regard, the electrocatalytic activity and performance of pristine graphene are discussed in the first place followed by the introduction of some design strategies to improve its efficiency. Then, various hybrid structures are profiled highlighting the role of 3D graphene as a great support. Finally, the future outlook and main challenges of this emerging field are discussed in the last section to offer an approach for further investigations.

Keywords 3D graphene · Hydrogen production · Water splitting · Renewable energy sources · Electrocatalyst

---

F. Khodabandeh
School of Metallurgy and Materials Engineering, College of Engineering, University of Tehran, North Kargar, 1417614411 Tehran, Iran

M. R. Golobostanfard (✉)
Ecole Polytechnique Fédérale de Lausanne (EPFL), Institute of Microengineering (IMT), Photovoltaics and Thin-Film Electronics Laboratory (PV-Lab), Rue de La Maladiere, 2000 Neuchâtel, Switzerland
e-mail: mohammadreza.golobostanfard@epfl.ch

© The Author(s), under exclusive license to Springer Nature Switzerland AG 2023
R. K. Gupta (ed.), *3D Graphene*, Carbon Nanostructures,
https://doi.org/10.1007/978-3-031-36249-1_19

1 Introduction

Due to the limited resources and environmental issues associated with fossil fuels, enormous efforts have been devoted to developing a renewable alternative. Molecular hydrogen (H_2), with its higher gravimetric energy capacities and pollution-free nature, is deemed to be an attractive candidate to fulfill modern society's demands. However, for a complete replacement of traditional fuels, economical and scalable hydrogen production is highly crucial. In stark contrast, industrial hydrogens evolution methods like steam reforming and coal gasification produce gigantic amounts of greenhouse gases contributing to global warming and air pollution [1].

Among various possible green approaches for hydrogen production, electrochemical water splitting is regarded to be a promising option since it only needs water as raw material, which is totally abundant and renewable and leaves no hazardous by-product. This method basically relies on a series of electrochemical reactions [2]: oxygen and hydrogen evolution reactions (HER and OER). Despite all the intriguing features of this method, the sluggish kinetics of the reactions hinders its widespread application. In this manner, the implementation of a high efficiency electrocatalyst is of significant importance. Precious Pt-group metals (PGM) have always represented great electrocatalytic behavior. Nevertheless, the scarcity and high cost of noble metals bound their practical usage for mass H_2 production. In recent years, massive research is going on in the development of cost-effective and more abundant electrocatalysts such as carbon-based nanostructures and transition metal compounds to replace PGMs.

The glamorous and charismatic properties of graphene such as its large specific surface area, high intrinsic conductivity, and great durability in an aqueous environment have paved the way for efficient and economical hydrogen production [3]. Graphene has a multifunctional structure and not only can be utilized as an electrocatalyst, but it can provide a proper support for other active materials. However, the considerable van der Waals force between its layers leads to the aggregation of graphene sheets. This phenomenon extremely reduces the accessibility of active sites and blocks electron transfer and gas diffusion to a high extent [4]. Therefore, it is necessary to overcome this challenge to realize the commercialization of graphene-based electrocatalysts. The construction of a three-dimensional (3D) network out of graphene sheets is a facile and novel solution to this problem. 3D graphene inherits the outstanding features of graphene and its hierarchical network and porous structure even make it a more reliable catalyst and support. The various interconnected pores in this framework expose more active sites to the reactants and simultaneously promote the diffusion of gas products. By precisely taking advantage of the aforementioned merits, 3D graphene-based materials can further optimize the electrocatalytic water splitting technique [5].

Regardless of all opportunities that 3D graphene provides, bare graphene has poor catalytic activity due to its zero-bandgap property and falls short of scalable fuel production [6]. In this regard, multitudes of strategies have been introduced to address this inferior performance. Chemical heteroatom doping of its lattice structure can highly improve its catalytic capability by manipulating the electronic structure. From another point of view, 3D graphene can be a fantastic support, and the hybridization of graphene sheets with other earth-abundant catalysts is a more practical and feasible route.

This chapter reviews recent progress made by 3D graphene as an electrocatalyst for water splitting process. First, the electrochemical water splitting mechanism and the functional properties of 3D graphene for the electrolysis reactions are explained. Then, the mostly utilized strategies to improve the catalytic activity of graphene are discussed including heteroatom doping of graphene and fabrication of various hybrid structures. Although substantial progress has been made inspired by the mentioned benefits, such investigations are still in their infancy and 3D graphene hybrids cannot yet compete with their Pt-based counterparts. Accordingly, challenges for the commercialization of 3D graphene-based electrocatalysts and future perspectives for their widespread applications are summarized in the last section.

2 Electrochemical Water Splitting Mechanism

Electrochemical water splitting is an eco-friendly and facile approach to store electrical energy as a chemical fuel. This conversion process involves a couple of electrochemical redox reactions. These reactions take place in an electrochemical cell consisting of (1) working electrodes, (2) electrolyte, and (3) external power supply as illustrated in Fig. 1a [7]. After the application of an external voltage to the electrodes, water molecules split into gaseous H_2 and O_2 on cathode and anode, respectively. The reaction mechanisms on each electrode in different media are as follows [8]:

Overall water splitting reaction:

$$H_2O \rightarrow H_2 + 0.5_2$$

In acidic medium:

$$2H^+ + 2e^- \rightarrow H_2(\text{cathode})$$

$$H_2O \rightarrow 2H^+ + 0.5O_2 + 2e^-(\text{anode})$$

In neutral and alkaline medium:

$$H_2O + 2e^- \rightarrow 2OH^-(\text{cathode})$$

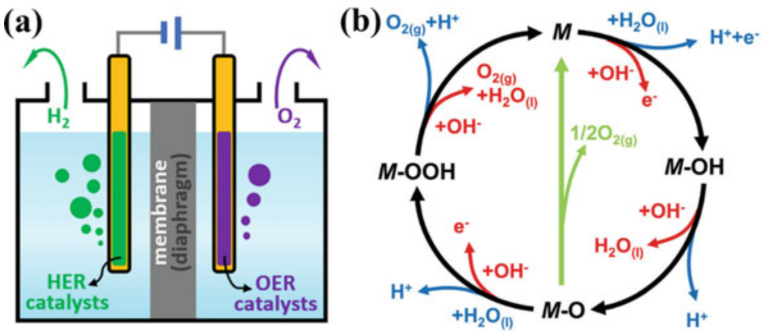

Fig. 1 **a** Schematic representation of an electrochemical water splitting cell. Adapted with permission [16]. Copyright (2018) American Chemical Society. **b** OER mechanism (Blue and red lines represent acidic and alkaline media, respectively). Adapted with permission [17]. Copyright (2017) Royal Society of Chemistry

$$2OH^- \rightarrow H_2O + 0.5O_2 + 2e^-(\text{anode})$$

In acidic medium, a proton obtains an electron to produce a H_{ads} in the Volmer step ($X + H^+ \rightarrow X\text{-}H_{ads}$, X is an active site), and after that, there are two possible reactions for HER resulting in two different mechanisms. The second step can be either Heyrovsky ($X\text{-}H_{ads} + H^+ + e^- \rightarrow X + H_2$) or Tafel ($X–H_2 + X–H_2 \rightarrow 2X + H_2$) reaction depending on the coverage of H_{ads}. However, in alkaline conditions, the aforementioned reactions will be $X + H_2O + e^- \rightarrow X\text{-}H_{ads} + OH^-$, $X\text{-}H_{ads} + H_2O + e^- \rightarrow X + H_2 + OH^-$, and $X–H_{ads} + X–H_{ads} \rightarrow 2X + H_2$, respectively [9]. In comparison, HER is quite faster in acidic medium and consumes less energy since there is no need for water molecules dissociation. In contrast to hydrogen production, the OER mechanism in both acidic and alkaline media is so complicated and involves many factors. Many research groups have investigated OER mechanism in different media and the most widely accepted one is shown in Fig. 1b; however, the precise OER mechanism is still an ongoing issue.

The Gibbs free energy of the overall water splitting reaction is ~237 kJ/mol [10]. Therefore, the minimum required voltage for a continuous water electrolysis under standard conditions (25 °C and 1 atm) is ~1.23 V. Practically, greater applied potentials are needed to overcome ohmic potential drop and other overpotentials associated with this process to produce hydrogen with an acceptable rate. Consequently, it is essential to coat electrodes with stable and active electrocatalysts to lower the overpotentials and accelerate the slow kinetics of both decomposition reactions. Although accelerating the HER on cathode is the major goal of water electrolysis, it is so important to develop efficient electrocatalysts for OER as it is the rate controlling reaction in most cases. The slow kinetics of OER arises from its multi-step procedure, which highly degrades the total performance of the cell. To date, IrO_2 [11] and RuO_2 [12] are known to be the two most efficient and stable catalysts to lower the high overpotential for oxygen evolution.

To promote an energy-saving and affordable water splitting process, electrocatalysts should possess certain characteristics regardless of the electrolyte medium. Factors including free energy of hydrogen adsorption (ΔG_H), Tafel slope, Faradic efficiency, turnover frequency (TOF), and overpotential are some of the functional criteria for material selection. ΔG_H of an electrocatalyst is its most decisive property indicating whether an electrocatalyst is qualified or not [13]. While a high binding energy between H atoms and catalyst surface is critical for the adsorption step (Volmer), a weak bonding is more favorable for electrochemical (Heyrovsky) and chemical (Tafel) desorption reactions. Taking this trade-off into account, a near-zero ΔG_H is considered to be the most ideal and this is the reason why Pt is the best electrocatalyst for HER under acidic circumstances [14]. Furthermore, the exchange current density is also another important property of electrocatalysts, and the relation between these two parameters is determined by the famous volcano diagram represented in Fig. 2, which is a great tool for estimating the catalytic performance of different materials. In addition to all these thermodynamic and kinetic factors, an electrocatalyst should also have a high mass transport ability, conductivity, number of active sites with suitable electron density, abundance, and stability in electrolyte to serve as a promising candidate.

It is well established that PGM-based electrocatalysts have always been the front runners for water splitting catalysis. However, these materials also have some problems, i.e., heavy anodic potential oxidizes RuO_2 to RuO_4 and reduces its active sites [15]. More importantly, their limited natural reserve and high cost hamper their practical and commercial applications. Therefore, it is urgent to develop earth-abundant and cost-effective substitutions with performance comparable to that of PGMs. In

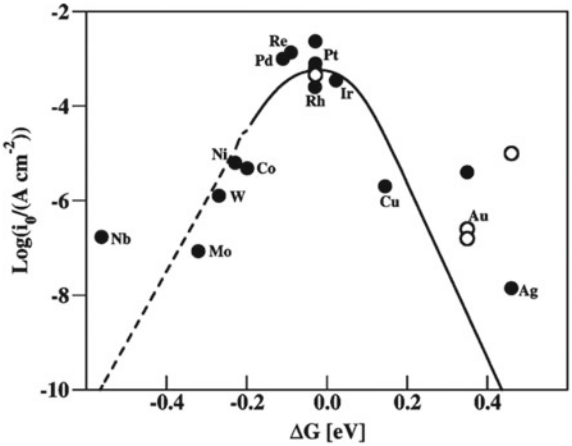

Fig. 2 Volcano diagram for HER exhibiting the relation between exchange current density and ΔG_H at U = 0 V. The solid line is a prediction depicted by a kinetic model and the dashed line represents the metals which usually form oxides at U = 0 V. The open circles are for (111) surface data and the filled circles are polycrystalline. Adapted with permission [18]. Copyright (2010) American Chemical Society

this regard, transition metal compounds such as chalcogenides, nitrides, carbides, and phosphides as well as carbon-based materials have been introduced, though their efficiency still lags behind that of noble metals.

3 Properties of 3D Graphene for Electrocatalytic Water Splitting

Outstanding physicochemical properties and conductivity of carbon materials have made them great candidates for PGM replacement [19]. Compared with transition metal compounds, carbon-based electrocatalysts introduce less pollution to the environment and are indeed less expensive making them superior options for mass production. The 2D member of this large family, graphene, has drawn much more researcher interests due to its extraordinary characteristics [3]. Theoretically, the specific surface area of graphene is incredibly high (2630 m^2/g), which facilitates the diffusion of electrolytes to the active sites and the release of reaction products. In addition, being a zero-bandgap semimetal endows graphene with a high electrical conductivity, which extremely increases reactions kinetics. Moreover, graphene is chemically stable and preserves its integrity even under harsh media. Finally, high thermal and mechanical stability of graphene can also be some interesting features for industrial applications.

Despite all these distinctive merits, ideal graphene is electrochemically inert and exhibits low catalytic performance [6]. The poor catalytic activity of a high-quality graphene originates from its special electronic structure and lack of any dangling bonds on its surface. Inspired by this limitation, diverse modification methods have been implemented to regulate the electronic structure and increase its chemical activity. Chemical doping by different elements and the introduction of defects to graphene lattice can effectively improve its performance since they can serve as active sites. On top of that, graphene can also be a fantastic support for the dispersion of other active materials.

In addition to inherent poor catalytic activity, graphene-based electrocatalysts cannot overcome the van der Waals forces between adjacent layers and tend to restack [20]. As a consequence, the number of active sites remarkably drops and all of the intriguing properties of graphene vanish, simultaneously. The development of a 3D framework out of graphene nanosheets can be a brilliant solution to alleviate this obstacle as it surpasses the reaggregation of graphene sheets and provides a suitable platform for the growth of other active materials. Another attractive feature of 3D graphene is that the interconnected pores in this structure surprisingly increase the surface area and available active sites compared with its 2D counterpart resulting in a much faster diffusion and HER rate. Additionally, this hierarchical network offers more pathways for electron transfer and lowers the overpotential for gas evolution reactions [4]. Coexistence of the advantages that this 3D scaffold brings along with functional inherent properties of graphene makes 3D graphene a reliable electrocatalyst for water electrolysis process.

4 3D Graphene as an Electrocatalyst for Water Splitting

In the past few years, numerous research have been focused on developing a novel method to trigger the intrinsic electrocatalytic capability of graphene. Chemical doping with heteroatoms, surface engineering, defect's introduction, and functionalization are some of the most feasible approaches to tailor the electronic properties of graphene sheets. However, heteroatom doping by non-metals has gained more attention in the case of 3D graphene.

4.1 Heteroatom Doping by Non-metals

Among all recommended techniques for boosting the weak catalytic activity of pristine graphene, heteroatom doping by non-metals is realized to be more practical [21]. The introduction of dopants to the graphene lattice furnishes abundant active sites to this structure and activates adjacent C atoms. In more detail, the foreign atoms effectively modulate the local electronic structure and contribute to charge redistribution in this hierarchical network, thus, promoting electrocatalytic performance. Electronegativity difference with carbon is the reason behind this activity improvement, and accordingly, elements including N, S, P, B, O, and Cl have been studied more frequently [4, 6, 22–24]. A schematic representation of various doping configurations of some common elements is demonstrated in Fig. 3.

When N is added to graphene planes, its lone electron pairs highly distort the planner structure by the formation of sp^2 and sp^3 hybridization. Additionally, high electronegativity of nitrogen leads to a noticeable polarization effect. Shen et al.

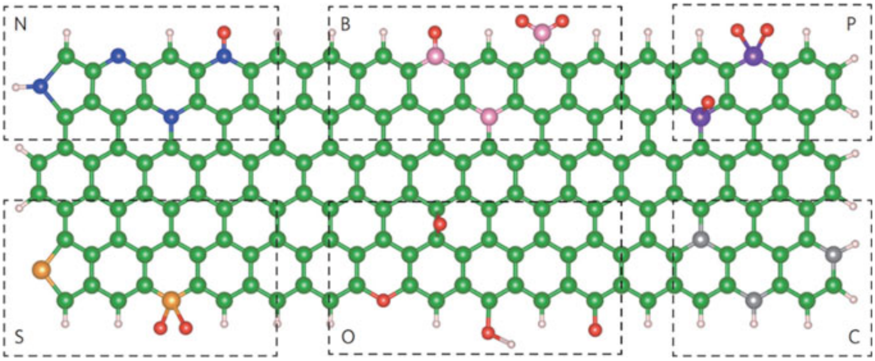

Fig. 3 A schematic representation of various doping configurations; from top and left: pyrrolic N, pyridinic N, graphitic N, B-2C-O, B-3C, B-C-2O, P-3C(-O), P-2C(-2O), th-S, S-2O, py-O, C–O–C, C–OH, C=O, g-C, z–C, and a-C. (C: Green/Gray, N: Blue, B: Pink, P: Purple, S: Gold, O: Red, and H: White). Adapted with permission [27]. Copyright (2016) Nature Publishing Group

[25] synthesized a 3D $Ti_3C_2T_x$/N-doped graphene (NG) hydrogel through a co-assembly approach using $NH_3.H_2O$ as a nitrogen source for graphene doping. A complex N 1 s spectrum in X-ray photoelectron spectroscopy results confirmed the presence of pyridinic, pyrrolic, and graphitic nitrogen in graphene sheets, and the catalytic activity of the first two provided so many active sites for HER. The sample containing 35% of MXene phase exhibited the lowest onset potential of 354 mV and overpotential of 474 mV to produce 10 mA/cm^2 in comparison with undoped graphene, bare samples, and the ones with different $Ti_3C_2T_x$ contents. The poor performance of blank 3D graphene and bare $Ti_3C_2T_x$ was ascribed to the inadequacy of active sites, while the introduction of nitrogen solved this issue. In the case of phosphorous, electronegativity is not the key factor, and the larger size of P atoms as well as its extra orbitals can impose distortion to the lattice and lead to a higher catalytic activity. However, boron and carbon have almost similar electronegativity and size and a modest change in bond length is responsible for catalytic performance enhancement.

Compared with other dopants, nitrogen has drawn much more attention for both HER and OER, though it is not still comparable with noble and transition metals. This inferior performance is mostly attributed to a nonideal ΔG_H and weak binding energy between hydrogen atoms and the catalyst surface. An elaborate strategy to further optimize ΔG_H of 3D graphene is dual or even multiatom doping. In such a case, a synergistic effect is induced in the procedure, which greatly improves the overall efficiency. Ito et al. [26] fabricated a nitrogen and sulfur codoped 3D nanoporous graphene catalyst through chemical vapor deposition method based on Ni template using pyridine and thiophene as N and S sources, respectively. Undoped, single-doped, and dual-doped samples were all synthesized under various temperatures for comparison and their HER polarization curves are illustrated in Fig. 4a. From samples prepared at 800 °C, it can easily be comprehended that HER activity has drastically increased after doping and a gradual decrease in onset potential is evident from undoped, N-doped, S-doped to N and S-doped graphene. Thus, doped samples exhibited a better electrocatalytic activity and the codoped catalyst had a superior performance, hence, showed the lowest Tafel slope of 105 mV/dec. In all, the best HER activity belonged to the codoped sample prepared in 500 °C with a Tafel slope of 80.5 mV.dec^{-1} and overpotential of 0.28 V at 10 mA/cm^2 comparable to that of chalcogenide catalysts. Furthermore, the electrochemical impedance spectroscopy (EIS) results indicated that the resistance of samples decreased after doping and it reached a minimum after doping with both N and S. As a result, the enhanced catalytic activity of doped samples could be attributed to this phenomenon. Reaction pathway of different samples achieved by density functional theory (DFT) calculations is shown in Fig. 4b. These results disclosed that ΔG_H of undoped graphene is positive, which means that adsorption of H_{ads} on its surface is not very favorable, while it is negative in the case of single-doped samples making it difficult for hydrogen desorption. However, N and S-doped graphene had the smallest value (0.12 eV) near to that of Pt. Therefore, the combination of positive and negative active sites created by N and S dopants, respectively, guaranteed fast electron transfer for HER.

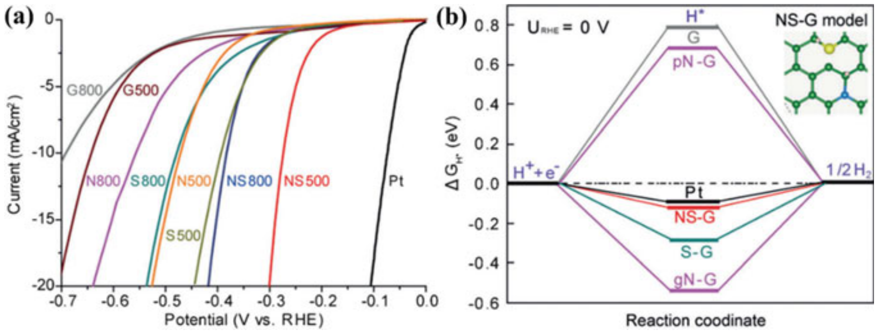

Fig. 4 **a** Cyclic voltammetry (CV) curves of the undoped and doped samples prepared at different temperatures, **b** Reaction pathways of undoped and doped samples achieved by DFT calculations. The inset shows a codoped graphene structure with a sulfur (yellow), nitrogen (blue), and hydrogen atom (white). Adapted with permission [26]. Copyright (2015) Wiley–VCH

In a nutshell, heteroatom doping of 3D graphene has undeniably opened a new door toward efficient metal-free catalysts for water electrolysis. Engineering the electronic structure of graphene to improve its catalytic activity and ΔG_H by non-metallic dopants has become an accepted method in recent decades. However, it is worth noting that although distortion of the ideal structure of graphene and tailoring its intrinsic characteristics are beneficial for catalytic activity, other exceptional properties of graphene, especially conductivity, degrade in exchange. Subsequently, an optimum dopant concentration should be employed for water splitting purpose.

5 3D Graphene as Electrocatalysts Support

Contrary to all the progress made by chemical doping in 3D graphene-based catalysts, they are not still among commercial candidates due to their unsatisfactory performance and high cost of the doping process. However, as it is already mentioned, graphene has got great potentials to be a support for other active materials. In this case, the high conductivity of graphene can contribute to the hybrid structure to dramatically increase the electron transfer kinetics. Meanwhile, the synergistic interaction of introduced materials with graphene modulates the electronic structure of active sites increasing their catalytic activity. Furthermore, graphene highly increases the number of exposed active sites by complete dispersion and controlling the morphology of the active material. Interestingly enough, these hybrid structures are greatly more durable in comparison with bare ones since graphene hinders their aggregation and bleaching after immersion in the electrolyte.

5.1 3D Graphene/Metals

It is well established that metal-based catalysts have always been the front runner for water electrolysis and their limited resources are the major bottleneck for their commercialization. A promising strategy to lower the metal consumption is to integrate them into a suitable support like 3D graphene [4]. A uniform dispersion of metal nanoparticles on the porous structure of graphene increases their exposed active sites and they definitely outperform due to the fascinating properties of 3D graphene mentioned in Sect. 2. From the stability point of view, graphene encapsulates dispersed nanoparticles and hinders their direct contact with electrolyte resulting in a more durable catalyst. Finally, metal particles regulate the electron density of graphene and make graphene itself catalytically more active. In the context, two bifunctional electrocatalysts based on Co-CoO/3D hierarchical porous graphene (Co-CoO/3DHPG) and Ni-NiO/3DHPG were investigated for HER and OER using cobalt nitrate and nickel acetate as Co and Ni sources, respectively [28]. The onset potential of Co-CoO/3DHPG, Ni-NiO/3DHPG, and 3DHPG electrodes obtained from the linear sweep voltammetry (LSV) plots were −0.26, −0.18, and -0.33 V_{RHE}, respectively, and the order of electrocatalytic activity was calculated to be Ni-NiO/3DHPG > Co-CoO/3DHPG > 3DHPG. Expectedly, overpotentials of samples at 10 mA/cm^2 for Co-CoO/3DHPG, Ni-NiO/3DHPG, and 3DHPG were −0.402, −0.31, and −0.45 V_{RHE}, respectively, and Tafel slopes were 65, 85, and 225 mV. Obviously, the presence of metal nanoparticles enhanced the catalytic performance of 3D graphene and Ni element was a better option for HER, while Co particles were more preferred for OER. It is worth noting that high electron density at the metal/oxide and graphene interface was advantageous for water splitting.

Hybrid structures of multiple metals alloys anchored on 3D graphene substrates have also been investigated for further improvements compared with single metals. In this respect, Zhong et al. [29] investigated the coupling of Pt_3Ni alloy nanoparticles with 3D N-doped graphene (Pt_3Ni/3DNG) for HER in alkaline media (1 M KOH). The transmission electron microscopy (TEM) image of Pt_3Ni/3DNG structure is illustrated in Fig. 5a. LSV curves in Figure 5b indicated that the Pt_3Ni/3DNG electrode produced the highest current density compared with Pt/3DG, Pt_3Ni/3DG, and even benchmark 40 wt.% Pt/C electrocatalysts. Importantly, Pt_3Ni/3DNG sample exhibited a very limited HER performance loss after 10,000 cycles in the alkaline electrolyte. This significant difference between catalytic performance of Pt_3Ni/3DNG and its non-alloy Pt/3DNG counterpart and other catalysts was attributed to the generation of a tensile strain and a ligand effect on active sites, which promoted the dissociation of water molecules and adsorption of H_{ads} species, respectively. Noteworthily, doping graphene before the introduction of single metal atoms or alloys can significantly improve the coordination of these catalysts and it was completely proved in the mentioned investigation.

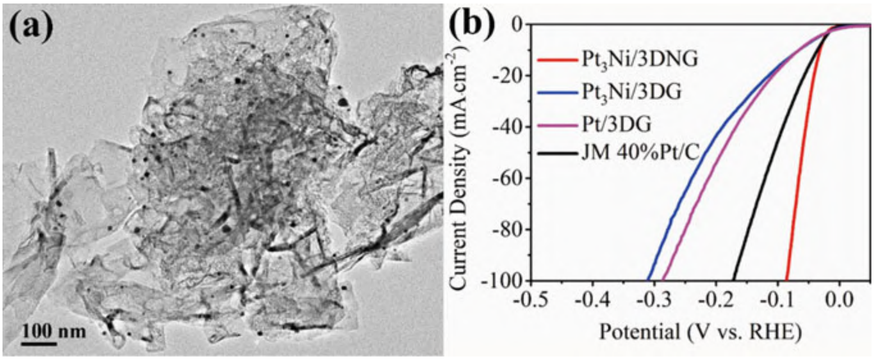

Fig. 5 **a** TEM image of Pt_3Ni/3DNG structure, **b** LSV polarization curves of Pt_3Ni/3DNG, Pt_3Ni/3DG, Pt/3DG, and commercial JM 40%Pt/C (with IR compensation). Adapted with permission [29]. Copyright (2022) Elsevier

5.2 3D Graphene/Dichalcogenides

Among countless electrocatalysts suggested for noble metals substitution, transition metal dichalcogenides (TMDCs) are the most likely candidates [30]. Their high catalytic activity and stability along with the economical synthesis process have attracted much attention in energy conversion and storage applications. In this regard, transition metal oxides, sulfides, and selenides have been studied more recently due to their high active sites and defects. Their inferior performance to that of PGMs arises from their low electrical conductivity, morphology transformation during catalysis, and high aggregation tendency [31]. Implementing a suitable support like 3D graphene for TMDCs increases not only their durability, but also electrocatalytic activity. It has been reported that graphene significantly prevents TMDCs from dissolution and aggregation while its high conductivity compensates that of TMDCs to some extent. The extremely high active sites and strong synergistic effect inherent in 3D graphene/TMDCs hybrid structures ensure a stable and efficient water electrolysis [4].

Among different kinds of TMDCs, sulfides, especially MoS_2, have represented adequate exciting breakthroughs. The binding energy between S atoms on the active edge sites and H^+ is so strong, providing a high HER rate. Furthermore, heteroatom doping is usually employed to improve catalytic activity of graphene; as a result, it can be a great way to develop a better support as well. Taking this approach, MoS_2/3D N-doped reduced graphene oxide (N-rGO) hydrogels were prepared as HER electrocatalysts by vertical integration of MoS_2 sheets to graphene planes [32]. N atoms in the graphene lattice served as nucleation sites for the vertical growth of MoS_2 sheets. A schematic representation of this process is shown in Fig. 6.

Figure 6 MoS_2/N-rGO had the lowest onset potential of 119 mV while N-rGO electrode exhibited negligible HER activity. Overpotential of this hybrid structure was 188 mV to approach 10 mA/cm^2, while it was a lot higher for pure MoS_2

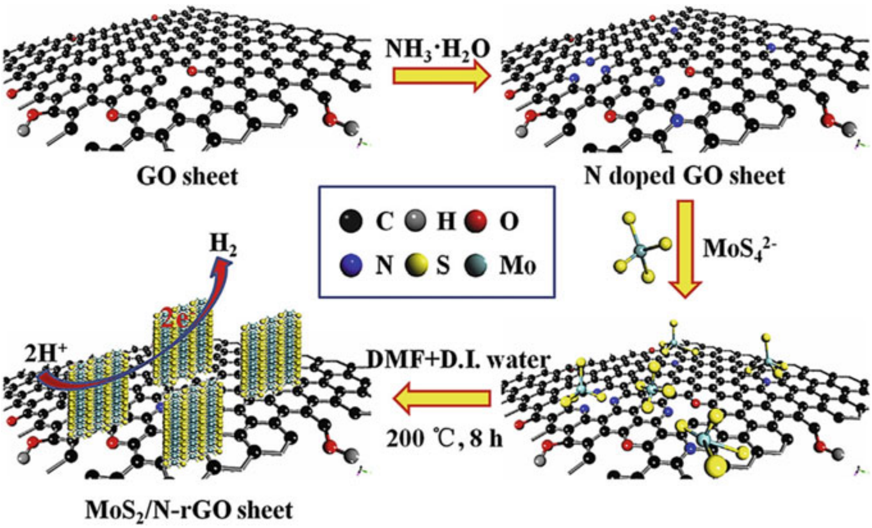

Fig. 6 Schematic representation of the synthesis process of MoS_2/N-rGO electrocatalyst. Adapted with permission [32]. Copyright (2017) Elsevier

(270 mV), confirming the superior performance of MoS_2/N-rGO to the non-hybrid electrodes. The incorporation of N atoms was also useful for the stability of electrodes and increased it for 1000 cycles (comparing MoS_2/N-rGO and MoS_2/rGO). In addition to MoS_2, other transition metal sulfides like WS_2 [33, 34] and CoS_2 [35] have also been supported on 3D graphene substrate and represented promoted electrocatalytic activities. Unlike sulfides, selenide and oxide compounds have rarely been studied.

Noticeably, hybrid structures based on two chalcogenides composed of two different metal elements can increase the number of active sites and accelerate the electron transfer rate. Recently, Kuang et al. [36] investigated interactions between MoS_2-NiS_2 nanoparticles and 3D N-doped graphene foam (NGF) and the performance of the electrode based on them toward water splitting reactions. The overpotential (172 mV) of this structure to obtain 10 mA/cm^2 was a lot lower than those of MoS_2/NGF, NiS_2/NGF, and bare NGF electrodes which was attributed to the synergistic effect between graphene and the bimetallic sulfides and the resultant abundant active sites. Moreover, the EIS results demonstrated a reduced semicircle in low frequency for MoS_2-NiS_2/NGF/nickel foam indicating the accelerated interfacial reaction and charge-transfer kinetics. Luckily, MoS_2-NiS_2/NGF hybrid structure exhibited acceptable OER activity in alkaline medium as well making it a bifunctional electrocatalyst for complete water electrolysis reactions. A two-electrode cell employing MoS_2-NiS_2/NGF as both electrodes needed 1.64 V to deliver 10 mA/cm^2 current density which is quite comparable to that of commercial noble metals and it was highly stable.

5.3 3D Graphene/Phosphides

Hydrogenase-like catalytic mechanism of transition metal phosphides is considerably advantageous for water splitting reactions. However, challenges like their low stability in electrolyte and poor electron transfer hamper further applications. In this vein, 3D graphene as a support can enhance their electron transfer capability while providing a large specific surface area to disperse them. Phosphides including Co_2P [37], FeP [38], and Ni_2P/Ni_5P_4 [39] have extensively been studied for this purpose.

5.4 Others

Although great progress has been made toward the electrocatalytic performance of compounds discussed in the above sections, developing robust and efficient novel catalysts for water splitting reactions is still an urgent demand. A plethora of different compounds, especially nitrides [40], carbides [41], layered double hydroxides [42], etc. have represented great potentials when integrated with 3D graphene. In addition to metallic compounds, polymeric catalysts have also received enormous attentions in recent years. However, low conductivity and poor stability of these materials are thoroughly detrimental to electrocatalytic operations. Coupling active polymers with highly conductive and stable 3D graphene has paved the way for their practical use. Graphitic carbon nitride ($g\text{-}C_3N_4$) is a relatively stable polymer and its low-cost synthesis process along with tunable chemical structure make it a fascinating option in this field. Electrochemical performance of $Cu_2P/g\text{-}C_3N_4$ nanocomposite merged with 3D graphene was assessed in 1 M H_2SO_4 [43]. This electrode disclosed a very low onset potential of 5 mV in comparison with bare graphene. Investigations revealed that the nitrogen functionalities of $g\text{-}C_3N_4$ served as active sites and the protonated phosphate groups of Cu_3P contributed to electron transfer between $g\text{-}C_3N_4$ and the support. Pure Cu_3P or $g\text{-}C_3N_4$-based electrocatalysts delivered poor cathodic current densities confirming the role of the graphene network for electron and mass transfer.

6 Self-Supported 3D Graphene Electrodes

Although the implementation of 3D graphene instead of 2D sheets extremely increased surface area and number of active sites, deposition of this structure on 2D substrates like F-doped tin oxide and glassy carbon electrode greatly restricts this advantage. From another respect, if a polymeric binder is used for better adhesion of graphene powder to substrate, diffusion of gas products is blocked and conductivity reduces significantly. Replacing 2D substrates with 3D frameworks such as carbon cloth (CC) and metal foams leads to the formation of self-supported free-standing electrodes with superior performance. Zhang et al. [44] integrated MoS_2 nanosheets with vertical graphene-coated CC (MDNS/VG/CC) and assessed its HER performance in comparison with CC, VG/CC, and MDNS/CC. The fabrication process of MDNS/VG/CC sample and its final microstructure is demonstrated in Fig. 7a–d. The MDNS/VG/CC electrode possessed the lowest onset potential (50 mV) and overpotential (78 mV). Furthermore, it produced 95 mA/cm^2 at 300 mV, which was 4 and 2 times higher than that of VG/CC and MDNS/CC electrodes, respectively. In addition, EIS results indicated a significant decrease in charge-transfer resistance of MDNS/VG/CC to 5.0 Ω from 85, 50, and 130 Ω for VG/CC, MDNS/CC, and CC, respectively. This improvement in HER activity for MDNS/VG/CC was attributed to the high conductivity of graphene, hence, faster electron transfer kinetics between MoS_2 edges and the support. Ni foam has always been regarded as a great support for other active materials and graphene sheets due to its high surface area and conductivity. Riyajuddin et al. [45] supported superhydrophilic $Ni_2P - CuP_2$ on Ni foam-graphene-carbon nanotubes heterostructure (NGCNC) through an electrochemical process shown in Fig. 7e. Impressively, NGCNC showed outstanding HER performance with an ultralow overpotential of 12 mV at 10 mA/cm^2 comparable with Ni − Pt/C (10 mV). Chronopotentiometry measurement at 100, 200, and 500 mA/cm^2 for 10 days disclosed a negligible (3%) fluctuation in potential, which indicates the superstability of NGCNC in acidic media. TOF values of NGCNC reached 1, 2, and 3 s^{-1} at low overpotentials of 100, 141, and 174 mV, respectively, illustrating its exceptional electrochemical HER activity. The superior performance of NGCNC electrode was attributed to the in-situ growth of graphene and bimetallic phosphides on Ni foam which prevented the use of any binder and formation of multiphases minimizing the series resistance.

7 Conclusion and Outlook

The development of an active, robust, and earth-abundant electrocatalyst for hydrogen fuel production is still known to be the most critical challenge for the industrialization of water electrolysis technique. Benefiting from its unique physical and chemical features, 3D graphene has been regarded as a promising candidate to address this issue. In this chapter, the inherent catalytic activity of graphene was estimated with emphasis on some practical modifications like heteroatom doping of the structure. As pristine graphene suffers poor catalytic activity and chemical doping results are not yet desirable, performances of several heterostructures were also reviewed in brief in which 3D graphene is mainly utilized as a support. However, there are still numerous issues to be dealt with in the way of practical applications and mass production and some of them are as follows.

Current methods employed for 3D graphene synthesis, either template-based or not, are not at all capable of large-scale applications. The exploitation of economical and less complicated strategies with more controllable synthesis conditions is considered essential to achieve products with desired properties, porosity, and morphology.

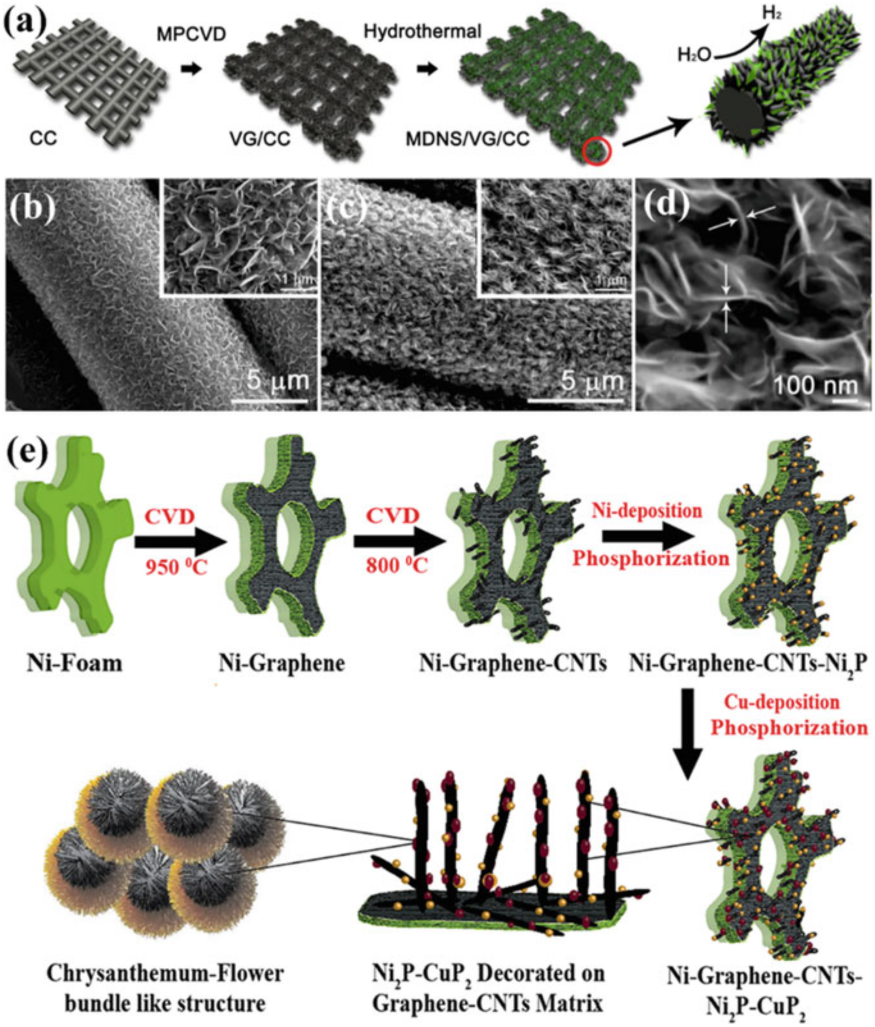

Fig. 7 **a** Schematic representation of the fabrication process of MDNS/VG/CC electrode, Low and high magnification SEM images of **b** VG/CC, **c**, **d** MDNS/VG/CC. Adapted with permission [44]. Copyright (2015) Elsevier. (e) Schematic illustration of the synthesis steps of NGCNC electrode. Adapted with permission [45]. Copyright (2021) American Chemical Society

Furthermore, doping is an efficient route to increase catalytic activity and stability of graphene even for hybrid structures, but it is too difficult to control the dopant content and existing methods are mostly expensive. Therefore, it is of great importance to attempt various methods to realize a controllable doping process.

Stability of the hybrid structures in harsh media is another long-standing obstacle for the scientific community. Although graphene plays a crucial role in increasing the durability of the whole structure, they still cannot compete with commercial electrocatalysts. Designing more stable composites applicable in less harsh electrolytes is considered necessary. On top of these, new research direction and enhancement strategies are needed rather than doping and compositing to regulate the electronic structure of graphene while maintaining its own properties to improve catalytic performance.

One of the most important reasons behind the poor performance of 3D graphene-based electrocatalysts is definitely the lack of information about the catalysis mechanism and active sites on the atomic scale and the blind design of catalysts. Moreover, DFT calculations are so simple and limited to the three steps mentioned in Sect. 2, which cannot provide sufficient information of more complex reaction intermediates formed on reaction sites. Development of more precise theoretical models toward the water spitting system and in-situ detecting technologies for characterization of the real reaction environment can provide a deep understanding of the whole process. Consequently, a more rational design of graphene-based electrocatalysts with faster reaction kinetics and higher stabilities becomes possible.

Acidic media accelerate HER kinetics while an alkaline environment is more favorable for OER; thus, bifunctional electrocatalysts which can be utilized for both reactions are more preferred options for future applications. In this regard, searching for electrodes that can catalyze the water splitting reactions in neutral pH values is a more preferred solution due to the stability issues. However, graphene-based bifunctional electrocatalysts are not yet efficient enough for widespread hydrogen production and require much more optimizations.

In total, bearing in mind all the fascinating opportunities that 3D graphene provides along with the challenges discussed above, one can make sure that this structure is an ideal choice for renewable electrochemical energy conversion and is worth much more investigations to march forward. In this connection, massive theoretical studies and experimental works should be devoted to the existing and future problems. In this unstoppable trend for the construction of the most efficient electrocatalyst for commercial water splitting, 3D graphene is undeniably a realistic candidate.

References

1. Chu, S., Majumdar, A.: Opportunities and challenges for a sustainable energy future. Nature **488**, 294–303 (2012)
2. Ibrahim, H., Ilinca, A., Perron, J.: Energy storage systems—characteristics and comparisons. Renew. Sustain. Energy Rev. **12**, 1221–1250 (2008)
3. Geim, A.K., Novoselov, K.S.: The rise of graphene. Nat. Mater. **6**, 183–191 (2007)
4. Kuang, P., Sayed, M., Fan, J., Cheng, B., Yu, J.: 3D graphene-based H2-production photocatalyst and electrocatalyst. Adv. Energy Mater. **10**, 1903802 (2020)
5. Cui, H., Guo, Y., Zhou, Z.: Three-dimensional graphene-based macrostructures for electrocatalysis. Small **17**, 2005255 (2021)
6. Zhang, X., Gao, J., Xiao, Y., Wang, J., Sun, G., Zhao, Y., Qu, L.: Regulation of 2D graphene materials for electrocatalysis. Chem. Asian J. **15**, 2271–2281 (2020)

7. Bard, A.J., Faulkner, L.R., White, H.S.: Electrochemical Methods: Fundamentals and Applications. Wiley (2022)
8. Schalenbach, M., Zeradjanin, A.R., Kasian, O., Cherevko, S., Mayrhofer, K.J.J.: A perspective on low-temperature water electrolysis–challenges in alkaline and acidic technology. Int. J. Electrochem. Sci. **13**, 1173–1226 (2018)
9. de Chialvo, M.R.G., Chialvo, A.C.: The resolution of the volmer-heyrovsky-tafel mechanism with a normal distribution of the standard gibbs energy of adsorption. J. Braz. Chem. Soc. **5**, 137–143 (1994)
10. Godula-Jopek, A.: Hydrogen Production: by Electrolysis. Wiley (2015)
11. Fierro, S., Nagel, T., Baltruschat, H., Comninellis, C.: Investigation of the oxygen evolution reaction on Ti/IrO_2 electrodes using isotope labelling and on-line mass spectrometry. Electrochem. Commun. **9**, 1969–1974 (2007)
12. Audichon, T., Napporn, T.W., Canaff, C., Morais, C., Comminges, C., Kokoh, K.B.: IrO2 coated on RuO2 as efficient and stable electroactive nanocatalysts for electrochemical water splitting. J. Phys. Chem. C. **120**, 2562–2573 (2016)
13. Nørskov, J.K., Bligaard, T., Logadottir, A., Kitchin, J.R., Chen, J.G., Pandelov, S., Stimming, U.: Trends in the exchange current for hydrogen evolution. J. Electrochem. Soc. **152**, J23 (2005)
14. Trasatti, S.: Work function, electronegativity, and electrochemical behaviour of metals: III. Electrolytic hydrogen evolution in acid solutions. J. Electroanal. Chem. Interfacial Electrochem. **39**, 163–184 (1972)
15. Kötz, R., Lewerenz, H.J., Stucki, S.: XPS studies of oxygen evolution on Ru and RuO_2 anodes. J. Electrochem. Soc. **130**, 825 (1983)
16. You, B., Sun, Y.: Innovative strategies for electrocatalytic water splitting. Acc. Chem. Res. **51**, 1571–1580 (2018)
17. Suen, N.-T., Hung, S.-F., Quan, Q., Zhang, N., Xu, Y.-J., Chen, H.M.: Electrocatalysis for the oxygen evolution reaction: recent development and future perspectives. Chem. Soc. Rev. **46**, 337–365 (2017)
18. Skúlason, E., Tripkovic, V., Björketun, M.E., Gudmundsdóttir, S., Karlberg, G., Rossmeisl, J., Bligaard, T., Jónsson, H., Nørskov, J.K.: Modeling the electrochemical hydrogen oxidation and evolution reactions on the basis of density functional theory calculations. J. Phys. Chem. C. **114**, 18182–18197 (2010)
19. Serp, P., Figueiredo, J.L.: Carbon Materials for Catalysis. Wiley (2009)
20. Qiu, B., Xing, M., Zhang, J.: Recent advances in three-dimensional graphene based materials for catalysis applications. Chem. Soc. Rev. **47**, 2165–2216 (2018)
21. Duan, J., Chen, S., Jaroniec, M., Qiao, S.Z.: Heteroatom-doped graphene-based materials for energy-relevant electrocatalytic processes. Acs Catal. **5**, 5207–5234 (2015)
22. Li, J., Zhao, Z., Ma, Y., Qu, Y.: Graphene and their hybrid electrocatalysts for water splitting. ChemCatChem **9**, 1554–1568 (2017)
23. Nemiwal, M., Zhang, T.C., Kumar, D.: Graphene-based electrocatalysts: Hydrogen evolution reactions and overall water splitting. Int. J. Hydrogen Energy. **46**, 21401–21418 (2021)
24. Kumar, R., Sahoo, S., Joanni, E., Singh, R.K., Maegawa, K., Tan, W.K., Kawamura, G., Kar, K.K., Matsuda, A.: Heteroatom doped graphene engineering for energy storage and conversion. Mater. Today. **39**, 47–65 (2020)
25. Shen, B., Huang, H., Liu, H., Jiang, Q., He, H.: Bottom-up construction of three-dimensional porous MXene/nitrogen-doped graphene architectures as efficient hydrogen evolution electrocatalysts. Int. J. Hydrogen Energy. **46**, 29984–29993 (2021)
26. Ito, Y., Cong, W., Fujita, T., Tang, Z., Chen, M.: High catalytic activity of nitrogen and sulfur co-doped nanoporous graphene in the hydrogen evolution reaction. Angew. Chemie. **127**, 2159–2164 (2015)
27. Jiao, Y., Zheng, Y., Davey, K., Qiao, S.-Z.: Activity origin and catalyst design principles for electrocatalytic hydrogen evolution on heteroatom-doped graphene. Nat. Energy. **1**, 1–9 (2016)
28. Ullah, N., Zhao, W., Lu, X., Oluigbo, C.J., Shah, S.A., Zhang, M., Xie, J., Xu, Y.: In situ growth of M-MO (M=Ni, Co) in 3D graphene as a competent bifunctional electrocatalyst for OER and HER. Electrochim. Acta. **298**, 163–171 (2019)

29. Zhong, H., Luo, X., Chen, H., Huang, S., Chen, Y.: Pt3Ni alloy catalyst coupled with three-dimensional nitrogen-doped graphene for enhancing the alkaline hydrogen evolution. Electrochim. Acta. **429**, 141030 (2022)
30. Peng, X., Pi, C., Zhang, X., Li, S., Huo, K., Chu, P.K.: Recent progress of transition metal nitrides for efficient electrocatalytic water splitting, Sustain. Energy Fuels. **3**, 366–381 (2019)
31. Xia, B., Yan, Y., Wang, X., Lou, X.W.D.: Recent progress on graphene-based hybrid electrocatalysts. Mater. Horizons. **1**, 379–399 (2014)
32. Zhao, L., Hong, C., Lin, L., Wu, H., Su, Y., Zhang, X., Liu, A.: Controllable nanoscale engineering of vertically aligned MoS2 ultrathin nanosheets by nitrogen doping of 3D graphene hydrogel for improved electrocatalytic hydrogen evolution. Carbon N. Y. **116**, 223–231 (2017)
33. Qi, F., Li, P., Chen, Y., Zheng, B., Liu, J., Zhou, J., He, J., Hao, X., Zhang, W.: Three-dimensional structure of WS2/graphene/Ni as a binder-free electrocatalytic electrode for highly effective and stable hydrogen evolution reaction. Int. J. Hydrogen Energy. **42**, 7811–7819 (2017)
34. Duan, J., Chen, S., Chambers, B.A., Andersson, G.G., Qiao, S.Z.: 3D WS2 nanolayers@ heteroatom-doped graphene films as hydrogen evolution catalyst electrodes. Adv. Mater. **27**, 4234–4241 (2015)
35. Pawar, R.C., Kang, S., Khan, H., Han, H., Lee, C.S.: Study of multi-faceted CoS2 introduced graphene aerogel hybrids via chemical approach for an effective electrocatalytic water splitting. Curr. Appl. Phys. **32**, 78–85 (2021)
36. Kuang, P., He, M., Zou, H., Yu, J., Fan, K.: 0D/3D MoS2-NiS2/N-doped graphene foam composite for efficient overall water splitting. Appl. Catal. B Environ. **254**, 15–25 (2019)
37. Li, G., Yu, J., Jia, J., Yang, L., Zhao, L., Zhou, W., Liu, H.: Cobalt-Cobalt phosphide nanoparticles@ nitrogen-phosphorus doped carbon/graphene derived from cobalt ions adsorbed saccharomycete yeasts as an efficient, stable, and large-current-density electrode for hydrogen evolution reactions. Adv. Funct. Mater. **28**, 1801332 (2018)
38. Venugopal, N.K.A., Yin, S., Li, Y., Xue, H., Xu, Y., Li, X., Wang, H., Wang, L.: Prussian blue-derived iron phosphide nanoparticles in a porous graphene aerogel as efficient electrocatalyst for hydrogen evolution reaction. Chem. Asian J. **13**, 679–685 (2018)
39. Ding, G., Zhang, Y., Dong, J., Xu, L.: Fabrication of Ni2P/Ni5P4 nanoparticles embedded in three-dimensional N-doped graphene for acidic hydrogen evolution reaction. Mater. Lett. **299**, 130071 (2021)
40. Song, G., Luo, S., Zhou, Q., Zou, J., Lin, Y., Wang, L., Li, G., Meng, A., Li, Z.: Doping and heterojunction strategies for constructing V-doped Ni 3 FeN/Ni anchored on N-doped graphene tubes as an efficient overall water splitting electrocatalyst. J. Mater. Chem. A. **10**, 18877–18888 (2022)
41. Wang, J., Xia, H., Peng, Z., Lv, C., Jin, L., Zhao, Y., Huang, Z., Zhang, C.: Graphene porous foam loaded with molybdenum carbide nanoparticulate electrocatalyst for effective hydrogen generation. Chemsuschem **9**, 855–862 (2016)
42. Shen, B., Huang, H., Jiang, Y., Xue, Y., He, H.: 3D interweaving MXene–graphene network–confined Ni–Fe layered double hydroxide nanosheets for enhanced hydrogen evolution. Electrochim. Acta. **407**, 139913 (2022)
43. Riyajuddin, S., Tarik Aziz, S.K., Kumar, S., Nessim, G.D., Ghosh, K.: 3D-graphene decorated with g-C3N4/Cu3P composite: a noble metal-free bifunctional electrocatalyst for overall water splitting. ChemCatChem. **12**, 1394–1402 (2020)
44. Zhang, Z., Li, W., Yuen, M.F., Ng, T.-W., Tang, Y., Lee, C.-S., Chen, X., Zhang, W.: Hierarchical composite structure of few-layers MoS2 nanosheets supported by vertical graphene on carbon cloth for high-performance hydrogen evolution reaction. Nano Energy **18**, 196–204 (2015)
45. Riyajuddin, S., Azmi, K., Pahuja, M., Kumar, S., Maruyama, T., Bera, C., Ghosh, K.: Super-hydrophilic hierarchical Ni-foam-graphene-carbon nanotubes-Ni2P–CuP2 nano-architecture as efficient electrocatalyst for overall water splitting. ACS Nano **15**, 5586–5599 (2021)

3D Graphene as a Photocatalyst for Water Splitting

Rozan Mohamad Yunus, Nurul Nabila Rosman,
and Nur Rabiatul Adawiyah Mohd Shah

Abstract Hydrogen production by photoelectrochemical (PEC) water splitting has attracted considerable interest because it is a promising clean source of energy for improving the earth's climate in the future. Owing to the excellent properties of graphene, the use of graphene in photocatalysis for green hydrogen production has attracted remarkable interest. 3D graphene, which can act as a co-catalyst and transfer agent to enhance photocatalytic hydrogen production, is a potential component for PEC electrodes due to its substantial surface area, fast electron transfer, high electron conductivity, low mass density, mechanical stability, interconnected and hierarchical structure. The use of 3D-graphene-based photocatalysts in PEC water-splitting applications is highlighted and discussed in this chapter. Various strategies and approaches for the synthesis of 3D graphene are also presented. Efforts have been made in the incorporation of 3D graphene with metal oxides, transition-metal dichalcogenides (TMDCs), or other semiconductor materials wherein the synergistic effect between these materials can suppress the recombination of photogenerated electron–hole pairs to enhance PEC water-splitting performance considerably. This chapter presents an inclusive review of the photocatalytic characteristics and current development of 3D graphene-based photocatalysts for water-splitting applications.

Keywords 3D graphene · Photocatalysts · Photoelectrochemical water splitting · Hydrogen production

1 Introduction

Graphene, the thinnest material, is an independent carbon material. It has a highly crystalline structure that is composed of a monolayer of carbon atoms packed tightly into a two-dimensional (2D) honeycomb lattice via sp^2-hybridized carbon–carbon bonds in a hexagonal arrangement, thus forming a strong and unique long-range π-conjugation structure. Graphene has extraordinary physicochemical properties

---

R. M. Yunus (✉) · N. N. Rosman · N. R. A. M. Shah
Fuel Cell Institute, Universiti Kebangsaan Malaysia, 43600 Bangi, Selangor, Malaysia
e-mail: rozanyunus@ukm.edu.my

© The Author(s), under exclusive license to Springer Nature Switzerland AG 2023

R. K. Gupta (ed.), *3D Graphene*, Carbon Nanostructures,
https://doi.org/10.1007/978-3-031-36249-1_20

that include high theoretical specific surface area (2630 m^2/g), ultrahigh intrinsic carrier mobility (≈200 000 $cm^2/V/s$), high mechanical strength (breaking strength of 42 N/m), outstanding high Young's modulus (≈1 TPa), good thermal conductivity (3000–5000 W/m/K), excellent optical transparency (≈97.7%), and strong chemical stability, all of which assist in attenuating the effect of wide band gaps and the recombination of electron–hole pairs in photocatalysts [1–4].

Graphene has highly attractive physical properties. Many studies on 2D materials have been conducted because of graphene's excellent properties. In 2004, Novoselov and Geim discovered the first 2D graphene sheets, which are the building blocks of graphite [5]. In the last decade, numerous 2D structures of π-conjugated carbon-based materials, such as graphene, graphene oxide (GO), reduced GO (rGO), and graphene/carbon quantum dots, have been introduced as efficient, attractive, and valuable substrates/templates/supports for catalysts and semiconducting nanomaterials. Additionally, many studies have reported that graphene can enhance the photocatalytic efficiency of photoelectrochemical (PEC) water splitting due to its unique 2D conjugated structure and electronic properties. However, producing high-quality 2D graphene, especially single-layer and free-defect graphene, on a large scale is difficult because it tends to aggregate and restack, thus decreasing its specific surface area, causing the loss of its distinct properties, and consequently resulting in poor photocatalytic performance [1, 2, 4, 6].

One effective solution to overcome these problems is the assembly of 2D layers of graphene into three-dimensional (3D) structures known as 3D graphene. Interestingly, interconnected 3D graphene structures retain the outstanding properties of 2D graphene and are free from aggregation or restacking. Therefore, their photocatalytic properties can be enhanced by increasing light adsorption, providing additional accessible active sites, and improving charge transport [1, 2, 4]. 3D graphene is also known as foams, sponges, aerogels, or hydrogels. Surface area, electrical conductivity, thermal properties, and mechanical stability are determined by synthesis methods, which include the hydrothermal, chemical vapor deposition (CVD), and self-assembly methods (Fig. 1). Understanding the important factors that influence the properties and nucleation and growth mechanism of 3D structures is required particularly when tuning the functionalization of 3D graphene structures [2].

3D graphene is suitable for application in PEC water hydrogen production due to its main properties, such as its porous structure, large surface area, outstanding mechanical properties, and rapid electron transport. The incorporation of 3D graphene with metal oxides, transition-metal dichalcogenides (TMDCs), and other semiconductor materials has been explored to improve photocatalytic properties for water splitting. Photocatalysts/photoelectrodes that can employ a wide solar spectrum, suppress the recombination of photogenerated electron–hole pairs, and improve system stability are expected to be obtained through these combinations. Thus, recent advancements in this effort are addressed in the last part of this book chapter.

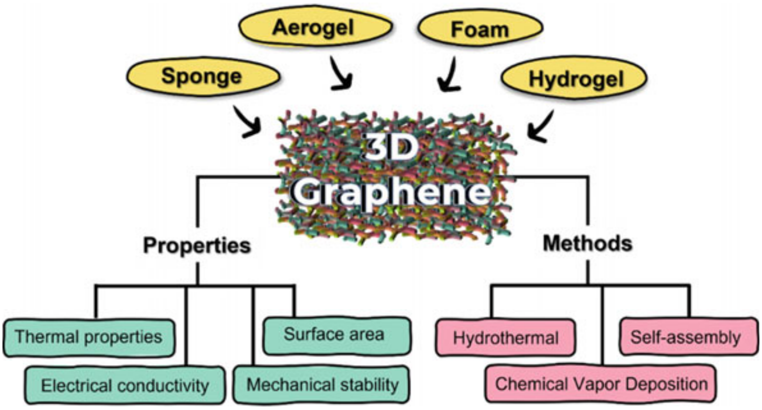

Fig. 1 Structures, properties, and synthesis methods related to 3D graphene

2 Properties of 3D Graphene

3D graphene structures can be classified into two types: (1) microscopic structures (less than 100 μm in all dimensions), which are typically in the form of macroscopically sized powders with 3D structures on the micrometer or nanometer scale and (2) macroscopic or macrostructures (more than 100 μm in all dimensions), such as macro 3D graphene monoliths, film, fibers, and millispheres [1, 2]. Graphene walls should be composed of not more than 10 layers of graphene and must preserve the basic properties of graphene. 3D graphene structures can be divided into two types depending on the form of connections: (1) joint 3D graphene, wherein several single-layer graphene sheets/cells are interknitted primarily through van der Waal's forces, and (2) integrated 3D graphene, in which chemical bonds continuously connect carbon atoms. Between these two structures, integrated 3D graphene structures exhibit excellent conductivity and mechanical robustness [2]. 3D graphene structures provide a solution to the challenge posed by graphene sheet aggregation and restacking. Such a solution is important for ion transfer in water splitting. 3D graphene not only has the intrinsic properties of graphene sheets, but it also has a variety of advantages, including very small mass density, high specific surface area and porosity, an interconnected and hierarchical structure, and excellent mechanical stability that allows for increased access to active sites by providing additional pathways for rapid mass and electron transport kinetics in photocatalysis. Given its ability to create new functionalities through cross-interactions, 3D graphene has been referred to as a bridge connecting the nano- and macroworlds. Considering its above distinguishing properties, 3D graphene has great potential for photocatalytic water-splitting applications [1, 4].

2.1 Surface Area

The number of nanosized (typically 1–100 nm) pores and the thickness of the graphene wall [2, 7] are important factors determining the surface area of 3D graphene. Several parameters, such as reaction time, temperature, and inlet gas flow rate, can be controlled to adjust the wall thickness and specific surface area of graphene [4, 7–13]. The template, substrate, scaffold, or catalyst used also influences the properties of 3D graphene [4, 14]. Generally, 3D graphene has a density of less than 0.1 g/cm, a surface area of 500–1000 m^2/g, and pore sizes ranging from several micrometers to several nanometers [2]. Min et al. prepared 3D graphene by using a conventional nickel foam template with a specific surface area of approximately 145 m^2/g and a density of 0.073 g/cm^3 [7]. Even after annealing at 1500 °C, the specific surface area of 3D graphene increased from 336.5 m^2/g to 440.8 m^2/g. A high proportion of mesopores were found in a narrow range of 3 nm to 5 nm with a peak pore diameter of approximately 3.8 nm (Fig. 2a, b) [11]. Meanwhile, the hierarchical interconnected structure of 3D graphene prepared by a 3D printed silica sacrificial template has obtained a higher BET surface area (994.2 m^2/g) as shown in Fig. 2c) [9]. Following template etching, 3D graphene maintained a porous structure with a large area. Freeze–drying is crucial for maintaining the structure of 3D porous graphene without considerable aggregation [7, 12, 13]. Shen et al. discovered that from a theoretical perspective, the graphene sheet size determines the microstructure and density of 3D graphene. Reducing the graphene sheet size to 2 nm facilitated the stacking and action as building blocks of 3D graphene with a density and pore value of 1.49 g/cm^3 and 5–10 nm, respectively. The graphene sheet became staggered and bent as its size increased, resulting in its low density [15]. Consequently, protecting the structure of 3D graphene photocatalysts from restacking, aggregation, staggering, or bending is essential to acquire a high surface area that increases the exposure of active sites for water-splitting reactions. However, obtaining graphene sheets with a uniform thickness remains challenging.

2.2 Electrical Conductivity

3D graphene has excellent electrical conductivity due to its porous interconnected structure and high-quality graphene walls. The electrical conductivity of 3D graphene can be measured by using a two-or four-probe method and generally ranges from 2 S/cm to 1600 S/cm [2, 9, 11, 16–18]. 3D graphene has an electrical conductivity of approximately 2.39 S/cm due to its highly continuous structure that comprises few- and multilayered graphene [9]. Figure 3a shows that even when synthesized from powder templates, 3D graphene has a good electrical conductivity of 13.84 S/cm [18]. Furthermore, a conductivity of 17.5 S/cm was obtained with more than five layers of graphene with wrinkled and folded morphologies [7]. The bulk electrical conductivities of 3D graphene increased from 14.4 S/m to 53.7 S/m with

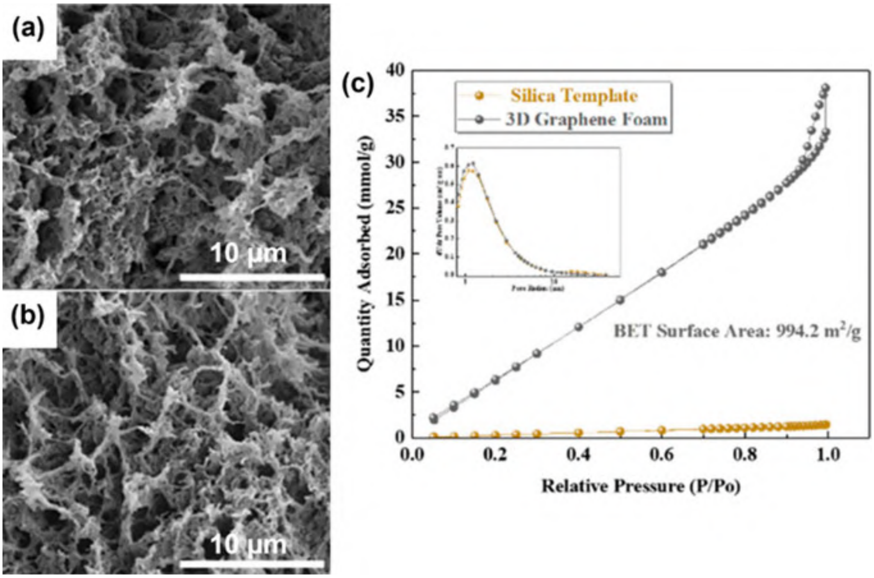

Fig. 2 FESEM image of 3D graphene (aerogel) **a** before and **b** after annealing. Adapted with permission [11], Copyright (2017), Scientific Reports. **c** Comparison of the BET surface areas of the silica template and 3D graphene (foam). Adapted with permission [9], Copyright (2020), American Chemical Society

the increase in bulk density and increased to 53.5–157.3 S/m after annealing (Fig. 3b) [11]. Xia et al. applied 3D microporous copper as a catalyst to grow graphene. The resulting 3D graphene had a high density and strong structure without any support, allowing for a high conductivity of approximately 1600 S/cm with a resistance of ~2.6 Ω (Fig. 3c) [16]. However, cross-linking agents with the function of strengthening the porous structure must be carefully selected to maintain the electrical conductivity of 3D graphene [1].

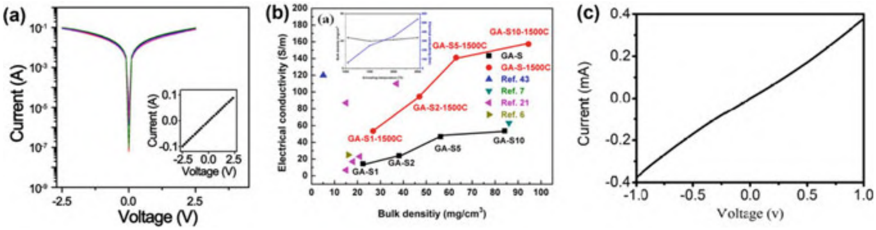

Fig. 3 **a** Current–voltage curve of 3D graphene (foam). Adapted with permission from [18], copyright (2016), American Chemical Society. **b** Electrical conductivities of 3D graphene (aerogel) before and after annealing. Adapted with permission [11], Copyright (2017), Scientific Reports. **c** Current–voltage measurement of 3D graphene. Adapted with permission [16], Copyright (2017), Journal of Physical Chemistry C

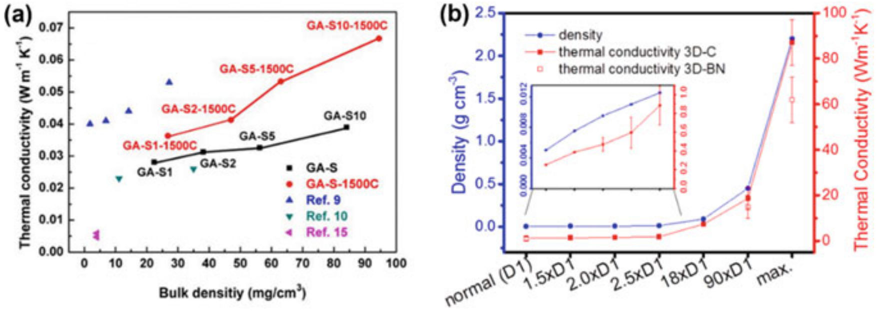

Fig. 4 **a** Thermal conductivities of 3D graphene (aerogel) before and after annealing. Adapted with permission [11], Copyright (2017), Scientific Reports. **b** Density and thermal conductivity measurements of 3D graphene (foam) (as 3D-C). Adapted with permission [20], Copyright (2017), American Chemical Society

2.3 Thermal Properties

Effective thermal conductivity is (κ) is calculated as $\kappa = K_{sample} \times L/A$, where L is the sample length, and A is the sample cross-sectional area. It is mainly influenced by two morphological factors: (1) primary structure, namely, building blocks, and (2) secondary structure, namely, assembled building blocks [19]. As shown in Fig. 4a, Cheng et al. discovered that 3D graphene had a thermal conductivity of 0.0281–0.0390 W/m/K after losing approximately 15% of its weight, and its thermal conductivity slightly increased to 0.0363–0.0667 W/m/K after being annealed at high temperatures (1500 °C) [11]. Moreover, 3D graphene with a density of 5 mg/cm^3 had a thermal conductivity of 1.2 W/m/K. As its density increased, its thermal conductivity increased to 86 ± 10 W/m/K (Fig. 4b) [20]. This finding demonstrated that in 3D graphene, thermal conductivity is directly proportional to mass density and could be improved without increasing graphene wall thickness [21]. Another approach for increasing mass density is to compress 3D graphene materials, which also can enhance the intrinsic thermal properties of 3D graphene as a photocatalyst [19]. In addition, the etchant solution used in substrate/template/support removal and the reaction temperature could affect the thermal conductivity of 3D graphene by reducing defects and defect-induced phonon scattering [2]. Nevertheless, 3D graphene exhibits hydrophobic properties, particularly after being etched away from the substrate/template/support.

2.4 Mechanical Stability

3D graphene photocatalysts can be obtained after the optimization of processing parameters that affect microscopic geometry and mass density. Interestingly, 3D graphene retains its freestanding structure after being etched from its template or supported substrate (regardless of thickness) due to the superior mechanical strength of graphene [2, 4]. A theoretical study by Li et al. demonstrated that triangle-like 3D graphene structures (only sp^2–sp^2 carbon bond, armchair, and zigzag) are strongly dependent on structural size. The in-plane Young's moduli (x and y directions) of the sp^2–sp^2 carbon bond, armchair, and zigzag can reach 505.20–578.51, 504–583.46, and 640.22–744.32 GPa, respectively [22]. 3D graphene is likely stable because multilayered graphene is highly crystallized and carbon shells are connected by a 2D graphene layer structure. 3D graphene with a density of 18 mg/cm^3 had Young's modulus of approximately 239.7 kPa, and its stress remained nearly constant at 55% compression strain for different loops, reflecting its flexibility and elasticity [9]. Moreover, Young's modulus and yield strength of 3D graphene rose to 1.02–17.29 and 0.08–1.05 MPa, respectively, after annealing [11]. Sha et al. reported that 3D graphene had remarkably similar morphologies before and after loading with weights, emphasizing its structural resiliency (Fig. 5) [18]. Hence, the porous structure of 3D graphene as a photocatalyst is crucial in providing intimate structural interconnectivities, a pathway for electron/phonon transport, high surface area, and strong mechanical properties.

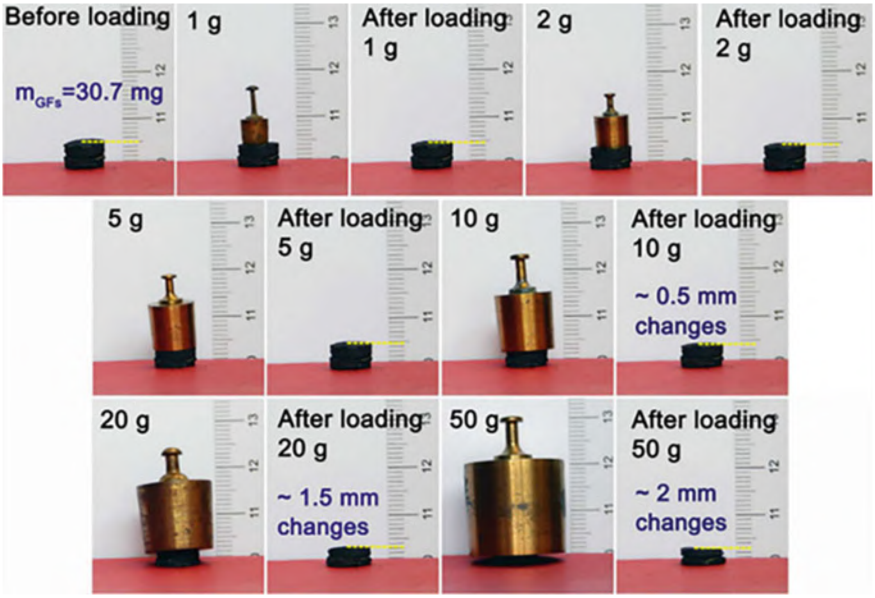

Fig. 5 Digital photos of 3D graphene (foam) before and after weight loading. Adapted with permission [18], Copyright (2016), American Chemical Society

2.5 Other Properties

Given its zero-band gap and strong Dirac fermion interactions with electromagnetic radiation, graphene has superior optical properties and thus can absorb photons from the visible to infrared spectrum. Xu et al. reported that 3D graphene has no response in the visible spectrum [23]. Its optical properties vary depending on the growth reaction temperature [24]. Furthermore, its in-plane pores provide numerous edge defects, resulting in additional active sites and efficient transport pathways. The substrate/template/support used, the hydrocarbon precursor, and the annealing and growth duration all have an effect on the in-plane properties of 3D graphene.

3 Methods for 3D Graphene Synthesis

Functionalized 3D graphene-based materials can be successfully self-assembled by using graphene and its functionalized derivatives and typical 2D structures as the building blocks. The usefulness of graphene in technologies is anticipated to increase as 3D graphene frameworks are developed [25]. 3D graphene foams (GFs) provide a number of benefits, including an expansive surface area, improved catalytic performance, reduced thermal conductivity, and moderate electronic conductivity [26]. A variety of terms, including “sponge”, “foam”, “aerogel”, “hydrogel”, “network”, “bead”, and “monolith”, have been used to define 3D graphene-based structures. The manufacture of 3D graphene utilizes a variety of templates, including polystyrene spheres, nickel foam, and copper foam [27]. Direct synthesis from carbon sources and solution-based synthesis methods, such as CVD and hydrothermal synthesis, can be used to create 3D porous graphene [27]. The direct fabrication method can provide the appropriate quality for the development of pore density, size, and distribution in 3D structures. Nevertheless, it has high production costs. The solution-based manufacturing process offers some advantages, including elemental functionalization, possible scalability, improved production efficiency, and cheap manufacturing costs, despite resulting in the dispersion of pore structure [28]. The template-based synthesis of the 3D porous network typically involves three processes: (1) precursors of the reaction are incorporated into the template, (2) the solid form is continuously grown in and on the surface of the template, and (3) a 3D porous structure is created by removing the template in a variety of ways [27]. Both synthesis methods are discussed in subsequent sections.

3.1 Hydrothermal Method

An aqueous solution that is being utilized as a reaction system is heated and pressurized in a particular closed reaction vessel to create a high-temperature and high-pressure reaction environment. In this process, a chemical that is weakly soluble or insoluble under normal conditions is dissolved and then recrystallized [29]. For example, Men et al. used the hydrothermal method to fabricate free-standing rGO foam for photocurrent generation and photocatalytic activity. Morphologically, the produced rGO/nickel foam had a porous structure. After the template was removed, the rGO foam demonstrated an interpenetrating 3D porous structure. The pore size of the rGO foam was in the order of approximately hundreds of micrometers, which was comparable with that of nickel foam (Fig. 6a, b) [13]. Zhou et al. synthesized a covalent 3D graphene network via the hydrothermal method by using an aromatic diamine, such as 2,2′-dimethyl-4,4′-biphenyldiamine (DMPDA), 4,4′-diaminodiphenylmethane (MDA), and benzidine, as a cross-linker to functionalize GO at ambient temperature. The treatment of stiff benzidine molecules with 2D GO flakes prevented face-to-face stacking because the surface of GO-benzidine was rougher and more porous than that of GO. GO-benzidine had a smaller surface area than GO-DMPDA and GO-MDA but 5.4 times higher photocatalytic activity than noncovalent 3D graphene. This finding showed that the particular surface area of 3D graphene did not have a significant effect on the production of hydrogen in the form of H_2 during photocatalysis [4, 30]. Meanwhile, GO hydrogels were fabricated by using a hydrothermal technique with exfoliated GO, which can be obtained through a modified Hummer method [31]. Graphene hydrogels can be turned into graphene aerogels by eliminating water through freeze–drying [32, 33]. The 3D porous network structure of graphene aerogel was clearly defined and connected by many micrometers of interconnected pores. A 3D graphene-based geometric framework with embedded nanoparticles had been shown to improve interface contact, reduce nanoparticle aggregation and dissolution, and increase stability and PEC performance [33].

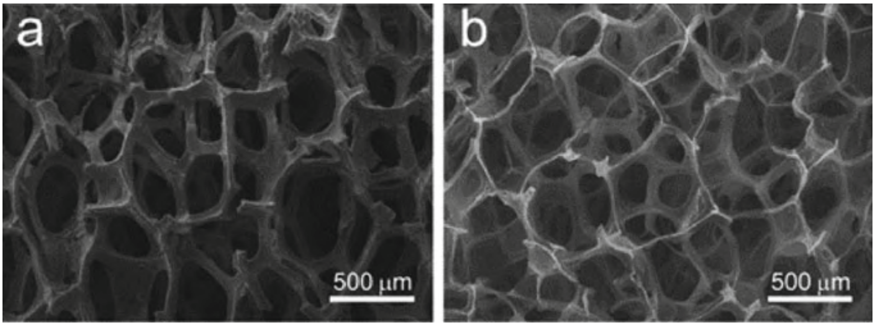

Fig. 6 SEM images **a** rGO/nickel foam and **b** free-standing rGO foam. Adapted with permission [13], Copyright (2016), Elsevier

3.2 CVD

CVD is the process of depositing nanomaterial in the form of a thin film from vapor species onto substrates through chemical reactions [34]. CVD has been widely used and is the current method for the molecular synthesis of graphene because it can produce graphene with high surface areas. In the CVD method, a thin metal substrate is placed into a furnace and heated to high temperatures (900 °C–1000 °C) under a low vacuum. Hydrogen gas and carbon from methane gas must flow through the chamber to ignite a reaction between methane and the surface of the metal film, such as copper, nickel, or cobalt film [35]. Chen et al. synthesized 3D GF on a nickel foam substrate by using the CVD method at 1000 °C under ambient pressure. Then, the nickel foam was etched away by using 3 M hydrochloric acid to produce free-standing GF. Ripples and wrinkles develop on the graphene films as a result of the differing thermal expansion coefficients of nickel and graphene. The wrinkling and ripples in composite materials produced when a GF is combined with a polymer are expected to promote mechanical interlocking between polymer chains, which improves adhesion. This effect is similar to the effect of the wrinkles in chemically produced graphene sheets. However, the building blocks of monolayer GF tend to collapse and break when copper foams are used as a template due to their inability to withstand the liquid capillary force exerted by acetone evaporation [36]. Meanwhile, Cai et al. synthesized a 3D GF to enhance the photocatalytic activity of ZnO. The morphological structure of 3D GF showed that additional ZnO nanorod nucleation sites were provided by the oxygen-containing functional groups of 3D graphene; thus ZnO nanorods were dispersed randomly and were well-separated from one another on 3D GF [37]. Flower-like 3D porous graphene (FG) can also be synthesized by using transformer-coupled plasma-enhanced CVD in a chamber wherein methane and argon had been introduced as precursors. The graphene framework features a densely packed and consistently dispersed flower-like structure as shown in Fig. 7a, b. The fold width was typically 200 nm. FG displays porous structures that might make it an ideal photocatalyst support material. The photocurrent performance of ZnS was approximately 4.4 times higher than that of bare ZnS after the addition of FG. Thus, FG can perform as an electron acceptor that can enhance separation and reduce the recombination of the photogenerated charge carriers of the ZnS/FG composite, permitting additional charge carriers to generate reactive species [38].

3.3 Self-Assembly Method

Self-assembly is one of the natural methods for building complex living structures in the nano-, micro-, and macro dimensions. Self-assembly has been widely acknowledged as a "bottom-up" nanotechnology approach. This method generates extensive molecular structures from molecules sustainably. The top-down chemical and mechanical exfoliation processes of natural graphite are used to create nano- and

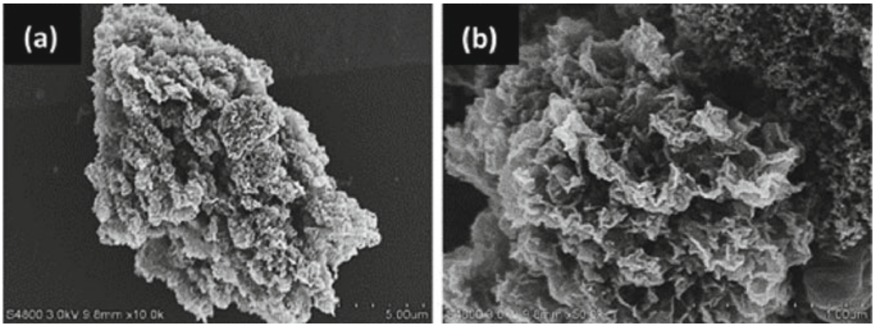

Fig. 7 FESEM images **a** FG **b** enlarged image of FG. Adapted with permission [38], Copyright (2017), Elsevier

microscale graphene sheets that can be employed as building blocks in self-assembly [39]. 3D structures of graphene can be self-assembled through $\pi-\pi$ interactions with ecofriendly phenolic acids. The hydrogels derived from assembling graphene into 3D frameworks were approximately 20 mm in height and 15 mm in diameter. After water removal through freeze–drying, the ultralight aerogels revealed consistently interconnected micrometer pores. This 3D graphene material has a variety of uses due to its unique mix of superhydrophobicity, high porosity, outstanding electrical conductivity, and exceptional mechanical properties [40]. *L*-cysteine also can be utilized as a template and reducing agent in the self-assembly of 3D graphene materials [41]. Graphene aerogel has a hierarchical pore structure with pore sizes ranging from a few hundred nanometers to micrometers. Thin graphene nanosheets serve as the building blocks for pore walls, and their overlapping helps create 3D porous networks. Interestingly, 3D graphene generated through self-assembly exhibits exceptional mechanical strength and thermal stability despite its low density.

4 Current Progress in Water-Splitting Applications

The incorporation of 3D graphene with metal oxides, transition-metal dichalcogenides (TMDCs), and other semiconductor materials is certainly an efficient approach for increasing utilization effectiveness and photocatalytic hydrogen evolution reaction (HER) performance because it enhances 3D graphene's ability as a co-catalyst to absorb incident light and provide numerous channels for gas diffusion, ion transfer, and electron transport. Yoon et al. used the hydrothermal method to synthesize 3D graphene inverse opal (GIO) nanostructures with α-Fe_2O_3. GIO was directly grown on a glass surface under low-temperature conditions, yielding 3D conducting networks for electron movement and photon-trapping effects. The activity of α-Fe_2O_3/GIO was 1.4 times higher than that of bare α-Fe_2O_3, indicating that the close proximity of the conducting electrode to the active components in the α-Fe_2O_3/GIO composite materials reduced electron–hole recombination and promoted quick electron transport [42].

Recently, Men et al. prepared free-standing ZnO/3D GF to study its photocatalytic performance in the energy field. ZnO nanorods acted as the active material that can most effectively optimize dimensions and interfaces. Meanwhile, the 3D self-supporting and hierarchical porous graphene structure served as the conductive substrate that would allow the solution to travel through itself. The photocurrent performance of ZnO/rGO foam was higher than that of rGO itself due to the simultaneous enhancement in light harvesting and charge transfer of ZnO/rGO foam [13]. Lu et al. fabricated TiO_2 nanoparticles on 3D graphene by using a hot electron mechanism. The H_2 generation efficiencies of TiO_2/3DG were 4.46 and 17.72 times greater than those of pure 3DG and TiO_2, respectively, due to the high synergetic effects between TiO_2 and 3DG [43].

3D graphene also can be incorporated with dual photoactive nanomaterials to further improve its photocatalytic HER performance. For example, Han et al. synthesized 3D-like ternary TiO_2/MoS_2/graphene aerogel via the hydrothermal reaction to enhance photocatalytic activities. The photocurrent activity of the TiO_2/MoS_2/graphene aerogel was 6 times higher than that of the pure TiO_2, implying that the good synergetic effect between the three composite materials and 3D graphene aerogel/MoS_2 nanosheets played a key role in enhancing active adsorption sites and photocatalytic reaction centers [44]. Shah et al. reported that the photocurrent density of 3D graphene on Ni foam incorporated with ZnO through the combination of CVD and the hydrothermal method was approximately 8.06 higher than that of the photocatalyst without graphene on Ni foam. This significant increase was due to the important role of 3D graphene as a co-catalyst for electron and hole transport in ZnO [45]. Various types of 3D graphene materials synthesized through different methods with their corresponding photocatalytic activities in PEC water splitting are summarized in Table 1.

Numerous studies have reported that pure metal oxide photocatalysts have poor PEC performances due to their rapid photogenerated electron–hole pair recombination. Loading graphene as a co-catalyst is an efficient approach for reducing the recombination of electron–hole pairs, which corresponds to the increased efficiency of PEC water splitting. The current trend in designing novel materials for photocatalysis is the incorporation of 3D graphene with materials, such as metal oxides and TMDCs and other semiconductor materials. Catalysts on 3D self-supported photoelectrodes have improved diffusion kinetics and a larger contact area with the electrolyte, resulting in their significantly superior performance compared with their planar counterparts and conventional 2D photoelectrodes. The combination of TMDCs with graphene enhances the features of the materials, such as stability, charge separation, and transport capabilities, which can improve the total photocatalytic PEC hydrogen generation. Additionally, the performance of the photocatalytic process can be improved by simplifying charge transfer between materials by using 3D porous graphene structures. Although several synthetic techniques can be applied, the physicochemical characteristics of the produced graphene materials differ greatly.

Table 1 Fabrication methods and photocatalytic activities of several 3D graphene-based composite materials

Type of 3D graphene	Composite materials	Fabrication method	Photocurrent density (mA/cm^2)	Hydrogen production rate (mmol/g/h)	References
GIO	α-Fe_2O_3	Hydrothermal	1.62 at 1.5 V versus RHE	–	[42]
Graphene aerogel	TiO_2/MoS_2	Hydrothermal	37.45 at + 0.6 V	–	[44]
3D graphene	Silicon	CVD	37.6 at + 0.16 V	–	[46]
3D graphene	ZnO	CVD and Hydrothermal	108.2 at 0–1.0 V versus Ag/AgCl	–	[45]
GF	ZnO	Hydrothermal	0.041 at 0 V versus Ag/AgCl	–	[13]
GF	TiO_2	Hot/free electron mechanism	–	1.205	[43]
Graphene aerogel	N-doped	Hydrothermal	–	0.013	[47]
Graphene aerogel	Cu	Gas exfoliation	–	4.87	[48]

The highest photocurrent density and hydrogen production rate of 3D graphene for pyramid-like graphene/p-Si Schottky junctions were approximately 37.6 mA/cm^2 and 11.60 mmol/g/h, respectively, at + 0.16 V. [45] Consequently, graphene-based 3D materials not only act as supports to increase the photoelectrocatalytic performance of composite materials, but also build a small skeleton framework that results in an increased surface area and hence a superior photoelectrocatalytic performance.

5 Summary

Graphene is an attractive material for photocatalysis applications. It is particularly attractive as a co-catalyst and transfer agent that can assist in reducing the effect of the wide band gaps of semiconducting materials and the recombination of electron–hole pairs in photocatalysts owing to its excellent intrinsic properties. Interconnected 3D graphene structures are a promising solution to the restacking or aggregation issues of 2D graphene in photocatalysis applications while still preserving the outstanding properties of 2D graphene. 3D graphene can exist in the form of foams, sponges, aerogels, or hydrogels. The current research trend in designing novel materials for photocatalysis is the incorporation of 3D graphene with metal oxides, TMDCs, and other semiconductor materials. The use of 3D graphene-based materials as a co-catalyst and catalyst support to enhance the performance of PEC water splitting can be ascribed to their large surface areas, porosity, effective transport, and improved reaction site accessibility. Many efforts have been made to synthesize 3D graphene-based photocatalysts for PEC water-splitting applications, and the number of researchers involved in this area has considerably increased. The properties, synthesis methods, and current progress in the water-splitting applications of 3D graphene-based photocatalysts reported to date were discussed thoroughly in this chapter. Nevertheless, the performance and stability of the photocatalyst still need further exploration. Thus, the design of 3D graphene-based photocatalysts with high photoelectrochemical efficiency and good stability is needed to realize the use of 3D graphene in practical PEC water-splitting applications.

Acknowledgments The authors would like to acknowledge the financial support given for this book chapter by FRGS/1/2019/STG07/UKM/02/2 from the Ministry of Higher Education, Malaysia.

References

1. Kuang, P., Sayed, M., Fan, J., Cheng, B., Yu, J.: 3D graphene-based H2-production photocatalyst and electrocatalyst. Adv. Energy Mater. **10**, 1–53 (2020)
2. Sun, Z., Fang, S., Hu, Y.H.: 3D graphene materials: from understanding to design and synthesis control. Chem. Rev. **120**, 10336–10453 (2020)
3. Cui, H., Guo, Y., Zhou, Z.: Three-dimensional graphene-based macrostructures for electrocatalysis. Small **17**, 1–19 (2021)
4. Mohd, N.R.A., Mohamad, R., Rosman, N.N., Wong, W.Y., Arifin, K., Jeffery, L.: Current progress on 3D graphene-based photocatalysts: from synthesis to photocatalytic hydrogen production. Int. J. Hydrogen Energy **46**, 9324–9340 (2021)
5. Novoselov, K.S., Geim, A.K., Morozov, S.V., Jiang, D., Zhang, Y., Dubonos, S.V., Grigorieva, I.V., Firsov, A.A.: Electric field effect in atomically thin carbon films. Nat. Mater **6**, 666–669 (2004)
6. Bramhaiah, K., Bhattacharyya, S.: Challenges and future prospects of graphene-based hybrids for solar fuel generation: moving towards next generation photocatalysts. Mater Adv **3**, 142–172 (2022)
7. Min, B.H., Kim, D.W., Kim, K.H., Choi, H.O., Jang, S.W., Jung, H.-T.: Bulk scale growth of CVD graphene on Ni nanowire foams for a highly dense and elastic 3D conducting electrode. Carbon N Y **80**, 446–452 (2014)
8. Kamedulski, P., Skorupska, M., Binkowski, P., Arendarska, W., Ilnicka, A., Lukaszewicz, J.P.: High surface area micro-mesoporous graphene for electrochemical applications. Sci. Rep. **11**, 1–12 (2021)
9. Xu, X., Guan, C., Xu, L., Tan, Y.H., Zhang, D., Wang, Y., Zhang, H., Blackwood, D.J., Wang, J., Li, M., Ding, J.: Three dimensionally free-formable graphene foam with designed structures for energy and environmental applications. ACS Nano **14**, 937–947 (2020)
10. Tsai, H.C., Vedhanarayanan, B., Lin, T.W.: Freestanding and hierarchically structured Au-dendrites/3D-graphene scaffold supports highly active and stable Ni3S2 electrocatalyst toward overall water splitting. ACS Appl. Energy Mater **2**, 3708–3716 (2019)
11. Cheng, Y., Zhou, S., Hu, P., Zhao, G., Li, Y., Zhang, X., Han, W.: Enhanced mechanical, thermal, and electric properties of graphene aerogels via supercritical ethanol drying and high-Temperature thermal reduction. Sci. Rep. **7**, 1–11 (2017)

12. Cui, C., Li, S., Qiu, Y., Hu, H., Li, X., Li, C., Gao, J., Tang, W.: Fast assembly of Ag3PO4 nanoparticles within three-dimensional graphene aerogels for efficient photocatalytic oxygen evolution from water splitting under visible light. Appl. Catal B Environ. **200**, 666–672 (2017)
13. Men, X., Chen, H., Chang, K., Fang, X., Wu, C., Qin, W., Yin, S.: Three-dimensional free-standing ZnO/graphene composite foam for photocurrent generation and photocatalytic activity. Appl. Catal B Environ. **187**, 367–374 (2016)
14. Banciu, C.A., Nastase, F., Istrate, A.I., Veca, L.M.: 3D Graphene foam by chemical vapor deposition: synthesis, properties, and energy-related applications. Molecules, 27 (2022)
15. Shen, Z., Ye, H., Zhou, C., Kröger, M., Li, Y.: Size of graphene sheets determines the structural and mechanical properties of 3D graphene foams. Nanotechnology **29**, 1–13 (2018)
16. Xia, D., Yi, K., Zheng, B., Li, M., Qi, G., Cai, Z., Cao, M., Liu, D., Peng, L., Wei, D., Wang, Z., Yang, L., Wei, D.: Solvent-free process to produce three dimensional graphene network with high electrochemical stability. J. Phys. Chem. C **121**, 3062–3069 (2017)
17. Drieschner, S., Weber, M., Wohlketzetter, J., Vieten, J., Makrygiannis, E., Blaschke, B.M., Morandi, V., Colombo, L., Bonaccorso, F., Garrido, J.A.: High surface area graphene foams by chemical vapor deposition. 2D Mater **3**, 1–10 (2016)
18. Sha, J., Gao, C., Lee, S.K., Li, Y., Zhao, N., Tour, J.M.: Preparation of three-dimensional graphene foams using powder metallurgy templates. ACS Nano **10**, 1411–1416 (2016)
19. O'Neill, C., Johnson, M.B., DeArmond, D., Zhang, L., Alvarez, N., Shanov, V.N., White, M.A.: Thermal conductivity of 3-dimensional graphene papers. Carbon Trends **4**, 100041 (2021)
20. Loeblein, M., Tsang, S.H., Pawlik, M., Phua, E.J.R., Yong, H., Zhang, X.W., Gan, C.L., Teo, E.H.T.: High-density 3D-boron nitride and 3D-graphene for high-performance nano-thermal interface material. ACS Nano **11**, 2033–2044 (2017)
21. Pettes, M.T., Ji, H., Ruoff, R.S., Shi, L.: Thermal transport in three-dimensional foam architectures of few-layer graphene and ultrathin graphite. Nano Lett. **12**, 2959–2964 (2012)
22. Li, X.L., Guo, J.G., Zhou, L.J.: The Young's modulus of triangle-like three-dimensional graphene under uniaxial tension: Finite element method and theoretical model. J. Phys. Chem. Solids **161**, 110473 (2022)
23. Xu, Z., Jiang, J., Zhang, Q., Chen, G., Zhou, L., Li, L.: 3D graphene aerogel composite of 1D–2D Nb2O5-g-C3N4 heterojunction with excellent adsorption and visible-light photocatalytic performance. J. Colloid Interface Sci. **563**, 131–138 (2020)
24. Bayram, O.: A study on 3D graphene synthesized directly on Glass/FTO substrates: Its Raman mapping and optical properties. Ceram Int **45**, 16829–16835 (2019)
25. Zeng, M., Wang, W.L., Bai, X.D.: Preparing three-dimensional graphene architectures: review of recent developments. Chinese Phys. B 22 (2013)
26. Thiyagarajan, P.: A review on three-dimensional graphene: synthesis, electronic and biotechnology applications-the unknown riddles. IET Nanobiotechnol. **15**, 348–357 (2021)
27. Baig, N., Saleh, T.A.: Electrodes modified with 3D graphene composites: a review on methods for preparation, properties and sensing applications. Microchim Acta 185 (2018)
28. Hiew, B.Y.Z., Lee, L.Y., Lee, X.J., Thangalazhy-Gopakumar, S., Gan, S., Lim, S.S., Pan, G.T., Yang, T.C.K., Chiu, W.S., Khiew, P.S.: Review on synthesis of 3D graphene-based configurations and their adsorption performance for hazardous water pollutants. Process Saf. Environ. Prot. **116**, 262–286 (2018)
29. Yang, G., Park, S.J.: Conventional and microwave hydrothermal synthesis and application of functional materials: a review. Materials (Basel) **12**, 1177 (2019)
30. Zhou, X., Cui, S.C., Liu, J.G.: Three-dimensional graphene oxide cross-linked by benzidine as an efficient metal-free photocatalyst for hydrogen evolution. RSC Adv. **10**, 14725–14732 (2020)
31. Ding, Y., Zhou, Y., Nie, W., Chen, P.: MoS2 -GO nanocomposites synthesized via a hydrothermal hydrogel method for solar light photocatalytic degradation of methylene blue. Appl. Surf. Sci. **357**, 1606–1612 (2015)
32. Cao, X., Guo, W., Li, A., Du, J., Du, L., Zhang, G., Liu, H.: Facile synthesis of reduced graphene oxide/CdS nanowire composite aerogel with enhanced visible-light photocatalytic activity. J. Nanoparticle Res. **22**, 81 (2020)

33. Han, W., Ren, L., Gong, L., Qi, X., Liu, Y., Yang, L., Wei, X., Zhong, J.: Self-assembled three-dimensional graphene-based aerogel with embedded multifarious functional nanoparticles and its excellent photoelectrochemical activities. ACS Sustain. Chem. Eng. **2**, 741–748 (2014)
34. Saeed, M., Alshammari, Y., Majeed, S.A., Al-Nasrallah, E.: Chemical vapour deposition of graphene-synthesis, characterisation, and applications: a review. Molecules **25**, 3856 (2020)
35. Bhaviripudi, S., Jia, X., Dresselhaus, M.S., Kong, J.: Role of kinetic factors in chemical vapor deposition synthesis of uniform large area graphene using copper catalyst. Nano Lett. **10**, 4128–4133 (2010)
36. Chen, Z., Ren, W., Gao, L., Liu, B., Pei, S., Cheng, H.M.: Three-dimensional flexible and conductive interconnected graphene networks grown by chemical vapour deposition. Nat. Mater **10**, 424–428 (2011)
37. Cai, R., Wu, J.G., Sun, L., Liu, Y.J., Fang, T., Zhu, S., Li, S.Y., Wang, Y., Guo, L.F., Zhao, C.E., Wei, A.: 3D graphene/ZnO composite with enhanced photocatalytic activity. Mater Des. **90**, 839–844 (2016)
38. Chang, C.J., Wei, Y.H., Huang, K.P.: Photocatalytic hydrogen production by flower-like graphene supported ZnS composite photocatalysts. Int. J. Hydrogen Energy **42**, 23578–23586 (2017)
39. Nine, M.J., Tung, T.T., Losic, D.: Self-assembly of graphene derivatives: methods, structures, and applications. Compr. Supramol. Chem. II **9**, 47–74 (2017)
40. Wang, J., Shi, Z., Fan, J., Ge, Y., Yin, J., Hu, G.: Self-assembly of graphene into three-dimensional structures promoted by natural phenolic acids. J. Mater. Chem. **22**, 22459–22466 (2012)
41. Zhang, X., Liu, D., Yang, L., Zhou, L., You, T.: Self-assembled three-dimensional graphene-based materials for dye adsorption and catalysis. J. Mater. Chem. A **3**, 10031–10037 (2015)
42. Yoon, K.Y., Lee, J.S., Kim, K., Bak, C.H., Kim, S.I., Kim, J.B., Jang, J.H.: Hematite-based photoelectrochemical water splitting supported by inverse opal structures of graphene. ACS Appl. Mater. Interfaces **6**, 22634–22639 (2014)
43. Lu, Y., Ma, B., Yang, Y., Huang, E., Ge, Z., Zhang, T., Zhang, S., Li, L., Guan, N., Ma, Y., Chen, Y.: High activity of hot electrons from bulk 3D graphene materials for efficient photocatalytic hydrogen production. Nano Res. **10**, 1662–1672 (2017)
44. Han, W., Zang, C., Huang, Z., Zhang, H., Ren, L., Qi, X., Zhong, J.: Enhanced photocatalytic activities of three-dimensional graphene-based aerogel embedding TiO2 nanoparticles and loading MoS2 nanosheets as Co-catalyst. Int. J. Hydrogen Energy **39**, 19502–19512 (2014)
45. Mohd, N.R.A., Yunus, R.M., Rosman, N.N., Wong, W.Y., Arifin, K., Minggu, L.J.: Synthesis of ZnO on 3D Graphene/Nickel Foam for Photoelectrochemical Water Splitting. Malaysian J. Anal. Sci. **26**, 546–553 (2022)
46. Ku, C.K., Wu, P.H., Chung, C.C., Chen, C.C., Tsai, K.J., Chen, H.M., Chang, Y.C., Chuang, C.H., Wei, C.Y., Wen, C.Y., Lin, T.Y., Chen, H.L., Wang, Y.S., Lee, Z.Y., Chang, J.R., Luo, C.W., Wang, D.Y., Hwang, B.J., Chen, C.W.: Creation of 3D textured Graphene/Si Schottky junction photocathode for enhanced photo-electrochemical efficiency and stability. Adv. Energy Mater **9**, 1–9 (2019)
47. Qiao, H., Huang, Z., Liu, S., Tao, Y., Zhou, H., Li, M., Qi, X.: Novel mixed-dimensional photocatalysts based on 3D graphene aerogel embedded with TiO2/MoS2 hybrid. J. Phys. Chem. C **123**, 10949–10955 (2019)
48. Wang, Y., Song, T., Zhang, P., Huang, T., Wang, T., Wang, T., Zeng, H.: Gas-exfoliation assisted fabrication of porous graphene nanosheets derived from plumeria rubra for highly efficient photocatalytic hydrogen evolution. ACS Sustain. Chem. Eng. **6**, 11536–11546 (2018)

3D Graphene for Flexible Electronics

Arpana Agrawal

Abstract Three-dimensional graphene structures are nowadays grabbing enormous research interest due to their porous structures exhibiting high conductivity, high specific surface area, and low density, hence making them excellent materials for flexible electronic applications including flexible wearable sensors, flexible electrodes for metal–ion batteries, supercapacitors, human body compatible e-skins, etc. Accordingly, the present chapter provides an overview of various three-dimensional graphene architectures (foams, hydrogels, aerogels, sponges, and films). A brief discussion of the various preparation methods has also been presented. A few examples of the applications of three-dimensional graphene structures for flexible electronics, particularly for flexible sensor-based applications (strain/pressure sensors, electronic skins, etc.) and flexible energy storage device applications (flexible supercapacitors, metal-based batteries such as lithium–ion, lithium–sulfur, etc.) have been highlighted critically. Finally, the concluding remarks and perspectives are presented.

Keywords 3D graphene structures · Porous structures · Flexible electronics · Supercapacitors · Sensors

1 Introduction

2D graphene is an exceptional material because of its several fascinating properties and is a planar sheet (one-atom-thick) where carbon atoms with sp^2 hybridization are bounded with each other in a honeycomb lattice. Apart from 2D graphene layers, 3D graphene structures are nowadays attracting immense research interest. Such structures can be termed as sponges/foams/aerogels and exhibit excellent porosity, encouraging conductivity, high specific surface area and hence are considered as promising materials for various electronic device applications. Owing to the highly

---

A. Agrawal (✉)
Department of Physics, Shri Neelkantheshwar Government Post-Graduate College,
Khandwa 450001, India
e-mail: agrawal.arpana01@gmail.com

© The Author(s), under exclusive license to Springer Nature Switzerland AG 2023

R. K. Gupta (ed.), *3D Graphene*, Carbon Nanostructures,
https://doi.org/10.1007/978-3-031-36249-1_21

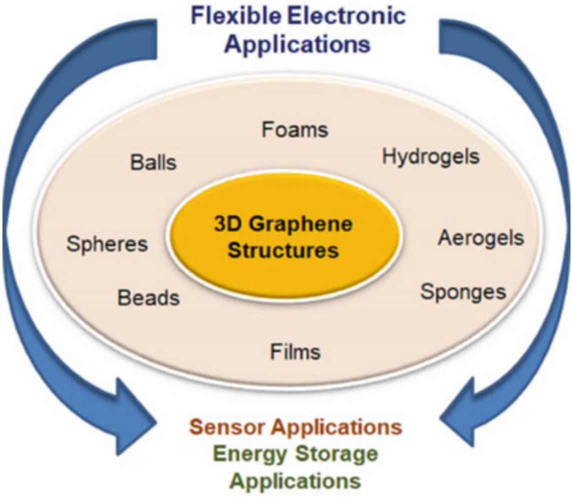

Fig. 1 Various 3D graphene structures along with their flexible electronic applications

porous structure of 3D graphene structures with excellent conductivity and encouraging compatibility with various polymeric materials possessing high elasticity, they are one of the potential candidates, particularly for flexible electronics including flexible electrodes, conductors, metal–ion batteries, metal–air batteries, wearable and flexible sensors, etc. Figure 1 pictorially shows the various 3D graphene structures along with their flexible electronic applications.

So far, various 3D graphene architectures have been reported including graphene spheres, graphene networks (foams, hydrogels, aerogels, sponges) and films, etc., and can be fabricated via a number of techniques such as self-assembly method, template-assisted method, electro-spinning/spraying, chemical vapor deposition (CVD), etc. In the spray assembly method, 3D graphene structures were prepared via gelation of graphene oxide dispersion which then undergo a reduction process to form reduced graphene oxide, whereas, in the template-assisted method, 3D templates of polystyrene or SiO_2 were utilized which can be easily removed from the 3D graphene structure. Electro-spinning/spraying facilitates the formation of 3D graphene structures in the form of fibers, spheres, or beads with diameters ranging from a few micrometers to nanometers and CVD allows straightforward deposition of 3D graphene architectures. Chen et al. [1] reported the growth of highly flexible and conducting 3D graphene networks employing CVD approach. Shehzad et al. [2] presented a critical review of various 3D macrostructures of 2D nanomaterials. An extensive review of the CVD growth of 3D graphene foam was also presented by Banciu et al. [3], along with their fascinating properties and various energy applications. Another review in this area deals with the preparation and morphological studies of various 3D graphene composites along with their numerous applications [4]. Li and Shi [5] also described various 3D graphene structures. Wu et al. [6] also reported a highly compressive 3D graphene sponge possessing near-zero Poisson's ratio. Hu et al. [7] discussed the growth of highly compressible and lightweight graphene aerogels. Li et al. [8] discussed the preparation method of a compressible 3D graphene sponge. Han et al. [9] reported a method to strengthen 3D graphene sponges using an ammonia solution.

It is worth mentioning here that in contrast to 2D graphene materials which exhibit outstanding mechanical strength, 3D graphene structures are usually reported to possess poor mechanical properties and hence are unfit for flexible device applications in as it is formed. The performance of flexible electronic devices fabricated from these structures in pristine form would get deteriorated after various deformable situations. However, to utilize 3D graphene structures for flexible electronics, they are combined with several polymeric materials. The very first report on flexible conductors based on template-assisted chemical vapor-deposited 3D graphene foam is with polydimethylsiloxane (PDMS). Wang et al. [10] have also reported the preparation of a 3D graphene-polymer-based composite. The preparation of 3D graphene/polymer composite not only provides flexibility and stretchability but also helps in improving their conductivity, and hence there is a utility for flexible electronics. Another fascinating property of 3D graphene structures is their ability to prepare composites via doping with other materials which adds further dimensions to the utility.

Accordingly, the present chapter provides an overview of various 3D graphene architectures (foams, hydrogels, aerogels, sponges, films) along with a few examples of their applications for flexible electronics, particularly for flexible sensor-based applications (strain/pressure sensors, electronic skins, etc.) and flexible energy storage device applications (flexible supercapacitors, metal–ion batteries such as lithium–ion battery, lithium–sulfur battery, sodium–ion battery, etc.).

2 3D Graphene for Flexible Electronic Applications

Several researchers have discussed the applications of 3D graphene structures including foams, sponges, aerogels, nanowalls, etc. for flexible electronics, particularly for sensor applications (flexible pressure/strain sensors/electronic skin) of energy storage applications (flexible capacitor/supercapacitors/fuel cells/metal–ion batteries), etc. This section will focus on a few applications of 3D graphene-based structures, particularly for sensor applications and energy storage applications.

2.1 3D Graphene for Sensor Applications

3D graphene-based structures have extensively been employed for sensor applications. Samad et al. [11] reported sensor applications of graphene foam composite having to regulate the sensitivity. 3D interconnecting structures of reduced graphene/polyimide nanocomposite-based flexible strain sensor applications with excellent elasticity, flexibility, and mechanical strength were reported by Qin et al. [12]. An et al. [13] fabricated a flexible wearable sensor utilizing graphene aerogel which was prepared via micro-extrusion printing technology using an ink obtained by dissolving graphene oxide in water. The prepared ink was loaded in a syringe and then patterned on the PET substrate which then undergoes a vacuum freeze-drying process to obtain GO aerogel followed by chemical reduction to produce reduced graphene oxide aerogel. Finally, to prepare a graphene aerogel-based wearable sensor, the aerogel allows electrodes to be glued to it and is packaged with PDMS. It should be noted here that the morphology of graphene aerogels strongly depends on the concentration of the graphene oxide inks and the fabricated sensor facilitates 3D multi-recognition and multi-deformation responses with excellent performances.

Fabrication of wearable and flexible pressure and strain sensors utilizing graphene porous structures is also reported by Pang et al. [14]. Highly compressible composite of graphene/thermoplastic polyurethane foam possessing high conductivity is also reported to be useful for piezoresistive sensing applications [15]. Facilely grown 3D graphene foam composite was employed to fabricate strain sensors [16]. Flexible sensors with self-healing properties were also reported to be fabricated using composite material composed of 3D graphene and polyborosiloxane (PBS) polymer where PBS acts as the self-healing material [17]. This sensor has an excellent capacity of sensing pressure and flexion angle and can automatically heal for 6–8 cycles. However, the fabricated sensor is unsuitable under harsh environmental conditions because of the poor mechanical strength of PBS polymer. Li et al. [18] have also reported the applications of reduced graphene oxide/polyurethane composite for healable flexible electronics.

An efficient lightweight, wearable, sensitive, and squeezable piezoresistive sensor was fabricated by Sengupta et al. [19], employing graphene-PDMS composite foam. To prepare this sensor, initially, the PDMS foam was prepared as a base material then the graphene nanoflakes were loaded in it. For this, a conductive graphene suspension was prepared by suspending graphene nanoflakes in N, N-dimethylformamide (DMF) solution which undergoes sonication followed by dipping of porous PDMS sponges in it for 1 h. This leads to the formation of graphene-coated PDMS sponges which then dried in oven at 60 °C for 1 h. The same steps continue for six cycles to prepare porous graphene-PDMS composite foam. Figure 2a shows the overall fabrication process of graphene-PDMS composite foam. Finally, to fabricate the sensor with all the electrical connections, conductive silver epoxy was coated on the sides of the prepared composite foam (Fig. 2b). The squeezability and lightweight of the developed sensor were demonstrated in Fig. 2c and d, respectively. Figure 2e and f shows the scanning electron microscopy images of the PDMS foam before loading and after loading of graphene nanoflakes, respectively, which clearly shows the penetration of graphene nanoflakes within the PDMS foam.

In order to examine the applicability of the developed graphene-PDMS-based sensor for flexible and wearable device applications, they have examined the developed sensor under several strain-loading circumstances. In their experimental setup as shown in Fig. 3a, the squeezable graphene-PDMS foam-based sensor was compressed using pistons doubling as electrodes which are connected to a Wheatstone bridge and hence the data is acquainted. The response of the sensor was obtained at different compressive stain loadings varying from 10 to 50% and the change in

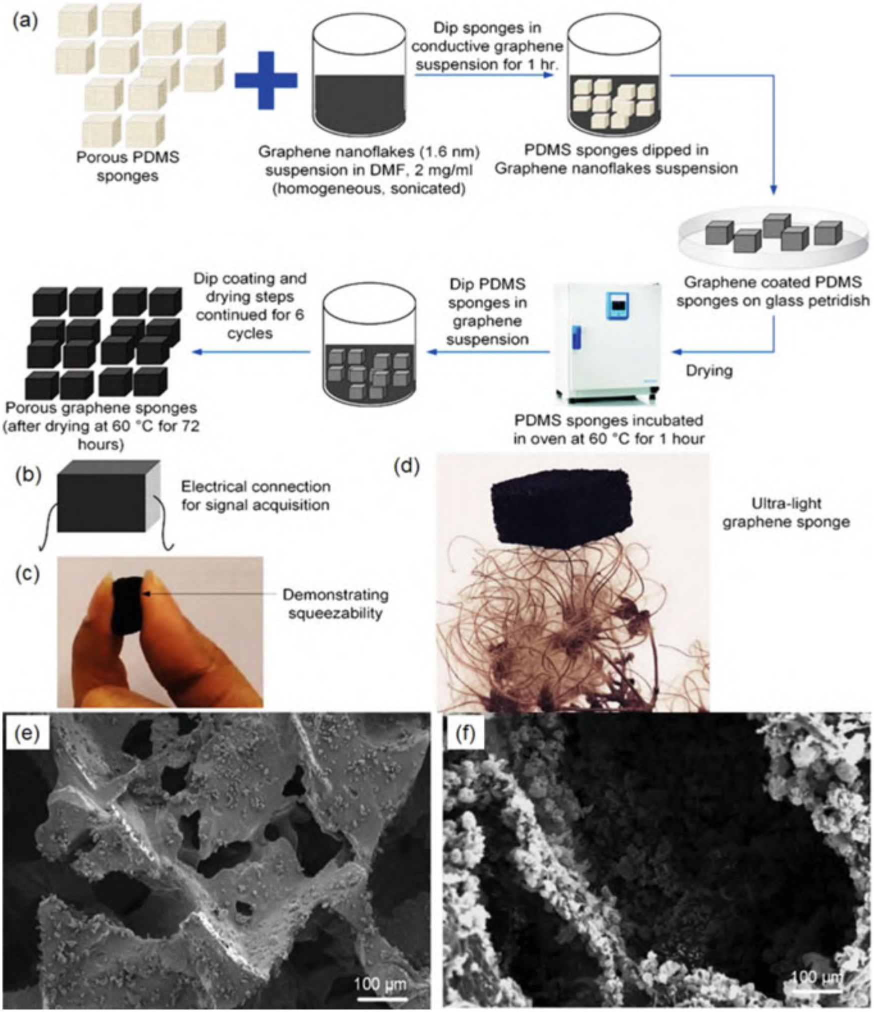

Fig. 2 **a** Schematic illustration of the overall fabrication process of graphene-PDMS composite foam. **b** Electrical connections to fabricate the sensor for signal acquisition. **c**, **d** Demonstration of squeezability (**c**) and lightweight (**d**) of the developed sensor. **e**, **f** SEM images of the PDMS foam before loading (**e**) and after loading (**f**) of graphene nanoflakes. Adapted with permission [19]. Copyright (2019) Copyright The Authors, some rights reserved; exclusive licensee ACS Publications. Distributed under a Creative Commons Non-Commercial No Derivative Works (CC-BY-NC-ND) Attribution License

the normalized resistance as a function of time is obtained as represented in Fig. 3b. They have further examined the applications of the developed sensor for real-time human foot pressure monitoring where the developed sensor was attached to the shoe sole at intense and low-pressure points of the foot mainly the toe ball, heels, and foot arch, respectively, as illustrated in Fig. 3c. The real-time response of the sensor while walking is then recorded as shown in Fig. 3d. The response of the sensor during the movements of the index finger and wrist was also examined (Fig. 3e, f), which clearly shows the feasibility of the developed sensor for flexible wearable health monitoring devices.

The same group has also designed piezoelectric 3D graphene-PDMS foam-based pressure sensors for smart gloves applications for Internet of things-enabled wearable pressure monitoring devices [20]. The photographs of the developed pressure sensor attached to a nitrile glove are represented in Fig. 4a where four identical 3D graphene-PDMS foam-based pressure sensors were attached to the thumb, index finger, middle finger, and ring finger. To cover and protect the attached sensors from foreign elements, another nitrile layer was employed (Fig. 4a). Finally, these gloves were used to hold a paper cup and the response in terms of resistance change was recorded. However, to convert this resistance change into voltage signals, a voltage divider is also connected to the sensor. Figure 4b depicts the sensor response obtained while holding a paper cup in terms of the voltage signal, suggesting its utility for wearable smart gloves as pressure-sensing devices.

Yang et al. [21] reported the fabrication of extremely flexible, stretchable, skin-compatible, and highly sensitive electronic nose utilizing 3D graphene microstructured nanowalls and PDMS substrate. Graphene nanowalls were grown onto a silicon substrate employing a plasma-enhanced CVD method using methane and hydrogen gases. Finally, the grown nanowall structures were loaded with PDMS polymer followed by solidification in a vacuum oven. Thereafter, the graphene nanowalls were transferred to PDMS substrate via a peeling off approach. Finally, to prepare electrodes for graphene nanowalls-PDMS-based e-skin, silver paste was polished on the edges of the grown structure. They have also examined the applications of the developed e-skin in the bending motion of joints of the human body including knee joints, elbow, fingers, eye movements, and voice sensations. It was found that the developed graphene nanowalls-PDMS-based e-skin shows excellent sensitivity toward stretching and bending motions with a gauge factor ~65.9 under 100% stretching conditions.

2.2 3D Graphene for Energy Storage Applications

In addition to sensor applications, 3D graphene structures are widely employed for energy storage applications. Several energy storage devices including supercapacitors, fuel cells, or metal–ion batteries particularly lithium–ion batteries have been reported to be fabricated from 3D graphene structures. Electrodes prepared from

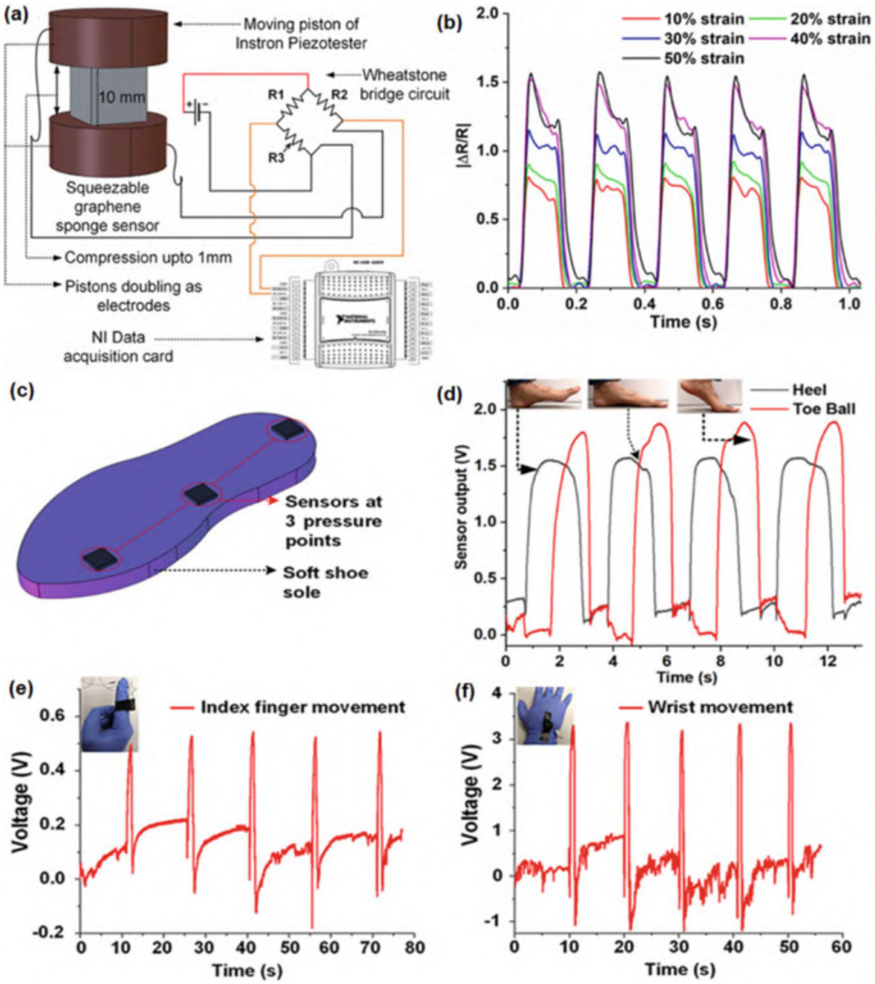

Fig. 3 **a** Schematic depiction of the experimental setup for performing the piezoresistivity measurements. **b** The response of the sensor in terms of change in the normalized resistance as a function of time at different compressive stain loadings varying from 10 to 50%. **c** Attachment of the developed sensor on the shoe sole at intense and low-pressure points of the foot, mainly toe ball, heels, and foot arch. **d** The real-time response of the sensor while walking for the demonstration of real-time human foot pressure monitoring. Response of the developed sensor in terms of voltage signals during the movements of the index finger (**e**) and wrist (**f**). Adapted with permission [19]. Copyright (2019) Copyright The Authors, some rights reserved; exclusive licensee ACS Publications. Distributed under a Creative Commons Non-Commercial No Derivative Works (CC-BY-NC-ND) Attribution License

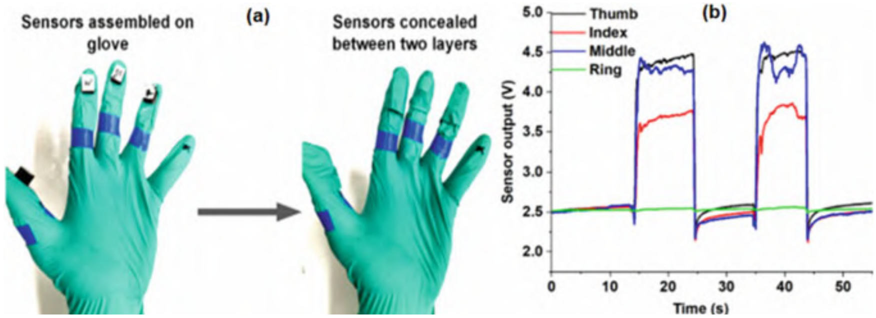

Fig. 4 **a** The photographs of four identical pressure sensors attached on a nitrile glove at fingertip regions with another nitrile layer to shield the attached sensors from foreign elements. **b** Sensor response obtained while holding a paper cup in terms of voltage signal. Adapted with permission [20]. Copyright (2022) Copyright The Authors, some rights reserved; exclusive licensee IOP Publishing. Distributed under a Creative Commons Attribution License 4.0

3D graphene were reported to be employed for fabricating high-performance pseudocapacitors and supercapacitors. Wang et al. [22] utilized electrodes made up of 3D graphene nickel oxide nanoflakes for pseudocapacitors while Dong et al. [23] employed electrodes of 3D graphene cobalt oxide for supercapacitors. Xu et al. [24] have reported the fabrication of highly flexible solid-state supercapacitors. Herein, the electrolyte was a mixture of polyvinyl alcohol (PVA) and sulfuric acid (H_2SO_4) and the electrode was made up of graphene hydrogel film having a thickness of 120 μm. The fabricated supercapacitor exhibits excellent performance with gravimetric capacitance ~186 Fg^{-1} at 1 Ag^{-1}. Flexible supercapacitors were also fabricated by Zheng et al. [25], employing hybrid aerogels composed of cellulose nanofibril, reduced graphene oxide, and carbon nanotubes. Highly flexible and efficient solid-state supercapacitors are also reported to be fabricated from nanoporous graphene films [26]. Fabrication of high-rate capability electrodes for supercapacitors made up of a composite material comprising of nanostructured 3D graphene and Ni_3S_2 was also demonstrated [27]. He et al. [28] also demonstrated flexible and ultralight supercapacitor electrodes obtained from graphene/MnO_2 composite.

Apart from supercapacitors, 3D graphene structures-based composites serving as either anodes or cathodes are extremely utilized for metal-based batteries (lithium–ion batteries or lithium–sulfur batteries, sodium–ion batteries, etc.). Generally silicon (Si)-based anodes were employed for lithium–ion batteries. However, one of the major drawbacks of using Si anodes is their extended volume variations while lithiation. To circumvent this drawback, Phadatare et al. [29] have prepared a Si-nanographite aerogel anode where an aerogel fabrication approach was employed to grow Si nanoparticles on nanographite flakes. The prepared electrode exhibits excellent cycle stability with a specific capacity of 455 $mAhg^{-1}$ at 100 mAg^{-1}. Ji et al. [30] have also employed 3D conductive networks serving as an anode for fabricating lithium–ion batteries which comprises a Si/graphene composite grown on ultrathin graphene foam. A critical review was presented by Zhang et al. [31], demonstrating the potentiality of 3D nanoarchitecture as anode materials for various lithium or sodium storage applications. TiO_2/graphene composite was also reported to exhibit high photocatalysis activity with excellent stability and capability [32]. Herein, to prepare the composite, TiO_2 nanocrystals were hydrothermally grown on graphene aerogels (001). Wei et al. [33] have also examined the utility of Fe_3O_4 nanospheres encapsulated in 3D graphene foam for encouraging lithium storage applications.

Mo et al. [34] have reported the fabrication of a highly flexible, sensitive, and efficient lithium–ion battery with long cycling capacity for flexible electronic applications using a 3D porous structured nitrogen-incorporated graphene foam (NGF) encapsulated with germanium quantum dots (QD)/nitrogen-incorporated graphene (NG) yolk–shell nanostructure (Ge-QD@ NG/NGF). This porous structure facilitates the large volumetric expansion of germanium due to the presence of internal void spaces and easy access to electrolytes because of the open channels. The template-assisted technique was employed to prepare the desired 3D graphene composite structure. Figure 5a schematically illustrates the overall growth process of Ge-QD@NG/NGF/PDMS yolk–shell nanoarchitecture. Here, 3D interconnected porous Ni foam was used as the template to grow N-doped graphene via the CVD method which then undergoes a hydrothermal process in presence of $GeCl_4$ to prepare GeO_2-decorated N-doped graphene on Ni foam. The obtained product was then undergoing electroless Ni deposition to form N-doped graphene with GeO_2@Ni on Ni foam which again undergoes a CVD process followed by Ar/H_2 annealing. This process leads to the preparation of N-doped graphene with Ge quantum dot@Ni@N-doped graphene on Ni foam. Thereafter, Ni etching was done to prepare yolk–shell nanoarchitecture and finally coated with PDMS to prepare the end product mainly Ge-QD@NG/NGF/PDMS yolk–shell electrode.

The electrochemical performances of the fabricated lithium–ion battery employing Ge-QD@NG/NGF/PDMS were examined by obtaining the galvanostatic charging–discharging and cycling response of the battery. Figure 5b depicts the galvanostatic charging–discharging behavior of the battery containing Ge-QD@NG/NGF yolk–shell nanoarchitecture for several cycles at 1 C which clearly shows a discharge and charge capacity of 1,597 $mAhg^{-1}$ and 1,220 $mAhg^{-1}$, respectively, for the first cycle. Figure 5c shows the cycling response of Ge/Cu electrode, Ge/NGF/PDMS electrode, and prepared Ge-QD@NG/NGF/PDMS yolk–shell electrode for 1000 cycles at 1 C. In pristine Ge/Cu electrode, fast capacity fading was observed which is mainly attributed to the greater size of the Ge nanoparticles resulting in pitiable strain relaxation, while in the case of Ge/NGF/PDMS electrode, added space was available to load the electrode material resulting in the formation of the interconnected conductive network. However, in contrast to both these electrodes, encouraging cycle stability was observed in the prepared Ge-QD@NG/NGF/PDMS yolk–shell electrode. Figure 5d schematically represents the assembled electrochemical cell comprising of lithium foil, Ge-QD@NG/NGF/PDMS yolk–shell nanoarchitecture as electrodes, and the experimental setup for in situ Raman measurements. In situ Raman experiment was performed using laser light (operating wavelength = 532 nm) for the working electrochemical cell before and during the lithiation process and the obtained results were shown in Fig. 5e. It was found that the first-order Raman band

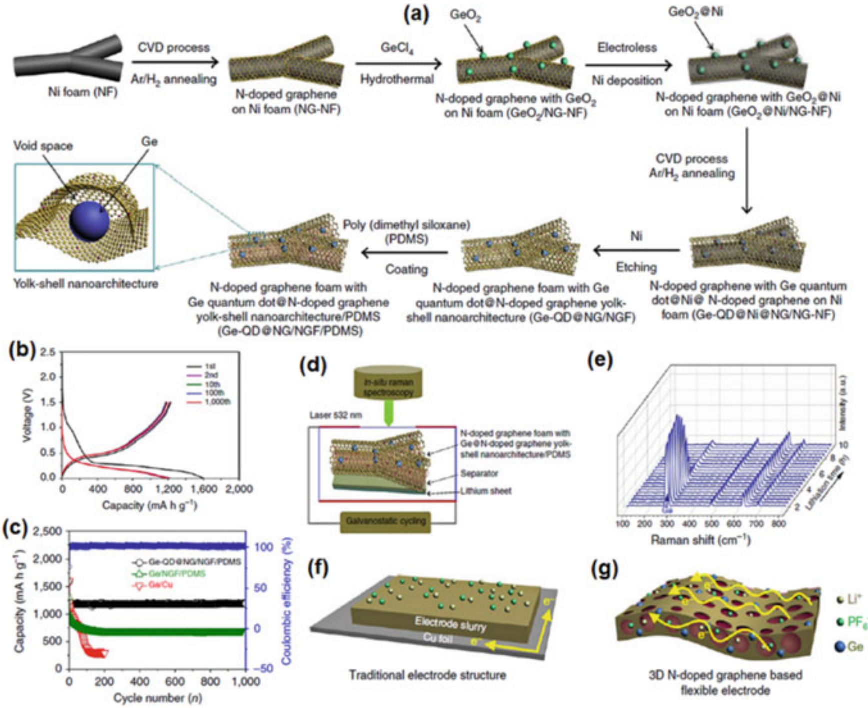

Fig. 5 **a** Pictorial demonstration of the overall growth process of Ge-QD@NG/NGF/PDMS yolk–shell-based nanoarchitecture. **b** Galvanostatic charging–discharging behavior of the fabricated battery containing Ge-QD@NG/NGF yolk–shell nanoarchitecture electrode for several cycles at 1 C. **c** Cycling response of Ge/Cu electrode, Ge/NGF/PDMS electrode and prepared Ge-QD@NG/NGF/PDMS yolk–shell electrode for 1000 cycles at 1 C. **d** Schematic representation of the assembled electrochemical cell comprising of lithium foil, Ge-QD@NG/NGF/PDMS yolk–shell nanoarchitecture as electrodes and separator along with the experimental setup for in situ Raman measurements. **e** In situ Raman spectra obtained using 532 nm laser light for the working electrochemical cell before and during lithiation process. Design of the traditional electrode (Ge/Cu) (**f**) and the flexible 3D N-doped graphene-based electrode (**g**). Adapted with permission [34]. Copyright (2017) Copyright The Authors, some rights reserved; exclusive licensee Nature Publishing. Distributed under a Creative Commons Attribution License 4.0 (CC BY)

appeared at 296 cm^{-1} for the fabricated battery before the start of lithiation along with a few other Raman peaks appearing due to the electrolyte or the packaging material. The difference between the design of the traditional electrode and the flexible 3D N-doped graphene-based electrode is also shown in Fig. 5f, g.

The same group has also reported the construction of lithium–ion batteries using Ge nanoparticles encapsulated in a 3D double-walled ultrathin graphite tube serving as a potential anode [35]. The superior electrochemical performance was observed with cycle stability up to 1000 cycles, a specific capacity of 1338 mAhg^{-1}, and a rate performance of 752 mAhg^{-1} at 40 C. It should be noted that other than PDMS, polyaniline (PANI) polymer was also reported to be a compatible polymer for 3D graphene structures. Zhang et al. [36] discussed the fabrication of lithium–ion batteries using electrodes comprising of SnO_2@PANI core–shell nanorod arrays grown on graphite foam. For this, initially, the SnO_2 nanorod arrays were grown on graphite foam which was then uniformly coated with a PANI layer to prepare SnO_2@PANI core–shell structure and hence the electrode. This prepared electrode shows enhanced electrochemical responses.

Cathode prepared from sulfur/3D network-structured graphene foam was also reported to be employed for the fabrication of lithium–sulfur batteries [37]. This cathode was synthesized by sulfur solution infiltration approach where sulfur was loaded on a 3D graphene structure. Herein, initially, the 3D network graphene structure was prepared via the CVD method employing template-assisted approach without using any binder. Ni foam was used as the sacrificial template and can be easily etched away after growth. The fabricated lithium–sulfur battery containing sulfur/3D network-structured graphene foam as cathode exhibits excellent electrochemical stability. Ji et al. [38] have reported the use of lithium iron phosphate-loaded 3D network of ultrathin graphite foam as a potential, economic, and compatible cathode material for fabricating lithium–ion batteries. This battery possesses high current density and a specific capacity of 1280 mAg^{-1} and 70 $mAhg^{-1}$, respectively. Lithium–sulfur batteries exhibiting excellent electrochemical properties were also fabricated using 3D Li_2S/graphene serving as a potential cathode [39]. Chang et al. [40] demonstrated the utility of 3D graphene-based N-incorporated carbon composites as efficient anode materials for sodium–ion batteries. Another report on the utility of composite electrodes made up of N-incorporated graphene on graphite foam serving as anode material for lithium–ion batteries was presented where an encouraging specific capacity of 1687 $mAhg^{-1}$ was observed [41]. 3D N-incorporated graphene foam was also reported to be synthesized by the green synthesis method and can be employed for electrochemical applications [42].

3D graphene structures are also employed for the purpose of detection devices mainly photodetectors. Li et al. [43] reported the utility of 3D graphene foam for fabricating photodetectors working from ultraviolet to microwave region. Highly sensitive photodetectors constructed from flexible 3D graphene/organic-based hybrid material were also reported for photodetection purposes in the visible to mid-infrared regime [45]. For the fabrication of an ultraviolet photodetector, Boruah et al. [44] have demonstrated the applications of ZnO nanowires grown on 3D graphene foam.

Overall, 3D graphene structures are one of the important classes of materials for flexible device applications owing to their various fascinating characteristics such as ultrathin, lightweight compatibility with various polymers that help in enhancing their flexibility, and ability to combine with other materials to synthesize composites. All these properties suggests their potential as electrode materials for energy storage applications including batteries, supercapacitors, lightweight sensors, and photodetectors.

3 Conclusion

In conclusion, an overview of various 3D graphene architectures mainly foams, hydrogels, aerogels, sponges, and films are provided. Various growth techniques employed to prepare these 3D graphene structures are also briefly discussed. Various flexible devices fabricated by utilizing such 3D graphene structures are critically highlighted with a particular focus on flexible sensor-based applications and flexible energy storage device applications including flexible supercapacitors, metal–ion batteries such as lithium–ion battery, etc. However, further work is still required to apprehend the commercialization of such flexible devices obtained from 3D structures because of the lack of standardization of the growth technique and/or fabrication technique. Constant efforts along with scientific innovations in this field will certainly lead to the fabrication of highly efficient flexible electronic devices.

References

1. Chen, Z.P., Ren, W., Gao, L., Liu, B., Pei, S., Cheng, H.-M.: Three-dimensional flexible and conductive interconnected graphene networks grown by chemical vapour deposition. Nat. Mater. **10**, 424–428 (2011)
2. Shehzad, K., Xu, Y., Gao, C., Duan, X.: Three-dimensional macro-structures of two-dimensional nanomaterials. Chem. Soc. Rev. **45**, 5541–5588 (2016)
3. Banciu, C.A., Nastase, F., Istrate, A.I., Veca, L.M.: 3D graphene foam by chemical vapor deposition: synthesis, properties, and energy-related applications. Molecules **27**, 3634 (2022)
4. Xiao, W., Li, B., Yan, J., Wang, L., Huang, X., Gao, J.: Three dimensional graphene composites: preparation, morphology and their multi-functional applications. Compos. Part A: Appl. Sci. Manuf. **154**, 107335 (2022)
5. Li, C., Shi, G.: Three-dimensional graphene architectures. Nanoscale **4**, 5549–5563 (2012)
6. Wu, Y., Yi, N., Huang, L., Zhang, T., Fang, S., Chang, H., Li, N., Oh, J., Lee, J.A., Kozlov, M.: Three-dimensionally bonded spongy graphene material with super compressive elasticity and near-zero poisson's ratio. Nat. Commun. **6**, 6141 (2015)
7. Hu, H., Zhao, Z., Wan, W., Gogotsi, Y., Qiu, J.: Ultralight and highly compressible graphene aerogels. Adv. Mater. **25**, 2219–2223 (2013)
8. Li, J., Zhao, S., Zhang, G., Gao, Y., Deng, L., Sun, R., Wong, C.-P.: A facile method to prepare highly compressible three-dimensional graphene-only sponge. J. Mater. Chem. A **3**, 15482–15488 (2015)
9. Han, Z., Tang, Z., Li, P., Yang, G., Zheng, Q., Yang, J.: Ammonia solution strengthened three-dimensional macro-porous graphene aerogel. Nanoscale **5**, 5462–5467 (2013)
10. Wang, M., Duan, X., Xu, Y., Duan, X.: Functional three-dimensional graphene/polymer composites. ACS Nano **10**, 7231–7247 (2016)
11. Samad, Y.A., Li, Y., Alhassan, S.M., Liao, K.: Novel graphene foam composite with adjustable sensitivity for sensor applications. ACS Appl. Mater. Interfaces **7**, 9195–9202 (2015)
12. Qin, Y., Peng, Q., Ding, Y., Lin, Z., Wang, C., Li, Y., Xu, F., Li, J., Yuan, Y., He, X.: Lightweight, superelastic, and mechanically flexible graphene/polyimide nanocomposite foam for strain sensor application. ACS Nano **9**, 8933–8941 (2015)
13. An, B., Ma, Y., Li, W., Su, M., Li, F., Song, Y.: Three-dimensional multi-recognition flexible wearable sensor via graphene aerogel printing. Chem. Commun. **52**, 10948–10951 (2016)
14. Pang, Y., Tian, H., Tao, L., Li, Y., Wang, X., Deng, N., Yang, Y., Ren, T.-L.: Flexible, highly sensitive, and wearable pressure and strain sensors with graphene porous network structure. ACS Appl. Mater. Interfaces **8**, 26458–26462 (2016)

15. Liu, H., Dong, M., Huang, W., Gao, J., Dai, K., Guo, J., Zheng, G., Liu, C., Shen, C., Guo, Z.: Lightweight conductive graphene/thermoplastic polyurethane foams with ultrahigh compressibility for piezoresistive sensing. J. Mater. Chem. C **5**, 73–83 (2017)
16. Li, J., Zhao, S., Zeng, X., Huang, W., Gong, Z., Zhang, G., Sun, R., Wong, C.-P.: Highly stretchable and sensitive strain sensor based on facilely prepared three-dimensional graphene foam composite. ACS Appl. Mater. Interfaces **8**, 18954–18961 (2016)
17. D'Elia, E., Barg, S., Ni, N., Rocha, V.G., Saiz, E.: Self-healing graphene-based composites with sensing capabilities. Adv Mater. **27**, 4788–4794 (2015)
18. Li, J., Zhang, G., Sun, R., Wong, C.-P.: A covalently cross-linked reduced functionalized graphene oxide/polyurethane composite based on diels–alder chemistry and its potential application in healable flexible electronics. J. Mater. Chem. C **5**, 220–228 (2017)
19. Sengupta, D., Pei, Y., Kottapalli, A.G.P.: Ultralightweight and 3D squeezable graphene polydimethylsiloxane composite foams as piezoresistive sensors. ACS Appl. Mater. Interfaces **11**, 35201–35211 (2019)
20. Sengupta, D., Kamat, A.M., Smit, Q., Jayawardhana, B., Kottapalli, A.G.P.: Piezoresistive 3D graphene–PDMS spongy pressure sensors for IoT enabled wearables and smart products. Flex. Print. Electron. **7**, 015004 (2022)
21. Yang, J., Ran, Q., Wei, D., Sun, T., Yu, L., Song, X., Pu, L., Shi, H., Du, C.: Three-dimensional conformal graphene microstructure for flexible and highly sensitive electronic skin. Nanotechnol. **28**, 115501 (2017)
22. Wang, C.D., Xu, J., Yuen, M.-F., Zhang, J., Li, Y., Chen, X., Zhang, W.: Hierarchical composite electrodes of nickel oxide nanoflake 3D graphene for high-performance pseudocapacitors. Adv. Funct. Mater. **24**, 6372–6380 (2014)
23. Dong, X.C., Xu, H., Wang, X.-W., Huang, Y.-X., Chan-Park, M.B., Zhang, H., Wang, L.-H., Huang, W., Chen, P.: 3D graphene cobalt oxide electrode for high-performance supercapacitor and enzymeless glucose detection. ACS Nano **6**, 3206–3213 (2012)
24. Xu, Y., Lin, Z., Huang, X., Liu, Y., Huang, Y., Duan, X.: Flexible solid-state supercapacitors based on three-dimensional graphene hydrogel films. ACS Nano **7**, 4042–4049 (2013)
25. Zheng, Q., Cai, Z., Ma, Z., Gong, S.: Cellulose Nanofibril/reduced graphene oxide/carbon nanotube hybrid aerogels for highly flexible and all-solid-state supercapacitors. ACS Appl. Mater. Interfaces **7**, 3263–3271 (2015)
26. Qin, K., Kang, J., Li, J., Liu, E., Shi, C., Zhang, Z., Zhang, X., Zhao, N.: Continuously hierarchical nanoporous graphene film for flexible solid-state supercapacitors with excellent performance. Nano Energy **24**, 158–164 (2016)
27. Wang, M., Wang, Y., Dou, H., Wei, G., Wang, X.: Enhanced rate capability of nanostructured three-dimensional graphene/Ni_3S_2 composite for supercapacitor electrode. Ceram. Int. **42**, 9858–9865 (2016)
28. He, Y., Chen, W., Li, X., Zhang, Z., Fu, J., Zhao, C., Xie, E.: Freestanding three-dimensional graphene/MnO_2 composite networks as ultralight and flexible supercapacitor electrodes. ACS Nano **7**, 174–182 (2013)
29. Phadatare, M., Patil, R., Blomquist, N., Forsberg, S., Örtegren, J., Hummelgård, M., Meshram, J., Hernández, G., Brandell, D., Leifer, K., Sathyanath, S.K.M., Olin, H.: Silicon-nanographite aerogel-based anodes for high performance lithium ion batteries. Sci. Rep. **9**, 14621 (2019)
30. Ji, J.Y., Ji, H., Zhang, L.L., Zhao, X., Bai, X., Fan, X., Zhang, F., Ruoff, R.S.: Graphene-encapsulated Si on ultrathin-graphite foam as anode for high capacity lithium-ion batteries. Adv. Mater. **25**, 4673–4677 (2013)
31. Zhang, Z., Chen, Y., Sun, S., Sun, K., Sun, H., Li, H., Yang, Y., Zhang, M., Li, W., Chou, S., Liu, H., Jiang, Y.: Recent progress on three-dimensional nanoarchitecture anode materials for lithium/sodium storage. J. Mater. Sci. Technol. **119**, 167–181 (2022)
32. Qiu, B.C., Xing, M.Y., Zhang, J.L.: Mesoporous TiO_2 nanocrystals grown in situ on graphene aerogels for high photocatalysis and lithium-ion batteries. J. Am. Chem. Soc. **136**, 5852–5855 (2014)
33. Wei, W., Yang, S., Zhou, H., Lieberwirth, I., Feng, X., Müllen, K.: 3D graphene foams cross-linked with pre-encapsulated Fe_3O_4 nanospheres for enhanced lithium storage. Adv. Mater. **25**, 2909–2914 (2013)

34. Mo, R., Rooney, D., Sun, K., Yang, H.Y.: 3D nitrogen-doped graphene foam with encapsulated germanium/nitrogen-doped graphene yolk-shell nanoarchitecture for high-performance flexible Li-ion battery. Nat. Commun. **8**, 13949 (2017)
35. Mo, R., Lei, Z., Rooney, D., Sun, K.: Three-dimensional double-walled ultrathin graphite tube conductive scaffold with encapsulated germanium nanoparticles as a high-areal-capacity and cycle-stable anode for lithium-ion batteries. ACS Nano **13**, 7536–7544 (2019)
36. Zhang, F., Yang, C., Gao, X., Chen, S., Hu, Y., Guan, H., Ma, Y., Zhang, J., Zhou, H., Qi, L.: SnO_2@PANI core-shell nanorod arrays on 3d graphite foam: a high-performance integrated electrode for lithium-ion batteries. ACS Appl. Mater. Interfaces **22**, 9620–9629 (2017)
37. Xi, K., Kidambi, P.R., Chen, R., Gao, C., Peng, X., Ducati, C., Hofmann, S., Kumar, R.V.: Binder free three-dimensional sulphur/few-layer graphene foam cathode with enhanced high-rate capability for rechargeable lithium sulphur batteries. Nanoscale **6**, 5746–5753 (2014)
38. Ji, H., Zhang, L., Pettes, M.T., Li, H., Chen, S., Shi, L., Piner, R., Ruoff, R.S.: Ultrathin graphite foam: a three-dimensional conductive network for battery electrodes. Nano Lett. **12**, 2446–2451 (2012)
39. He, J., Chen, Y., Lv, W., Wen, K., Li, P., Qi, F., Wang, Z., Zhang, W., Li, Y., Qin, W., He, W.: Highly-flexible 3D Li_2S/graphene cathode for high-performance lithium sulfur batteries. J. Power Sources **327**, 474–480 (2016)
40. Chang, B., Chen, J., Zhou, M., Zhang, X., Wei, W., Dai, B., Han, S., Huang, Y.: Three-dimensional graphene-based n-doped carbon composites as high-performance anode materials for sodium-ion batteries. Chem Asian J. **13**, 3859–3864 (2018)
41. Ji, J., Liu, J., Lai, L., Zhao, X., Zhen, Y., Lin, J., Zhu, Y., Ji, H., Zhang, L.L., Ruoff, R.S.: In situ activation of nitrogen-doped graphene anchored on graphite foam for a high-capacity anode **9**, 8609–16 (2015)
42. Yu, H., Ye, D., Butburee, T., Wang, L., Dargusch, M.: Green synthesis of porous three-dimensional nitrogen-doped graphene foam for electrochemical applications. ACS Appl. Mater. Interfaces **8**, 2505–2510 (2016)
43. Li, Y., Zhang, Y., Yu, Y., Chen, Z., Li, Q., Li, T., Li, J., Zhao, H., Sheng, Q., Yan, F., Ge, Z., Ren, Y., Chen, Y., Yao, J.: Ultraviolet-to-microwave room-temperature photodetectors based on three-dimensional graphene foams. Photonics Res. **8**, 368–374 (2020)
44. Ge, Z., Xu, N., Zhu, Y., Zhao, K., Ma, Y., Li, G., Chen, Y.: Visible to Mid-Infrared photodetection based on flexible 3D graphene/organic hybrid photodetector with ultrahigh responsivity at ambient conditions. ACS Photonics **9**, 59–67 (2022)
45. Boruah, B.D., Mukherjee, A., Sridhar, S., Misra, A.: Highly dense ZnO nanowires grown on graphene foam for UV photodetection. ACS Appl. Mater. Interfaces **7**, 10606–10611 (2015)

3D Graphene for Capacitive De-ionization of Water

Sara Madani and Cavus Falamaki

Abstract Herein we consider the use of 3D graphene structures in the so-called capacitive de-ionization (CDI) process of water. The topic is hot and the need for such structures is explained by presenting a brief description of CDI technology including the latest configurations and discussing the most important and recent steps taken so far to use 3D graphene as an electrode material. The advantages and disadvantages of using 3D structures as electrode materials to be implemented in the CDI process of water are discussed. The state of art related to 3D graphene-only electrodes, 3D graphene composites with carbonaceous materials, and 3D graphene composites with non-carbonaceous materials are discussed in detail. The future perspective is briefly addressed and considers the use of 3D printing, pseudocapacitive layered materials and introduces 3D graphene/3D non-graphene structures. The use of new 3D graphene materials in the field of CDI is constantly increasing. Accordingly, this chapter can serve as a motivational tool to encourage researchers to focus on the development of new 3D graphene-based materials for CDI electrodes to combat the increasing scarcity of drinking water worldwide.

Keywords 3D graphene · Capacitive de-ionization · Water desalination · Hierarchical pore structure · Graphene-based electrode

1 Why CDI?

Water scarcity is becoming a crucial problem for humanity in recent decades [1]. Therefore, desalination technologies have been intensively developed as desirable solutions in recent years. Currently, thermal desalination technologies including multi-stage flash distillation (MSF), multi-effect distillation (MED), mechanical vapor compression (MVC), and multi-effect solar stills (MESS), and membrane-based technologies such as reverse osmosis (RO) and electrodialysis (ED) have been

---

S. Madani (✉) · C. Falamaki
Chemical Engineering Department, Amirkabir University of Technology (Tehran Polytechnic), Tehran, Iran
e-mail: sm.saramadani@gmail.com

© The Author(s), under exclusive license to Springer Nature Switzerland AG 2023

R. K. Gupta (ed.), *3D Graphene*, Carbon Nanostructures,
https://doi.org/10.1007/978-3-031-36249-1_22

widely developed. However, these established techniques suffer from high costs, poor efficiency, and pollution, and require large amounts of energy in the form of thermal and/or electrical energy [2]. To reduce energy consumption, several new technologies such as forward osmosis (FO) [3], membrane distillation (MD) [4], reverse electrodialysis (RED) [5], and capacitive de-ionization (CDI) [6] have evolved and may soon approach full commercialization. CDI is known as an environmentally friendly desalination technology with lower energy consumption and lower capital costs compared to traditional desalination methods. The use of high-pressure pumps and membranes is not required, and no secondary waste is generated during the process in these systems. In addition, a wide range of applications from water softening and water desalination to selective ion removal has been established for CDI systems [6].

2 CDI Technology in Brief

In 1960, Blair and Murphy first explored the idea of electrochemical desalination of water [7]. The pioneering work of CDI was continued by Murphy and Caudle [8] in the mid-1960s. In 1971, the theory of ion transport in porous carbon electrodes in CDI and ion storage based on the capacitor mechanism was introduced [9]. In 1996, Farmer et al. improved the performance of a carbon aerogel electrode CDI device [10]. After introduction of this first 3D carbonaceous structure as electrode material, CDI process development underwent an unprecedented accelerated rapid growth.

Basically, the term capacitive de-ionization denotes two main functions: The term capacitive is used to indicate that charged ions are adsorbed by water and stored on the inner surface of porous electrodes, while de-ionization causes the removal of cations and anions from the water. In fact, CDI is an electrochemically controlled technique for removing salt from salt water. In a basic design (Fig. 1), salt water flows between a pair of large surface area electrodes and simultaneously a small potential difference (<2 V) is applied across them. The potential window should not exceed the water splitting potential point [11]. Charged ions are pulled toward the electrode with contrary polarity during a charge cycle, while they are expelled to the secondary stream during a discharge cycle when application of voltage to the electrodes is discontinued or reversed.

Two important types of CDI have been studied extensively: symmetric and asymmetric. The most common CDI configuration is flow-through CDI (Fig. 2a), first proposed by Blair et al. [7]. Later, this configuration was widely used in a variety of research and works. In another configuration, referred to as osmotic CDI, the feed current flows directly through the osmotic electrodes. This configuration was first reported in 1970 by Johnson et al. (Fig. 2b) [12]. This type of CDI was used to study key performance parameters and showed more rapid cell charging compared to flow-through CDI. In 2012, two battery electrodes for desalination in a desalination battery were presented as a novel CDI design (Fig. 2c). Although a desalination battery is a desirable configuration for high salinity water desalination, this type of

Fig. 1 Schematic diagram of a traditional CDI system

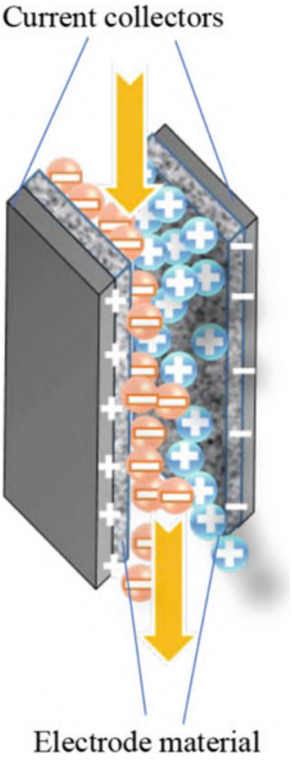

CDI suffers from instability due to Faraday reactions. A novel CDI design is the flow electrode CDI (Fig. 2d), which may offer compact, low-resistance systems using slurry or flow electrodes [13]. Carbon suspensions were used as a novel suspension electrode in the CDI system (Fig. 2e) for desalination of brackish and sea water [14]. Asymmetric CDI has been subject of emerging research in recent years due to its better performance compared to symmetric CDI.

Materials with different potential of zero charge (PZC), surface functional groups, surface charges [12, 15, 16], electrode thicknesses [17], and even different ion removal mechanisms [18] can increase desalination performance and system capacity. One of the most popular asymmetric configurations is membrane-assisted capacitive de-ionization (MCDI), which is a combination of ion-exchange membranes with classic forms of CDI (flow-by, flow-through) configurations [19]. Anion and cation exchange membranes were applied to the anode and cathode electrodes, respectively. Covalently attached groups allow easy access of the ions to the counter-electrode while repelling co-ions. Ion-exchange membranes can be installed free-standing [19] or ion-selective groups can be grafted directly onto porous electrodes [20]. When the co-ions are expelled from the electrodes, they must not move toward the spacer channel. Thus, co-ions remain on the electrode side and accumulate in higher concentrations in the macropores. Charge neutrality in macropores

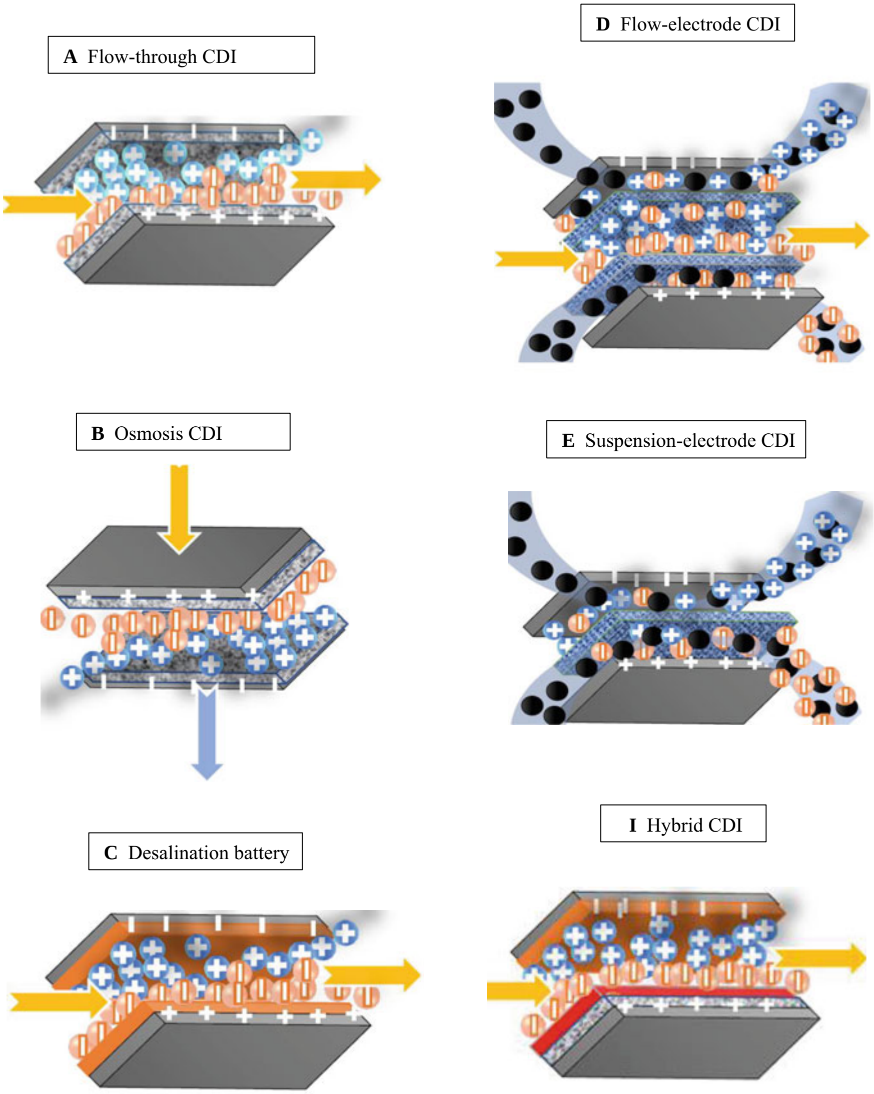

Fig. 2 **a** Various CDI configurations (A to E). **b** Various CDI configurations (F to K). **c** Legend

also requires the accumulation of counter-ions. This eventually improves the charging efficiency.

The remarkably fast recovery of the electrodes due to the application of a reverse voltage in the regeneration cycle is another advantage of MCDI over CDI. Finally, membranes prevent the electrode from disintegrating in the long term [21]. Inverted-CDI (i-CDI) as another modified CDI guarantees the desalination stability and efficiency of the CDI over time. Unlike traditional CDI, ion adsorption and desorption

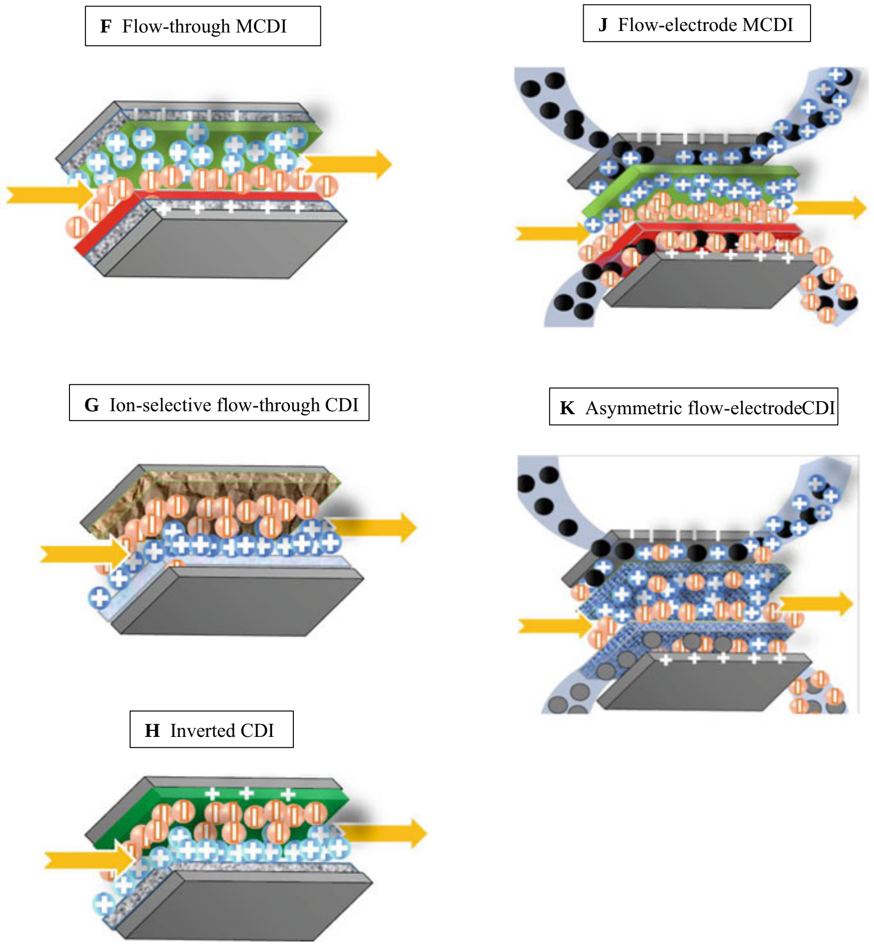

F Flow-through MCDI

G Ion-selective flow-through CDI

H Inverted CDI

J Flow-electrode MCDI

K Asymmetric flow-electrodeCDI

Fig. 2 (continued)

occur during the discharge and charge time of i-CDI, respectively [15]. A combination of faradic and capacitive electrodes in a CDI structure is called hybrid-CDI (HCDI) [18]. Hybrid systems exhibit a higher sorption capacity for ion removal than a typical CDI system. Flowing suspension carbon was used as the electrode material in a membrane CDI to desalinate water with high salinity. In another similar configuration, activated carbon suspension is used in combination with metal oxide to create an asymmetric structure to increase the voltage window. Consequently, SAC with this configuration is much higher than that of a typical flow electrode CDI.

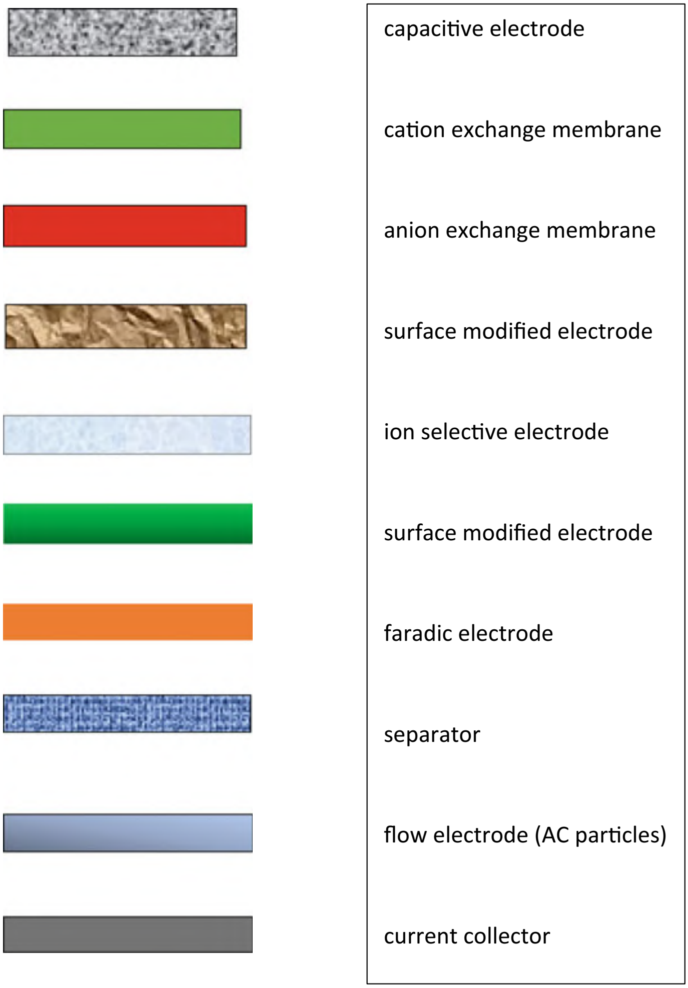

Fig. 2 (continued)

2.1 *Electrode Material: A Key Component*

Electrode material is a key component in CDI configuration, and affects ion sorption capacity, de-ionization rate, and system reliability. An ideal CDI electrode material possesses high electrical conductivity and surface area, and proper wettability that benefits from continuous electron transfer pathways, rich active sites, and fast ion transport pathways to form an efficient electrochemical double layer [23, 24].

Therefore, abundant accessible surface areas and hierarchical pore morphology are key properties for the electrode materials. In addition, good electrode candidates are inexpensive, scalable, and easy-to-process materials [25]. Members of the carbon family of materials as ideal CDI electrode materials are conductive with easily tunable properties that exhibit excellent chemical/electrochemical stability and diverse morphology. So far, activated carbon, ordered mesoporous carbon, carbon nanotubes, carbon nanofibers, carbon aerogels, carbon nanospheres, and graphene and their composites have been widely used as electrode material in CDI systems [26–28]. Graphene as the newest class of carbon material with exceptional characteristics such as high theoretical surface area of 2630 $m^2\ g^{-1}$, high carrier mobility up to 10 000 $m^2\ V^{-1}\ s^{-1}$, substantially high conductivity (7200 $S\ m^{-1}$), high electron and thermal mobility, tunable surface properties and morphology, and excellent physical and chemical properties has attracted the attention of researchers for large-scale CDI applications [22, 29].

Graphene is the two-dimensional layer of carbon atoms with hexagonal crystalline arrangement, which has created promising perspectives in a variety of applications due to its unique physicochemical properties. The history of using graphene in CDI systems dates back to 2009 when Li et al. used reduced graphene oxide as the electrode material in a CDI for the first time [30]. They hypothesized that corrugated sheets of reduced graphene oxide (RGO) create a porous structure to facilitate ion storage. Although the obtained electrosorption capacity superseded that of activated carbon (AC) in the similar experimental conditions, the salt adsorption capacity (SAC) value for reduced graphene oxide was not satisfactory. The low specific surface area (14.2 m^2g^{-1}) due to the aggregation of the graphene nanosheets was the main cause resulting in low electrosorption capacity. The same group performed another study and increased the specific surface area of RGO nanoflakes from 222 to 254 $m^2\ g^{-1}$, while the achieved NaCl removal capacity remained at about 1.35 mg g^{-1} under the same experimental conditions [31].

One of the possible solutions to increase the electrosorption capacity was to propose a novel reduction method such as solar irradiation and/or thermal shock reduction. For example, in the solar irradiance reduction method, the sunlight focused on graphene oxide (GO) causes a sudden temperature rise that decomposes GO into RGO, CO_2, and marginal H_2O. The pressurized CO_2 promoted exfoliation of the graphene, resulting in a structural transition from a dense structure to a fluffy/fuzzy structure. The folded and crumpled structure of the obtained RGO creates a large surface area that can generate up to a high SAC of 22.4 mg g^{-1} in a 5844 mg L^{-1} NaCl solution at 1 V [32]. The SAC growth of RGO electrodes has been mainly attributed to microstructure modification such as in-plane porous structures or curve morphology and surface functional groups like oxygenates. However, creation of 3D porous graphene structure and surface modification of graphene are considered as more promising solutions, which are discussed in the following section.

3 3D Structures in Water Treatment: Advantages and Challenges

In general, low-dimensional nanomaterials show enormous potential for water treatment; however, these material agglomerates not only cause a loss of activity in water, but their recovery is difficult and expensive. In addition, nanomaterials potentially remaining in drinking water cause many health concerns. 3D macrostructures made from low-dimensional nanomaterials inherit the special properties of their corresponding nanoscale building blocks. Unlike nanomaterials themselves, 3D structures can be easily recovered and recycled without using membrane separation techniques. Thus, these material classes improve the application of low-dimensional nanomaterials and make the treatment process more economical to carry out. The likelihood of release (leaching) of nanomaterials in the water treatment process decreases significantly, eliminating health concerns related to treated water consumption. Instead of using expensive and environmentally harmful processes such as thermal treatment or chemical washing, environmentally friendly regeneration techniques can be used. It also gives the treatment system a good opportunity to design the flow units in a continuous mode of operation. Last but not least, a 3D structure of graphene resembles a scaffold, and other functional groups or nanomaterials can be grafted onto these unique structures to build macro-sized multifunctional nanocomposites to simultaneously separate different contaminants. Therefore, making a 3D structure from low-dimensional material is very important. These multifunctional nanocomposites can be synthesized by mixing other nanomaterial with the precursor or by accommodating it on graphene's 3D structural surface. While the fabrication of low-dimensional material is a tedious, time-consuming process that makes its large-scale application problematic, the fabrication of 3D graphene-based macrostructures (3D GBMs) is simple and inexpensive.

The cause of graphene sheet aggregation and restacking lies in interplanar van der Waals forces and strong π–π interactions of the basal planes of graphene sheets. In a CDI system, the physisorption process is responsible for NaCl electrosorption on graphene electrodes. Two key strategies can be considered to prevent graph restacking; as already mentioned, the first and main solution is to fabricate a 3D porous structure to promote accessibility to separate graphene layers and increase the surface area in the system meaningfully, and the second way is to apply spacer material such as carbon nanotube (CNT) and mesoporous carbon between layers of graphene, which is not our focus.

3.1 3D Graphene-Based Electrodes

Till now, different methods have been adopted to manufacture 3D structures of graphene as a CDI electrode, such as aerogels, hydrogels, foams, scaffolds, and sponges. Depending on the GO synthesis method and 3D structure, GO concentration, pH of the GO suspension, reduction method, pre-treatments or post-treatments, chemicals used in the production stages, treatment time, and temperature, the structures produced differ in specific surface area and pore size distribution, porosity, internal structure, wettability, and electrical and mechanical properties. Hence, we will observe different reported results for the application of different 3D structures of graphene in CDI systems under the same test conditions.

Graphene hydrogel as one of these 3D structures is a jelly-like macroporous material. Water is trapped within the pores of graphene hydrogels (GHs) and they have hydrophilic nature. GO as a starting material is used to produce GH using chemical reduction or cross-linking processes. Graphene aerogels (GAs) have been produced through controlled dehydration of GHs without appreciable volume shrinkage or by chemical vapor deposition on 3D porous scaffolds. GAs and GHs fulfill ideal CDI electrode properties such as high specific surface area and conductivity, appropriate hydrophilicity, and connected porous structure. GAs and GHs benefit from a hierarchical pore structure which can play different key roles in the electrosorption process. They can be easily adapted to the required electrode architecture based on synthesis methods and their parameters. Macropores/mesopores are mainly responsible for providing efficient pathways to transport ions, while mesopores resemble storage reservoirs for adsorbed ions. Furthermore, micropores in this structure provide high surface area ions for EDL formation. Wang and co-workers used GAs as the electrode material in a CDI and achieved a SAC of 5.39 mg g^{-1} at 2.0 V and an initial NaCl concentration of 105 μS cm^{-1} [33].

Graphene oxide layers undergo self-assembly provided their concentration is higher than a critical value that leads to the formation of liquid crystals as a result of nematic phase separation [34]. Therefore, the GO concentration is crucial to determine the morphology of the hydrogel. Drying the hydrogel in direct contact with air disintegrates the 3D structure due to capillary forces. Drying methods such as freeze-drying or supercritical drying are commonly used to remove water from the hydrogel, and the aerogel produced does not show any significant reduction in volume or collapse of the internal structure. As ice crystals grow, RGO layers are pushed to align along the moving freezing front, creating a well-organized cellular structure through the freezing process. Interconnected layers of GA create a highly compressible/elastic structure (in one or all directions) called sponges or graphene foams. Polyurethane-templated technique was used to fabricate a spongy graphene with a specific surface area of 305 m^2 g^{-1} in 2014, whose SAC was 4.95 mg g^{-1} in 1 mL of aqueous NaCl at 1.5 V [35].

In another study, a graphene sponge was fabricated by directly freeze-drying the GO suspension and then annealing it in a nitrogen atmosphere [36]. The reported SAC for this electrode material was about 14.9 mg g^{-1} at 1.2 V in 500 mg L^{-1}

NaCl solution, ca. 3.2 times the capacity of pristine graphene (4.64 mg g^{-1}). Such a high capacitance value is obtained not only for a relatively large specific surface area (356.0 m^2 g^{-1}), but also because of the accessible 3D cross-linked porous structure (pore volume of 1.51 cm^3 g^{-1} versus 0.83 cm^3 $g^{-1}$for pristine graphene) and low charge transfer resistance. Because the EDLs are formed at the electrode surface, a higher quantity of charges is adsorbed eventually leading to a superb capacitance. Therefore, effectively increasing the surface area has been known as one of the solutions to improve the CDI operation.

KOH activation is considered a traditional method to increase the surface area of activated carbon (AC), CNT, and carbon nanofibers. Zhuo et al. applied the KOH-activated graphene electrode with a 3D porous structure in a CDI system, which possess an unusual specific surface area of 3513 m^2 g^{-1} and an electrical conductivity of 104 S m^{-1} [37]. The thermal shock in the first step of the fabrication process leads to the decomposition of most of the oxygenate groups, generating pressurized gas in a very short time that promotes exfoliation of the graphene sheets (Fig. 3). This process was followed by a KOH treatment to etch the graphene layers and form in-plane micropores. The ion removal capacity of this electrode was 11.86 mg g^{-1} at 2 V in 70 mg L^{-1} NaCl solution, which is much better than that of activated carbon, CNT- and RGO-based electrodes under the same experimental conditions until then (2015). In addition, the de-ionization rate for activated graphene is much higher than for RGO. The de-ionization process with the KOH-activated graphene is completed in less than 20 min, while the same process for RGO takes almost 50 min.

On the other hand, the etching process creates a lot of surface (or edge) carbon, which has a much larger specific capacity than that of the graphene basal plane, resulting in a significant increase in the overall electrosorption capacity. The interconnected structure forms a conductive percolated network that guarantees rapid electrosorption and good mechanical robustness. In 2015, another research group constructed a 3D graphene architecture with nanopores using an H_2O_2-induced chemical etching process of the graphene ground plane [38]. Graphene carbon atoms were etched and then enlarged into nanopores with H_2O_2. The 3D holey graphene hydrogel was a connected highly porous 3D architecture of huge surface area due to numerous in-plane pores (NP-3DG). This electrode showed a large SAC of 17.1 mg g^{-1} at 1.6 V in 500 mg L^{-1} NaCl solution. NP-3DG showed a much higher salt removal capacity (15 mg g^{-1}) than that of 3D graphene (3DG) structure (8.3 mg g^{-1}) under the same experimental conditions (1.4 V and 500 mg L^{-1}). 3D holey graphene contained in-plane macropores and nanopores, which provided ions with larger available surface area (3DG structure having a specific surface area of 247 m^2 g^{-1}) and efficient pathways for ion transport. In fact, the interconnected macropores of the graphene matrix improve demineralization process by storing ions to decrease the diffusion paths from the outer electrolyte to the inner surface.

Increasing the voltage increases the driving force on ions, causing more micropores to participate in improving the SAC of the electrode. For this reason, some studies report high SAC values, however, when actually evaluating and comparing the results of different studies, voltage and other experimental parameters such as initial concentration should be taken into account. The voltage should not be too

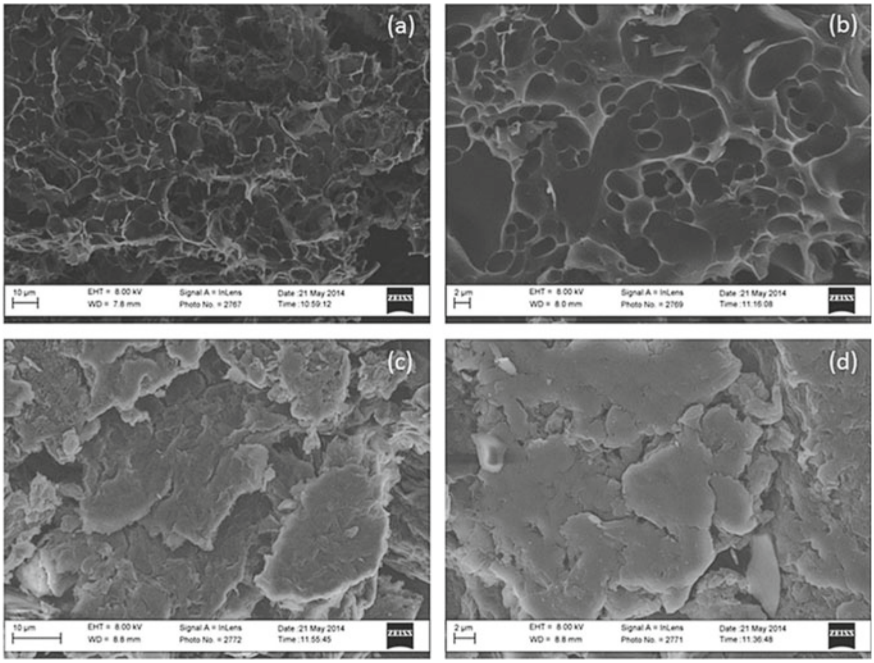

Fig. 3 SEM images of **a**, **b** KOH-activated graphene and **c**, **d** reduced graphene oxide. Adapted with permission from [37]. Copyright (2023) Elsevier

high to exceed the hydrolysis voltage. In a study, a high-hole graphene framework (HGF) was successfully applied as the CDI electrode material using lyophilization and heat treatment at 200 °C [39]. The reported SACs of HGF were 8.0, 16.9, and even 29.6 mg g^{-1} in different NaCl concentrations of 80, 270, and 572 mg L^{-1}, respectively. Such values are substantially larger than those reported for other carbon-based materials at 2.0 V. A higher NaCl concentration increased the ions transportation rate within the pores and decreased overlaying phenomena of EDL, therefore the cell SAC improved with increasing NaCl concentration under the same experimental conditions (constant applied voltage). However, in another study, scientists obtained the high NaCl level of 9.13 mg g^{-1} at 2.0 V in an ultra-low salt concentration of 50 mg L^{-1} NaCl solution using surface microporous graphene (SMG) [40]. This shows that structural manipulation of the graphene surface without using heteroatoms or pseudocapacitive material can be an essential tool to increase the system performance even in very low concentration. The excellent CDI performance at such a low salt concentration is due to the rich active sites with short ion transport distance in the surface micropore structure.

The existence of an original 3D structure incorporated in a hierarchical hole system in HGF is a major factor enhancing CDI performance. The 3D graphene with hierarchical porous structure (3DHGR) has been fabricated as an effective CDI electrode material [41]. These electrodes were fabricated using a template-controlled process in combination with the in situ defect etching process (oxometalate etching). 3DHGR consists of 3D graphene entities containing many micro-mesopores over the associated macroporous walls. 3DHGR has been reported to have a large SAC of 14.7 mg g^{-1} in 500 ppm NaCl solution at 1.2 V and good regeneration performance in repeated charge–discharge cycles and a speedier salt adsorption rate compared to 3D graphene under the same conditions. Although macropores in 3DHGR impose a short diffusion path by screening ions, micro- and mesopores play the key role in providing accessible surfaces and adsorption sites and facilitating ion transport in macroporous 3D graphene. The charge efficiency (Λ) is one of the main parameters for determining the proportion of salt take up to charge transfer. The calculated charging efficiency of 3DHGR is 0.63. This is significantly larger compared to 3DGR (0.28).

In 2018, Ma et al. compared the performance of RGO hydrogel and graphene aerogel in the CDI system, achieving exceptional electrosorption capacities of 49.34 and 45.88 mg g^{-1} (at an initial concentration of 500 mg L^{-1} and a voltage of 2.0 V) for GH and GA, respectively [42]. The specific surface area of GH and its average pore size are higher than that of GA. The hydrophilicity and electrical conductivity of GH are higher than that of GA, however, the function of water is a cornerstone of the performance dissimilarities. The SAC of GH is 49.34 mg g^{-1}, larger than that of GA (45.88 mg g^{-1}) at 2.0 V with an initial NaCl concentration of 500 mg L^{-1}. Water has the function of supporting and transferring: water can reduce graphene rearrangement (supports) and facilitate ion transport from the inner pores to the outside. Many of the techniques mentioned above involve templating processes, which are somewhat complex and time-consuming. In addition, the desalination performance needs to be improved to be economical and practical.

One of the simple ways to fabricate a 3D hierarchically porous graphene is a merging of H_2O_2-assisted hydrothermal and microwave processes [43]. An ultrahigh CDI capacitance of 21.58 mg g^{-1} in a 500 ppm NaCl solution at 1.4 V was obtained with this unique hierarchically porous 3D graphene (GO-Mw-Hyd). The charging efficiency of the system is 0.73, which is excellent compared to GO ($\Lambda = 0.41$) and AC ($\Lambda = 0.37$).

3.2 3D Graphene Composite with Carbonaceous Material

Researchers have constructed various carbonaceous composites using 3D graphene macrostructures in association with other carbon family members such as AC, carbon nanotubes (CNT), and carbon spheres to create the large specific surface area with porous structure and improve demineralization operation. CNTs are used to play the role of spacer material when used with GO to prevent the agglomeration of GR layers. Several successful studies have been conducted with GR and CNT. One of them was an analogy between the CDI operation of 3D graphene hydrogel in combination with single-walled CNT (SWCNT) and multi-walled CNT (MWCNT) as electrode materials [44]. This research showed that SWCNTs/RGO hydrogel had a larger specific surface area of 308.37 m^2 g^{-1} (lower internal resistance) and a larger

SAC of 48.73 mg g^{-1} compared to MWCNTs/RGO with a capacity of 39.53 mg g^{-1} at 2 V in a 300 mg L^{-1} NaCl solution.

In 2020, microwave-irradiated graphene oxide (mwGO) 3D-CDI electrode materials with CNT deposited on RVC by the dip-coating method were constructed and evaluated [45]. The optimized composition (9-CNT/mwGO/RVC) showed 100% cycling stability and the amount of water produced per day for this electrode rose by a factor of 1.67 in comparison with CNT/RVC in a full desalination process. The maximum electrosorption capacity in 500 mg L^{-1} NaCl feed concentration was 10.84 mg g^{-1} for this optimal electrode, while this value is 65% of the theoretically calculated highest value (16.59 mg g^{-1}) of this composition. In another case study, a 3D graphene network embellished with microporous carbon spheres (3DGF-MCS) showed a maximum SAC of 19.8 mg g^{-1} at 1.2 V in a NaCl concentration of 100 mg L^{-1} [46]. Hybrid aerogel electrodes composed of graphene and nitrogen-doped multi-walled carbon nanotubes (Gr-MWCNT) (N-Gr-MWCNT) were fabricated using a facile hydrothermal synthesis method [47]. The large SAC of 20.1–22.5 mg g^{-1} at 1.8 V in 0.5 g L^{-1} NaCl solution was attributed to an interconnected network of graphene sheets with hierarchical porosity, uniform structure, outstanding electrical conductivity, large specific surface area, and high wettability.

Graphene composite carbon aerogels (GCCAs) have been synthesized under ambient pressure drying methods as electrode material for a CDI system [48]. Rational design of pore structure and highly conductive network resulted in a high SAC of 26.9 mg g^{-1} and 18.9 mg g^{-1} in NaCl solutions with concentrations of 500 mg L^{-1} and 250 mg L^{-1}, respectively.

3.3 3D Graphene Composites with Non-carbonaceous Material

In CDI, ion storage occurs by two main phenomena: capacitive ion storage and pseudocapacitive ion storage. Based on these mechanisms, the electrode material should be developed to achieve a proper de-ionization performance. Although carbonaceous electrodes have shown a gradual improvement in adsorption capacity, they are still not completely amenable to commercialization. Redox and faradic active intercalation materials have emerged as the latest class of proposed materials to search for better electrode materials capable of surpassing the electrosorption capacity of EDL-powered electrodes with fast electrosorption/desorption properties. So far, many pseudocapacitive materials from metal oxides and conducting polymers to heteroatoms such as nitrogen and phosphorus have been extensively used in combination with graphene in the 3D structures to significantly increase the performance of CDI due to their synergistic effects. Metal oxide nanoparticles such as TiO_2, MnO_2, ZnO_2, Fe_3O_4, and Co_3O_4 can inhibit the association of RGO sheets, and their proper physicochemical characteristics like high hydrophilicity enhance electrode wettability.

In 2013, Tang et al. applied a flexible technique to construct 3D graphene aerogel/metal oxide using various metal oxide nanoparticles (TiO_2, CeO_2, Fe_2O_3, and Mn_3O_4) [49]. The properties of low toxicity, good stability, low cost, easy anchoring in the carbon structure, and large dielectric constant for containing a higher amount of electric charges make TiO_2 a desirable candidate for the graphene/metal oxide nanocomposite. They could achieve the high capacity of 15.1 mg g^{-1} at 1.2 V (500 ml g^{-1} NaCl solution) for graphene aerogel/TiO_2, which is 1.5 and 12.6 times the capacity of GA and AC, respectively. For a NaCl concentration of 6000 mg L^{-1}, the CDI adsorption was 24.2 mg g^{-1} for the same electrode, representing the 1.6- and 7.3-fold that of GA (15.4 mg g^{-1}) and AC (3.3 mg g^{-1}). Among the transition metal oxides, MnO_2 has a high theoretical specific capacity (1,400 F g^{-1}), natural occurrence, and environmental friendliness, making it a potential candidate for modification of carbon-based composite electrodes. Conductive polymers are known as another important class of CDI electrode materials that improve CDI performance. Polyaniline (PANI), polypyrrole (PPy), and polyvinyl alcohol (PVA) are widely utilized in graphene composites because of their high electrical conductivity and acceptable chemical stability, ease of synthesis process, and being economical. On the other hand, the incorporation of polymers can reduce restacking of graphene sheets. In a research study, a three-dimensional electrode with a hierarchically porous structure was fabricated using RGOs, polypyrrole, and MnO_2 (RGO-PPy-Mn) [27]. This electrode exhibited a large specific surface area and specific capacity, which was the result of inserting two active materials (PPy and MnO_2) into the graphene network. The RGO-PPy-Mn hydrogels have a distinct porous network that optimizes ion diffusion in the electrode network. The high electrosorption capacity of 18.4 mg g^{-1} for RGO-PPy-Mn can be attributed to the synergistic effect of these components' capacitive properties and improved ion transport. Increased electrochemical capacity and excellent SAC show that the RGO-PPy-Mn electrode is fully suitable for CDI embracing both high performance and low energy consumption.

In another research, carbonization of GO-MF composites leads to 3D-RGO-melamine–formaldehyde (3D-RGO-MF) composites synthesized via electrostatic attraction between GO and MF nanoparticles [50]. Hierarchical porous structure of this composite (specific surface area of 352 m^2 g^{-1}) with high nitrogen doping level of 10.86% gives an extraordinarily high value of the electrosorption capacity of 21.93 mg g^{-1} at a potential of 2.0 V in NaCl solution. Low internal resistance and high reversibility prove that the 3D-RGO-MF electrodes can be a proper contender for high-performance CDI. In addition, a study showed that GO/PPy on a copper–nickel foam (CNF) could remove Rhodamine B (RhB) with a unique capacity of 270.3 mg g^{-1} and a rate of 3.762 mg g^{-1} min^{-1}.

Ensuring high electrical conductivity and hydrophilicity at the same time is a challenge that needs to be considered to achieve high-performance CDI. On the one hand, the surface functional groups of GO sheets should be removed as much as possible during a reduction process to preserve the conjugated structure of graphene sheets and increase conductivity. On the other hand, the elimination of the oxygenate groups leads to a decrease in hydrophilicity, which is essential in the capacitive deionization of salt water. Doping heteroatoms such as nitrogen into graphitic networks is considered to be one of the most effective methods to address the problem and fabricate n-type conductive materials of enhanced conductivity. In this way, the ions can straightforwardly be adsorbed by the electrode materials, and the salt uptake rate is accelerated. Nitrogen-doped graphene is usually produced by thermal conversion of various nitrogen precursors, plasma and flame, and hydrothermal treatment.

In 2015, a simple and economical strategy to produce nitrogen-doped sponge graphene (NGS) on a large scale was proposed [51]. GO was simply freeze-dried and annealed in an NH_3 atmosphere instead of the template method or hydrothermal technique. The prepared NGS showed an ultrahigh SAC of 21.0 mg g^{-1} at 1.5 V in a NaCl solution of about 500 mg L^{-1}, which is about 1.4 and 4.6 times that of graphene sponge (GS) (14.6 mg g^{-1}) and PG (4.5 mg g^{-1}), respectively. An increased specific surface area (526.7 m^2 g^{-1}) and increased pore volume (3.13 cm^3 g^{-1}) provide short ion diffusion paths and more accessible spaces for receiving and storing ions. In addition, pseudocapacitance is increased by doping with nitrogen. Doping also increases the electrical conductivity of graphene, and increases the wettability of the electrode–electrolyte interface. This can reduce the internal resistance of the electrodes and lead to promoting the electrosorption performance of NGS.

An easy and inexpensive method has been used to first synthesize 3D intercalated graphene sheet-sphere nanocomposite architectures (Fig. 4) [52]. Since 3D graphene nanospheres between graphene layers prevent stacking of graphene layers, this structure guarantees a high specific surface area, a well-defined/favorable pore size distribution, and high conductivity. An outstanding electrosorption capacity of 22.09 mg g^{-1} is obtained in a 500 mg L^{-1} NaCl solution at 1.2 V using graphene oxide and $[Ni_2(EDTA)]$ as precursors in a rational assembly of a 3D structure. The salt removal percentage was about 90% and the electrodes show excellent de-ionization stability and regeneration performance. This unique structure was fabricated using a two-step process of direct thermal conversion of GO and the Ni^{+2} coordination complex and acid etching without using additional templates, catalysts, or CVD processes. This work presents a promising scalable method to fabricate efficient CDI electrode materials for brackish and seawater desalination.

4 Future Perspective

3D graphene is establishing itself as a fundamental pillar in the architecture of CDI systems. Development of advanced 3D structures embracing all the desired characteristics like high SAC, low energy consumption, and high charging efficiency at the same time remains a tricky challenge. Some new researches are oriented toward the use of 3D printing [53], doping with heteroatoms [54], using pseudocapacitive layered transition metal sulfides (like MoS_2) [54] and nitrides (MXenes) [55], and combining 3D graphene structures with other non-graphene 3D structures (like 3D Prussian Blue) [56].

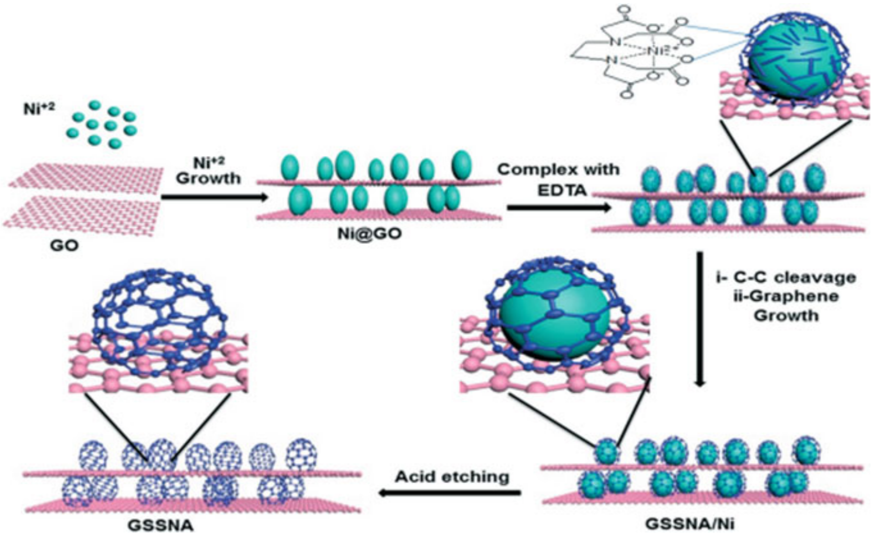

Fig. 4 Schematic of fabrication process of 3D multi-layered mesoporous GR sheet-sphere-like microstructure. Adapted with permission from [52]. Copyright (2023) Royal Society of Chemistry

References

1. Woo, Y.C., Kim, S.H., Shon, H.K., Tijing, L.D.: Introduction: membrane desalination today, past, and future (2018)
2. Kokabian, B., Gude, V.G.: Microbial desalination systems for energy and resource recovery. In: Microbial Electrochemical Technology, pp. 999–1020. Elsevier (2019)
3. Phuntsho, S., Lotfi, F., Hong, S., Shaffer, D.L., Elimelech, M., Shon, H.K.: Membrane scaling and flux decline during fertiliser-drawn forward osmosis desalination of brackish groundwater. Water Res. **57**, 172–182 (2014)
4. Kebria, M.R.S., Rahimpour, A.: Membrane distillation: basics, advances, and applications. In: Advances in Membrane Technologies (2020)
5. Tian, H., Wang, Y., Pei, Y., Crittenden, J.C.: Unique applications and improvements of reverse electrodialysis: a review and outlook. Appl. Energy **262**, 114482 (2020)
6. Gupta, S.S., Islam, M.R., Pradeep, T.: Capacitive Deionization (CDI): An Alternative Cost-Efficient Desalination Technique, pp. 165–202. Advances in Water Purification Techniques. Elsevier (2019)
7. Blair, J.W., Murphy, G.W.: Electrochemical Demineralization of Water with Porous Electrodes of Large Surface Area. ACS Publications (1960)
8. Murphy, G., Caudle, D.: Mathematical theory of electrochemical demineralization in flowing systems. Electrochim. Acta **12**(12), 1655–1664 (1967)
9. Johnson, A.M., Newman, J.: Desalting by means of porous carbon electrodes. J. Electrochem. Soc. **118**(3), 510 (1971)
10. Farmer, J.C., Fix, D.V., Mack, G.V., Pekala, R.W., Poco, J.F.: Capacitive deionization of NaCl and $NaNO_3$ solutions with carbon aerogel electrodes. J. Electrochem. Soc. **143**(1), 159 (1996)
11. Tong, Y., Zhou, S., Zhou, J., Zhang, G., Li, X., Zhao, C., Liu, P.: Advances in efficient desalination technology of capacitive deionization for water recycling. J. Water Reuse Desalin. **11**(2), 189–200 (2021)

12. Johnson, A., Venolia, A., Newman, J., Wilbourne, R., Wong, C., Gillam, W., Johnson, S., Horowitz, R.: Electrosorb process for desalting water, Office of Saline Water Research and Development Progress Report No. 516, US Dept, Interior Pub 200(056) 31 (1970)
13. Jeon, S.-I., Yeo, J.-G., Yang, S., Choi, J., Kim, D.K.: Ion storage and energy recovery of a flow-electrode capacitive deionization process. J. Mater. Chem. A **2**(18), 6378–6383 (2014)
14. Hatzell, K.B., Iwama, E., Ferris, A., Daffos, B., Urita, K., Tzedakis, T., Chauvet, F., Taberna, P.-L., Gogotsi, Y., Simon, P.: Capacitive deionization concept based on suspension electrodes without ion exchange membranes. Electrochem. Commun. **43**, 18–21 (2014)
15. Gao, X., Omosebi, A., Landon, J., Liu, K.: Surface charge enhanced carbon electrodes for stable and efficient capacitive deionization using inverted adsorption–desorption behavior. Energy Environ. Sci. **8**(3), 897–909 (2015)
16. Han, L., Karthikeyan, K., Anderson, M., Wouters, J., Gregory, K.B.: Mechanistic insights into the use of oxide nanoparticles coated asymmetric electrodes for capacitive deionization. Electrochim. Acta **90**, 573–581 (2013)
17. Porada, S., Bryjak, M., Van Der Wal, A., Biesheuvel, P.: Effect of electrode thickness variation on operation of capacitive deionization. Electrochim. Acta **75**, 148–156 (2012)
18. Lee, J., Kim, S., Kim, C., Yoon, J.: Hybrid capacitive deionization to enhance the desalination performance of capacitive techniques. Energy Environ. Sci. **7**(11), 3683–3689 (2014)
19. Biesheuvel, P., Zhao, R., Porada, S., Van der Wal, A.: Theory of membrane capacitive deionization including the effect of the electrode pore space. J. Colloid Interface Sci. **360**(1), 239–248 (2011)
20. Kim, Y.-J., Choi, J.-H.: Improvement of desalination efficiency in capacitive deionization using a carbon electrode coated with an ion-exchange polymer. Water Res. **44**(3), 990–996 (2010)
21. Porada, S., Zhao, R., van der Wal, A., Presser, V., Biesheuvel, P.M.: Review on the science and technology of water desalination by capacitive deionization. Prog. Mater. Sci. **58**(8), 1388–1442 (2013)
22. Liu, P., Yan, T., Shi, L., Park, H.S., Chen, X., Zhao, Z., Zhang, D.: Graphene-based materials for capacitive deionization. J. Mater. Chem. A **5**(27), 13907–13943 (2017)
23. Sun, M.-H., Huang, S.-Z., Chen, L.-H., Li, Y., Yang, X.-Y., Yuan, Z.-Y., Su, B.-L.: Applications of hierarchically structured porous materials from energy storage and conversion, catalysis, photocatalysis, adsorption, separation, and sensing to biomedicine. Chem. Soc. Rev. **45**(12), 3479–3563 (2016)
24. Wu, Z.-S., Sun, Y., Tan, Y.-Z., Yang, S., Feng, X., Müllen, K.: Three-dimensional graphene-based macro-and mesoporous frameworks for high-performance electrochemical capacitive energy storage. J. Am. Chem. Soc. **134**(48), 19532–19535 (2012)
25. Porada, S., Borchardt, L., Oschatz, M., Bryjak, M., Atchison, J.S., Keesman, K.J., Kaskel, S., Biesheuvel, P.M., Presser, V.: Direct prediction of the desalination performance of porous carbon electrodes for capacitive deionization. Energy Environ. Sci. **6**(12), 3700–3712 (2013)
26. Madani, S., Falamaki, C., Kazemzadeh, M., Rahmanifard, A., Aboutalebi, S.H.: Conceptual circuit model for the prediction of electrochemical performance of carbonaceous electrodes containing reduced ultra large graphene oxide. J. Electrochem. Soc. **169**(4), 040554 (2022)
27. Gu, X., Yang, Y., Hu, Y., Hu, M., Huang, J., Wang, C.: Facile fabrication of graphene–polypyrrole–Mn composites as high-performance electrodes for capacitive deionization. J. Mater. Chem. A **3**(11), 5866–5874 (2015)
28. Huang, Z.-H., Yang, Z., Kang, F., Inagaki, M.: Carbon electrodes for capacitive deionization. J. Mater. Chem. A **5**(2), 470–496 (2017)
29. Rao, C.N.R., Sood, A.K., Subrahmanyam, K.S., Govindaraj, A.: Graphene: the new two-dimensional nanomaterial. Angewandte Chemie Int. Edn. **48**(42), 7752–7777 (2009)
30. Li, H., Lu, T., Pan, L., Zhang, Y., Sun, Z.: Electrosorption behavior of graphene in NaCl solutions. J. Mater. Chem. **19**(37), 6773–6779 (2009)
31. Li, H., Zou, L., Pan, L., Sun, Z.: Novel graphene-like electrodes for capacitive deionization. Environ. Sci. Technol. **44**(22), 8692–8697 (2010)
32. Mohanapriya, K., Ghosh, G., Jha, N.: Solar light reduced graphene as high energy density supercapacitor and capacitive deionization electrode. Electrochim. Acta **209**, 719–729 (2016)

33. Wang, H., Zhang, D., Yan, T., Wen, X., Zhang, J., Shi, L., Zhong, Q.: Three-dimensional macroporous graphene architectures as high performance electrodes for capacitive deionization. J. Mater. Chem. A **1**(38), 11778–11789 (2013)
34. Madani, S., Falamaki, C., Alimadadi, H., Aboutalebi, S.H.: Binder-free reduced graphene oxide 3D structures based on ultra large graphene oxide sheets: high performance green micro-supercapacitor using NaCl electrolyte. J. Energy Storage **21**, 310–320 (2019)
35. Yang, Z.Y., Jin, L.J., Lu, G.Q., Xiao, Q.Q., Zhang, Y.X., Jing, L., Zhang, X.X., Yan, Y.M., Sun, K.N.: Sponge-templated preparation of high surface area graphene with ultrahigh capacitive deionization performance. Adv. Func. Mater. **24**(25), 3917–3925 (2014)
36. Xu, X., Pan, L., Liu, Y., Lu, T., Sun, Z., Chua, D.H.: Facile synthesis of novel graphene sponge for high performance capacitive deionization. Sci. Rep. **5**(1), 1–9 (2015)
37. Li, Z., Song, B., Wu, Z., Lin, Z., Yao, Y., Moon, K.-S., Wong, C.: 3D porous graphene with ultrahigh surface area for microscale capacitive deionization. Nano Energy **11**, 711–718 (2015)
38. Kong, W., Duan, X., Ge, Y., Liu, H., Hu, J., Duan, X.: Holey graphene hydrogel with in-plane pores for high-performance capacitive desalination. Nano Res. **9**, 2458–2466 (2016)
39. Li, J., Ji, B., Jiang, R., Zhang, P., Chen, N., Zhang, G., Qu, L.: Hierarchical hole-enhanced 3D graphene assembly for highly efficient capacitive deionization. Carbon **129**, 95–103 (2018)
40. Chang, L., Hu, Y.H.: Surface-microporous graphene for high-performance capacitive deionization under ultralow saline concentration. J. Phys. Chem. Solids **125**, 135–140 (2019)
41. Wang, H., Yan, T., Liu, P., Chen, G., Shi, L., Zhang, J., Zhong, Q., Zhang, D.: In situ creating interconnected pores across 3D graphene architectures and their application as high performance electrodes for flow-through deionization capacitors. J. Mater. Chem. A **4**(13), 4908–4919 (2016)
42. Ma, J., Wang, L., Yu, F.: Water-enhanced performance in capacitive deionization for desalination based on graphene gel as electrode material. Electrochim. Acta **263**, 40–46 (2018)
43. Dianbudiyanto, W., Liu, S.-H.: Outstanding performance of capacitive deionization by a hierarchically porous 3D architectural graphene. Desalination **468**, 114069 (2019)
44. Cao, J., Wang, Y., Chen, C., Yu, F., Ma, J.: A comparison of graphene hydrogels modified with single-walled/multi-walled carbon nanotubes as electrode materials for capacitive deionization. J. Colloid Interface Sci. **518**, 69–75 (2018)
45. Aldalbahi, A., Rahaman, M., Almoiqli, M., Meriey, A.Y., Periyasami, G.: Efficiency improvement of a capacitive deionization (CDI) system by modifying 3D SWCNT/RVC electrodes using microwave-irradiated graphene oxide (mwGO) for effective desalination. J. Nanomater. **2020**, 1–14 (2020)
46. Xu, X., Liu, Y., Wang, M., Zhu, C., Lu, T., Zhao, R., Pan, L.: Hierarchical hybrids with microporous carbon spheres decorated three-dimensional graphene frameworks for capacitive applications in supercapacitor and deionization. Electrochim. Acta **193**, 88–95 (2016)
47. Gupta, S., Henson, A., Evans, B., Meek, R.: Graphene-based aerogels with carbon nanotubes as ultrahigh-performing mesoporous capacitive deionization electrodes for brackish and seawater desalination. Water Desal. Treat. **162**, 97–111 (2019)
48. Zhang, C., Wang, X., Wang, H., Wu, X., Shen, J.: Ambient pressure-dried graphene–composite carbon aerogel for capacitive deionization. Processes **7**(1), 29 (2019)
49. Yin, H., Zhao, S., Wan, J., Tang, H., Chang, L., He, L., Zhao, H., Gao, Y., Tang, Z.: Three-dimensional graphene/metal oxide nanoparticle hybrids for high-performance capacitive deionization of saline water. Adv. Mater. **25**(43), 6270–6276 (2013)
50. Gu, X., Yang, Y., Hu, Y., Hu, M., Huang, J., Wang, C.: Nitrogen-doped graphene composites as efficient electrodes with enhanced capacitive deionization performance. RSC Adv. **4**(108), 63189–63199 (2014)
51. Xu, X., Sun, Z., Chua, D.H., Pan, L.: Novel nitrogen doped graphene sponge with ultrahigh capacitive deionization performance. Sci. Rep. **5**(1), 11225 (2015)
52. Khan, Z.U., Yan, T., Shi, L., Zhang, D.: Improved capacitive deionization by using 3D intercalated graphene sheet–sphere nanocomposite architectures. Environ. Sci. Nano **5**(4), 980–991 (2018)

53. Vafakhah, S., Sim, G.J., Saeedikhani, M., Li, X., y Alvarado, P.V., Yang, H.Y.: 3D printed electrodes for efficient membrane capacitive deionization. Nanoscale Adv. **1**(12), 4804–4811 (2019)
54. Han, B., Cheng, G., Wang, Y., Wang, X.: Structure and functionality design of novel carbon and faradaic electrode materials for high-performance capacitive deionization. Chem. Eng. J. **360**, 364–384 (2019)
55. Bo, Z., Huang, Z., Xu, C., Chen, Y., Wu, E., Yan, J., Cen, K., Yang, H., Ostrikov, K.K.: Anion-kinetics-selective graphene anode and cation-energy-selective MXene cathode for high-performance capacitive deionization. Energy Storage Mater. **50**, 395–406 (2022)
56. Vafakhah, S., Guo, L., Sriramulu, D., Huang, S., Saeedikhani, M., Yang, H.Y.: Efficient sodium-ion intercalation into the freestanding Prussian blue/graphene aerogel anode in a hybrid capacitive deionization system. ACS Appl. Mater. Interfaces. **11**(6), 5989–5998 (2019)

The Evolution of 3D Graphene and Its Derivatives for Theranostic Applications

Aditya Srivastava, Akshit Rajukumar Prajapati, Sunil Venkanna Pogu, and Aravind Kumar Rengan

Abstract Beginning with the humble pencil, graphene has evolved to play a vital role in nanomedicine, particularly in the early detection of abnormalities and effective treatments thereof. Graphene and its derivatives have recently attracted much interest in various fields, including biomedicine, due to their exceptional physical and electrochemical properties. Owing to the high customizability, tuneability, and potential to functionalize using multiple biomolecules, the prospect of graphene to realize theranostic applications holds great promise for the advancement of modern healthcare. Theranostic applications like biosensing, drug delivery, "hybrid theranostics", etc., benefit significantly from the said functionalization. This is because they enhance graphene's solubility, stability, and loading capacity, among other properties. Recent applications also include multi-modal imaging and imaging-guided therapy, particularly in the case of Cancer. In this chapter, various aspects of 3D graphene-based theranostic modules, including fabrication and functionalization techniques, have been discussed, along with multiple applications and advantages. The recent advancements and challenges faced therein have also been elaborated upon.

Keywords 3D graphene · Graphene · Theranostics · Bioimaging · Graphene oxide · Reduced graphene oxide · Quantum dots · Drug delivery · Photothermal therapy · Photodynamic therapy

1 Introduction

In the case of materials sciences, almost all innovations and advances are the culmination of the merger between pre-existing technologies. The same is true for theranostics, a field that extensively applies both materials science and biomedicine. Despite the inherent complexity, theranostics is now one of the foremost strategies for multifunctional nano-engineered systems, more so because of the incessant need

---

A. Srivastava · A. R. Prajapati · S. V. Pogu · A. K. Rengan (✉)
Department of Biomedical Engineering, Indian Institute of Technology Hyderabad, Telangana 502285, India
e-mail: aravind@bme.iith.ac.in

© The Author(s), under exclusive license to Springer Nature Switzerland AG 2023

R. K. Gupta (ed.), *3D Graphene*, Carbon Nanostructures,
https://doi.org/10.1007/978-3-031-36249-1_23

for novel theranostic modalities to facilitate fast and accurate diagnosis of complex diseases. Theranostic modalities are rapid, cost-effective, and minimally invasive, hence advantageous over traditional diagnosis strategies that are slow, tedious, and costly. The said theranostic modalities must be not only extremely sensitive but also highly specific to distinguish between diseases exhibiting similar biomarkers and pathophysiology. These may also prove pivotal to the success of surgical interventions by enabling accurate pre-surgical guidance imaging and post-surgical confirmation of the absence of cancers.

Ever since the discovery of graphene in 2002 and the subsequent Nobel Prize awarded for the same in 2010, various attempts have been made to determine the full extent of the potential of graphene and derivatives thereof (alone or modified with nanoparticles) in various advanced fields like quantum physics; nanoelectronics; and, obviously, biomedicine [1]. Due to the versatility of its structure, it has rightfully been called the “mother of all carbon materials”, as it is the prime component of numerous carbon allotropes [2], and complex structures like carbon nanotubes (both single-layered and multi-layered), graphene oxide (GO), reduced graphene oxide (rGO), etc., and more carbon-based materials like “nanoribbons” [3] can be synthesized from it. An added advantage is the ease of fabrication and cost-effectiveness of these materials. Furthermore, a plethora of inorganic nanostructures can be cultivated from nanographene due to its remarkable surface properties, giving rise to various functional nanocomposites with equally impressive unique properties. Hence, it can be said that graphene has the potential to be the precursor for multiple theranostic modalities, some of which can also be multifunctional. In addition, various cargoes like drugs, nucleic acids, biomolecules, chromophores, fluorescent probes, etc. can be easily loaded onto graphene and its derivatives.

1.1 Strengths of Graphene

Graphene can be defined as a 2D monolayered, honeycomb-latticed nano-sheet of sp^2 hybridized carbons, having high intrinsic mobility. This unique arrangement confers some supreme properties to graphene, making it a novel, promising theranostic modality. Graphene nanostructures can be detected rapidly even at very low sensitization, and the sensing is highly specific and precise [4]. Recently, graphene nanostructures have even been employed in the diagnosis of COVID-19 [1]. Some of the most prominent features of graphene have been enumerated as follows:

1. **Ultra-high Surface Area**: Single-layered graphene sheets have an extremely high surface area because of the exposure of each atom, thereby providing free bonds for efficacious molecular loading and biological conjugation. This also opens graphene to functionalization, allowing the modifications to improve biocompatibility, enabling biosensing and cargo delivery.
2. **High Aromaticity**: Graphene has an abundance of delocalized π electrons, which significantly increase its aromaticity while also enabling functionalization and, in

turn, loading of various cargoes like drugs, genes, biomolecules, and even therapeutic cells. Higher aromaticity in rGOs makes them better at photosensitization than GOs.

3. **Oxygen-containing Functional Groups**: Most GOs and rGOs have an abundance of defects and functional groups enriched with oxygen. This improves the overall stability in a physiological sense and improves biological functionalization. Oxygen-rich functional groups also have an enhancing effect on the solubility of GOs. Graphene derivatives can easily be functionalized using polymeric agents like PEG, chitosan, and even biomolecules like peptides and antibodies.
4. **NIR and Fluorescent Optical Properties**: Graphene and its derivatives show impeccable inherent optical properties, both as fluorescent activity and NIR range excitation. This makes them highly suited for biosensing, bioimaging, and photothermal and photodynamic applications at both in vitro and in vivo levels [5]. The excitation and emission characteristics can also be tailored during synthesis [6]. The most common agents that can find use in fluorescence imaging are carbon nanotubes and quantum dots.
5. **Biocompatibility and Toxicity**: Graphene (and derivatives thereof) shows high biocompatibility and low toxicity but only after surface and size modifications, as seen in a few in vivo studies [7], wherein the ADME characteristics of nanographene were studied.

Apart from these properties, graphene also shows many intrinsic properties like high conductivity; high sensitivity; selectiveness; intrinsic mobility [1]; and other structural, optical, and electromagnetic properties surpassing other carbon and plasmonic nanomaterials. Some structures have also been known to show photoacoustic properties, enabling their usage in ultrasound-based therapies. Several attempts have been made to enhance the passivation, solubility, and biocompatibility of graphene.

2 Classification and Fabrication of Common Graphene-Based Theranostic Modalities

Several nanomaterials can be incorporated with graphene to create various nanosystems, which can find use in a plethora of biomedical applications, and there are numerous ways to obtain them. Classic examples of synthetic techniques include exfoliation (both chemical and mechanical), GO reduction, chemical vapor deposition (CVD), and organic synthesis. Despite the persistent lack of consensus when it comes to the classification of graphene-based theranostic modalities, some attempts have been made by a few. A broad classification of the said modalities has been shown in Fig. 1.

The synthesis of some common graphene-derivative theranostic materials has been discussed as follows.

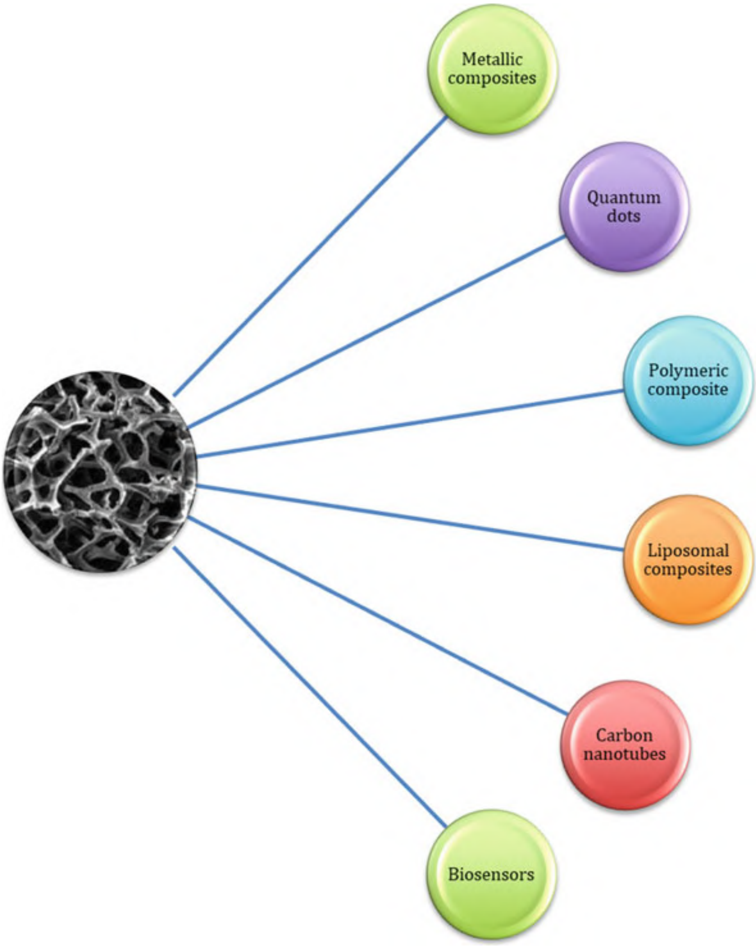

Fig.1 Overview of the classification of graphene-based theranostic modalities

2.1 Graphene-Based Metallic Nanocomposites

Metal nanoparticles are incorporated into graphene during synthesis to create innovative nanocomposites and other hybrid materials. This enables the possibility of nano-structuring remarkable nanoscale building blocks for new materials based on graphene derivatives. While there are many ways to manufacture graphene, most of them pose many stacking-related issues, which emerge from the consecutive layers having intermediate Van der Waals interactions, resulting in a loss of many valuable properties, and decreased utility. This problem can easily be rectified by functionalizing or modifying surface characteristics. These "stacking interactions" can efficiently be culled using metal or metal oxide nanosystems [8].

A vast variety of fabrication techniques are applicable in the synthesis of graphene-based metal nanocomposites, including bonding interactions (covalent or otherwise), growth methods (hydrothermal or solvothermal), reduction, microwave irradiation, and electrochemical deposition. It goes unsaid that each of these methods has its own set of advantages and disadvantages, and the choice of fabrication method can crucially affect the quality of the product obtained.

2.2 Graphene-Based Quantum Dots

"Graphene quantum dots", or GQDs, are fundamentally composed of triangular, zero-dimension (less than 10nm) forms of graphene. Drug delivery and theranostics benefit from GQDs because of their robust quantum confinement and edge effects. If their diameter is smaller than 30 nm, graphene balls produced from tens of graphene layers can also be considered GQDs. GQDs are an attractive replacement for semiconductor QDs, which are based on heavy metals. Compared to heavy metals, GQDs have been proven to be far more stable, easy to prepare, and benign to the environment. It is also possible to tailor GQDs for specific uses.

Carbon and hydrogen make up the bulk of the molecules in GQDs. GQDs can take on a variety of shapes, including spherical, oval, hexagonal, and even pyramidal ones. Carbonyl, carboxyl, hydroxyl, and epoxy groups, as well as the essential elements (C, O, and H) found in graphene, can be introduced to the surface of GQDs. To create GQDs having desired shapes, sizes, and homogeneity, attempts are being made to develop various simple and environment-friendly methods.

2.2.1 Top-Down Approaches

In these methods, GQDs are formed by partitioning larger GO sheets into smaller ones and rearrangement. Typical examples of such methods are chemical ablation and exfoliation, electron beam lithography, acidic and hydrothermal exfoliation, oxidation, laser ablation, etc.

2.2.2 Bottom-Up Approaches

In bottom-up methods, GQDs are built from organic molecular building blocks. Examples of such strategies are carbonization of organic precursors, solution chemistry, comprehensive utilization strategy, solvothermal synthesis, ultrasonic method, irradiation method, etc.

2.3 Graphene-Based Polymeric Nanocomposites

Nanomedicine has advanced leaps and bounds with the advent of novel modalities like polymeric nanocomposites, graphene included. A multiphase solid polymer nanocomposite has one phase with dimensions less than 100 nm. Polymeric nanocomposites contain therapeutic components in a polymer matrix. These nanocomposites can be made from cellulose and derivatives thereof, PET, polyamides and imides, polyethylene, and polycarbonates. In certain plastics, graphene can also be employed as a nanofiller [9]. Polymeric nanocomposites' physicochemical qualities depend on the polymer graphene layer distribution in the polymer matrix, and the interfacial connectivity. In its purest state, graphene does not produce composites with complete consistency. Chitosan coating on GO reduced hemolysis and increased erythrocyte compatibility [10].

The molecular weight, polarity, and hydrophobicity of the component material may affect the preparation procedure. Numerous technologies have produced polymer/graphite composites. Polymers are combined with graphite and intercalated between graphite layers.

Standard methods to synthesize polymeric nanocomposites of graphene include the non-covalent dispersion method, intercalation (solution-based or melting-based), in situ polymerization, in situ emulsion polymerization, and compounding.

2.4 Graphene-Based Liposomal Nanocomposites

To emulate the fluid mosaic structure and cell membrane features, liposomes have emerged as bio-inspired nano-platforms. Phospholipid-GO hybrids have only been described in a small number of investigations, including some that reported GO functionalized with a phospholipid monolayer, and studied its interactions with negatively charged, positively charged, and neutral liposomes. When compared to neutral or cationic liposomes, it was discovered that negatively charged liposomes were more stable in an aqueous solution [11].

Sonicating graphite in a liposomal suspension is one of the simplest methods used to create graphene-based liposomes. This is achieved due to the resultant nanoscale sheets of graphene being produced by sonication, which are then sandwiched between alkyl chains of phospholipids.

2.5 Graphene-Based Carbon Nanotubes (CNTs) and CNT-Hybrids

1D carbon nanotubes (CNTs), like 2D graphene, have inspired theoretical and practical research due to their large surface area and biological versatility. CNTs are certainly bigger in size and are structurally durable, but structural disruptions often tend to reduce their electric conductivity. Graphene-carbon nanotube hybrid films overcome this limitation, as graphene inhibits CNTs from clumping while carbon nanotubes prevent graphene sheets from restacking, making the hybrid stable. Among carbon nanostructures, graphene-CNT has the maximum edge density per unit area. Single-walled or multi-walled CNT hybrids have a certain number of carbon layers based on their diameter and catalyst size. Single-walled CNTs are usually cylindrical and 2–5 nm wide, whereas multi-walled CNTs are cylinders made of several graphene layers with a diameter between 2 and 100 nm [12].

Numerous methods like ultrasonication, chemical vapor deposition (CVD), layering-based assembly, or even self-assembly can be used to create graphene-CNT hybrid nanomaterials.

2.6 Graphene Nanocrystal Hybrids

The term "nanocrystal" refers to any substance composed of a crystalline lattice while being in the nanoscale range in at least one dimension. Graphene or its derivatives can be conjugated, integrated physically, or bonded chemically to form nanocrystal hybrids having the best of both worlds, i.e., the favorable characteristics of both parent substances. Nanocrystals (NCs) adorn a core made of graphene, creating a hybrid material with remarkable properties. Semiconducting nanocrystals can be made by using materials having singular or multi-crystalline arrangements of atoms. This particular arrangement confers various properties like broadened absorption bands, and efficacy in signal transduction and conversion, which result in enhanced photophysical, photochemical, and biological properties. Graphene-nanocrystal hybrids are now being studied for their potential in theranostics and targeted delivery.

Methods such as a direct method, oxidation method, in situ method, assembly method, and solution phase synthesis can be used to synthesize nanocrystals.

2.7 Graphene-Based Biosensors

Graphene and its derivative materials are especially advantageous as biosensors, owing to the transduction of various optical, thermal, and electrochemical signals enabled by them. Thus, many graphene-based biosensors can be fabricated based on the desired applicability and method of detection, with electrochemical biosensors being used more frequently than optical biosensors [1]. Apart from cancer theranostics, graphene-based biosensors are also being explored for other diseases like Diabetes mellitus [13].

Direct coating is the most frequent method for making biosensors because it is simple, cost-effective, and requires no special equipment [1]. In this method, electrodes can be directly coated, as the name suggests, using a graphene-rich gel or solution. Methods like blade coating, drip coating, spin coating, or drop-casting can be chosen for this purpose, based on the desired effects. Other parameters like surface area, film thickness, and homogeneity also play a key role in defining the properties of the product. Despite being highly convenient, some have pointed toward the wastefulness and time-consuming nature of this method [14].

Of late, 3D printers have introduced printing-based fabrication technologies. Printing techniques are desirable because of large-scale fabrication, cost-savings, and low processing temperature requirements, among other favorable factors, which facilitate the convenient incorporation of materials such as graphene. Various 3D printing methods like ink-jet or nozzle-jet printing, laser scribing, or screen printing can be employed.

Growing nanoparticles on electrodes is another biosensor fabrication process. This approach gained popularity due to adjustable manufacturing factors, which include time-related, thermal, pH, barometric, and concentration-based parameters. This method uses thermal, hydrothermal, and chemical degradation and anodization to accelerate nanomaterial development on electrode surfaces [1]. Due to restricted direct growth to the electrode surface, these approaches are given limited attention for fabricating graphene-based biosensors.

3 Novel Graphene-Based Nanocomposites

Recent years have seen the rise of many hybrid modalities, wherein the most advantageous properties of two or more systems (one of them being graphene based) have been combined to obtain superior properties. The utility of these systems is certainly not limited to theranostic applications but also tissue engineering and other such fields.

Hydrogels are desirable due to their properties like high moldability and water content. Add to that the structural reinforcement and other properties of graphene, and we get superior hybrid hydrogels that compensate for the lack of biocompatibility of graphene. These hybrid gels can act as scaffolds, model ECMs, with applicability in wound healing purposes, and even as drug delivery models, among various other applications [15].

Nowadays, a novel concept called “Organic dots” or “O-dots” has started gaining momentum. O-dots are basically graphene and other carbon derivatives that are dependent on other moieties like oxygen, hydrogen, and nitrogen for their optical properties [6]. Owing to their minuscule sizes, O-dots have been known to be highly photostable even after extended exposure to radiation. A variety of O-dots-based hybrid nanosystems find use in cancer theranostics.

The shortcomings of traditional magnetic nanoparticles (MNPs) manifesting as a lack of biocompatibility and overall low biofunctionalization can also be corrected using graphene-based nanosystems. Carbon-based magnetic nanosystems have been widely explored recently owing to their various interesting properties and potential for synergistic and image-guided therapy. Hybrid graphene-MNPs combine the best properties of both graphene and magnetic nanosystems, enabling utility in various domains like biosensing, MRI, hyperthermia, etc. Other novel materials like graphene nano-diamonds are also being explored [16].

4 Biocompatibility

The composition of graphene is mainly the carbon element, which is also a major component of body biomolecules that reduces the chances of tissue toxicity and its related complications. Multiple literature have reported the biocompatibility of graphene materials using various in vitro and in vivo analyses. For example, Jianfeng Li et al. bioprinted gelatine-supported alginate 3D scaffold coated with ascorbic acid-reduced graphene oxide to evaluate its adhesion property and cytocompatibility toward human adipose stem cells (ADSCs). It was found that reduced graphene oxide displayed superior cytocompatibility and supported the proliferation and differentiation of ADSCs (Fig. 2), which can be useful in autologous implant generation [17]. Similarly, Lee et al. reported the biocompatibility of graphene quantum dots (GQDs) against hepatocytes using a cell viability assay. It was found that GQDs-treated hepatocytes displayed no variation in cell viability for 48 h of treatment, and the extracellular aminotransferase, lactate dehydrogenase, and intracellular reactive oxygen species concentration also remained similar to the untreated cells [18]. In another study, graphene-coated polyimide electrodes were fabricated and their biocompatibility as a retinal implant was evaluated, and it was found that graphene-coated electrodes were more biocompatible as compared to uncoated electrodes. Through the histopathological studies, it was observed that graphene-coated electrodes attracted or activated less number of microglial cells compared to uncoated polyimide electrodes [19]. Another recent study has shown the enhanced biocompatibility of composite scaffolds with GOs, besides improvement in mechanical properties for the development of bone scaffolds [20].

5 Theranostic Applications of 3D Graphene

Graphene and its derivatives have recently garnered much attention in the scientific community due to its unique physical and chemical properties, including high mechanical strength, thermal stability, and electrical conductivity. These properties make graphene a promising material for various applications in electronics, energy, and biomedical fields. In recent years, 3D graphene-based nanostructures have emerged as a new class of materials that combine the advantages of graphene with those of 3D structures, making them ideal for use in theranostics. Theranostics, a rapidly growing field, refers to the development of multifunctional materials that can be used for both diagnosis and therapy of diseases, particularly cancer. Most of these applications can broadly be classified as follows.

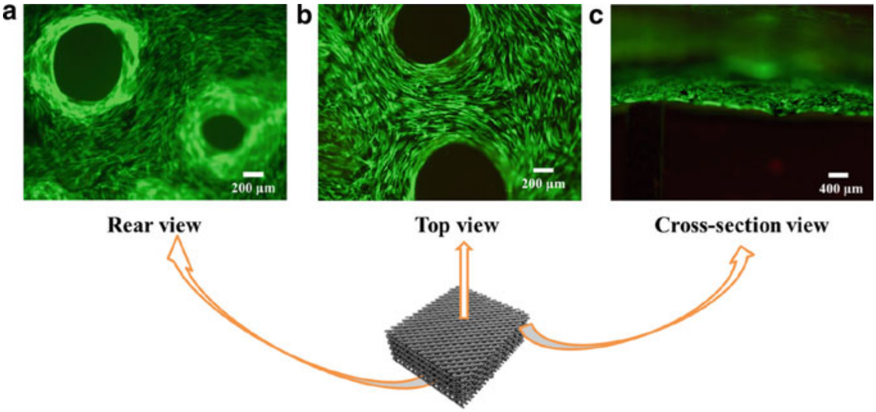

Fig. 2 Cell viability and adhesion on the 3D RGO/Alg scaffolds. Fluorescence microscope images of live/dead ADSC staining on 3D RGO/Alg scaffolds from **a** rear view, **b** top view, and **c** cross-sectional view following 7-day culture. Adapted with permission [17], Frontiers in Bioengineering and Biotechnology

5.1 Imaging-Based Theranostics

There are various imaging modalities that stand to benefit from the inclusion of graphene-based imaging agents. This is because of the excellent optical properties of graphene, which make it highly suitable for imaging in vivo. MRI contrast imaging is a widely used modality for cancer diagnosis and uses contrast agents to enhance the visibility of tumors. Multiple studies have shown the potency of nanographene entities in MRI imaging, and even in synergy with photodynamic activity [21]. Photoacoustic imaging (PAI) is a newer imaging modality that combines light and sound to generate images of biological tissues. Graphene-based nanostructures show high photoacoustic activity, thereby facilitating efficient imaging. A recent study shows the use of gallium-modified graphene nanobodies for photoacoustic and photothermal activities [22]. The proposed nanosystem could convert more than 42% of the incident light into heat.

Fluorescence imaging is a powerful tool for in vivo imaging, and can be used to visualize biological tissues and cells. Graphene-based modalities have the potential to further the progress of fluorescence imaging in cancer theranostics owing to the enhanced binding of fluorescent probes, as demonstrated in recent attempts [23]. Safe and efficiently targeted imaging of tumors has also been demonstrated recently using GO-based QDs [24].

X-ray CT imaging is a widely used diagnostic tool that uses X-rays to generate images of internal tissues and organs. 3D graphene-based nanostructures have the potential to act as contrast agents for X-ray CT imaging due to their high X-ray absorption properties, as shown in recent research [25]. Anjusha et al. showed the efficacy of amino acid-conjugated graphene nanosystems in simultaneous X-ray

CT imaging and PDT [26]. Certain multi-modal imaging platforms involving other techniques like Positron Emission Tomography imaging have also been developed.

5.2 Therapy-Enabling Applications

In recent years, various therapeutic applications of 3D graphene-based nanostructures have been investigated, including photothermal therapy, photodynamic therapy, hyperthermia therapy, chemotherapy, radiation therapy, immunotherapy, and gene therapy. Photothermal therapy is a method in which 3D graphene-based nanostructures are utilized as photothermal converters to convert light energy into heat, thereby destroying cancer cells. Quite literally, a vast number of graphene-based PTT agents have been shown to have a high therapeutic index in cancer therapy. Examples of such systems include both particulate and hydrogel-based PTT modalities [27, 28]. On the other hand, photodynamic therapy is a method in which a photosensitizer is activated by light to produce reactive oxygen species that can destroy cancer cells. The potential of graphene nanostructures to facilitate the same has been verified experimentally [29]. Along similar lines, hyperthermia therapy is a method in which heat is used to destroy cancer cells, which can also be enabled by various graphene-based nanosystems.

Chemotherapy is a method in which drugs are used to destroy cancer cells. 3D graphene-based nanostructures can be used to improve the efficacy of chemotherapy drugs by increasing drug accumulation in cancer cells. This also coincides with drug-delivery-related applications.

Radiation therapy is a method in which high-energy radiation is used to destroy cancer cells. A recent study shows the implementation of the same in facilitating terahertz wave ablation using a graphene-based antennary nanosystem [30].

Immunotherapy is a method in which the immune system is activated to fight cancer cells. Graphene-based nanostructures can be used to improve immunotherapy efficacy by enhancing antigen presentation and T-cell activation [31]. On the other hand, gene therapy is a method in which genes are introduced into cells to treat cancer. 3D graphene-based nanostructures can be used as gene delivery vehicles to improve gene transfection efficiency and therapeutic efficacy [32].

5.3 Application in Drug Delivery

The surface characteristics of graphene enable high tunability and surface engineering, which can be harnessed to facilitate the delivery of drugs and other active agents. Targeted drug delivery refers to the delivery of drugs specifically to the site of disease, such as a tumor, with the aim of maximizing therapeutic efficacy and minimizing side effects. 3D graphene-based nanostructures have been functionalized with targeting ligands such as antibodies, peptides, and small molecules to enhance their specificity for cancer cells. For example, a recent study utilized a 3D graphene-based nanostructure functionalized with folic acid to target and deliver doxorubicin to cancer cells [33]. The nanostructure showed improved therapeutic efficacy and reduced systemic toxicity compared to free doxorubicin while simultaneously enabling imaging as well.

Similarly, imaging-guided drug delivery involves the use of imaging techniques to monitor the distribution and efficacy of the therapeutic agents in real time. 3D graphene-based nanostructures can be conjugated with imaging agents such as fluorescent dyes, radionuclides, and near-infrared dyes to enable non-invasive imaging. Such nanosystems can be used as highly efficient delivery systems, while also providing the advantages of imaging.

Graphene-based nanomaterials are also highly applicable in developing various diagnosing point-of-care devices as graphene itself is a good electrical signal conductor. Concerning this, Tutku Beduk et al. developed a rapid point-of-care device based on the laser-scribed graphene technique. This device detects the change in electrical signal on the binding of the virus on antibody-coated gold nanostructures [34]. Similarly, Zahra et al. fabricated an aptamer-based biosensor using 3D graphene hydrogel and gold nanoparticles composites for diagnosing breast cancer markers' carcinoembryonic antigen (CEA) and cancer antigen 15–3 [35].

The excellent biocompatibility property of graphene-based material makes it suitable for disease diagnosis, drug delivery, and as a coating material for implants and 3D scaffolds (Fig. 3). In a study reported by Maria Romero et al., graphene oxide nanocomposites coated with PEG-folic acid, Indocyanine green, and Rhodamine B were synthesized. These nanocomposites were preferentially accumulated at tumor region visualized using in vivo imaging techniques, and under NIR light irradiation, nanocomposites displayed significant rise in temperature which aided in reducing the tumor size [36]. Graphene oxide displays an antimicrobial property and coating these on implants or surgical instruments can reduce the chances of microbial infection occurring during the post-surgical period. Similar to these contexts, Sofia Melo et al. fabricated poly caprolactone 3D scaffold with or without incorporating graphene oxide. 3D scaffold with graphene oxide displayed more bactericidal effect against *S. epidermidis* and *E. coli* and allowed adhesion of human cells [37]. Similarly, another study reported that incorporating graphene oxide in polylactic acid-based scaffolds had increased its cytocompatibility and mechanical properties [38].

6 Challenges and Shortcomings

According to recent market trends, 3D graphene theranostic systems have high commercialization potential, with immense growth rates by 2023. However, their commercialization certainly warrants the resolution of challenges that hinder their full use [1]. Scaling and mass-producing graphene-based theranostic systems are tedious and demand dedicated and skilled personnel for any significant pharmacological enterprise, which seems to be the prime cause for the lack of a clinically

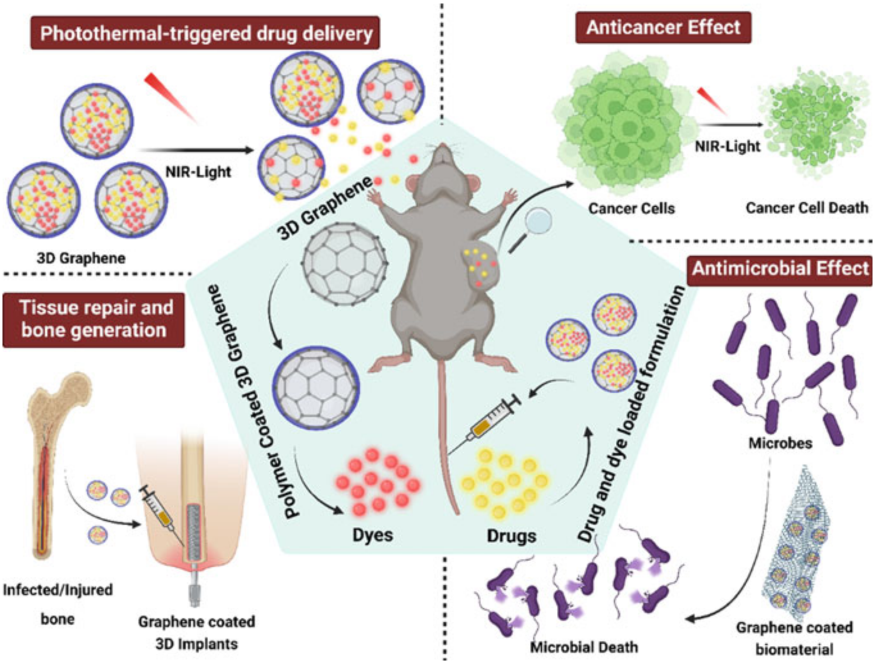

Fig. 3 Theranostic applications of 3D graphene

significant product. The synthesis parameters, although minimalistic and thoroughly explored, have a lot of anomalies and non-standardized protocols which in turn lead to batch inconsistency [39]. Most recent research studies lack significant data about various parameters like the size and stability of various systems. There are various parameters that affect the biocompatibility, including timing of intervention, release profiles, and even concentrations [40]. Size-toxicity relations are still not fully understood, worsening the situation even further. Thus, a crucial optimization of the said parameters needs to be done to establish and standardize protocols, only after which the up-scaling and industrialization of therapeutic modalities are possible [41]. This is not limited to synthesis alone—surface engineering and functionalization approaches are still daunting for many [6]. This is further problematic because the surface properties have a significant role in culling magnetic interactions and preventing aggregation of nanosystems.

Perhaps the most challenging aspect of most graphene-based systems seems to be that of toxicity and biocompatibility. Many of the recently published articles have shown the potential of these systems in vitro, but fall short of results on actual histological or in vivo levels [39]. Furthermore, such systems are also known to frequently elicit inflammatory responses [16]. Many experts in this field have reported weak fluorescence and photon yield [3] and false positives due to errant or unintended surface characteristics [1], worsened by other disadvantages like low solubility [42]. Magnetic nanoparticles have also been known to give false results, especially in viability tests like the MTT assay [41]. Recently, significant questions have been raised about the bioresponsiveness and rapid clearance of these systems and the effect of exposure routes on immune response and toxicity [43]. Some studies go even further, showing that these systems may be teratogenic or even foeticidal [44]. Incidences of disruption of membranes have also been reported in some cases [45]. Traditional in vivo approaches to screen for toxicity and other issues are limited by financial and time-related confinements [46]. All these issues necessitate resolution before these modalities can be put to clinical use without endangering the well-being of the patient. Approaches like biomicrofluidics and stealth functionalization [47] can be used as possible ways to achieve adequate biosafety. A recent study has shown the amelioration of graphene toxicity using Ginsenoside Rg3 in a therapeutic approach against liver and breast cancer cell lines [48]. Furthermore, in silico algorithms with good predictability are also being developed, which can provide another layer of validation for the development of new theranostic modalities [46].

7 Conclusion and Future Prospects

In recent years, graphene and its derivatives have been used as prime components to develop multiple theranostic modalities [49]. Various methods have been discovered for synthesizing the said systems, including both top-down and bottom-up approaches. The many remarkable properties of these modalities make them rather versatile and applicable in a diverse array of applications ranging from sensing and diagnosis, to drug delivery and photosensitization-based therapies [50]. Various novel systems like radio-labeled graphene and graphene nanoribbons have been proposed, with great therapeutic potential. Other modalities like sonodynamic therapy [43] and photoacoustic imaging [3] have also emerged as novel non-invasive theranostic strategies. Graphene-based theranostic systems are superior because of the inherent superior properties which enable tuneability and customization.

Despite the remarkable advantages and versatility associated with graphene-derived systems, there are various drawbacks that hinder their full usage potential and bench-to-bedside translation. Most of these hindrances are due to batch inconsistencies, dicey biocompatibility, and an overall inadequacy of clinically significant research in this direction. However, this is being rectified by the numerous research groups who are working on developing novel modalities and improving the existing ones. Upconversion [42, 43], 3D-bioprinting, and green synthesis are only a few of the new avenues being explored, apart from existing areas like synergistic therapy, radiotherapy, and even photoacoustic and sonodynamic therapy. As most market trends reveal, redressal of the drawbacks is well underway, and the day is not far when graphene-based theranostic modalities will emerge with commercial success.

References

1. Alhazmi, H.A., Ahsan, W., Mangla, B., Javed, S., Hassan, M.Z., Asmari, M., Al Bratty, M., Najmi, A.: Graphene-based biosensors for disease theranostics: development, applications, and recent advancements. Nanotechnol Rev. **11**, 96–116 (2021)
2. Sharma, J., Sharma, S., Ajay, K., Sharma, L.K.: Role of graphene in biomedical applications. Mater. Today Proc. **63**, 542–546 (2022)
3. Lee, S.Y., Kwon. M., Raja. I.S., Molkenova. A., Han. D.W., Kim. K.S.: Graphene-based nanomaterials for biomedical imaging, pp. 125–148 (2022)
4. Peña-Bahamonde, J., Nguyen, H.N., Fanourakis, S.K., Rodrigues, D.F.: Recent advances in graphene-based biosensor technology with applications in life sciences. J Nanobiotechnol. **16**, 75 (2018)
5. Cheung, F.: Engineering of new graphene-based materials as potential materials to assist near-infrared photothermal therapy cancer treatment. Heliyon **6**, e04131 (2020)
6. Shiralizadeh Dezfuli, A., Kohan, E., Tehrani Fateh, S., Alimirzaei, N., Arzaghi, H., Hamblin, M.R.: Organic dots (O-dots) for theranostic applications: preparation and surface engineering. RSC Adv. **11**, 2253–2291 (2021)
7. Yang, K., Feng, L., Shi, X., Liu, Z.: Nano-graphene in biomedicine: theranostic applications. Chem. Soc. Rev. **42**, 530–547 (2013)
8. Manolata Devi, M., Sahu, S.R., Mukherjee, P., Sen, P., Biswas, K.: Graphene-metal nanoparticle hybrids: electronic interaction between graphene and nanoparticles. Trans. Indian Inst. Met. **69**, 839–844 (2016)
9. Das, T.K., Prusty, S.: Graphene-based polymer composites and their applications. Polym. Plast. Technol. Eng. **52**, 319–331 (2013)
10. Miculescu, M., Thakur, V.K., Miculescu, F., Voicu, S.I.: Graphene-based polymer nanocomposite membranes: a review. Polym. Adv. Technol. **27**, 844–859 (2016)
11. Shim, G., Kim, M.-G., Park, J.Y., Oh, Y.-K.: Graphene-based nanosheets for delivery of chemotherapeutics and biological drugs. Adv. Drug Deliv. Rev. **105**, 205–227 (2016)
12. Shahriary, L., Ghourchian, H., Athawale, A.A.: Graphene-multiwalled carbon nanotube hybrids synthesized by gamma radiations: application as a glucose sensor. J. Nanotechnol. **2014**, 1–10 (2014)
13. Wang, C., Raza, S.A., Adebayo, T.S., Yi, S., Shah, M.I.: The roles of hydro, nuclear and biomass energy towards carbon neutrality target in China: a policy-based analysis. Energy **262**, 125303 (2023)
14. Sun, C.-L., Lai, S.-Y., Tsai, K.-J., Wang, J., Zhou, J., Chen, H.-Y.: Application of nanoporous core–shell structured multi-walled carbon nanotube–graphene oxide nanoribbons in electrochemical biosensors. Microchem. J. **179**, 107586 (2022)
15. Sangam, S., Garg, P., Sanyal, T., Pahari, S., Khurana, S.M.P., Mukherjee, M.: Graphene quantum dots and their hybrid hydrogels: a multifaceted platform for theranostic applications. In: Synthesis and Applications of Nanoparticles, pp. 417–453. Springer Nature Singapore, Singapore (2022)
16. Jiang, H., Xia, C., Lin, J., Garalleh, H.A.L., Alalawi, A., Pugazhendhi, A.: Carbon nanomaterials: a growing tool for the diagnosis and treatment of diabetes mellitus. Environ. Res. **221**, 115250 (2023)
17. Li, J., Liu, X., Crook, J.M., Wallace, G.G.: 3D printing of cytocompatible graphene/alginate scaffolds for mimetic tissue constructs. Front. Bioeng. Biotechnol. **8**, 1–11 (2020)
18. Lee, N.E., Jeong, J.M., Lim, H.S., Lee, S.Y., Cho, S.O.: Ultraviolet/blue light emitting high-quality graphene quantum dots and their biocompatibility. Carbon NY **170**, 213–219 (2020)
19. Nguyen, D., Valet, M., Dégardin, J., Boucherit, L., Illa, X., de la Cruz, J., del Corro, E., Bousquet, J., Garrido, J.A., Hébert, C., Picaud, S.: Novel graphene electrode for retinal implants: an in vivo biocompatibility study. Front. Neurosci. **15**, 1–10 (2021)
20. Sahafnejad-Mohammadi, I., Rahmati, S., Najmoddin, N., Bodaghi, M.: Biomimetic polycaprolactone-graphene oxide composites for 3D printing bone scaffolds. Macromol. Mater. Eng. 2200558 (2023)

21. Hassani, S., Gharehaghaji, N., Divband, B.: Chitosan-coated iron oxide/graphene quantum dots as a potential multifunctional nanohybrid for bimodal magnetic resonance/fluorescence imaging and 5-fluorouracil delivery. Mater. Today Commun. **31**, 103589 (2022)
22. Zhang, Y., Guo, Z., Zhu, H., Xing, W., Tao, P., Shang, W., Fu, B., Song, C., Hong, Y., Dickey, M.D., Deng, T.: Synthesis of liquid gallium@reduced graphene oxide core-shell nanoparticles with enhanced photoacoustic and photothermal performance. J. Am. Chem. Soc. **144**, 6779–6790 (2022)
23. Chen, C.Y., Chiu, H.Y., Chang, S.J., Yeh, N.L., Chan, C.H., Shih, C.C., Chen, S.L., Yang, J.W., Huang, C.Y., Chen, G.Y.: Enhanced probe bonding and fluorescence properties through annealed graphene oxide nanosheets. ACS Biomater. Sci. Eng. (2022) acsbiomaterials 1c01044
24. Ouyang, A., Zhao, D., Wang, X., Zhang, W., Jiang, T., Li, A., Liu, W.: Covalent RGD–graphene–phthalocyanine nanocomposite for fluorescence imaging-guided dual active/passive tumor-targeted combinatorial phototherapy. J. Mater. Chem. B **10**, 306–320 (2022)
25. Mirrahimi, M., Alamzadeh, Z., Beik, J., Sarikhani, A., Mousavi, M., Irajirad, R., Khani, T., Davani, E.S., Farashahi, A., Ardakani, T.S., Bulte, J.W.M., Ghaznavi, H., Shakeri-Zadeh, A.: A 2D nanotheranostic platform based on graphene oxide and phase-change materials for bimodal CT/MR imaging, NIR-activated drug release, and synergistic thermo-chemotherapy. Nanotheranostics **6**, 350–364 (2022)
26. Anjusha, A.J., Thirunavukkarasu, S., Resmi, A.N., Jayasree, R.S., Dhanapandian, S., Krishnakumar, N.: Multifunctional amino functionalized graphene quantum dots wrapped upconversion nanoparticles for photodynamic therapy and X-ray CT imaging. Inorg. Chem. Commun. **149**, 110428 (2023)
27. Costa, F.J.P., Nave, M., Lima-Sousa, R., Alves, C.G., Melo, B.L., Correia, I.J., de Melo-Diogo, D.: Development of Thiol-Maleimide hydrogels incorporating graphene-based nanomaterials for cancer chemo-photothermal therapy. Int. J. Pharm. **635**, 122713 (2023)
28. Lei, Z., Fan, J., Li, X., Chen, Y., Shi, D., Xie, H., Liu, B.: Biomimetic graphene oxide quantum dots nanoparticles targeted photothermal-chemotherapy for gastric cancer. J. Drug Target. **31**, 320–333 (2023)
29. Vinothini, K., Dhilip Kumar, S.S., Abrahamse, H., Rajan, M.: Synergistic effect of polymer functionalized graphene oxide system for breast cancer treatment. Int. J. Pharm. 632, 122556 (2023)
30. Geyikoglu, M.D., Koc, H., Çavusoglu, B., Ertugrul, M., Abbasian, K.: Designing graphene-based antenna for terahertz wave ablation (TWA) system. Erzincan Üniversitesi Fen Bilimleri Enstitüsü Dergisi **15**, 507–514 (2022)
31. Shi, C., Fu, W., Zhang, X., Zhang, Q., Zeng, F., Nijiati, S., Du, C., Liu, X., Wang, M., Yao, Y., Huang, H., Zheng, N., Chen, X., Wu, B., Zhou, Z.: Boosting the immunoactivity of T cells by resonant thermal radiation from electric graphene films for improved cancer immunotherapy. Adv. Ther. (Weinh) 2200163 (2022)
32. Demirel, E., Yuksel Durmaz, Y.: PEGylated reduced graphene oxide as nanoplatform for targeted gene and drug delivery. Eur. Polym. J. **186**, 111841 (2023)
33. Kang, H., Wang, T., Liu, W., Tian, D.: Folic acid modified graphene quantum dots from konjac glucomannan for cell imaging and targeted drug delivery. ChemistrySelect **7** (2022)
34. Beduk, T., Beduk, D., de Oliveira Filho, J.I., Zihnioglu, F., Cicek, C., Sertoz, R., Arda, B., Goksel, T., Turhan, K., Salama, K.N., Timur, S.: Rapid point-of-care covid-19 diagnosis with a gold-nanoarchitecture-assisted laser-scribed graphene biosensor. Anal. Chem. **93**, 8585–8594 (2021)
35. Shekari, Z., Zare, H.R., Falahati, A.: Dual assaying of breast cancer biomarkers by using a sandwich–type electrochemical aptasensor based on a gold nanoparticles–3D graphene hydrogel nanocomposite and redox probes labeled aptamers. Sens. Actuators B Chem. **332**, 129515 (2021)
36. Romero, M.P., Buzza, H.H., Stringasci, M.D., Estevão, B.M., Silva, C.C.C., Pereira-Dasilva, M.A., Inada, N.M.: Bagnato versus graphene oxide theranostic effect: conjugation of photothermal and photodynamic therapies based on an in vivo demonstration. Int. J. Nanomed. **16**, 1601–1616 (2021)

37. Melo, S.F., Neves, S.C., Pereira, A.T., Borges, I., Granja, P.L., Magalhães, F.D., Gonçalves, I.C.: Incorporation of graphene oxide into poly(ε-caprolactone) 3D printed fibrous scaffolds improves their antimicrobial properties. Mater. Sci. Eng. C 109 (2020)
38. Belaid, H., Nagarajan, S., Teyssier, C., Barou, C., Barés, J., Balme, S., Garay, H., Huon, V., Cornu, D., Cavaillès, V., Bechelany, M.: Development of new biocompatible 3D printed graphene oxide-based scaffolds. Mater. Sci. Eng. C **110**, 110595 (2020)
39. Roy, S., Jaiswal, A.: Graphene-based nanomaterials for theranostic applications. Rep. Adv. Phys. Sci. **01**, 1750011 (2017)
40. Huang, S., Zhong, Y., Fu, Y., Zheng, X., Feng, Z., Mo, A.: Graphene and its derivatives: “one stone, three birds” strategy for orthopedic implant-associated infections. Biomater. Sci. **11**, 380–399 (2023)
41. Lage, T., Rodrigues, R.O., Catarino, S., Gallo, J., Bañobre- López, M., Minas, G.: Graphene-based magnetic nanoparticles for theranostics: an overview for their potential in clinical application. Nanomaterials **11**, 1073 (2021)
42. Kansara, V., Tiwari, S., Patel, M.: Graphene quantum dots: a review on the effect of synthesis parameters and theranostic applications. Colloids Surf B Biointerfaces **217**, 112605 (2022)
43. Geetha Bai, R., Ninan, N., Muthoosamy, K., Manickam, S.: Graphene: a versatile platform for nanotheranostics and tissue engineering. Prog Mater Sci **91**, 24–69 (2018)
44. Xu, S., Zhang, Z., Chu, M.: Long-term toxicity of reduced graphene oxide nanosheets: effects on female mouse reproductive ability and offspring development. Biomaterials **54**, 188–200 (2015)
45. Liao, C., Li, Y., Tjong, S.: Graphene nanomaterials: synthesis, biocompatibility, and cytotoxicity. Int. J. Mol. Sci. **19**, 3564 (2018)
46. Wang, T., Russo, D.P., Bitounis, D., Demokritou, P., Jia, X., Huang, H., Zhu, H.: Integrating structure annotation and machine learning approaches to develop graphene toxicity models. Carbon NY **204**, 484–494 (2023)
47. Belling, J.N., Jackman, J.A., Yorulmaz Avsar, S., Park, J.H., Wang, Y., Potroz, M.G., Ferhan, A.R., Weiss, P.S., Cho, N.-J.: Stealth immune properties of graphene oxide enabled by surface-bound complement factor H. ACS Nano **10**, 10161–10172 (2016)
48. Rahimi, S., van Leeuwen, D., Roshanzamir, F., Pandit, S., Shi, L., Sasanian, N., Nielsen, J., Esbjörner, E.K., Mijakovic, I.: Ginsenoside Rg3 reduces the toxicity of graphene oxide used for pH-responsive delivery of doxorubicin to liver and breast cancer cells. Pharmaceutics **15**, 391 (2023)
49. Zhang, L., Dong, Q., Zhang, H., Xu, J., Wang, S., Zhang, L., Tang, W., Li, Z., Xia, X., Cai, X., Li, S., Peng, R., Deng, Z., Donovan, M.J., Chen, L., Chen, Z., Tan, W.: A magnetocatalytic propelled cobalt–platinum@graphene navigator for enhanced tumor penetration and theranostics. CCS Chem. **4**, 2382–2395 (2022)
50. Atiyah, N.A., Albayati, T.M., Atiya, M.A.: Functionalization of mesoporous MCM-41 for the delivery of curcumin as an anti-inflammatory therapy. Adv. Powder Technol. (2022)

Toxicity, Stability, Recycling, and Risk Assessments

Raunak K. Tamrakar, Kanchan Upadhyay, Judith Gomes, and Sunil Kumar

Abstract As the production of graphene has increased and its range of uses has expanded, worries about the possible harmful effects that its derivative nanoparticles and materials may have on human health have come to the fore. Numerous studies have demonstrated that graphene, in whatever shape it takes, affects a wide range of living things. Prokaryotic bacteria, viruses, plants, micro- and macro-invertebrates, mammalian and human cells, and whole creatures in vivo are some of these organisms. However, there is frequently a great deal of disagreement, if not outright controversy, regarding the results of the studies that have been carried out. As a result, we present in this paper a critical analysis of the most recent reports that have been gathered in the area of the biocompatibility and toxicology of materials related to graphene. Our objective is to provide information on the most current developments, new trends, and potential career opportunities in this area. Graphene exposure scenarios like inhalation through the respiratory system, ingestion through the digestive tract, administration via the parenteral route, and topical exposure through the skin are examined in the context of the experiment results using a variety of in vitro and in vivo model systems.

Keywords Graphene · Graphene derivatives · Health · Environment · Cytotoxicity

1 Introduction

Carbonaceous nanomaterials are being used in an increasing number of applications, thoroughly evaluating the risks associated with them and identifying strategies to reduce those risks of the utmost importance from the standpoint of human health and safety. Since the announcement of the Nobel Prize in this field in 2010, graphene has been at the forefront of 2D representatives and as such deserves a special level of merit and scrutiny. In many publications, graphene toxicity has been explored in

---

R. K. Tamrakar (✉) · K. Upadhyay · J. Gomes · S. Kumar
Bhilai Institute of Technology (Seth Balkrishan Memorial), Near Bhilai Power House, Durg, Chhattisgarh, India
e-mail: rounak.tamrakar@bitdurg.ac.in; raunak.ruby@gmail.com

© The Author(s), under exclusive license to Springer Nature Switzerland AG 2023

R. K. Gupta (ed.), *3D Graphene*, Carbon Nanostructures,
https://doi.org/10.1007/978-3-031-36249-1_24

terms of various issues including synthesis method, environmental exposure, tissue engineering, biological applications, its physiochemical behavior, a new system for nano-drug delivery, and its use in the advanced treatment or as a theranostic tool [1].

The toxicity study of the 3D graphene material has not been studied in detail; however, new experimental evidence shows that our current understanding of the biocompatibility, toxicity, and potential applications of graphene-based nanomaterials is still lacking clarity and, at times, even controversy. This is due in large part to the wide variety of graphene forms currently on hand, but it is also attributable to differences in experimental setups and approaches between research centers. Graphene is a 2D carbon nanomaterial consisting of a single layer, and it is characterized by the formation of strong covalent bonds between its constituent carbon atoms in sp2 hexagonal networks [2]. These hexagonal networks are the building blocks of 3D graphite, while 2D carbon nanotubes are created by rolling up sheets. Graphene materials have different dimensions and are interconnected with each other as described in Fig. 1. When comparing the edge effects and surface chemistries of these materials, we will find that they are vastly distinct. It is the edges and defects in graphene that facilitate bio-interactions, but the hydrophilic surface of graphene oxide makes it a stable dispersion in water [3]. We have attempted to provide a more thorough overview of the most recent developments in this field here in order to cast light on the cutting-edge trends and future prospects in the field of graphene-related biocompatibility and toxicology. Graphene and its derivatives are being used more frequently in advanced structures and technologies for applications in electronics, catalysis, computing, and health care. In this situation, one must consider the potentially harmful effects of graphene materials on the environment and human health when released from the devices at the end of their useful lives, with a focus primarily on the assessment of potential risks connected to the individual components and implemented materials of the devices themselves. The idea behind a number of novel drug delivery methods is that the drug will come into direct touch with human cells either after topical application or after systemic administration. The identification and characterization of the potential hazards are anticipated to make use of the maximum physicochemical characterization of the questioned nanomaterial, which includes physicochemical factors.

However, there are numerous safety concerns surrounding graphene materials. Although the potential toxicity of GBMs has been brought to light, there are only a small number of toxicity studies available, and the threat they pose to human health is largely unexplored. Workplace exposure to GBMs appears to pose the greatest threat to human health at this time, while their uses are still in the testing phase. Humans are most likely to be exposed to GBMs during industrial or small-scale production and waste discharge through inhalation, cutaneous, and ocular routes due to the proximity of the respiratory tract, skin, and eyes to the work environment. It is also possible to ingest GBMs through secondary inhalation and accidental oral ingestion.

A thorough description and classification for 3D graphene architectures have not yet been established, despite the rapid development of 3D graphene materials over the past 10 years and the exploration of many new synthesis techniques and

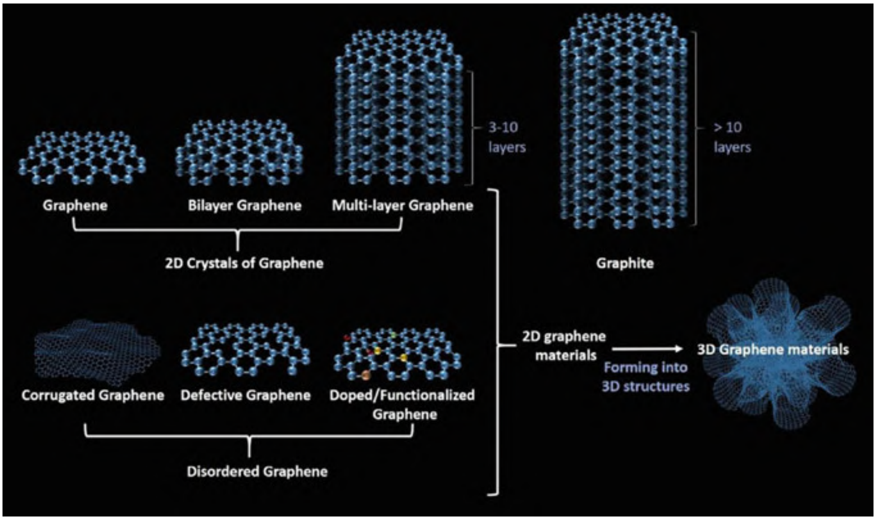

Fig. 1 Relationships among graphene, 2D graphene materials, 3D graphene materials, and graphite. Reproduced with permission [1], Copyright 2020, American Chemical Society

application fields. It's true despite the fact that both of those things have been tried. Furthermore, there were clear differences in the features of 3D graphene materials made with various methods, leading to a wide range of performances when applied to various contexts. The formation mechanism for each 3D graphene family and the key steps that influence the properties of the 3D architectures must all be thoroughly understood in order to fine-tune the functionalization of a 3D graphene structure and maximize its performance for specific applications. Several excellent reviews of methods for producing large, three-dimensional graphene monoliths were published in the early years of the field (one type of 3D graphene materials). The most recent, relevant studies have primarily focused on 3D graphene-based composite materials for a variety of applications. Further research into the 3D graphene family is still needed [4].

The safe and effective management of nanoparticles is a topic that must be revisited frequently to ensure that any risks to respiratory health are mitigated or eliminated. As graphene nanomaterials continue to gain in popularity, it's important that information about potential risks and how to mitigate them is regularly updated and made accessible. And this is even though studies are being run on the topic. In this chapter, we assess the potential for mitigating the risks associated with graphene-based materials, and we look at ways to do so, such as by making use of graphene's physicochemical properties, surface modifications, and potential catabolic degradation pathways. Finally, we offer an in-depth evaluation of recent developments in health care, diagnostics, and novel therapeutic approaches that are enabled by graphene.

2 Toxicity and Exposure Route of Graphene-Based Nanoparticles

Different exposure methods or routes of administration allow GFNs to enter the body or cells, where they can cause toxicity both in vivo and in vitro (Fig. 2). The degree of GFN toxicity may depend on factors such as the administration route, the route of entry, the tissue distribution and excretion, and the pattern of cell uptake [4]. Therefore, it may be useful to clarify them in order to better comprehend the rules governing the emergence and evolution of GFNs' toxicity.

For the most comprehensive toxicological information, bio-persistence and accumulation patterns of nanomaterials as well as the effects of acute and chronic long-term exposure need to be fully investigated. In light of the aforementioned factors, we assess the most current information on the toxicity of graphene.

2.1 *Respiratory Exposure*

One of the most probable exposure routes is through the respiratory system (inhalation), with potential applications in both industrial manufacturing settings and in the event that graphene is unintentionally exposed to people through the environment. Han et al. [5] investigated the effects of a single 6-h nasal inhalation method at doses of 0.46 and 3.76 mg/m3 on the lungs of Sprague–Dawley rats. Following graphene exposure, there were no appreciable changes in body weight, food intake, or organ weight during the 2-week recovery interval. The findings of the study demonstrate

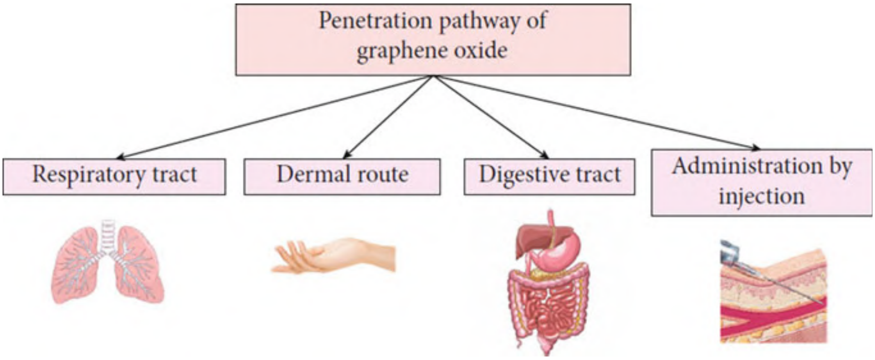

Fig. 2 Exposure route of graphene materials. Adapted from [4]. Copyright © 2021 Asmaa Rhazouani et al. This is an open-access article distributed under the Creative Commons Attribution License, which permits unrestricted use, distribution, and reproduction in any medium, provided the original work is properly cited

that even at concentrations that are relatively high in comparison to the possible realistic environmental equivalent, graphene oxide's pulmonary toxicity is low following either a single dose or a series of doses over an extended period of time.

In order to investigate the potential pro-inflammatory effects of graphene nanoplatelets and their accumulation in the mediastinal lymph nodes of rats, a different intratracheal instillation paradigm and the context of variable surface functionalization of nanomaterials by carboxylic acid groups were used. Even though it was discovered that all particle types had dose-dependent, unidirectional impacts, only the positively charged graphene nanoplatelets significantly increased neutrophil counts after 24 h. In other words, the acute pro-inflammatory effect that was noticed was not sustained, and cell counts had already returned to normal by the end of the first week. No matter how the surface charge was modified, nanomaterial eventually built up in the local lymph nodes [6]. It is clear that there is an urgent need for researchers in the field to agree on a long-awaited unified approach to dose-exposure calculations in nanotoxicology studies, including those involving animals. This is because different authors in the aforementioned studies estimated exposure dose in different ways.

2.2 *Oral Exposure*

In Sprague–Dawley rats, the effects of oral graphene oxide doses varying from 10 to 40 mg/kg have been studied [7]. The findings demonstrated that superoxide dismutase, catalase, and glutathione peroxidase activities increased in the kidneys of rats in a dose-dependent manner and that the accumulation of hydrogen peroxide and lipid hydroperoxide was also substantially elevated. All in all, these results provide strong evidence for oxidative stress's role in inducing nephrotoxicity in experimental animals, calling for more thorough research into the topic. The authors suggest that reduced graphene oxide exposure may have an influence on the activity of serum superoxide dismutase, which may explain the transient changes in the animals' behavior observed after ingestion of the compound. In contrast, there is hardly any evidence that a person's explorer, anxious, learner, or memory behaviors alter [8]. However, it is difficult to extrapolate from these reports the conceivable exposure doses for humans in the workplace or through consumer products.

This is the first major study to determine the effects of administering multilayered pristine graphene intragastrically to mice on a daily basis for 4 weeks. It was surprising to learn, in light of the review's discussion of graphene's antibacterial properties, that exposure to the material increased the diversity of gut microbiota and shifted the microbial community in favor of G-bacteria. This may be due to the fact that different microorganisms are more or less sensitive to oxidative stress and have varying degrees of membrane stability after coming into contact with graphene. Antibiotic-resistant genes in the gut microbiota of mice were found to be significantly more numerous and diverse after exposure to graphene. The results of this study should be considered in the development of new graphene-based drugs for oral administration, and similar groundbreaking discoveries are likely to be made in the near future.

2.3 Cutaneous Exposure

The literature is growing in favor of the utilization of graphene nanomaterials in cutting-edge applications for various skin-related issues which include wearable skin sensors, diagnostic devices, and transdermal patches for medicine delivery, tissue engineering, and regenerative systems [9]. While it is common knowledge that carbonaceous nanomaterials are associated with an elevated risk of skin illnesses. Surprisingly little research has been done into the impacts of graphene on dermal toxicity and the functional state of its cellular components in vivo. Out of all the studies only one has reported that the antibacterial cotton textiles infused with graphene oxide were found to be over 90% effective against bacteria even after being washed 100 times without causing irritation to rabbit skin [10]. The impacts of graphene and its derivatives, such as PEGylated graphene oxide/polypropylene fumarate nanocomposites, on dermal fibroblasts, an important cellular component of the skin, have only been studied in vitro so far. In both studies, graphene was determined to be safe for fibroblasts. However, Wang et al. [11] discovered that graphene oxide actually inhibits the adhesion, cytotoxicity, and apoptosis of human fibroblasts at concentrations higher than 50 g/mL. More research is required because this exposure scenario is still largely unexplored, particularly in light of the conflicting experimental data that are presently available.

2.4 Intravenous Exposure

Graphene oxide's acute and chronic dose-dependent toxicity in mice following systemic intravenous administration was previously reported by Wang et al. In animal studies, no acute or chronic toxicity was observed at doses up to 0.25 mg/animal. At a higher dose of 0.4 mg/animal graphene accumulated inside the organs due to insufficient clearance, causing chronic toxicity manifestations like lung granuloma formation [11]. There was no accumulation of unmodified, pristine few-layered graphene in the brain, heart, or testes after 3 months of monitoring in a study using similar high doses (20 mg/kg). Regardless of the surface chemistry, the accumulation of graphene materials in the organs caused significant cellular and organ damage, as evidenced by the development of necrotic and fibrotic foci and dysfunction in glomerular filtration.

Recently, comparable outcomes were seen after injecting graphene oxide functionalized with poly sodium 4-styrene sulfonate into the veins. This injected graphene material shows persistent accumulation for 6 months inside the internal organs liver, lungs, etc. and results in chronic specific organ inflammation. By using a novel administration method, intraperitoneal parenteral, Kurantowicz et al. investigated the biodistribution of several carbonaceous nanomaterials. The connective tissue of the epidermis, muscles, and peritoneum of the abdominal cavity, as well as the injection location, all contained significant aggregates of the nanomaterials [12]. Despite the significance of these findings from a mechanistic and experimental standpoint, this route of administration is unlikely to be used in humans.

3 Biological Fate of Graphene Materials

A number of variables, including administration methods, physicochemical characteristics, particle agglomeration, and surface coating, have a major influence on the biological fate including biodistribution, biotransformation, and excretion of graphene materials. The effect of graphene materials on different organs has been shown in Fig. 3. After giving mice GO intravenously, Zhang et al. [13] found that the substance was securely retained in a number of organs, including the lungs, liver, spleen, and bone marrow. GO caused pulmonary edema in rodents when administered intravenously at a dose of 10 mg/kg body weight [13]. Due to its increased chemical reactivity, GO can be biotransformed to significantly alter its physicochemical properties [14]. Qi and coworkers demonstrated that GO could undergo a substantial physicochemical transformation in Gamble's solution and artificial lysosomal fluid, both of which mimic human lung fluids (ALF). The carbonyl and epoxy groups in GO were converted to phenolic groups after being treated with lung fluids, resulting in a smaller molecule. This alteration got rid of macrophages, which slowed down the endocytosis of GO. In addition, the changes occurring in Gamble's solution lessened GO's interaction with cells and allowed for its precipitation. But modifications to the ALF improved the adhesion of large sheet-like GO aggregates to the plasma membrane in the absence of cell uptake [15]. Biotransformation of GO in blood plasma has been shown to affect toxicity, according to other studies. Analyses of metabolic pathways revealed that biotransformation mitigated oxidative stress caused by GO by primarily modifying fatty acid metabolism and decreasing galactose metabolism. New research has shown that the interaction of GO particles with the digestive fluids and the acidic pH of the stomach causes them to aggregate. Oral absorption of GO does not result in biotransformation, as no structural changes or degradation have been observed [16]. In different organs, GO is eliminated in different ways. Difficult to clear from the lungs, GO triggers inflammation, cell infiltration, granuloma formation, and pulmonary edema. Following the bile duct from the duodenum, GO nanoparticles are excreted from the body via the hepatobiliary pathway in the liver [17]. The functional derivatives of GO polyethylene glycol tend to build up in the liver, while the spleen can be eliminated gradually, most likely via the kidneys and fecal excretion. Although the precise mechanisms by which GO is excreted in vivo remain unclear, it appears that the kidneys and the intestines play a significant role in its elimination. There have been a number of conflicting findings about where and how much of this nanomaterial is excreted so far.

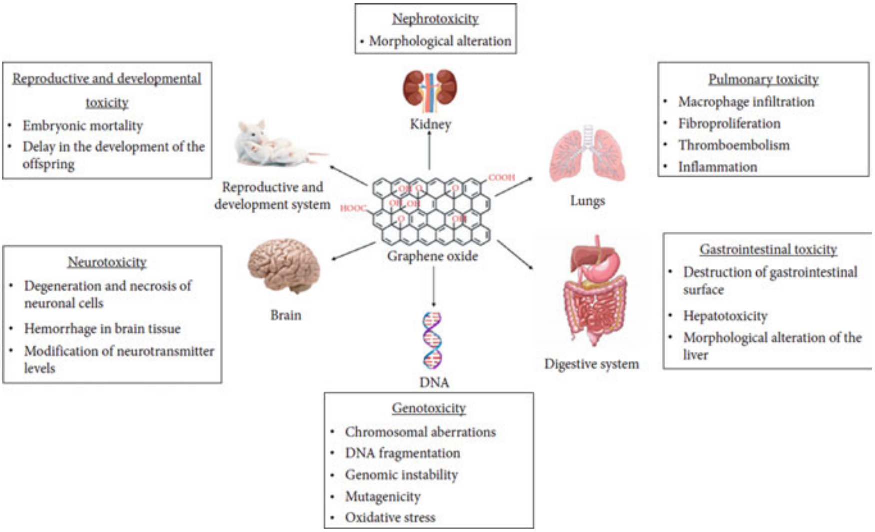

Fig. 3 Toxic effect of graphene oxide in different organs. Adapted from [4]. Copyright © 2021 Asmaa Rhazouani et al. This is an open-access article distributed under the Creative Commons Attribution License, which permits unrestricted use, distribution, and reproduction in any medium, provided the original work is properly cited

Sasidharan et al. prepared FLG and two of its derivatives (carboxylated FLG-COOH and PEGylated FLG-PEG) to investigate the biodistribution of these compounds over a 24-h period (lateral dimension: 100,200 nm, thickness: 0.8 nm) [18]. FLG-COOH accumulated more in the lungs than FLG-PEG did anywhere else over the period of 24 h, whereas FLG-PEG accumulated in the lungs first and then moved on to the liver and spleen. To assess their biodistribution in both small and large GO sheets, researchers in another study intravenously injected mice with 125I-labeled GO sheets for 180 min. It was discovered that small GO had a longer blood circulation period than large GO. While only a trace amount of small GO sheets were identified in the lungs and spleen, they accumulated mainly in the liver (with a peak at 5 min and a gradual decline through 180 min) rapidly disappearing from these organs [19].

All told, these studies have helped researchers better understand the fate of different GBMs after being administered in different ways. Several different GBMs have been shown to overcome normal physiological barriers and spread to distant secondary organs. However, it is still too soon to draw definitive conclusions with respect to relationships between physicochemical features and the biodistribution patterns of GBMs due to the paucity of published data and the lack of systematic investigations. What happens to GBMs over time at the site where they tend to accumulate is also crucial. To generate such information, however, is not simple; it necessitates labeled materials that can be followed and measured quantitatively over extended periods of time, even as GBMs undergo biotransformation or degradation within the body.

4 Toxicity Mechanism

One of the key elements significantly affecting the biocompatibility of nanomaterials, independent of their ex-synthesis composition, is biocorona formation upon contact with the biological milieu, which contains a broad range of biomolecules, including a profusion of proteins. Since the word was first coined nearly 10 years ago, numerous reports have established the significance of the phrase “protein corona” for the functional behavior of nanoparticles and their ensuing effects at the cellular and organismal levels [20].

However, a nanoparticle core containing a coat of surface functionalized substances can also significantly affect the biocorona’s dynamic makeup. It was discovered that one instance of a surface change that improves biocompatibility in vitro and in vivo involves the functionalization of GO with PAA (poly acrylic acid). When compared to the pristine or PEGylated graphene oxide nanomaterials, this surface modification significantly decreased the cytotoxicity and other significant biological and pathological changes in the internal organs of mice that are typically induced by graphene oxides. According to the authors’ hypotheses, differences in the amount of platelet depletion in blood, the formation of thrombi during short-term exposure, and the known pro-inflammatory effects following long-term exposure are caused by the different protein corona compositions, particularly immunoglobulin G, which form on the surface of nanoparticles and regulate their interactions with cell membranes and cellular uptake [21]. These findings are in line with research suggesting that covering graphene oxide with a protein like BSA can lessen the cytotoxicity of the material by preventing it from penetrating cell membranes. Due to a reduction in accessible surface area and unfavorable steric effects, the interaction between the graphene surface and the phospholipids in the cell membrane is reduced in order to achieve this [22]. Similar to this, it was discovered using a simulation-based molecular dynamics method that graphene oxide strongly binds to proteins via pi-pi stacking interactions with aromatic protein residues. This raised the theoretical possibility of reduced cytotoxicity of reduced graphene oxide nanosheets and graphene oxide after coating with major high abundance blood proteins, a finding that has since been experimentally verified [23].

However, it is still debatable and uncertain exactly how the biocorona’s composition affects the toxicity of graphene. In light of this, the possibility of reducing the toxicity of these biological secretions was complexed with graphene, which resulted in modified nanoplatelets.

4.1 Risk Assessment Methods

Risks and uncertainties related to the commercialization of graphene-enabled products (GEP) need to be evaluated thoroughly on a macro-, micro-, and nano-scale basis. In particular, it is essential to reduce risks associated with development costs, regulatory requirements, and environmental concerns before introducing novel materials and products to the market (i.e., health and safety aspects). Since graphene is an advanced material with many potential uses, it can be difficult to determine whether or not the material poses any significant risks to consumers, workers, or the environment. The aforementioned discussion also shows that GEP can vary widely in its physicochemical properties depending on the application to which it is ultimately put. As a result, GEP risk assessment can be very time-consuming and resource-intensive if dedicated separately to each product. Due to this, the scientific, industrial, and regulatory communities have been working very hard over the past 10 years to develop the necessary characterization cascades, quality assurance tools, and frameworks for risk assessments, management, and monitoring of emerging products containing advanced materials. Most of the time, the improvement is linked to some characteristic of the materials being used that operates at the nano-scale [24].

The incorporation of a tiered safe-by-design method [25] can be used as a de-risking strategy to identify uncertainties and risks during the early stages of GEP development. Standardization of graphene characterization is necessary for improved customer trust, reproducibility, and quality assurance. In addition, the risk assessment procedure can be prioritized with the help of newly introduced safety thresholds for each GEP component. Those who pose the greatest health risks are screened first, as this is where the bulk of the data is gathered and analyzed. Dekkers et al. developed a non sepcific risk assesment strategy [26] and put into practice for the benefit of consumers and, in the case of medical goods, patients.

4.2 Optimal Physical and Chemical Properties

The best way to reduce the dangers brought on by graphene exposure depends on a number of important considerations. By utilizing basic physical properties, graphene's toxicity is influenced by how much of it has been oxidized; less oxidized graphene has been shown to produce more reactive oxygen species, cytotoxicity, and apoptosis, which can have a big impact. One of the most recent and intriguing findings is the possibility of making use of the chiral characteristics of graphene quantum dots.

4.3 Surface Functionalization

It has been demonstrated that coating with chitosan is one of the earliest documented simple methods to reduce the harmful impact of graphene oxide on red blood cells and is a nearly 100% effective method of eliminating this type of toxicity [27]. Recent research suggests that the hydrophilicity and weak inductive nature of a novel hydroxylated graphene derivative promote cell adhesion and growth of stromal cells derived from rat adipose tissue. Because of the ease of this method, industrial quantities of this graphene derivative can be produced in the kilogram range [28]. It has been demonstrated that amine-modified graphene oxide is a much safer functionalized material than its unmodified graphene oxide or reduced graphene oxide counterparts in terms of its possible thrombogenic and hemolytic effects in mice in vivo [29].

4.4 Modified Degradation

GO nanoparticles tweaked with PEG and branched PEE when introduced in biological systems as nano-drug carriers join plasmid DNA through electrostatic interaction to create a stable nano-complex. After being absorbed by cells, the complex can quickly leave endosomes by photothermally converting graphene oxide after being exposed to near-infrared light and causing endosome disruption. The reduced intracellular environment enables polymer dissociation and rapid gene release, increasing transfection efficacy and lowering toxicity when compared to non-reducible amide-functionalized graphene nanocarriers. Additionally, the exposed disulfide bonds in the de-PEGylated graphene oxide nanocarriers boost phagocyte engulfment and facilitate macrophage degradation [30]. In order to create biocompatible and seemingly biodegradable structures with the potential to act as sensitive T2 contrast agents, Zan et al. have created a novel technique for creating water-dispersible nanocomposites with iron oxide nanoparticles attached to graphene. These composites are non-toxic, according to the writers, because the body's metabolic processes excrete them [31]. As the biodegradation process, in this case, was only related to the iron oxide component of the complex, this study emphasizes the importance of implementing the aforementioned safe-by-design approach [25], which must be strictly adhered to from the very early stages of the development of new nanomedicines in relation to all the constituent components. It ensures that cutting-edge diagnostic and therapeutic preparations are risk-free, successful in healing their intended cells, and have the least possible impact on unrelated cells.

5 Stability and Sustainability of 3D Graphene

Graphene is an extraordinary substance; it has been hailed as a wonder substance with the potential to revolutionize the entire industry. The potential to revolutionize entire sectors and our built environment lies in a one-atom-thick layer of carbon that is 200 times stronger than steel, transparent, flexible, and extremely thermally and electrically conductive. Thus, we can say graphene carries the property of higher conductivity, higher mechanical strength than steel, and a dense packing structure along with the flexibility of modifying them in the form of other nanotubes. This makes a tremendous impact in every field, whether it is a medical, chemical, or any other industrial application. Graphene has been praised as one of the most important material advancements since the plastics revolution more than a century ago since its discovery in 2004. Early predictions suggested that the kinds of goods and technologies are seen in science fiction movies would almost instantly be made possible by graphene. After more than 15 years, that has yet to take place [32].

Graphene is a form of carbon that could bring us bulletproof armor and space elevators, improve medicine, cell phone batteries, headphones, and even bridges and make the Internet run faster. In 15 years of the journey of graphene and its applicability, consumers have been hearing about this wonder material and all the ways it could change everything. Graphene opened a new window in materials science in 3D materials and has enormous properties and has the potential to use in electronics in aerospace industries. The main constraint is its mass production and production cost [33]. The main reason why manufacturing doesn't produce the desired products is that growth frequently only produces thin flakes of various sizes. There are a lot of tiny flakes, but we need big sheets so that we can use them for electronics. But that's really challenging. The flash technique only produces flakes, as do the items shown, which is useful if you need just flakes for some reason. The biggest advance, however, will come from the production of huge sheets of pure single-layer graphene. Although many people are working on it, nobody has had much luck with it [34].

From solar cells to computer chips, graphene is set to disrupt many industries. This is because the biggest hurdle to overcome is not science but mass production. There are several companies working on graphene materials to be used in a vast array of markets. These companies are on the cutting edge and getting closer by the day to unlocking the key to mass-producing graphene. Sustainability is now a priority, and we should concentrate on graphene applications that already separate waste from other waste streams, applications that can increase the operational lifetime, and integration with materials from which graphene can be recovered most easily [34]. As a sustainable material, graphene has enormous potential. This includes sustainable methods of producing graphene from either natural or waste sources, as well as using graphene to reduce material usage (and reducing the carbon footprint of these materials in the process). Many people talk about graphene in high-tech applications, but it is in these fundamental applications where graphene can be used as an additive that the graphene market will be propelled forward. 3D graphene is expected to be a sustainable, autonomous wearable devices that could be biodegradable or compostable and would rely on Graphene Flagship developments in the electronic components, powering of the device, and also the sensors which are integrated into that device in years to come. Future graphene research anticipates new directions as the demand for environmental protection and sustainable alternatives grows. So, we know graphene hasn't changed the world yet but is truly on the verge of skyrocketing the changes by revolutionizing the world. The future of graphene appears bright, but we must ensure that the world we live in is taken into account when making decisions about graphene applications.

6 Conclusion and Future Prospects

Graphene is a wonder material with properties like a diamond, 200 times stronger than steel, has high elasticity, is lighter than aluminum, and is a pure substance that has a very large surface area and carries some semi-conductor properties and can be stretched 20 to 25% of its original length. Graphene with such quality can be mixed with other materials to make extraordinary composites. Graphene has a very high thermal conductivity ratio which is even better than that of silver and copper and even has good electrical conductivity. Due to its flat hexagonal lattice structure, it has low resistance and hence has electrical conductivity 13 times higher than that of copper and very near to that of superconductors. Graphene has higher electron mobility as compared to semi-conductors like silicon and thus is very useful in the electronic industry on a large scale and it will revolutionize the electronic industry and technology as a whole. Graphene is super thin and almost completely transparent and can transmit 97 to 99% of light and hence has super optical properties, thus in the future it can be used in the optical industry and even can be used as a perfect material for solar panels, LCDs, touch screens, etc. Graphene is already started being used in new forms of energy storage devices like supercapacitors and water filters and can reduce pressure on the planet by helping us turn ocean water into safe drinking water.

With constraints of mass production for commercial purposes, it is expected that bottom-up and top-down graphene production methods will solve the commercial production of graphene in coming years with the different types of graphene, and very soon in coming years, we can expect to see the different types of graphene in products.

References

1. Sun, Z., Fang, S., Hu, Y.H.: 3D graphene materials: from understanding to design and synthesis control. Chem. Rev. **120**, 10336–10453 (2020)
2. Malard, L.M., Pimenta, M.A., Dresselhaus, G., Dresselhaus, M.S.: Raman spectroscopy in graphene. Phys. Rep. 473, 51–87 (2009)
3. Russier, J., Treossi, E., Scarsi, A., Perrozzi, F., Dumortier, H., Ottaviano, L., Meneghetti, M., Palermo, V., Bianco, A.: Evidencing the mask effect of graphene oxide: a comparative study on primary human and murine phagocytic cells. Nanoscale **5**, 11234–11247 (2013)
4. Asmaa, R., Halima, G., Mounir, E.A., Khalid, A., Lhoucine, G., Md Sahab, U., Faissal, A.: Synthesis and toxicity of graphene oxide nanoparticles: a literature review of in vitro and in vivo studies. BioMed Res. Int. **2021** (2021), Article ID 5518999
5. Han, S.G., Kim, J.K., Shin, J.H., Hwang, J.H., Lee, J.S., Kim, T.G., Lee, J.H., Lee, G.H., Kim, K.S., Lee, H.S., Song, N.W., Ahn, K., Yu, I.J.: Pulmonary responses of sprague-dawley rats in single inhalation exposure to graphene oxide nanomaterials. Biomed. Res. Int. **2015**, 376756 (2015)
6. Lee, J.K., Jeong, A.Y., Bae, J., Seok, J.H., Yang, J.Y., Roh, H.S., Jeong, J., Han, Y., Jeong, J., Cho, W.S.: The role of surface functionalization on the pulmonary inflammogenicity and translocation into mediastinal lymph nodes of graphene nanoplatelets in rats. Arch. Toxicol. **91**(2), 667–676 (2016)
7. Patlolla, A.K., Randolph, J., Kumari, S.A., Tchounwou, P.B.: Toxicity evaluation of graphene oxide in kidneys of sprague-dawley rats. Int. J. Environ. Res. Public Health **13**, 380–388 (2016)
8. Zhang, D., Zhang, Z., Liu, Y., Chu, M., Yang, C., Li, W., Shao, Y., Yue, Y., Xu, R.: The short- and long-term effects of orally administered high-dose reduced graphene oxide nanosheets on mouse behaviors. Biomaterials 68, 100–113 (2015)
9. Ding, X., Liu, H., Fan, Y.: Graphene-based materials in regenerative medicine. Adv. Healthc. Mater. **4**, 1451–1468 (2015)
10. Zhao, J., Deng, B., Lv, M., Li, J., Zhang, Y., Jiang, H., Peng, C., Li, J., Shi, J., Huang, Q., Fan, C.: Graphene oxide-based antibacterial cotton fabrics. Adv. Healthc. Mater. **2**(9), 1259–66 (2013)
11. Wang, K., Ruan, J., Song, H., Zhang, J., Wo, Y., Guo, S., Cui, D.: Biocompatibility of graphene oxide. Nanoscale Res. Lett. **6**, 8 (2011)
12. Kurantowicz, N., Strojny, B., Sawosz, E., Jaworski, S., Kutwin, M., Grodzik, M., Wierzbicki, M., Lipinska, L., Mitura, K., Chwalibog, A.: Biodistribution of a high dose of diamond graphite, and graphene oxide nanoparticles after multiple intraperitoneal injections in rats. Nanoscale Res. Lett. **10**, 398 (2015)
13. Zhang, X., Yin, J., Peng, C., Hu, W., Zhu, Z., Li, W., Fan, C., Huang, Q.: Distribution and biocompatibility studies of graphene oxide in mice after intravenous administration. Carbon **49**, 986–995 (2011)
14. Raslan, A., Burgo, L.S.D., Ciriza, J., Pedraz, J.L.: Graphene oxide and reduced graphene oxide-based scaffolds in regenerative medicine. Int. J. Pharm. **580**, 119226 (2020)
15. Qi, Y., Liu, Y., Xia, T., Xu, A., Liu, S., Chen, W.: The biotransformation of graphene oxide in lung fluids significantly alters its inherent properties and bioactivities toward immune cells. NPG Asia Mater. **10**(5), 5385–5396 (2018)
16. Guarnieri, D., Sánchez-Moreno, P., Del Rio Castillo, A.E., Bonaccorso, F., Gatto, F., Bardi, G., Martín, C., Vázquez, E., Catelani, T., Sabella, S., Pompa, P.P.: Small **14**, 1800227 (2018)
17. Hirn, S., Semmler-Behnke, M., Schleh, C., Wenk, A., Lipka, J., Schäffler, M., Takenaka, S., Möller, W., Schmid, G., Simon, U., Kreyling, W.G.: Particle size dependent and surface charge-dependent biodistribution of gold nanoparticles after intravenous administration. Eur. J. Pharm. Biopharm. **77**(3), 407–416 (2011)
18. Sasidharan, A., Swaroop, S., Koduri, C.K., Girish, C.M., Chandran, P., Panchakarla, L.S., Somasundaram, V.H., Gowd, G.S., Nair, S., Koyakutty, M.: Comparative in vivo toxicity, organ biodistribution and immune response of pristine, carboxylated and PEGylated few-layer graphene sheets in swiss albino mice: a three month study. Carbon **95**, 511–524 (2015)

19. Liu, J.-H., Yang, S.-T., Wang, H., Chang, Y., Cao, A., Liu, Y.: Effect of size and dose on the biodistribution of graphene oxide in mice. Nanomedicine **7**, 1801–1812 (2012)
20. Volkov, Y.: Quantum dots in nanomedicine: recent trends, advances and unresolved issues. Biochem. Biophys. Res. Commun. **468**, 419–27 (2015)
21. Xu, M., Zhu, J., Wang, F., Xiong, Y., Wu, Y., Wang, Q., Weng, J., Zhang, Z., Chen, W., Liu, S.: Improved in vitro and in vivo biocompatibility of graphene oxide through surface modification: poly(acrylic acid)-functionalization is superior to PEGylation. ACS Nano **10**, 3267–3281 (2016)
22. Duan, G., Kang, S.G., Tian, X., Garate, J.A., Zhao, L., Ge, C., Zhou, R.: Protein corona mitigates the cytotoxicity of graphene oxide by reducing its physical interaction with cell membrane. Nanoscale **7**, 15214–15224 (2015)
23. Chong, Y., Ge, C., Yang, Z., Garate, J.A., Gu, Z., Weber, J.K., Liu, J., Zhou, R.: Reduced cytotoxicity of graphene nanosheets mediated by blood-protein coating. ACS Nano **9**, 5713–5724 (2015)
24. Mu, L., Gao, Y., Hu, X.: Characterization of biological secretions binding to graphene oxide in water and the specific toxicological mechanisms. Environ. Sci. Technol. **50**(16), 8530–8537 (2016)
25. Movia, D., Gerard, V., Maguire, C.M., Jain, N., Bell, A.P., Nicolosi, V., O'Neill, T., Scholz, D., Gun'ko, Y., Volkov, Y., Prina-Mello, A.: A safe-by-design approach to the development of gold nanoboxes as carriers for internalization into cancer cells. Biomaterials **35**, 2543–2557 (2014)
26. Dekkers, S., Oomen, A.G., Bleeker, E.A., Vandebriel, R.J., Micheletti, C., Cabellos, J., Janer, G., Fuentes, N., Vazquez-Campos, S., Borges, T., Silva, M.J., Prina-Mello, A., Movia, D., Nesslany, F., Ribeiro, A.R., Leite, P.E., Groenewold, M., Cassee, F.R., Sips, A.J., Dijkzeul, A., van Teunenbroek, T., Wijnhoven, S.W.: Towards a nanospecific approach for risk assessment. Regul. Toxicol. Pharmacol. **80**, 46–59 (2016)
27. Liao, K.H., Lin, Y.S., Macosko, C.W., Haynes, C.L.: Cytotoxicity of graphene oxide and graphene in human erythrocytes and skin fibroblasts. ACS Appl. Mater. Interfaces **3**, 2607–2615 (2011)
28. Sun, J., Deng, Y., Li, J., Wang, G., He, P., Tian, S., Bu, X., Di, Z., Yang, S., Ding, G., Xie, X.: A new graphene derivative: hydroxylated graphene with excellent biocompatibility. ACS Appl. Mater. Interfaces **8**, 10226–10233 (2016)
29. Singh, S.K., Singh, M.K., Kulkarni, P.P., Sonkar, V.K., Gracio, J.J., Dash, D.: Amine-modified graphene: thrombo-protective safer alternative to graphene oxide for biomedical applications. ACS Nano **6**, 2731–2740 (2012)
30. Kim, H., Kim, J., Lee, M., Choi, H.C., Kim, W.J.: Stimuli-regulated enzymatically degradable smart graphene-oxide-polymer nanocarrier facilitating photothermal gene delivery. Adv. Healthc. Mater. **5**, 1918–1930 (2016)
31. Zan, P., Yang, C., Sun, H., Zhao, L., Lv, Z., He, Y.: One-pot fabricating Fe_3O_4/graphene nanocomposite with excellent biocompatibility and non-toxicity as a negative MR contrast agent. Colloids Surf. B Biointerfaces **145**, 208–16 (2016)
32. Barbhuiya, N.H., Kumar, A., Singh, A., Chandel, M.K., Arnusch, C.J., Tour, J.M., Singh, S.P.: The future of flash graphene for the sustainable management of solid waste. ACS Nano **15**(10), 15461–15470 (2021)
33. Shukla, S., Khan, I., Bajpai, V.K., Lee, H., Kim, T., Upadhyay, A., Tripathi, K.M.: Sustainable graphene aerogel as an ecofriendly cell growth promoter and highly efficient adsorbent for histamine from red wine. ACS Appl. Mater. Interfaces **11**, 18165−18177 (2019)
34. Zhang, X., Wang, L., Lu, Q., Kaplan, D.L.: Mass production of biocompatible graphene using silk nanofibers. ACS Appl. Mater. Interfaces **10**, 22924–22931 (2018)